Universität Hamburg
DER FORSCHUNG | DER LEHRE | DER BILDUNG

Light-Mediated Liquid-Gas Reactions:

Photooxidation and Photocarbonylation Chemistry

an der Universität Hamburg eingereichte Dissertation

zur Erlangung des Doktorgrades der Naturwissenschaften

Dr. rer. nat.

an der Fakultät für Mathematik, Informatik und Naturwissenschaften

Fachbereich Chemie

Institut für Anorganische und Angewandte Chemie

der Universität Hamburg

vorgelegt von

Robin Stuhr

September 2024

The experimental part of this work was performed from December 2020 to July 2024 at the Institute of Inorganic and Applied Chemistry, University of Hamburg. This work was supervised by Prof. Dr. Axel Jacobi von Wangelin.

„Und man hat Recht;

so ein bisschen Bildung ziert den ganzen Menschen"

<div align="right">-   Heinrich Heine in „Reisebilder"</div>

I.   List of Publications

[1] S. Bettermann, R. Stuhr, H.-U. Moritz, W. Pauer
Customizable 3D-printed stirrers for investigation, optimization and scale-up processes of batch emulsion copolymerizations
Chem. Eng. Sci. **2019**, *206*, 50–62, DOI 10.1016/j.ces.2019.05.026.

[2] E. González, R. Stuhr, J. M. Vega, E. García-Lecina, H.-J. Grande, J. R. Leiza, M. Paulis
Assessing the Effect of CeO_2 Nanoparticles as Corrosion Inhibitor in Hybrid Biobased Waterborne Acrylic Direct to Metal Coating Binders
Polymers **2021**, *13*, 848, DOI 10.3390/polym13060848.

[3] R. Stuhr, P. Bayer, C. B. W. Stark, A. Jacobi von Wangelin
Light-Driven Waste-To-Value Upcycling: Bio-Based Polyols and Polyurethanes from the Photo-Oxygenation of Cardanols
ChemSusChem **2021**, *14*, 3325–3332, DOI 10.1002/cssc.202101175.

[4] R. Stuhr, P. Bayer, A. Jacobi von Wangelin
The Diverse Modes of Oxygen Reactivity in Life & Chemistry
ChemSusChem **2022**, *15*, e202201323, DOI 10.1002/cssc.202201323.

[5] R. Stuhr, A. Jacobi von Wangelin
Organic Photoredox Carbonylation of Arenediazonium under Mild Conditions
Synlett **2024**, 35, 1889–1892, DOI 10.1055/s-0042-1751531.

[6] A. Pulcinella, S. Bonciolini, R. Stuhr, D. Diprima, M. T. Tran, M. Johansson, A. Jacobi von Wangelin, T. Noël
Deoxygenative Photochemical Alkylation of Secondary Amides Enables a Streamlined Synthesis of Substituted Amines
Under revision.

II. Table of Contents

III.   List of Abbreviations

acac	acetylacetonato		**ESI**	electron spray ionization
An	4-methoxyphenyl		**Et**	ethyl
AN	acid number		**EY**	eosin Y
Ar	aryl		**FID**	flame ionization detector
ATR	attenuated total reflection		**FEP**	fluorinated ethylene propylene
[bmim]	1-butyl-3-methylimidazolium		**FT**	fourier transformation
Bipy	2,2′-bipyridine		**GC**	gas chromatography
Bu	butyl		**GHS**	globally harmonized system
BVO	Baeyer-Villiger oxidation		**GPC**	gel permeation chromatography
CA	cardanyl acetate		**HALS**	hindered amine light stabilizer
Cat	catalyst		**HAT**	hydrogen atom transfer
CC	cyclic carbonate		**[hmim]**	1-hexyl-3-methylimidazolium
ClPh	4-chlorophenyl		**HPLC**	High-performance liquid chromatography
COgen	9-methyl-9*H*-fluorene-9-carbonyl chloride		**HYP**	hydroperoxide
D	donor		**iPr**	*iso*-propyl
DO	trimethylene glycol dioleate		**IR**	infrared
DABCO	1,4-diazabicyclo[2.2.2]octane		**LED**	light emitting diode
DABSO	1,4-diazabicyclo[2.2.2]octane-*bis*(sulfur dioxide)		**LMCT**	ligand to metal charge transfer
DEET	*N,N*-diethyl toluamide		**Me**	methyl
DSC	dynamic scanning calorimetry		**Mes-Acr⁺**	9-mesityl-10-methylacridinium
EI	electron impact		*m***CPBA**	*meta*-chloroperbenzoic acid
EpAlc	epoxy alcohol		**MO**	methyl oleate

MS	mass spectrometry	**ROS**	reactive oxygen species
MW	molecular weight	**Ref.**	reference
MWD	molecular weight distribution	**r.t.**	room temperature
NIPU	non-isocyanate polyurethane	**SCE**	standard calomel electrode
NMR	nuclear magnetic resonance	**Sens**	photosensitizer
Nu	nucleophile	**SET**	single electron transfer
OA	oleyl alcohol	**SHE**	standard hydrogen electrode
OAcr	oleyl acrylate	**SR**	sacrificial reductant
OlA	oleic acid	**TCB**	1,2,4-trichlorobenzene
OPEW	oxidized polyethylene wax	**TEMPO**	2,2,6,6-tetramethylpiperidine *N*-oxide
PC	photocatalyst	**TGA**	thermogravimetric analysis
PDI	polydispersity index	**TLC**	thin layer chromatography
PE	polyethylene	**TMS**	trimethylsilyl
PFA	perfluoroalkoxy alkanes	**TO**	triolein
Ph	phenyl	**TPP**	tetraphenylporphyrin
PP	polypropylene	**UV**	ultraviolet
PU	polyurethane	**Vis**	visible radiation

1. Abstract

The aim of this work is the exploration and investigation of new light-mediated liquid-gas reactions, with focus on photooxygenation and photocarbonylation chemistry. Particular interest lies in the aspects of sustainability and technical implementation.

A concise introduction to the field of light-mediated liquid-gas reactions is given in **Chapter 3**. Advantages and challenges of using gaseous reagents, photochemistry and combinations thereof are discussed. Additionally, different reactor types are presented.

Chapter 4 gives an overview of the importance of oxygen in life and chemistry. The different forms of molecular oxygen (triplet oxygen $^3O_2$, ozone O_3 and singlet oxygen $^1O_2$) and their occurrence, role in nature, application in industry, as well as chemical reactivity are reviewed. Additionally, physical data and practical advice on their handling are compiled.

A modular approach towards the photooxidative degradation of waste polyethylene (PE) and transformation into diverse value-added products is presented in **Chapter 5**. End-of-life PE is converted into oxidized polyethylene waxes under O_2 atmosphere and violet light irradiation (405 nm) using inexpensive and abundant $FeCl_3$ as catalyst. The process features simultaneous introduction of oxygen functionalities (ketones, carboxylic acids, lactones) and chain scission. The total oxidation degree and by extension the product properties can be modulated by variation of reaction time, catalyst loading and oxygen concentration. The obtained PE waxes can be used as materials or be further degraded via Baeyer-Villiger oxidation into low-molecular-weight feedstock chemicals (diols, diacids, and ω-hydroxy acids).

In **Chapter 6** a three-step one-pot procedure for the formation of bio-based cyclic carbonates using only O_2 and CO_2 as stoichiometric reagents is presented. Unsaturated fatty acid derivatives are reacted with $^1O_2$ (generated by photosensitization) in a photo-flow reactor to quantitatively yield allyl hydroperoxides. These products undergo self-epoxidation to epoxy alcohols in the presence of inexpensive and non-toxic catalyst $VO(acac)_2$. After addition of pyridine (10 mol%) and treatment with CO_2 (4 bar, 90 °C) hydroxy cyclic carbonates are obtained in high yields with excellent atom-economy. Finally, the application of these products as monomers in the formation of non-isocyanate polyurethanes is shown.

An improved metal-free photocarbonylation of arenediazonium salts to benzoyl derivatives is reported in **Chapter 7**. Using the organic photocatalyst 9-mesityl-10-methylacridinium perchlorate, the reaction gives access to esters, amides, benzoic acids and anhydrides under mild conditions (20 bar CO, 25 °C, 4 h, blue 450 nm LED) in an autoclave. In **Chapter 8** the photocarbonylation is further developed by transfer to flow conditions: the reaction time is decreased (10 min residence time) and scalability and safety are significantly improved. The flow approach allows for the formation of reactive intermediates (acyl chlorides, -azides, -cyanides) that can be used for follow-up reactions without the need for an intermediate work-up. This modular approach allows access to products that are not accessible by direct photocarbonylation and rapid diversification of the product scope. Thus, benzoyl derivatives have been synthesized using O, N, S, Cl, F, P, H and C-nucleophiles. The work is concluded with mechanistical investigations.

2. Zusammenfassung

Das Ziel dieser Arbeit ist die Untersuchung neuartiger, licht-vermittelter Flüssig-Gas-Reaktionen mit Fokus auf Photooxygenierungen und Photocarbonylierungen. Besonderes Interesse besteht dabei an den Aspekten der Nachhaltigkeit und technischen Umsetzung.

Eine kurze Einleitung wird in **Kapitel 3** gegeben. Die Vorteile und Herausforderungen der Nutzung von gasförmigen Reagenzien, der Photochemie, sowie der Kombination von beiden werden diskutiert. Im Anschluss werden verschiedene Reaktortypen präsentiert.

In **Kapitel 4** wird ein Überblick über die Bedeutung von Sauerstoff für das Leben und die Chemie gegeben. Die verschiedenen Formen von molekularem Sauerstoff (Triplett-Sauerstoff $^3O_2$, Ozon O_3 und Singulett-Sauerstoff $^1O_2$), ihre Vorkommen, Rollen in der Natur, Anwendungen in der Industrie und chemische Reaktivität werden vorgestellt. Zusätzlich sind physikalische Daten und praktische Hinweise für ihre Handhabung zusammengestellt.

Ein modularer Ansatz zum photooxidativen Abbau von Abfall-Polyethylen (PE) und dessen Transformation in diverse Produkte wird in **Kapitel 5** präsentiert. Hochmolekulares *end-of-life* PE wird unter O_2 Atmosphäre und violettem Licht (405 nm LED) mithilfe des günstigen Katalysators $FeCl_3$ in oxidiertes PE-Wachs umgewandelt. Dabei erfolgt zugleich der Einbau von Sauerstofffunktionalitäten (Ketone, Carbonsäuren, Lactone) und Kettenbruch. Der Oxidationsgrad und dadurch auch die Produkteigenschaften können durch Variation von Reaktionszeit, $FeCl_3$-Menge und O_2-Konzentration gesteuert werden. Die PE-Wachse können als Produkte genutzt werden oder durch Baeyer-Villiger Oxidation zu niedermolekularen *feedstock* Chemikalien (Diole, Disäuren, ω-Hydroxysäuren) abgebaut werden.

In **Kapitel 6** wird eine *one-pot* Synthese von biobasierten cyclischen Carbonaten mit O_2 und CO_2 als einzigen stöchiometrischen Reagenzien präsentiert. Derivate von ungesättigten Fettsäuren werden mit $^1O_2$ (erzeugt durch Photosensibilisierung) in einem Flussreaktor quantitativ zu Allylhydroperoxiden umgesetzt. Diese Produkte bilden Epoxyalkohole in Gegenwart des günstigen und ungiftigen Katalysators $VO(acac)_2$. Durch Zugabe von Pyridin (10 mol%) und Reaktion mit CO_2 (4 bar, 90 °C) werden cyclische Carbonate in hohen Ausbeuten und mit exzellenter Atomökonomie erhalten. Zuletzt wird die Anwendung einiger Produkte als Monomere in der Synthese von *non-isocyanate polyurethanes* gezeigt.

Eine verbesserte metallfreie Photocarbonylierung von Diazoniumsalzen zu Benzoylderivaten wird in **Kapitel 7** berichtet. Unter Verwendung des organischen Katalysators Mes-Acr ClO_4 werden Ester, Amide, Benzoesäuren und Anhydride unter milden Bedingungen (20 bar CO, 25 °C, 4 h, 450 nm LED) in einem Autoklav erhalten. In **Kapitel 8** wird die Reaktion durch die Durchführung im Flussreaktor weiterentwickelt: die Reaktionszeit wird verkürzt (10 min Verweilzeit) und die Skalierbarkeit und Sicherheit erhöht. Reaktive Intermediate (Acylazide, -chloride, -cyanide) können im Flussreaktor gebildet und danach ohne Aufarbeitung weiterreagiert werden. Dieser modulare Ansatz erlaubt den Zugang zu Produkten, die nicht durch direkte Photocarbonylierung gebildet werden können, sowie schnelle Diversifizierung. O, N, S, Cl, F, P, H und C-Nucleophile wurden zur Synthese von Benzoylderivaten genutzt. Mechanistische Untersuchungen schließen die Arbeit ab.

3. Principles of Light-Mediated Liquid-Gas Reactions

3.1   Introduction

Currently, humankind is confronted with multiple global challenges, including climate change, environmental pollution, and resource depletion. An encompassing paradigm change towards more sustainability in all parts of society, economy, and life in general will be necessary to overcome these issues. Chemistry – the study of matter and the changes that substances undergo[1] – can clearly not be exempted from this essential transformation. Chemical research and industry have played an ambivalent role in the past; laying the ground for societal progress (nitrogen fixation by Haber-Bosch process, introduction of polymeric materials, etc.), but simultaneously contributing to environmental decline through the release of harmful waste products (e.g. ozone-depleting chlorofluorocarbons, persistent organic pollutants, …). While further chemical production and innovation are necessary for the flourishing of human society, negative ecological impacts need to be either prevented or at least minimized. The growing environmental awareness led to the postulation of the "12 principles of green chemistry" by Anastas et al. *(*Scheme 3.1) as guidelines for increasing the sustainability of chemical reactions and processes. This includes, *inter alia*, the evaluation of used chemicals (e.g. renewable feedstock, safer solvents), reaction design (catalysis, reducing derivatives, atom economy), processes (e.g. waste prevention, energy efficiency), and consideration of environmental implications (design for degradation).[2–4]
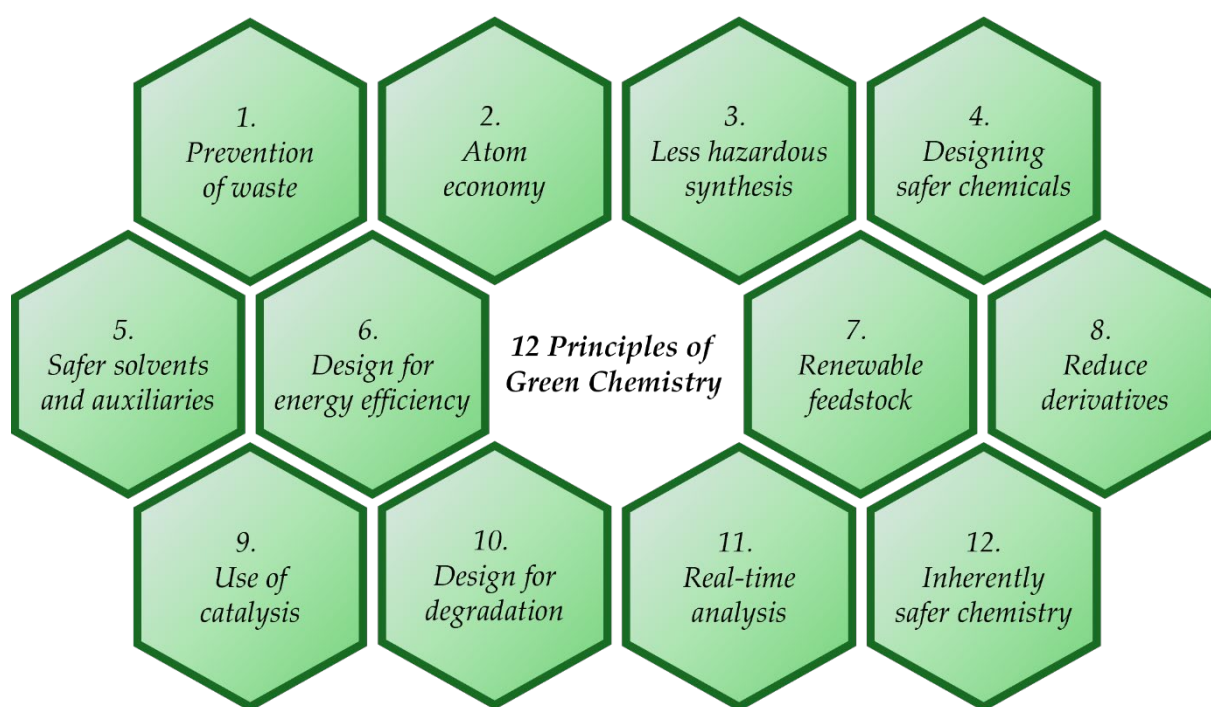

Scheme 3.1. 12 principles of green chemistry.

Both, the improvement of existing procedures and the development of new "green" synthesis strategies, bear an enormous potential for turning chemistry more sustainable. In this context, it should be noted that the 12 principles are points of reference rather than rigid rules; adapting a procedure to each point is often neither possible nor suitable. Sometimes, comparably few

changes (such as the use of a more sustainable solvent, principle 5) can significantly improve a reaction's "greenness". In industrial settings, economic factors regularly impose a stricter barrier to the implementation of more sustainable process solutions. Therefore, approaches that combine sustainability with economic benefits are especially promising.

Low-molecular weight gases – e.g. O_2, CO, CO_2, etc. – are interesting building blocks for organic synthesis, both in terms of green chemistry and economic efficiency (Scheme 3.2). They are inexpensive and (nearly) inexhaustible. Oxygen is present in the air (21% of the atmosphere), while other gases such as carbon dioxide, carbon monoxide, sulfur dioxide, and nitrogen oxides are easily accessible from industrial exhaust emissions or other large-scale processes. The use of these gaseous reagents can enable highly atom-economical introduction of functional groups into organic molecules (e.g. carbonyl motifs from CO, sulfones from SO_2, etc.). Furthermore, gases can be removed in a traceless manner from reaction mixtures, thereby simplifying the product purification.[5]

Light gases find application in the large-scale synthesis of bulk chemicals such as sulfuric acid (contact process), nitric acid (Ostwald process), ammonia (Haber-Bosch process) or hydrocarbons (Fischer-Tropsch process). These processes are often gas phase reactions that are conducted under harsh reaction conditions (high temperature and/or pressure) in the presence of heterogenous catalysts. However, such conditions are only suitable for a limited range of base chemicals.[1]
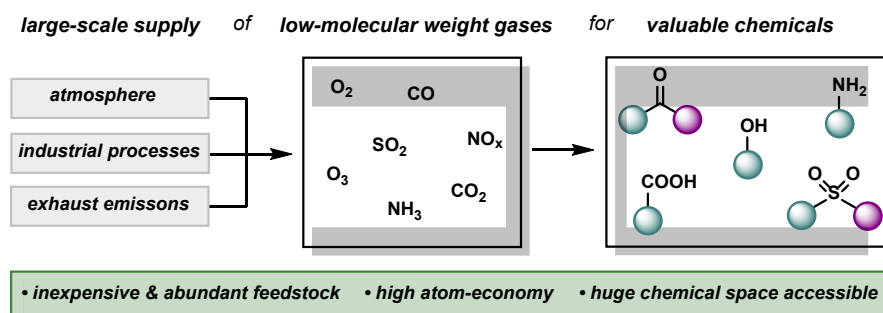

Scheme 3.2. Potential advantages of low-molecular weight gases in organic synthesis.

In the synthesis of small organic molecules and fine chemicals under mild conditions, there are also some well-established procedures involving gases, such as hydrogenations or palladium-catalyzed carbonylations. The main challenge in gas-liquid reactions is usually the proper mixing of the two phases. The gas is applied via the reaction vessels headspace. The low solubility of most gases in organic solvents and the comparably slow diffusion across the gas-liquid phase interface lead to a low local concentration of dissolved gas in the reaction mixture. This could decrease reaction kinetics, negatively affect reaction equilibria, or give rise to undesired side reactions. The diffusion rate can be increased to a certain extent by efficient stirring or gas sparging in order to enlarge the surface area. Application of pressure to the system can significantly raise the gas solubility. For such purposes, however, specialized equipment (pressure tubes, autoclave, etc.) is necessary. In general, handling gases with toxic, corrosive, flammable or oxidizing properties requires special care, training and safety measures, especially under elevated pressure.[5–7]

Recently, solid precursors that can release low molecular weight gases *in situ* or *ex situ* have gained increasing popularity. For example, CO can be generated by controlled Pd-catalyzed decarbonylation of COgen, and DABSO, the adduct of 1,4-diazobicyclo[2.2.2]octane and SO_2, is a solid source of sulfur dioxide.[8,9] Their main advantages are easy handling and precise dosing of the crystalline substances, and increased safety by lowering the effective amounts of the toxic gases in the system. The handling and storage of gas bottles are also completely omitted. On the other hand, these precursors are much more expensive than the respective gases, and their use decreases the atom economy significantly (Scheme 3.3).

The main obstacle for the use of gaseous reagents is generally the availability of reaction technologies that enable affordable, efficient, and safe handling of liquid-gas reactions. These issues can be addressed by the utilization of flow chemistry (*vide infra*); consequently, a multitude of new reaction protocols "in flow" have been developed in the last years.[5–7]
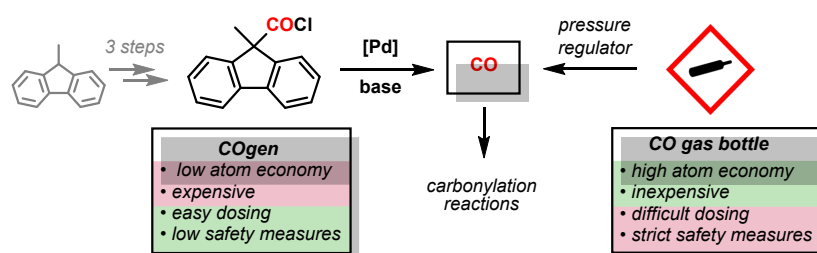
Scheme 3.3. Advantages and disadvantages of CO generated from COgen, and CO gas bottles.

The use of light to promote chemical reactions has been known since the 19th century, and organic photochemistry was established as an independent branch of chemistry by the works of Giacomo Ciamician and Paul Silber in the beginning of 20th century.[10] Procedures such as Paternò-Büchi reaction, Schenck-ene reaction or photoisomerization have been part of the standard repertoire of organic chemists for many decades. In recent years, the introduction of photoredox and photo hydrogen atom transfer (HAT) catalysis have caused a new surge in the interest in photochemistry.[11]

Light is an inexpensive and sustainable resource. Nowadays, affordable high-power LEDs of many wavelengths in the visible and near-UV light range are commercially readily available. Notably, these lamps show a high degree of energy efficiency. In most cases, photochemical reaction conditions are exceptionally mild (room temperature). Furthermore, photocatalysis enables completely new reactivities and previously unknown reactivity pathways. Irradiation with light of specific wavelengths makes targeted and selective excitation of certain molecules possible, in contrast to the unselective thermal activation. The coupling of photochemistry with transition-metal catalysis or electrochemistry further extends the scope of possible transformations.[12]

Nevertheless, the implementation of photochemistry comes with multiple challenges. The light intensity in a reaction solution decreases exponentially (with respect to penetration depth) due to absorbance by photoactive species (Lambert-Beer law). As a result, the photoreaction can take place only in the well-illuminated edges of a reaction vessel; large parts of the inner reaction volume do not receive meaningful amount of irradiation. This problem becomes more severe during the scale-up of reactions because the surface-to-volume ratio decreases for larger

containers. Therefore, photochemistry is conducted extensively in lab-scale but finds hitherto few applications on larger scale. The absorption problem can be circumvented using flow technology (*vide infra*). However, also photo flow reactors are not prevalent in industrial contexts (yet).[12]

Photocatalytic reactions can be divided into different types according to their principal mechanism. The most important are photosensitization, photoredox catalysis and photo HAT catalysis (Scheme 3.4).

Scheme 3.4. Types of photochemistry and common catalysts. D = donor, A = acceptor.
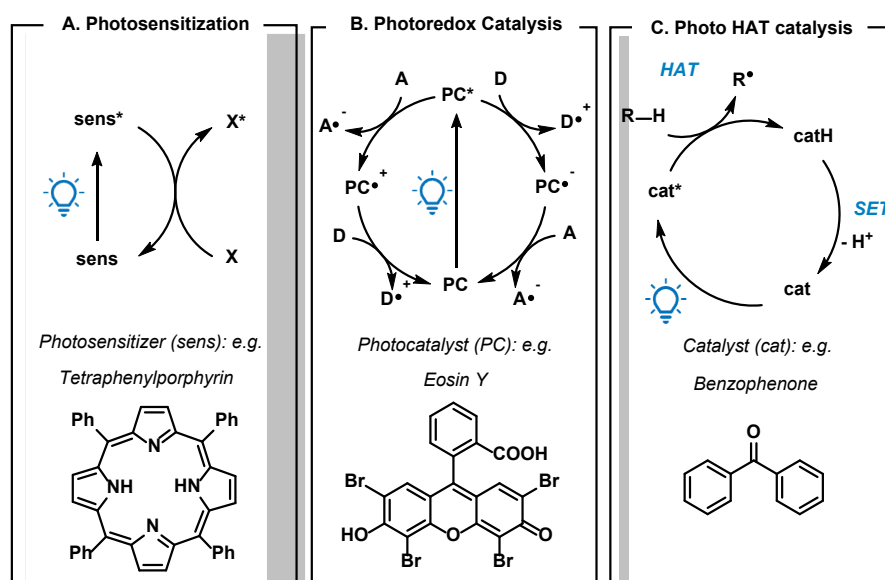
Photosensitization (Scheme 3.4, left) is based on energy transfer processes. A photosensitizer (sens) is promoted into its excited triplet state by photon absorption and subsequent intersystem crossing. The triplet energy of typical sensitizers lies around 30–60 kcal/mol. This energy can be transferred to another molecule, restoring the donor to its energetic ground-state. The newly excited molecule can undergo intramolecular rearrangement, intermolecular reaction with other substrates or unproductive deactivation (phosphorescence, thermal deactivation, etc.). Typical sensitizers are metal complexes (e.g. chlorophyll), or organic dyes such as methylene blue, porphyrins or xanthones. Notable applications of photosensitization are the generation of singlet oxygen as a versatile reagent or the *E/Z*-isomerization of double bonds.[13,14]

Photoredox catalysis (Scheme 3.4, middle) has aroused a lot of interest in recent years due to the large scope of applications. The excitation of a photocatalyst (PC) creates a species with new electronic properties (PC*) that can act either as photooxidant or photoreductant and react with donors (D) or acceptors (A), respectively, via single-electron transfer (SET). Another SET-reduction or oxidation step restores the catalyst. If the catalyzed reaction is redox-neutral, both redox reactions occur with substrate species at different parts of the catalytic cycle. But if the reaction is net-oxidative or reductive, cheap sacrificial oxidants/reductants (e.g. amines, O_2, etc.) are added to restore the catalyst. Typical photocatalysts are (noble) metal complexes such as $[Ru(bipy)_3]^{2+}$, or organic dyes (e.g. eosin Y, acridinium salts, cyanoarenes).[15,16] The redox

properties of these molecules can be modified by variation of ligands or substituents (electron donating or withdrawing groups), thus enabling the synthesis of tailor-made catalysts.[17,18]

In photo HAT catalysis (Scheme 3.4, right), the excited catalyst can abstract an H-atom (simultaneously proton and electron) from a substrate to generate a reactive radical. The catalyst is regenerated either by back-HAT or separate transfer of electron and proton. Common catalysts are benzophenones, polyoxometallates (e.g. decatungstate) and the uranyl cation. Metal chlorides such as $FeCl_3$ or $CuCl_2$ have recently emerged as new class of HAT catalysts. Upon irradiation, ligand-to-metal charge transfer (LMCT) leads to the reduction of the metal center and formation of a chlorine radical. The latter acts as the actual HAT agent; reoxidation of the metal ion regenerates the catalyst. Photo HAT reactions are of special interest because they enable C–H bond activation.[19]

3.2   Technological Implementation

Light-mediated liquid-gas reactions combine the advantages of photochemistry and gaseous reagents: the use of abundant and inexpensive feedstock, high atom-economy, efficient energy source, mild reaction conditions, and new, innovative reaction pathways (Scheme 3.5). These features are in alignment with the 12 principles of green chemistry, thereby enabling sustainable reactions. On the other hand, the difficulties presented by each individual component are also combined. The main challenge is to create a dispersion of the three entities light, gas and liquid to overcome the limitations of gas solubility, diffusion, and light absorption (*vide supra*). For this purpose, a variety of reaction set-ups is available.
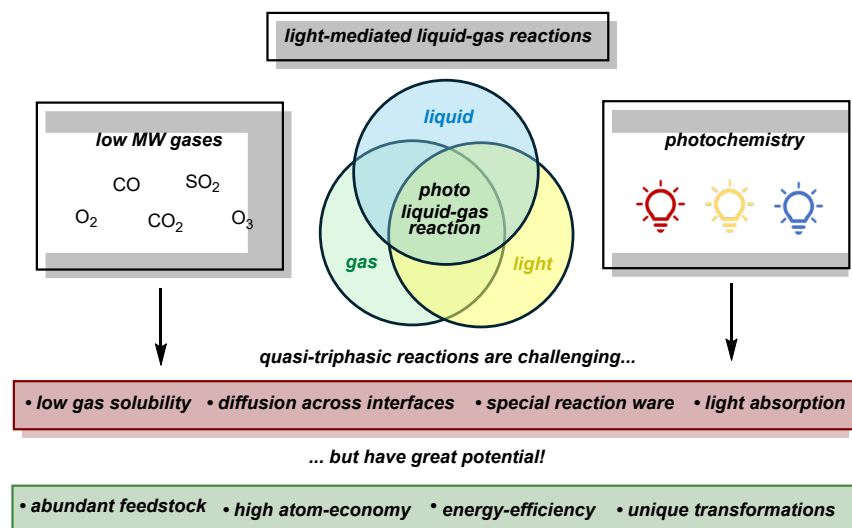
Scheme 3.5. Challenges and potential of light-mediated gas-liquid reactions.

The choice and the optimization of reaction set-ups are crucial in the development of light-mediated liquid-gas reactions. Different concepts are available depending on the specific demands of a reaction (pressure, temperature, etc.). The most common reaction set-ups are batch-type under atmospheric pressure, autoclaves and flow reactors (Scheme 3.6). It is necessary to include transparent components such as glass or certain polymers (e.g. polytetrafluoroethylene) to enable the illumination of the reaction solution. LEDs are popular light sources because of their energy efficiency, availability in many wavelengths, and high

light intensity. Sunlight would be the optimal energy source in terms of sustainability. Solar photochemistry, however, struggles with inconsistent irradiation due to influences of the weather (clouds), the alternation of day and night, and seasonal differences.[20]
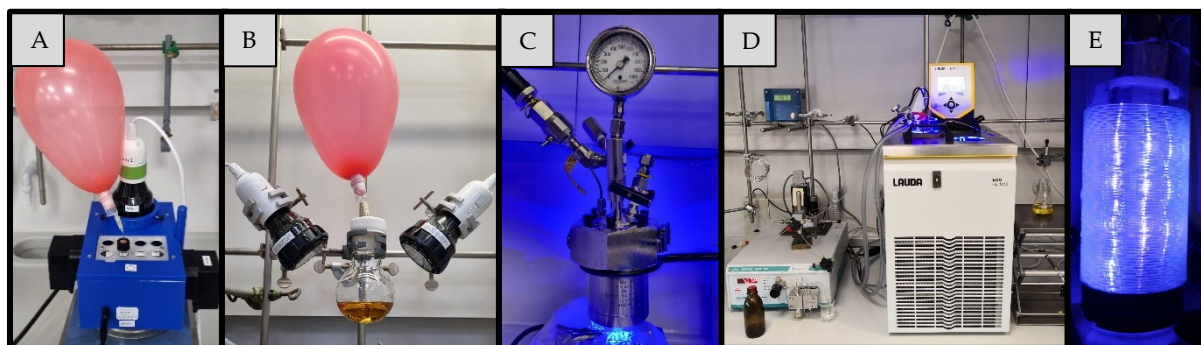
Scheme 3.6. Comparison of reactor set-ups for light-mediated liquid-gas reactions: vial (A) or round bottom flask with balloon (B), autoclave (C), and flow reactor (D) with illuminated coil (E).

The simplest solution on lab-scale is the use of standard glass reaction ware and supply of the gas via an attached balloon. LEDs or other light sources can be mounted next to it easily whereas the use of multiple lamps or mirrors can provide a more homogenous illumination. Such batch set-ups allow a wide variation of reaction conditions such as elevated temperatures, the handling of suspensions, precipitation, and highly reactive reagents. On the other hand, the general limitations of photochemistry and gas handling apply. The maximum system pressure (<2 bar) does not enable high gas concentration in solution. Constant sparging to increase diffusion is only practical for inexpensive and non-toxic gases. The light intensity decrease by absorption complicates scale-up attempts. Therefore, these batch set-ups are most suitable for reactions that are conducted on small scale, run at low gas concentrations, and/or use catalysts with low molar extinction coefficients. Examples include Pd-catalyzed carbonylations with CO, carboxylations with CO_2 or oxidations with O_2.[21–23] Also, photoreactions with solid gas-precursors (e.g. COgen) are conducted in related fashion.[24]

Autoclaves with integrated glass plates allow for high gas pressures (>80 bar) and simultaneous illumination. However, this specialized equipment is expensive and not very widespread. The reaction space is limited by the autoclave size, and this restricts the number and scale of the performed reactions. Also, the illumination is not ideal because it can occur only from one side. Extensive use of corrosive gases (e.g. SO_2) might also damage the stainless-steel equipment. There is a rather small number of reports using autoclaves and they are mainly focused on carboxylations with CO_2 and metal-free carbonylations with CO.[25–27]

In recent years, flow chemistry has been established as a useful methodology in organic laboratories and has been proven to be highly advantageous for photochemical reactions, the use of gaseous reagents and the combination of both. There are several types of flow set-ups for this kind of chemistry, such as falling film, tube-in-tube, and spinning disc reactors. Additionally, tube reactors are widespread; this equipment is commercially available but can also be built by yourself. A typical set-up consists of transparent polymer tubing – such as perfluoroalkoxy alkanes (PFA), or fluorinated ethylene propylene (FEP) – with a small inner diameter (d < 0.5 cm) wrapped into a reactor coil. These polymers show good chemical resistance against most reactive compounds and corrosive gases. HPLC, syringe or peristaltic

pumps are used to pump the reaction solution through the tubing. The gas is added and dosed via a mass flow controller. Both phases are combined through a T-mixer to create slug flow conditions: discrete gas bubbles separated by solvent droplets, with a thin liquid layer on the tube surface (Scheme 3.7). Tube reactors can be pressurized up to 50 bar to increase the solubility of the gas in the organic solvent. Additionally, the large interfacial areas between the two phases and the short pathways enable fast gas diffusion. The light source shines on the inside or outside of the reactor coil while the high surface-to-volume ratio (small diameter) allows uniform illumination throughout the whole reactor volume. However, since the tubing is prone to clogging due to its small diameter, reagents or products susceptible to precipitation should be avoided.[28–30]
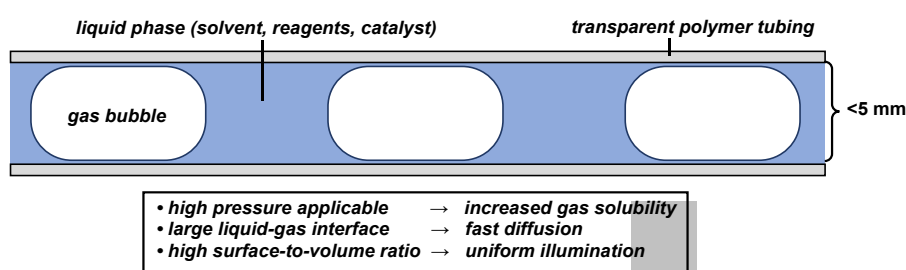
Scheme 3.7. Structure and advantages of tube reactor under slug flow conditions.

The use of flow reactors can overcome many limitations of light-mediated liquid gas reactions and facilitate their application. Reactions with many different gases have been performed successfully under flow conditions (e.g. O_2, CO, CO_2, SF_6, CH_4, etc), and even with mixtures of multiples gases (alkanes/CO, alkanes/SO_2, etc).[28,31,32]

3.3   Motivation and Thesis Outline

The motivation of the thesis in hand is to showcase the possibilities of light-mediated liquid-gas reactions in terms of sustainability, efficiency and diversity, and how to overcome the involved technological challenges. To this end, reactions with different gases (O_2, CO, CO_2), various photochemical activation modes (photosensitization, photoredox and HAT-catalysis) and diverse substrate scopes (fine chemical synthesis, monomer formation, waste valorization) are investigated and optimized (Scheme 3.8) in line with the twelve principles of green chemistry.
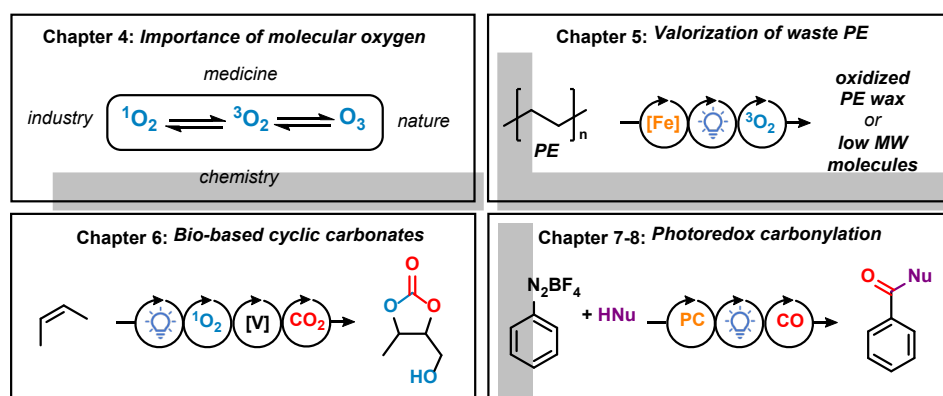
Scheme 3.8. Graphical outline of this thesis.

First, **Chapter 4** provides an overview of the importance of the different forms of *molecular oxygen* (triplet oxygen, ozone, and singlet oxygen) in life and chemistry. Their roles in nature and applications in industry and especially in chemistry are highlighted. This compilation of reactivities, physical data and handling advices would hopefully encourage the further use of the various oxygen species as *sustainable reagents* in organic chemistry. Triplet and singlet oxygen-based reactions are accordingly employed in the following chapters.

Chapter 5 deals with the photooxidative valorization of *end-of-life polyethylene* (PE). In this *waste stream utilization* approach, solutions of PE are treated with the inexpensive and abundant photocatalyst *FeCl₃* under (triplet) *oxygen* atmosphere. The photooxidation follows an HAT-mechanism and leads to the introduction of carbonyl functions and chain scission. Different *value-added products* – oxidized polyethylene wax or dicarboxylic acids and diols – can be obtained depending on the reaction conditions and post-treatment. The reactions are performed in a batch approach under moderate temperature and ambient pressure.

In **Chapter 6**, a new, *solvent-free* synthesis approach towards bio-based cyclic carbonates is introduced. *Renewable* fatty acid derivatives are transformed by *singlet oxygen* into hydroperoxides in a flow reactor. After vanadium-catalyzed rearrangement into epoxy alcohols, the insertion of CO_2 yields the cyclic carbonate products. The reactions with almost quantitative yields show exceptional *atom-economy*. A non-isocyanate polyurethane was formed by the reaction of a multi-functional cyclic carbonate with a diamine, demonstrating the possible use of the products as *monomers*.

Chapter 7 and **8** deal with the *metal-free* photoredox carbonylation of aryl diazonium salts using *CO*. Both a batch (autoclave) and a flow procedure with mild reaction conditions are presented. The further development of a *modular flow approach* allows the access to virtually any aroyl derivatives either by direct reaction or via the formation of reactive benzoyl chlorides as intermediates. Additionally, the applicability of the flow set-up for gram-scale synthesis of *fine chemicals* is shown. The work is finalized by mechanistical investigations.

In the end, this work, with the combination of diverse projects, shall hopefully contribute to the further development and popularization of light-mediated liquid-gas reactions.

3.4   References

[1]   A. F. Holleman, E. Wiberg, N. Wiberg, *Anorganische Chemie*, Walter De Gruyter, Berlin, **2017**.

[2]   P. Anastas, N. Eghbali, *Chem. Soc. Rev.* **2010**, *39*, 301–312.

[3]   M. K. M. Lane, H. E. Rudel, J. A. Wilson, H. C. Erythropel, A. Backhaus, E. B. Gilcher, M. Ishii, C. F. Jean, F. Lin, T. D. Muellers, T. Wang, G. Torres, D. E. Taylor, P. T. Anastas, J. B. Zimmerman, *Nat. Sustain.* **2023**, *6*, 502–512.

[4]   P. Marion, B. Bernela, A. Piccirilli, B. Estrine, N. Patouillard, J. Guilbot, F. Jérôme, *Green Chem.* **2017**, *19*, 4973–4989.

[5]   C. J. Mallia, I. R. Baxendale, *Org. Process Res. Dev.* **2016**, *20*, 327–360.

[6]   A. A. H. Laporte, T. M. Masson, S. D. A. Zondag, T. Noël, *Angew. Chem. Int. Ed.* **2024**, *63*, DOI 10.1002/anie.202316108.

[7]   L. Capaldo, Z. Wen, T. Noël, *Chem. Sci.* **2023**, *14*, 4230–4247.

[8]   S. D. Friis, A. T. Lindhardt, T. Skrydstrup, *Acc. Chem. Res.* **2016**, *49*, 594–605.

[9]   H. Woolven, C. González-Rodríguez, I. Marco, A. L. Thompson, M. C. Willis, *Org. Lett.* **2011**, *13*, 4876–4878.

[10]   H. D. Roth, *Angew. Chem. Int. Ed.* **1989**, *28*, 1193–1207.

[11]   L. Marzo, S. K. Pagire, O. Reiser, B. König, *Angew. Chem. Int. Ed.* **2018**, *57*, 10034–10072.

[12]   L. Buglioni, F. Raymenants, A. Slattery, S. D. A. Zondag, T. Noël, *Chem. Rev.* **2022**, *122*, 2752–2906.

[13]   F. H. Quina, G. T. M. Silva, *J. Photochem. Photobiol.* **2021**, *7*, 100042, DOI 10.1016/j.jpap.2021.100042.

[14]   J. Corpas, P. Mauleón, R. Gómez Arrayás, J. C. Carretero, *Adv. Synth. Catal.* **2022**, *364*, 1348–1370.

[15]   N. A. Romero, D. A. Nicewicz, *Chem. Rev.* **2016**, *116*, 10075–10166.

[16]   C. K. Prier, D. A. Rankic, D. W. C. MacMillan, *Chem. Rev.* **2013**, *113*, 5322–5363.

[17]   E. Speckmeier, T. G. Fischer, K. Zeitler, *J. Am. Chem. Soc.* **2018**, *140*, 15353–15365.

[18]   C. Fischer, C. Kerzig, B. Zilate, O. S. Wenger, C. Sparr, *ACS Catal.* **2020**, *10*, 210–215.

[19]   H. Cao, X. Tang, H. Tang, Y. Yuan, J. Wu, *Chem Catalysis* **2021**, *1*, 523–598.

[20]   M. Oelgemöller, *Chem. Rev.* **2016**, *116*, 9664–9682.

[21]   C. S. Yeung, *Angew. Chem. Int. Ed.* **2019**, *58*, 5492–5502.

[22]   B. Cai, H. W. Cheo, T. Liu, J. Wu, *Angew. Chem. Int. Ed.* **2021**, *60*, 18950–18980.

[23]   M. W. Logan, Y. A. Lau, Y. Zheng, E. A. Hall, M. A. Hettinger, R. P. Marks, M. L. Hosler, F. M. Rossi, Y. Yuan, F. J. Uribe-Romo, *Catal. Sci. Technol.* **2016**, *6*, 5647–5655.

[24]   K. S. Mühlfenzl, M. Sardana, T. Skrydstrup, C. S. Elmore, *ChemistrySelect* **2022**, *7*, DOI 10.1002/slct.202203582.

[25]   S. R. Mangaonkar, H. Hayashi, H. Takano, W. Kanna, S. Maeda, T. Mita, *ACS Catal.* **2023**, *13*, 2482–2488.

[26]   B. Lu, Z. Zhang, M. Jiang, D. Liang, Z. W. He, F. S. Bao, W. J. Xiao, J. R. Chen, *Angew. Chem. Int. Ed.* **2023**, *62*, DOI 10.1002/anie.202309460.

[27]   M. Majek, A. Jacobi von Wangelin, *Angew. Chem. Int. Ed.* **2015**, *54*, 2270–2274.

[28]   D. Cambié, C. Bottecchia, N. J. W. Straathof, V. Hessel, T. Noël, *Chem. Rev.* **2016**, *116*, 10276–10341.

[29]   N. J. W. Straathof, Y. Su, V. Hessel, T. Noël, *Nat. Protoc.* **2016**, *11*, 10–21.

[30]   J. Schachtner, P. Bayer, A. Jacobi von Wangelin, *Beilstein J. Org. Chem.* **2016**, *12*, 1798–1811.

[31]   D. Nagornîi, F. Raymenants, N. Kaplaneris, T. Noël, *Nat. Commun.* **2024**, *15*, DOI 10.1038/s41467-024-49322-w.

[32]   F. Raymenants, T. M. Masson, J. Sanjosé-Orduna, T. Noël, *Angew. Chem. Int. Ed.* **2023**, *62*, DOI 10.1002/anie.202308563.

4. Oxygen and its Role in Life and Chemistry

diverse reactivity through allotropes and electronic configurations
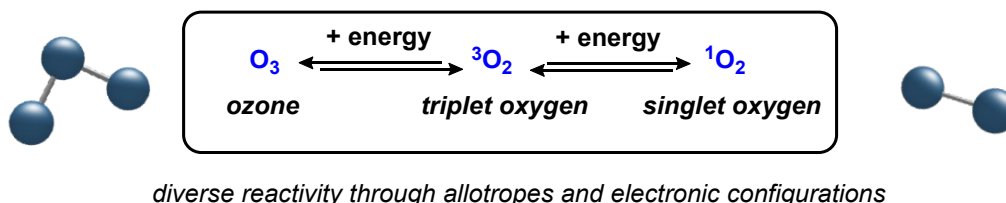
Abstract. Oxygen is a molecule of utmost importance in our lives. Beside its vital role for the respiration and sustaining of organisms, oxygen is involved in numerous chemical and physical processes. Upon combination of the different forms of molecular oxygen species with various activation modes, substrates, and reaction conditions an extremely wide chemical space can be covered that enables rich applications of diverse oxygenation processes. This Chapter provides an instructive overview of the individual properties and reactivities of oxygen species and illustrates their importance in nature, everyday life, and in the context of chemical synthesis.

Author contributions: **Robin Stuhr**: writing – original draft (lead); writing – review & editing (equal). **Patrick Bayer**: writing – original draft (supporting). **Axel Jacobi von Wangelin**: conceptualization; supervision; writing – review & editing (equal).

4.1   Introduction

Oxygen (atomic number 8) is the most abundant element by mass in the earth's crust, hydrosphere, and biosphere. Bonded oxygen is a major component of minerals (such as silicates, oxides, carbonates, sulfates, phosphates, nitrates, etc.), water, and biomolecules (carbohydrates, lignin, proteins, fats) (Figure 4.1). Oxygenated species constitute the key components of all global biogeochemical cycles (such as carbon, nitrogen, phosphorus, sulfur).[1] Despite the undeniable importance of all these compounds, this overview focuses on elemental oxygen, the most widely dispersed and mobile member of the oxygen family tree.
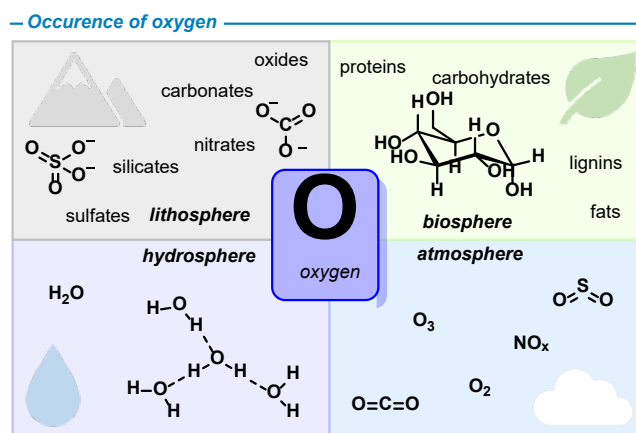
Figure 4.1. Occurrence of oxygen in the lithosphere, biosphere, hydrosphere, and atmosphere.

Elemental oxygen exists in different allotropes, the most important species being molecular dioxygen O_2 (hereafter also referred to as *oxygen*) that makes up 21% of the earth's atmosphere. It was first recognized as a chemical element in 1774 and given the name *oxygène* (from the Greek *oxys*: "acid producer") in 1777 by Antoine Lavoisier. Despite its simple structure, typically but wrongly drawn O=O, it exhibits rather unusual properties regarding its magnetic behavior, energy-transfer abilities, and chemical reactivities toward various compounds.

Sixteen electrons are filled into the molecular orbitals of O_2 according to the *Aufbau* principle (orbitals are filled starting at the lowest possible energy levels), the Pauli exclusion principle (no two electrons can have the same set of quantum numbers), and Hund's rule (which states that energy is lowest when degenerate orbitals are occupied by two electrons singly and with the same spin before, for the second-lowest energetic state, they are filled in one orbital as a pair). Three electronic configurations of molecular oxygen are depicted in Figure 4.2: the biradical triplet ground state $^3\Sigma_g^-$, the first excited singlet state $^1\Delta_g$, and the second excited singlet state $^1\Sigma_g^+$. Unlike the vast majority of molecules we know, O_2 has a paramagnetic triplet ground state (called "triplet oxygen" and denoted $^3O_2$). The ground state ($^3\Sigma_g^-$) has two unpaired electrons, a phenomenon that typically encourages other radicals or biradicals to stabilize themselves by forming bonds to each other, and to neighboring oxygen or hydrogen atoms (Figure 4.2, top).[2] In contrast, the lowest-energy excited electronic configuration of oxygen is a singlet spin state (commonly called "singlet oxygen" and denoted $^1O_2$) featuring a significantly different but not less rich chemistry which is characterized by several rather selective transformations.[3] Distinct reactivities are known for $^3O_2$ and $^1O_2$, as well as the trioxygen allotrope ozone (O_3) (Figure 4.2, center).[4–6] The individual reactivity profiles include

significantly different rates of reactions with several chemical compounds and even diverging reactivities with identical substrates (hydrocarbons, radical species, metals, furans). An especially striking example is the reaction of oxygen species with furan derivatives. Ozone effects the oxidative cleavage of the C=C bonds; cycloaddition with the diene component operates with $^1O_2$; oxidative homocoupling to a furan dimer is observed when reacting furans with aerial $^3O_2$ in the presence of a metal catalyst (Figure 4.2, bottom).[7–9]
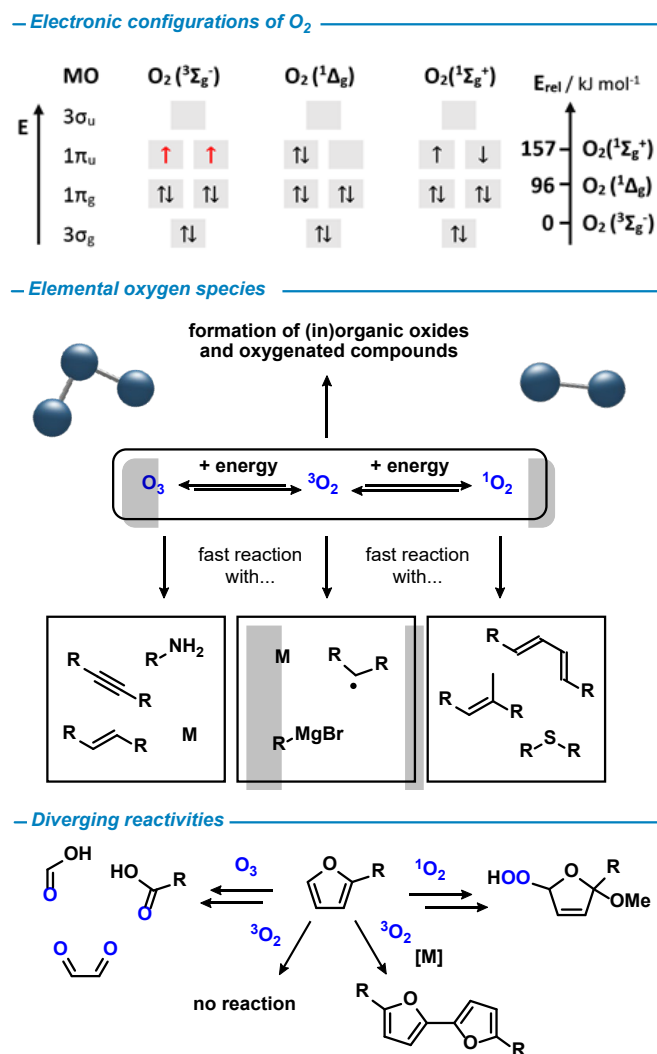
Figure 4.2. Molecular orbital occupation of ground and excited states of O_2. MOs are sorted by energy in ascending order; $(1\sigma_g)^2(1\sigma_u)^2(2\sigma_g)^2(2\sigma_u)^2$ were omitted for simplicity (top). The reactivity of elemental oxygen species (middle). Different reaction pathways of oxygen species with furans (bottom).

Further species such as the high-energy second excited singlet oxygen and allotropes like the oxygen atom, O_4, or O_8 are only short-lived or require special conditions and therefore have little applications.[10–12] This overview is intended to provide exemplary insights into the nature, properties, chemical reactivities, and technical applications of the three most prominent molecular oxygen species $^3O_2$, O_3, and $^1O_2$. Major emphasis is placed on diverse applications from various fields, important aspects of modern research, and instructive experiments for education purposes. The short-lived allotropes and the so-called "reactive oxygen species" (ROS, e.g. H_2O_2, O_2^-, OOH,.) will not be covered in this chapter.[13,14]

4.2 Triplet Oxygen – $^3O_2$

General   Aerial oxygen is a color- and odorless gas at standard conditions; in liquid (b.p. -183 °C) and solid state (m.p. -218 °C) it appears blueish.[1] Triplet oxygen is especially reactive in contact with other radicals while it is kinetically persistent toward reactions with most other compounds. Triplet oxygen does not (readily) abstract hydrogen atoms to form $HOO^{\cdot}$ under reaction conditions where the more reactive peroxyl radicals $ROO^{\cdot}$ easily engage in such H atom transfer (HAT). This is due to the very large resonance stabilization energy of $^3O_2$ that effects strong π-bonding and can be explained by valence bond and molecular orbital theory.[2] It is important to note that $^3O_2$, however, has an exothermic energy balance in reactions with almost every compound or element on the surface of our planet. In that sense, oxygen is an energetic molecule which is only held back from rapid reactions by high activation barriers, *i.e.* at best it reacts with very slow rates. The hydrogen balloon exploding in a chemistry class does not go off until activation energy in form of a spark is present; likewise paper does not ignite spontaneously in air until it reaches a temperature of about 230 °C. The combustion of organic compounds occurs via a series of exothermic radical pathways.[15,16] A fine dispersion of combustible compounds in O_2/air (flour, coal dust, organic solvent vapors, etc.) can form explosive mixtures due to the very large surface area. Flames burn stronger in pure oxygen than in air; a fact that is used to detect oxygen (or other oxidizing gases) by the glowing splint test in school labs. Therefore, reactions with pure oxygen have to be handled with greatest care. Even greater reactivities are observed in liquid oxygen: For example, the mixture of solid lithium hydride and liquid oxygen is an explosives of much greater power than trinitrotoluene (TNT).[17] Many rather standard chemicals, including car fuels or other hydrocarbons become very powerful explosives when treated with liquid oxygen.[18]

Nature   The oxygen content of the earth's atmosphere originates from the oxidation of water via photosynthesis processes over the course of millions of years. Today, approximately 170 Gt of biomass are formed by photosynthesis each year. All higher life forms on earth are directly dependent on the constant availability of oxygen. The reduction of $^3O_2$ to water is a key step of the aerobic respiration and responsible for the generation of ATP (adenosine triphosphate), the cellular "energy currency" that drives many reactions in living cells. The oxidation of iron to rust is a process that is known to everyone. A closely related reaction of oxygen with an iron atom is the transport of oxygen into the cells of almost all vertebrates which operates via the reversible binding to the iron-containing protein hemoglobin in red blood cells (Figure 4.3).[19]
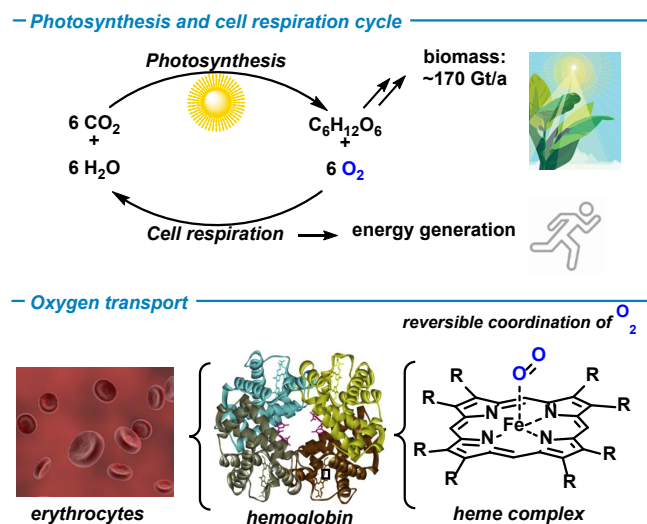
Figure 4.3. Photosynthesis and cell respiration cycle (top), oxygen transport in the blood (bottom), structure of hemoglobin. Reprinted from ref.[20]. Copyright (2021), with permission of Springer Nature.

Furthermore, oxygen is an important substrate in many enzyme-catalyzed biosynthetic pathways that convert molecules for energy and heat release, digestion, detoxification, signaling pathways etc. Oxidases, monooxygenases, and dioxygenases utilize $^3O_2$ as oxidant and source of incorporation of one or two oxygen atoms into biomolecules, respectively. Among other oxidative mechanisms, enzymatic hydroxylations and epoxidations are especially frequent.[21,22] A rather special application of $^3O_2$ is its role in the glowing of fireflies (Figure 4.4). The enzyme luciferase catalyzes the reaction of molecular oxygen with luciferin, forming an instable 4-membered ring, the dioxetane intermediate. Elimination of CO_2 gives oxyluciferin in a thermally excited state. The transition into the ground state is accompanied by the emission of a photon. As a result, the firefly glows. Similar oxygen-dependent bioluminescence processes can be found, *inter alia*, in bacteria, algae, jellyfishes and squids.[23]
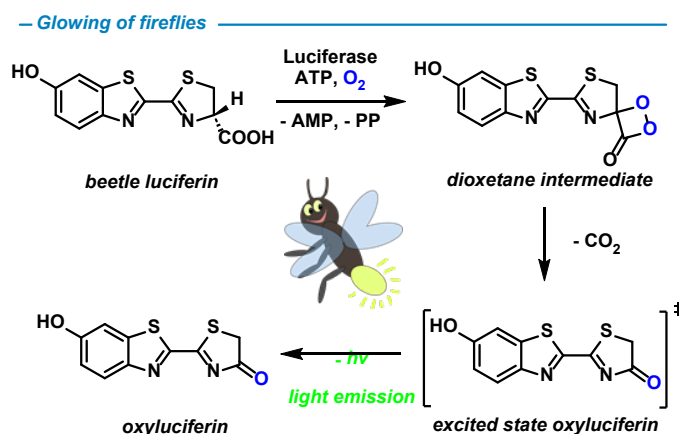
Figure 4.4. Role of oxygen in the signaling mechanism of fireflies.

Technology   Oxygen, hydrogen and their reaction product water constitute the basis of the so-called "hydrogen economy", a hypothetical future scenario of a carbon emission-free economy (Figure 4.5, top). Firstly, water, a renewable resource, is electrolytically split into gaseous hydrogen and oxygen. This reaction must be powered by energy from renewable resources in order to be fully sustainable. The produced hydrogen gas can then be stored and

distributed to its individual applications. There, hydrogen is oxidized or "burned" by oxygen in fuel cells that produce no other emissions than water. Both electrolysis and fuel cell reaction require advanced catalysts, whose development is a vibrant research topic.[33] In electrolysis, the oxygen evolution reaction (OER) is the most challenging step due to its significant overpotential.[34,35] On the other hand, the oxygen reduction reaction (ORR) is most critical in the fuel cell operations (Figure 4.5, bottom). Beside metals, new research is directed at metal-free and molecular catalysts.[36–38]
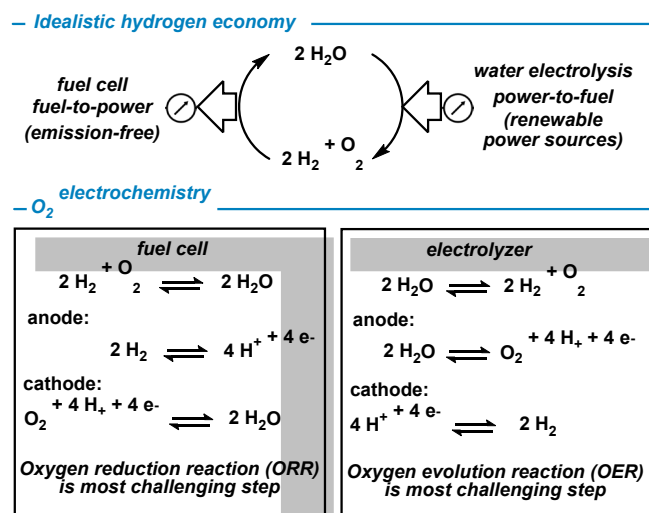
Figure 4.5. Idealistic hydrogen economy (top) and involved electrochemistry (bottom).

Molecular oxygen is also involved in the large-scale synthesis of many inorganic (sulfuric acid, nitric acid, titanium dioxide) and organic bulk chemicals such as ethylene oxide, acrylic acid and terephthalic acid (Figure 4.6). These reactions are usually performed as gas-phase reactions at elevated temperature and pressure in the presence of heterogenous metal(oxide) catalysts. The annual production volume of these chemicals is in the multimillion-ton scale.[24]
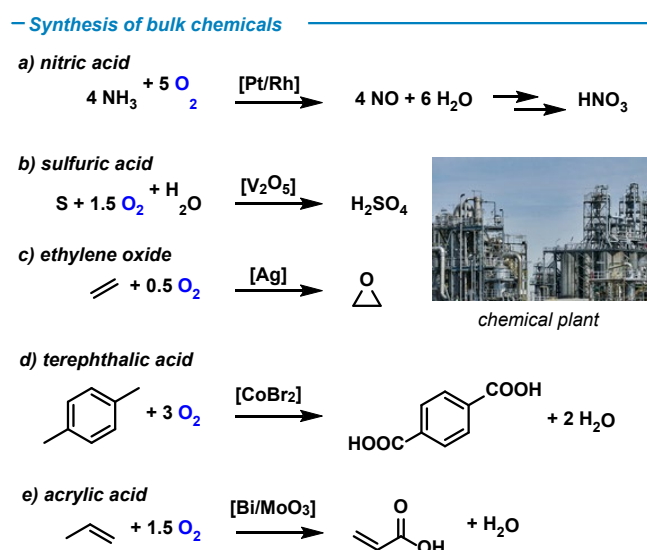
Figure 4.6. Oxygen in the synthesis of selected bulk chemicals.

Synthesis   In organic synthesis, $^3O_2$ is employed in diverse mechanistic settings paralleling the biological mode of oxidations: as stochiometric oxidant or as source for the introduction of oxygen atoms into organic molecules.

Triplet oxygen has a high oxidizing power, its standard electrode potential (vs. standard hydrogen electrode, SHE) ranges from +0.401 V to +1.229 V in basic to acidic aqueous media, respectively. A highly instructive visualization of the redox properties of oxygen is the blue-bottle experiment (Figure 4.7). An aqueous solution of the organic dye methylene blue and a reducing agent (e.g. glucose) is filled into a bottle. Upon standing, the dye is reduced into its colorless leuco-form leading to the discoloration of the solution. Shaking the bottle transfers oxygen from the gas phase into the solution; the dye is reoxidized and the blue color reappears. This cycle can be repeated several times until the reducing agent is fully consumed.[30]
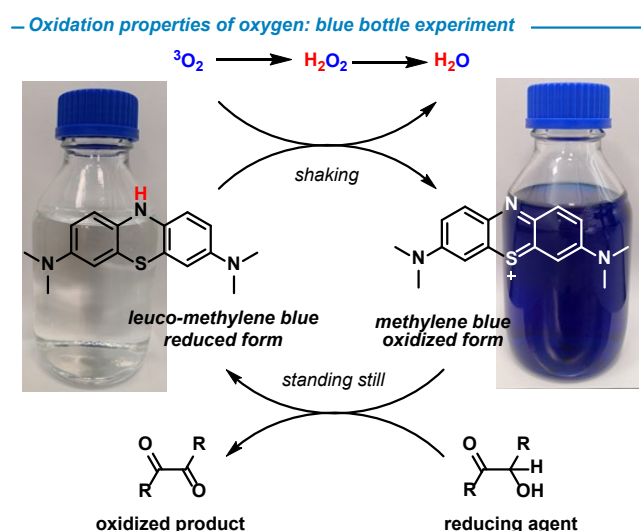
Figure 4.7. Applications of $^3O_2$ as oxidant: Blue bottle experiment.

$^3O_2$ is often employed as the stochiometric oxidant of a reaction cascade without reacting directly with the substrate, but rather with a redox mediator or catalyst. Many transition metal complexes mediate oxidation processes during which the metal undergoes net reduction. The role of $^3O_2$ is the oxidation and regeneration of the active metal species into the original oxidation state to enable a catalytic reaction. A prominent example is the Wacker oxidation of olefins to aldehydes (Figure 4.8, top). The industrial wacker process comprises the homogenous oxidation of ethylene to acetaldehyde by a palladium(II) catalyst. During the reaction, Pd(II) is reduced to Pd(0); the active Pd(II) species is regenerated by oxidation by a Cu(II) salt. The resulting Cu(I) is then in turn reoxidized by $^3O_2$ to Cu(II). Molecular oxygen is therefore the terminal oxidant, while the two metal salts act as redox shuttles.[31] Another technical application of oxygen redox is the H_2O_2 production in the anthraquinone process (Figure 4.8, bottom). An organic substrate such as ethyl anthraquinone is hydrogenated by gaseous H_2 to its hydroquinone form. Subsequent reaction with O_2 yields hydrogen peroxide and regenerates the quinone.[32]
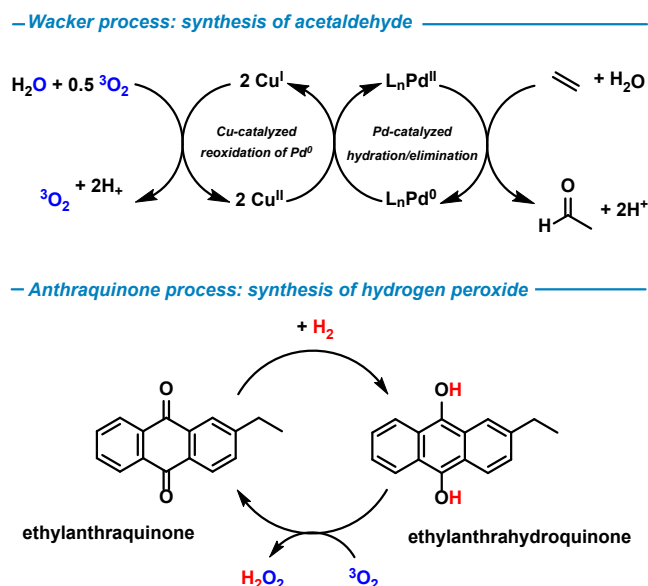
Figure 4.8. Applications of $^3O_2$ as oxidant: Wacker process (top), anthraquinone process (bottom).

$^3O_2$ can act as source of oxygen atoms for the introduction into organic molecules (usually being also an oxidation process). The introduction of -O–O- peroxy-functions follows a free-radical chain mechanism initiated by H-atom abstraction from RH by an initiator. The resulting substrate radical rapidly recombines with a molecule $^3O_2$ to give a peroxo radical. H-atom abstraction from another substrate propagates the chain reaction and delivers the hydroperoxide product ROOH. The formation of cumyl hydroperoxide from cumene follows exactly this mechanism. It is a key step in the industrial Hock process that produces most of the world's phenol (Figure 4.9, top). The obtained cumyl hydroperoxide is cleaved in a Hock rearrangement to give acetone and phenol.[39] The unwanted ageing of ethers to hazardous peroxides by air and sunlight (especially from diisopropyl ether, diethyl ether, THF) also proceeds via such H-atom abstraction processes (Figure 4.8, middle).[40] The resultant hydroperoxides tend to polymerize in condensation reactions and pose serious hazard potential; spontaneous detonation regularly causes accidents and injuries.[40] In nature, a closely related process (the so-called autoxidation) is an important part of food (e.g. oil) spoilage processes, as unsaturated fatty acids are prone to hydroperoxide formation (Figure 4.9, bottom). Their subsequent decomposition to short-chain aldehydes, alcohols and acids gives the characteristic odor of rancid food.[41] However, synthetic applications of free radical chain reactions with $^3O_2$ that operate with good selectivity and high yields are rather rare in chemical laboratories.
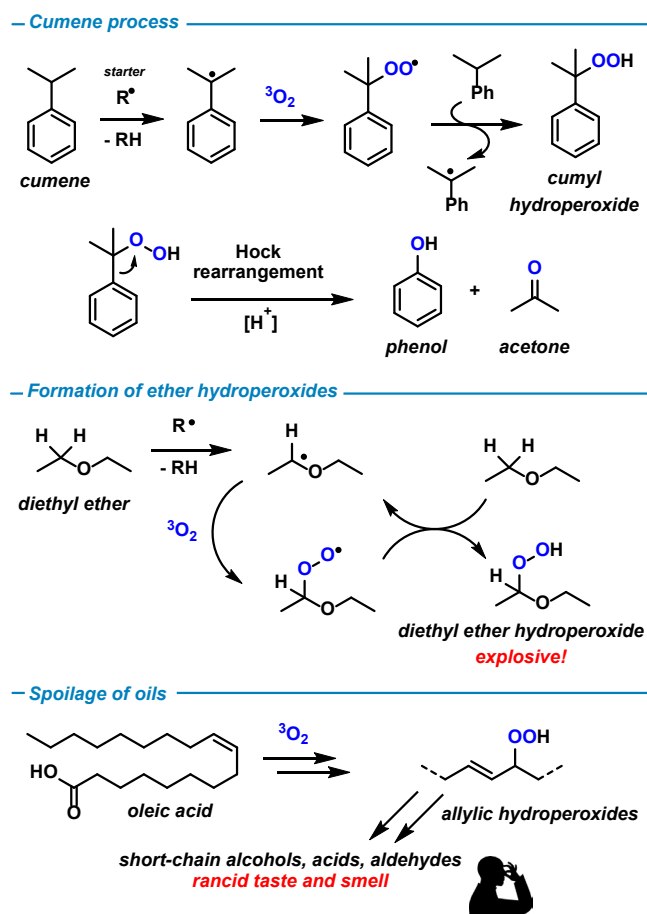
Figure 4.9. Free radical chain reactions of oxygen: cumene process (top), formation of ether hydroperoxides (middle), spoilage of oils (bottom).

The oxidative and radical behavior of $^3O_2$ demands that air and oxygen must be excluded when safely handling metallic or organometallic compounds or conducting metal-catalyzed reactions involving reductants (H_2, silanes, CO), low-valent reduced metal complexes (Pd/C, Ni(cod)$_2$, Wilkinson catalyst, etc.), or free radical intermediates (cross-coupling, radical polymerization). An example of a rather selective radical reaction with triplet oxygen is the two-step mechanism with Grignard reagents that operates via single-electron transfer (SET) from the metal to oxygen followed by fast radical-radical coupling. This procedure can be exploited in the synthesis of substituted phenols.[42] A range of polyoxometallates, a class of large metal oxide anions, are capable of H-atom abstraction from hydrocarbons; the resulting carbon-centered radicals rapidly react with $^3O_2$ to give various oxygenation products.[43]

Many modern applications of $^3O_2$ in lab-scale synthetic chemistry involve the role as low-molecular-weight, abundant and inexpensive oxidant and/or oxygen source in transition metal-catalyzed (homocoupling of arenes, oxidative brominations, oxidative annulations, etc.)[44] and photocatalyzed reactions that themselves operate via open-shell or radical intermediates.[45,46] The individual mechanisms are very diverse but conceptually related to those of the reactions shown above. Many of these recently developed catalytic oxidations mirror biological processes of oxidation and oxygenation but have been tailored to proceed with different catalysts under non-biological reaction conditions to enable wider substrate scopes and specific mechanistic scenarios (e.g. stereocontrol, tolerance of sensitive functional

22

groups, larger scale production). For example, the eosin Y-catalyzed oxygenation of diphenylmethane to benzophenone is speculated to run via the diphenylmethane radical cation and the superoxide anion (Figure 4.10, top).[47] Superoxide and the radical cation recombine to the hydroperoxide; benzophenone is formed after elimination of water.

With several metal complexes, $^3O_2$ shows good coordination ability. The biological respiration mechanisms based on Fe-O_2 heme complexes such as hemoglobin are the most prominent applications from which many synthetic models have been derived from (Figure 4.3). By choice of the metal, ligands, and reaction conditions, fine tuning of the reactivity of the metal-oxygen complexes can be achieved so that a wide range of selective reactions can be realized. As example of the rapidly developing field of metal-catalyzed C–H bond oxidation, the Pd-catalyzed hydroxylation of isonicotinic acid is shown in Figure 4.10, bottom. This electronic state of metal-bonded oxygen selectively oxidizes the C–H bond neighboring the carboxylic acid function, while leaving the pyridine-N and other C–H bonds intact.[48]

Recently, the often unselective reactions with triplet oxygen due to over-oxidations have been transferred to new reactor setups, most notably flow reactors. These conditions involve effective mixing of gas phase (O_2) and liquid phase (substrates, catalysts), enable wide variation of reaction parameters (O_2 pressure, reaction times, temperature), facilitate product separation, and most importantly can be tuned so that over-oxidations are suppressed. Simple home-made reactors can be built from inexpensive laboratory equipment (syringes, syringe/HPLC pumps, polymer tubing, valves).[49]
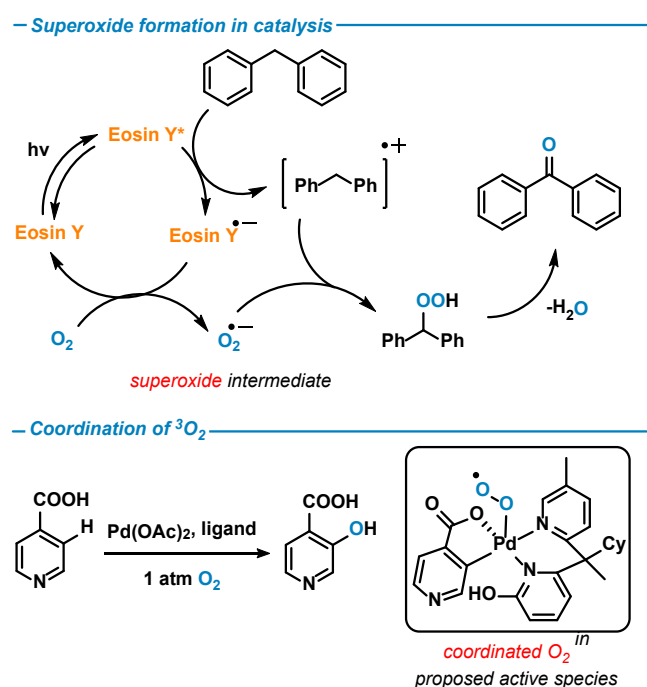
Figure 4.10. Selected reactivities in synthetic chemistry: Formation of superoxide in photoredox catalysis (top), reactivity by coordination (bottom).

4.3 Ozone – O_3

General Ozone, the triatomic allotrope of oxygen, is less stable than triplet oxygen and also much more reactive toward alkenes and alkynes.[50] The molecule adopts a bent dipolar structure. At standard conditions, O_3 is a pale blue gas with a low paramagnetic moment. It has a half-life time between minutes and hours depending on the atmospheric conditions. Its distinctive unpleasant smell has a threshold of about 0.01–0.02 ppm for humans.[51] Ozone is a strong oxidant with a standard electrode potential of +2.08 V *vs.* SHE. Liquid and solid ozone (b.p. -112 °C, m.p. -193 °C) are extremely explosive.

Nature Ozone mainly occurs in the stratosphere where it forms the so-called "ozone layer" that absorbs most of the ultraviolet part of the sunlight (Figure 4.11). Both the formation and decomposition of O_3 are induced by the absorption of UV-B and UV-C light, which also effects irreversible DNA damage in higher organisms when hitting the earth's surface. The emission of chlorofluorocarbons led to the anthropogenic ozone layer depletion in the stratosphere. As a result, the amount of solar UV radiation at the earth's surface increased. The use of many ozone-depleting substances has been banned by the Montreal protocol.[52] On the other hand, the formation of ozone at the earth surface level, induced by a combination of air pollutants such as nitrogen oxides and hydrocarbons and light, causes serious health threats. The inhalation of O_3 can lead to vertigo, nosebleed, chest pains, bronchitis, and pulmonary edema.[53] The reaction of ozone with organic compounds in the atmosphere such as terpenes can induce the formation of secondary organic aerosols which are toxic to the human health.[54] The presence of highly reactive O_3 in the troposphere cause damage to many materials such as rubber.[55] Therefore, the search for efficient catalysts for the removal of tropospheric ozone is of high interest.[56]
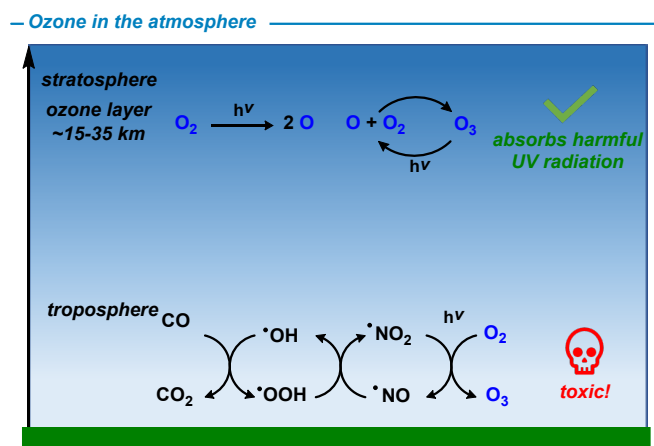
Figure 4.11. Ambivalent role of ozone in the atmosphere.

Technology For commercial use, O_3 is typically generated from diatomic oxygen by exposition to an electrical field or UV light. Low concentrations of ozone can be inadvertently formed via the same processes by household appliances such as air purifiers or printing devices which is easily perceived by the characteristic smell.[57] Due to a maximum half-life of about one day, ozone is typically generated spatially separated from the site of usage in an ozone generator.[58] The gas feed of the generator consists of either pure oxygen or pressurized air. Only a small amount of dioxygen is transformed into ozone; typically, an O_2/O_3 stream is

fed to the application. The oxidizing properties of ozone are exploited in many application such as chemical oxidations, disinfections, bleaching, or detoxifications (e.g. of cyanide waste) (Figure 4.12).[51] Ozone finds application in environmental remediation; the gas can be injected into the ground to chemically degrade pollutants (aromatics, etc.).[26]
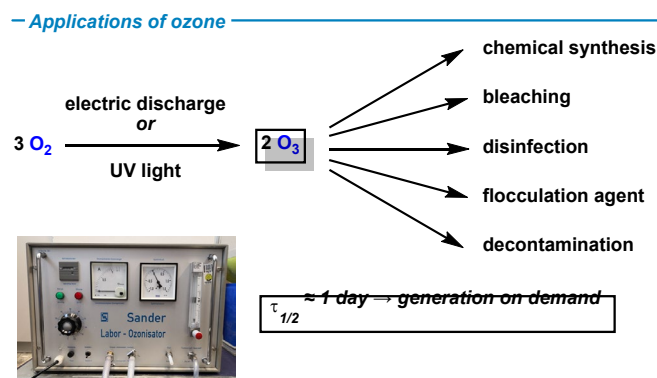
Figure 4.12. Generation and applications of ozone.

Synthesis   Ozone is regularly applied in chemical analyses and chemical syntheses.[59] The ozonolysis of alkenes is the major synthesis method involving ozone. Electron-rich C=C double bonds are primarily attacked due to the electrophilicity of ozone. Alkynes and aromatic compounds are less reactive and only oxidized after consumption of all double bonds. The ozonolysis of alkenes is initiated by a [4+2] cycloaddition yielding a primary ozonide heterocycle. Cycloreversion affords a carbonyl and a so-called Criegee intermediate (which can be a biradical or zwitterion). Secondary ozonides are formed by cross-recombination of the two fragments at the other ends (Figure 4.13). The reaction needs to be terminated with a redox reaction that cleaves the weak O-O bond of the primary oxidation products.[60] The work-up procedure determines the products. Aldehydes and alcohols are accessible under reductive conditions, whilst the use of oxidative reagents leads to the formation of carboxylic acids. The presence of short-chain alcohols (methanol, ethanol, etc.) during ozonolysis induces the formation of intermediate hydroperoxyl acetals instead of ozonides. Subsequent work-up however delivers the same oxidation products as above.[61] Ozonolysis reactions are usually conducted at low temperatures down to -78 °C to stabilize the labile intermediates. The temperature must not drop below the condensation or freezing point of ozone (-112 °C and -193 °C respectively), since liquid and solid ozone may evaporate explosively. Suitable solvents for ozonolysis reactions include alkanes, halogenated alkanes, ethers, acetone, and short-chain alcohols. The tolerance of oxidation-sensitive functional groups is very low: Amines are converted to nitro compounds and amine-*N*-oxides, phosphines to phosphine oxides, and sulfides to sulfoxides and sulfones. Heteroaromatic compounds (e.g. pyrrole, furan) often decompose in the presence of ozone.[62,63]
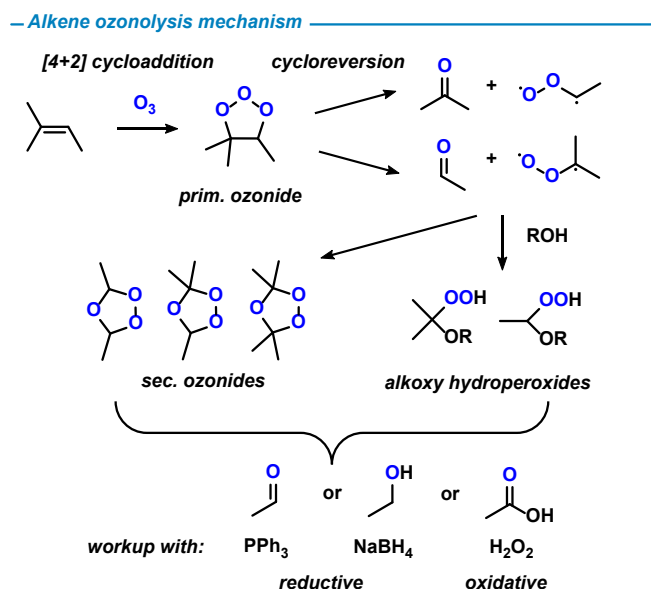
Figure 4.13. Mechanism of the oxidative C=C cleaving alkene ozonolysis.

The ozonolysis of the renewable, bio-based resource oleic acid is run on industrial scale (Figure 4.14, top). Oxidative work-up is achieved with hydrogen peroxide and provides the two carboxyl acids azelaic acid (ointments, polymers) and nonanoic acid (flavorings, plasticizers, herbicides).[64,65] Vanillin is one of the most important food flavor with production scales of more than 20,000 tons annually, mostly from chemical synthesis. An early synthetic approach was based on isoeugenol (available from the plant-based eugenol by acid-catalyzed isomerization). Ozonolysis and reductive work-up give vanillin and acetaldehyde (Figure 4.14).[66] Today, more efficient routes have replaced this synthesis. The reaction of ozone with alkynes is far less utilized. Similar intermediates as in the alkene ozonolysis are assumed. Oxidative work-up procedures cleave the intermediates into two carboxylic acids. In case of terminal alkynes, one molecule carbon dioxide is formed.[67] Reductive conditions enable the formation of α-diketones from acetylenes; an example of which is the synthesis of benzil from diphenylacetylene (Figure 4.14). This synthetically useful reactivity makes O_3 an alternative to more hazardous alkyne oxidizing reagents such as permanganate, $RuO_2/NaIO_4$, mercuric salts, Ru/t-BuOOH.[68] Ozone selectively converts furan derivatives into carboxylates so that furans serves as placeholders for carboxylic acid functions in many synthesis endeavors (Figure 4.14). The electron-rich furan is more rapidly attacked by O_3 than arene rings.[9] Further examples of selective ozonolyses of organic molecules have been compiled in the recent literature.[6,69]

The progress of ozonolysis reactions can often be tracked visually. Quantitative conversion of the substrate is achieved when the reaction mixture develops a blueish color due to the enrichment with unreacted ozone. Alternatively, brightly colored azo dyes such as Sudan III can be added as indicators (Figure 4.14, bottom). The diazo groups have a lower reactivity with ozone than C=C double bonds. Upon full consumption of the substrate, the diazo group is oxidized and the dye is fragmented into colorless molecules. Therefore, the discoloration of the red solution indicates the end point of the reaction.[70,71]
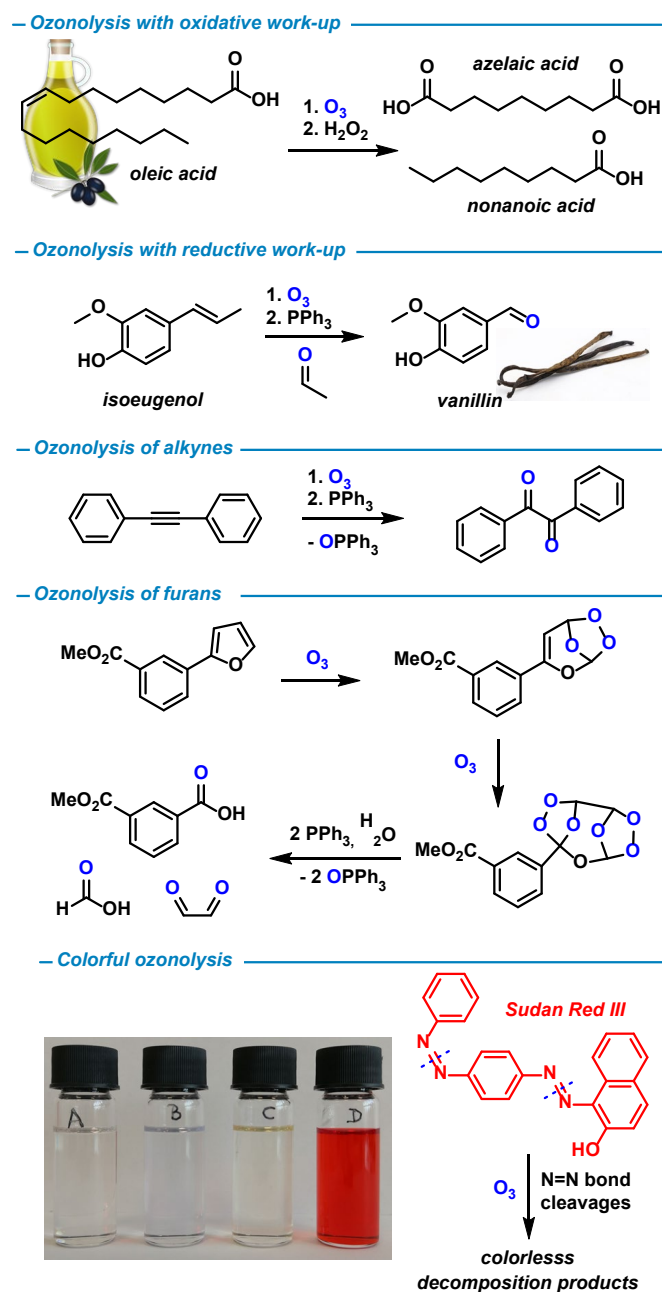
Figure 4.14. From top to bottom: Ozonolysis of alkenes, alkynes, and furans. Bottom: Visual analysis of reaction courses (A: CH_2Cl_2, B: O_3 in CH_2Cl_2, C: decomposed Sudan Red III solution, D: Sudan Red III in CH_2Cl_2).

4.4 Singlet Oxygen – $^1O_2$

General The existence of an "active oxygen species" was first proposed by Kautsky already in the 1930s. General interest in this form of oxygen, the singlet oxygen state $^1O_2$, however started only after the seminal work of Foote and Wexler in 1964. Singlet oxygen is an electrophilic species and reacts preferably with electron-rich C=C π-bonds and lone pairs of heteroatoms (N, S, P, Se). In contrast to reactions with the radical reactions of triplet oxygen $^3O_2$ and bond cleavage reactions of ozone O_3, reactions with $^1O_2$ display rather good selectivities under mild reaction conditions. Singlet oxygen has, however, a short lifetime, it returns to its ground state ($^3O_2$) via radiative deactivation or physical quenching interactions

27

with other molecules. The quenching rate is highly dependent on the stereoelectronic properties of the quencher molecules. Typical lifetimes of $^1O_2$ are in the range of milli- to microseconds ($\tau = 10^{-1}$ s in CCl_4, 10^{-2} s in air, 10^{-4} s in CH_2Cl_2, $5 \cdot 10^{-5}$ s in liquid O_2, 10^{-5} s in MeOH, 10^{-6} s in H_2O). C–H, N–H and especially O–H induce rapid electronic-to-vibrational energy transfer. Further quenching modes are charge-transfer deactivation (e.g. by amines) and electronic energy transfer (e.g. by carotenoids).[72–74] Due to the short lifetime, effective reactions require the generation of $^1O_2$ *in situ* and proximal to its reaction partner. The direct generation of singlet oxygen from triplet oxygen by light absorption is not very effective due to the low concentration and low extinction coefficient ε of gaseous oxygen.[75] Other methods of generation include the catalyzed decomposition of hydrogen peroxide,[76] the deoxygenative release from dioxygen carriers such as anthracenes, and probably the most widely applied technique, the photosensitized production from $^3O_2$ catalyzed by an organic dye molecule under visible light irradiation (Figure 4.15).[4,77] Photo-sensitizers (such as methylene blue, rose bengal, and tetraphenylporphyrin) with high extinction coefficients (500,000 L mol^{-1} cm^{-1}) and quantum yields (well above 0.5) for $^1O_2$ generation are described in literature and readily available.[78,79]
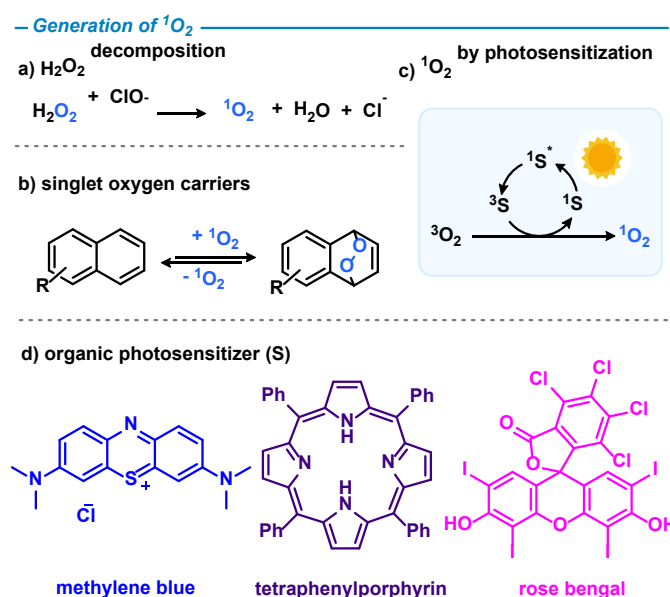
Figure 4.15. Generation of singlet oxygen (top) and common organic photosensitizers (bottom).

Nature   In nature, the photoexcitation of $^3O_2$ to $^1O_2$ is a secondary process during the photosynthesis in plant cells with chlorophyll acting as photosensitizer. The high reactivity of $^1O_2$ causes oxidative damage to biomolecules such as in the lipid peroxidation or DNA damage and can ultimately lead to programmed cell death (Figure 4.16, top).[80] Singlet oxygen can add to DNA bases such as guanine to form endoperoxides. The presence of such labile intermediates and their decomposition products lead to erroneous base pairing and mutations (Figure 4.16, middle).[81] Quenching strategies protect the cell structures up to a certain level. Carotenoids act as physical quenchers that deactivate $^1O_2$ and dissipate the released energy into heat. Ascorbate, flavonoids, and vitamin B_6 are chemical quenchers that react preferably with $^1O_2$ and therefore protect more valuable structures. The quenching mechanism of vitamin B_6 is shown in Figure 4.16, bottom.[82] The presence of $^1O_2$ initiates chloroplast-to-nucleus retrograde signaling followed by, *inter alia*, increased synthesis of quenching molecules. Thus,

it contributes to plant stress responses. The mode of action of certain herbicides is based on an increased $^1O_2$ formation that results in cell death and ultimately the death of the plant.[83–85]

Technology   Photodynamic therapies fighting, among others, certain types of cancer mimic the mode of action of oxidative stress in plant cells (Figure 4.16, top). A medication such as Verteporfin that can act as a photosensitizer is injected intravenously to the patient and disperses throughout the body. Then, the targeted areas are stimulated with a laser inducing the formation of $^1O_2$ that effects cell death only in the irradiated areas. Many surgeries and associated treatments can be avoided using photodynamic therapy (Figure 4.16). In a very similar fashion, photosensitizers can be used to form $^1O_2$ for water decontamination.[86,87]
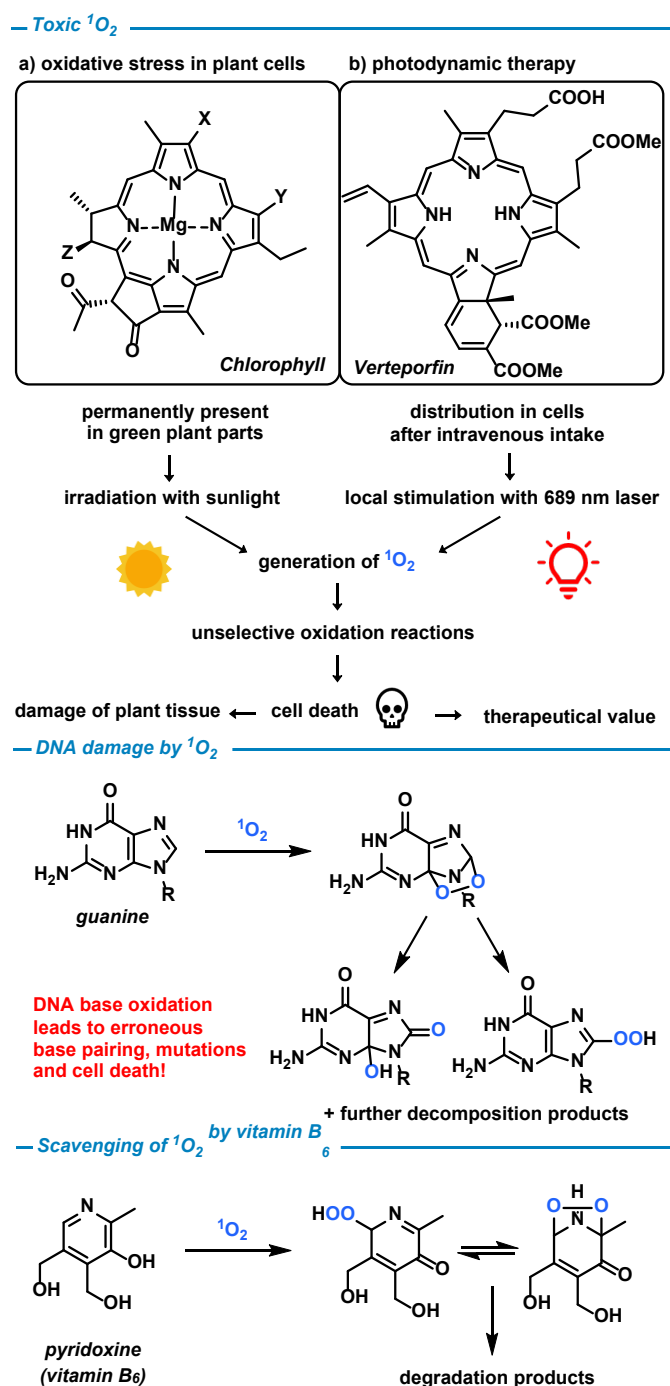
Figure 4.16. Role of $^1O_2$ in oxidative plant stress and photodynamic therapy.

$^1O_2$ also bears a high synthetic value in the synthesis of functional molecules, natural products, and drugs.[94] Notable examples are the production of rose oxide and artemisinin (*vide supra*). However, applications on industrial scales are very rare, mostly due to low selectivities, short $^1O_2$ lifetimes, and poor mixing of such gas-liquid-light reaction settings. Singlet oxygen has a long lifetime in especially harmful and expensive solvents such as $CDCl_3$ or CCl_4. A promising approach is the use of microreactors that ensure high dispersion of gas, liquid, light and short diffusion pathways.[4,77]

Synthesis Singlet oxygen displays different reaction modes with reactive alkene and heteroatom functions (Figure 4.17). $^1O_2$ engages in [4+2] cycloadditions with conjugated *s-cis*-dienes to form endoperoxides which are often unstable or even explosive. The [2+2] cycloaddition with alkenes affords 1,2-dioxetanes that are typically even more unstable and decompose to aldehydes accompanied by UV light irradiation. Isolation of these products is sometimes possible at low temperatures. Furthermore, the singlet oxygen-ene reaction (also called Schenck ene reaction) constitutes a synthetically versatile oxygenation; it was discovered in 1943 by Günther Otto Schenck.[88,89] The ene reaction of $^1O_2$ with alkenes allows the introduction of hydroperoxyl groups. The reaction proceeds via electrophilic attack of $^1O_2$ at the double bond followed by abstraction of an allylic hydrogen. The transition state is described as perepoxide, zwitterion or biradical in nature. The reactivity of an olefin in the ene reaction depends on the electron density and the availability of properly oriented allylic H-atoms in accessible conformations. High levels of regio- und stereocontrol can be achieved under certain conditions, especially in the proximity to directing groups such as amides, alcohols, *tert*-butyl groups, and arenes. Heteroatom-oxidation is a further reaction mode of $^1O_2$. Electron-rich sulfides and phosphines are especially suitable. The oxidation of methylphenylsulfide yields methylphenylsulfoxide and tris(4-methoxyphenyl)phosphine oxide is obtained by the oxidation of tris(4-methoxyphenyl)phosphine.[90] The oxidation of metal complexes by $^1O_2$ has not been studied in great details, possibly due to the standard procedures of organometallic and coordination chemistry that typically involve oxygen-free conditions. The formation of oxo complexes has been observed.[91] Poorly nucleophilic organometallic reagents may be stable toward $^1O_2$; an example is the observed ene reaction of allyltin derivatives while the C–Sn bond remained intact.[92]
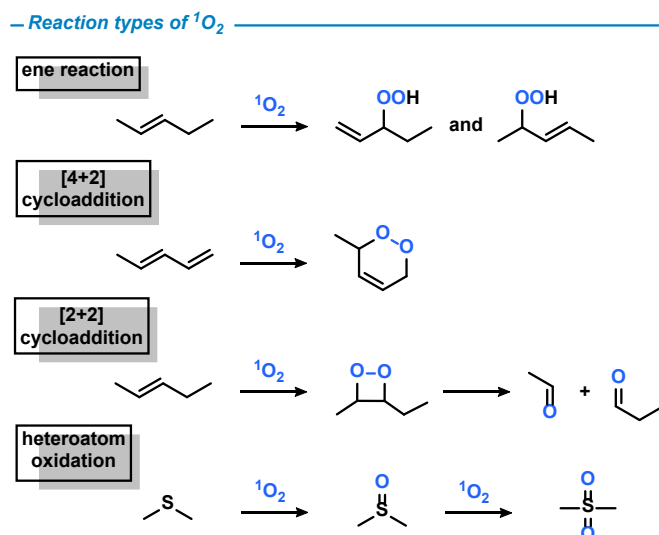
Figure 4.17. Reactivities of singlet oxygen with organic molecules.

The different reaction modes of $^1O_2$ with olefins may directly compete with one another. The ene reaction is usually faster by several orders of magnitude than the [2+2]-cycloaddition to an extent that the dioxetane products are not observable. Compounds that lack allylic hydrogen atoms cannot undergo ene reactions and are therefore preferred substrates for [2+2]-cycloaddition. In a similar fashion, [4+2]-cycloaddition is usually preferred to the [2+2]-reaction in conjugated dienes. An interesting exemption is the reaction of $^1O_2$ with *trans*-resveratrol (Figure 4.18). The incorporation of one double bond into the aromatic system slows down the [4+2]-cycloaddition, about 60% of the substrate is transformed into the endoperoxide. Only 40% material is converted by the [2+2]-cycloaddition; the intermediate dioxetane is highly instable and decomposes into aldehydes.[93]
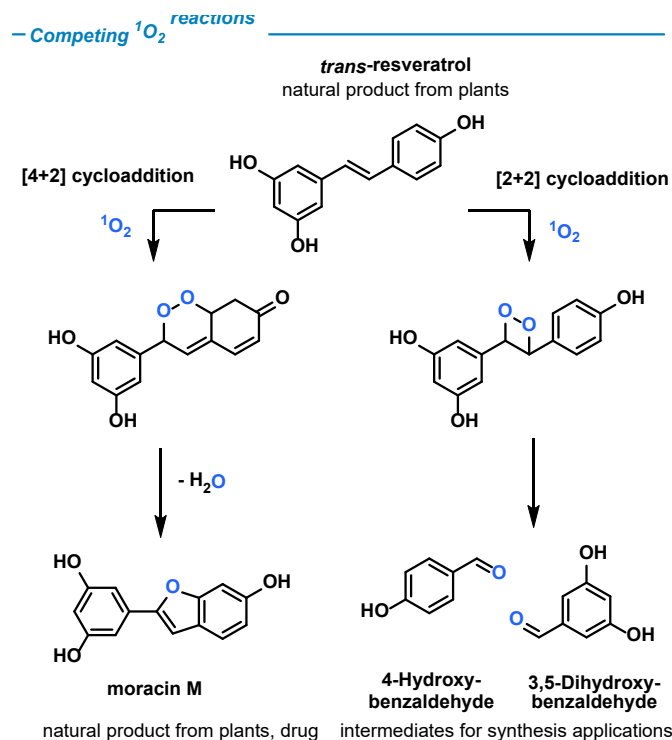
Figure 4.18. Competing [4+2]- and [2+2]-cycloaddition of $^1O_2$ with *trans*-resveratrol.

A prominent example of a selective industrial synthesis with singlet oxygen is the annual multi-ton production of rose oxide (Figure 4.19, top). Singlet oxygen is reacted with β-citronellol to produce allyl hydroperoxides via the Schenck ene allylic oxygenation reaction; two regioisomers are formed in equal amounts. The reduction of the reaction mixture with sodium sulfite affords two sets of allylic alcohols. Only one of the isomers is used in the subsequent acid-catalyzed rearrangement followed by the elimination of water to give rose oxide as *cis* and *trans* isomers. The product is an important technically produced fragrance.

Research has recently also untapped the potential use of $^1O_2$ in the transformation of biomass into feedstock chemicals (Figure 4.19, bottom). Furfural, that can be easily produced from various glucose-based renewable resources, rapidly reacts with $^1O_2$ in methanol solution via [4+2]-cycloaddition to hydroxybutenolide. Etherification with different alcohols affords alkoxybutenolides that were successfully used for coatings. Alternatively, the hydroxy-butenolide can be transformed in few steps into the important monomer building block acrylic acid. This synthesis is an alternative to the industrial petrochemical route to acrylates.[95,96]
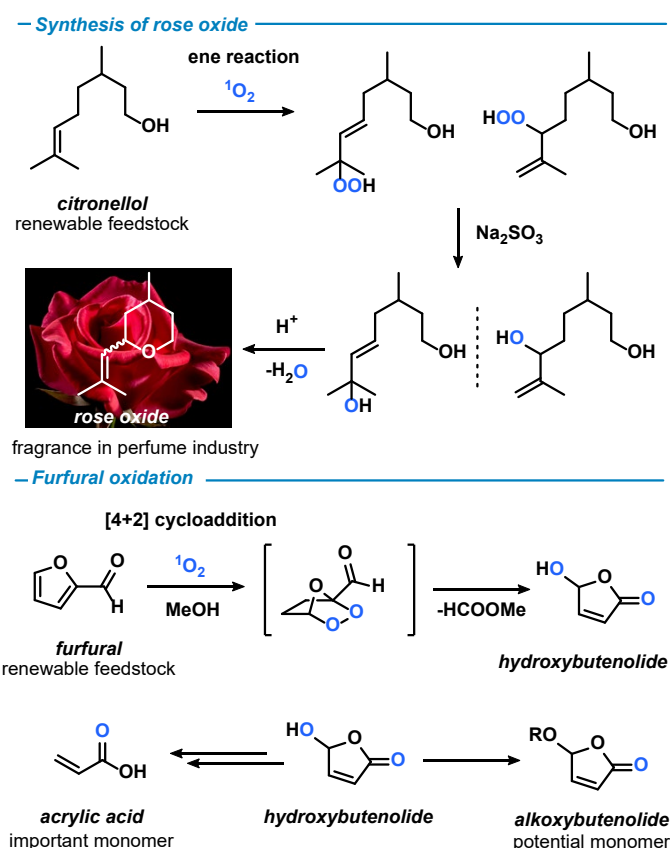
Figure 4.19. Synthesis of rose oxide from citronellol (top). Furfural oxidation (bottom).

Singlet oxygen is also used in the synthesis of pharmaceuticals. Ascaridole was the first discovered naturally occurring peroxide and was used as medication against intestinal worms. It can be synthesized by treatment of the natural resource α-terpinene with $^1O_2$ via [4+2]-cycloaddition (Figure 4.20, top). This process was also the first commercial synthesis employing $^1O_2$ and chlorophyll as photosensitizer. Today, the use of ascaridole is limited due to its medical side effects.[97] Artemisinin, another endoperoxide-based medication, is an important anti-malaria drug. The direct extraction from *artemisia annua* has a low yield and is

very expensive. Therefore, semisynthetic pathways have been developed (Figure 4.20, bottom). Dihydroartemisinic acid, a more cost-efficient natural precursor, reacts via an $^1O_2$-ene pathway to the allyl hydroperoxide. Hock cleavage, subsequent reaction with $^3O_2$, and water elimination afford artemisinin. This synthesis is a rare example of an oxidation route that includes both oxygen species, $^1O_2$ and $^3O_2$.[98]
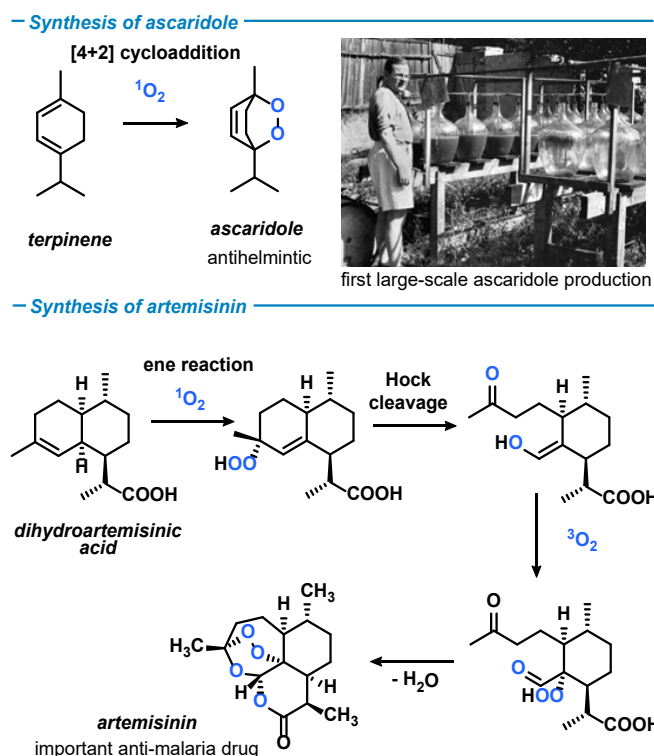
Figure 4.20. Synthesis of pharmaceuticals: ascaridole (top left) and artemisinin (bottom). G. O. Schenck with ascaridole synthesis "plant", photograph reprinted from ref.[99] Copyright (2003), with permission from Wiley-VCH.

4.5   Key Data of Molecular Oxygen Species for Synthesis Application

The three oxygen species $^3O_2$, $^1O_2$, and O_3 differ in many physical, chemical characteristics, their range of applications, and the operating procedures. The most important information on the reactivity, generation and handling of the oxygen species are compiled in Table 4.1. The choice of solvent is an important factor in reaction design of the most important mode of reactions where substrates, catalyst, additives are in solution phase and the gaseous oxygen species is purged into the solution. For reactions with oxygen in general, both the boiling and the flash point of the solvent are important to evaluate the danger of formation of explosive vapor mixtures. A high gas solubility is desirable; oxygen is generally better soluble in nonpolar than in polar solvents. The solubility can be increased by applying gas pressure. The Ostwald coefficient is defined as the ratio of dissolved gas volume (*L*) per gas-free solvent volume (*L*) at standard conditions. The melting point of a solvent has to be considered in ozone reactions because they are conducted at low temperatures, and the solvent must not react with ozone. For singlet oxygen reactions, solvents that enable long $^1O_2$ lifetimes are favorable. Additionally, environmental and sustainability criteria should be considered. Table 4.2 gives an overview of the most critical properties of solvents in the context of reactions with oxygen.

Tab. 4.1. Compilation of key chemical data of the generation, handling, and reactivities of oxygen species.

	Triplet oxygen $^3O_2$	Ozone O_3	Singlet oxygen $^1O_2$
Main reactivities	radical coupling oxidation CH abstraction	cleavage of multiple bonds (alkene, alkyne, arene, ...) heteroatom oxidation (N, P, S)	addition to C=C bonds ene reaction heteroatom oxidation (P, S)
Temperature range of applications	broad	-78 - 0 °C	room temperature
Supply, generation	O_2 gas cylinder, compressed air or ambient air	O_2 gas cylinder/compressed air fed to ozone generator on-site	O_2 gas cylinder/compressed air with photosensitizer, light source or chemical generation *in situ*
Typical reaction additives	radical starter or catalyst (transition metal, photo, etc.)	none	none
Treatment of excess gas	not necessary	reduction of excess ozone, e.g. $Na_2S_2O_3$	not necessary
Hazards	oxidizing, formation of explosive atmospheres	toxic, oxidizing, formation of explosive atmospheres	oxidizing, formation of explosive atmospheres

Tab. 4.1 Selected physical data of common solvents used for reactions with oxygen species.

Solvent	„greenness"[a]	m.p. [°C]	b.p. [°C]	Flash point [°C]	Ostwald coefficient O₂ [b]	¹O₂ Life-time [μs] [b]	Reaction with O₃
Acetic Acid	yellow	17	118	40	0.18	25	no
Acetone	green	-95	56	-20	0.28	40	no
Acetonitrile	yellow	-45	82	2	0.20	81	no
Benzene	red	6	80	-11	0.22	32	yes
Benzonitrile	n.d.	-13	190	75	n.d.	40	yes
tert-Butanol	green	25	82	11	0.20	34	no[c]
Chloroform	red	-63	61	-	0.28	240	no
1,2-Dichloroethane	dark red	-36	84	13	0.18	63	no
Dichloromethane	dark red	-97	40	-	0.26	100	no
Diethylether	dark red	-116	35	-45	0.45	34	no
Dimethylformamide	red	-61	153	58	0.11	23	no
Dimethylsulfoxide	yellow	19	189	89	0.051	6	yes
Dioxane	red	12	101	12	0.17	25	no
Ethanol	green	-114	78	14	0.23	10	no[c]
Ethyl acetate	green	-84	77	-4	0.31	43	no
n-Hexane	red	-95	69	-26	0.37	30	no
Methanol	green	-98	65	12	0.20	10	no[c]
Isopropanol	green	-89	83	12	0.25	n.d.	no[c]
Tetrahydrofuran	red	-108	66	-14	0.25	20	no
Toluene	green	-95	111	4	0.22	29	yes
1,2,4-Trichlorobenzene	n.d.	17	213	110	n.d.	94	yes
Water	green	0	100	-	0.030	2	no

[a] Solvent classification based on diverse criteria including availability, physical properties, safety, health, and environmental aspects. Green: recommended, yellow: problematic, red: hazardous, deep red: highly hazardous. For a detailed analysis, see ref. [100]. [b] Rounded average values, limited comparability due to different analytical methods. For Ostwald coefficient of O₂, see ref. [101,102] For ¹O₂ lifetimes, see ref. [103–109]. [c] Formation of alkoxy hydroperoxides instead of secondary ozonides possible.

35

4.6   Summary and Outlook

Molecular oxygen in its different forms plays a pivotal role in many aspects of biology, medicine, technology and chemistry as it is the most abundantly available, most inexpensive, and smallest molecule for oxidative transformations on the surface of our planet. The three molecular species $^3O_2$, O_3, and $^1O_2$ display distinct physical behavior and chemical reactivities; they can be easily transformed into each other so that a wide variety of applications can be accessed. Numerous transformations of biomass, technical chemicals, pharmaceuticals, household products, foods, and materials rely on oxygen as oxidant (in electronic redox processes) or as oxygen source (for the incorporation of O atoms into molecules). The importance of molecular oxygen in chemistry will most likely increase as its use as an atom-efficient, virtually inexhaustible, inexpensive and environmentally benign reagent aligns well with the Principles of Green Chemistry and the Sustainability Development Goals of the United Nations. The most important challenges for the use of molecular oxygen species in the realm of modern chemical synthesis revolve around the precise control of their reactivities and reaction mechanisms, the suppression of unwanted over-oxidations or by-product formations, and technological aspects (safety, phase mixing, etc.). The rapid development of ever more effective catalysts, spectroscopic tools, and technological advances such as the implementation of (micro)flow technologies will certainly enable direct oxygenations with the abundantly available and inexpensive molecular oxygen species move to the forefront of modern oxygenation technologies. Future technologies (biomass utilization, waste degradation and recycling, fuel cells, selective chemicals production, medicinal treatments etc.) will highly depend on oxygen-driven reactions.

4.7   References

[1]   E. Wiberg, A. F. Holleman, N. Wiberg, *Inorganic Chemistry*, Academic Press, San Diego, **2001**.

[2]   W. T. Borden, R. Hoffmann, T. Stuyver, B. Chen, *J. Am. Chem. Soc.* **2017**, *139*, 9010–9018.

[3]   P. R. Ogilby, *Chem. Soc. Rev.* **2010**, *39*, 3181–3209.

[4]   S. Nonell, C. Flors, *Singlet Oxygen: Applications in Biosciences and Nanosciences*, RSC Publishing, Cambridge, **2016**.

[5]   I. Pibiri, S. Buscemi, A. Palumbo Piccionello, A. Pace, *ChemPhotoChem* **2018**, *2*, 535–547.

[6]   G. Audran, S. R. A. Marque, M. Santelli, *Tetrahedron* **2018**, *74*, 6221–6261.

[7]   N. N. Li, Y. L. Zhang, S. Mao, Y. R. Gao, D. D. Guo, Y. Q. Wang, *Org. Lett.* **2014**, *16*, 2732–2735.

[8]   K. Gollnick, A. Griesbeck, *Tetrahedron* **1985**, *41*, 2057–2068.

[9]   M. D. Roydhouse, W. B. Motherwell, A. Constantinou, A. Gavriilidis, R. Wheeler, K. Down, I. Campbell, *RSC Adv.* **2013**, *3*, 5076–5082.

[10]   H. Richter, C. Buchbender, R. Güsten, R. Higgins, B. Klein, J. Stutzki, H. Wiesemeyer, H.-W. Hübers, *Commun. Earth Environ.* **2021**, *2*, 19, DOI 10.1038/s43247-020-00084-5.

[11]   F. Cacace, G. De Petris, A. Troiani, *Angew. Chem. Int. Ed.* **2001**, *40*, 4062–4065.

[12]   L. F. Lundegaard, G. Weck, M. I. McMahon, S. Desgreniers, P. Loubeyre, *Nature* **2006**, *443*, 201–204.

[13]   Y. Nosaka, A. Y. Nosaka, *Chem. Rev.* **2017**, *117*, 11302–11336.

[14]   C. C. Winterbourn, *Nat. Chem. Biol.* **2008**, *4*, 278–286.

[15]   C. K. Westbrook, F. L. Dryer, *Prog. Energy Combust. Sci.* **1984**, *10*, 1–57.

[16]   H. J. Curran, *Proc. Combust. Inst.* **2019**, *37*, 57–81.

[17]   L. Bretherick, *Bretherick's Handbook of Reactive Chemical Hazards*, Butterworth-Heinemann, Boston, **1990**.

[18]   *Fire Protection Guide to Hazardous Materials*, National Fire Protection Association, Quincy, **2002**.

[19]   H. Decker, K. E. Van Holde, *Oxygen and the Evolution of Life*, Springer Science & Business Media, Berlin, Heidelberg, **2010**.

[20]   M. K. Safo, M. H. Ahmed, M. S. Ghatge, T. Boyiri, *Biochim. Biophys. Acta* **2011**, *1814*, 797–809.

[21]   T. D. H. Bugg, *Tetrahedron* **2003**, *59*, 7075–7101.

[22]   D. Monti, G. Ottolina, G. Carrea, S. Riva, *Chem. Rev.* **2011**, *111*, 4111–4140.

[23]   E. H. White, M. G. Steinmetz, J. D. Miano, P. D. Wildes, R. Morland, *J. Am. Chem. Soc.* **1980**, *102*, 3199–3208.

[24]   M. J. Kirschner, A. Alekseev, S. Dowy, M. Grahl, L. Jansson, P. Keil, G. Lauermann, M. Meilinger, W. Schmehl, H. Weckler, C. Windmeier, *Oxygen* in: Ullmann's Encyclopedia of Industrial Chemistry, Wiley-VCH Verlag GmbH & Co. KGaA, Weinheim, **2017**.

[25]   B. Ferrández-Gómez, A. Sánchez, J. D. Jordá, E. S. Fonfría, C. Bordehore, M. Cerdán, *Environ. Geochem. Health* **2021**, *43*, 4975–4986.

[26]   M. L. Brusseau in *Environmental and Pollution Science* (Eds.: M. L. Brusseau, I. L. Pepper, C. P. Gerba), Academic Press, **2019**, pp. 329–354.

[27]   C. C. Azubuike, C. B. Chikere, G. C. Okpokwasili, *World J. Microbiol. Biotechnol.* **2016**, *32*, 180, DOI 10.1007/s11274-016-2137-x.

[28]   Y. J. Chan, M. F. Chong, C. L. Law, D. G. Hassell, *Chem. Eng. J.* **2009**, *155*, 1–18.

[29]   C. E. Boyd, E. L. Torrans, C. S. Tucker, *J. World Aquac. Soc.* **2018**, *49*, 7–70.

[30]   T. Limpanuparb, C. Areekul, P. Montriwat, U. Rajchakit, *J. Chem. Educ.* **2017**, *94*, 730–737.

[31]   J. Tsuji, *Synthesis* **1984**, *5*, 369–384.

[32]   T. Nishimi, T. Kamachi, K. Kato, T. Kato, K. Yoshizawa, *Eur. J. Org. Chem.* **2011**, 4113–4120.

[33]   I. Katsounaros, S. Cherevko, A. R. Zeradjanin, K. J. J. Mayrhofer, *Angew. Chem. Int. Ed.* **2014**, *53*, 102–121.

[34]   E. Fabbri, T. J. Schmidt, *ACS Catal.* **2018**, *8*, 9765–9774.

[35]   T. Noor, L. Yaqoob, N. Iqbal, *ChemElectroChem* **2021**, *8*, 447–483.

[36]   X. Wang, Z. Li, Y. Qu, T. Yuan, W. Wang, Y. Wu, Y. Li, *Chem* **2019**, *5*, 1486–1511.

[37]   L. Dai, Y. Xue, L. Qu, H. J. Choi, J. B. Baek, *Chem. Rev.* **2015**, *115*, 4823–4892.

[38]   S. Dey, B. Mondal, S. Chatterjee, A. Rana, S. Amanullah, A. Dey, *Nat. Rev. Chem.* **2017**, *1*, 0098.

[39]   R. J. Schmidt, *Appl. Catal. A Gen.* **2005**, *280*, 89–103.

[40]   S. Di Tommaso, P. Rotureau, O. Crescenzi, C. Adamo, *Phys. Chem. Chem. Phys.* **2011**, *13*, 14636–14645.

[41]   M. H. Brodnitz, *J. Agric. Food Chem.* **1968**, *16*, 994–999.

[42] Z. He, T. F. Jamison, *Angew. Chem. Int. Ed.* **2014**, *53*, 3353–3357.

[43] I. A. Weinstock, R. E. Schreiber, R. Neumann, *Chem. Rev.* **2018**, *118*, 2680–2717.

[44] Z. Shi, C. Zhang, C. Tang, N. Jiao, *Chem. Soc. Rev.* **2012**, *41*, 3381–3430.

[45] C. Bian, A. K. Singh, L. Niu, H. Yi, A. Lei, *Asian J. Org. Chem.* **2017**, *6*, 386–396.

[46] Y. Zhang, W. Schilling, S. Das, *ChemSusChem* **2019**, *12*, 2898–2910.

[47] C. Bo, Q. Bu, J. Liu, B. Dai, N. Liu, *ACS Sustain. Chem. Eng.* **2022**, *10*, 1822–1828.

[48] K. Yeung, W. R. Ewing, J. Yu, *Science* **2021**, *372*, 1452–1457.

[49] a) C. A. Hone, C. O. Kappe, *Top. Curr. Chem. (Z)* **2019**, *377*, 2, doi.org/10.1007/s41061-018-0226-z. b) J. Schachtner, P. Bayer, A. Jacobi von Wangelin, *Beilstein J. Org. Chem.* **2016**, *12*, 1798–1811.

[50] P. S. Bailey, *Ozonation in Organic Chemistry, Volume I: Olefinic Compounds*, Academic Press, London, **1978**, pp. 1–2.

[51] M. J. Kirschner, *Ozone* in: Ullmann's Encyclopedia of Industrial Chemistry, Wiley-VCH Verlag GmbH & Co. KGaA, Weinheim, **2012**.

[52] P. W. Barnes, C. E. Williamson, R. M. Lucas, S. A. Robinson, S. Madronich, N. D. Paul, J. F. Bornman, A. F. Bais, B. Sulzberger, S. R. Wilson, A. L. Andrady, R. L. McKenzie, P. J. Neale, A. T. Austin, G. H. Bernhard, K. R. Solomon, R. E. Neale, P. J. Young, M. Norval, L. E. Rhodes, S. Hylander, K. C. Rose, J. Longstreth, P. J. Aucamp, C. L. Ballaré, R. M. Cory, S. D. Flint, F. R. de Gruijl, D. P. Häder, A. M. Heikkilä, M. A. K. Jansen, K. K. Pandey, T. M. Robson, C. A. Sinclair, S. Å. Wängberg, R. C. Worrest, S. Yazar, A. R. Young, R. G. Zepp, *Nat. Sustain.* **2019**, *2*, 569–579.

[53] D. Nuvolone, D. Petri, F. Voller, *Environ. Sci. Pollut. Res.* **2018**, *25*, 8074–8088.

[54] T. Wainman, J. Zhang, C. J. Weschler, P. J. Lioy, *Environ. Health Perspect.* **2000**, *108*, 1139–1145.

[55] T. Zheng, X. Zheng, S. Zhan, J. Zhou, S. Liao, *Polym. Degrad. Stab.* **2021**, *186*, 109514, DOI 10.1016/j.polymdegradstab.2021.109514.

[56] Z. B. Sun, Y. N. Si, S. N. Zhao, Q. Y. Wang, S. Q. Zang, *J. Am. Chem. Soc.* **2021**, *143*, 5150–5157.

[57] C. Guo, Z. Gao, J. Shen, *Build. Environ.* **2019**, *158*, 302–318.

[58] J. D. McClurkin, D. E. Maier, K. E. Ileleji, *J. Stored Prod. Res.* **2013**, *55*, 41–47.

[59] S. G. Van Ornum, R. M. Champeau, R. Pariza, *Chem. Rev.* **2006**, *106*, 2990–3001.

[60] R. Brückner, *Organic Mechanisms*, Springer, Berlin, Heidelberg, **2010**.

[61] W. Chao, Y. H. Lin, C. Yin, W. H. Lin, K. Takahashi, J. J. M. Lin, *Phys. Chem. Chem. Phys.* **2019**, *21*, 13633–13640.

[62] A. Tekle-Röttering, S. Lim, E. Reisz, H. V. Lutze, M. S. Abdighahroudi, S. Willach, W. Schmidt, P. R. Tentscher, D. Rentsch, C. S. McArdell, T. C. Schmidt, U. von Gunten, *Environ. Sci. Water Res. Technol.* **2020**, *6*, 976–992.

[63] S. Lim, C. S. McArdell, U. von Gunten, *Water Res.* **2019**, *157*, 514–528.

[64] R. G. Ackman, M. E. Retson, L. R. Gallay, F. A. Vandenheuvel, *Can. J. Chem.* **1961**, *39*, 25–28.

[65] L. Rebrovic, *J. Am. Oil Chem. Soc.* **1992**, *69*, 159–165.

[66] M. B. Rubin, *Helv. Chim. Acta* **2003**, *86*, 930–940.

[67] J. G. Cannon, L. L. Darko, *J. Org. Chem.* **1964**, *29*, 3419–3420.

[68]   J. L. Alterman, D. X. Vang, M. R. Stroud, L. J. Halverson, G. A. Kraus, *Org. Lett.* **2020**, *22*, 7424–7426.

[69]   T. J. Fisher, P. H. Dussault, *Tetrahedron* **2017**, *73*, 4233–4258.

[70]   T. Veysoglu, L. A. Mitscher, J. K. Swayze, *Synthesis* **1980**, *10*, 807–810.

[71]   M. Gao, Z. Zeng, B. Sun, H. Zou, J. Chen, L. Shao, *Chemosphere* **2012**, *89*, 190–197.

[72]   C. Schweitzer, R. Schmidt, *Chem. Rev.* **2003**, *103*, 1685–1757.

[73]   D. R. Kearns, *Chem. Rev.* **1971**, *71*, 395–427.

[74]   S. Jockusch, N. J. Turro, E. K. Thompson, M. Gouterman, J. B. Callis, G. E. Khalil, *Photochem. Photobiol. Sci.* **2008**, *7*, 235–239.

[75]   C. Long, D. R. Kearns, *J. Chem. Phys.* **1973**, *59*, 5729–5736.

[76]   H. H. Seliger, *Anal. Biochem.* **1960**, *1*, 60–65.

[77]   T. Noël, M. Escriba Gelonch, K. Huvaere, in *Photochemical Processes in Continuous-Flow Reactors*, (Ed. T. Noël), World Scientific, New Jersey, **2017**, pp. 245–267.

[78]   M. DeRosa, R. J. Crutchley, *Coord. Chem. Rev.* **2002**, *233–234*, 351–371.

[79]   A. Kashyap, E. Ramasamy, V. Ramalingam, M. Pattabiraman, *Molecules* **2021**, *26*, 2673, DOI 10.3390/molecules26092673.

[80]   P. Di Mascio, G. R. Martinez, S. Miyamoto, G. E. Ronsein, M. H. G. Medeiros, J. Cadet, *Chem. Rev.* **2019**, *119*, 2043–2086.

[81]   J. Cadet, T. Douki, J. P. Pouget, J. L. Ravanat, *Methods Enzymol.* **2000**, *319*, 143–153.

[82]   B. K. Ohta, C. S. Foote, *J. Am. Chem. Soc.* **2002**, *124*, 12064–12065.

[83]   W. Czarnocka, S. Karpiński, *Free Radic. Biol. Med.* **2018**, *122*, 4–20.

[84]   V. Dogra, M. Li, S. Singh, M. Li, C. Kim, *Nat. Commun.* **2019**, *10*, 2834, DOI 10.1038/s41467-019-10760-6.

[85]   C. Triantaphylidès, M. Havaux, *Trends Plant Sci.* **2009**, *14*, 219–228.

[86]   R. Saini, N. Lee, K. Liu, C. Poh, *Cancers (Basel)* **2016**, *8*, 83, DOI 10.3390/cancers8090083.

[87]   L. Villén, F. Manjón, D. García-Fresnadillo, G. Orellana, *Appl. Catal. B Environ.* **2006**, *69*, 1–9.

[88]   G. O. Schenck, *Verfahren zur Herstellung von Pinocarveylhydroperoxyd*, **1943**, DE933925 C.

[89]   M. Prein, W. Adam, *Angew. Chem. Int. Ed.* **1996**, *35*, 477–494.

[90]   D. Zhang, B. Ye, D. G. Ho, R. Gao, M. Selke, *Tetrahedron* **2006**, *62*, 10729–10733.

[91]   M. Selke, C. S. Foote, *J. Am. Chem. Soc.* **1993**, *115*, 1166–1167.

[92]   H.-S. Dang, A. G. Davies, *J. Chem. Soc. Perkin Trans. 2* **1991**, 2011–2020.

[93]   J. A. Celaje, D. Zhang, A. M. Guerrero, M. Selke, *Org. Lett.* **2011**, *13*, 4846–4849.

[94]   A. A. Ghogare, A. Greer, *Chem. Rev.* **2016**, *116*, 9994–10034.

[95]   J. G. H. Hermens, T. Freese, K. J. Van den Berg, R. Van Gemert, B. L. Feringa, *Sci. Adv.* **2020**, *6*, eabe0026.

[96]   J. G. H. Hermens, A. Jensma, B. L. Feringa, *Angew. Chem. Int. Ed.* **2022**, *61*, e202112618.

[97]   G. O. Schenck, *Angew. Chem.* **1952**, *64*, 12–23.

[98]   F. Lévesque, P. H. Seeberger, *Angew. Chem. Int. Ed.* **2012**, *51*, 1706–1709.

[99]   K. Schaffner, *Angew. Chem. Int. Ed.* **2003**, *42*, 2932–2933.

[100]   D. Prat, A. Wells, J. Hayler, H. Sneddon, C. R. McElroy, S. Abou-Shehada, P. J. Dunn, *Green Chem.* **2015**, *18*, 288–296.

[101]   *Oxygen and Ozone*, IUPAC Solubility Data Series, Vol. 7 (Ed. R. Battino), Pergamon Press, Oxford, **1981**.

[102] H. Lawrence Clever, R. Battino, H. Miyamoto, Y. Yampolski, C. L. Young, *J. Phys. Chem. Ref. Data* **2014**, *43*, 033102.

[103] J.-M. Aubry, B. Mandard-Cazin, M. Rougee, R. V. Bensasson, *J. Am. Chem. Soc.* **1995**, *117*, 9159–9164.

[104] R. H. Young, D. Brewer, R. A. Keller, *J. Am. Chem. Soc.* **1973**, *95*, 375–379.

[105] K. I. Salokhiddinov, I. M. Byteva, G. P. Gurinovich, *J. Appl. Spectrosc.* **1981**, *34*, 561–564.

[106] M. Bregnhøj, M. Westberg, F. Jensen, P. R. Ogilby, *Phys. Chem. Chem. Phys.* **2016**, *18*, 22946–22961.

[107] J. R. Hurst, J. D. McDonald, G. B. Schuster, *J. Am. Chem. Soc.* **1982**, *104*, 2065–2067.

[108] S. Oelckers, T. Hanke, B. Röder, *J. Photochem. Photobiol. A Chem.* **2000**, *132*, 29–32.

[109] R. C. R. Gonçalves, J. Pina, S. P. G. Costa, M. M. M. Raposo, *Dye. Pigment.* **2021**, *196*, 109784, DOI 10.1016/j.dyepig.2021.109784.

5. Photooxidative Degradation and Valorization of Waste Polyethylene
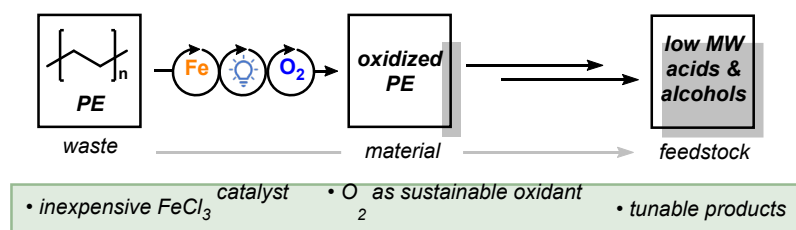
Abstract. Polyethylene, the most important commodity polymer, is produced and discarded annually in the Mt scale. Currently, chemical recycling approaches to harness this resource are heavily underrepresented. Here, a proof-of-concept study for the degradation and valorization of waste polyethylene is presented. The utilization of abundant molecular oxygen, purple light and inexpensive and non-toxic catalyst FeCl₃ allows the transformation of PE into valuable oxidized polyethylene waxes. Furthermore, downstream functionalization enables the breakdown into low-molecular feedstock chemicals.

5.1 Introduction

Polyethylene (PE) is the world's most important commodity plastic (production capacity >100 Mt/a) and accounts for almost 30 % of all annual polymer production by weight.[1] It is industrially produced by polymerization of the inexpensive, but non-sustainable monomer ethene (obtained from fossil sources). Currently, the use of bio-based ethene plays only a negligible role. The skeletal backbone of PE – consisting only of inert sp^3-C–C and C–H bonds and lacking functional groups – provides the polymer with advantageous properties such as high chemical stability and electrical insulation. Therefore, polyethylene has a wide range of applications as valuable low-cost material, e.g. in construction, textile sector, electrical and mechanical engineering. Its main use, however, is the production of packaging and single-use items with short lifetimes, thereby leading to the generation of large amounts of waste PE. The chemical inertness of polyethylene – previously a desirable material property – then impedes both the degradation and valorization of the waste. As of today, most end-of-life PE is stored on landfills or is incinerated. On the other hand, mechanical recycling of pure and clean PE to give new products with decreased mechanical properties plays only a minor role.[2]

In times of climate change and depleting fossil resources, however, end-of-life polyethylene should not only be considered as waste, but as an inexpensive and easily accessible potential feedstock for the production of chemicals. This double-purpose approach reduces pollution effects, and also harnesses an alternative, more sustainable raw material source than oil and gas. Hence, there has been a growing research interest in the development of new strategies for the strongly underdeveloped chemical utilization and valorization of PE waste.

Two main strategies for the chemical valorization can be identified in the recently reported literature: break-down of PE into low-molecular weight hydrocarbons or oxidative degradation. The pyrolysis of polyethylene under high temperatures (>350 °C) and exclusion of oxygen yields mixtures of small alkanes and alkenes.[3] Hydrogenolysis approaches, mostly catalyzed by ruthenium on solid supports, operate under somewhat milder, but still harsh conditions (250 °C, 50 bar H_2) and transform polyethylene mainly into liquid alkanes.[4,5] Abu-Omar et al. reported a multi-step approach for the formation of α,ω-divinyl oligomers from PE. Double-bonds were introduced into the polymer backbone by a bromination-elimination sequence. Then, metal-catalyzed metathesis with ethene led to the breakdown of PE into oligomeric structures.[6] Similarly, PE-pentane mixtures were transformed into low-molecular weight alkanes by a dehydrogenation-metathesis approach.[7] In 2022, the groups of Hartwig and Guironnet independently published dehydrogenation/isomerization-metathesis strategies under ethene atmosphere that selectively produced propylene, albeit with high loadings of noble metal catalysts (Ir/Pd/Ru, Pt/Re) under harsh conditions.[8,9] Thermo-oxidative treatment of polyethylene with nitric acid under microwave irradiation yielded mixtures of short-chain dicarboxylic acids (mainly C_3-C_6).[10,11]

Very recently, the use of oxygen as inexpensive, abundant and sustainable reagent in the oxidative degradation of PE has sparked new interest. These oxidations follow radical pathways and yield complex product mixtures, mostly dicarboxylic acids. The comparability of the results of different reports is limited due to inconsistent specification and definition of key values such as yield, conversion, mass recovery, etc. In 2022, Rabot et al. reported PE

oxidation with a ternary catalyst system (5 wt% $Co(NO_3)_2$, 5 wt% $Mn(NO_3)_2$ and 5 wt% *N*-hydroxyphthalimide) in acetic acid with 16 bar O_2 pressure at 150 °C. Solvent oxidation was observed in certain cases. The main (identified) products were dicarboxylic acids (C_4-C_{12}).[12] The Huang group used a Ru/TiO_2 catalyst (50 wt%) to transform polyethylene (15 bar air, 160 °C, water) into long-chain diacids (M_w ~650 g/mol).[13] Zhang et al. developed an oxidation procedure with Co-MCM-41 (cobalt-functionalized molecular sieve) in 2024. They obtained dicarboxylic acids (C_3-C_{20}) under neat conditions with 10 wt% catalyst (10 bar O_2, 125 °C). The weight distribution of the acids could be influenced by the cobalt content of the catalyst.[14] However, the described reactions all require high pressure of oxygen or air at elevated temperatures and high catalyst loadings. In 2024, Zhao et al. reported the oxidation of polyethylene to short-chain (di)carboxylic acids at atmospheric pressure with 3 mol% $CoCl_2$, 3 mol% $MnSO_4$ and 6 mol% HBr in butyl acetate. The reaction was performed for 48 h at 120 °C (b.p. butyl acetate 126 °C, flash point 22 °C) under a continuous stream of oxygen, which raises safety concerns. Additionally, significant amount of solvent oxidation was observed.[15] The Wang group recently disclosed an oxidative PE degradation procedure at atmospheric pressure using a dichlorido tris(pyrazol-1-yl)methane iron complex $[FeCl_2\{k^3\text{-}HC(pz)_3\}]$ (14 wt%) and xylene as reactive solvent. The rather expensive ligand (>100 €/g) is commercially available. Potential uses of the oxygenated oligomeric products e.g. as emulsifying agents or hydrogel formation were reported.[16]

Additionally, methods for the introduction of low amounts of oxygen functionalities into (virgin) PE [17–19] or PE film surfaces [20–22] without chain scission were reported. The obtained polymers show, *inter alia*, improved adhesive properties.

Until now, the polyethylene valorization strategies are dependent on harsh reaction conditions (high temperature/pressure) and/or the use of expensive and hazardous reagents, while high-volume low-value chemicals are formed; this discrepancy hampers economic utility of the processes. However, the enormous availability of polyethylene encourages the development of a range of complementary valorization methods to maximize the potential product range.[23–25]

In nature, polyethylene undergoes slow photooxidative degradation in presence of sunlight and oxygen. This slow, but self-accelerating process initially leads to the introduction of peroxo functions via an H-atom transfer cycle; degradation of these peroxides causes the formation of hydroxy and carbonyl functions as well as chain scission. As a result, PE becomes brittle and loses its mechanical properties.[26] In recent years, light-induced hydrogen atom transfer (HAT) catalysis for functionalization of sp^3 C–H bonds has gained a lot of interest; various catalytic systems were developed, such as polyoxometalates (decatungstate),[27] metal chlorides ($FeCl_3$, $CuCl_2$)[28] or organic dyes (eosin Y, benzophenones)[29,30]. Iron(III) chloride is a non-toxic, readily available, and inexpensive compound; it has been successfully employed e.g. for HAT-catalyzed alkylations and aminations. Light irradiation causes a ligand-to-metal charge transfer (LMCT) and liberation of a chlorine radical that acts as the actual HAT agent.[31] Importantly, $FeCl_3$ is able to catalyze the oxygenation of C–H bonds with molecular oxygen as sustainable and abundant oxidant. Applications of this reactivity include the photooxygenation of low molecular weight alkanes[32–34] and the photodegradation and postfunctionalization of polystyrene[35–37] and polyethers.[38]

In this work we present a new, modular valorization strategy of waste polyethylene into oxygenated chemical feedstock. Inspired by natural PE photodegradation, we use inexpensive and abundant $FeCl_3$, visible light and molecular oxygen for HAT-catalyzed oxygenation of C–H bonds, followed by C–C bond scission. The obtained oxygenated fragments can be used as waxes or be further transformed into feedstock chemicals by "classical" chemistry.
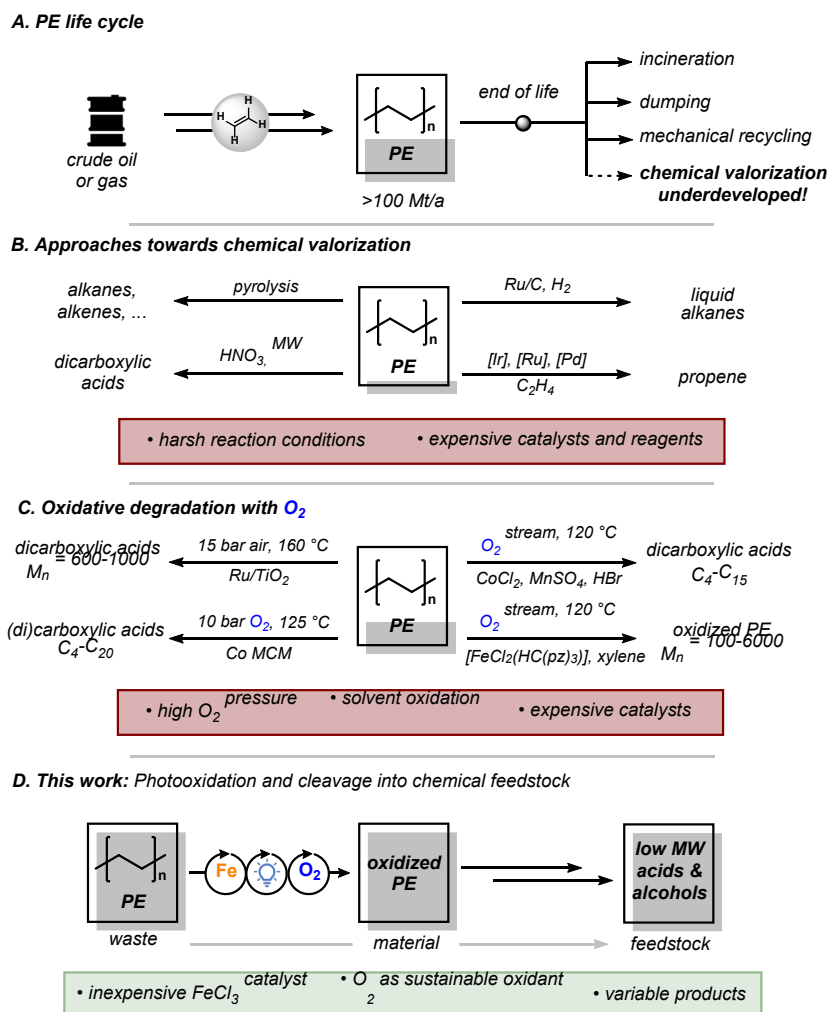
Scheme 5.1. A. PE life cycle, B. approaches towards chemical valorization, C. oxidative degradation approaches with O_2, D. This work.

5.2   Results and Discussion

This work serves as a proof-of-concept study for the development of a modular valorization approach for end-of-life polyethylene (Scheme 5.2). Waste stream PE as starting material is available in almost unlimited quantity; therefore, it is especially profitable if the designed method can give controllable access to a variety of value-added products. In this case, the photooxidation of PE with the inexpensive, abundant and non-toxic catalyst iron(III) chloride, oxygen and light produces oxidized polyethylene. The material´s characteristics are close to commercial oxidized polyethylene waxes (OPEW), and it could find application e.g. as dispersing agents or surface modifiers. The properties and application areas depend on the oxidation degree. Due to the introduced oxygen functionalities, the oxidized PE could be further degraded by classical chemical reactions such as Baeyer-Villiger-Oxidation. This

reaction gives then access to low-molecular weight diacids, diols and ω-hydroxyacids that serve as chemical feedstock. Their chain lengths depend, again, on the amount of functionalization in the photooxygenation step. Therefore, the understanding of the reaction and the control of the oxidation degree is key in the transformation of waste PE into a large portfolio of useful products.
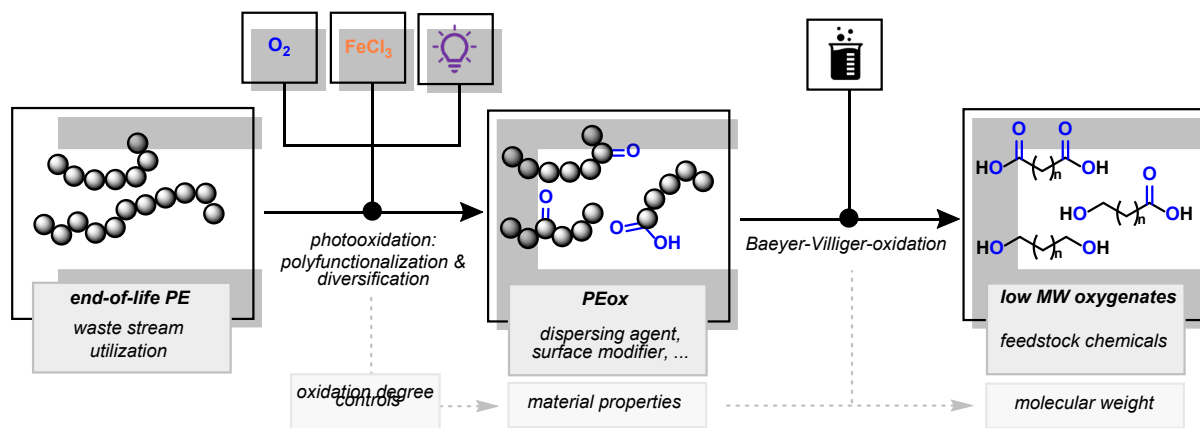
Scheme 5.2. Concept of this work.

At first, applicable reaction conditions for the photooxidation of PE had to be identified. In literature, most $FeCl_3$-catalyzed HAT-reactions are conducted in polar solvents such as acetonitrile or acetone.[39–41] However, polyethylene is completely insoluble in these systems. The chemical inertness and resistance against organic solvents make PE a valuable material but prevent its dissolution and thereby complicate its chemical functionalization and degradation. Initial photooxidation experiments with suspended, finely dispersed, or emulsified PE in acetonitrile showed no oxidation at all. These results implicated the need for a homogenous reaction system. Good solvents for PE are rare, and available choices are mostly limited to hydrocarbons and aromatics at elevated temperature. On the other hand, the selection of reaction media for Photo HAT reactions is also limited. The solvent must not have easily abstractable H-atoms to prevent side reactions. Also, organic solvent vapors in an oxygen atmosphere can easily form explosive or highly flammable mixtures. The use of either inflammable media or those with high boiling and flame point would be the safe choice.

Therefore, the search for a proper solvent (mixture) to carry out the $FeCl_3$ catalyzed oxidation of PE was challenging. The solvent has to fulfill the following requirements: a) ability to solubilize nonpolar PE, b) ability to dissolve polar $FeCl_3$, c) resistance towards H-atom abstraction, d) low flammability. After an extensive screening of solvent combinations, a 1:1 mixture of 1,2,4-trichlorobenzene (TCB) and benzonitrile (PhCN) at 120 °C was identified as promising solution that complies with the aforementioned conditions (Table 5.1). A special focus has to be put on the recyclability of the solvents due to their comparable higher price and environmental concerns.

Table 5.1. Solvents and their potential use in PE photooxidation.

Solvent (mixture)	PE solubility	FeCl₃ solubility	HAT resistance	Low flammability
Ethers	No	No	No	No
Acetone, MeCN	No	Yes	Yes	No
Alcohols	No	Yes	No	No
Haloalkanes	~	No	No	Yes
Toluene, xylene	Yes	No	No	No
TCB	Yes	No	Yes	Yes
PhCN	No	Yes	Yes	~
TCB/PhCN (1/1)	**Yes**	**Yes**	**Yes**	**Yes**

Polyethylene has no activated or preferential sites for H-atom abstraction, unlike polystyrene or polyethers. Thus, the photooxidation can be expected to be rather unselective and to yield complex product mixtures. Potentially formed functionalized polymers or oligomers can be difficult to analyze and characterize (limited solubility, irregular structures, etc.). Therefore, first investigations on reactivity and selectivity of the photooxidation were conducted on low molecular weight alkanes. Then, PE was reacted under the same conditions and analyzed in consideration of the previous findings (Scheme 5.3).

Cyclododecane was chosen as suitable model substrate; the formation of only a single regioisomer during the monooxidation simplifies the reaction analysis. Furthermore, the negligible ring-strain is not expected to have an influence on the reactivity. Additional photooxidation experiments were conducted with *n*-decane to study the distribution of regioisomers. These reactions were not optimized for yield but analyzed qualitatively to study the chemo- and regioselectivity.

The photooxidation of cyclododecane (0.1 M) in TCB/PhCN (1/1) was conducted under oxygen atmosphere (solution sparged with O₂; balloon attached to vial) with 5 mol% FeCl₃ · 6 H₂O at 120 °C and irradiation of two 405 nm LED lamps for 4 hours. The formation of cyclododecanone as main product, minor amounts of diketones, and traces of cyclododecanol was observed. Dodecanedioic acid (detected as methyl ester after treatment with TMS-diazomethane) was found due to chain scission reactions. When the reaction was conducted at room temperature, no acids were detected. No reaction occurred in the absence of light. Also, under nitrogen atmosphere, no oxidation products were formed; instead traces of chlorocyclododecane could be detected proving the presence of chlorine radicals. The observed product distribution contrasts previous literature reports that found significant alcohol formation, although under different reaction conditions (MeCN, room temperature, halogen arc lamp 300 W >400 nm)[42]. Cyclododecanol as starting material was completely transformed into cyclododecanone with our procedure. Therefore, it can be rationalized that intermediately formed alcohols are rapidly oxidized to ketones. The photooxidation of decane

showed the same trends as for cyclododecane. An approximately equimolar mixture of regioisomeric ketones (2-, 3-, 4-, 5-decanone) was obtained under standard conditions. Furthermore, minor amounts of multiply oxygenated products and traces of alcohols (all regioisomers) and decanal were detected. The presence of decanoic acid was proven by detection of decanoic acid methyl ester after treatment with TMS-diazomethane. The functionalization of both primary and secondary carbon positions is characteristic for reactions of the unselective chlorine radical. Triphenyl phosphine was added to the reaction mixture after the photooxidation to test for residual hydroperoxides. No triphenyl phosphine oxide formation could be observed, excluding the presence of peroxides.

Next, a practical photooxidation procedure for polyethylene was developed. A round-bottom flask was purged with oxygen, charged with PE and TCB, and heated to 150 °C until the PE was completely dissolved. Then, a solution of $FeCl_3 \cdot 6 H_2O$ in PhCN was added. After a clear, orange solution was obtained, the temperature was decreased to 120 °C, an oxygen balloon was connected to the flask and the system was irradiated by 405 nm LEDs. The reaction was terminated by turning off the lamps and cooling to room temperature. Reaction products could be obtained by precipitation with cold methanol or solvent evaporation under reduced pressure.

We chose commercial PE gloves (used e.g. for handling food in stores) as starting material. They are representative single-use items, and typically contain negligible amounts of additives. The analysis of the gloves by GPC, IR and ^1H NMR confirmed a high molecular weight ($3.4 \cdot 10^5$ g/mol), and the absence of oxygen functionalities as well as additives in detectable amounts. Then, the photooxidation was conducted with PE gloves (0.6 g) as starting material dissolved in 20 mL TCB/PhCN (1/1), a catalyst loading of 3 wt% $FeCl_3 \cdot 6 H_2O$ for four hours. Addition of cold methanol (0 °C) to the reaction mixture led to the precipitation of a beige solid that was filtered and dried in air (PEox, 0.39 g, 65 wt%). Solvent (TCB, PhCN, MeOH) removal under reduced pressure gave an oil-like residue. The product was analyzed by GPC, IR, ^1H and ^{13}C NMR spectroscopy (Scheme 5.3).

The GPC analysis of PEox reveals a strong decrease of the chain length from $M_w = 3.4 \cdot 10^5$ to $M_w = 1.7 \cdot 10^3$ g/mol. This indicates to a multitude of chain scission events, typically known from α-scission of radicals (see mechanistical discussion below). Additionally, the polydispersity index (PDI) decreased from 8.0 to 2.8. IR spectroscopy shows the appearance of strong, superimposed bands in the range from 1600 to 1820 cm^{-1}, corresponding to a variety of carbonyl and carboxyl species. The maximum is located at 1714 cm^{-1}, the characteristic band of isolated keto functions. Also, the formation of γ-lactones (band at 1770 cm^{-1}) can be observed. The IR band of carboxylic acids (1710 cm^{-1}) is only noticeable as shoulder due to the strong overlap in this wave number range. However, treatment of PEox with TMS-diazomethane led to the appearance of a new band at 1735 cm^{-1} (see experimental section for more details), which shows the formation of methyl esters and confirms the initial occurrence of carboxylic acids. These findings were further confirmed by high-temperature ^1H NMR spectroscopy. Protons adjacent to carbonyl and carboxyl groups (2.35–2.55 ppm) can be observed; the broad multiplet is formed by overlap of the signals of chemically different ketones and carboxylic acids. The signal at 4.5 ppm can be assigned to the γ-proton of 5-membered lactones. After functionalization of PEox with TMS-diazomethane, the characteristic signals of carboxylic acid

methyl esters (singlet at 3.7 ppm, triplet at 2.3 ppm) can be observed in the NMR spectrum. Unfortunately, the quality of the baseline is low due to the low solubility of the sample and the presence of many chemically different species. Therefore, quantification of the functional groups by integration is not reliably possible. ^{13}C NMR signals are hardly detectable due to high chemical variance in the sample. No hydroxy or hydroperoxy functions could be found by any analytical method as expected from the model substrate studies. The assignment of functional groups corresponds with previous systematic investigations of PE oxidation products.[43]

The molecular weight of PEox is in the typical range for oxidized polyethylene waxes (OPEW). These are commercially produced by the high-temperature oxidation of virgin PE and find use, *inter alia*, as dispersing agents, polishes or softening agents.[44–46] The acid number (AN) of PEox, determined by titration, is 48 and slightly above the typical range of OPEW (5–45).

Next, the residue obtained after solvent evaporation, consisting of the methanol-soluble product fraction, was treated with TMS-diazomethane and analyzed by GC-MS. Various small molecules (<C$_{20}$) could be detected and identified. The two main groups of products are dicarboxylic acid methyl esters (C$_4$–C$_{16}$) and ω-(γ-lactone) carboxylic acid methyl esters (C$_7$–C$_{12}$). Additionally, derivatives of these groups with further keto groups were found. The indubitable identification of all detected products was not possible. The identified molecules and functional groups are in alignment with the previous analysis of PEox. The residue also contained small amounts of degradation products from the solvent, namely benzamide from the hydrolysis of benzonitrile, and hydroxylated and dimerized aromatics.

The presented analysis proved that the photooxidation process transformed waste polyethylene into PEox with decreased molecular weight and introduced carbonyl, carboxyl and lactone functionalities. Furthermore, based on the properties, the obtained product PEox has potential commercial use as OPEW.
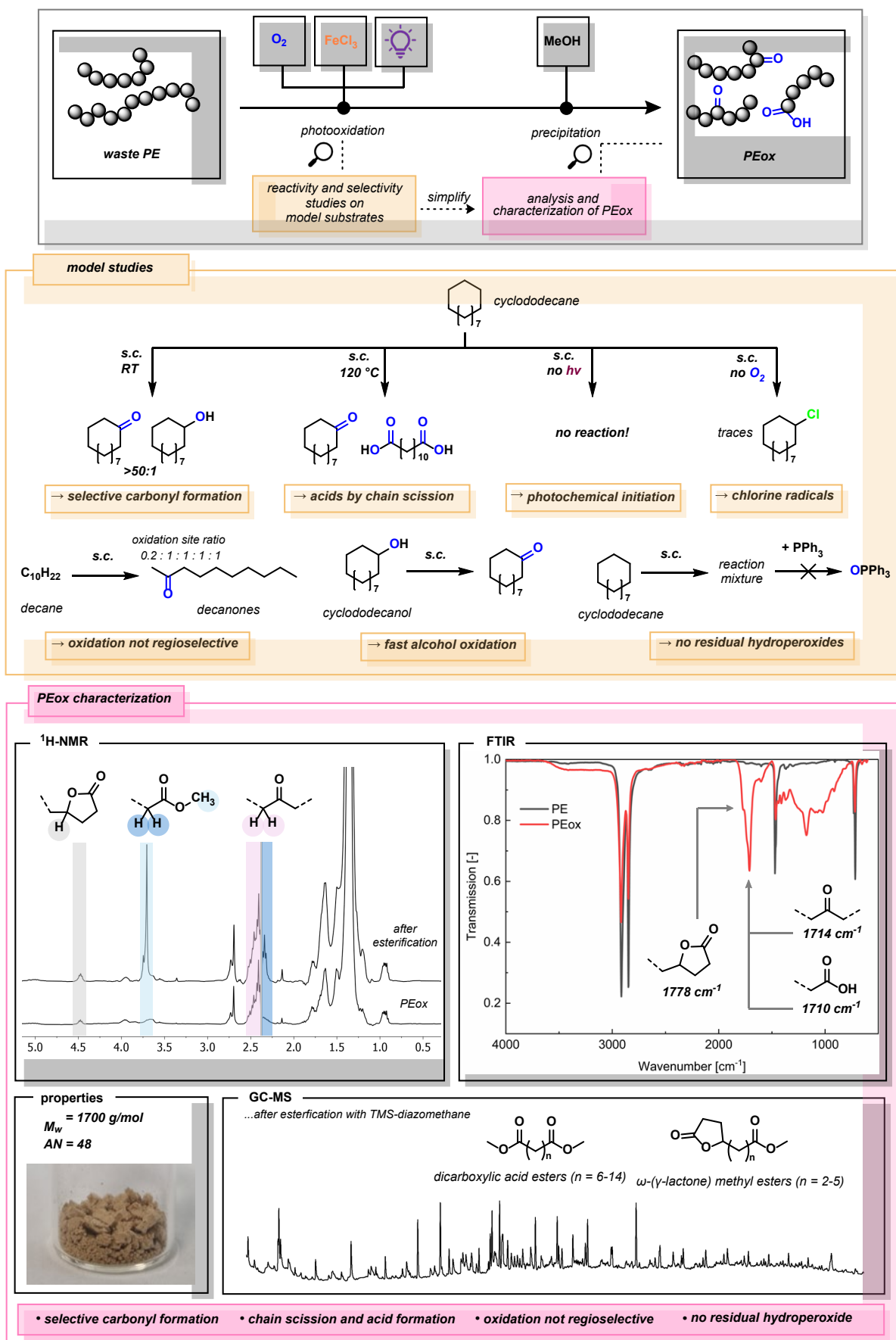
Scheme 5.3. Model studies for photooxidation and characterization of PEox. s.c.: standard conditions: substrate (0.1 M) in TCB/PhCN 1/1, 5 mol% FeCl$_3$ · 6 H$_2$O, 120 °C, 405 nm LED, 4 h.

The oxidation degree of PEox defines the final product properties. Therefore, various influences on the reaction were investigated (Scheme 5.4). First, the progress of the photooxidation under standard conditions was followed for 16 hours. Samples were taken after 0.5 h, 1 h, 2 h, 4 h, 8 h and 16 h reaction time and treated as previously described. The weight of recovered, solid PEox (by precipitation) decreased due to the higher formation of methanol-soluble short molecules. These species could be detected by GC-MS. The acid number of PEox steadily increased from AN = 0 for virgin PE to AN = 15 (0.5 h), 30 (1 h), 40 (2 h) and 48 (4 h). Comparable final values are reported for OPEW formation from virgin PE.[47] The progressing oxidation of PEox could also be tracked by IR spectroscopy: the intensity of the C–H stretch and deformation bands (2915, 2850, 1460 cm^{-1}) steadily decreased, while the C=O and C–O stretch bands (~1715, 1170 cm^{-1}) increased. The analysis by GPC further confirms a continuous decline of the molecular weight during the photooxidation. For the products with longer reaction time (t = 8, 16 h) neither acid number determination by titration nor investigation by GPC were possible due to low solubility in the respective non-polar solvents (xylene, TCB). This indicates high polarity of the products due to prolonged oxidation.

Next, the role of the catalyst loading in the reaction was investigated. The photooxidation was conducted with variation of iron(III) chloride hexahydrate amount between 1.5–6 wt%. PEox samples were obtained, analyzed and compared to the standard product. An increased amount of iron catalyst corresponds to a larger oxidation degree in the same reaction time, without other apparent changes in the composition (no other functionalities detected). This result is especially visible in the IR spectra. Lastly, the reaction was conducted in both pure oxygen atmosphere (O$_2$ balloon) and under air (open reflux condenser attached to the flask). Again, the properties of obtained PEox were compared. The use of air instead of pure O$_2$ led to the formation of significantly less carbonyl and carboxyl functionalities in the same time frame, observable by IR spectroscopy. This is most likely due to the lower availability of oxygen in the reaction solution. However, the lower concentration of O$_2$ in air decreases the risk of the formation of flammable atmosphere during the reaction.

In conclusion, the oxidation degree and therefore the product properties of PEox can be tuned by three independently controllable factors: oxygen concentration, loading of FeCl$_3$ and the reaction time. This flexibility is highly advantageous in the development of a modular process and gives facile access to products for different applications.
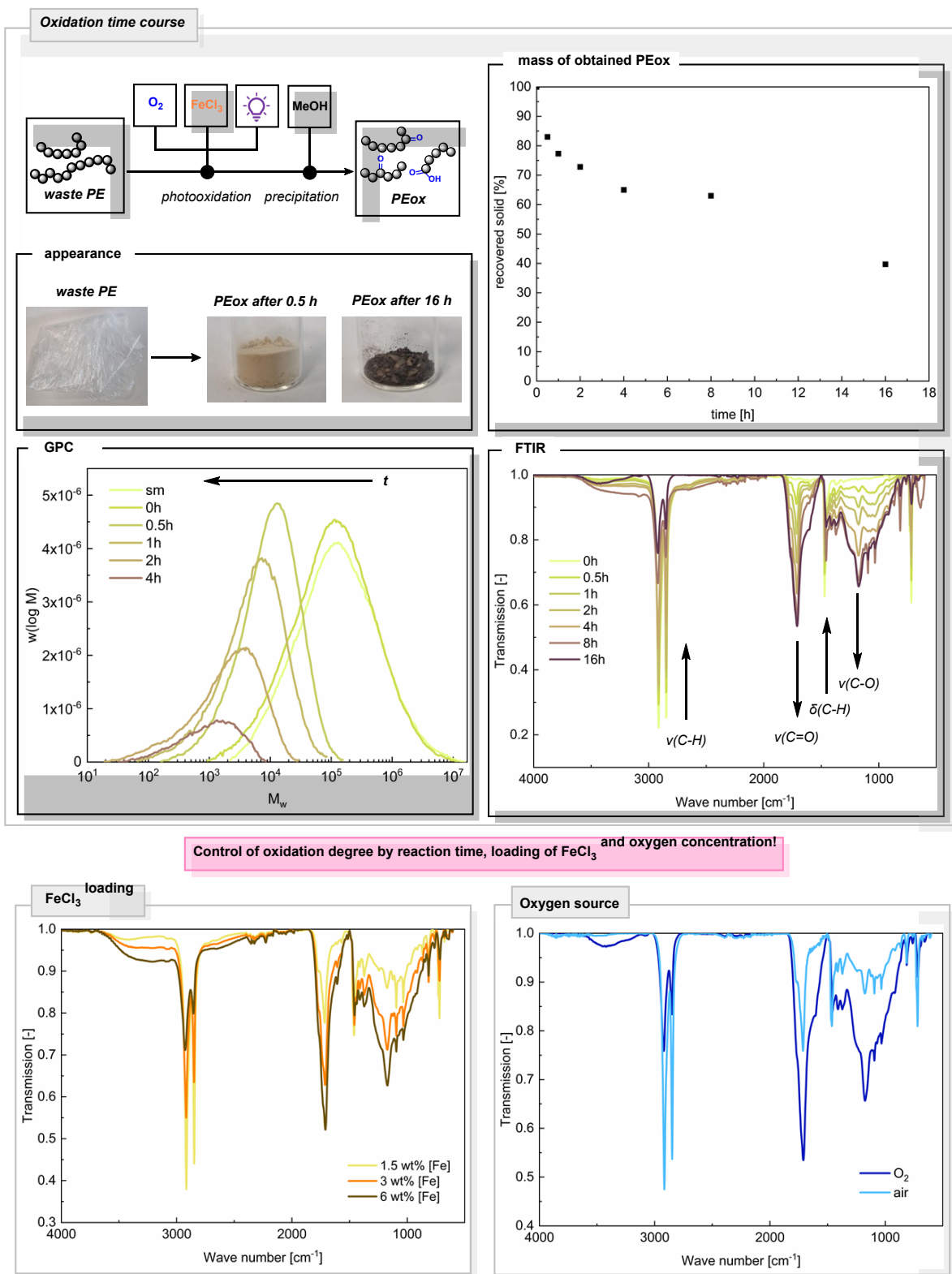
Scheme 5.4. Time course of the PE oxidation (top), influence of FeCl$_3$ loading and O$_2$ source (bottom).

The transformation of PE into low molecular weight feedstock is an interesting addition to the previously described production of oxidized PE waxes in order to maximize product variety. The photooxidation approach yields, even after prolonged reaction times, mostly polyfunctional oligomers or polymers and only small amounts of defined low-molecular weight molecules. However, PEox contains carbonyl, carboxyl and lactone moieties that enable further functionalization by "classical" organic chemistry. The Baeyer-Villiger oxidation (BVO) is a valuable reaction that transforms ketones into esters. For PEox, full carbonyl conversion followed by solvolysis would lead to further decrease of the molecular weight and give mainly monofunctional or α,ω-difunctionalized products. BVO is rather challenging for linear aliphatic ketones; therefore, strong reagents were used for this proof-of-concept. Multiple strategies for the transformation of carbonyl functions in polymers into esters by Baeyer-Villiger oxidation have already been reported.[48–50]

The following BVO procedure was developed for the transformation of oxidized polyethylene: PEox was dissolved or suspended in dichloromethane, then trifluoroacetic anhydride and urea hydrogen peroxide adduct were added at room temperature. Pertrifluoroacetic acid was formed as active reagent *in situ*. After 12 hours, solid Na_2SO_3 and methanol were added, the mixture was heated to reflux and stirred for 12 hours. After cooling to room temperature, the suspension was filtered, and the solvent was removed under reduced pressure. A viscous residue, the "Baeyer-Villiger product", was obtained and analyzed.

The product was characterized by ^{1}H NMR and IR spectroscopy and GC-MS analysis (Scheme 5.5). The NMR spectrum showed new signals in the range of 3.4 to 3.8 ppm indicating the formation of alcohols and methyl esters. Additionally, the signal intensity around 2.3 ppm (ketones and carboxylic acids) decreased compared to PEox. Consistent results were obtained from IR analysis. The maximum of the carbonyl band shifted from 1714 cm^{-1} (isolated aliphatic ketone) to 1736 cm^{-1} (aliphatic ester). Furthermore, the strong, broad band around 1040–1100 cm^{-1} can be assigned to C–O stretch vibrations of alcohols. Several low-weight molecules could be identified by GC-MS such as 1,10-decanediol, 1,12-dodecanediol, methyl hexadecanoate and methyl octadecenoate. These results prove (at least partial) transformation of ketones into esters, followed by methanolysis and formation of low-molecular weight products. Thus, the proof-of-concept can be deemed successful.

This functionalization approach can be potentially extended to other types of reactions. The transformation of carbonyl groups in PEox into oximes followed by Beckmann rearrangement and hydrolysis would give access to diamines, diacids and amino acids. Examples for the formations of oximes in polymers can be found in literature.[51]

For potential commercial application, the reaction would have to be further optimized. Especially the use of less expensive reagents would be important; utilization of *in situ* generated peracetic or performic acid could be a potential solution. Also, the separation of the reaction products could be challenging. Oxidation or reduction of the reaction mixture could transform the products into either only alcohols or carboxylic acids, thus simplifying the work-up and application. However, such investigations are out of the scope of the work.
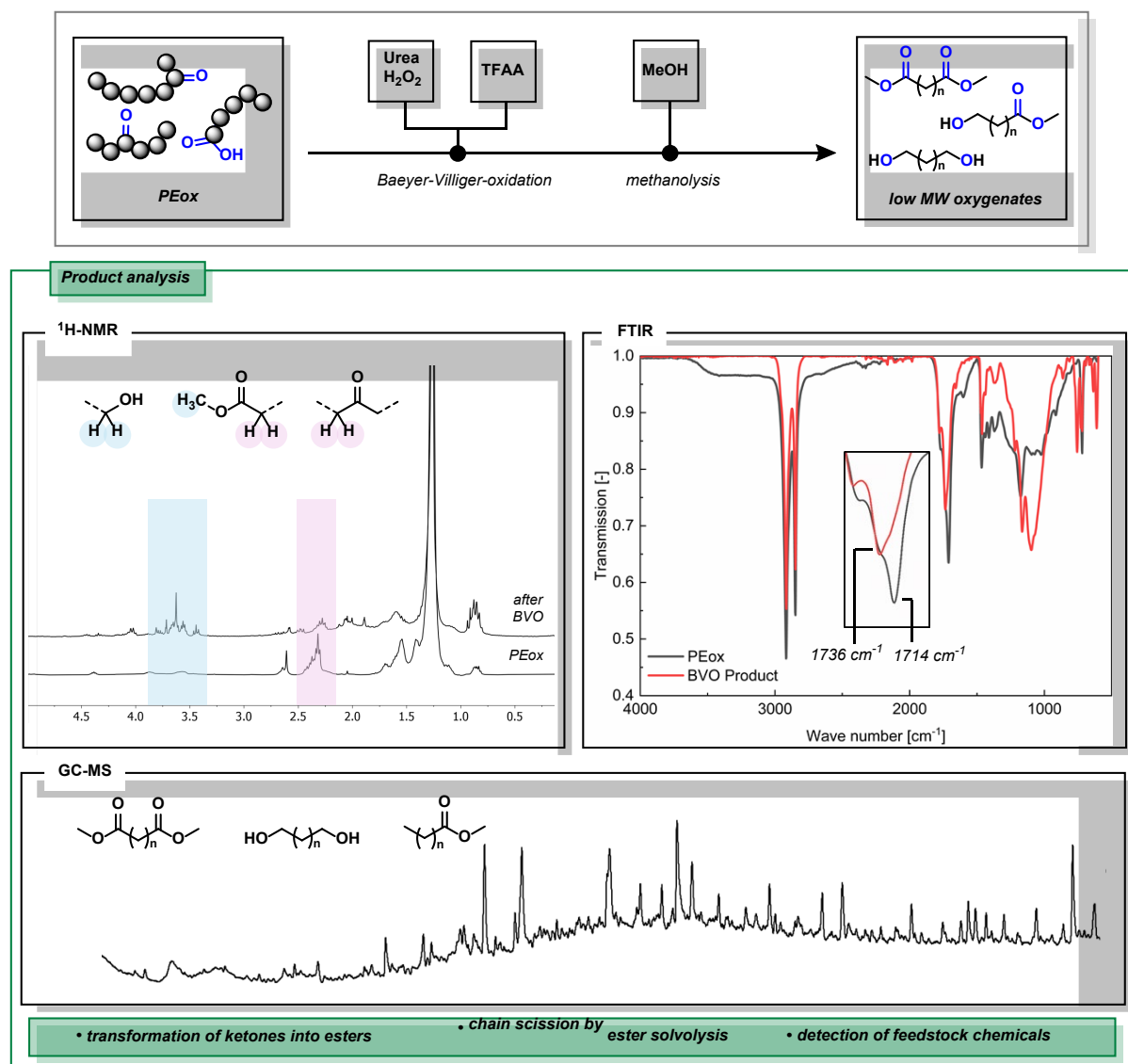
Scheme 5.5. Baeyer-Villiger oxidation of PEox.

The variation of the photooxidation conditions is the key to access different products. For the better control of this reaction, it is important to understand the reaction mechanism. It will most likely resemble the natural PE photooxidation; the here proposed pathways are based on literature reports and experimental observations (Scheme 5.6). First, the $FeCl_3$-catalyzed HAT reaction initiates a self-sustaining cycle and provides a steady flux of radicals. After irradiation and LMCT, Fe(III) is reduced to Fe(II) and a chlorine radical is liberated. This species can abstract a hydrogen atom from polyethylene, thereby creating an alkyl radical and hydrochloric acid. Oxidation of Fe(II) by dioxygen or peroxyradicals in presence of HCl leads to the regeneration of the catalytic Fe(III)Cl$_3$ species.[32] The detection of chlorocyclododecane in absence of oxygen confirms the presence of chlorine radicals. The previously formed alkyl radical recombines with dioxygen to a peroxyradical, and then abstracts a hydrogen atom from other PE chains to ultimately form a hydroperoxide. The simultaneously formed alkyl radical enters again the radical chain mechanism. The highly labile O–O bonds of the hydroperoxides can be split homolytically, e.g. by heat, UV light or metal catalysis. Their lifetime is going to be short under the reaction conditions. The split gives a hydroxy and an alkoxy radical. Both

species can abstract H-atoms from the PE chains, starting new radical chains and accelerating the photooxidation. Ketones are formed by the formal expulsion of water from hydroperoxides or by oxidation of the formed alcohols.[52,53] The presence of hydroxy radicals is confirmed by the detection of hydroxylation products of solvent molecules (PhCN, TCB).

The observed molecular weight decrease and the formation of carboxylic acids and lactone moieties can occur via various pathways. The previously described alkoxy radicals can undergo α-scission into either alkyl chain and acyl radical, or aldehyde and primary alkyl radical. The three latter species can all be oxidized to carboxylic acids by molecular oxygen. Lactone formation can be initiated by intramolecular H-atom abstraction of peroxo radicals from the 4-position of the same hydrocarbon chain. The resulting alkyl radical can then attack the hydroperoxide, thus leading to the expulsion of •OH and formation of a tetrahydrofuran moiety. The positions next to the ether oxygen are prone to hydrogen atom abstraction and peroxide formation. Lactones are then formed after α-scission. The same type of intramolecular attack can occur on a peroxo acid, the lactone is directly generated by displacement of •OH.[54] The photooxidation is highly complex and not completely understood; not all possible radical pathways can be described here. The presented reactions, however, cover the most important processes and explain the experimental findings.
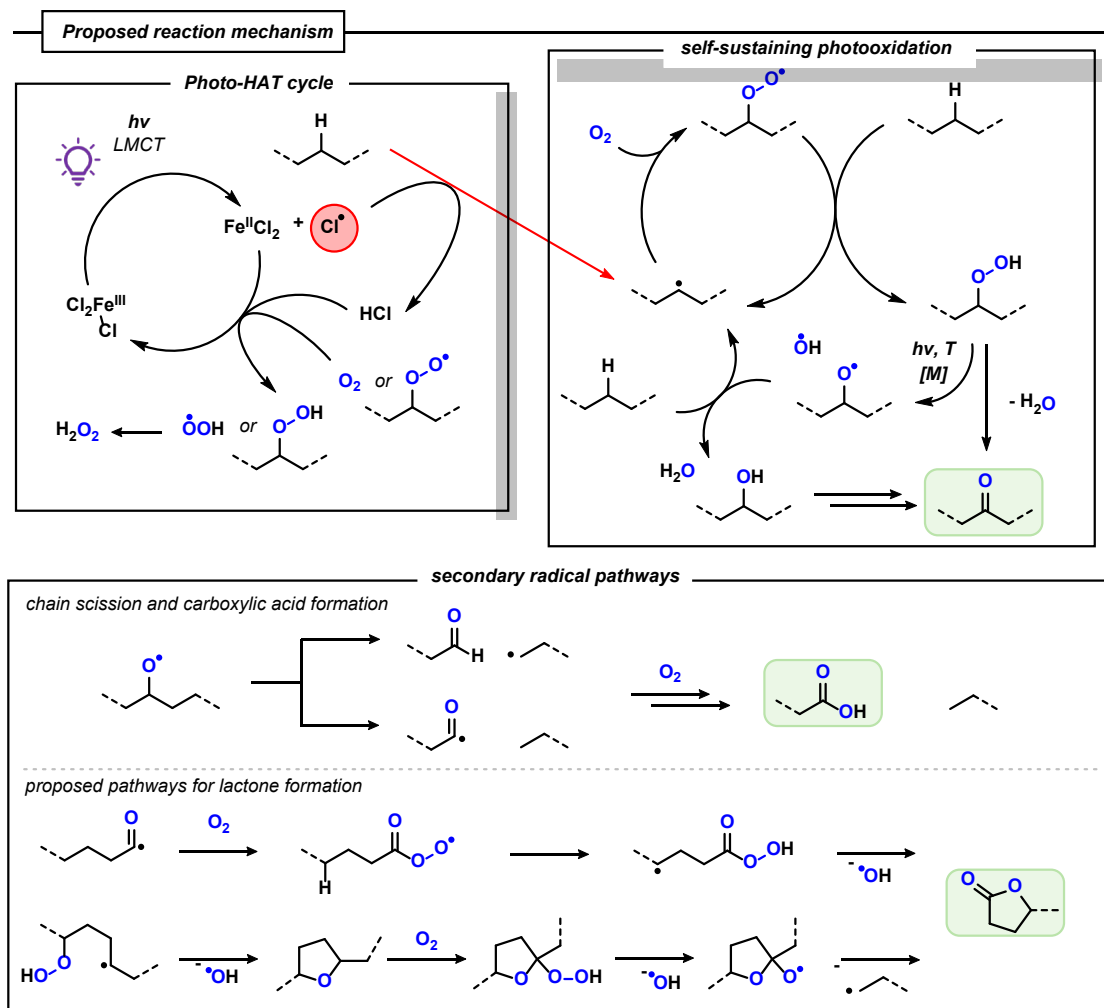
Scheme 5.6. Selected possible reaction pathways in the PE photooxidation. Experimentally detected functional groups marked in green.

The described natural photooxidation of polyethylene is a highly undesired process in commercial materials. Therefore, most PE products contain stabilizers and additives that preserve the material properties and enhance the lifetime of the goods (Scheme 5.7).[55] The main classes are radical scavenger, hindered amine light stabilizers, hydroperoxide scavengers, and UV absorbers. The PE products can contain different mixtures of these compounds depending on the intended use. Radical scavengers (e.g. pentaerythritol tetrakis[3-(3,5-di-*tert*-butyl-4-hydroxyphenyl)propionate] (PTTP)) are often hindered phenols, the phenolic hydrogen atom can be easily abstracted by radicals (hydroxy, peroxy, alkyl). The resulting radical is unreactive for further HAT due to steric hindrance and electronic stabilization; thus, the radical chain is interrupted. The molecules are consumed as stochiometric reagents, each phenol unit can deactivate only one radical. Hindered amine light stabilizers (HALS, e.g. bis(2,2,6,6,-tetramethyl-4-piperidyl)sebacate (BTPS)) also stop the photooxidation by interception of radical species. During the process they are converted into aminoxyl radicals, but they can be transformed back into the amines by a follow-up reaction sequence (Denisov cycle).[56] Therefore, HALS can deactivate multiple radicals. Hydroperoxide scavengers are often phosphite esters (such as tris(2,4-di-*tert*-butylphenyl)phosphite (TTPP)). They reduce hydroperoxides to the corresponding alcohols and in this way impede the generation of further radicals by O–O bond scission. The phosphite esters are consumed stoichiometrically. Finally, there are UV absorbers such as ethyl 2-cyano-3,3-diphenylacrylate (ECDA), octabenzone, and bumetrizole. The absorption of energy-rich irradiation inhibits many primary radical generation pathways that would initiate the photooxidation. Also, it prevents the scission of hydroperoxides by UV light. The absorption band should ideally end right before the visible light region to absorb all UV light while preventing unwanted coloration of the product.[55]
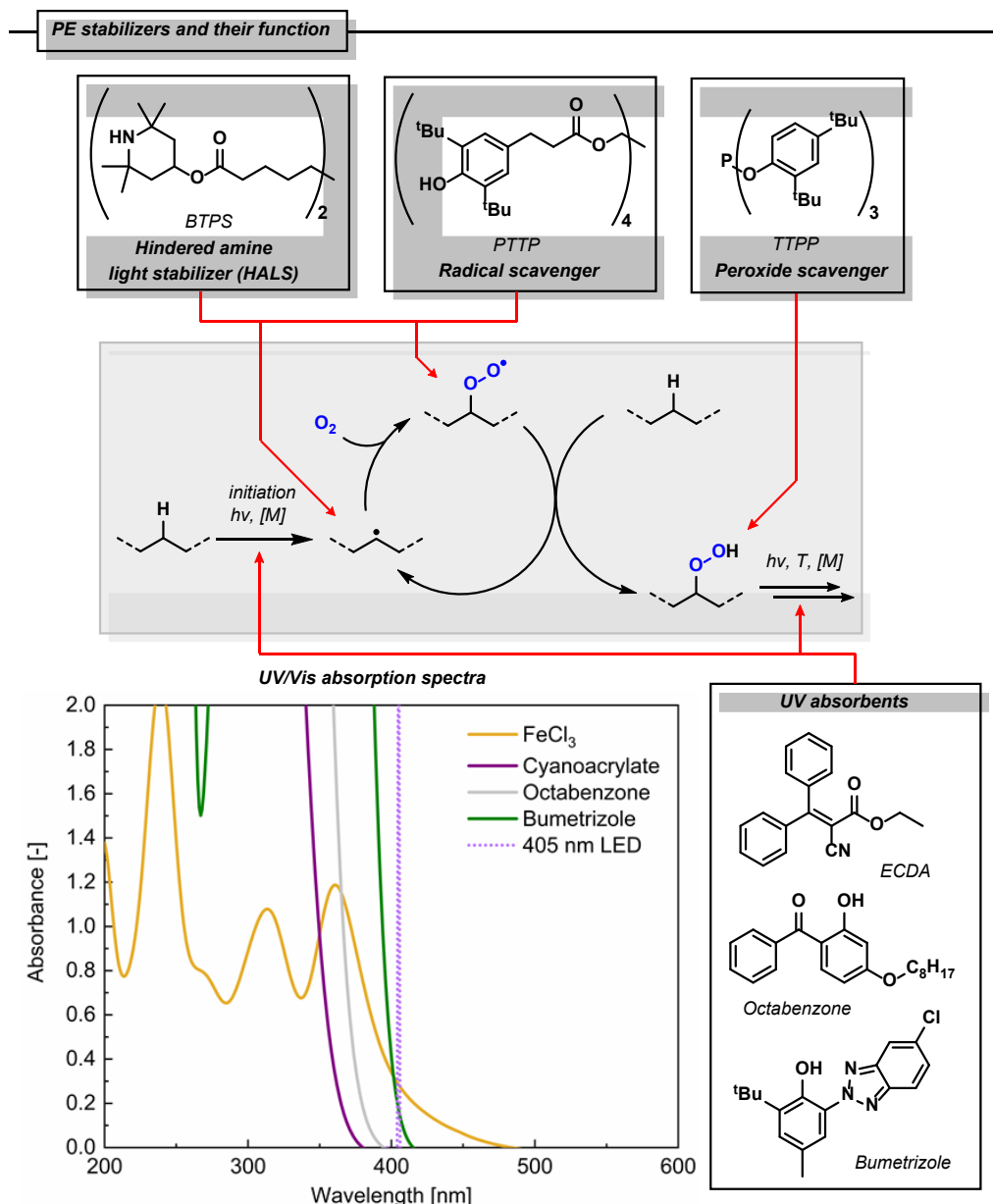
Scheme 5.7. Selected commercial PE stabilizers and their roles in oxidation inhibition.

The proposed photooxidation procedure must be practicable in presence of polymer stabilizers if it shall be applicable for real PE waste. Therefore, 1 wt% of different additives, which is in the common range for commercial products, were added to the reaction (table 5.2). Gratifyingly, most additives did not impede the photooxidation. The UV absorbents ECDA and octabenzone did not show any influence on the reaction, since their absorption spectra do not overlap with the used 405 nm LED. Bumetrizole, on the other hand, does absorb light until 415 nm. Consequently, a decrease of the oxidation degree was observed, but without stopping the reaction. Both, radical and hydroperoxide scavengers, were tolerated in the procedure. They were most likely rapidly consumed under the reaction conditions. HALS proved to be the most problematic additives, decreasing the PE oxidation to traces. These stabilizers are known to be sensitive to acidic conditions, after protonation the amine moiety does not interact with radicals. Indeed, the addition of six equivalents of hydrochloric acid (solution in MeOH)

to the reaction mixture deactivated the HALS. The tolerance of the photooxidation protocol against the commercial polymer stabilizers enables its use in the valorization of waste PE.

Table 5.2. Influence of additives and impurities on the photooxidation of PE.

Additive	Class	PE oxidation
ECDA (λ_{abs} < 380 nm)		Yes
Octabenzone (λ_{abs} < 395 nm)	UV absorbent	Yes
Bumetrizole (λ_{abs} < 415 nm)		decreased
TTPP	Peroxide scavenger	Yes
PTTP	Radical scavenger	Yes
BTPS	HALS	traces
		Yes[a]

a) after addition of 6 eq. HCl (2 M in MeOH, 0.15 μmol)

The reusability of the benzonitrile/trichlorobenzene mixture is an important factor to decrease the cost and environmental concerns of the process. Therefore, the recyclization was tested. First, the photooxidation was performed under standard conditions, PEox was obtained by precipitation with methanol. Then, MeOH was removed from the solvent mixture under reduced pressure and collected for later use. A new loading of polyethylene was dissolved in the residual PhCN/TCB/FeCl₃ solution. The photooxidation step was repeated and new PEox was obtained after addition of the previously collected MeOH. The properties of both batches were the same, proving the possibility to reuse all solvents and the catalyst.

Finally, a modular photooxidation process can be proposed based on the experimental results (Scheme 5.8). The reaction of polyethylene is conducted with variation of the three factors oxygen concentration, iron(III) chloride loading and reaction time. PEox with adaptable properties is obtained by precipitation with MeOH. The solvent/catalyst system can be recovered and reused in a closed cycle, thereby minimizing waste formation.
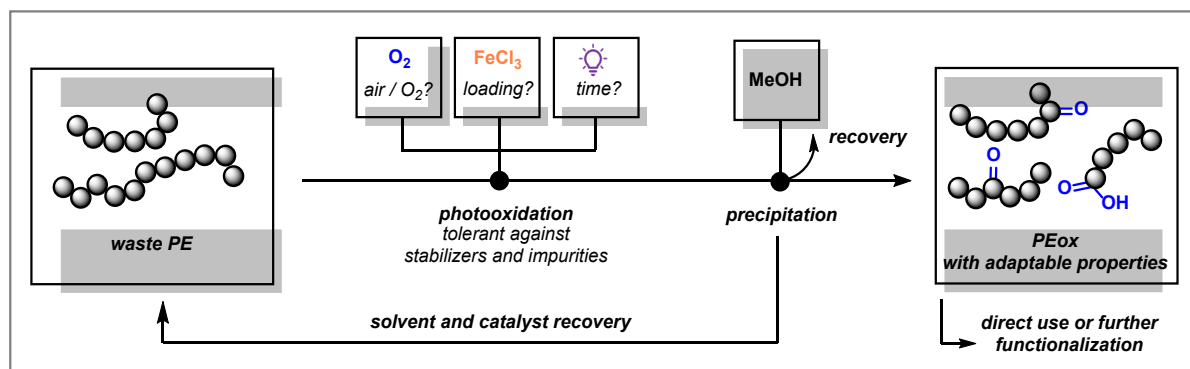
Scheme 5.8. Possible implementation of the PE photooxidation.

5.3   Conclusion and Outlook

The proof-of-concept study for a modular method for degradation and valorization of polyethylene into value-added products was successfully performed. The photooxidation of waste PE can be controlled by variation of the independently controllable factors $FeCl_3$ loading, reaction time and oxygen content. Oxidized polyethylene waxes with varying properties, depending on the oxidation degree, and potential commercial interest as OPEW are obtained. Furthermore, the product can be used as resource for further valorization. Baeyer-Villiger oxidation transformed the waxes into a mixture of diacids, diols and ω-hydroxy carboxylic acids that can serve as chemical feedstock. The oxidation degree determines the molecular weight distribution of the small oxygenates. Thus, different products can be obtained based on variation of the conditions.

The transfer from lab-scale to a potential technical process would include several challenges. First, photochemical reactions are well-established in chemical laboratories but underrepresented in industry. A competent set-up that allows the illumination of a large volume of (hot) solvent would need to be developed. For the Baeyer-Villiger oxidation, more economical reagents need to be found. Additionally, the obtained product mixtures are highly complex. Either an efficient separation method needs to be found, or potential application areas that do not require isolated products. However, these challenges could certainly be solved with further investigations and optimizations.

5.4   Experimental Section

5.4.1   Materials and Methods

Commercial chemicals (>95 % purity) were used as obtained without further purification. NMR spectral data was collected on a *Bruker* FourierHD (300 or 400 MHz for ^{1}H; 75 or 151 MHz for ^{13}C) at 25 °C. Spectra of polymers were measured in a mixture of TCE-d_2 and 1,2,4-trichlorobenzene at 90 °C. Low-resolution mass spectroscopy was conducted on an *Agilent* 6890N GC-system coupled to a 5975 MSD unit and H_2 as carrier gas. HP6890 GC-system with an injector 7683B and an *Agilent* 7820A system and N_2 as carrier gas was used for GC-FID analysis. UV/Vis spectra were measured on the Cary5000 spectrometer by *Agilent*. IR spectra were obtained on ALPHA Platinum ATR-IR and VERTEX 70 FTIR spectrometer by *Bruker*.
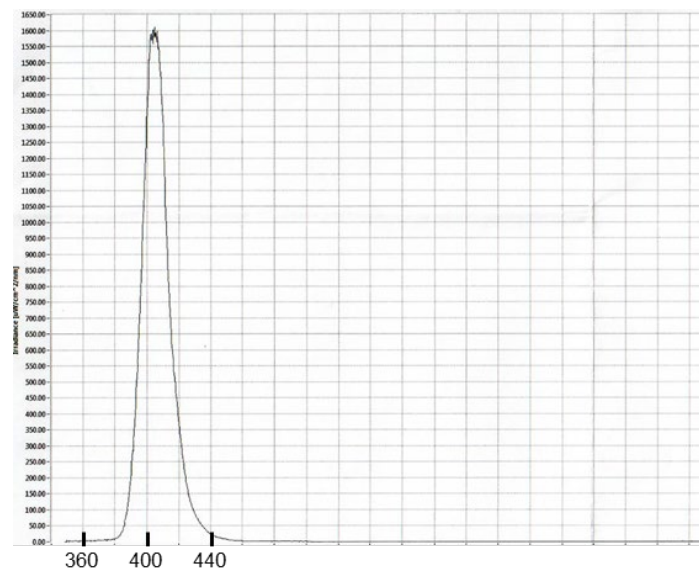
Figure 5.1. Emission spectrum of the used purple LED (λ_{max} = 405 nm).
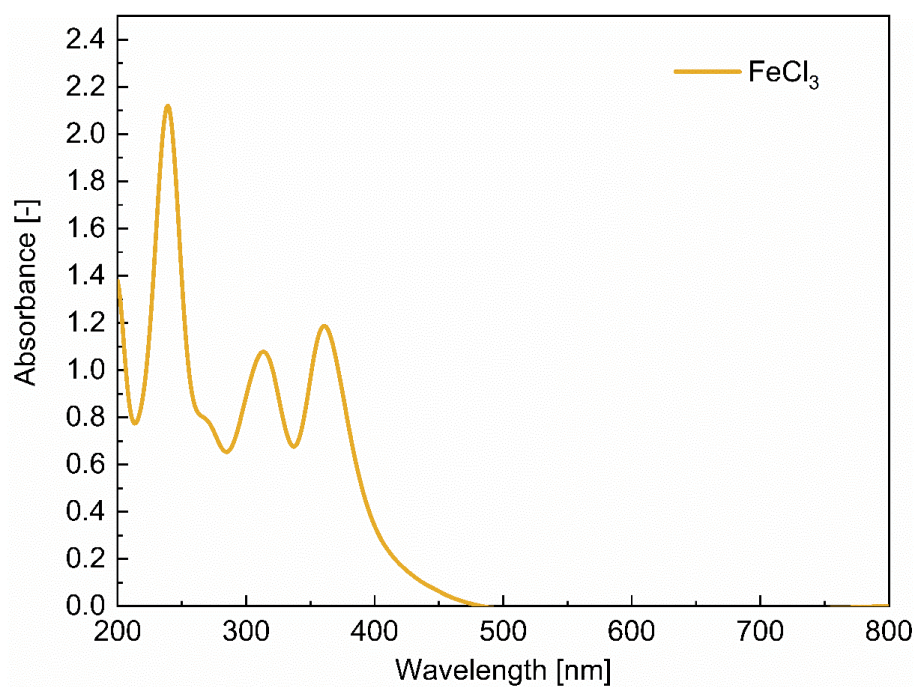
Figure 5.2. Absorption spectrum of FeCl₃.

Analysis of starting material

Commercial PE gloves (Figure 5.3) were chosen as starting material and analyzed by ^{1}H NMR spectroscopy, GPC, and IR spectroscopy prior to their use (Figure 5.4–5.6).

Figure 5.3. PE glove.

60
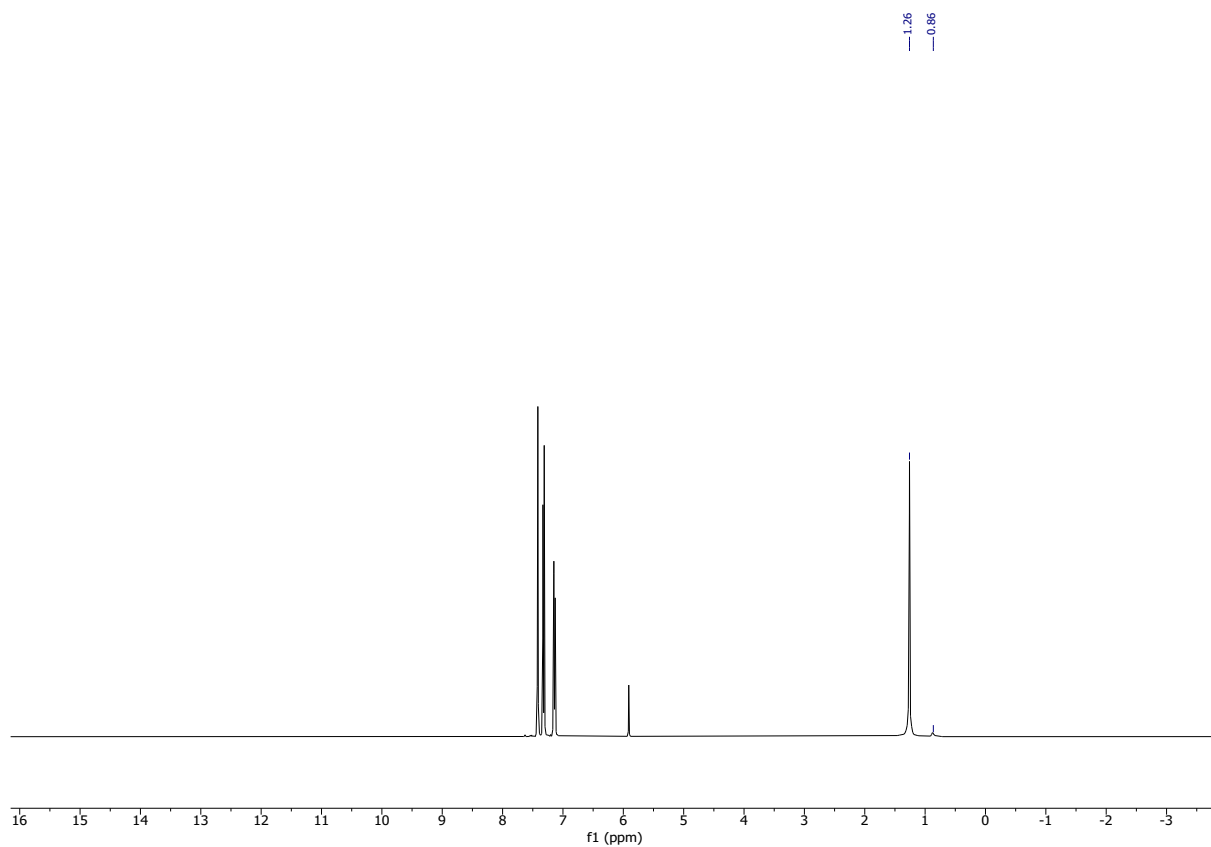
Figure 5.4. ¹H NMR (400 MHz, TCE-*d₂*+TCB) of PE glove.
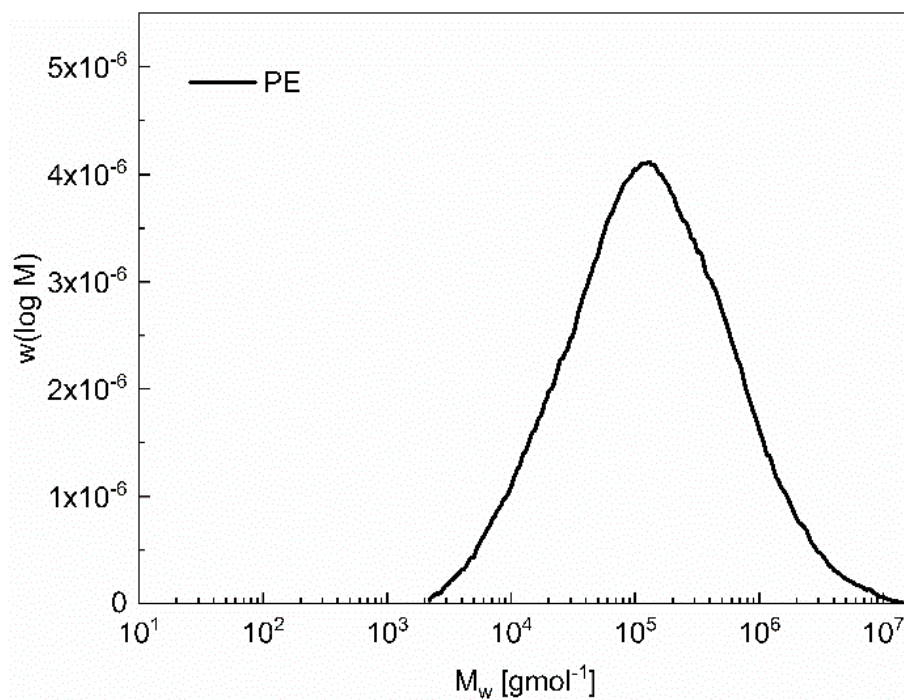
Figure 5.5. Molecular weight distribution of PE glove.
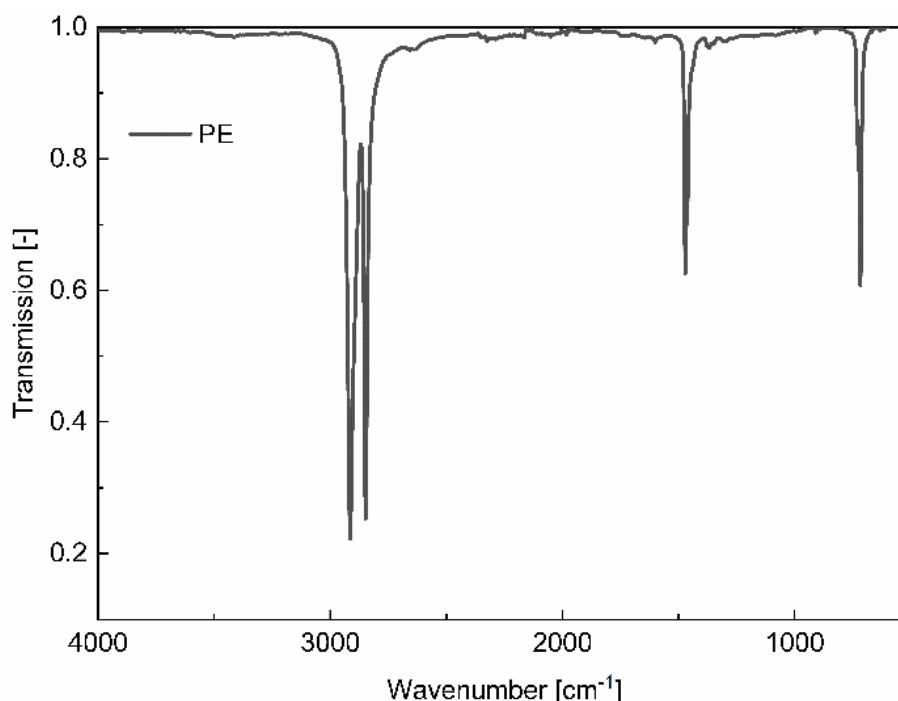
Figure 5.6. IR spectrum of PE glove.

5.4.2 General Procedures

General procedure photooxidation of model substrate (GP1)

Model substrate (0.2 mmol) and $FeCl_3 \cdot 6\ H_2O$ (5 mol%) were dissolved in a 1/1 mixture of TCB/PhCN (0.1 M), and the solution was purged with oxygen for two minutes. Then, the solution was heated to 120 °C, an oxygen balloon was connected to the flask and the system was irradiated by 405 nm LEDs for four hours. After cooling to room temperature, the reaction mixture was washed with diluted hydrochloric acid (0.1 M, 2x 2 mL) and filtered over a short silica plug. The sample was then analyzed by GC-FID. Assignment of the peaks was done by comparison with commercial products, and GC-MS analysis.

General procedure photooxidation of PE (GP2)

A round-bottom flask was purged with oxygen, charged with PE (0.6 g) and TCB (12 mL), and heated to 150 °C until the PE was completely dissolved. Then, $FeCl_3 \cdot 6\ H_2O$ (3 wt%, 18 mg), dissolved in PhCN (12 mL), was added. After a clear, orange solution was obtained, the temperature was decreased to 120 °C, an oxygen ballon was connected to the flask and the system was irradiated by 405 nm LEDs (0.5–16 h). The reaction was terminated by turning off the lamps and cooling to room temperature. Addition of cold methanol (0 °C) to the reaction mixture led to the precipitation of a beige solid that was filtered and dried in air (PEox). Solvent (TCB, PhCN, MeOH) removal under reduced pressure gave an oil-like residue.

General procedure esterification (GP3)

The compound (PEox, PEoil, BP or oxidation product of cyclododecane) was dissolved in toluene at 100 °C and cooled to room temperature. After dilution with methanol (5 vol%), TMS-diazomethane (0.6 mol/L solution in hexane) was added dropwise until a yellow color in

the solution persisted and no more gas evolution occurred. Excess TMS-diazomethane was quenched by dropwise addition of acetic acid until the yellow color vanished.

Acid number determination

The acid number was determined according to a modified version of ASTM D1386-15.[57]

Potassium hydroxide (0.56 g) was dissolved in distilled water (0.56 g) and diluted with 2-propanol (analytical grade) to 1000 mL. The solution was standardized by titration of benzoic acid. PEox (100 mg) was dissolved in warm xylene (40 mL) and three drops of phenolphthalein indicator solution were added. Then, the heated mixture was titrated with the alcoholic KOH-solution. The end point was taken when the pink color persisted for at least ten seconds. The titration was repeated three times, and the average value was taken. Additionally, the blank titration value was obtained by following the procedure without addition of PEox.

The acid number (AN) was calculated from the milliliters of alkali solution required for the titration of the sample (A) and the blank sample (B), the normality of the alkali solution (N) and the grams of sample used (C) (equation 1).

$$\text{Acid number} = (A - B) \cdot N \cdot 56.1/C \qquad \text{Eq. 1}$$

5.4.3 Photooxidation

Photooxidation of model substrates

Model substrates (0.2 mmol) were reacted according to GP1 and analyzed by GC-FID. A typical curve for the photooxidation of cyclododecane is shown in Figure 5.7.
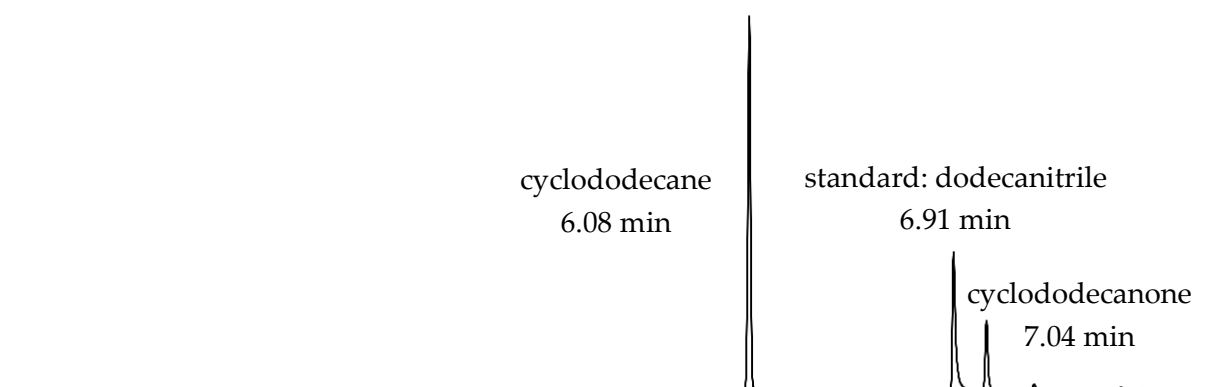
Figure 5.7. Section of GC-FID curve for the photooxidation of cyclododecane.

Photooxidation of PE (4 hours)

PE was reacted according to GP2 for 4 hours. Portions of obtained PEox and residue after solvent removal (20 mg each) were esterified following GP3. The samples were analyzed by ^{1}H NMR spectroscopy, IR spectroscopy and GC-MS.
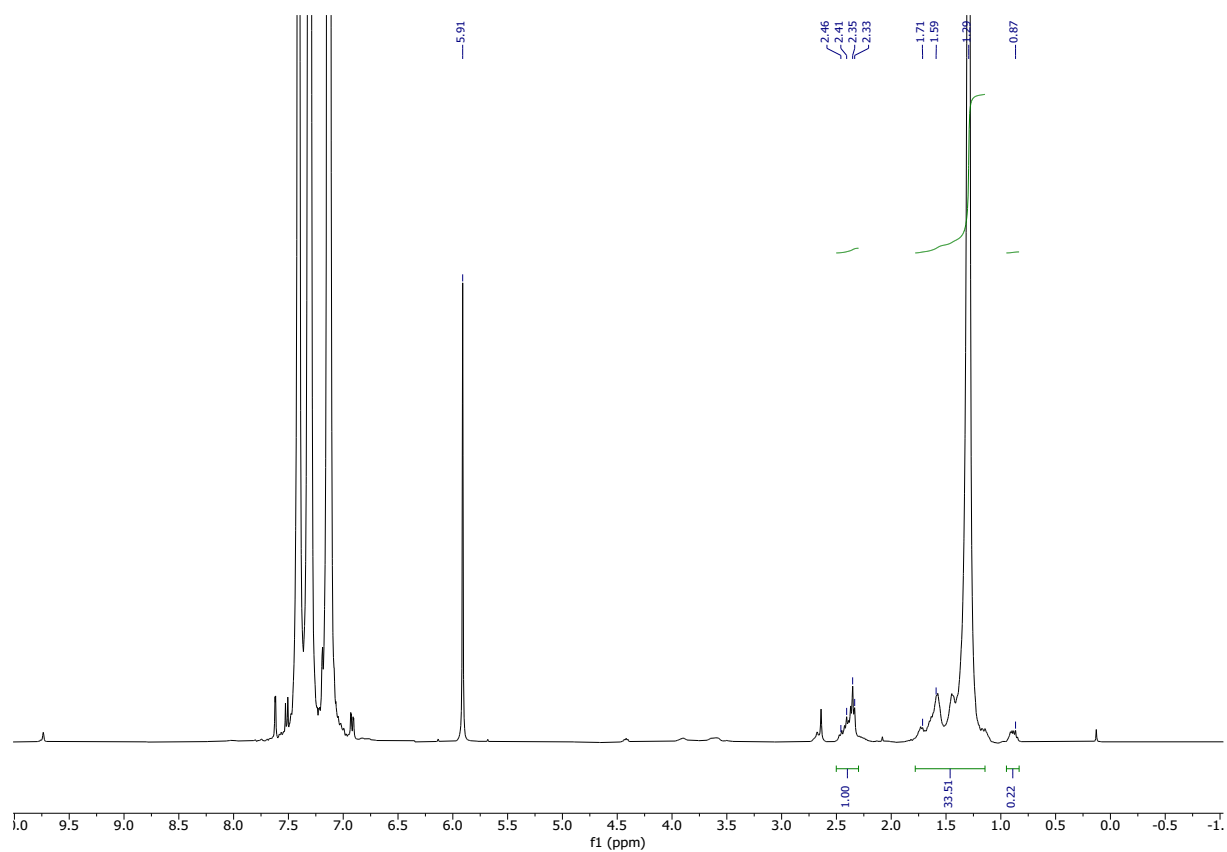
Figure 5.8. ^{1}H NMR (400 MHz, TCE-d_2+TCB) of PEox.
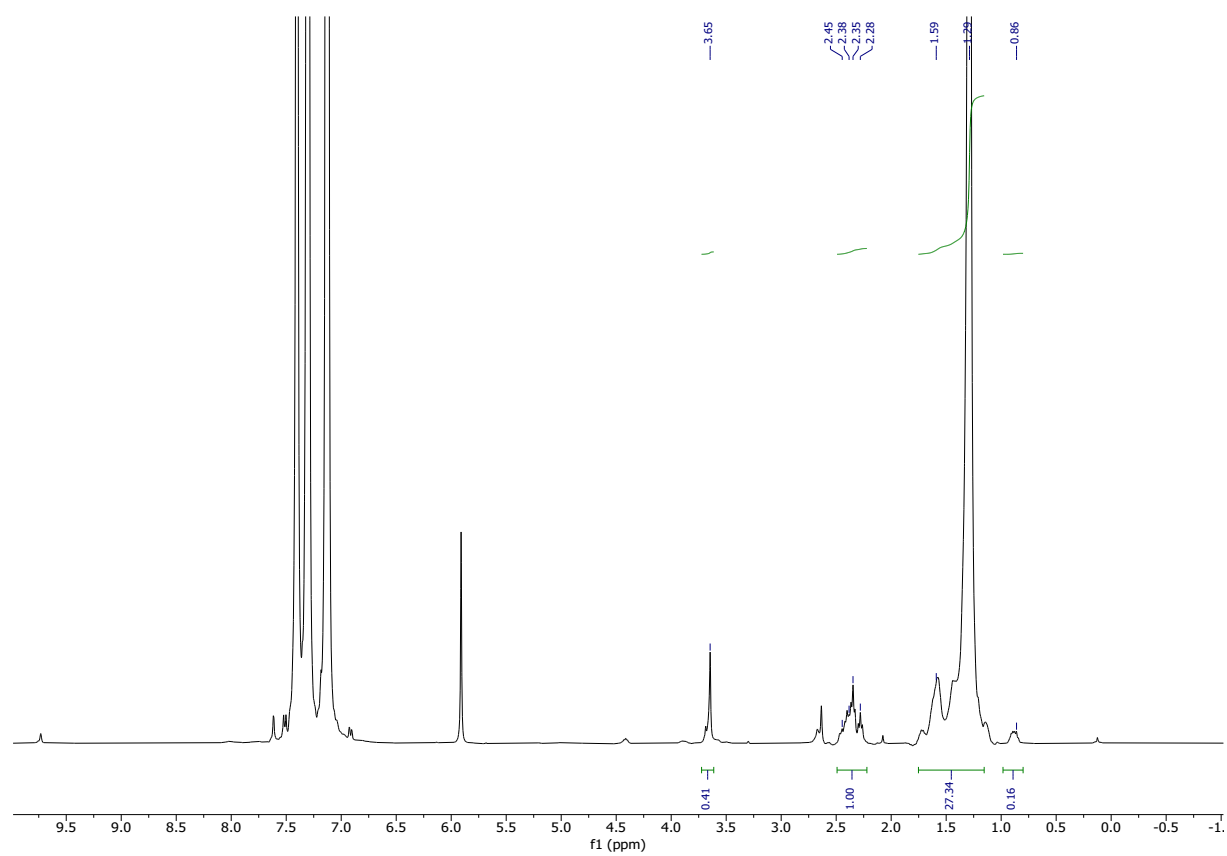
Figure 5.9. ^{1}H NMR (400 MHz, TCE-d_2+TCB) of PEox after esterification.
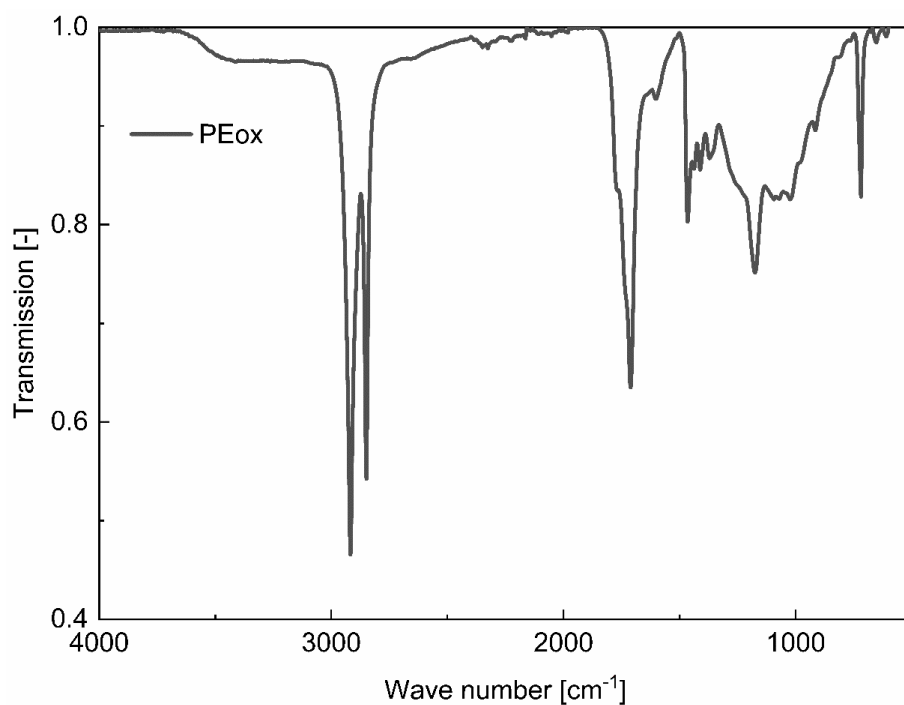
Figure 5.10. IR spectrum of PEox (4 hours photooxidation).
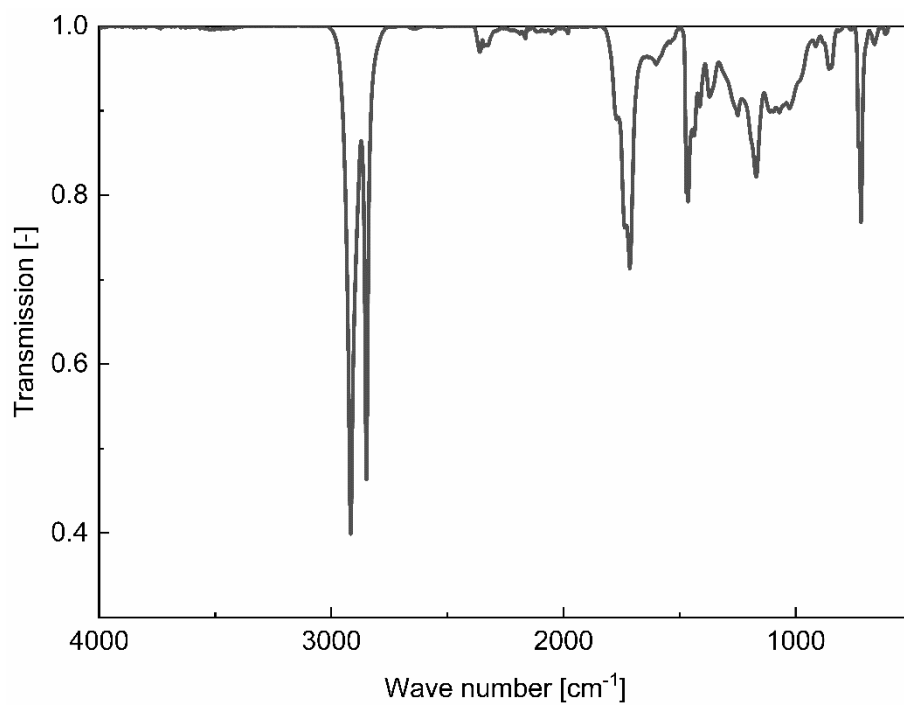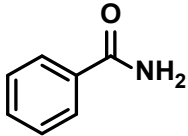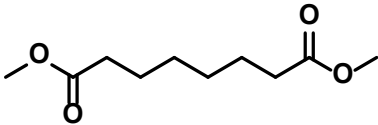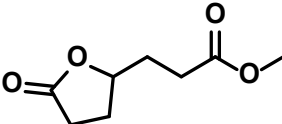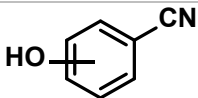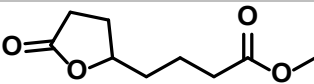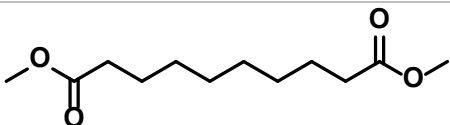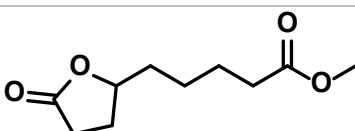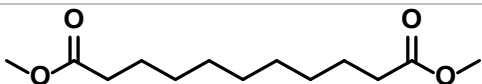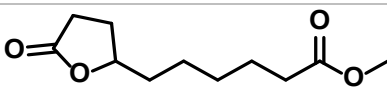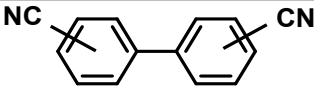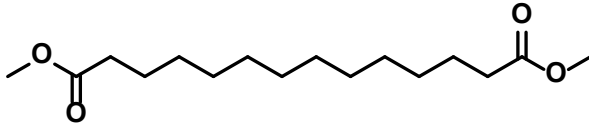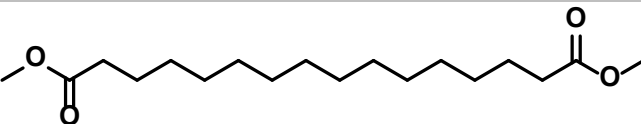
Figure 5.11. IR spectrum of PEox (4 hours photooxidation) after esterification with TMS-diazomethane.

Table 5.3. Selected oxidation products identified by GC-MS.

Name	Structure
Benzamide	
Dimethyl octanedioate	
Methyl 3-(5-oxotetrahydro-furan-2-yl)propanoate	
Hydroxy-benzonitriles	
Methyl 4-(5-oxotetrahydro-furan-2-yl)butanoate	
Dimethyl decanedioate	
Methyl 5-(5-oxotetrahydro-furan-2-yl)pentanoate	
Dimethyl undecanedioate	
Methyl 6-(5-oxotetrahydro-furan-2-yl)hexanoate	
Biphenyl-dicarbonitriles	
Dimethyl tetradecanedioate	
Dimethyl hexadecanedioate	

PE was reacted according to GP2 for 16 hours. Samples were taken after 0.5 h, 1 h, 2 h, 4 h, 8 h and 16 h. Portions of obtained PEox and of the residue after solvent removal (20 mg each) were esterified following GP3. The samples were analyzed by IR spectroscopy, GPC, and GC-MS. Additionally, the acid value was determined.
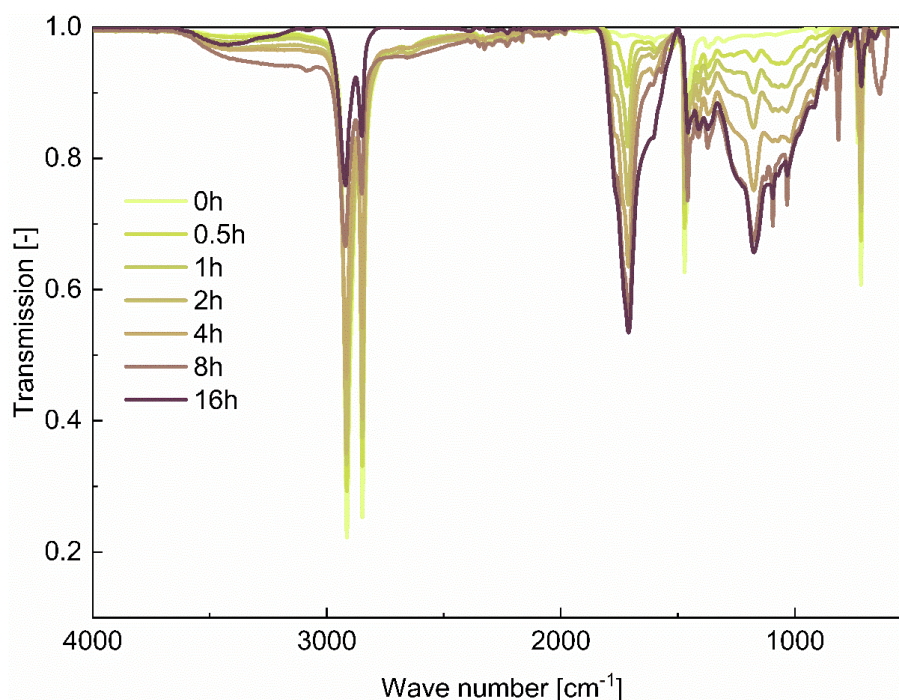
Figure 5.12. Stacked IR spectra of PEox after varying reaction time.
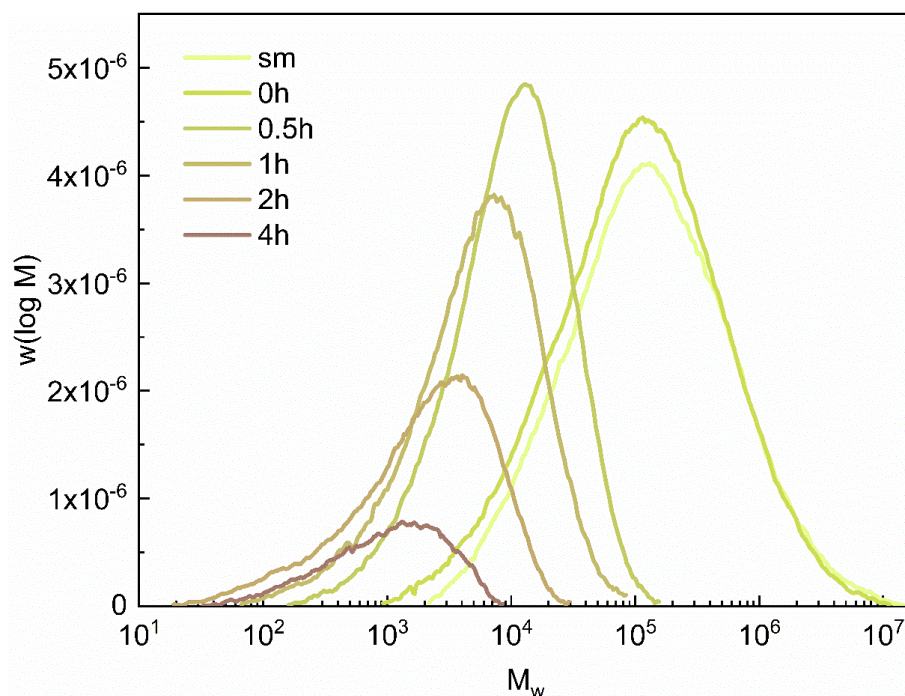
Figure 5.13. Molecular weight distributions of PEox after varying reaction time.

Table 5.4. Acid number and molecular weight of PEox after different reaction times.

Reaction time [h]	Acid number [-]	M_w [g·mol^{-1}]
0	0	290,000
0.5	15	n.d.
1	30	9,200
2	40	3,900
4	48	1,700
8	sample not soluble, analysis not possible	
16	sample not soluble, analysis not possible	

Photooxidation with variation of [Fe] loading

The photooxidation was conducted according to GP2 for four hours with 9 mg (1.5 wt%), 18 mg (3 wt%) and 36 mg (6 wt%) FeCl$_3$ · 6 H$_2$O. PEox was analyzed by IR spectroscopy.
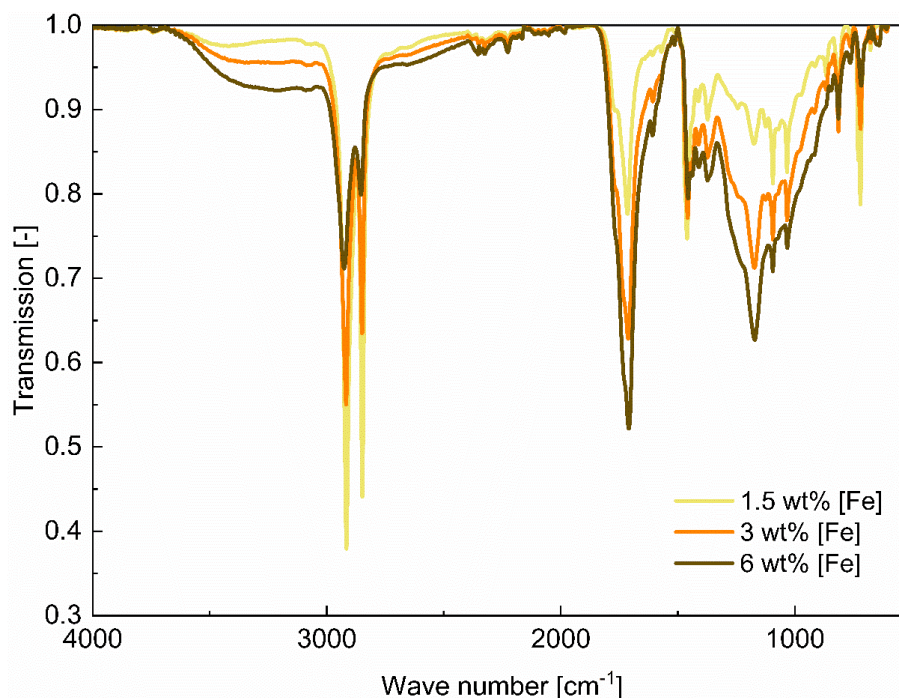
Figure 5.14. Stacked IR spectra of PEox after photooxidation with different FeCl$_3$ · 6 H$_2$O loading.

The photooxidation was conducted according to GP2 for four hours under oxygen atmosphere (connected to O_2-balloon) and under air (connected to open reflux condenser).
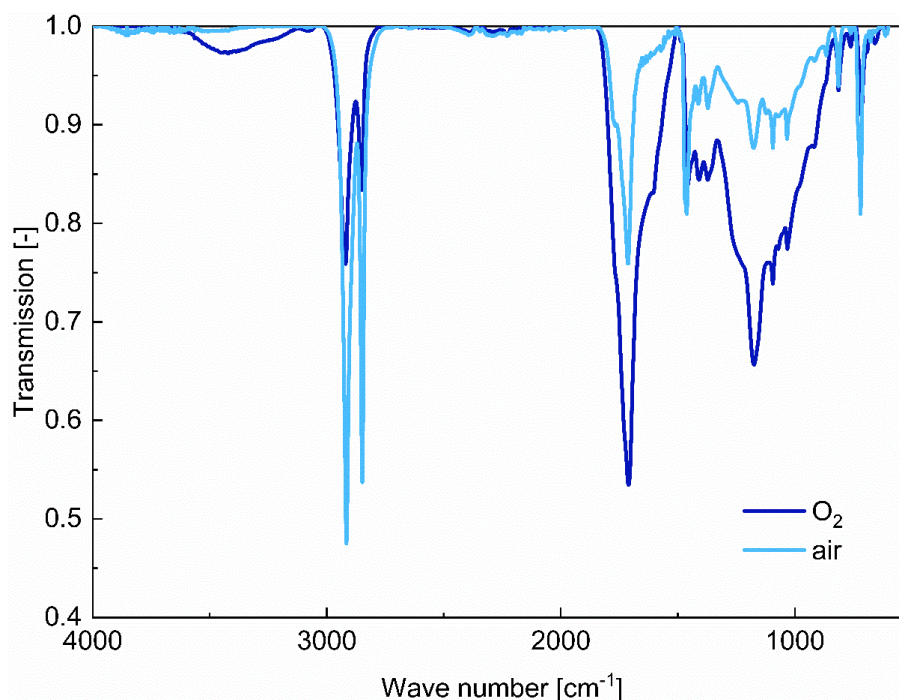
Figure 5.15. Stacked IR spectra of PEox after photooxidation with different oxygen sources.

5.4.4   Baeyer-Villiger Oxidation

Baeyer-Villiger-Oxidation

PEox (100 mg) was dissolved or suspended in dichloromethane (15 mL) and trifluoroacetic anhydride (0.26 mL) and urea hydrogen peroxide adduct (0.19 g) were added at room temperature. Pertrifluoroacetic acid was formed as active reagent *in situ*. After 12 hours, solid Na_2SO_3 (0.2 g) and methanol (10 mL) were added, the mixture was heated to reflux and stirred for 12 hours. After cooling to room temperature, the suspension was filtered, and the solvent was removed under reduced pressure. A viscous residue, the "Baeyer-Villiger product" (BP), was obtained and analyzed by GC-MS, IR and ¹H NMR spectroscopy.
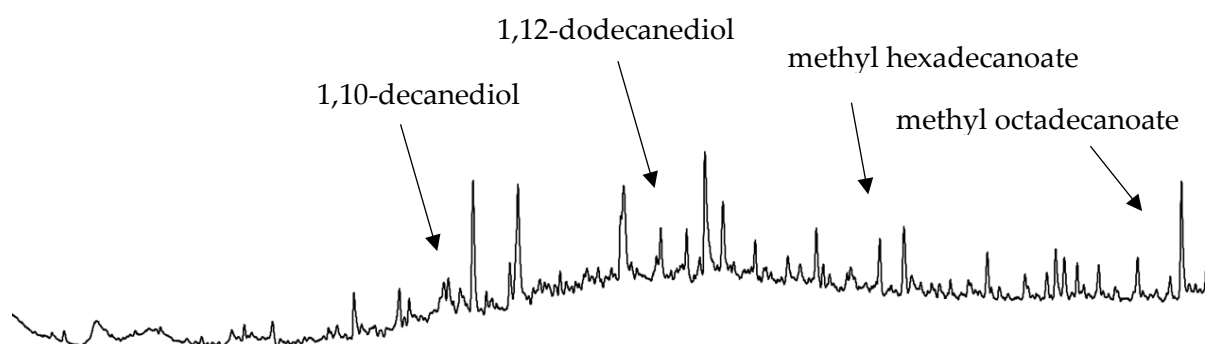
Figure 5.16. Section of GC-FID curve and assignment of selected peaks.
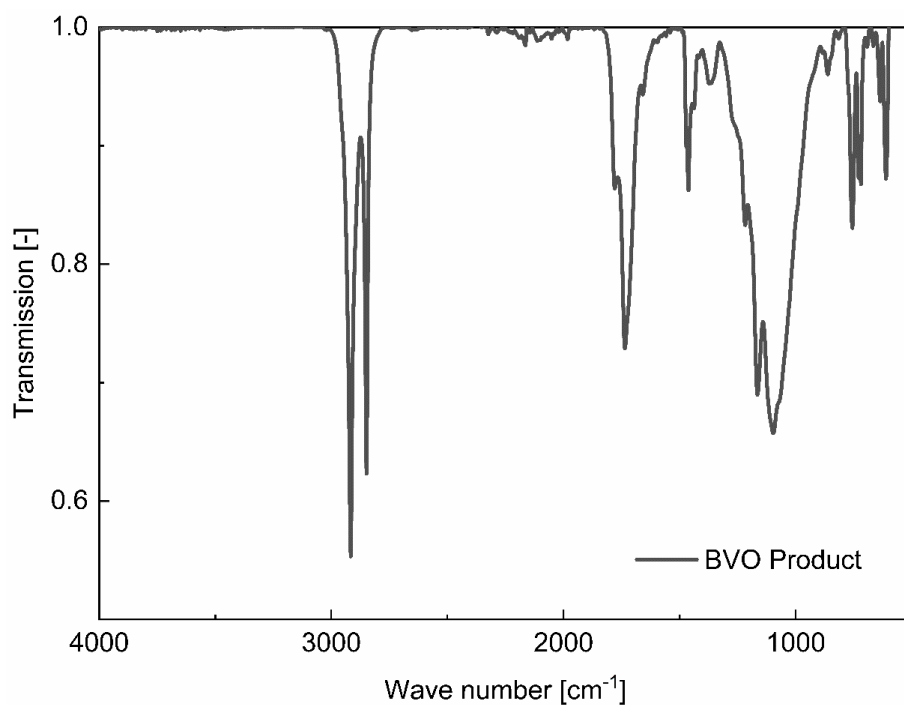
Figure 5.17. IR spectrum of Baeyer-Villiger product.
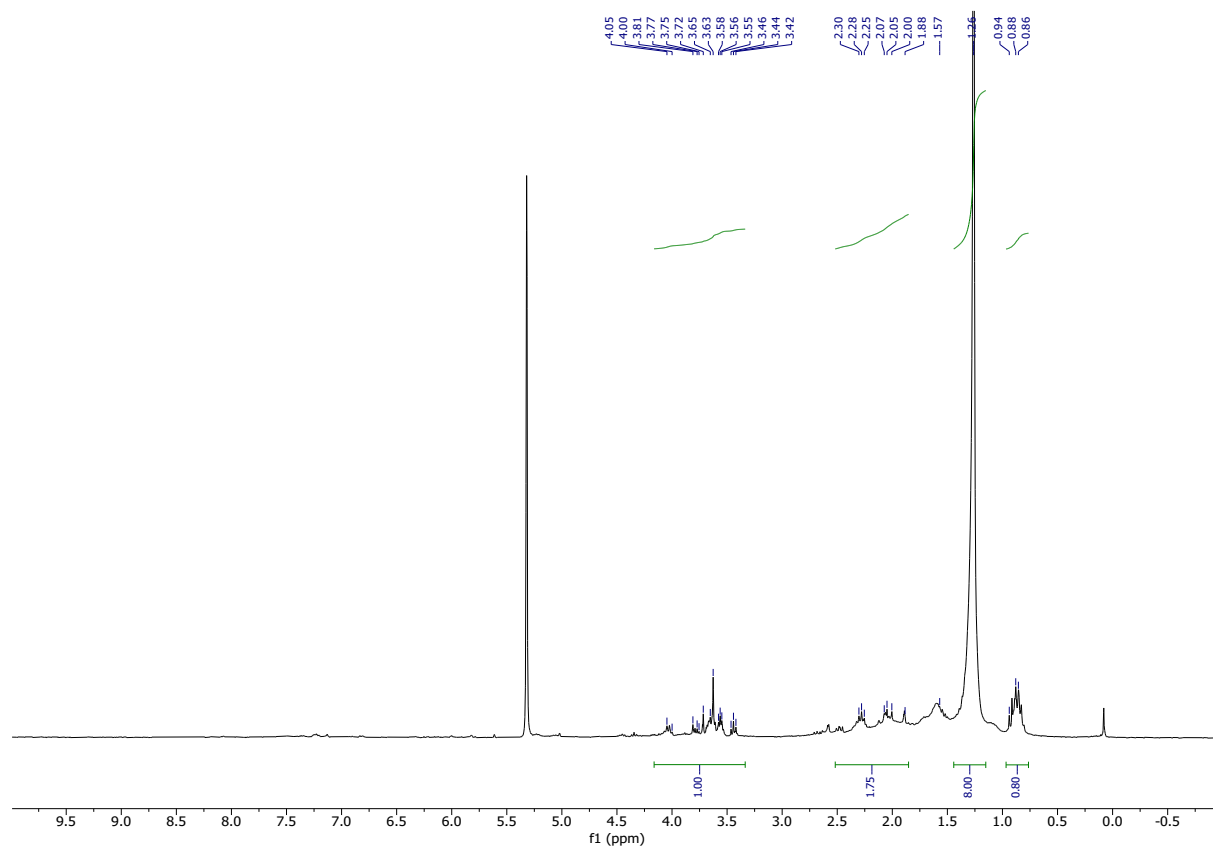
Figure 5.18. ¹H NMR (400 MHz, CD₂Cl₂) of Baeyer-Villiger product.

5.5   References

[1]   PlasticsEurope, *Plastics - the Fast Facts 2023*, **2024**, available in https://plasticseurope.org/knowledge-hub/plastics-the-fast-facts-2023/, last access **01.09.2024**.

[2]   D. Jeremic, *Polyethylene* in: Ullmann's Encyclopedia of Industrial Chemistry, Wiley-VCH Verlag GmbH & Co. KGaA, Weinheim, **2014**.

[3]   D. Zhao, X. Wang, J. B. Miller, G. W. Huber, *ChemSusChem* **2020**, *13*, 1764–1774.

[4]   J. E. Rorrer, G. T. Beckham, Y. Román-Leshkov, *JACS Au* **2021**, *1*, 8–12.

[5]   C. Wang, T. Xie, P. A. Kots, B. C. Vance, K. Yu, P. Kumar, J. Fu, S. Liu, G. Tsilomelekis, E. A. Stach, W. Zheng, D. G. Vlachos, *JACS Au* **2021**, *1*, 1422–1434.

[6]   M. Zeng, Y. H. Lee, G. Strong, A. M. Lapointe, A. L. Kocen, Z. Qu, G. W. Coates, S. L. Scott, M. M. Abu-Omar, *ACS Sustain. Chem. Eng.* **2021**, *9*, 13926–13936.

[7]   L. D. Ellis, S. V. Orski, G. A. Kenlaw, A. G. Norman, K. L. Beers, Y. Román-Leshkov, G. T. Beckham, *ACS Sustain. Chem. Eng.* **2021**, *9*, 623–628.

[8]   N. M. Wang, G. Strong, V. Dasilva, L. Gao, R. Huacuja, I. A. Konstantinov, M. S. Rosen, A. J. Nett, S. Ewart, R. Geyer, S. L. Scott, D. Guironnet, *J. Am. Chem. Soc.* **2022**, *144*, 18526–18531.

[9]   R. J. Conk, S. Hanna, J. X. Shi, J. Yang, N. R. Ciccia, L. Qi, B. J. Bloomer, S. Heuvel, T. Wills, J. Su, A. T. Bell, J. F. Hartwig, *Science* **2022**, *377*, 1561–1566.

[10]   K. Pinsuwan, P. Opaprakasit, A. Petchsuk, L. Dubas, M. Opaprakasit, *Polym. Degrad. Stab.* **2023**, *210*, DOI 10.1016/j.polymdegradstab.2023.110306.

[11]   E. Bäckström, K. Odelius, M. Hakkarainen, *Ind. Eng. Chem. Res.* **2017**, *56*, 14814–14821.

[12]   C. Rabot, Y. Chen, S. Bijlani, Y. M. Chiang, C. E. Oakley, B. R. Oakley, T. J. Williams, C. C. C. Wang, *Angew. Chem. Int. Ed.* **2023**, *62*, DOI 10.1002/anie.202214609.

[13]   K. Wang, R. Jia, P. Cheng, L. Shi, X. Wang, L. Huang, *Angew. Chem. Int. Ed.* **2023**, *62*, DOI 10.1002/anie.202301340.

[14]   Q. Zhang, J. He, X. Wei, C. Shen, P. Ye, W. An, X. Liu, H. Li, S. Xu, Z. Su, Y. Z. Wang, *Angew. Chem. Int. Ed.* **2024**, DOI 10.1002/anie.202407510.

[15]   B. Zhao, H. Tan, J. Yang, X. Zhang, Z. Yu, H. Sun, J. Wei, X. Zhao, Y. Zhang, L. Chen, D. Yang, J. Deng, Y. Fu, Z. Huang, N. Jiao, *Innovation* **2024**, *5*, DOI 10.1016/j.xinn.2024.100586.

[16]   Q. Zhang, X. Wei, C. Shen, P. Ye, W. An, X. Liu, S. Xu, Y. Z. Wang, *ACS Sustain. Chem. Eng.* **2024**, *12*, 5788–5798.

[17]   J. X. Shi, N. R. Ciccia, S. Pal, D. D. Kim, J. N. Brunn, C. Lizandara-Pueyo, M. Ernst, A. M. Haydl, P. B. Messersmith, B. A. Helms, J. F. Hartwig, *J. Am. Chem. Soc.* **2023**, *145*, 21527–21537.

[18]   A. Bunescu, S. Lee, Q. Li, J. F. Hartwig, *ACS Cent. Sci.* **2017**, *3*, 895–903.

[19]   L. Chen, K. G. Malollari, A. Uliana, D. Sanchez, P. B. Messersmith, J. F. Hartwig, *Chem* **2021**, *7*, 137–145.

[20]   O. Iguerb, S. Demoustier-Champagne, J. Marchand-Brynaert, D. Daoust, M. Sclavons, J. Devaux, *J. Appl. Polym. Sci.* **2006**, *100*, 1184–1197.

[21]   D. E. Bergbreiter, N. White, J. Zhou, *J. Polym. Sci. A. Polym. Chem.* **1992**, *30*, 389–396.

[22]   M. Azimi, E. Asselin, *ACS Appl. Mater. Interfaces* **2022**, *14*, 3601–3609.

[23]   L. D. Ellis, N. A. Rorrer, K. P. Sullivan, M. Otto, J. E. McGeehan, Y. Román-Leshkov, N. Wierckx, G. T. Beckham, *Nat. Catal.* **2021**, *4*, 539–556.

[24]   C. Jehanno, J. W. Alty, M. Roosen, S. De Meester, A. P. Dove, E. Y. X. Chen, F. A. Leibfarth, H. Sardon, *Nature* **2022**, *603*, 803–814.

[25] M. Chu, Y. Liu, X. Lou, Q. Zhang, J. Chen, *ACS Catal.* **2022**, *12*, 4659–4679.

[26] D. Feldman, *J. Polym. Environ.* **2002**, *10*, 163–173.

[27] M. D. Tzirakis, I. N. Lykakis, M. Orfanopoulos, *Chem. Soc. Rev.* **2009**, *38*, 2609–2621.

[28] F. Juliá, *ChemCatChem* **2022**, *14*, DOI 10.1002/cctc.202200916.

[29] X. Fan, J. Rong, H. Wu, Q. Zhou, H. Deng, J. Da Tan, C. Xue, L. Wu, H. Tao, J. Wu, *Angew. Chem. Int. Ed.* **2018**, *57*, 8514–8518.

[30] P. E. Krach, A. Dewanji, T. Yuan, M. Rueping, *Chem. Comm.* **2020**, *56*, 6082–6085.

[31] C. Yin, M. Wang, Z. Cai, B. Yuan, P. Hu, *Synthesis* **2022**, *54*, 4864–4882.

[32] G. B. Shulpin, G. V. Nizova, Y. N. Kozlov, *New J. Chem.* **1996**, *20*, 1243–1256.

[33] K. Takaki, J. Yamamoto, Y. Matsushita, H. Morii, T. Shishido, K. Takehira, *Bull. Chem. Soc. Jpn.* **2003**, *76*, 393–398.

[34] W. Wu, X. He, Z. Fu, Y. Liu, Y. Wang, X. Gong, X. Deng, H. Wu, Y. Zou, N. Yu, D. Yin, *J. Catal.* **2012**, *286*, 6–12.

[35] S. Oh, E. E. Stache, *J. Am. Chem. Soc.* **2022**, *144*, 5745–5749.

[36] M. Wang, J. Wen, Y. Huang, P. Hu, *ChemSusChem* **2021**, *14*, 5049–5056.

[37] G. Zhang, Z. Zhang, R. Zeng, *Chin. J. Chem.* **2021**, *39*, 3225–3230.

[38] D. L. Langer, S. Oh, E. E. Stache, *Chem. Sci.* **2023**, *15*, 1840–1845.

[39] Y. Jin, Q. Zhang, L. Wang, X. Wang, C. Meng, C. Duan, *Green Chem.* **2021**, *23*, 6984–6989.

[40] L. Ding, K. Niu, Y. Liu, Q. Wang, *ChemSusChem* **2022**, *15*, DOI 10.1002/cssc.202200367.

[41] J. L. Tu, A. M. Hu, L. Guo, W. Xia, *J. Am. Chem. Soc.* **2023**, *145*, 7600–7611.

[42] K. Takaki, J. Yamamoto, K. Komeyama, T. Kawabata, K. Takehira, *Bull. Chem. Soc. Jpn.* **2004**, *77*, 2251–2255.

[43] T. J. Smak, P. de Peinder, J. C. Van der Waal, R. Altink, I. Vollmer, B. M. Weckhuysen, *ChemSusChem* **2024**, *17*, DOI 10.1002/cssc.202301198.

[44] W. Wang, Y. Wang, Z. Liu, Y. Han, C. Wang, *Prog. Org. Coat.* **2019**, *136*, DOI 10.1016/j.porgcoat.2019.105294.

[45] Y. Zhang, Q. Song, Q. Lv, H. Wang, *Constr. Build. Mater.* **2021**, *302*, DOI 10.1016/j.conbuildmat.2021.124115.

[46] J. Shi, B. Jing, X. Zou, H. Luo, W. Dai, *J. Mater. Sci.* **2009**, *44*, 1251–1257.

[47] J. Zawadiak, B. Orliańska, A. A. Marek, *J. Appl. Polym. Sci.* **2013**, *127*, 976–981.

[48] M. Baur, N. K. Mast, J. P. Brahm, R. Habé, T. O. Morgen, S. Mecking, *Angew. Chem. Int. Ed.* **2023**, *62*, DOI 10.1002/anie.202310990.

[49] H. Yuan, K. Takahashi, S. Hayashi, M. Suzuki, N. Fujikake, K. I. Kasuya, J. Zhou, S. Nakagawa, N. Yoshie, C. Li, K. Yamaguchi, K. Nozaki, *J. Am. Chem. Soc.* **2024**, *146*, 13658–13665.

[50] P. Ma, C. M. Plummer, W. Luo, J. Pang, Y. Chen, L. Li, *Chem. Sci.* **2022**, *13*, 11746–11754.

[51] O. N. Golodkov, G. P. Belov, *Russ. Chem. Bull. Int. Ed.* **2013**, *62*, 2624–2625.

[52] A. Tidjani, Y. Watanabe, *Polym. Degrad. Stab.* **1995**, *49*, 299–304.

[53] J. Lacoste, D. J. Carlsson, S. Falicki, D. M. Wiles, *Polym. Degrad. Stab.* **1991**, *34*, 309–323.

[54] F. Gugumus, *Polym. Degrad. Stab.* **2007**, *92*, 143–157.

[55] B. Pelzl, R. Wolf, B. L. Kaul, *Plastics, Additives* in: Ullmann's Encyclopedia of Industrial Chemistry, Wiley-VCH Verlag GmbH & Co. KGaA, Weinheim, **2018**.

[56] J. L. Hodgson, M. L. Coote, *Macromolecules* **2010**, *43*, 4573–4583.

[57] *"Standard Test Method for Acid Number (Empirical) of Synthetic and Natural Waxes"*, ASTM D1386-15(2022), ASTM International, **2022**.

6. Sustainable Synthesis Route towards Bio-based Cyclic Carbonates

· **three-step one-pot reaction**   · O_2 and CO_2 **as stoichiometric reagents**   · **mild conditions**   · **valuable hydroxy cyclic carbonates**
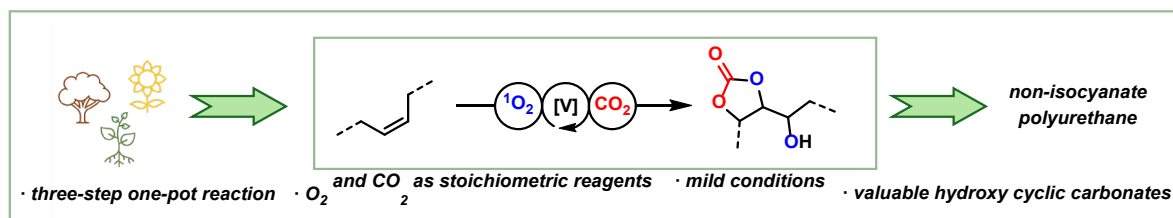
Abstract. The formation of cyclic carbonates from epoxides and CO_2 is a prime example of green chemistry. However, the sustainability aspect of the reaction is thwarted by the unfavorable epoxide formation. Here, a new, sustainable approach for the formation of bio-based cyclic carbonates from fatty acid derivatives, O_2 and CO_2 is presented. High yields and excellent atom-economy are achieved with the three-step one-pot reaction. The use of the obtained cyclic carbonates in the synthesis of non-isocyanate polyurethanes is demonstrated.

6.1   Introduction

Five-membered cyclic carbonates (CC) are valuable structural motifs of increasing importance for laboratory and industrial applications (Scheme 6.1). Ethylene and propylene carbonate, the most important examples, find widespread use as solvents, electrolyte components or chemical precursors. Low molecular weight CC are generally considered non-toxic and biodegradable. Carbonate units are also present in more complex and functionalized molecules and are used e.g. as protecting groups for diols or as synthetic intermediates. Functional groups in direct vicinity to the cyclic carbonate (e.g. hydroxy, amine, or vinyl groups) allow for facile diversification, modification or integration into larger systems. Molecules with multiple cyclic carbonate moieties can be used as monomers, together with diamines, in the formation of polyhydroxyurethanes (PHU), a sub-class of non-isocyanate polyurethanes (NIPU). These polymers, as the name suggests, avoid the use of the highly reactive and toxic diisocyanates in favor of the safer-to-handle carbonates.[1–5]

The synthesis of cyclic carbonates from epoxides and carbon dioxide, a constantly growing research field, is often mentioned as a prime example for the implementation of green chemistry. Indeed, the reaction features a high atom-economy, waste gas (CO_2) as reagent, and can be conducted *neat*; thus, adhering well to the "twelve principles of green chemistry".[6,7] A wide range of different catalyst types (e.g. metal complexes, organocatalysts, ionic liquids) has been reported.[8–10] The most common activation motif is the combination of a lewis-acid to activate the epoxide and a nucleophilic co-catalyst. Highly efficient catalytic systems continue to be developed, further optimizing the process.

However, the epoxides used as starting materials are often highly reactive, toxic and require problematic synthesis routes themselves (Scheme 6.1). Alkenes commonly undergo epoxidation by oxygen-transfer from peroxyacids (e.g. *meta*-chloroperoxybenzoic acid) or via metal-catalyzed reactions with alkyl hydroperoxides, such as cumyl hydroperoxide or *tert*-butyl hydroperoxide. These processes require handling of problematic reagents, additional isolation and purification steps and generate stoichiometric amounts of undesired by-products. Alternatively, epoxides can be formed from the intramolecular substitution of 1,2-functionalized alcohols (diols, halohydrins) under often harsh, basic conditions. These, in terms of green chemistry, unfavorable access routes to epoxides thwart the advertised sustainability of the cyclic carbonate formation by CO_2 insertion to a certain extent.[11–13]

Alternative synthesis routes towards epoxides utilizing milder reaction conditions and reagents would benefit the overall impact of CC formation. One approach is the photooxygenation of alkenes followed by a peroxide rearrangement giving access to epoxy alcohols: Oxygen can be excited to its singlet state ($^1O_2$) by photosensitization using inexpensive organic dyes and LEDs (cf. chapter 4).[14] The reactive singlet oxygen can then undergo a Schenck-ene reaction with an alkene and form allylic hydroperoxides.[15] This reaction mode is well-established and can be performed quantitatively in short reaction times in flow reactors. Our group reported the completely solvent-free photooxygenation of several readily available alkenes.[16] The obtained allylic hydroperoxide can undergo self-epoxidation reactions into epoxy alcohols in presence of inexpensive and non-toxic titanium or vanadium catalysts.[17] Both reactions have been successfully combined into one-pot processes.[16,18–20] This

transformation of alkenes into epoxy alcohols using only oxygen, light and a first-row transition metal catalyst is exceptionally mild and presents an attractive alternative towards common epoxidation strategies. Epoxy alcohols are well established substrates for the CO_2 insertion and yield hydroxy functionalized cyclic carbonates. The most prominent example is the transformation of glycidol into 1,2-glycerol carbonate. The role of the neighboring free hydroxy group in the insertion mechanism and possible isomerization reactions of the resulting cyclic carbonates have been investigated (*vide infra*).[21–23] To our best knowledge, there are no reports on the use of epoxy alcohols obtained from photooxygenation approaches in the CO_2 insertion reaction.

In this work, we report a highly atom-economical three-step approach for the transformation of unsaturated bio-based molecules into hydroxy cyclic carbonates in a one-pot fashion. Furthermore, their illustrative use in the synthesis of non-isocyanate polyurethanes (Scheme 6.1) is described. The process utilizes only inexpensive and abundant biomolecules, oxygen and carbon dioxide as stoichiometric reagents and operates under mild conditions.
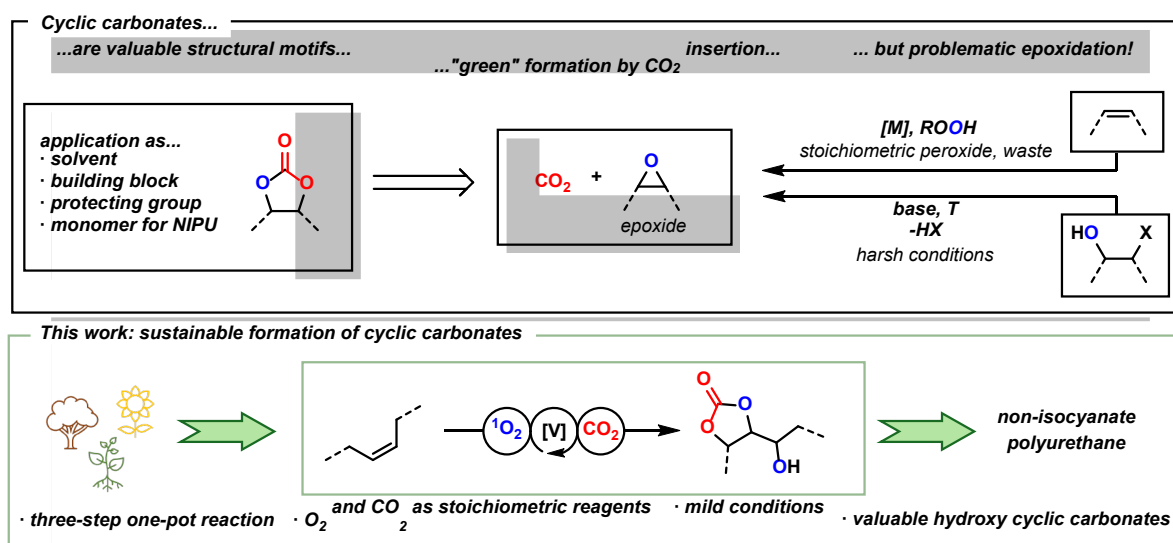
Scheme 6.1. Application and synthesis of cyclic carbonates (top), this work (bottom).

6.2   Results and Discussion

The proposed three-step one-pot reaction sequence for the synthesis of cyclic carbonates from bio-based alkenes consists of photooxygenation, epoxidation and CO_2 insertion (Scheme 6.2, bottom). The reactions are first investigated separately and then combined into a unified process that avoids the isolation of reactive and potentially hazardous intermediates.

Unsaturated molecules are ubiquitous in nature (Scheme 6.2); prominent examples are unsaturated fatty acids such as oleic acid. They are accessible in large quantities from vegetable oils; however, their chemical use is in competition with food production. Therefore, secondary sources such as waste cooking oil are of special interest.[24,25] Further non-edible substrates are e.g. ricinoleic acid, or phenolic lipids such as cardanol (from the waste product cashew nut liquid). Other unsaturated product classes include terpenes (limonene, pinene, …) and terpenoids (citronellol, geraniol, …).

Bio-based cyclic carbonates have been previously synthesized e.g. from triglycerides, castor oil, and limonene and their use as monomer in NIPUs was shown. However, the required epoxide intermediates are usually formed by the reaction of double bonds with peroxo species (*vide supra*), thus reducing the sustainability of the monomer.[26–29]

This work focusses on fatty acid derivatives as precursors for hydroxy functionalized cyclic carbonates. Initial experiments are conducted with symmetrical (Z)-4-octene as model substrate due to simplified analysis.
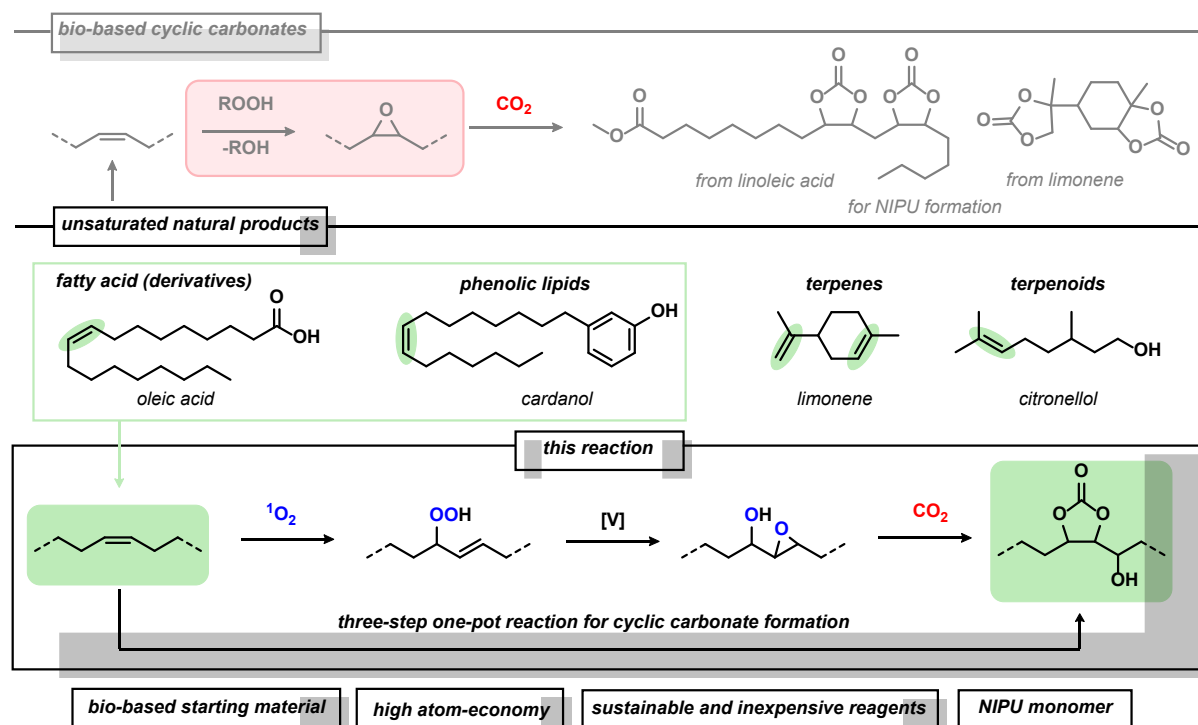
Scheme 6.2. Selected bio-based cyclic carbonates for NIPU formation (top), unsaturated natural products (middle), outline of the reported reaction sequence (bottom).

First, the photooxygenation (Schenck-ene reaction) to transform alkenes into allylic hydroperoxides was investigated (Scheme 6.3). Our group previously reported both solvent-based and solvent-free photooxidation procedures in a home-built flow reactor. [30,31] For this work, both reaction types are evaluated with the option to choose between them. The solvent-free oxygenation has advantages in terms of sustainability, waste prevention and space-time-yield. However, it is limited to liquid substrates and products, and the high concentration of peroxides can give security concerns. On the other hand, the use of solvent decreases the environmental sustainability of the reaction and its productivity, but the dilution of the hydroperoxide increases the safety. Solid substrates have to be reacted in solution in any case.

Tetraphenylporphyrins are popular photosensitizers. It has been shown that alkyl substituents in the para-position of the phenyl substituents increase the solubility in highly non-polar media significantly.[16] Therefore, tetra(4-isopropylphenyl)porphyrin was chosen as sensitizer for the solvent-free reaction. The stable, violet solid is easily accessible by Rothemund reaction of pyrrole and cuminaldehyde. The sensitizer was directly dissolved in the liquid substrate (1.5 mM). Alternatively in the solvent based process, the starting material (0.1 M) and

methylene blue (1 mM) were dissolved in an appropriate solvent (preferentially acetonitrile, very non-polar substrates in dichloromethane).

The photooxygenation was then carried out in the home-built flow reactor:[30] the reaction mixture (with or without solvent) was pumped through FEP capillary tubing (1/16" OD, 1/32" ID; irradiated tubing length 12.8 m) which is coiled around a glass cylinder (OD 65 mm) at flow rates between 0.20–0.50 mL/min by an HPLC pump (resulting residence times of 8–20 minutes). O₂ gas was supplied with a Brooks Instruments mass-flow control, the total system pressure was adjusted to 45 bar by an *IDEX* back-pressure cartridge. The O₂ flow rate was tuned so that a laminar slug flow resulted, and oxygen was not completely consumed when the solution left at the end of the reactor tubing. Temperature control (20 °C) was applied from the outside of the reactor coil by a temperature-controlled oil bath. The reactor coil was irradiated from the inside by 24 water-cooled white LEDs (λ_{max} = 630 nm).

The product was collected at the reactor outlet and analyzed. Full conversion of octene to the corresponding hydroperoxide was achieved after eight minutes for the reaction in solution and after 20 minutes for the solvent-free reaction (Scheme 6.3). No by-product formation was observed. The isolated peroxides are stable at room temperature for several days and can be stored at −30 °C indefinitely. Non-symmetrical long-chain substrates, such as methyl oleate, yield two equimolar regioisomers because there is no preferential hydrogen abstraction site (Scheme 6.3, bottom).[15] For the fatty acid derivatives, the isomers are not distinguishable in ¹H NMR and the products are not separable. However, two sets of signals are observed in the ¹³C NMR spectrum.
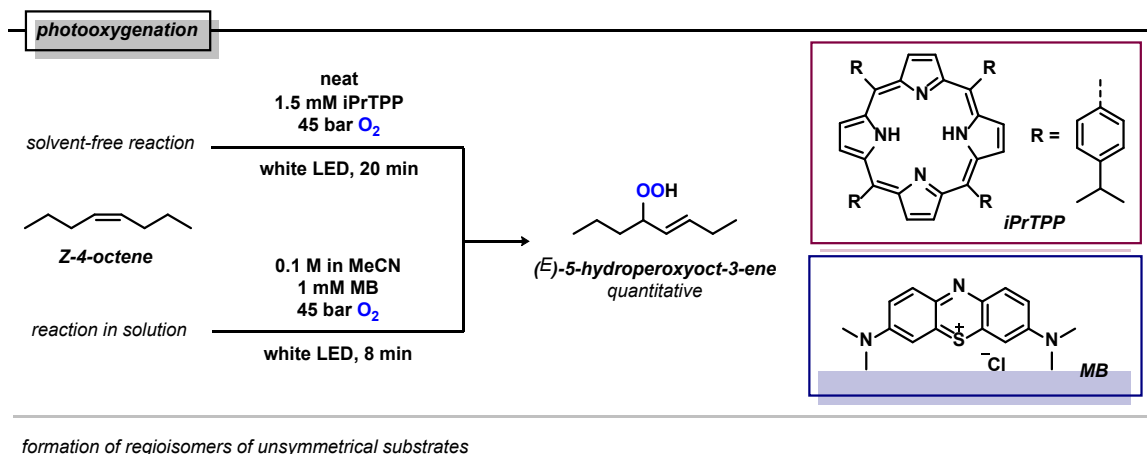
Scheme 6.3. Photooxygenation of (*Z*)-4-octene with and without solvent (top), formation of regioisomeric allyl hydroperoxides in the photooxygenation of methyl oleate (bottom).

The choice for the use or omission of solvent should be based on sustainability, productivity, and safety thoughts. The space-time yield (STY) is an important factor to describe the reaction and reactor efficiency, it is defined as mass of the formed product m_P per reactor volume V and residence time τ (equation 1).[32]

$$STY = \frac{m_P}{V \cdot \tau} \qquad \qquad \text{Eq. 1}$$

The active oxygen content (AO) describes the share of peroxidic oxygen (via number of peroxo groups n) of the molecular weight M; it is a useful number to estimate the sensitivity of a compound (equation 2).

$$AO = \frac{n \cdot 16 \text{ g·mol}^{-1}}{M} \qquad \qquad \text{Eq. 2}$$

The space-time yield was calculated for the photooxygenation of octene and methyl oleate with and without solvent, and the active oxygen content of the products was determined (Table 6.1).

Table 6.1. Active oxygen content, and space-time yields of 4-octene and methyl oleate.

Substrate	Peroxide AO	STY solvent-free [g·L^{-1}·h^{-1}]	STY 0.1 M solution [g·L^{-1}·h^{-1}]
4-octene	11.1 %	1550	60
Methyl oleate	4.9 %	1600	140

The space-time yield of the solvent-free reaction is more than ten times higher than the STY of the reaction in solution. The better values of methyl oleate compared to 4-octene can be explained by the larger molecular weight of the former. The active oxygen content of the octene hydroperoxide is 11.1 %, compared to only 4.9 % for methyl oleate. Lower values are generally considered safer (for comparable structures). Values below 5 % indicate, with reservations, rather unproblematic substance, while special care should be taken if the AO exceeds 10 %. In conclusion, for sustainability and productivity reasons, the solvent-free approach is highly advantageous. Fatty acid derived hydroperoxides are also expected to be rather safely manageable in *neat* conditions. Reactions in solution on the other hand, are required for solid substrates and those with a very low molecular weight to avoid high concentrations of hydroperoxides with high AO.[33,34]

Next, the self-epoxidation of the allylic peroxides into epoxy alcohols was investigated (Scheme 6.4). There are only limited literature reports on this reactivity, although the catalytic activity of titanium and vanadium complexes has been known for several decades.[17,35] Both metals are abundant, inexpensive and their complexes generally exhibit no to low toxicity, rendering them valuable reagents for a sustainable synthesis approach. Readily available VO(acac)₂ was chosen as catalyst due to good performance in previous works.[31] Again, a solvent-free process and a reaction in solution were investigated. The catalyst (1 mol%) was added to a cooled (0 °C) reaction mixture: either pure allylic hydroperoxide, or a solution (0.1 M) in acetonitrile. Full conversion was observed after 0.5 and 2 hours, respectively. The obtained epoxy alcohols consisted of different diastereomers (*syn* and *anti*-arrangement) in a ratio of 1:1, determined by ^{1}H NMR spectroscopy. Furthermore, the product contained two sets of regioisomers when the isomeric starting material was used. Possible side-products (e.g.

reduction to allylic alcohol or dehydration to the enone) were not detected. The solvent-free self-epoxidation of octene hydroperoxide occurred highly exothermic and led to the boiling of the reaction mixture. In comparison, this was not observed for methyl oleate. Therefore, the solvent-free approach is only recommended for small-scale reactions and/or the use of substrates with low active oxygen content. No reaction was observed if $VOSO_4 \cdot H_2O$ was used as the catalyst, most likely due to the very low solubility in non-polar media. The reaction mechanism of the vanadium-catalyzed peroxide rearrangement is not fully elucidated. It is assumed that the reaction occurs – analogous to the epoxidation of allylic alcohols with *tert*-butyl hydroperoxide – via the formation of a peroxovanadium complex, followed by the transfer of one oxygen atom to a double bond.[36,37] No additional mechanistical experiments have been conducted.
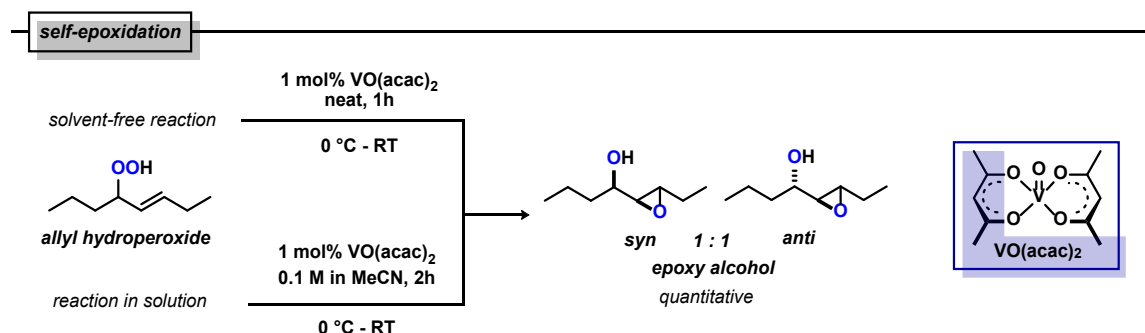
Scheme 6.4. Rearrangement of allylic hydroperoxides to epoxy alcohols.

Dual catalysts that are capable of both photooxygenation and epoxide rearrangement would allow the facile combination of the two steps. Metalloporphyrins are a potential catalyst class for this application, the organic porphyrin moiety is a known photosensitizer itself, and also complexes such as chlorophyll are capable of $^1O_2$ formation. The combination with a metal center (Ti, V) that can catalyze the rearrangement could create a dual catalyst. Therefore, TiO(iPrTPP) and VO(iPrTPP) were synthesized, both are purple to pink crystalline compounds that are readily soluble in nonpolar substrates or solvents. Both compounds were tested in a model reaction with (Z)-4-octene in the flow reactor (0.1 M in CH_2Cl_2, 1 mM sensitizer, 40 bar O_2, white LED, 8–20 minutes) (Scheme 6.5). No reaction was observed for TiO(iPrTPP). The excited state of the sensitizer might undergo fast non-productive deactivation pathways that inhibit the singlet oxygen generation. However, the exact reason is unclear. For VO(iPrTPP), the formation of 26 % epoxy alcohol and no residual hydroperoxide were detected after eight minutes (74 % unreacted starting material). Longer reaction times did not lead to improved conversion or yield. Also, the conduction under solvent-free conditions did not give better results. The photooxygenation step seems to stop after a certain amount of time, maybe a change of coordination or oxidation state in the vanadium center – caused by the rearrangement catalysis – leads to the loss of photosensitization properties. No further optimization attempts on the system were made. The previously described two-step process with the easily accessible catalysts methylene blue/iPrTPP and VO(acac)₂ is also satisfying.
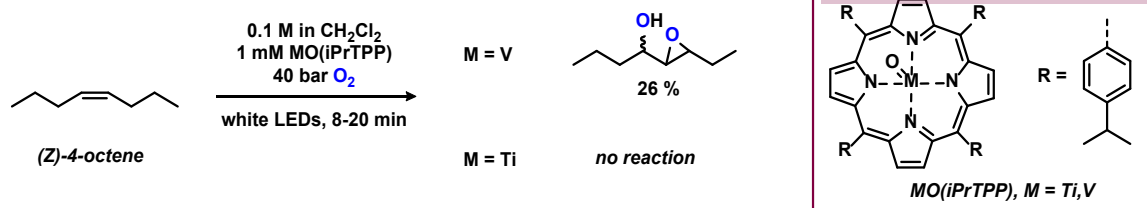
Scheme 6.5. Test of potential dual catalysts for photooxygenation and rearrangement.

The final step is the CO_2 insertion reaction into the epoxy alcohols to obtain the desired cyclic carbonates. Most commonly, combinations of lewis-acids and nucleophiles are used (Scheme 6.6). The epoxide is coordinated by the lewis-acid (e.g. a metal center) and thus activated for nucleophilic attack and ring-opening by the additive (e.g. bromide-ion). After coordination of CO_2 to the metal center, it is attacked by the alkoxide and forms a carbonate. The five-membered cycle is formed by an internal substitution reaction with the intermediate mono alkyl carbonate and expulsion of the nucleophile.[38] An alternative mechanism exists for epoxides with neighboring hydroxy groups. The alcohol can perform a base-assisted nucleophilic attack on carbon dioxide forming a carbonate. This moiety can then open the epoxide in an intramolecular substitution. Protonation of the formed alkoxide yields the cyclic carbonate. The reaction can be further promoted by a lewis-acid that coordinates and activates CO_2. In contrast to the "classical" mechanism, the cyclic carbonate is not in the same position as the former epoxide but is shifted to include the former hydroxy group. Both reaction mechanisms can occur in parallel leading to a mixture of regioisomers.[21,22] Additionally, internal attack of the hydroxy group on the carbonate moiety can lead to isomerization of the products.
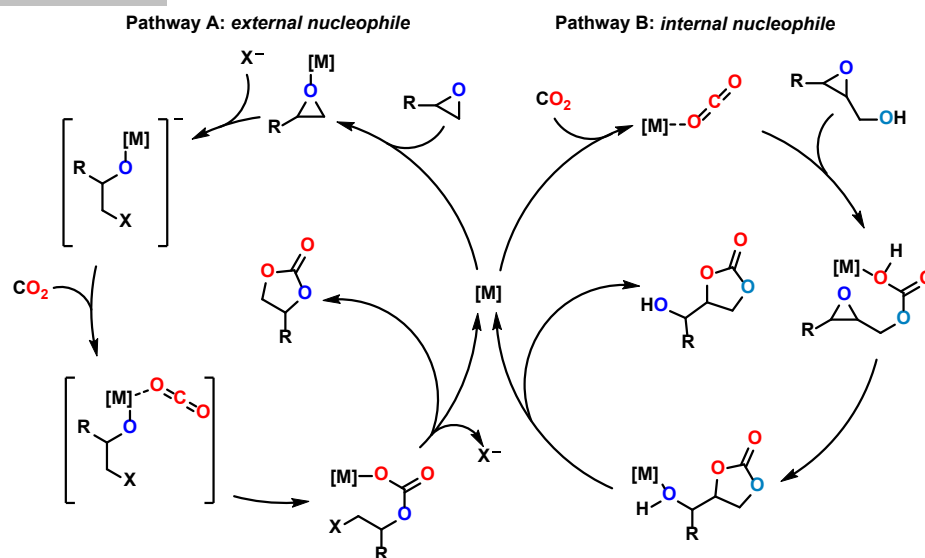
Scheme 6.6. Two possible reaction mechanisms for the CO_2 insertion reaction into epoxides.

The optimization for the CO_2 insertion was conducted with (*Z*)-4-octene derived epoxy alcohol in an autoclave (table 6.2). VO(acac)$_2$ was primarily tested as lewis-acid, already having the

one-pot approach in mind. Varying amounts of catalyst, CO_2 pressures and addition of nucleophiles and bases were screened. First experiments at high pressure (40 bar) with 2 mol% VO(acac)$_2$ and 5 mol% pyridine gave excellent ^{1}H NMR yield of cyclic carbonate (entry 1). The use of other bases such as triethylamine decreased the yield (entry 2). In following experiments, the pressure was decreased to 4 bar to increase the safety and reduce CO_2 input. High yield was obtained with 10 mol% pyridine under these conditions (entry 3). Halving of the catalyst amount (1 mol% [V], 5 mol% pyridine) led to a significant decrease of product formation (entry 4). The yield dropped further without VO(acac)$_2$ (entry 5). In absence of base only trace amounts of product were detected (entry 6), proving the importance of both the vanadium catalyst and pyridine. The substitution of base with tetraoctylammonium bromide gave inferior yields of cyclic carbonate (entry 7).

The optimized reaction conditions were *neat* epoxy alcohol with 2 mol% VO(acac)$_2$ and 10 mol% pyridine under 4 bar CO_2 at 90 °C for 24 hours.

Table 6.2. Insertion of CO_2 into epoxy alcohols and selected optimization experiments.

Entry	Deviation from optimized conditions[a]	Yield [%][b]
1	**5 mol% pyridine, 40 bar CO₂**	**93**
2	5 mol% Et₃N instead of pyridine, 40 bar CO₂	54
3	**-**	**91**
4	1 mol% VO(acac)₂, 5 mol% pyridine	35
5	no metal, 5 mol% pyridine	19
6	no base	traces
7	no base, 2.5 mol% tetraoctylammonium bromide	63

a) optimized conditions: 4 bar CO_2, 2 mol% VO(acac)$_2$, 10 mol% pyridine, *neat*, 90 °C; b) combined yield of both regioisomers determined by ^{1}H NMR spectroscopy with mesitylene as internal standard.

After successful optimization of the individual reaction steps, one-pot approaches without separation of the intermediates were developed (Scheme 6.7). For solvent-free reactions, the sensitizer iPrTPP was dissolved in the substrate (1 mM) and reacted in the flow reactor (20 minutes residence time, white LED, 45 bar O$_2$). The product was collected, cooled to 0 °C and 1 mol% of VO(acac)$_2$ was added. After one hour, 10 mol% of pyridine was added and the reaction vial was transferred into an autoclave, the device was filled with 4 bar CO_2 and stirred for 16 hours at 90 °C. The reaction in solution were conducted in a similar manner. The substrate (0.1 M) and methylene blue (1 mM) were dissolved in dichloromethane or

acetonitrile and then reacted in the flow reactor (8 minutes residence time, white LED, 45 bar O_2). The obtained reaction mixture was cooled to 0°C and 1 mol% of VO(acac)$_2$ was added. After two hours, the solvent was evaporated, and 10 mol% of pyridine was added to the *neat* substance. The CO_2 insertion was then carried out analogously to the solvent free procedure.
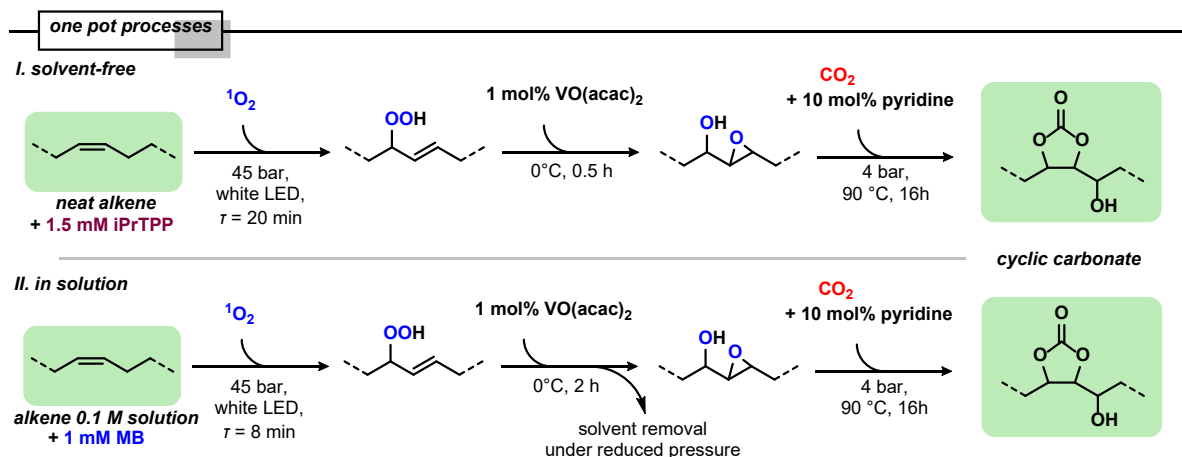
Scheme 6.7. One-pot processes: solvent-free method (top), and reaction in solution (bottom).

All three reaction steps – photooxygenation, peroxide rearrangement and CO_2 insertion – can yield regio- or stereoisomers, especially for rather low functionalized substrates. Therefore, the use of this approach for the synthesis of complex defined molecules is limited. On the other hand, for technical purposes, e.g. as monomer in polymer formation, surfactants, etc., the exact composition is often less important. Those are therefore highly interesting possible application areas.

The scope of the reaction was investigated with focus on inexpensive and readily available fatty acid derivatives (Scheme 6.8). Most natural lipids contain double bonds in *Z*-configuration; *E*-configured fatty acids ("*trans*-fat") can be formed by isomerization during heating or as a side reaction during technical hydrogenation. The reaction of (*E*)- and (*Z*)-4-octene yielded the same products, being an example for a convergent synthesis strategy. The merging occurs already during the photooxygenation step as the same hydroperoxide is formed for both starting materials (*vide supra*). Different derivatives of oleic acids were reacted to test the functional group tolerance of the reaction. Esters, free alcohols, and aromatic moieties (from cardanol) were tolerated in every reaction step and gave high isolated yields. Oleyl acrylate was successfully used in the sequence. Due to the ability to polymerize spontaneously, a radical stabilizer was added after the photooxidation. The cyclic carbonate product could find application as a crosslinking agent for hybrid polymer formulation because it is able to partake in both NIPU formation and radical polymerization. Oleic acid was transformed successfully to the epoxy alcohol. The CO_2 insertion, however, gave only an unidentifiable product mixture.

Scheme 6.8. Reaction scope of the three-step one-pot reaction. Isolated yields after three reaction steps given. a) yield of epoxy alcohol is given.

Molecules with multiple cyclic carbonate functionalities (*f*) were formed from trimethylene glycol dioleate (*f* = 2) and glyceryl trioleate (*f* = 3). These are potential monomers for the

formation of NIPUs. The combination of difunctional carbonates (f = 2) and diamines would give linear polymers, while polyfunctional monomers (f > 2) would lead to the formation of cross-linked polyurethane networks. Urethane bonds with two hydroxy groups in their vicinity are formed by the reaction of an amine with the hydroxy CC.[39,40]

The cyclic carbonate product of glyceryl trioleate (TO-CC) was chosen for exemplary NIPU formation (Scheme 6.9). The commercial starting material triolein contained saturated stearic acid impurities; therefore, the average number of double bonds and later cyclic carbonate moieties (f = 2.7, determined by ^{1}H NMR spectroscopy) in the molecule was below the theoretical amount. TO-CC, hexamethylene diamine (functional group ratio 1.1/1, slight excess of cyclic carbonate) and DABCO as catalyst were dissolved in dichloromethane at room temperature, the solution was then poured into an aluminium dish. After solvent evaporation, the polymer was cured at 90 °C for 48 hours. A clear, slightly orange polymeric film was obtained. FTIR analysis proved the formation urethane bonds (bands at 1714, 1530 cm^{-1}). Also, residual cyclic carbonate functions (band at 1793 cm^{-1}) were observed due to being the excess component. Thermogravimetic analysis (TGA) showed stability of the film up to at least 200 °C (less than 5 % weight loss). This aligns with reported decomposition temperatures of NIPUs in the range of 200–250 °C.[29] The glass-transition temperature of T_g = -4 °C was determined by Dynamic Scanning Calorimetry (DSC). Similar T_g values were obtained for fatty-acid based NIPUs by Boyer et al.[40] Due to the cross-linked structure no melting point was observed.

The analysis proves successful polymer formation. Further tests (dynamic mechanical analysis, rheometry, etc.) should be conducted to identify possible application areas. Based on these results, different bio-based NIPUs could be synthesized by variation of the cyclic carbonate or diamine component.
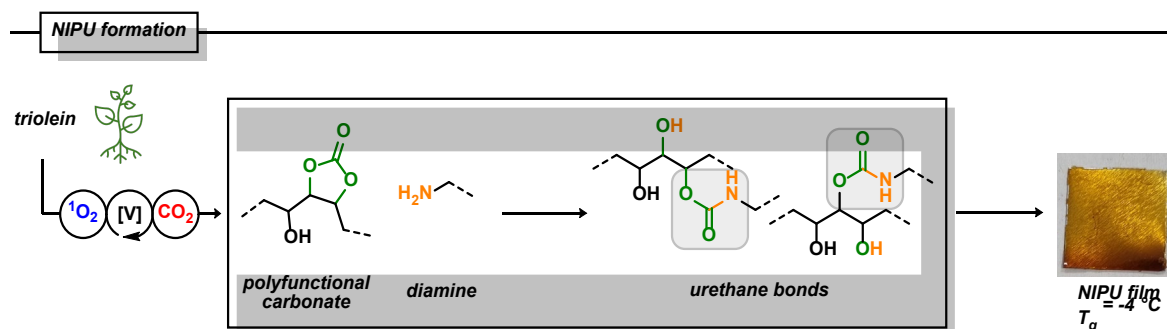
Scheme 6.9. Formation of bio-based cyclic carbonate and use in NIPU formation.

6.3   Conclusion

A three-step one-pot procedure for the transformation of unsaturated fatty acid derivatives into cyclic carbonates was successfully developed. The sequence of photooxygenation, self-epoxidation and CO_2 insertion can be performed under mild reaction conditions. O_2 and CO_2 are the only stoichiometric reagents, in combination with low amounts of inexpensive and mostly low-toxic catalysts and additives (methylene blue, iPrTPP, VO(acac)$_2$ and pyridine). Several cyclic carbonates were obtained in high yields and with excellent atom-economy. The procedure tolerated e.g. esters, free alcohols, aromatics and acryl moieties. Finally, the exemplary use of the hydroxy cyclic carbonate in the synthesis of NIPUs was shown.

6.4 Experimental Section

6.4.1 Materials and Methods

Commercial chemicals (>95 % purity) were used as obtained without further purification; triolein (65 %), oleyl alcohol (80 %) and oleic acid (90 %) were of lower purity. Technical NC-700 CNSL resin was obtained from *Cardolite* as a free sample. TLC was performed using commercial silica gel coated aluminum plates (DC Kieselgel 60 F254, *Merck*); visualization was done using UV light. Staining was realized with a solution of phosphomolybdic acid in ethanol. Product yields were determined from isolated materials after flash chromatography on silica gel (*Acros Organics*, mesh 35–70). NMR spectral data was collected on a *Bruker* FourierHD 300 (300 or 400 MHz for ^{1}H; 75 or 151 MHz for ^{13}C) at 25 °C. The quantification of ^{1}H cores was obtained by integration of resonance signals. Abbreviations used in 1H NMR spectra: s – singlet, d – doublet, t – triplet, m – multiplet. Low-resolution mass spectroscopy was conducted on an *Agilent* 6890N GC-system coupled to a 5975 MSD unit and H_2 as carrier gas. UV/Vis spectra were measured on the Cary5000 spectrometer by *Agilent*. High resolution mass spectrometry (HRMS) was carried out by the Central Analytics at the department of chemistry, University of Hamburg. IR spectra were obtained on ALPHA Platinum ATR-IR and VERTEX 70 FTIR spectrometer by *Bruker*. TGA was performed on *Netzsch* TG 209 F1 Libra with following temperature program: 25–150 °C with a heating rate of 20 K/min, 150–200 °C with 5 K/min, 200 °C 5 min hold at 200 °C. Dynamic scanning calorimetry was conducted on *Mettler Toledo* DSC 1, the sample was heated to 150 °C, cooled to -70 °C and again heated to 150 °C with a heating/cooling rate of 10 K/min. Data evaluation was performed with STARe software V16.10.
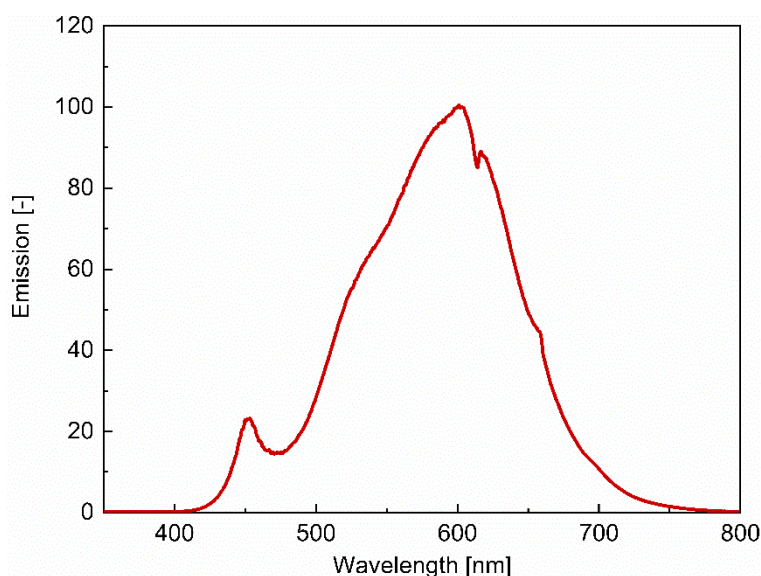
Figure 6.1. Emission spectrum of the used white LED.

6.4.2 Synthesis of Starting Materials and Catalysts

Methyl oleate (*MO*)
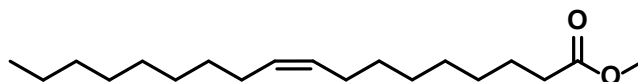
A solution of oleic acid (4.5 g, 16 mmol), trimethyl orthoformate (4.4 mL, 40 mmol) and one drop of sulfuric acid (96 %) in methanol (10 mL) was stirred for 16 hours at room temperature. The solvent was removed under reduced pressure and the red residue was diluted with diethyl ether (60 mL) and washed with sodium bicarbonate solution (2x 20 mL) and water (2x 20 mL). A dark brown oil formed while washing and was discarded. The organic phase was dried over sodium sulfate. After solvent removal under reduced pressure, the product was obtained as slightly yellow liquid (4.6 g, 15 mmol, 94 %).

¹H NMR (400 MHz, CDCl₃, ppm): δ = 5.40–5.26 (m, 2H), 3.65 (s, 3H), 2.29 (t, J = 7.5 Hz, 2H), 2.09–1.91 (m, 4H), 1.68–1.54 (m, 2H), 1.39–1.20 (m, 20H), 0.87 (t, J = 6.7 Hz, 3H).

The spectral data are consistent with literature values.[41]

Cardanyl acetate (*CA*)
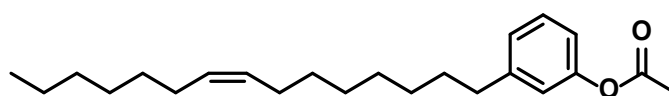
Cardanol monoene (0.51 g, 1.7 mmol) and triethylamine (0.34 mL, 2.4 mmol) were dissolved in dichloromethane (15 mL). Acetyl chloride (0.20 g, 0.18 mL, 2.2 mmol) dissolved in dichloromethane (1.5 mL) was slowly added to the reaction at 0 °C. After 16 hours stirring at room temperature, the solvent was removed from the reaction mixture under reduced pressure. The residue was redissolved in dichloromethane (10 mL) and the organic phase was washed with water (10 mL), hydrochloric acid (0.1 M, 3x 10 mL), half-saturated sodium bicarbonate solution (10 mL) and brine (10 mL). After drying over sodium sulfate, the solvent was removed under reduced pressure. Cardanyl acetate was obtained as orange oil (0.55 g, 1.6 mmol, 94 %).

¹H NMR (300 MHz, CDCl₃, ppm): δ = 7.30–7.24 (m, 2H), 7.05–7.03 (m, 2H), 6.92–6.87 (m, 2H), 5.38–5.32 (m, 2H), 2.63–2.58 (m, 2H), 2.29 (s, 3H), 2.04–1.98 (m, 4H), 1.63–1.58 (m, 2H), 1.35–1.24 (m, 16H), 0.90–0.86 (m, 3H). **¹³C NMR** (151 MHz, CDCl₃, ppm): δ = 169.7, 150.8, 144.8, 130.1, 130.0, 129.2, 126.1, 121.5, 118.8, 35.9, 31.9, 31.2, 29.9, 29.5, 29.4, 29.3, 29.1, 27.4, 27.3, 22.8, 21.3, 14.3.

Oleyl acrylate (*OAcr*)
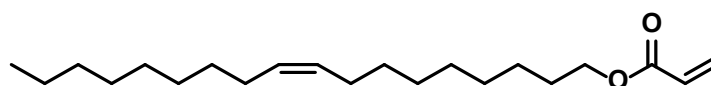
Oleyl alcohol (5.02 g, 18.6 mmol) and triethylamine (3.4 mL, 24 mmol) were dissolved in dichloromethane (185 mL). Acryloyl chloride (2.0 g, 1.8 mL, 22 mmol) dissolved in dichloromethane (15 mL) was slowly added to the reaction at 0 °C. After 16 hours stirring at room temperature, the solvent was removed from the reaction mixture under reduced pressure. The residue was redissolved in dichloromethane (10 mL) and the organic phase was washed with water (70 mL), hydrochloric acid (0.1 M, 3x 80 mL), half-saturated sodium bicarbonate solution (80 mL) and brine (80 mL). After drying over sodium sulfate, the solvent was removed under reduced pressure. Oleyl acrylate was obtained as yellow oil (5.56 g, 17.2 mmol, 92 %).

¹H NMR (500 MHz, CDCl₃, ppm): δ = 6.39 (dd, *J* = 17.4, 1.6 Hz, 1H), 6.11 (dd, *J* = 17.4, 10.5 Hz, 1H), 5.80 (dd, *J* = 10.4, 1.5 Hz, 1H), 5.41–5.29 (m, 2H), 4.14 (t, *J* = 6.8 Hz, 2H), 2.15–1.92 (m, 4H), 1.66 (m, 2H), 1.41–1.21 (m, 22H), 0.87 (t, *J* = 6.8 Hz, 3H).

The spectral data are consistent with literature values.[42]

Trimethylene glycol dioleate (*DO*)
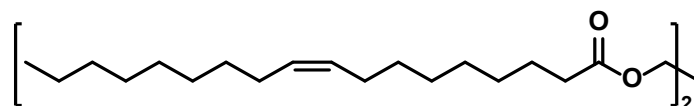
Thionyl chloride (8.4 mL, 115 mmol) was added dropwise to a cooled solution of oleic acid (25 g, 88 mmol) in chloroform (150 mL) and stirred for four hours. After solvent removal under reduced pressure, oleyl chloride was obtained by distillation (200 °C, 10 mbar). The purity was checked by ¹H NMR spectroscopy. The oleyl chloride (8.5 g, 28 mmol) was dissolved in chloroform (60 mL) and slowly added to a solution of 1,3-propandiol (1.0 mL, 14 mmol) and pyridine (3.0 mL, 38 mmol) in CHCl₃ (20 mL) and stirred for 16 hours at room temperature. The reaction mixture was washed with water (2x 100 mL), diluted hydrochloric acid (5%, 100 mL) and saturated NaHCO₃ solution (100 mL), and the solvent was removed under reduced pressure. After flash chromatography on silica with EA/pentane as eluent (gradient 1/500–1/10) trimethylene glycol dioleate was obtained as colorless oil (5.3 g, 8.7 mmol, 62 %)

¹H NMR (500 MHz, CDCl₃, ppm): δ = 5.36–5.33 (m, 4H), 4.12 (q, *J* = 7.1 Hz, 1H), 2.28 (t, *J* = 7.5 Hz, 1H), 2.06–1.98 (m, 8H), 1.64–1.59 (m, 4H), 1.30–1.25 (m, 42H), 0.97–0.74 (m, 6H). **¹³C NMR** (75 MHz, CDCl₃, ppm): δ = 173.9, 130.0, 129.8, 60.2, 34.4, 31.9, 29.8, 29.7, 29.5, 29.3, 29.2, 29.1, 29.1, 27.2, 27.2, 25.0, 22.7, 14.3, 14.1.

5,10,15,20-Tetrakis(4-*iso*propylphenyl)porphyrin (iPrTPP)
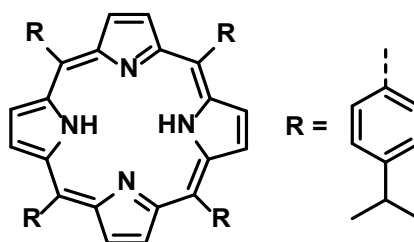
4-Isopropyl-benzaldehyde (1.48 g, 10 mmol) and pyrrole (0.7 mL, 10 mmol) were added to a hot mixture (120 °C) of acetic acid (75 mL) and nitrobenzene (50 mL). The temperature was maintained for 4 h, then the solution was cooled to room temperature to give crystals of the product porphyrin, which were filtered off and dried. Then, the dye dissolved in dichloromethane, methanol was added, only dichloromethane was carefully removed under reduced pressure, and the product was precipitated at -30 °C. The porphyrin was filtered and washed with methanol until the washing solution was colorless. Finally, the product was dried under reduced pressure to give dark pink crystals (492 mg, 0.63 mmol, 25 % yield).

¹H NMR (500 MHz, CDCl₃, ppm): δ = 8.87 (s, 8H), 8.15–8.13 (m, 8 H), 7.61–7.59 (m, 8H), 3.26 (sept, *J* = 7.0 Hz, 4H), 1.55 (d, *J* = 6.9 Hz, 24H), –2.75 (s, 2H). **¹³C NMR** (126 MHz, CDCl₃, ppm): δ = 148.3, 139.8, 134.9, 124.9, 120.3, 34.3, 24.4. **UV/Vis** (CHCl₃): λ$_{max}$ = 421, 518, 554, 593, 650 nm.

The spectral data are consistent with literature values.[43]

VO(iPrTPP)
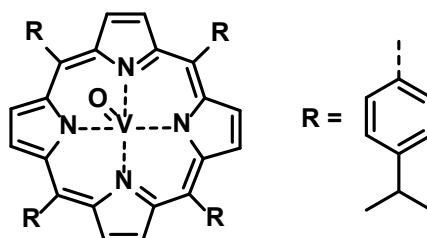
The reaction was conducted according to a modified procedure from Maurya et al.[44] iPrTPP (0.42 g, 0.54 mmol) was dissolved in *N,N*-dimethylformamide (50 mL). VOSO₄ · H₂O (1.0 g, 5.7 mmol) was added, and the reaction mixture was heated to reflux for 16 hours. After cooling the reaction mixture to room temperature, distilled water (150 mL) was added, and a purple precipitate was obtained. The solid was filtered and washed with distilled water (150 mL) and methanol (20 mL). The product was obtained after drying under reduced pressure as purple crystals in 86 % yield (0.39 g, 0.46 mmol).

IR (KBr): ṽ = 3022, 2958, 2866, 1915, 1497, 1458, 1337, 1004, 801 cm⁻¹. **UV/Vis** (CHCl₃): λ$_{max}$ = 427, 550, 587 nm.

TiO(iPrTPP)
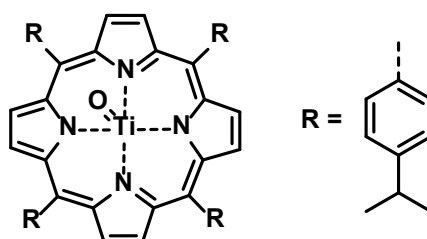
The reaction was conducted according to a modified procedure from Fournari et al.[45] iPrTPP (244 mg, 0.31 mmol) was dissolved in *N,N*-dimethylformamide (100 mL). To this, pyridine (2 mL) and TiCl₄ (1.7 mL, 15 mmol) were added under nitrogen atmosphere and the resulting reaction mixture was heated to reflux for 24 h. After cooling the reaction mixture to room temperature, distilled water (150 mL) was added, and a purple precipitate was obtained. The solid was filtered, washed with distilled water (3x 25 mL). Then, the product was dissolved in CHCl₃, stirred over sodium carbonate, filtered and concentrated. The addition of pentane led to the precipitation of the product. TiO(iPrTPP) was obtained after flash chromatography on silica with CHCl₃ as eluent as pink crystals (52 mg, 0.062 mmol, 20 % yield).

¹H NMR (500 MHz, CDCl₃, ppm): δ = 9.18 (s, 8H), 8.43–8.05 (m, 8H), 7.72–7.70 (m, 8H), 3.30 (sept, *J* = 6.9 Hz, 4H), 1.58 (d, *J* = 6.9 Hz, 24H). **¹³C NMR** (126 MHz, CDCl₃, ppm): δ = 148.8, 148.7, 139.3, 135.1, 134.6, 132.7, 125.2, 125.0, 123.8, 34.3, 24.4. **UV/Vis** (CHCl₃): λ$_{max}$ = 426, 553, 592 nm.

The spectral data are consistent with literature values.[45]

6.4.3 Optimization experiments

For the optimization of the CO_2 insertion reaction, a vial, equipped with a stirrer bar, was filled with epoxy alcohol (*EpAlc*, 0.6 mmol), metal catalyst, additive and mesitylene (10 mol%) and sealed with a crimp top, in which a cut-off canula was inserted. The autoclave, containing up to seven vials, was then filled with CO_2 and heated to 90 °C while stirring. After different time spans, the autoclave was cooled to 8 °C using an ice bath and depressurized slowly while stirring. The ratios of cyclic carbonate to epoxy alcohol (*CC:EpAlc*) is reported in table 6.3.

Table 6.3. Optimization experiments for CO_2 insertion.

Metal-catalyst	Additive	CO_2 [bar]	*t* [h]	*T* [°C]	*CC:EpAlc*
–	10 mol% DIPEA	40	48	90	79:21
1 mol% VO(acac)$_2$	2.5 mol% TOAB	40	48	90	94:6
1 mol% VO(acac)$_2$	10 mol% DIPEA	40	48	90	95:5
2 mol% VO(acac)$_2$	10 mol% DIPEA	40	48	90	95:5
2 mol% [VO(^{iPr}TPP)]	10 mol% DIPEA	40	48	90	80:20
2 mol% VO(acac)$_2$	10 mol% DIPEA	40	24	90	78:22
2 mol% VO(acac)$_2$	5 mol% DIPEA	40	24	90	70:30
2 mol% VO(acac)$_2$	5 mol% Et$_3$N	40	24	90	54:46
2 mol% VO(acac)$_2$	5 mol% pyridine	40	24	90	93:7
2 mol% VO(acac)$_2$	5 mol% DBU	40	24	90	97:3
2 mol% VO(acac)$_2$	5 mol% DABCO	40	24	90	94:6
–	5 mol% pyridine	4	24	90	19:81
1 mol% VO(acac)$_2$	5 mol% pyridine	4	24	90	35:65
2 mol% VO(acac)$_2$	10 mol% pyridine	4	24	90	91:9
2 mol% VO(acac)$_2$	2.5 mol% TOAB	4	24	90	63:37
2 mol% VO(acac)$_2$	2 mol% Na$_3$(citrate) · 2 H$_2$O	4	24	90	<5:95
5 mol% Ti(OiPr)$_4$	5 mol% pyridine	4	24	90	<5:95

| 5 mol% Ti(OiPr)$_4$ | – | | 4 | 24 | 90 | <5:95 |

6.4.4 General procedures

General procedure for solvent-free photooxygenation (GP1)

iPrTPP (1.5 mM) was dissolved in the starting material, ultrasonification was used to assure a homogenous and particle-free solution. The solution was then injected to the micro flow reactor developed by Schachtner et al.[30] at 20 °C and irradiated for 20 min with 24 white (λ_{max} = 630 nm) LEDs in an approximately 13 m long 1/16 inch (0.79 mm) inner diameter FEP tubing, together with oxygen at a pressure of roughly 45 bar. The O$_2$ flow rate was adjusted so that a laminar slug flow resulted, and the gas was not completely consumed when the solution left the back-pressure cartridge at the end of the tubing. For NMR analysis a small portion was taken, dissolved in ethyl acetate and filtered over silica to remove residual catalyst. The crude product was used as starting material in the following reaction. If not stated otherwise, quantitative yields of hydroperoxide were obtained.

General procedure for oxygenation in solution (GP2)

The starting material was dissolved in a solution of methylene blue (1 mM, in MeCN or dichloromethane) to give a 0.1 M solution of the substrate (1 mol% of MB sensitizer with respect to the substrate), ultrasonification was used to assure a homogenous and particle-free solution. The solution was then injected to the micro flow reactor developed by Schachtner et al.[30] at 20 °C and irradiated for 8 min with 24 white (λ_{max} = 630 nm) LEDs in an approximately 13 m long 1/16 inch (0.79 mm) inner diameter FEP tubing, together with oxygen at a pressure of roughly 45 bar. The O$_2$ flow rate was adjusted so that a laminar slug flow resulted and O$_2$ was not completely consumed when the solution left the back-pressure cartridge at the end of the tubing. For NMR analysis a small portion was taken and filtered over silica to remove residual catalyst. The crude product was used as starting material in the following reaction either in solution or neat after solvent removal. If not stated otherwise, quantitative yields of hydroperoxide were obtained.

General procedure for solvent-free self-epoxidation (GP3)

The substrate was cooled to 0 °C and stirred vigorously, then VO(acac)$_2$ (1 mol%) was added slowly. After 0.5 hours, full conversion was confirmed by TLC. For NMR analysis a small portion was taken, dissolved in ethyl acetate and filtered over silica to remove residual catalyst. The crude product was used as starting material in the following reaction. If not stated otherwise, quantitative yields of epoxy alcohols were obtained.

General procedure for self-epoxidation in solution (GP4)

The substrate was dissolved in dichloromethane or acetonitrile (0.1 M) and cooled to 0 °C. VO(acac)$_2$ (1 mol%) was added slowly under stirring and the mixture was allowed to warm to room temperature. After two hours, full conversion was confirmed by TLC. For NMR analysis a small portion was taken and filtered over silica to remove residual catalyst. After solvent removal under reduced pressure, the crude product was used as starting material in the following reaction. If not stated otherwise, quantitative yields of epoxy alcohols were obtained.

General procedure for CO₂ insertion (GP 5)

A vial, equipped with a stirrer bar, was filled with the corresponding epoxy alcohol (0.6 mmol), VO(acac)$_2$ (1 mol%, $6.0 \cdot 10^{-6}$ mol, 1.6 mg) and pyridine (10 mol%, $6.0 \cdot 10^{-5}$ mol, 4.8 μL), and sealed with a crimp top, in which a cut-off canula was inserted. The autoclave, containing up to seven vials, was then filled with CO_2 (4 bar) and heated to 90 °C while stirring. After 24 h, the autoclave was gradually cooled to 8°C using an ice bath and depressurized slowly while stirring.

6.4.5   Analytical Data of synthesized compounds

Reaction sequence for (Z)-4-octene and (E)-4-octene

trans-5-Hydroperoxyoct-3-ene (O-HYP)
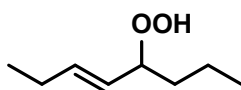
(Z)-4-octene (1.12 g, 10.0 mmol) was reacted according to GP2 in acetonitrile. ¹H NMR analysis showed quantitative conversion to O-HYP. The reaction solution was used in the following step without further purification. The reaction of (E)-4-octene (0.11 g, 1.0 mmol) following GP2 in acetonitrile also gave quantitative formation of O-HYP.

¹H NMR (300 MHz, CDCl₃, ppm): δ = 7.71 (br s, 1H), 5.83 (dt, J = 15.5, 6.2 Hz, 1H), 5.37 (m, 1H), 4.29 (dt, J = 8.3, 6.4 Hz, 1H), 2.18–2.04 (m, 2 H), 1.51–1.28 (m, 4 H), 1.02 (t, J = 7.5 Hz, 3H), 0.91 (t, J = 7.3, 3H). **¹³C NMR** (100 MHz, CDCl₃, ppm): δ = 138.7, 127.6, 87.0, 34.7, 25.5, 18.7, 14.1, 13.5.

The spectral data are consistent with literature values.[16]

1-(3-Ethyloxiran-2-yl)butan-1-ol (O-EpAlc)
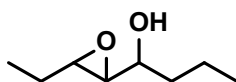
Following GP4, a crude solution of O-HYP (10.0 mmol) in acetonitrile was treated with VO(acac)₂ (26 mg). ¹H NMR analysis showed quantitative conversion to O-EpAlc. A mixture of diastereomeric products (*syn/anti*) can be observed in the NMR spectra.

¹H NMR (300 MHz, CDCl₃, ppm): δ = 3.85–3.72 (m, 1H, *syn*) 3.50–3.33 (m, 1 H, *anti*), 3.06–2.95 (m, 1H, *syn*), 2.94–2.85 (m, 1H, *anti*), 2.79–2.76 (m, 1H, *syn*), 2.75–2.72 (m, 1H, *anti*), 1.67–1.34 (m, 6 H), 1.04–0.86 (m, 6 H) ppm. **¹³C NMR** (151 MHz, CDCl₃, ppm): δ = 72.8, 71.4, 69.9, 68.3, 61.7, 61.6, 60.9, 60.8, 58.2, 56.9, 56.1, 54.9, 36.6, 35.8, 33.82, 33.81, 27.6, 26.6, 24.9, 24.8, 19.5, 19.4, 18. 7, 14.3, 14.2, 14.1, 10.0, 9.9, 9.84, 9.77 ppm.

### 4-(1-Hydroxypropyl)-5-propyl-1,3-dioxolan-2-one (O-CC)
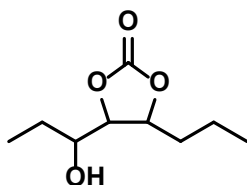
Following GP5, crude O-EpAlc (4.2 mmol) was used as starting material. After flash chromatography on silica with pentane/ethyl acetate as eluent, O-CC was obtained as yellow oil (0.73 g, 92 % yield).

¹H NMR (300 MHz, CDCl₃, ppm): δ = 4.75–4.57 (m, 1H), 4.16–4.10 (m, 1H), 3.88–3.73 (m, 1H), 2.22 (br s, 1H), 1.78–1.37 (m, 6H), 1.06–0.92 (m, 6H). **¹³C NMR** (101 MHz, CDCl₃, ppm): δ = 154.9, 83.2, 83.1, 80.3, 80.2, 79.0, 77.9, 72.3, 70.6, 70.0, 37.1, 36.5, 36.3, 35.0, 34.0, 31.1, 28.0, 27.4, 27.3, 26.2, 25.2, 22.5, 19.1, 18.8, 18.7, 18.14, 18.08, 18.0, 14.0, 13.8, 9.9, 8.9.

Reaction sequence for methyl oleate (MO)

Methyl *trans*-9-hydroperoxyoctadec-10-enoate and
Methyl *trans*-10-hydroperoxyoctadec-8-enoate (MO-HYP)
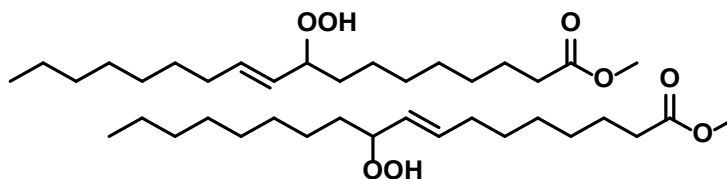
Methyl oleate (2.96 g, 10.0 mmol) was reacted according to GP1. ¹H NMR analysis showed quantitative conversion to MO-HYP. The crude reaction mixture was used in the following step without further purification.

¹H NMR (300 MHz, CDCl₃, ppm): δ = 8.06 (d, J = 18.6 Hz, 1H), 5.81–5.64 (m, 1H), 5.42–5.28 (m, 1H), 4.27–4.20 (m, 1H), 3.64 (s, 3H), 2.33–2.23 (m, 2H), 2.11–1.99 (m, 2H), 1.69–1.16 (m, 22H), 0.91–0.81 (m, 3H). **¹³C NMR** (126 MHz, CDCl₃, ppm): δ = 137.3, 136.8, 129.0, 128.6, 87.1, 87.1, 51.7, 51.6, 34.2, 34.1, 32.6, 32.5, 32.5, 32.3, 29.6, 29.6, 29.39, 29.35, 29.24, 29.19, 29.15, 29.1, 28.9, 28.84, 28.76, 25.5, 25.3, 24.98, 24.95, 22.8, 14.2. **GC-MS** (EI): m/z (%): 281 (18), 211 (2) [M⁺−H₂O−(C₂H₄COOMe)], 167 (24), 153 (13), 137 (16), 97 (21), 81 (25), 67 (36), 55 (58).

The spectral data are consistent with literature values.[46]

Methyl 9-(3-heptyloxiran-2-yl)-9-hydroxynonanoate and
Methyl 7-(3-(-1-hydroxynonyl)oxiran-2-yl)heptanoate (MO-EpAlc)
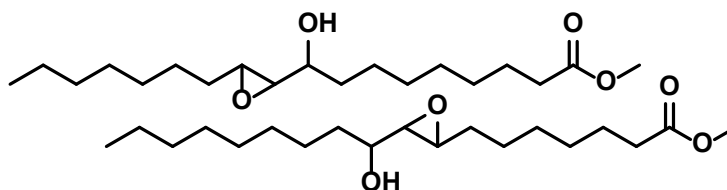
Following GP3, crude MO-HYP (10.0 mmol) was treated with VO(acac)₂ (26 mg). ¹H NMR analysis showed quantitative conversion to MO-EpAlc. A mixture of diastereomeric products (*syn/anti: 1/1*) can be observed in the NMR spectra. A fraction of the product mixture was

separated by flash chromatography on silica with pentane/ethyl acetate as eluent yielding the clean *syn*- and *anti*-diastereomers.

¹H NMR (300 MHz, CDCl₃, ppm): δ = 3.81–3.73 (m, 1H, *syn*), 3.64 (s, 3H), 3.48–3.37 (m, 1H, *anti*), 3.01–2.94 (m, 1H, *syn*), 2.87 (td, *J* = 5.5, 2.3 Hz, 1H, *anti*), 2.75–2.74 (m, 1H, *syn*), 2.70 (dd, *J* = 5.3, 2.3 Hz, 1H, *anti*), 2.32–2.27 (m, 2H), 2.09–1.98 (m, 1H), 1.71–1.19 (m, 24H), 0.87 (t, *J* = 6.6 Hz). **¹³C NMR** (101 MHz, CDCl₃, ppm): δ = 174.3, 71.4, 68.7, 68.6, 61.92, 61.88, 61.0, 57.0, 56.9, 55.1, 55.0, 51.40, 51.38, 34.3, 34.2, 34.0, 33.9, 33.6, 33.5, 31.8, 31.7, 31.60, 31.57, 31.52, 31.49, 29.64, 29.58, 29.5, 29.40, 29.35, 29.32, 29.31, 29.2, 29.14, 29.09, 29.00, 28.98, 28.9, 26.0, 25.9, 25.8, 25.7, 25.28, 25.25, 25.2, 24.82, 24.75, 22.61, 22.57, 14.04, 14.01.

Methyl *syn*-9-(3-heptyloxiran-2-yl)-9-hydroxynonanoate and
Methyl *syn*-7-(3-(-1-hydroxynonyl)oxiran-2-yl)heptanoate (MO *syn*-EpAlc)
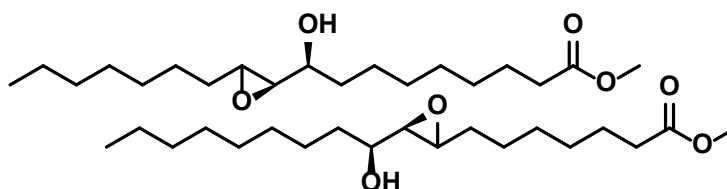
¹H NMR (300 MHz, CDCl₃, ppm): δ = 3.81–3.73 (m, 1H), 3.66 (s, 3H), 3.01–2.94 (m, 1H), 2.75–2.74 (m, 1H), 2.32–2.27 (m, 2H), 1.88 (br s, 1H), 1.71–1.19 (m, 24H), 0.87 (t, *J* = 6.6 Hz). **¹³C NMR** (101 MHz, CDCl₃, ppm): δ = 174.4, 174.3, 68.72, 68.65, 61.1, 55.11, 55.04, 51.60, 51.58, 34.2, 34.1, 33.7, 33.6, 32.0, 31.9, 31.74, 31.66, 29.8, 29.63, 29.57, 29.5, 29.4, 29.32, 29.26, 29.2, 29.1, 26.2, 26.0, 25.44, 25.37, 25.0, 24.9, 22.79, 22.75, 14.2. **GC-MS** (EI): m/z (%): 207 (30), 187 (12), 155 (47) [M⁺−H₂O−(C₈H₁₆COOMe)], 141 (70), 111 (23), 96 (42), 95 (60), 83 (48), 81 (65), 69 (54), 67 (64), 55 (100).

Methyl *anti*-9-(3-heptyloxiran-2-yl)-9-hydroxynonanoate and
Methyl *anti*-7-(3-(-1-hydroxynonyl)oxiran-2-yl)heptanoate (MO *anti*-EpAlc)
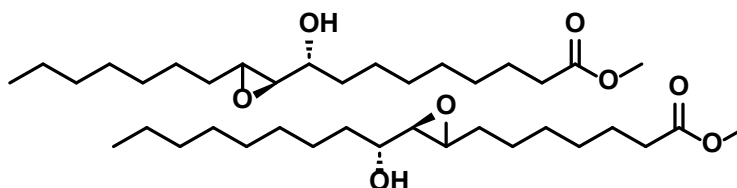
¹H NMR (300 MHz, CDCl₃, ppm): δ = 3.66 (s, 3H), 3.50–3.37 (m, 1H), 2.94–2.84 (m, 1H), 2.71 (dd, *J* = 5.1, 2.3 Hz, 1H), 2.30 (t, *J* = 7.5 Hz, 2H), 1.89 (br s, 1H), 1.70–1.49 (m, 8H), 1.48–1.99 (m, 16H), 0.87 (t, *J* = 6.5 Hz, 2H). **¹³C NMR** (101 MHz, CDCl₃, ppm): δ = 174.3, 71.5, 61.9, 57.1, 57.0, 51.6, 34.6, 34.5, 34.20, 34.15, 32.0, 31.9, 31.8, 31.7, 29.7, 29.6, 29.5, 29.4, 29.32, 29.27, 29.2, 29.1, 26.1, 25.9, 25.43, 25.35, 25.0, 24.9, 22.8, 22.8, 14.2. **GC-MS** (EI): m/z (%): 187 (8), 173 (17), 155 (25), 141 (100), 95 (48), 81 (29), 57 (42), 55 (58).

Methyl 9-(5-heptyl-2-oxo-1,3-dioxolan-4-yl)-9-hydroxynonanoate and regioisomers
(MO-CC)
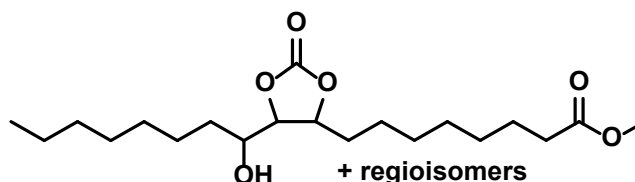
Following GP5, crude MO-EpAlc (4.2 mmol) was used as starting material. After flash chromatography on silica with pentane/ethyl acetate as eluent, O-CC was obtained as yellow oil (1.41 g, 90 % yield).

¹H NMR (300 MHz, CDCl₃, ppm): δ = 4.68–4.58 (m, 1H), 4.11–4.05 (m, 1H), 3.87–3.78 (m, 1H), 3.65 (s, 3H), 2.29 (t, *J* = 7.5 Hz, 2H), 1.81–1.12 (m, 24H), 0.86 (t, *J* = 6.4 Hz, 3H). **¹³C NMR** (101 MHz, CDCl₃, ppm): δ = 174.5, 155.0, 83.6, 78.0, 70.8, 51.6, 35.0, 34.1, 32.1, 32.0, 31.8, 29.5, 29.31, 29.29, 29.2, 29.03, 28.98, 28.9, 25.4, 24.9, 24.6, 22.74, 22.70, 14.2. **GC-MS** (EI): m/z (%): 207 (35), 173 (37), 155 (14), 141 (100), 95 (54), 83 (18), 69 (28), 55 (34).

Reaction sequence for oleyl alcohol (OA)

trans-9-Hydroperoxyoctadec-10-en-1-ol and *trans*-10-Hydroperoxyoctadec-8-en-1-ol (OA-HYP)
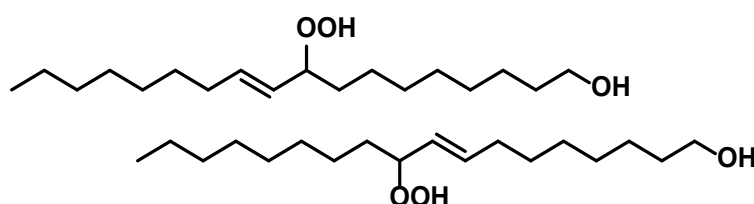
Oleyl alcohol (0.81 g, 3.0 mmol) was reacted according to GP1. ¹H NMR analysis showed quantitative conversion to OA-HYP. The reaction mixture was used in the following step without further purification.

¹H NMR (300 MHz, CDCl₃, ppm): δ = 8.56 (s, br, 1H), 5.81−5.72 (m, 1H), 5.36 (dd, *J* = 15.4, 8.2, 1H), 4.25–4.18 (m, 1H), 3.64 (t, *J* = 6.7, 2H), 2.15–1.98 (m, 2H), 1.64–1.18 (m, 24H), 0.85 (t, *J* = 6.4 Hz, 3H). **¹³C NMR** (101 MHz, CDCl₃, ppm): δ = 137.1, 136.9, 128.9, 128.7, 87.1, 63.2, 63.1, 32.8, 32.7, 32.59, 32.57, 32.5, 32.4, 31.98, 31.95, 29.82, 29.78, 29.74, 29.66, 29.6, 29.5, 29.41, 29.35, 29.3, 29.23, 29.17, 29.1, 29.0, 25.78, 25.75, 25.5, 25.4, 22.81, 22.78, 14.2.

1-(3-Heptyloxiran-2-yl)nonane-1,9-diol and 1-(3-(7-Hydroxyheptyl)oxiran-2-yl)nonan-1-ol (OA-EpAlc)
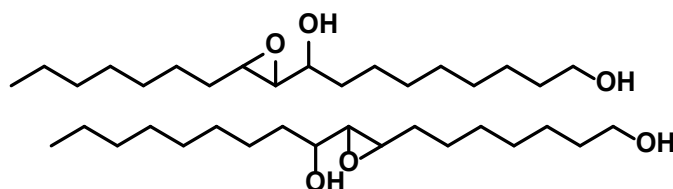
Following GP3, crude OA-HYP (3.0 mmol) was treated with VO(acac)₂ (8.0 mg). ¹H NMR analysis showed quantitative conversion to OA-EpAlc. A mixture of diastereomeric products (*syn/anti: 2/3*) can be observed in the NMR spectra.

¹H NMR (300 MHz, CDCl₃, ppm): δ = 3.81−3.73 (m, 1H, *syn*), 3.62 (t, *J* = 6.6 Hz, 2H), 3.46–3.40 (m, 1H, *anti*), 2.98 (td, *J* = 5.5, 2.2 Hz, 1H, *syn*), 2.89 (td, *J* = 6.7, 2.2 Hz, 1H, *anti*), 2.76–2.74 (m, 1H, *syn*), 2.71 (dd, *J* = 5.2, 2.3 Hz, 1H, *anti*), 1.99 (s, br, 1H), 1.62–1.21 (m, 26H), 0.92−0.82 (m, 3H). **¹³C NMR** (101 MHz, CDCl₃, ppm): δ = 71.5, 68.73, 68.68, 63.2, 63.10, 63.06, 62.01, 61.99, 61.2, 57.2, 57.1, 55.18, 55.16, 34.51, 34.48, 33.9, 33.70, 33.65, 32.91, 32.86, 32.8, 32.1, 32.0, 31.9, 31.8,

31.74, 31.71, 29.81, 29.78, 29.74, 29.70, 29.63, 29.59, 29.56, 29.5, 29.44, 29.40, 29.37, 29.3, 29.23, 26.15, 26.1, 26.0, 25.9, 25.82, 25.75, 25.4, 22.81, 22.78, 22.7, 14.22, 14.19.

4-(1-Hydroxyoctyl)-5-(8-hydroxyoctyl)-1,3-dioxolan-2-one and regioisomers **(OA-CC)**
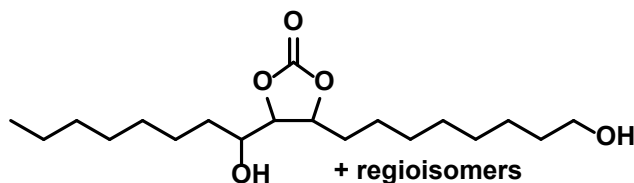
Following GP5, crude OA-EpAlc (1.8 mmol) was used as starting material. After flash chromatography on silica with pentane/ethyl acetate as eluent, OA-CC was obtained as yellow oil (0.53 g, 85 % yield).

^{1}H NMR (300 MHz, CDCl$_3$, ppm): δ = 4.67–4.56 (m, 1H), 4.16–4.13 (m, 1H, *diast.*), 4.11–4.08 (m, 1H, *diast.*), 3.87–3.82 (m, 1H, *diast.*), 3.63 (t, *J* = 6.6 Hz, 2 H), 3.60–3.55 (m, 1H, *diast.*), 1.90–1.80 (m, 2H), 1.78–1.70 (m, 1H), 1.69–1.62 (m, 2H), 1.59–1.44 (m, 5H), 1.40–1.20 (m, 19H), 0.88 (t, *J* = 6.7 Hz, 3H). **^{13}C NMR** (101 MHz, CDCl$_3$, ppm): δ = 155.1, 84.04, 84.01, 83.8, 79.13, 79.08, 78.31, 78.28, 71.3, 71.1, 71.0, 63.4, 63.3, 35.34, 35.28, 34.6, 34.1, 33.33, 33.30, 33.1, 33.0, 32.3, 32.2, 32.1, 29.8, 29.7, 29.6, 29.5, 29.4, 26.1, 26.02, 25.96, 25.9, 25.81, 25.75, 25.6, 25.0, 24.9, 24.8, 23.03, 22.99, 14.5. **HRMS** (ESI): *m/z* calculated for C$_{19}$H$_{36}$O$_5$+Na$^+$: 367.2460 [M+Na]$^+$; found 367.2449.

Reaction sequence for oleic acid (OlA)

***trans*-9-Hydroperoxyoctadec-10-enoic acid** and ***trans*-10-Hydroperoxyoctadec-8-enoic acid (OlA-HYP)**
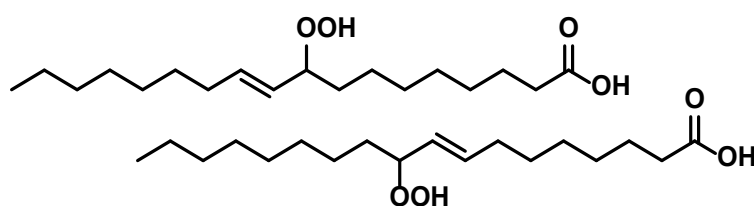
Oleic acid (0.85 g, 3.0 mmol) was reacted according to GP1 in dichloromethane. ^{1}H NMR analysis showed quantitative conversion to OlA-HYP. The reaction solution was used in the following step without further purification.

^{1}H NMR (300 MHz, CDCl$_3$, ppm): δ = 5.81−5.69 (m, 1H), 5.39−5.30 (m, 1H), 4.30–4.23 (m, 1H), 2.38−2.30 (m, 2H), 2.09–2.07 (m, 2H), 1.69−1.56 (m, 3H), 1.48−1.19 (m, 19H), 0.92−0.83 (m, 3H). **^{13}C NMR** (101 MHz, CDCl$_3$, ppm): δ = 180.1, 180.0, 137.4, 136.9, 128.9, 128.5, 87.21, 87.18, 34.12, 34.07, 32.6, 32.51, 32.46, 32.3, 31.98, 31.95, 29.7, 29.56, 29.39, 29.36, 29.3, 29.19, 29.16, 29.1, 28.9, 28.83, 28.75, 25. 5, 25.4, 24.73, 24.68, 22.8, 14.2.

The spectral data are consistent with literature values.[47]

9-(3-Heptyloxiran-2-yl)-9-hydroxynonanoic acid and
7-(3-(1-Hydroxynonyl)oxiran-2-yl)-heptanoic acid (OlA-EpAlc)
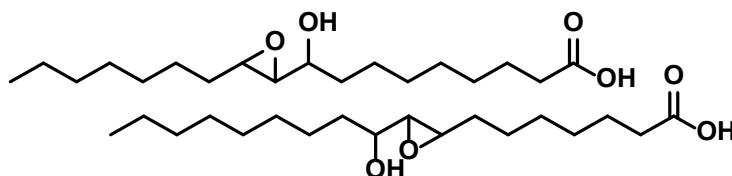
Following GP4, a crude solution of OlA-HYP (3.0 mmol) in dichloromethane was treated with VO(acac)$_2$ (8.0 mg). ^{1}H NMR analysis showed quantitative conversion to OlA-EpAlc. A mixture of diastereomeric products (*syn/anti: 3/2*) can be observed in the NMR spectra. OlA-EpAlc was isolated by flash chromatography on silica with pentane/ethyl acetate as eluent as off-white solid (0.80 g, 85 % yield).

^{1}**H NMR** (300 MHz, CDCl$_3$, ppm): δ = 3.84–3.73 (m, 1H, *syn*), 3.50–3.38 (m, 1H, *anti*), 3.05 – 2.96 (m, 1H, *syn*), 2.95–2.87 (m, 1H, *anti*), 2.79–2.70 (m, 1H), 2.33 (t, *J* = 7.3 Hz, 2H), 1.70–1.17 (m, 24H), 0.87 (t, *J* = 6.4 Hz, 3H). ^{13}**C NMR** (151 MHz, CDCl$_3$, ppm): δ = 179.7, 179.6, 71.5, 71.4, 68.7, 68.6, 62.14, 62.10, 61.3, 61.2, 57.3, 57.2, 55.3, 55.2, 34. 5, 34.4, 34.10, 34.08, 34.05, 33.7, 33.6, 33.5, 31.99, 31.96, 31.9, 31.73, 31.70, 31.66, 31.64, 31.61, 29.82, 29.79, 29.75, 29.7, 29.63, 29.60, 29.53, 29.48, 29.4, 29.33, 29.31, 29.23, 29.20, 29.11, 29.08, 29.0, 26.13, 26.05, 25.9, 25.9, 25.43, 25.36, 25.3, 25.2, 24.8, 24.70, 24.65, 22.78, 22.75, 14.23, 14.21.

Reaction sequence for cardanyl acetate (CA)

trans-**3-(8-Hydroperoxypentadec-9-en-1-yl)phenyl acetate** and
trans-**3-(9-Hydroperoxy-pentadec-7-en-1-yl)phenyl acetate (CA-HYP)**
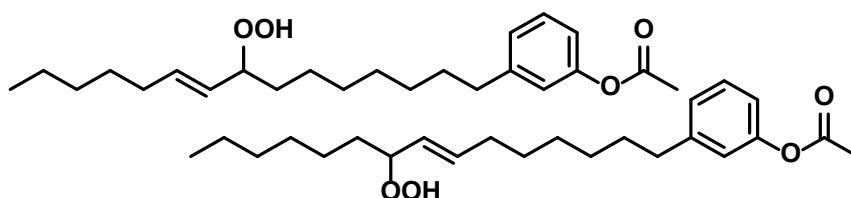
Cardanyl acetate (0.5 g, 1.5 mmol) was reacted according to GP2 in acetonitrile. ^{1}H NMR analysis showed quantitative conversion to O-HYP. The reaction solution was used in the following step without further purification.

^{1}**H NMR** (300 MHz, CDCl$_3$, ppm): δ = 7.66 (br s, 1H), 7.33–7.23 (m, 1H), 7.03 (d, *J* = 7.8 Hz, 1H), 6.93–6.86 (m, 2H), 5.85–5.69 (m, 1H), 5.42–5.30 (m, 1H), 4.30 – 4.23 (m, 1H), 2.63 – 2.57 (m, 2H), 2.29 (s, 3H), 2.12–1.99 (m, 2H), 1.70–1.20 (m, 18H), 0.93–0.83 (m, 3H). ^{13}**C NMR** (101 MHz, CDCl$_3$, ppm): δ = 150.7, 144.8, 137.3, 137.1, 129.3, 128.8, 128.6, 126.1, 121.6, 118.88, 118.85, 87.23, 87.21, 35.8, 32.60, 32.57, 32.44, 32.41, 31.9, 31.5, 31.24, 31.18, 29.5, 29.4, 29.33, 29.25, 29.12, 29.08, 29.0, 28.9, 25.9, 22.7, 22.6, 21.3, 14.2.

3-(8-Hydroxy-8-(3-pentyloxiran-2-yl)octyl)phenyl acetate and
3-(6-(3-(1-Hydroxyheptyl)-oxiran-2-yl)hexyl)phenyl acetate (CA-EpAlc)
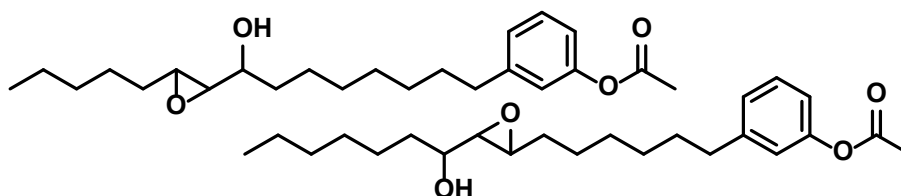
Following GP4, a crude solution of CA-HYP (1.0 mmol) in acetonitrile was treated with VO(acac)$_2$ (2.6 mg). ^{1}H NMR analysis showed quantitative conversion to CA-EpAlc. A mixture of diastereomeric products (*syn/anti: 1/1*) can be observed in the NMR spectra.

^{1}H NMR (300 MHz, CDCl$_3$, ppm): δ = 7.30–7.23 (m, 1H), 7.05–7.02 (m, 1H), 6.90–6.89 (m, 2H), 3.83–3.73 (m, 1H, *syn*), 3.49–3.39 (m, 1H, *anti*), 3.03–2.95 (m, 1H, *syn*), 2.93–2.86 (m, 1H *anti*), 2.78–2.69 (m, 1H), 2.60 (t, *J* = 7.8 Hz, 2H), 2.29 (s, 3H), 1.80 (s, br, 1H), 1.69–1.18 (m, 20H), 0.93–0.84 (m, 3H). **^{13}C NMR** (151 MHz, CDCl$_3$, ppm): δ = 169.7, 150.5, 144.7, 129.3, 126.1, 121.6, 118.9, 71.5, 68.69, 68.66, 61.88, 61.86, 61.1, 57.12, 57.05, 55.10, 55.05, 35.82, 35.78, 34.60, 34.56, 33.7, 33.6, 31.9, 31.7, 31.2, 31.1, 29.7, 29.6, 29.5, 29.4, 29.4, 29.3, 29.3, 29. 2, 26.14, 26.07, 25.41, 25.39, 22.7, 21.3, 14.2, 14.1.

3-(7-(5-Hexyl-2-oxo-1,3-dioxolan-4-yl)-7-hydroxyheptyl)phenyl acetate and regioisomers
(CA-CC)
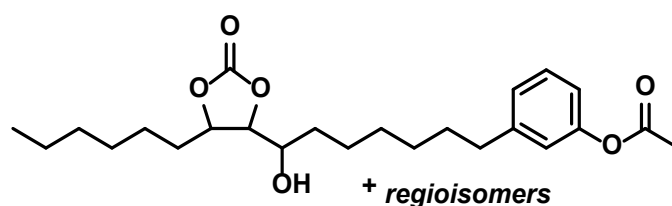
Following GP5, crude CA-EpAlc (0.6 mmol) was used as starting material. After flash chromatography on silica with pentane/ethyl acetate as eluent, O-CC was obtained as yellow oil (0.23 g, 93 % yield).

^{1}H NMR (300 MHz, CDCl$_3$, ppm): δ = 7.29–7.25 (m, 1H), 7.04–7.03 (m, 1H), 6.90–6.88 (m, 2H), 4.65–4.59 (m, 1H), 4.10–4.06 (m, 1H), 3.86–3.78 (m, 1H), 2.62–2.59 (m, 2H), 2.29 (s, 3H), 1.73–1.59 (m, 5H), 1.40–1.25 (m, 19H), 0.91–0.87 (m, 3H). **^{13}C NMR** (101 MHz, CDCl$_3$, ppm): δ = 151.1, 144.9, 144.7, 129.59, 129.56, 126.4, 121.9, 121.8, 119.20, 119.16, 119.1, 83.7, 78.3, 71.2, 71.0, 36.02, 35.94, 35.34, 35.30, 35.27, 35.2, 32.4, 32.3, 32.2, 32.1, 32.0, 31.7, 31.4, 31.3, 31.2, 29.54, 29.52, 29.45, 29.3, 29.1, 25.7, 25.6, 25.5, 25.4, 24.92, 24.87, 24.8, 24.6, 23.0, 22.9, 22.8, 21.6, 14.44, 14.38.

Reaction sequence for oleyl acrylate (OAcr)

trans-9-Hydroperoxyoctadec-10-en-1-yl acrylate and
trans-10-Hydroperoxyoctadec-8-en-1-yl acrylate (OAcr-HYP)
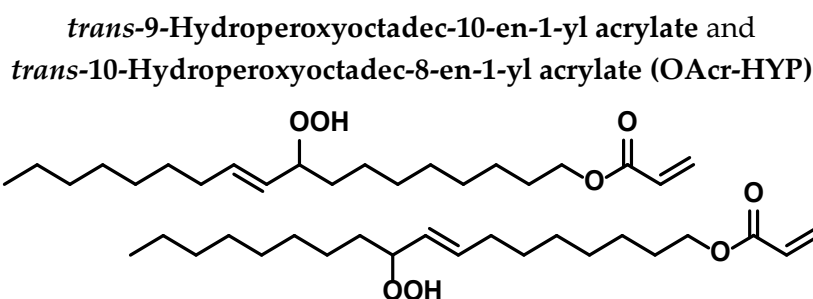
Oleyl acrylate (0.97 g, 3.0 mmol) was reacted according to GP2 in acetonitrile. ^{1}H NMR analysis showed quantitative conversion to OAcr-HYP. The reaction solution was used in the following step without further purification.

^{1}H NMR (300 MHz, CDCl$_3$, ppm): δ = 7.75–7.66 (m, 1H), 6.40 (d, *J* = 17.3 Hz, 1H), 6.12 (dd, *J* = 17.3, 10.4 Hz, 1H), 5.85–5.70 (m, 2H), 5.43–5.30 (m, 1H), 4.30–4.23 (m, 1H), 4.15 (t, *J* = 6.7 Hz, 2H), 2.11–2.04 (m, 2H), 1.72–1.56 (m, 4H), 1.49–1.18 (m, 20H), 0.88 (t, *J* = 6.4 Hz, 3H). **^{13}C NMR**

(151 MHz, CDCl$_3$, ppm): δ = 166.5, 137.4, 137.0, 130.7, 130.6, 128.84, 128.77, 128.75, 128.6, 87.2, 64.83, 64.79, 32.59, 32.56, 32.5, 32.4, 32.00, 31.96, 29.7, 29.6, 29.54, 29.47, 29.4, 29.3, 29.19, 29.15, 29.12, 29.06, 28.72, 28.70, 26.01, 25.97, 25.5, 25.4, 22.8, 14.2.

9-(3-Heptyloxiran-2-yl)-9-hydroxynonyl acrylate and 7-(3-(1-Hydroxynonyl)oxiran-2-yl)-heptyl acrylate (OAcr-EpAlc)
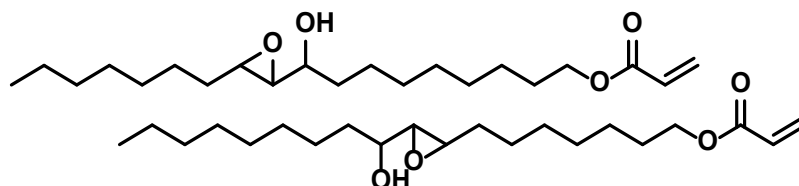
Following GP4, a crude solution of OAcr-HYP (3.0 mmol) in acetonitrile was treated with VO(acac)$_2$ (8.0 mg). ^{1}H NMR analysis showed quantitative conversion to OAcr-EpAlc. A mixture of diastereomeric products (*syn/anti: 5/4*) can be observed in the NMR spectra.

^{1}H NMR (300 MHz, CDCl$_3$, ppm): δ = 6.39 (dd, *J* = 17.3, 1.6 Hz, 1H), 6.11 (dd, *J* = 17.3, 10.4 Hz, 1H), 5.81 (dd, *J* = 10.4, 1.6 Hz, 1H), 4.14 (t, *J* = 6.7 Hz, 2H), 3.83–3.75 (m, 1H, *syn*), 3.49–3.39 (m, 1H, *anti*), 3.01–2.96 (m, 1H, *syn*), 2.92–2.87 (m, 1H, *anti*), 2.76–2.74 (m, 1H, *syn*), 2.73–2.70 (m, 1H, *anti*), 1.84 (s, br, 1H), 1.72–1.21 (m, 26H), 0.93–0.83 (m, 3H). **^{13}C NMR** (151 MHz, CDCl$_3$, ppm): δ = 166.5, 130.62, 130.59, 128.77, 128.75, 71.5, 68.68, 68.65, 64.8, 64.7, 61.90, 61.87, 61.1, 57.1, 57.0, 55.1, 55.0, 34.58, 34.55, 33.7, 33.6, 32.0, 31.9, 31.78, 31.75, 31.7, 29.82, 29.75, 29.7, 29.6, 29.52, 29.49, 29.41, 29.38, 29.33, 29.30, 29.26, 28.73, 28.70, 26.2, 26.1, 26.03, 25.95, 25.5, 25.43, 25.39, 22.80, 22.76, 14.24, 14.21.

8-(5-(1-Hydroxyoctyl)-2-oxo-1,3-dioxolan-4-yl)octyl acrylate and regioisomers (OAcr-CC)
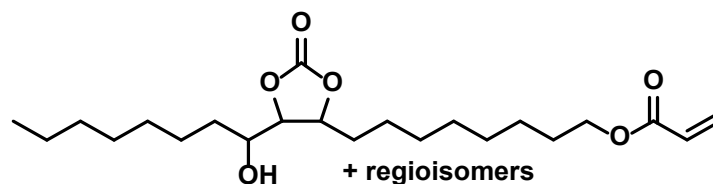
Following GP5, crude OAcr-EpAlc (1.2 mmol) was used as starting material. After flash chromatography on silica with pentane/ethyl acetate as eluent, O-CC was obtained as yellow oil (0.42 g, 88 % yield).

^{1}H NMR (300 MHz, CDCl$_3$, ppm): δ = 6.33 (d, *J* = 17.3 Hz, 1H), 6.05 (dd, *J* = 17.3, 10.4 Hz, 1H), 5.75 (d, *J* = 10.4 Hz, 1H), 4.62–4.56 (m, 1H), 4.10–4.02 (m, 3H), 3.82–3.76 (m, 1H), 2.55–2.54 (m, 1H), 1.62–1.21 (m, 26H), 0.83–0.79 (m, 3H). **^{13}C NMR** (101 MHz, CDCl$_3$, ppm): δ = 166.5, 155.0, 130.7, 128.7, 83.6, 78.0, 70.8, 64.7, 35.0, 32.1, 31.8, 29.5, 29.3, 29.2, 29.1, 29.0, 28.7, 25.9, 25.4, 24.6, 22.7, 14.2.

Reaction sequence for trimethylene glycol dioleate (DO)

Propane-1,3-diyl (10-*trans*,10'-*trans*)-bis(9-hydroperoxyoctadec-10-enoate) and isomers (DO-HYP)
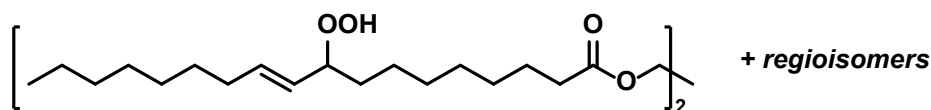
Trimethylene glycol dioleate (1.8 g, 3.0 mmol) was reacted according to GP2 in dichloromethane. ^{1}H NMR analysis showed quantitative conversion to DO-HYP. The reaction solution was used in the following step without further purification.

^{1}H NMR (300 MHz, CDCl$_3$, ppm): δ = 7.82 (d, J = 29.6 Hz, 1H), 5.76 (dq, J = 15.5, 6.5 Hz, 1H), 5.36 (dd, J = 15.5, 8.2 Hz, 1H), 4.26 (dt, J = 7.3, 6.8 Hz, 2H), 4.15 (t, J = 6.3 Hz, 4 H), 2.30 (td, J = 7.5, 2.1 Hz, 4H), 2.13–1.91 (m, 4H), 1.68–1.55 (m, 4H), 1.47–1.17 (m, 40H), 0.93–0.82 (m, 6H). **^{13}C NMR** (151 MHz, CDCl$_3$, ppm): δ = 174.00, 173.99, 137.3, 136.8, 129.0, 128.6, 87.2, 87.1, 61.0, 34.4, 34.3, 32.61, 32.57, 32.5, 32.3, 32.00, 31.96, 29.8, 29.7, 29.6, 29.42, 29.37, 29.27, 29.26, 29.20, 29.19, 29.1, 29.0, 28.9, 28.8, 28.1, 25.5, 25.4, 25.01, 24.97, 22.80, 22.79, 14.3.

Propane-1,2-diyl bis(9-(3-heptyloxiran-2-yl)-9-hydroxynonanoate) and regioisomers
(**DO-EpAlc**)
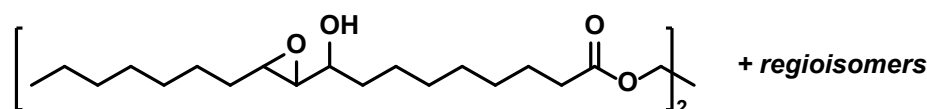
Following GP4, a crude solution of DO-HYP (3.0 mmol) in dichloromethane was treated with VO(acac)$_2$ (8.0 mg). ^{1}H NMR analysis showed quantitative conversion to O-EpAlc. A mixture of diastereomeric products (*syn/anti: 8/7*) can be observed in the NMR spectra.

^{1}H NMR (300 MHz, CDCl$_3$, ppm): δ = 4.12 (t, J = 6.3 Hz, 4H), 3.79–3.69 (m, 1H, *syn*), 3.47–3.36 (m, 1H, *anti*), 3.02–2.92 (m, 1H, *syn*), 2.89–2.83 (m, 1H, *anti*), 2.75–2.67 (m, 2H), 2.28 (t, J = 7.4 Hz, 4H,), 1.94 (p, J = 6.3 Hz, 2H), 1.66 – 1.18 (m, 48H), 0.86 (t, J = 6.7 Hz, 6H). **^{13}C NMR** (151 MHz, CDCl$_3$, ppm): δ = 173.8, 173.8, 71.44, 71.37, 68.8, 68.7, 62.0, 61.9, 61.1, 61.0, 57.1, 57.0, 55.2, 55.1, 34.5, 34.4, 34.3, 34.2, 33.7, 33.6, 32.0, 31.8, 31.7, 31.71, 31.65, 31.6, 29.8, 29.73, 29.70, 29.66, 29.6, 29.53, 29.48, 29.46, 29.4, 29.34, 29.29, 29.27, 29.2, 29.12, 29.07, 28.1, 26.1, 26.0, 25.94, 25.87, 25.4, 25.34, 25.32, 25.0, 24.9, 22.74, 22.71, 14.19, 14.17.

DO-CC
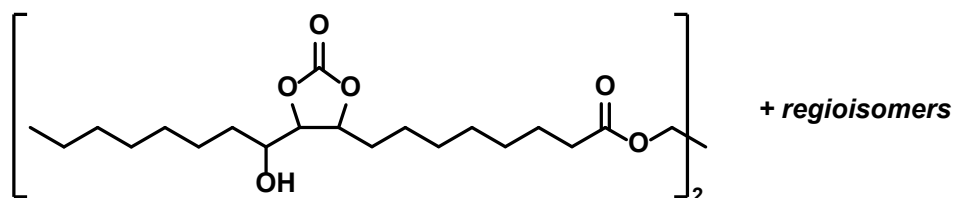
Following GP5, crude DO-EpAlc (1.8 mmol) was used as starting material. After flash chromatography on silica with pentane/ethyl acetate as eluent, O-CC was obtained as yellow oil (1.2 g, 87 % yield).

^{1}H NMR (300 MHz, CDCl$_3$, ppm): δ = 4.60–4.57 (m, 2H), 4.09–4.07 (m, 4H), 4.04–4.02 (m, 2H), 2.27–2.21 (m, 4H), 1.92–1.89 (m, 2H), 1.62–1.56 (m, 8H), 1.33–1.18 (m, 2H), 0.82–0.80 (m, 6H). **^{13}C NMR** (101 MHz, CDCl$_3$, ppm): δ = 173.9, 155.0, 153.2, 83.5, 78.1, 70.8, 60.4, 35.1, 35.0, 34.4,

34.3, 33.9, 32.1, 32.0, 31.91, 31.85, 31.8, 29.81, 29.77, 29.7, 29.6, 29.5, 29.4, 29.3, 29.2, 29.0, 28.8, 28.1, 25.4, 25.2, 25.1, 24.90, 24.85, 24.7, 24.6, 22.80, 22.76, 22.7, 14.2.

Reaction sequence for triolein (TO)
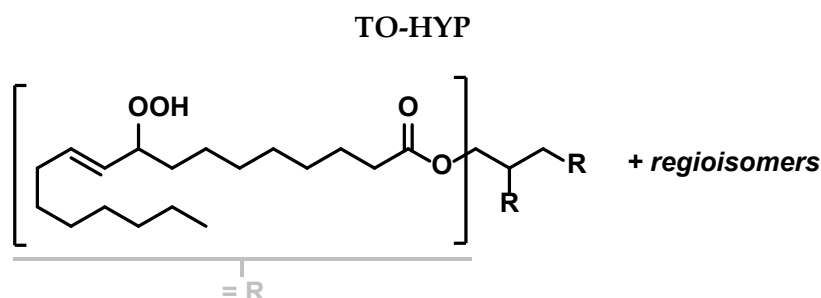
TO-HYP

Triolein (2.7 g, 3.0 mmol) was reacted according to GP1. ^{1}H NMR analysis showed quantitative conversion to TO-HYP. The reaction mixture was used in the following step without further purification.

^{1}H NMR (300 MHz, CDCl$_3$, ppm): δ = 7.85–7.71 (m, 3H), 5.75–5.63 (m, 3H), 5.30 (dd, J = 15.5, 8.1 Hz, 3H), 5.22–5.16 (m, 1H), 4.27–4.15 (m, 3H), 4.11–4.03 (m, 2H), 2.25 (t, J = 7.4 Hz, 1H), 2.05–1.95 (m, 5H), 1.61–1.46 (m, 10H), 1.36–1.14 (m, 57H), 0.81 (t, J = 6.5 Hz, 1H).
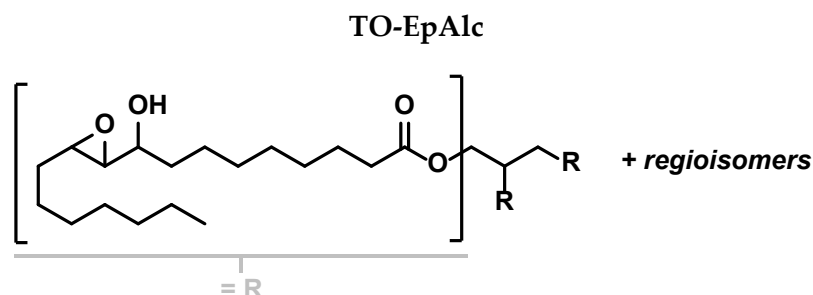
TO-EpAlc

Following GP3, crude TO-HYP (3.0 mmol) was treated with VO(acac)$_2$ (24 mg). ^{1}H NMR analysis showed quantitative conversion to TO-EpAlc. A mixture of diastereomeric products (*syn/anti: 4/5*) can be observed in the NMR spectra.

^{1}H NMR (300 MHz, CDCl$_3$, ppm): δ = 5.26–5.22 (m, 1H), 4.29–4.26 (m, 2H), 4.14–4.11 (m, 2H), 3.75–3.73+3.43–3.41 (m, 3H), 2.98–2.87 (m, 3H), 2.74–2.70 (m, 3H), 2.34–2.24 (m, 6H), 1.60–1.23 (m, 75H), 0.87–0.85 (m, 3H). **^{13}C NMR** (151 MHz, CDCl$_3$, ppm): δ = 173.7, 173.2, 71.7, 69.3, 69.1, 61.4, 57.4, 57.3, 55.4, 34.8, 34.6, 34.5, 34.4, 34.3, 34.0, 33.9, 32.31, 32.25, 32.23, 32.19, 32.15, 32.03, 32.01, 31.95, 30.09, 30.07, 30.01, 29.96, 29.90, 29.87, 29.77, 29.75, 29.64, 29.60, 29.58, 29.5, 29.4, 29.3, 26.42, 26.35, 26.2, 25.7, 25.2, 23.1, 23.0, 14.5.

TO-CC
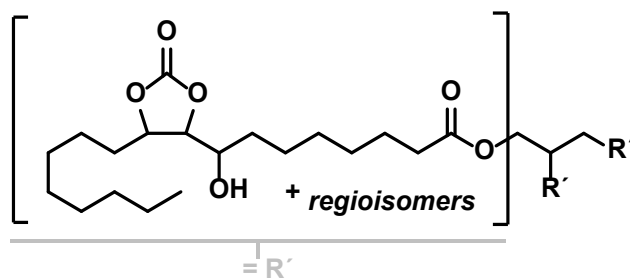
Following GP5, crude TO-EpAlc (2.4 mmol) was used as starting material. After flash chromatography on silica with pentane/ethyl acetate as eluent, O-CC was obtained as orange oil (2.2 g, 83 % yield).

¹H NMR (300 MHz, CDCl₃, ppm): δ = 5.29–5.23 (m, 1H), 4.72–3.58 (m, 12H), 2.35–2.28 (m, 6H), 1.73–1.24 (m, 76H), 0.88–0.85 (m, 9H). **¹³C NMR** (151 MHz, CDCl₃, ppm): δ = 173.3, 172.8, 154.6, 83.6, 83.4, 80.5, 78.8, 78.6, 78.1, 70.7, 70.4, 68.9, 68.6, 62.1, 34.94, 34.86, 34.2, 34.1, 34.0, 32.9, 32.0, 31.9, 31.8, 31.74, 31.66, 29.70, 29.66, 29.5, 29.4, 29.3, 29.2, 29.0, 28.9, 28.8, 25.7, 25.5, 25.3, 24.7, 24.6, 24.54, 24.48, 22.7, 22.6, 14.1.

6.4.6 NIPU formation

TO-CC (0.15 g, 0.13 mmol), hexamethylenediamine (0.019 g, 0.16 mmol) and DABCO (1.0 mg, 8.9 µmol) were dissolved in dichloromethane (3 mL) under vigorous stirring. The solution was poured into an aluminum pan and the solvent was slowly evaporated. Afterwards, the film was cured for 12 hours at 90 °C. The obtained orange NIPU-film was characterized by TGA (Figure 6.2), IR spectroscopy (Figure 6.4), and DSC (Figure 6.5).
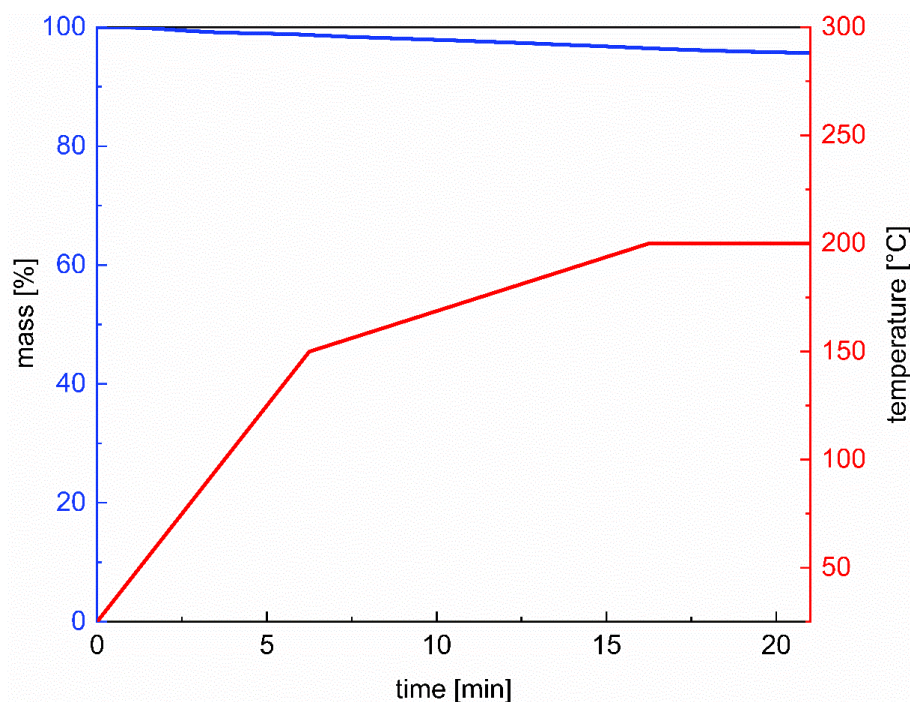
Figure 6.2. TGA of NIPU film.
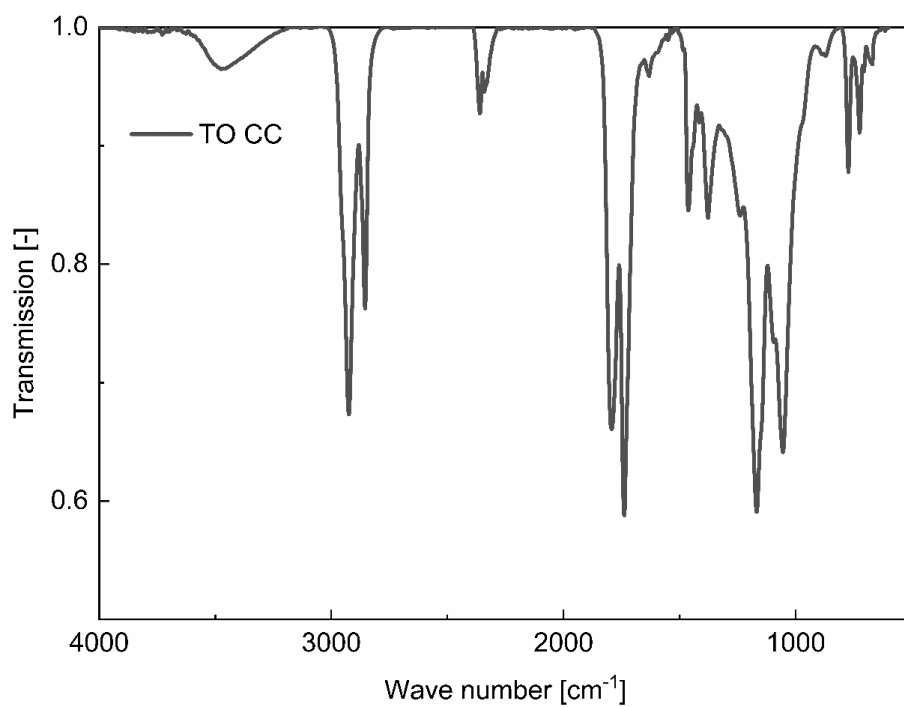
Figure 6.3. IR spectrum of monomer TO-CC.
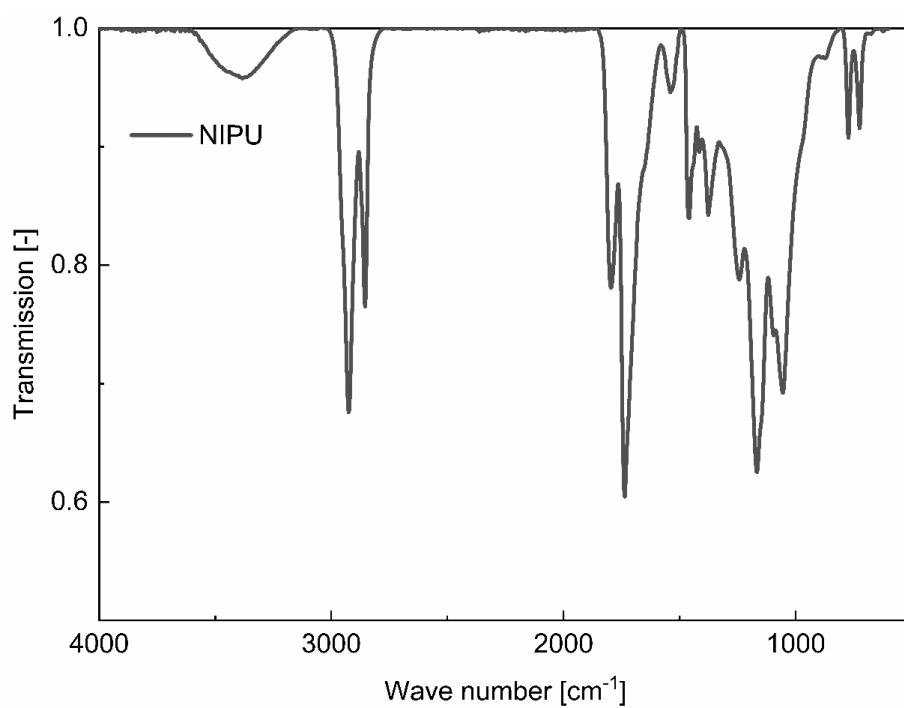
Figure 6.4. IR spectrum of NIPU film.
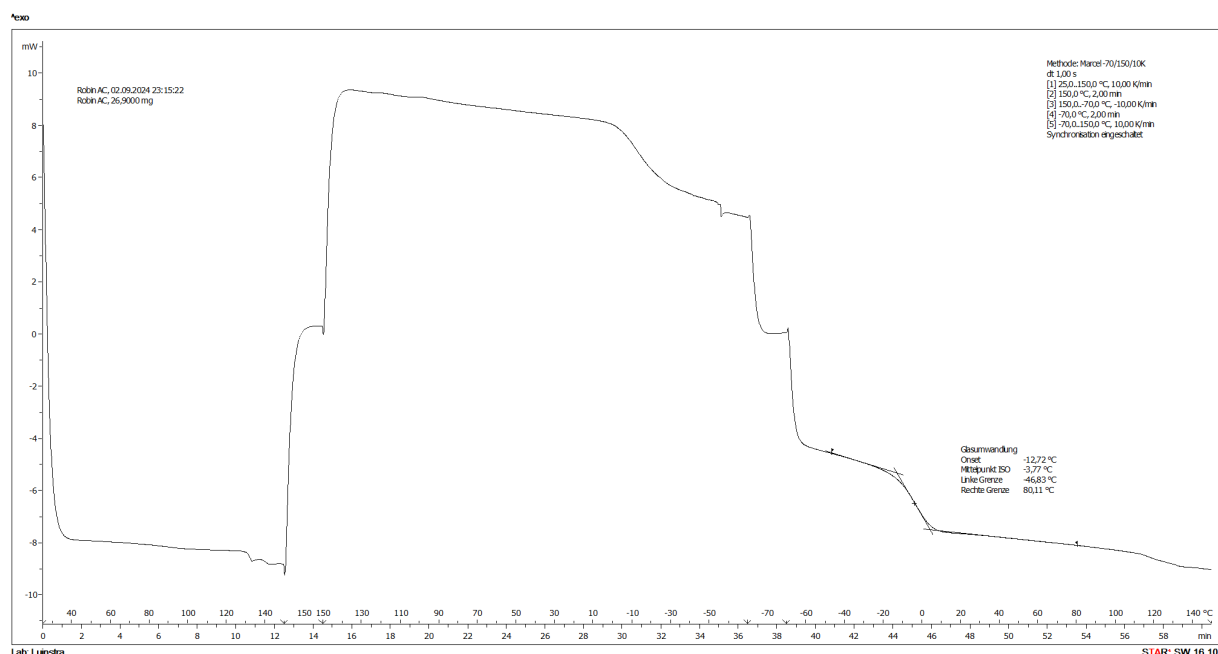
Figure 6.5. DSC measurement of NIPU film.

6.5   References

[1]   P. Rollin, L. K. Soares, A. M. Barcellos, D. R. Araujo, E. J. Lenardão, R. G. Jacob, G. Perin, *Appl. Sci.* **2021**, *11*, 5024.

[2]   L. Zuo, T. Liu, X. Chang, W. Guo, *Molecules* **2019**, *24*, 3930.

[3]   C. Ngassam Tounzoua, B. Grignard, C. Detrembleur, *Angew. Chem. Int. Ed.* **2022**, *61*, DOI 10.1002/anie.202116066.

[4]   W. Guo, J. E. Gómez, À. Cristòfol, J. Xie, A. W. Kleij, *Angew. Chem. Int. Ed.* **2018**, *57*, 13735–13747.

[5]   N. Yadav, F. Seidi, D. Crespy, V. D'Elia, *ChemSusChem* **2019**, *12*, 724–754.

[6]   F. Mundo, S. Caillol, V. Ladmiral, M. A. R. Meier, *ACS Sustain. Chem. Eng.* **2024**, *12*, 6452–6466.

[7]   P. Anastas, N. Eghbali, *Chem. Soc. Rev.* **2010**, *39*, 301–312.

[8]   M. Cokoja, M. E. Wilhelm, M. H. Anthofer, W. A. Herrmann, F. E. Kühn, *ChemSusChem* **2015**, *8*, 2436–2454.

[9]   J. W. Comerford, I. D. V. Ingram, M. North, X. Wu, *Green Chem.* **2015**, *17*, 1966–1987.

[10]   Z. Li, J. Sun, Q. Xu, J. Yin, *ChemCatChem* **2021**, *13*, 1848–1866.

[11]   B. R. Moser, S. C. Cermak, K. M. Doll, J. A. Kenar, B. K. Sharma, *J. Am. Oil. Chem. Soc.* **2022**, *99*, 801–842.

[12]   Y. Meng, F. Taddeo, A. F. Aguilera, X. Cai, V. Russo, P. Tolvanen, S. Leveneur, *Catalysts* **2021**, *11*, 765.

[13]   P. T. Wai, P. Jiang, Y. Shen, P. Zhang, Q. Gu, Y. Leng, *RSC Adv.* **2019**, *9*, 38119–38136.

[14]   M. C. DeRosa, R. J. Crutchley, *Coord. Chem. Rev.* **2002**, *233–234*, 351–371.

[15]   M. Prein, W. Adam, *Angew. Chem. Int. Ed.* **1996**, *35*, 477–494.

[16]   P. Bayer, A. Jacobi von Wangelin, *Green Chem.* **2020**, *22*, 2359–2364.

[17]   W. Adam, A. Griesbeck, E. Staab, *Angew. Chem. Int. Ed.* **1986**, *25*, 269–270.

[18] M. Unverferth, M. A. R. Meier, *Eur. J. Lipid Sci. Technol.* **2018**, *120*, DOI 10.1002/ejlt.201800015.

[19] J. E. Kim, G. E. Son, H. J. Lim, Y. S. Jang, C. H. Song, C. P. Park, *J. Org. Chem.* **2024**, *89*, 6960–6965.

[20] W. Adam, M. Braun, A. Griesbeck, V. Lucchini, E. Staab, B. Will, *J. Am. Chem. Soc.* **1989**, *111*, 203–212.

[21] J. Rintjema, R. Epping, G. Fiorani, E. Martín, E. C. Escudero-Adán, A. W. Kleij, *Angew. Chem. Int. Ed.* **2016**, *55*, 3972–3976.

[22] C. Maquilón, B. Limburg, V. Laserna, D. Garay-Ruiz, J. González-Fabra, C. Bo, M. Martínez Belmonte, E. C. Escudero-Adán, A. W. Kleij, *Organometallics* **2020**, *39*, 1642–1651.

[23] F. Della Monica, A. Buonerba, A. Grassi, C. Capacchione, S. Milione, *ChemSusChem* **2016**, *9*, 3457–3464.

[24] W. H. Foo, S. S. N. Koay, S. R. Chia, W. Y. Chia, D. Y. Y. Tang, S. Nomanbhay, K. W. Chew, *Fuel* **2022**, *324*, DOI 10.1016/j.fuel.2022.124539.

[25] A. Mannu, S. Garroni, J. Ibanez Porras, A. Mele, *Processes* **2020**, *8*, 366, DOI 10.3390/pr8030366.

[26] N. Tenhumberg, H. Büttner, B. Schäffner, D. Kruse, M. Blumenstein, T. Werner, *Green Chem.* **2016**, *18*, 3775–3788.

[27] L. Maisonneuve, A. S. More, S. Foltran, C. Alfos, F. Robert, Y. Landais, T. Tassaing, E. Grau, H. Cramail, *RSC Adv.* **2014**, *4*, 25795–25803.

[28] N. Narra, B. N. Prasad Rachapudi, S. Phani Babu Vemulapalli, P. V. Korlipara, *RSC Adv.* **2016**, *6*, 25703–25712.

[29] C. Carré, Y. Ecochard, S. Caillol, L. Avérous, *ChemSusChem* **2019**, *12*, 3410–3430.

[30] J. Schachtner, P. Bayer, A. Jacobi von Wangelin, *Beilstein J. Org. Chem.* **2016**, *12*, 1798–1811.

[31] R. Stuhr, P. Bayer, C. B. W. Stark, A. Jacobi von Wangelin, *ChemSusChem* **2021**, *14*, 3325–3332.

[32] C. A. Hone, C. O. Kappe, *Chemistry–Methods* **2021**, *1*, 454–467.

[33] E. S. Shanley, *J. Chem. Educ.* **1990**, *67*, A41.

[34] C. M. McCloskey, *Plant/operations progress* **1989**, *8*, 185–188.

[35] K. Allison, P. Johnson, G. Foster, M. B. Sparke, *Ind. Eng. Chem. Prod. Res. Dev.* **1966**, *5*, 166–173.

[36] A. O. Chong, K. B. Sharpless, *J. Org. Chem* **1977**, *42*, 1587–1590.

[37] J. Ferraz-Caetano, F. Teixeira, M. N. D. S. Cordeiro, *Int. J. Mol. Sci.* **2023**, *24*, 12299, DOI 10.3390/ijms241512299

[38] A. Rehman, F. Saleem, F. Javed, A. Ikhlaq, S. W. Ahmad, A. Harvey, *J. Environ. Chem. Eng.* **2021**, *9*, DOI 10.1016/j.jece.2021.105113.

[39] a) H. Tomita, F. Sanda, T. Endo, *J. Polym. Sci. A. Polym. Chem.* **2001**, *39*, 3678–3685. b) H. Tomita, F. Sanda, T. Endo, *J. Polym. Sci. A. Polym. Chem.* **2001**, *39*, 162–168.

[40] A. Boyer, E. Cloutet, T. Tassaing, B. Gadenne, C. Alfos, H. Cramail, *Green Chem.* **2010**, *12*, 2205–2213.

[41] Y. Fu, Y. Weng, W. X. Hong, Q. Zhang, *Synlett* **2011**, *6*, 809–812.

[42] A. Das, N. Chatani, *Chem. Sci.* **2021**, *12*, 3202–3209.

[43]   H. Sharghi, A. Hassani Nejad, *Tetrahedron* **2004**, 60, 1863–1868.

[44]   M.R. Maurya, V. Prakash, F. Avecilla, M. Sankar, *Eur. J. Inorg. Chem.* **2021**, *17*, 1685–1694.

[45]   P. Fournari, R. Guilard, M. Fontesse, *J. Organomet. Chem.* **1976**, 110, 205–217.

[46]   N. A. Porter, K. A. Mills, S. E. Caldwell, G. R. Dubay, *J. Am. Chem. Soc.* **1994**, 116, 6697–6705.

[47]   N. A. Porter, J. S. Wujek, *J. Org. Chem.* **1987**, 52, 5085–5089.

6.6   Experimental Spectra
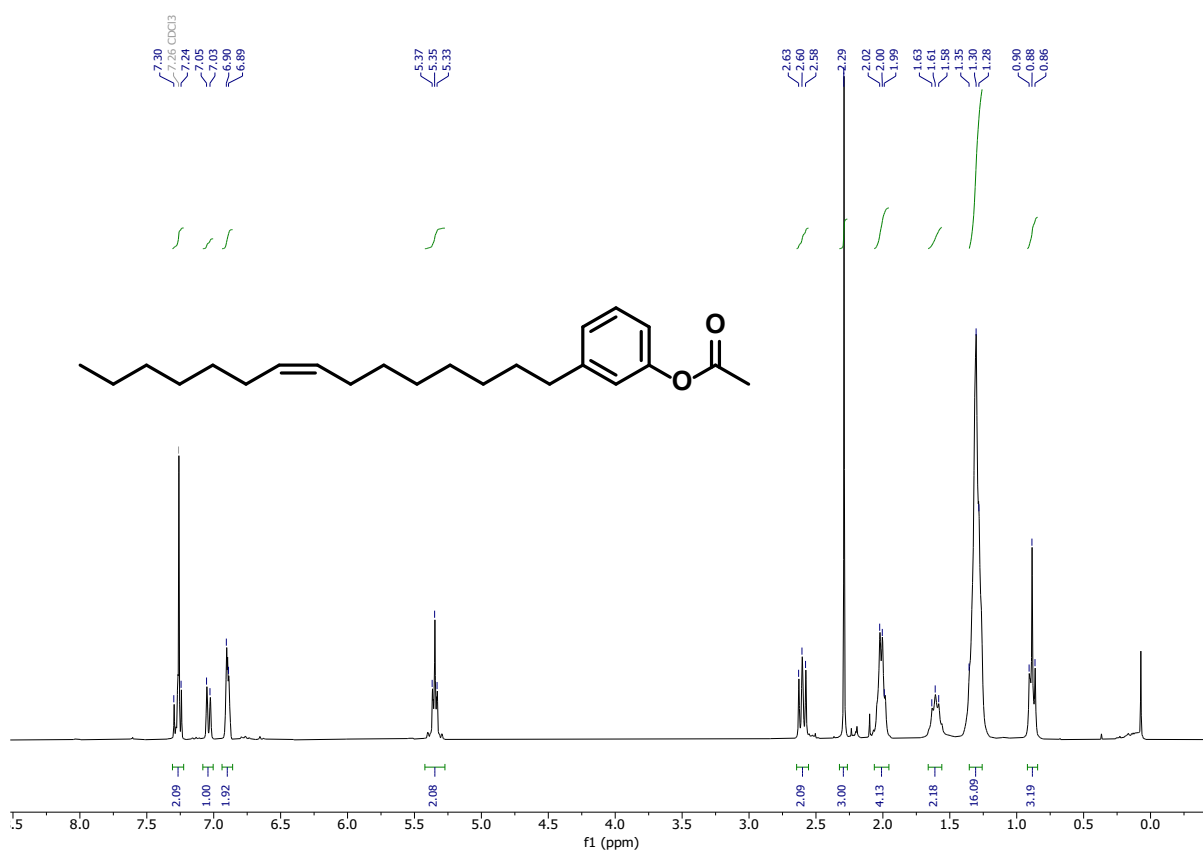
^{1}H NMR (300 MHz, CDCl$_3$) of cardanyl acetate (CA).
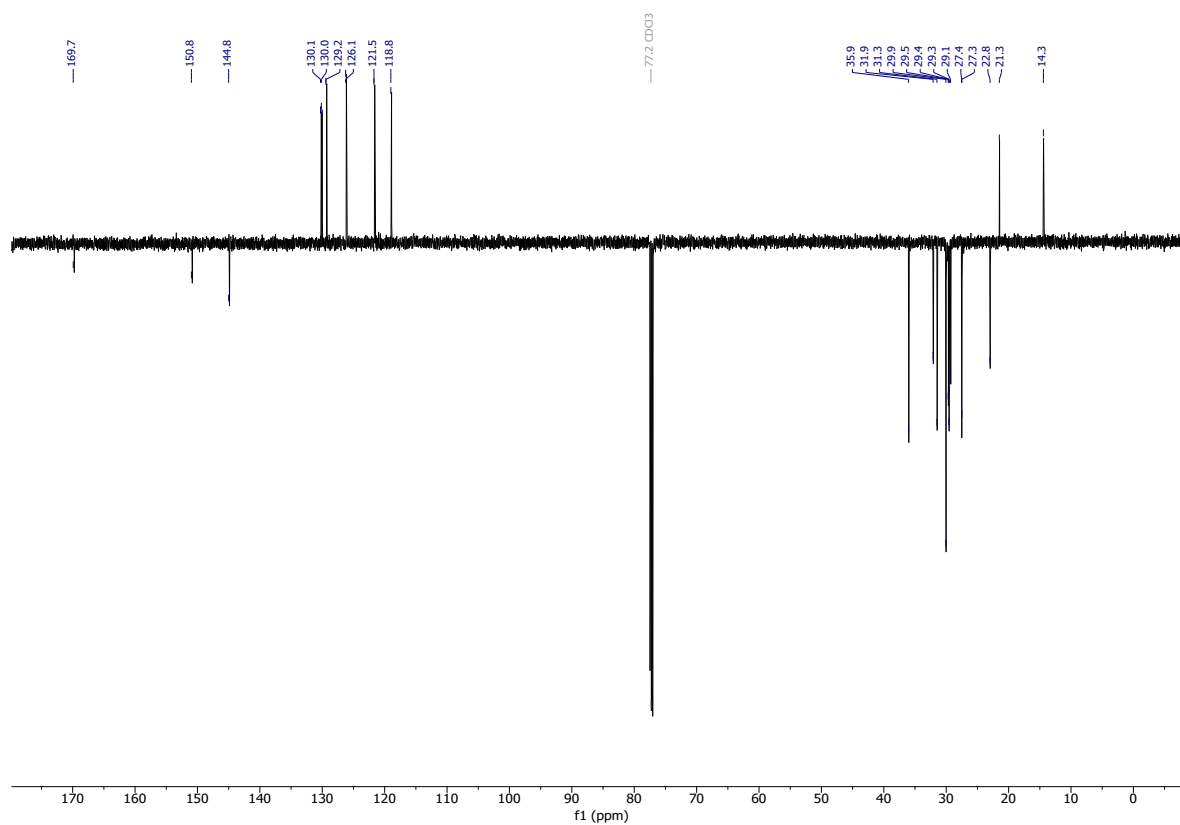
^{13}C NMR (151 MHz, CDCl$_3$) of cardanyl acetate (CA).
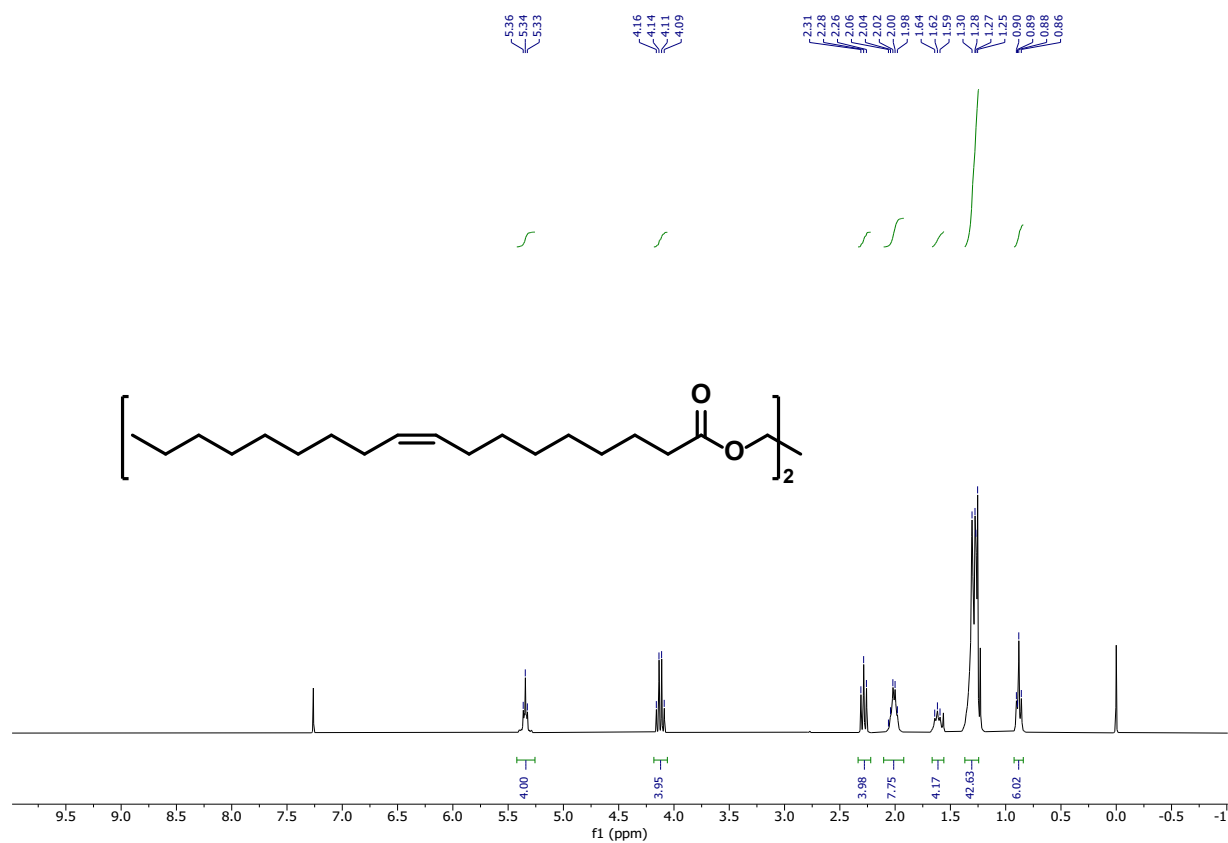
¹H NMR (300 MHz, CDCl₃) of trimethylene glycol dioleate (DO).
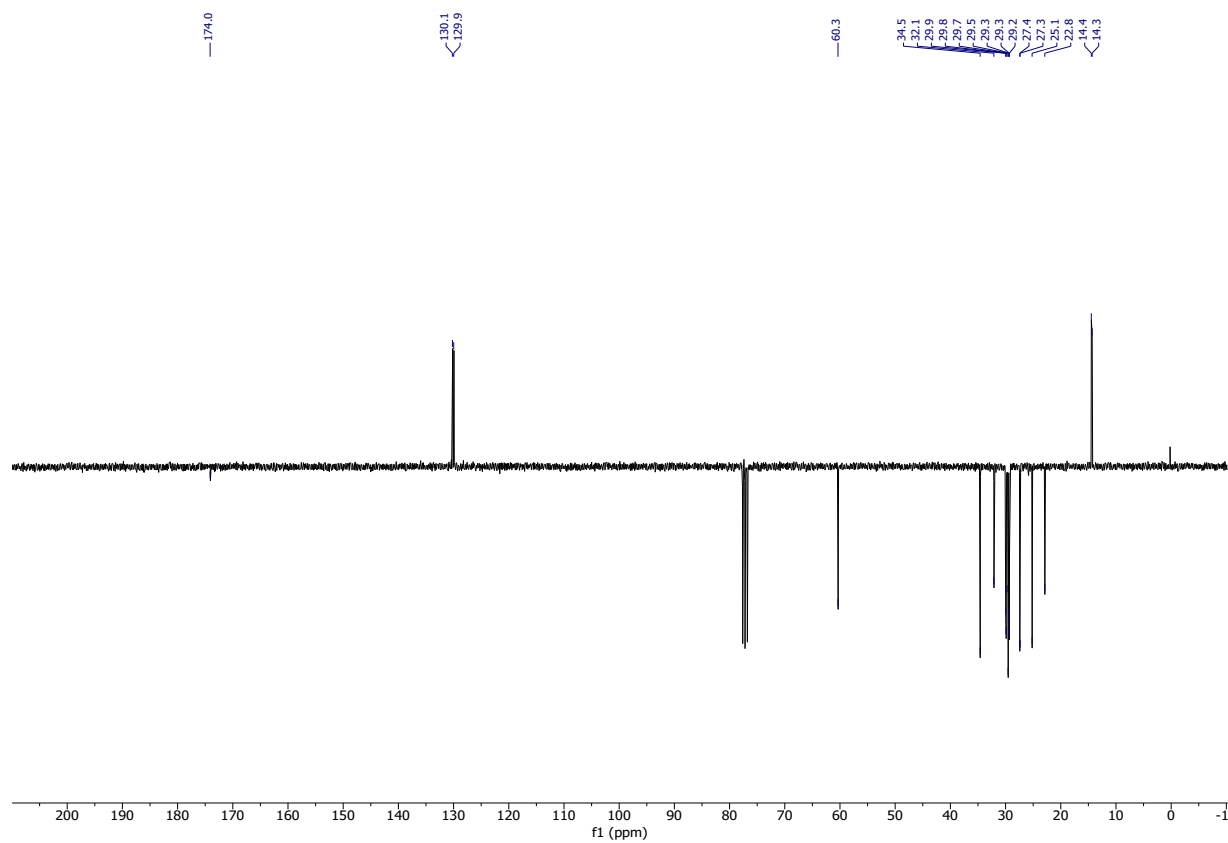
¹³C NMR (75 MHz, CDCl₃) of trimethylene glycol dioleate (DO).
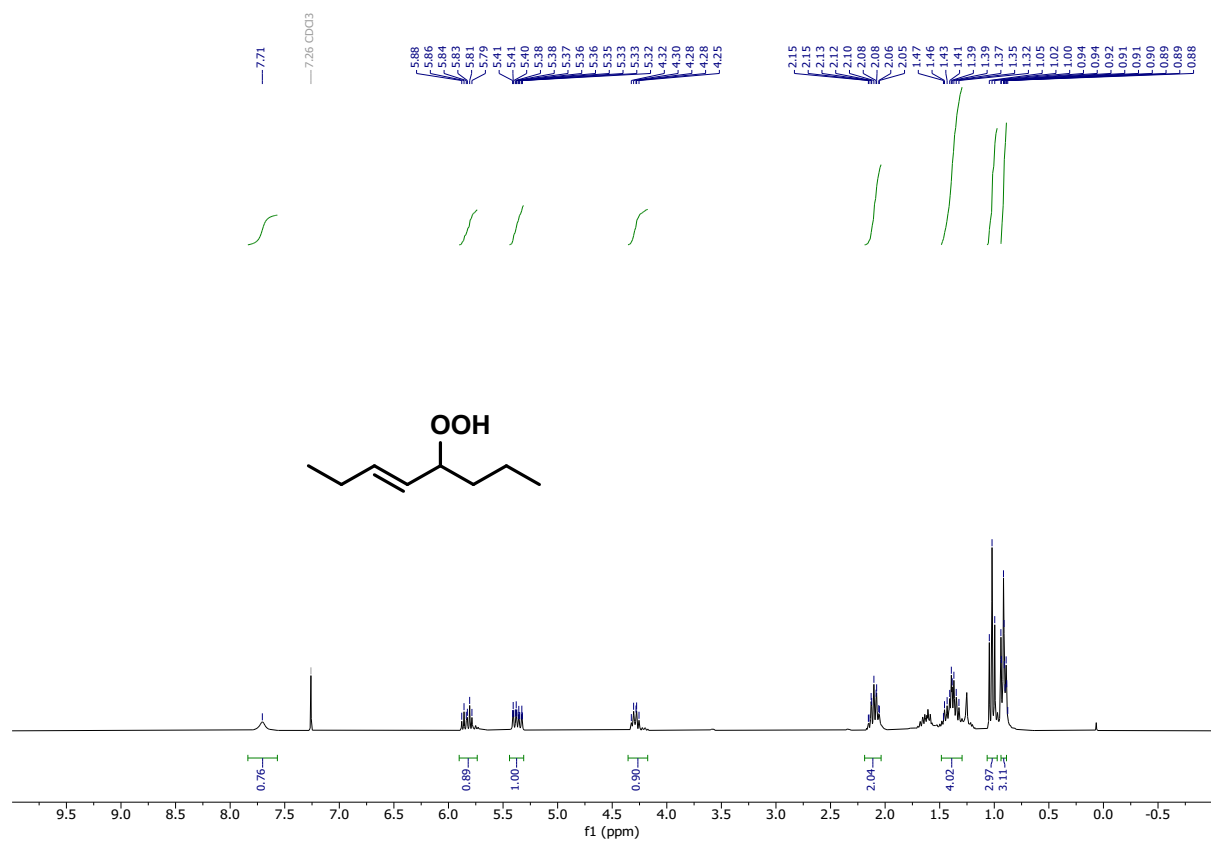
¹H NMR (300 MHz, CDCl₃) of O-HYP.
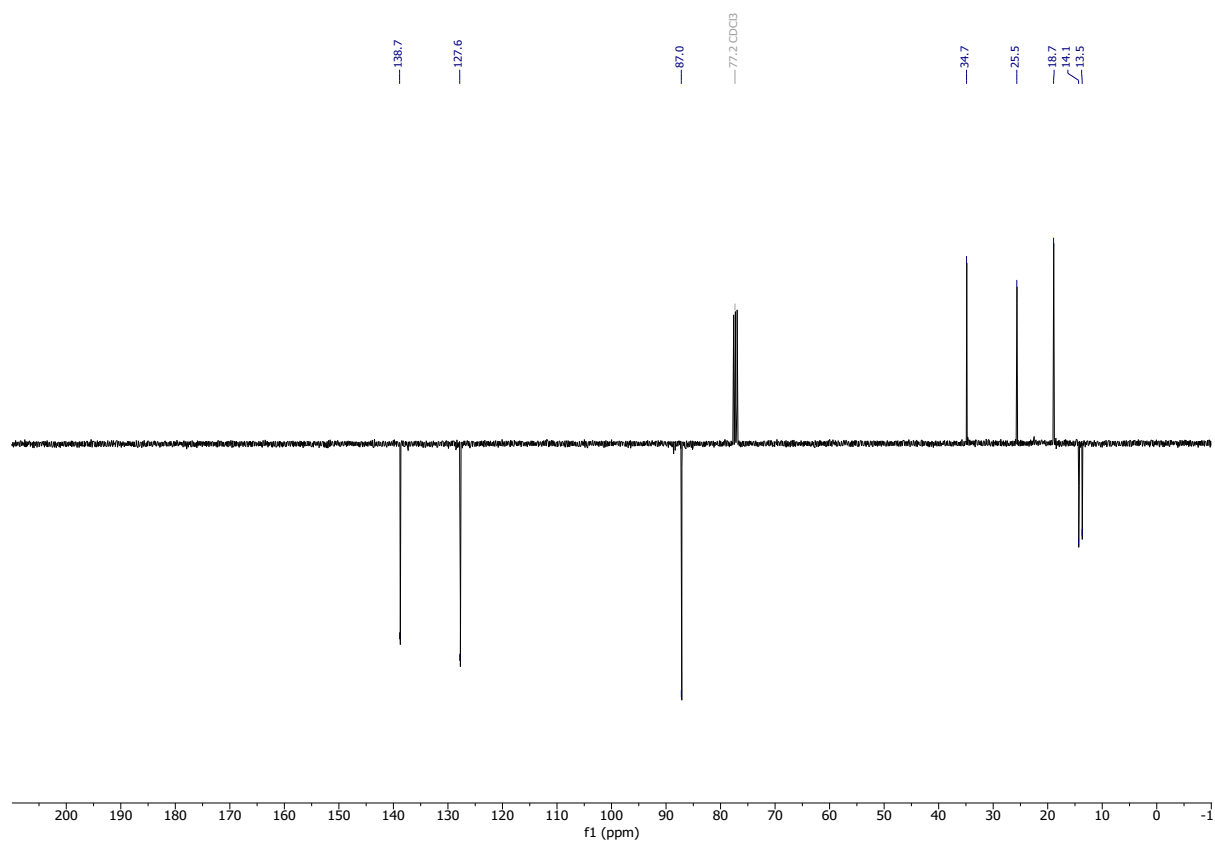
¹³C NMR (100 MHz, CDCl₃) of O-HYP.

^{1}H NMR (300 MHz, CDCl$_3$) of O-EpAlc.

^{13}C NMR (151 MHz, CDCl$_3$) of O-EpAlc.
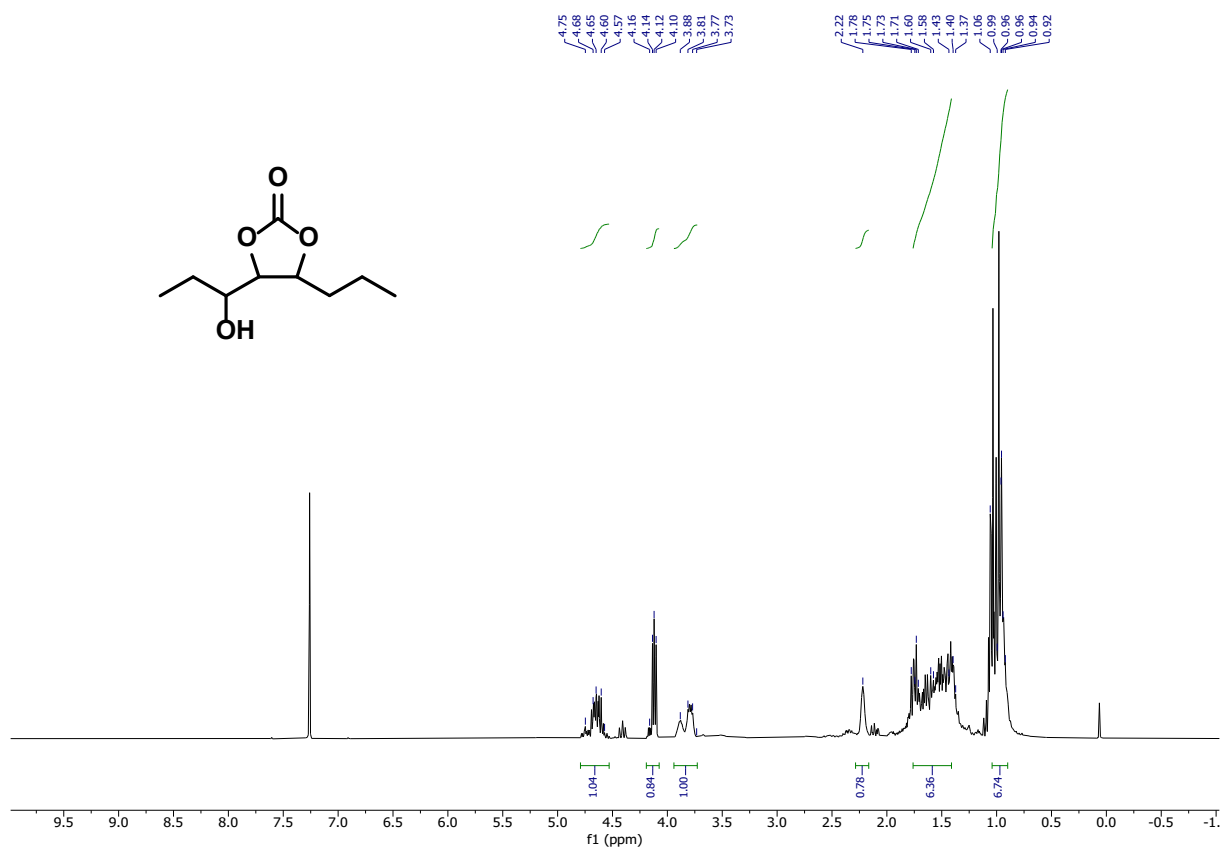
^{1}H NMR (300 MHz, CDCl$_3$) of O-CC.

^{13}C NMR (151 MHz, CDCl$_3$) of O-CC.

^{1}H NMR (300 MHz, CDCl$_3$) of MO-HYP.
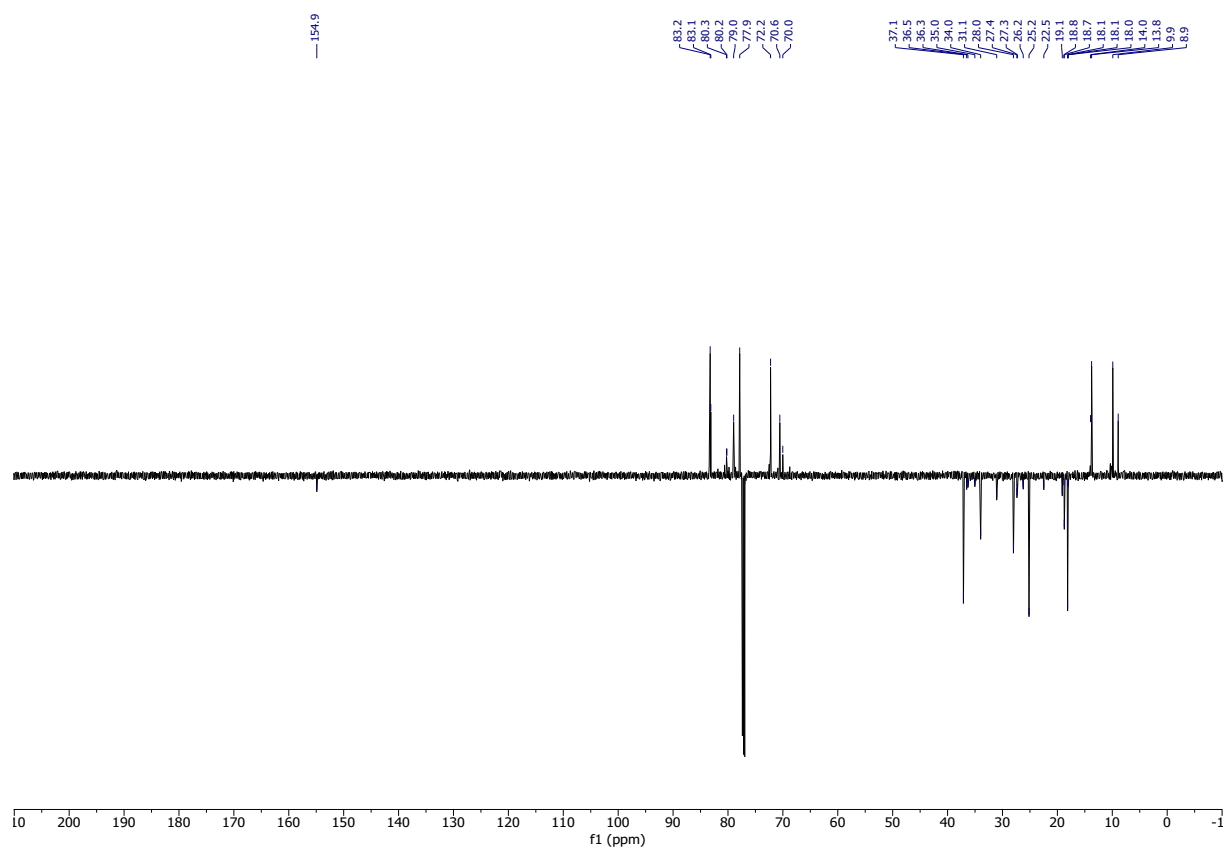
^{13}C NMR (126 MHz, CDCl$_3$) of MO-HYP.
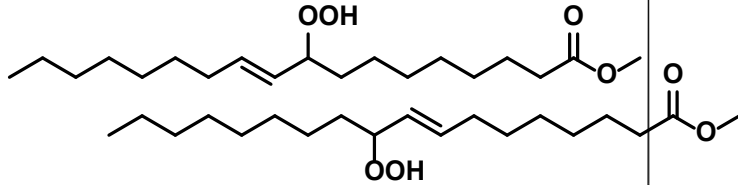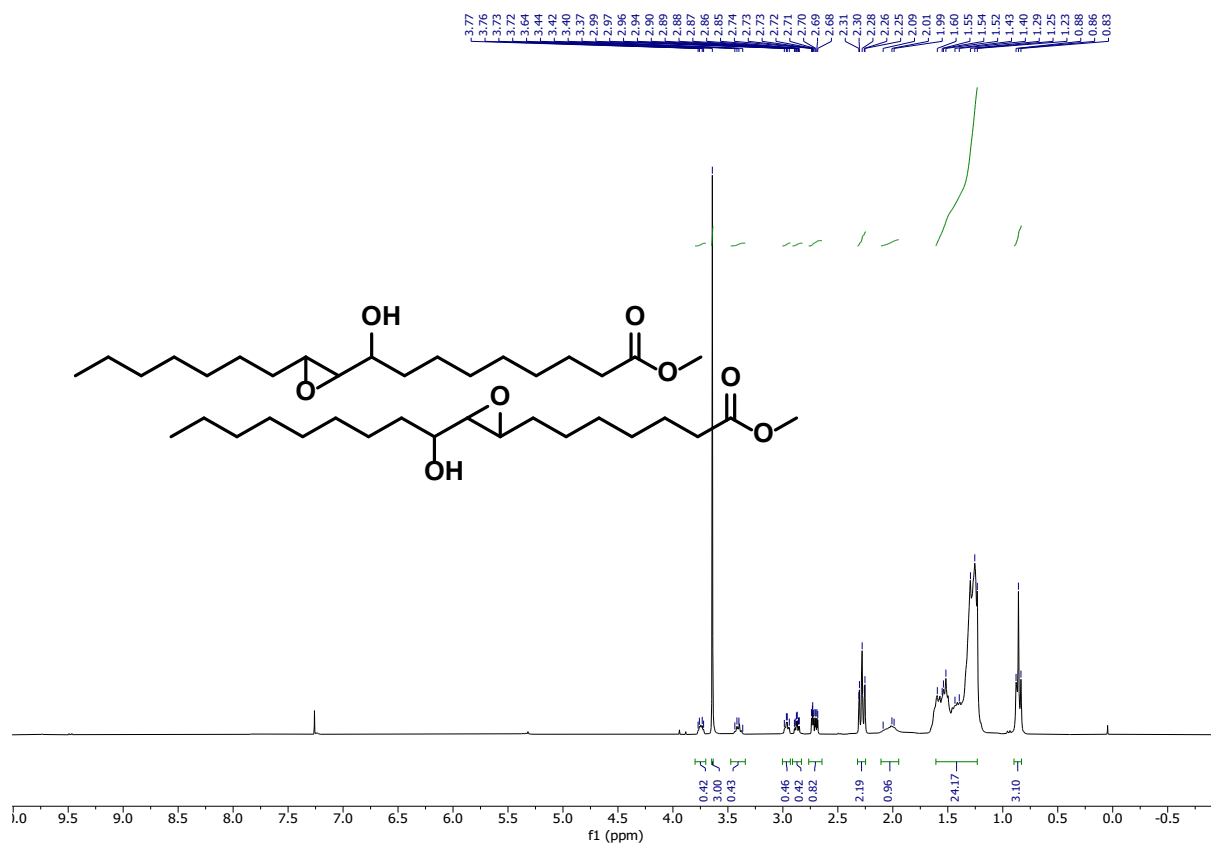
^{1}H NMR (300 MHz, CDCl$_3$) of MO-EpAlc.

^{13}C NMR (126 MHz, CDCl$_3$) of MO-EpAlc.

113

^{1}H NMR (300 MHz, CDCl$_3$) of MO-*syn*-EpAlc.

^{13}C NMR (101 MHz, CDCl$_3$) of MO-*syn*-EpAlc.

114
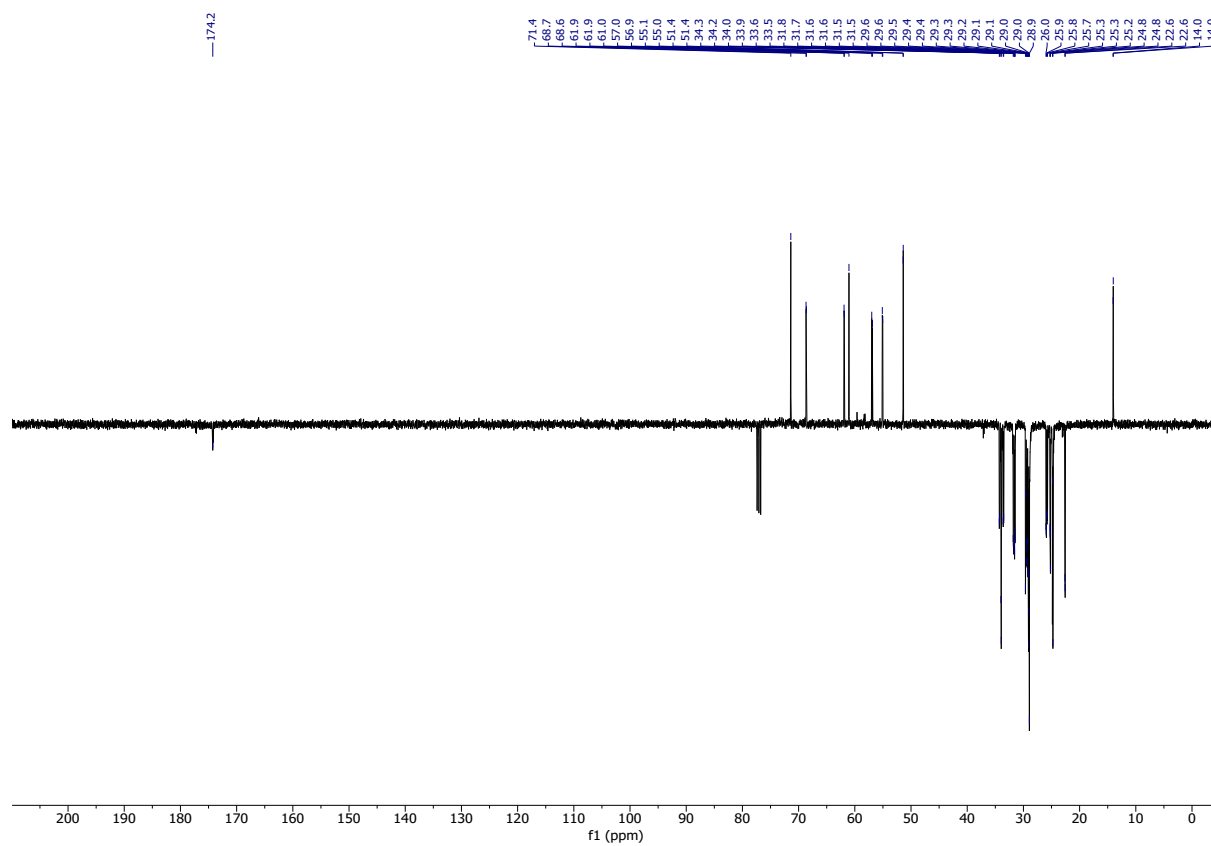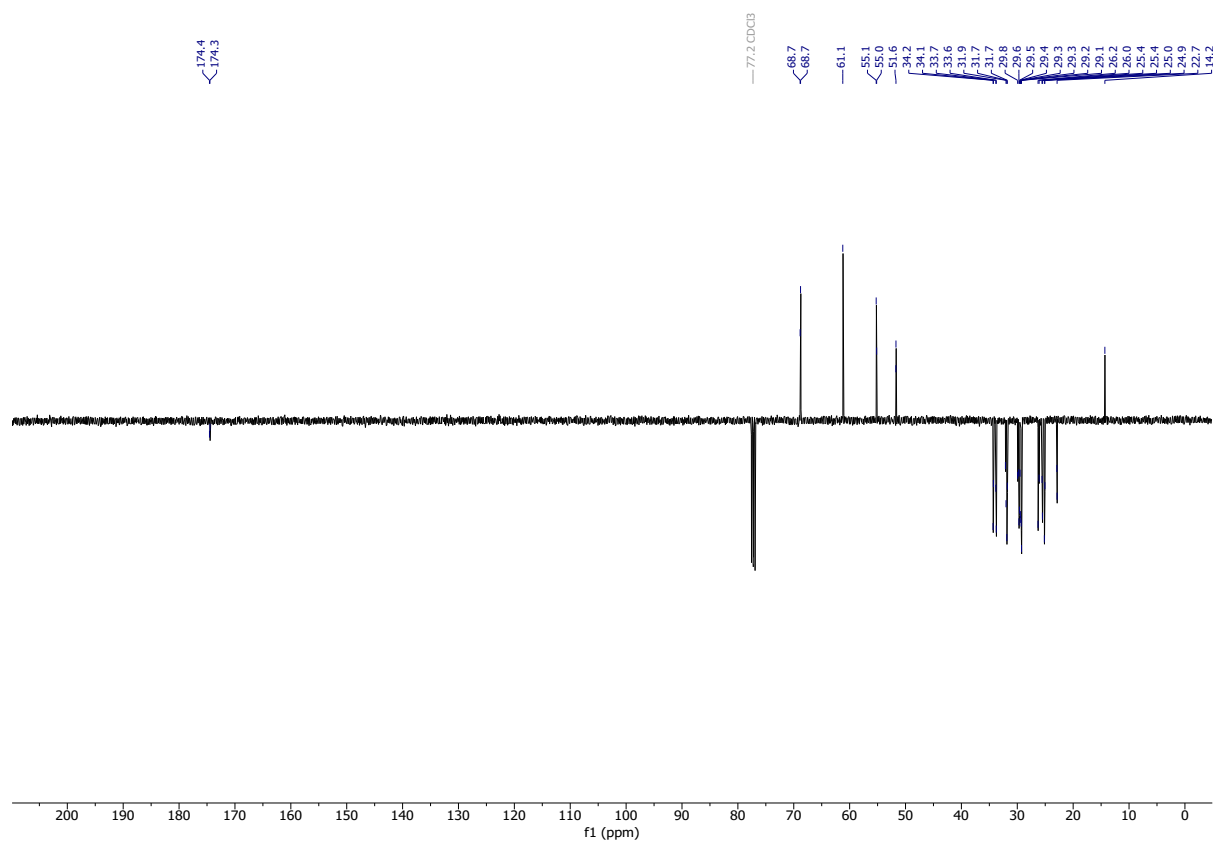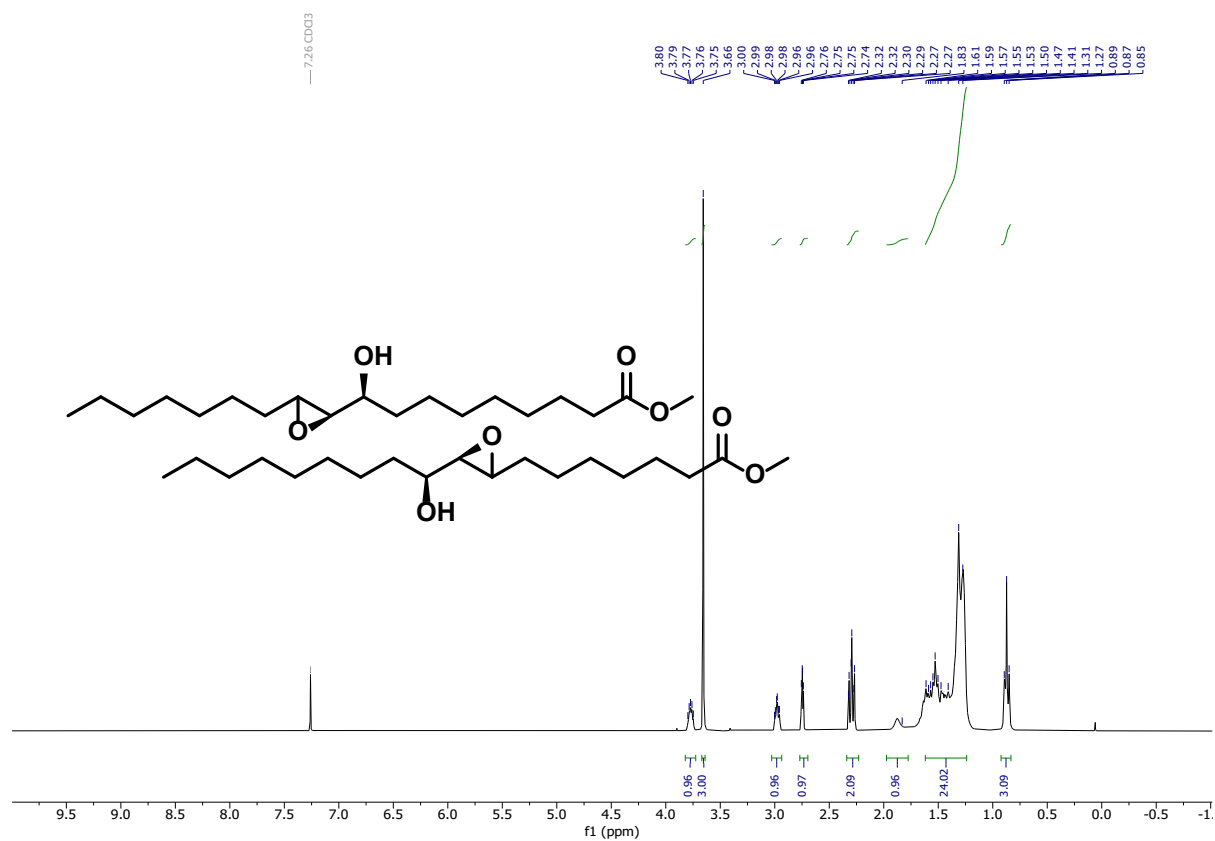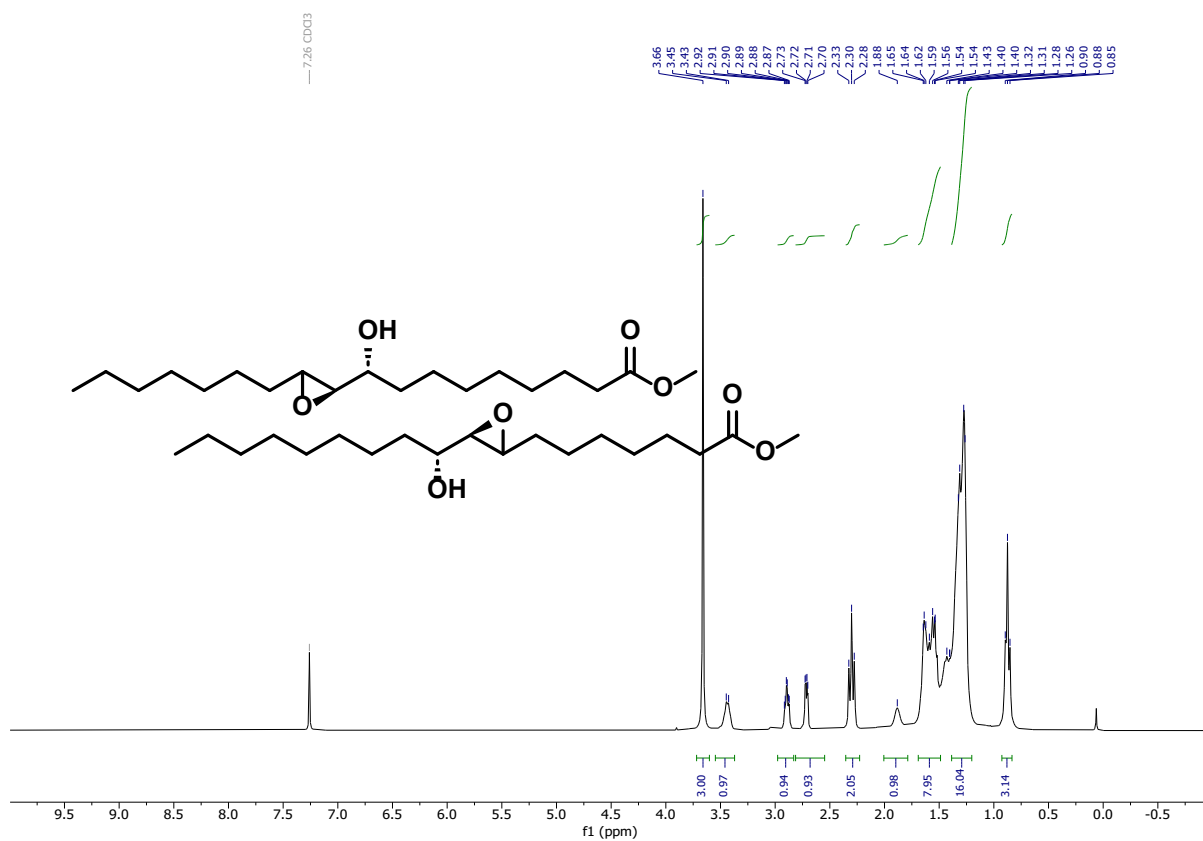
^{1}H NMR (300 MHz, CDCl$_3$) of MO-*anti*-EpAlc.
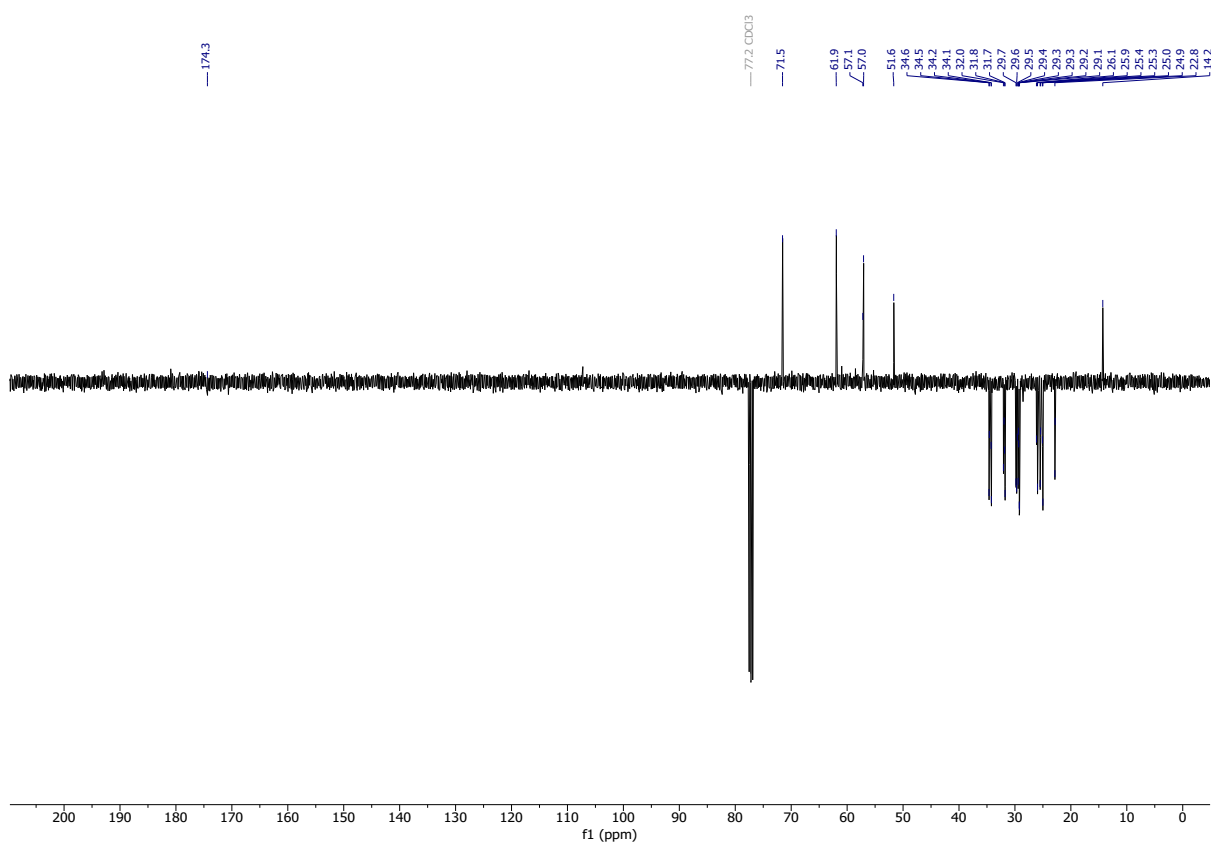
^{13}C NMR (101 MHz, CDCl$_3$) of MO-*anti*-EpAlc.
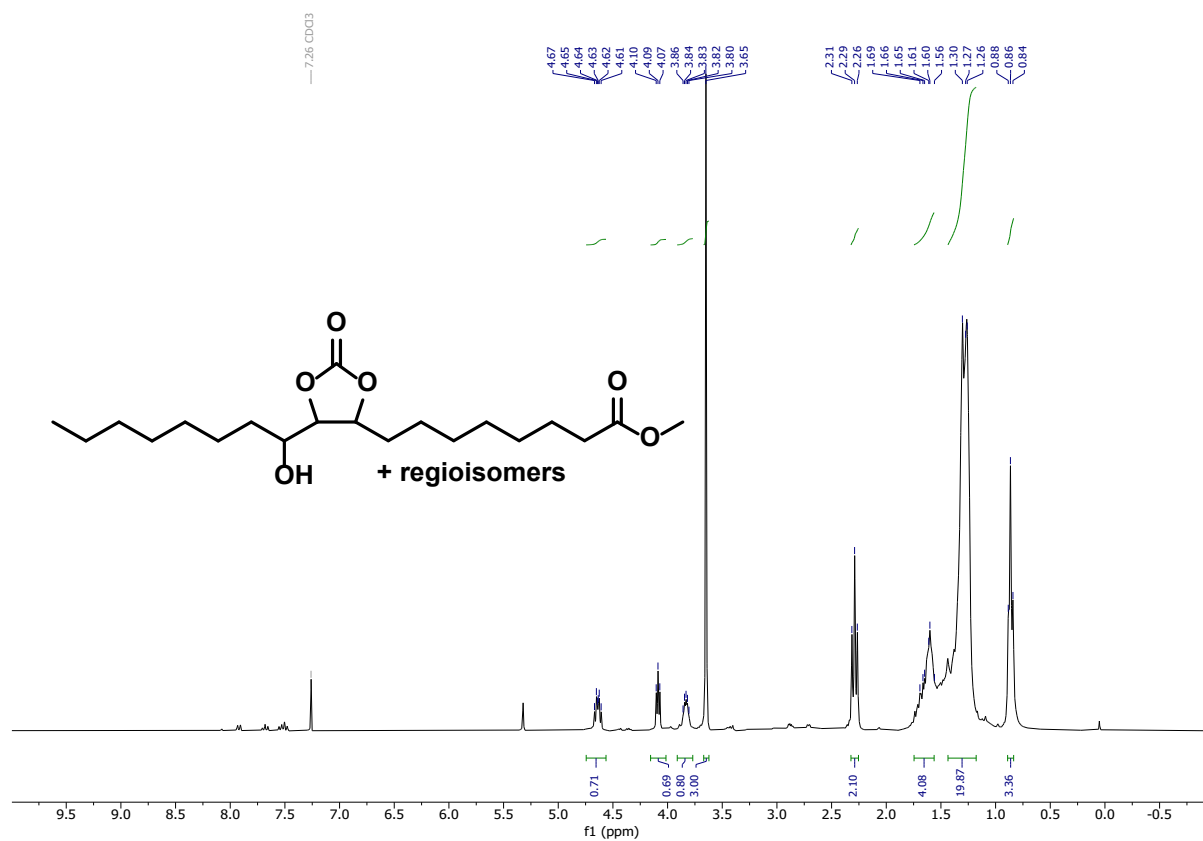
^{1}H NMR (300 MHz, CDCl$_3$) of MO-CC.
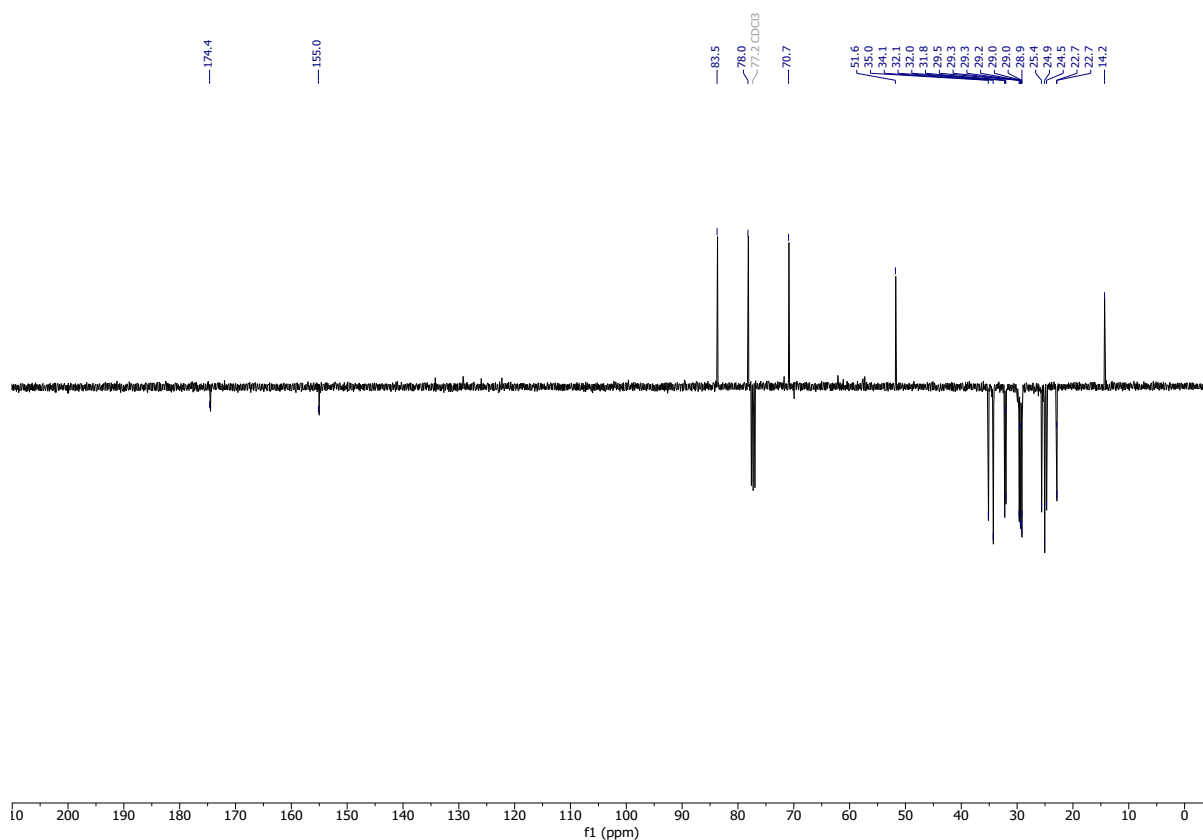
^{13}C NMR (101 MHz, CDCl$_3$) of MO-CC.
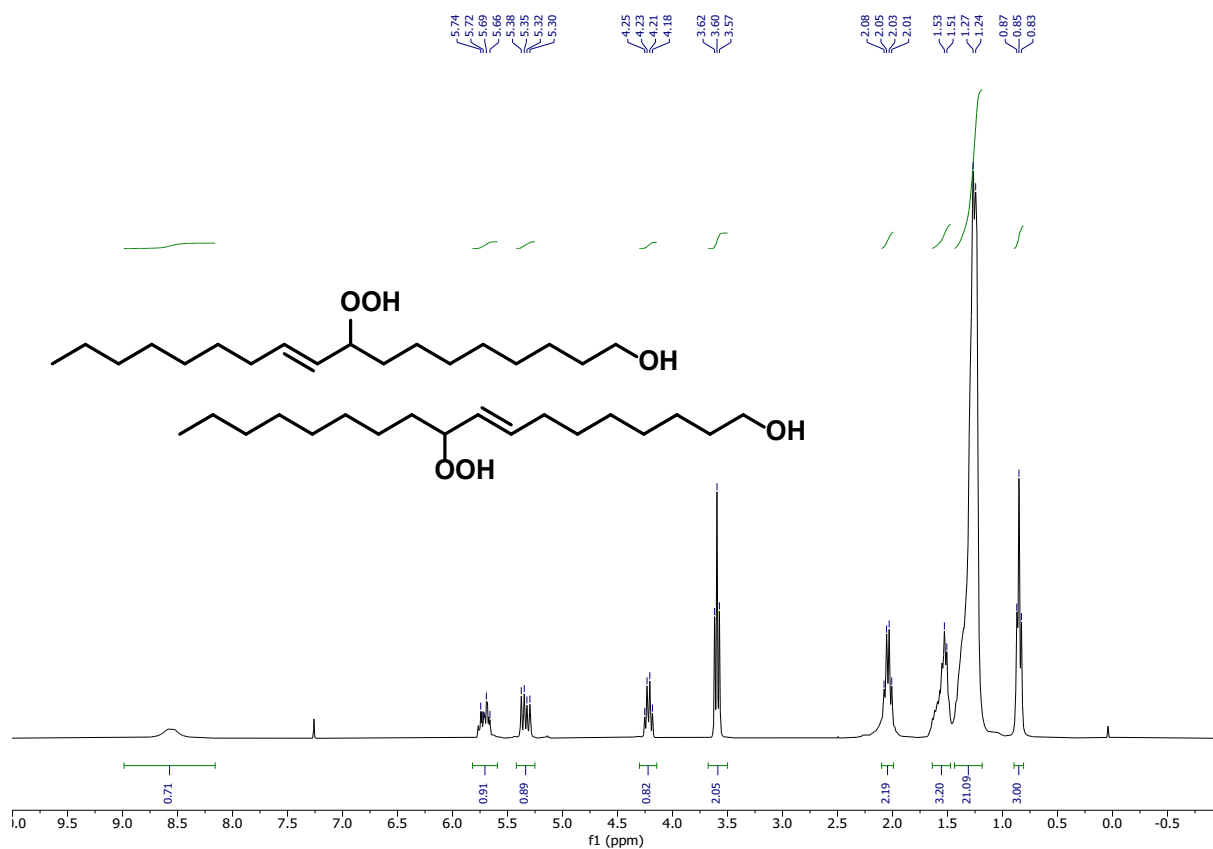
¹H NMR (300 MHz, CDCl₃) of OA-HYP.
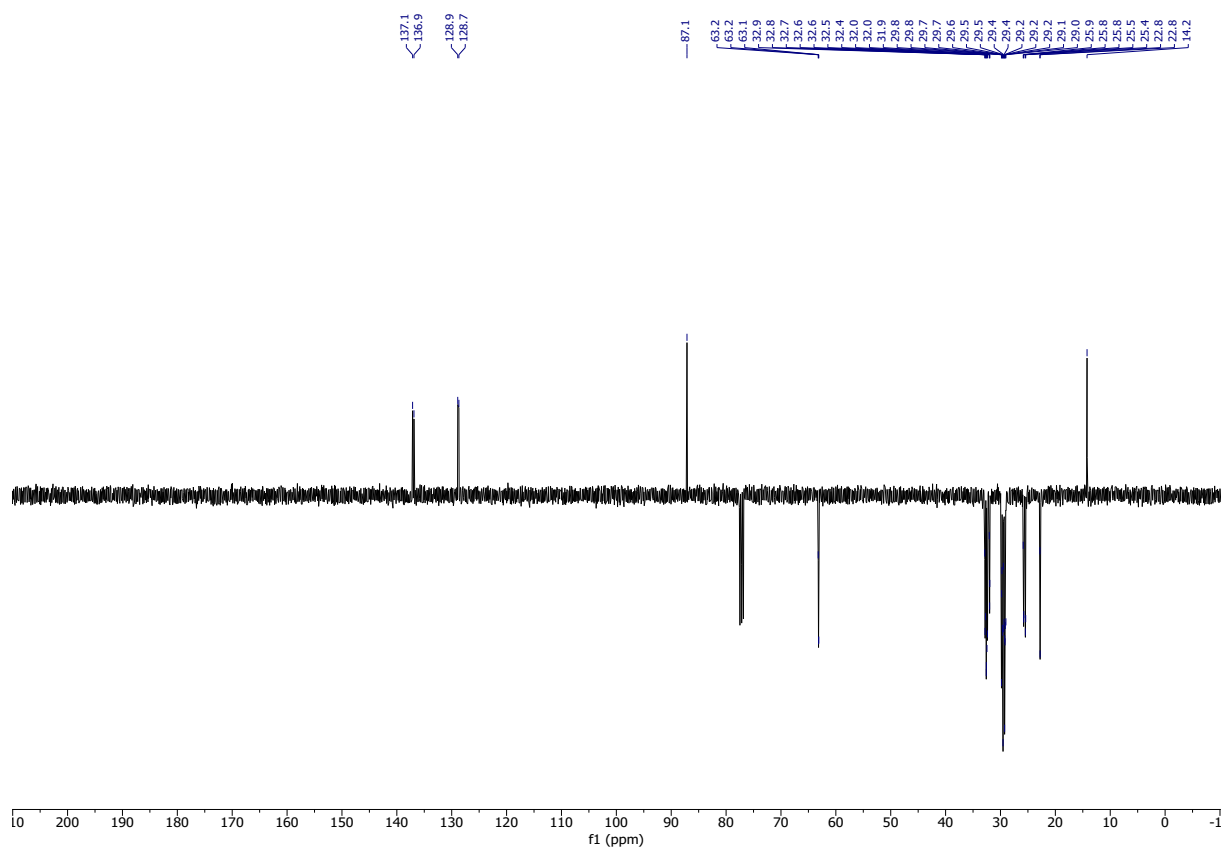
¹³C NMR (101 MHz, CDCl₃) of OA-HYP.
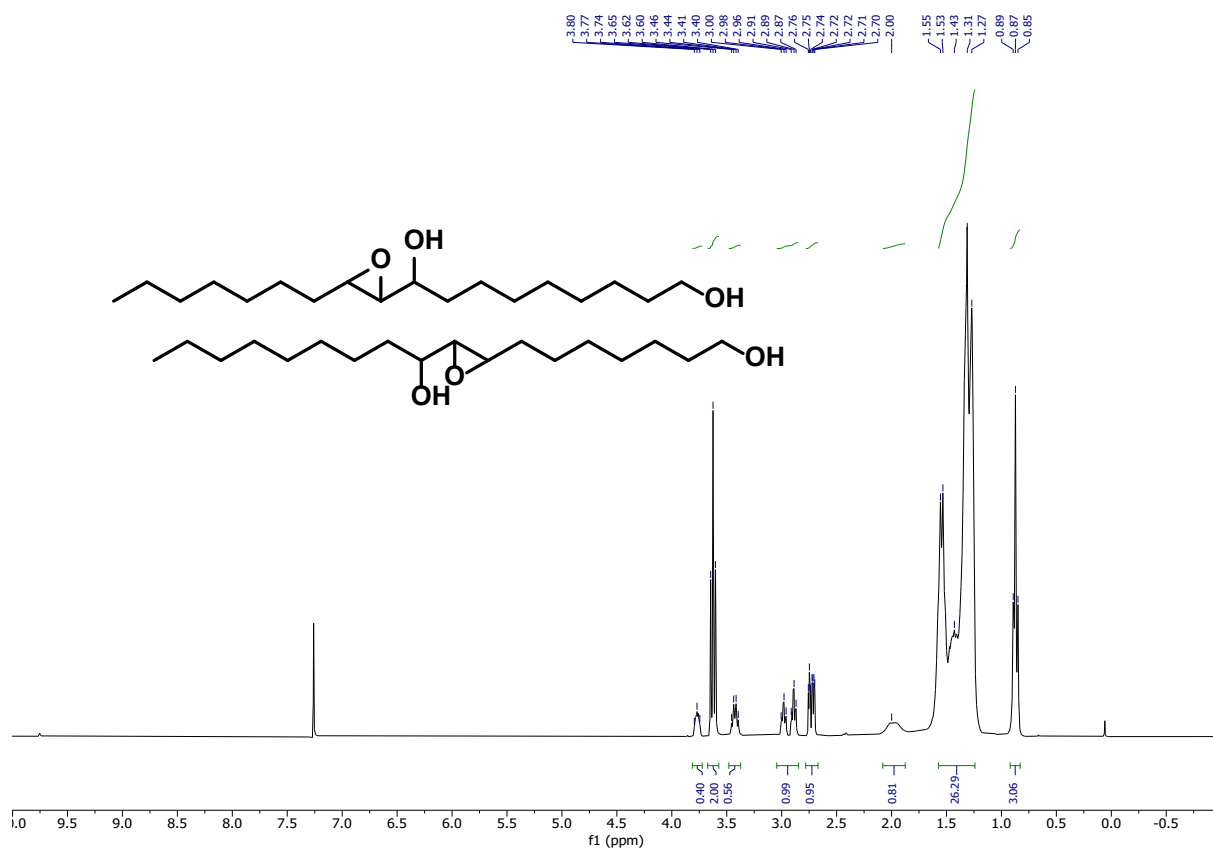
¹H NMR (300 MHz, CDCl₃) of OA-EpAlc.
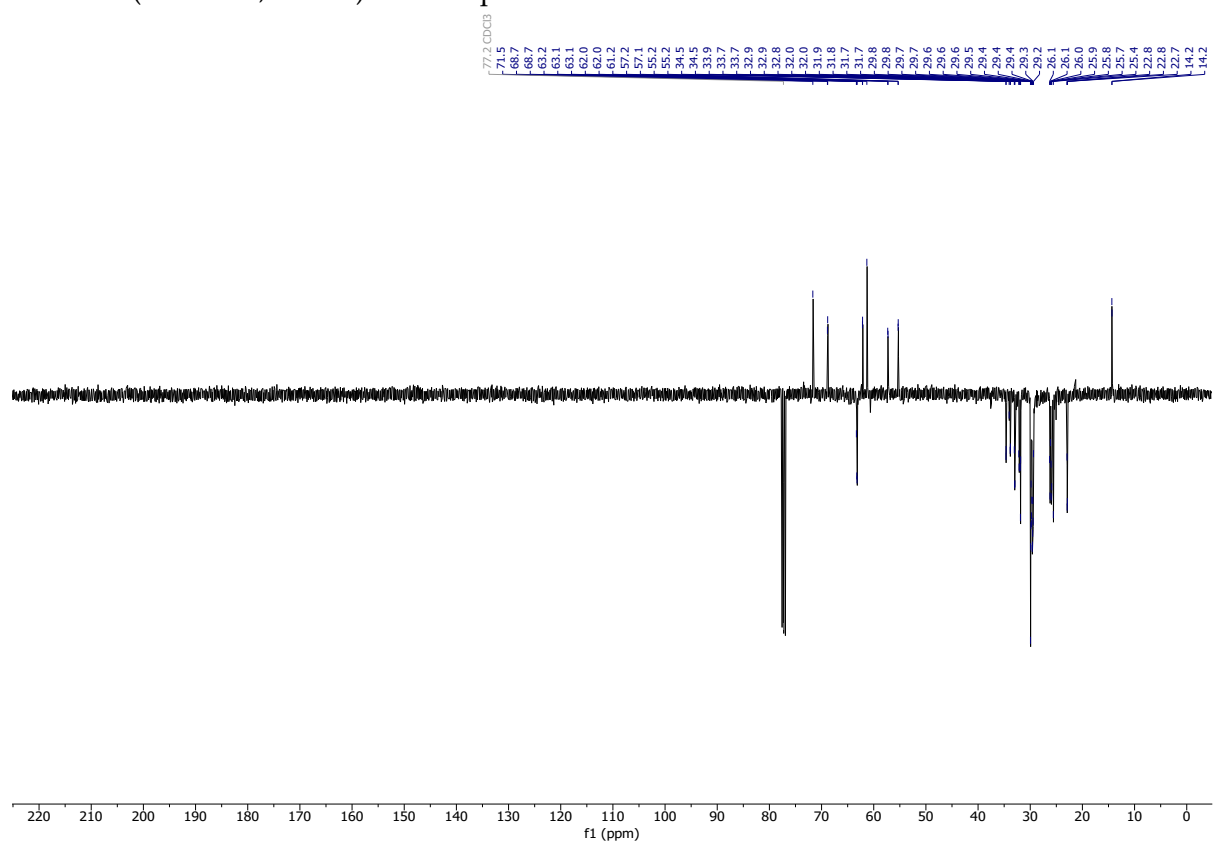
¹³C NMR (101 MHz, CDCl₃) of OA-EpAlc.
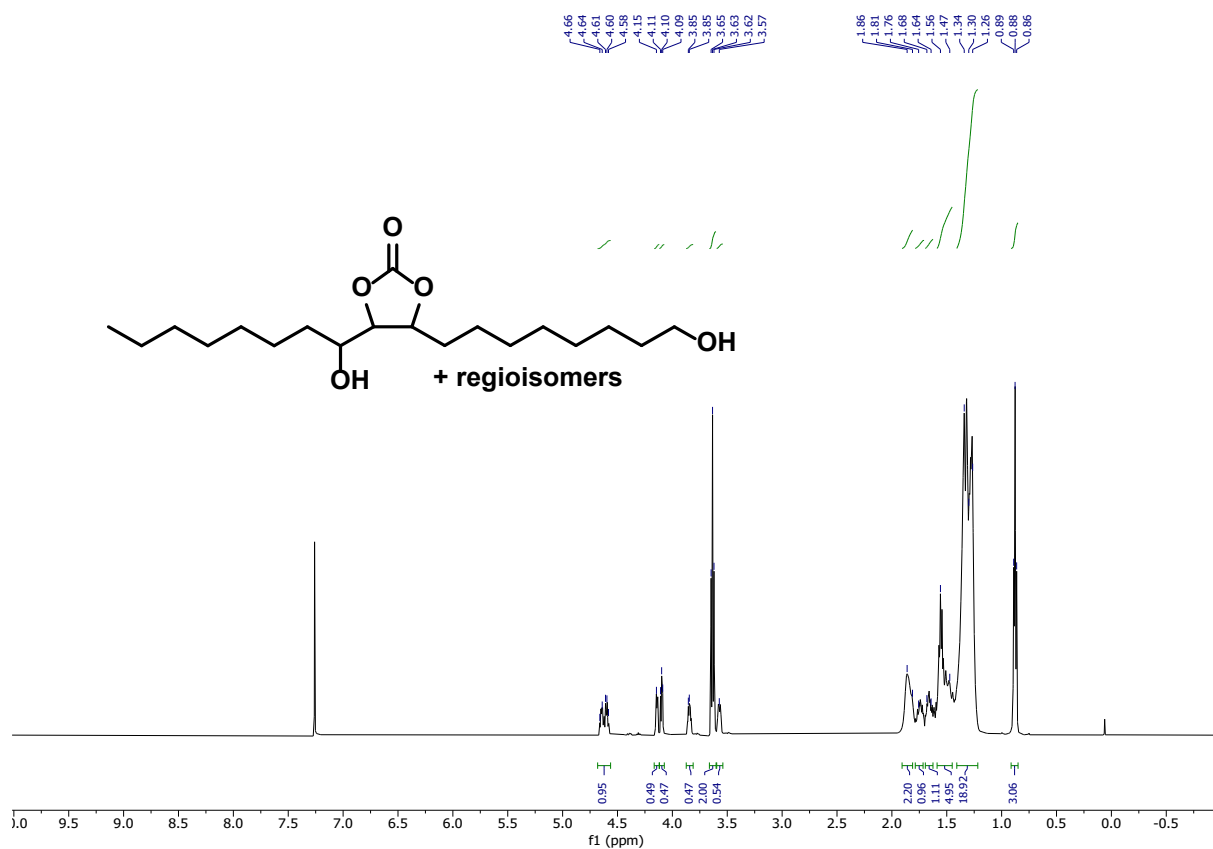
^{1}H NMR (300 MHz, CDCl$_3$) of OA-CC.
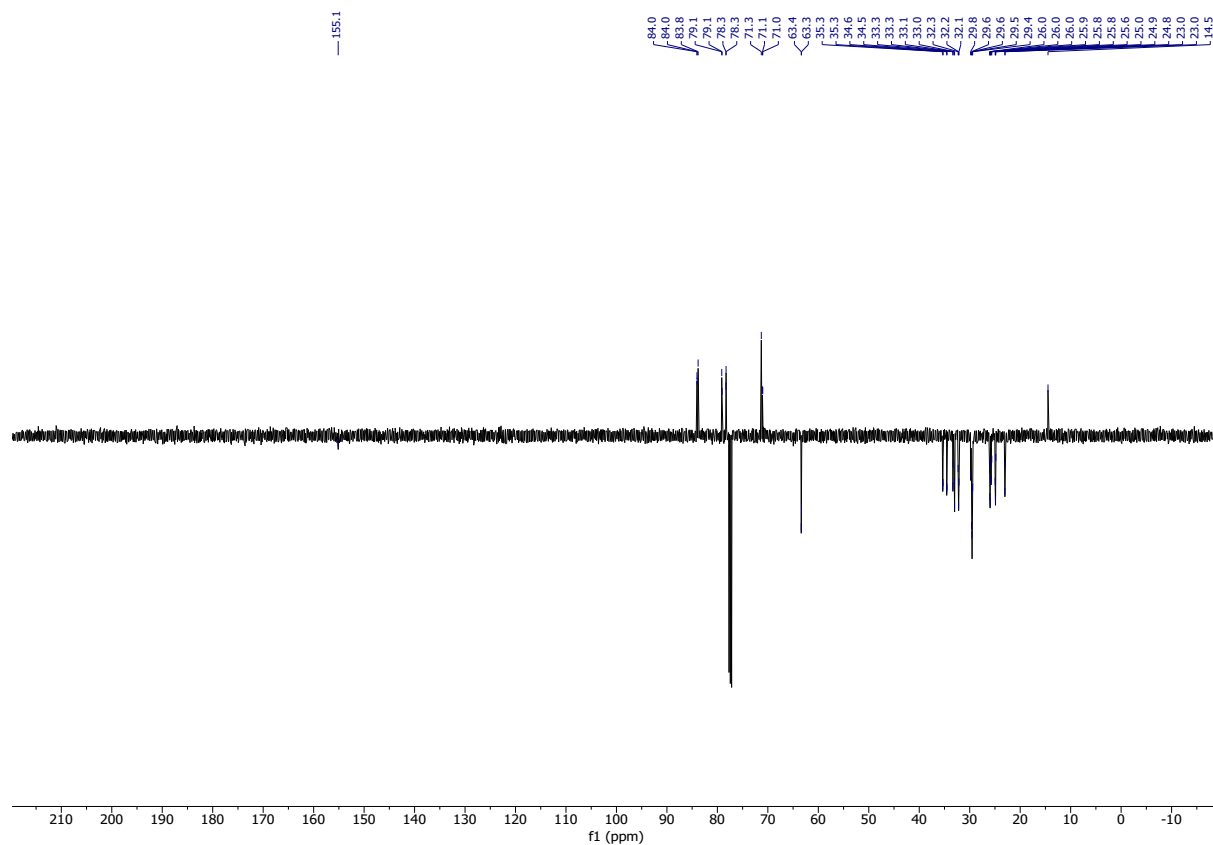
^{13}C NMR (101 MHz, CDCl$_3$) of OA-CC.
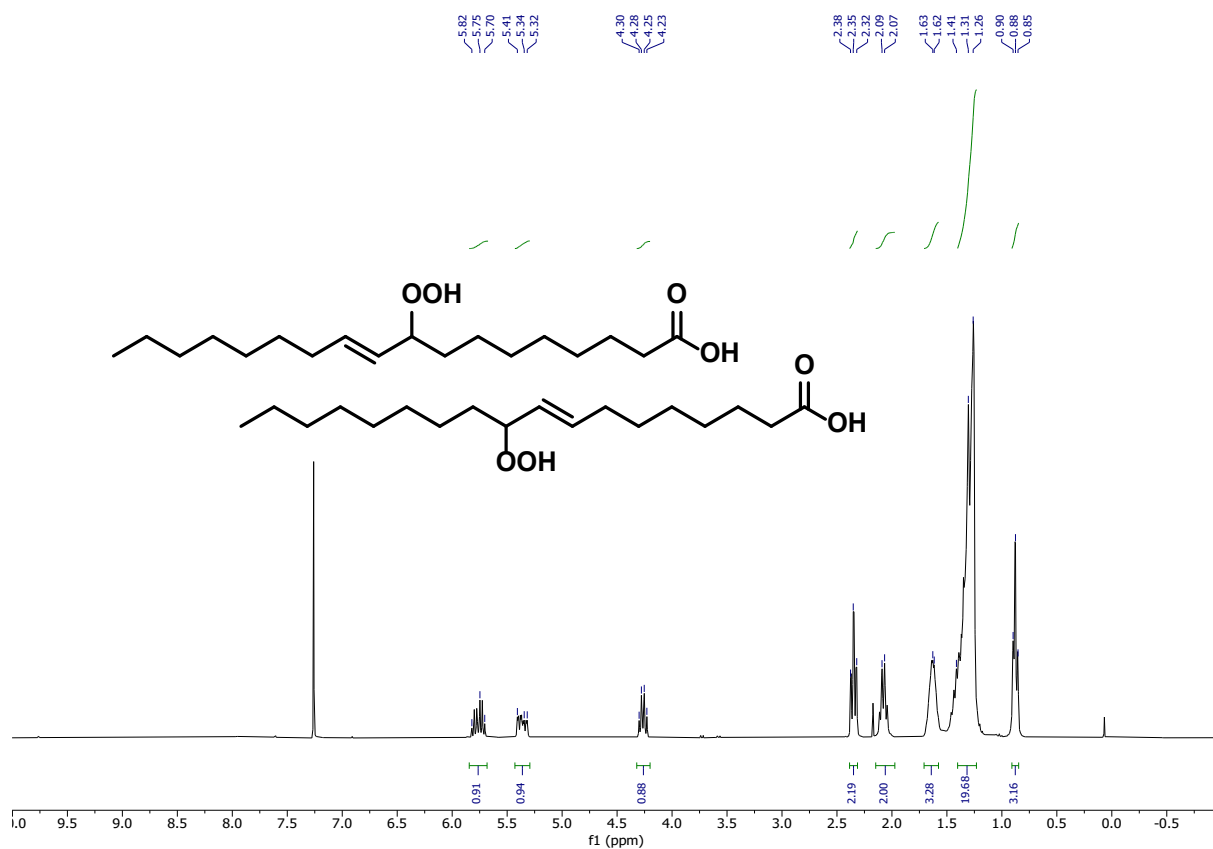
^{1}H NMR (300 MHz, CDCl$_3$) of OlA-HYP.
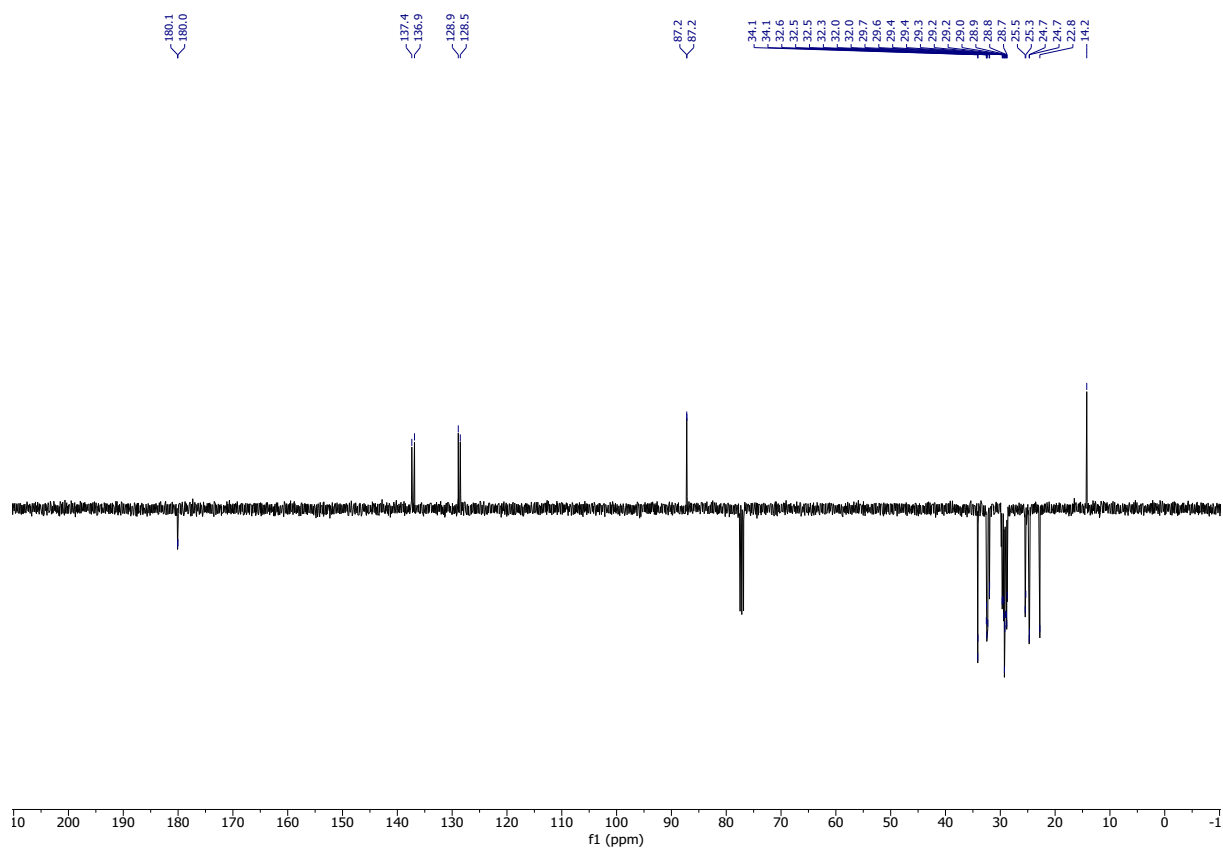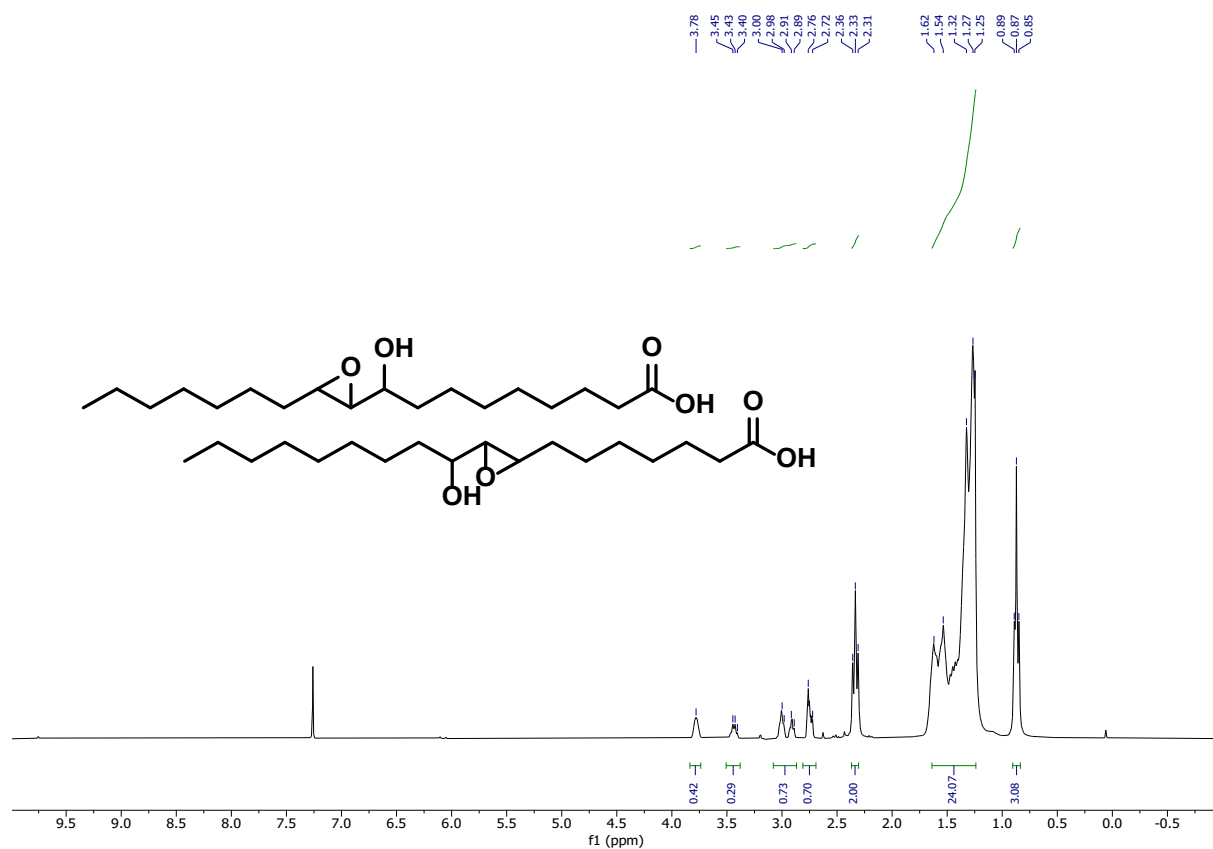
^{13}C NMR (101 MHz, CDCl$_3$) of OlA-HYP.

^{1}H NMR (300 MHz, CDCl₃) of OlA-EpAlc.

^{13}C NMR (151 MHz, CDCl₃) of OlA-EpAlc.

^{1}H NMR (300 MHz, CDCl$_3$) of OAcr-HYP.
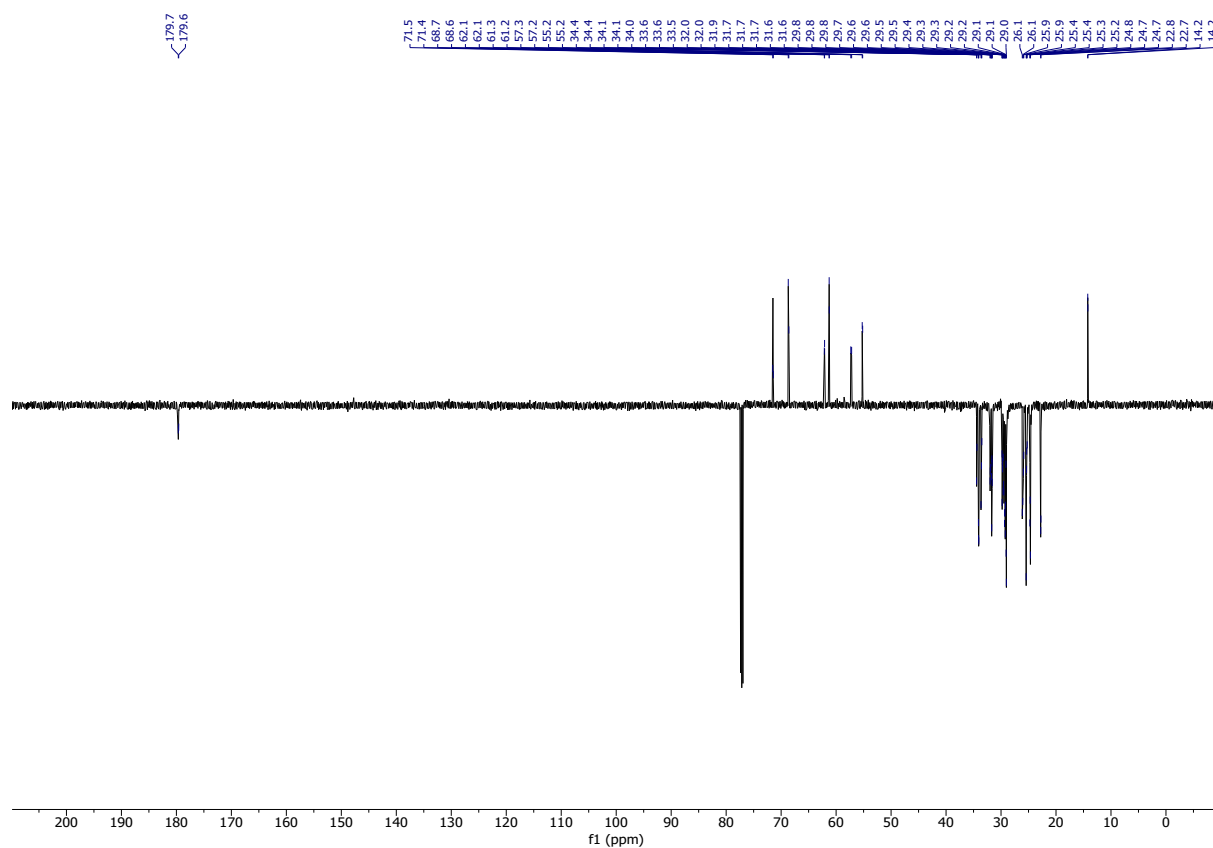
^{13}C NMR (151 MHz, CDCl$_3$) of OAcr-HYP.
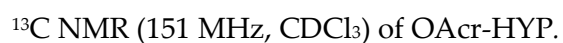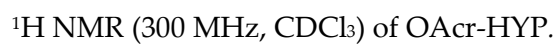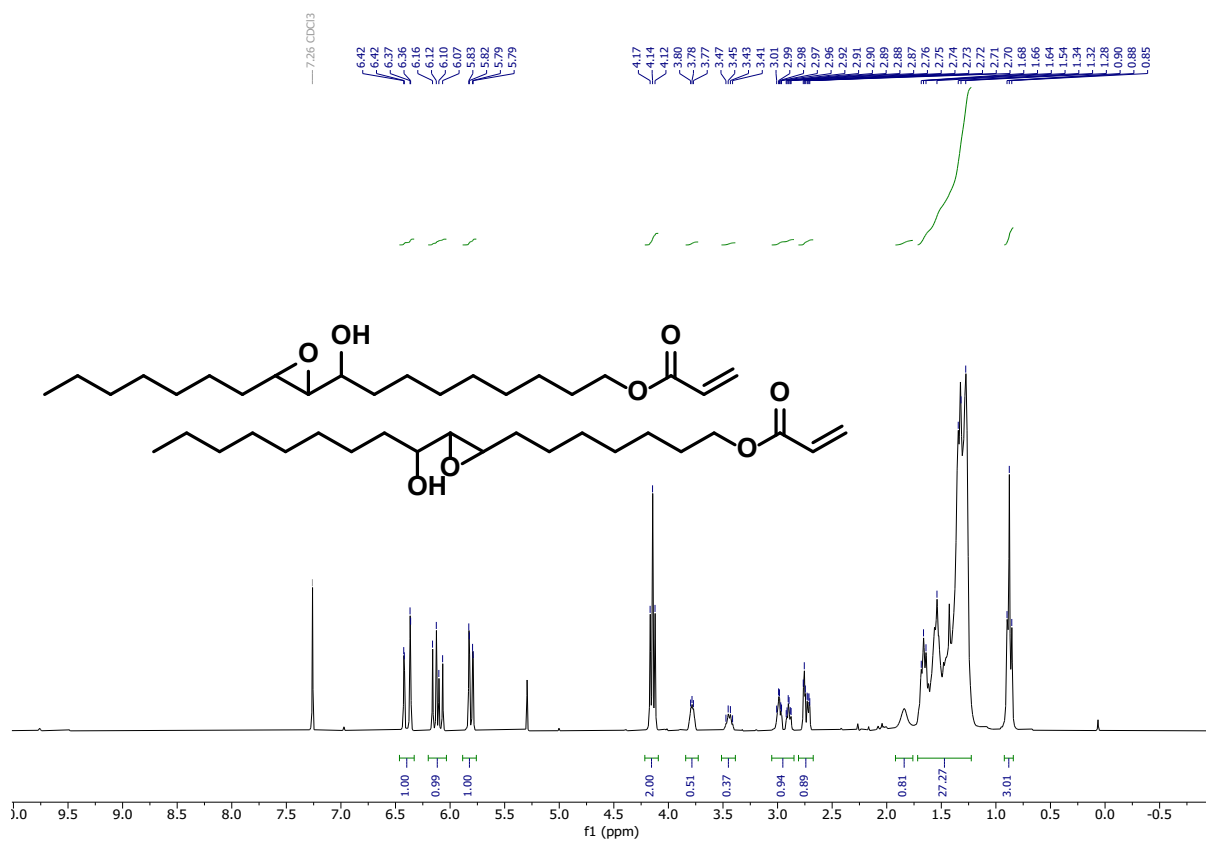
^{1}H NMR (300 MHz, CDCl$_3$) of OAcr-EpAlc.
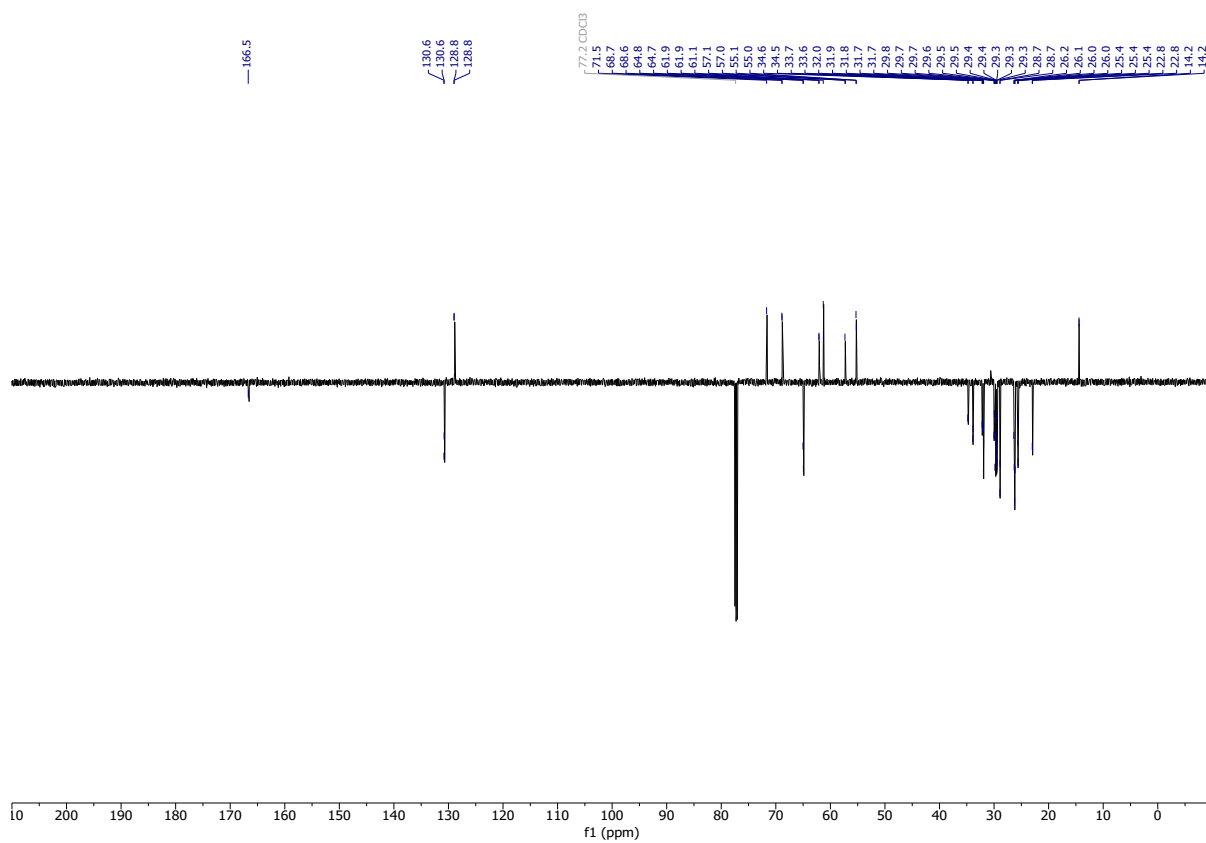
^{13}C NMR (151 MHz, CDCl$_3$) of OAcr-EpAlc.
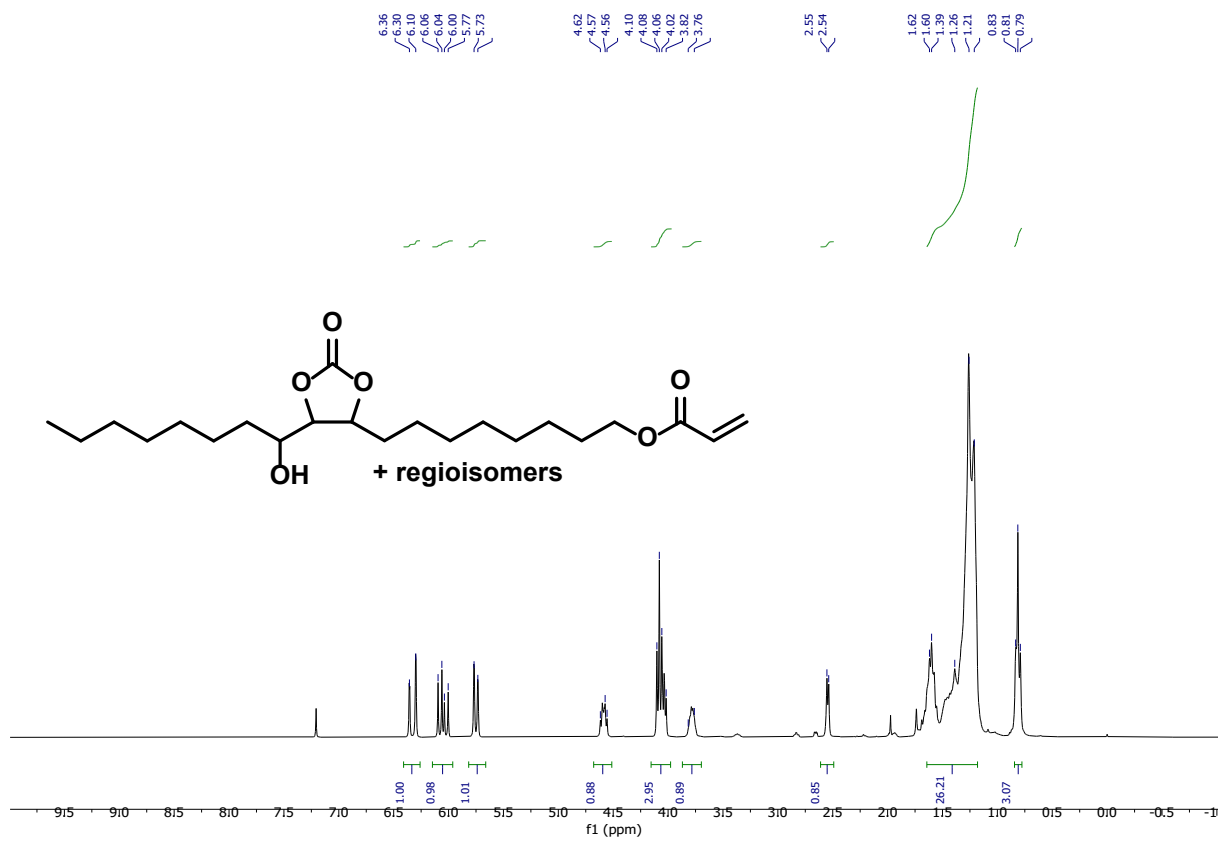
¹H NMR (300 MHz, CDCl₃) of OAcr-CC.
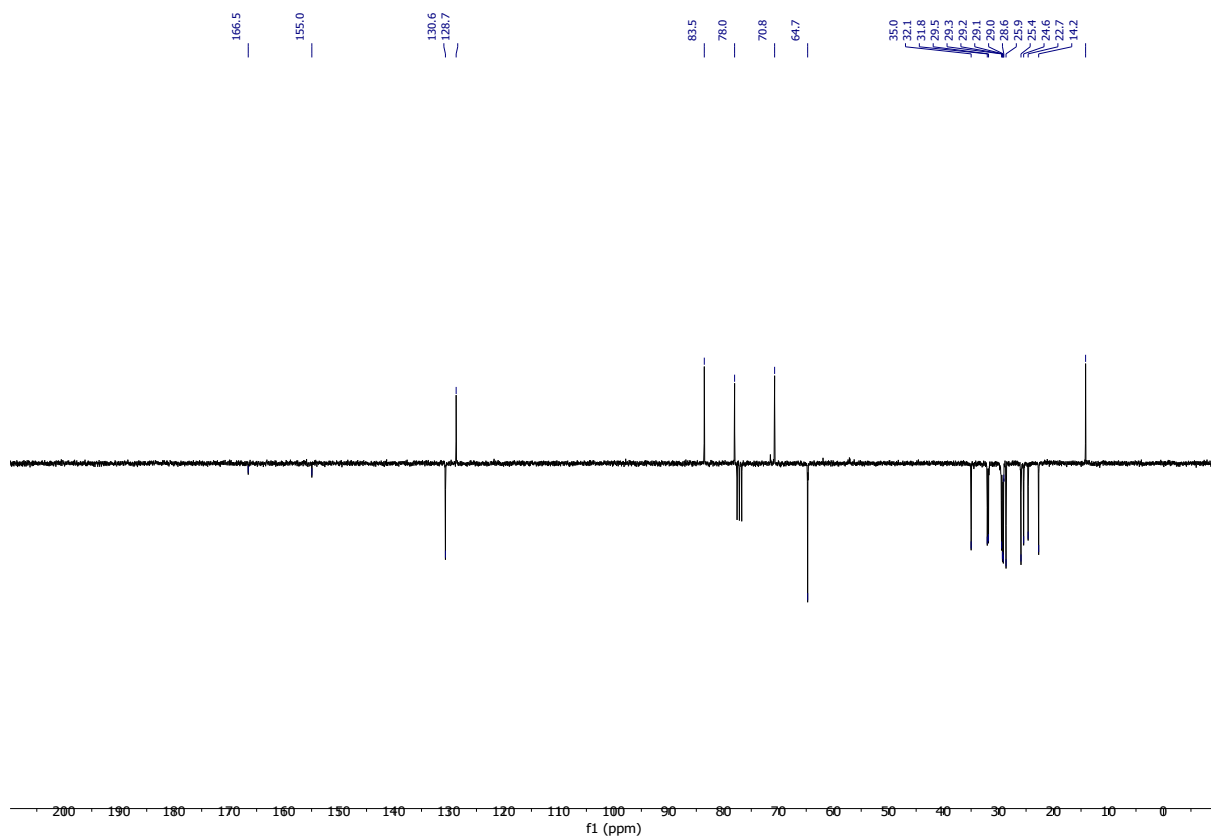
¹³C NMR (101 MHz, CDCl₃) of OAcr-CC.
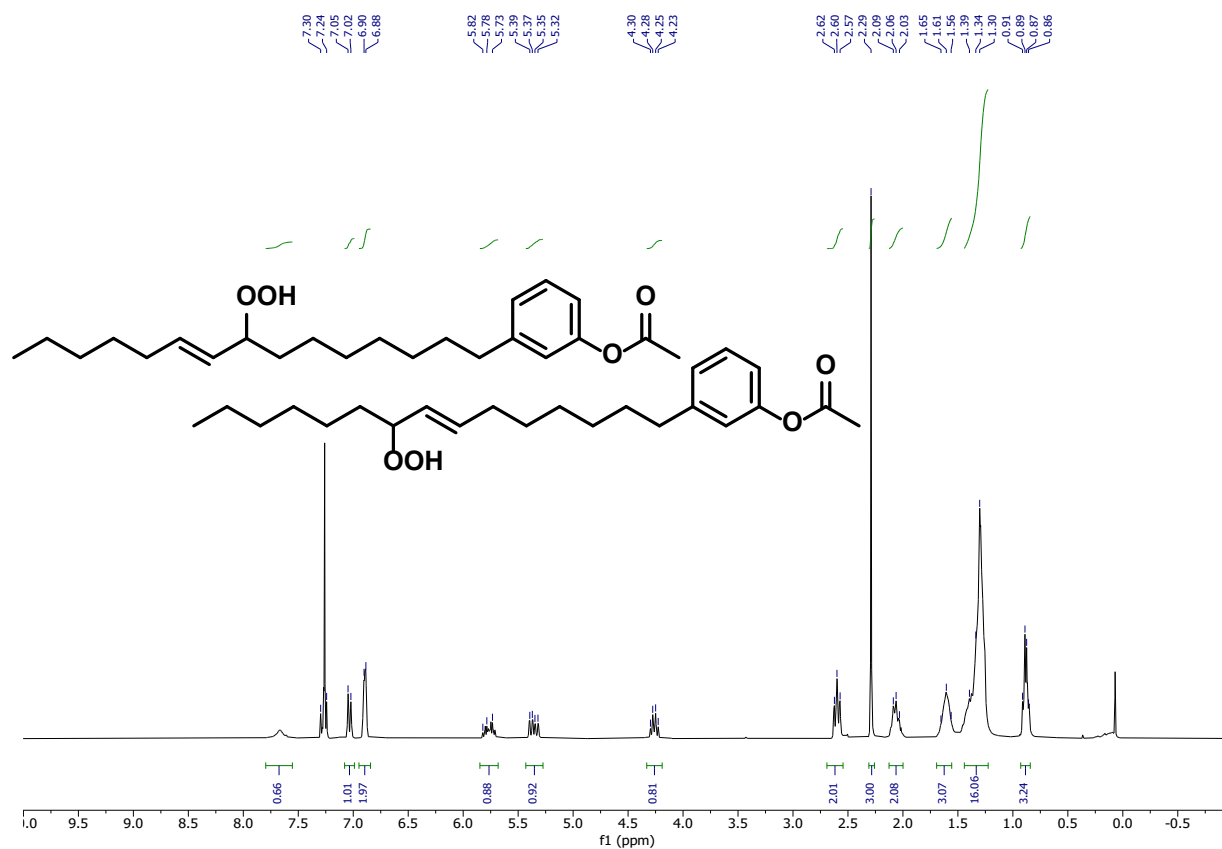
^{1}H NMR (300 MHz, CDCl$_3$) of CA-HYP.
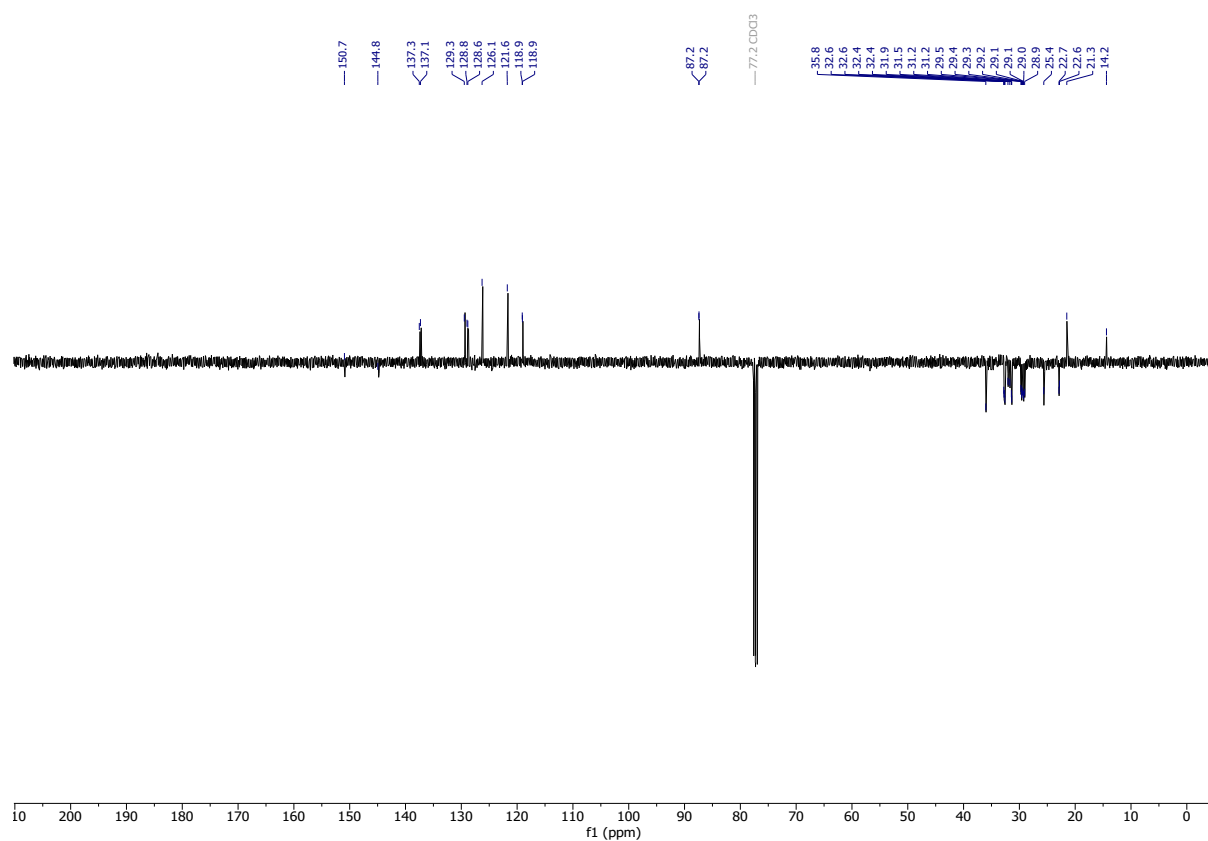
^{13}C NMR (101 MHz, CDCl$_3$) of CA-HYP.

125
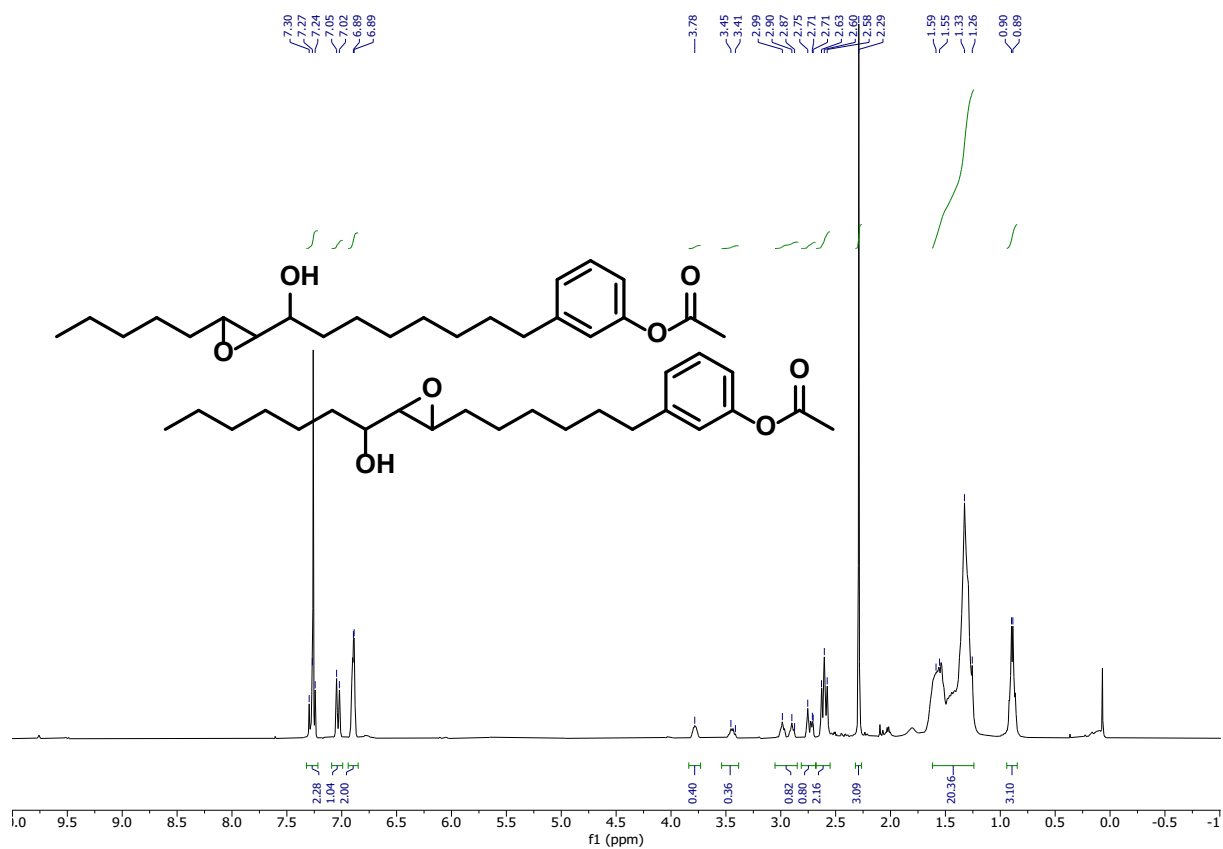
^{1}H NMR (300 MHz, CDCl$_3$) of CA-EpAlc.
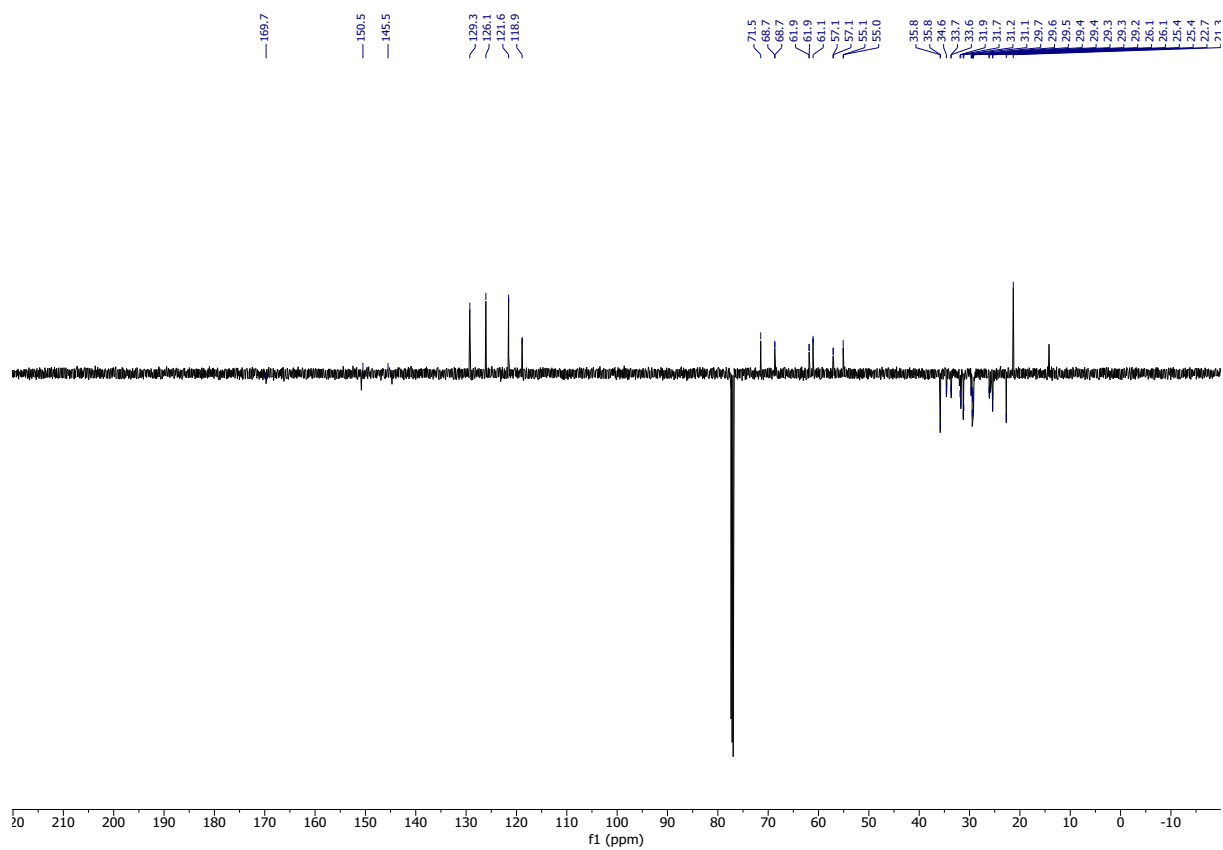
^{13}C NMR (151 MHz, CDCl$_3$) of CA-EpAlc.
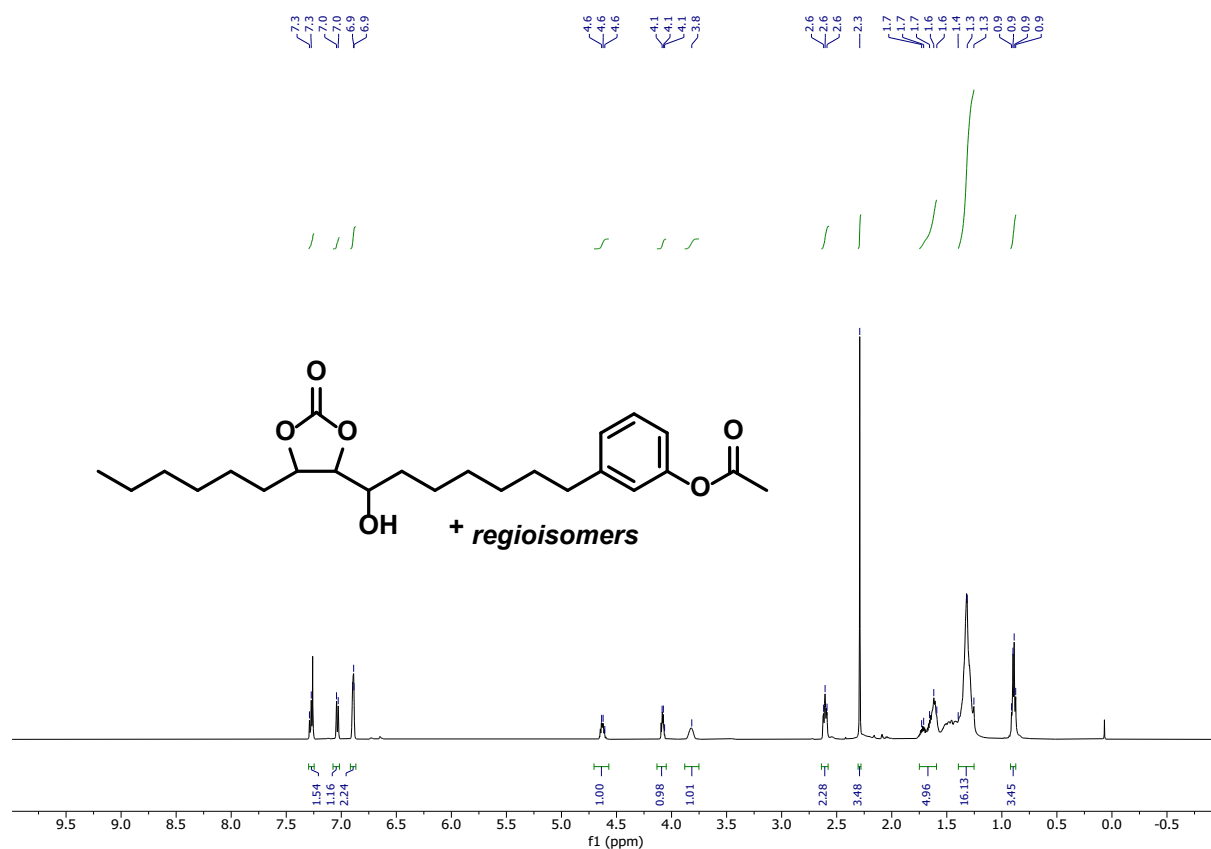
^{1}H NMR (300 MHz, CDCl$_3$) of CA-CC.
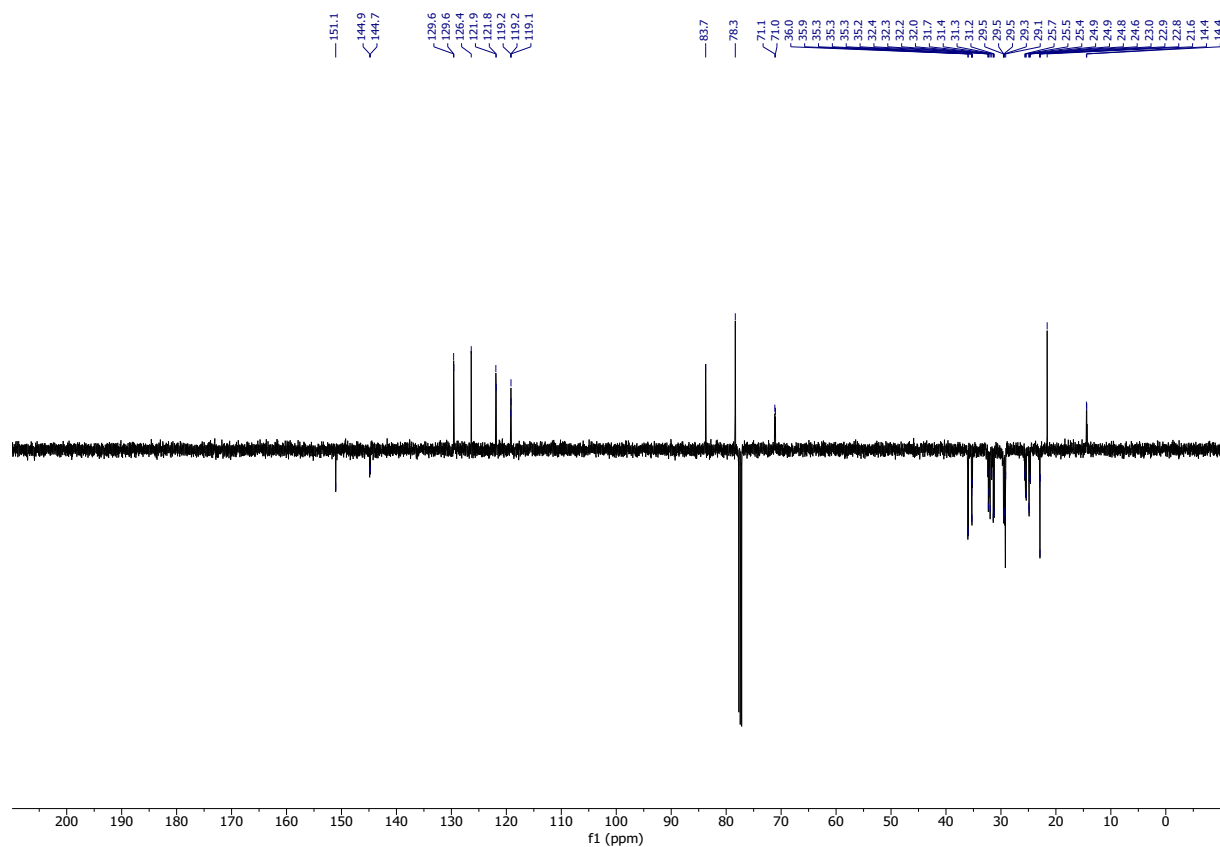
^{13}C NMR (101 MHz, CDCl$_3$) of CA-CC.
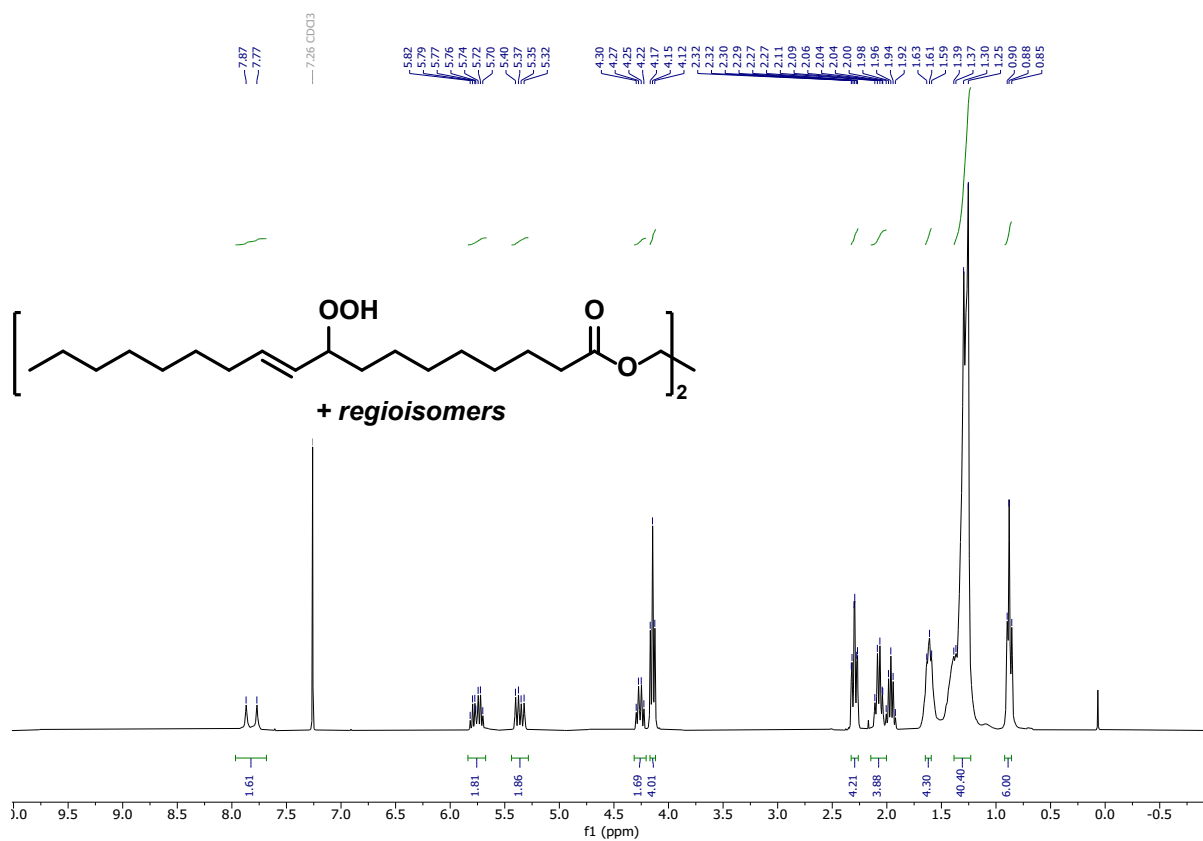
^{1}H NMR (300 MHz, CDCl$_3$) of DO-HYP.
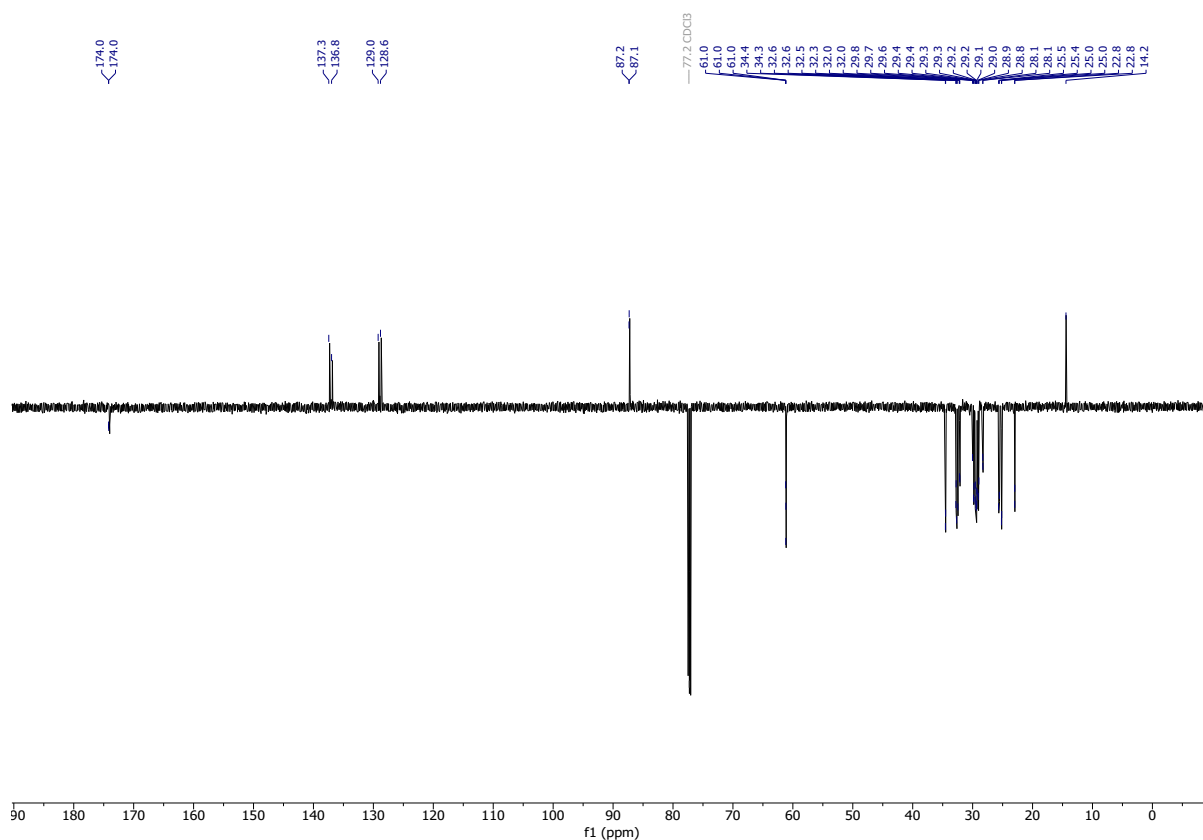
^{13}C NMR (151 MHz, CDCl$_3$) of DO-HYP.
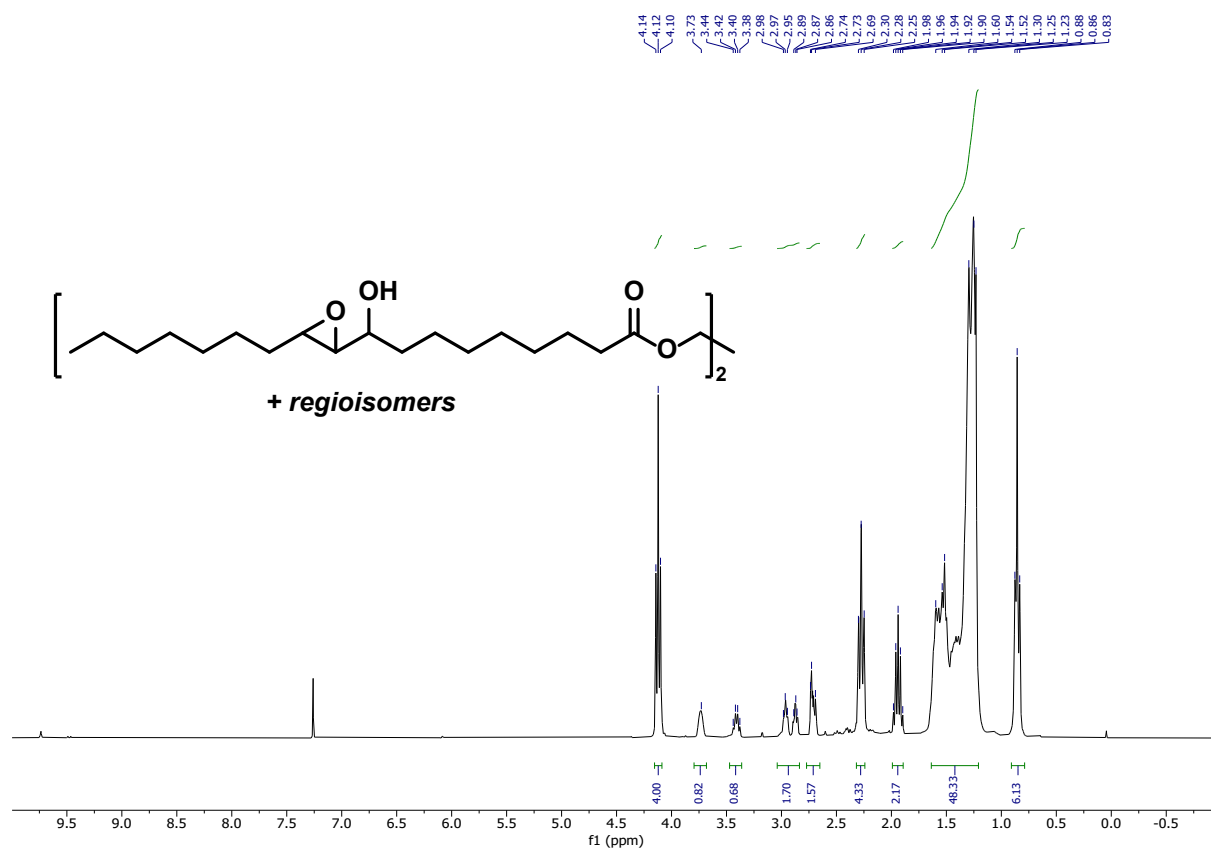
^{1}H NMR (300 MHz, CDCl₃) of DO-EpAlc.
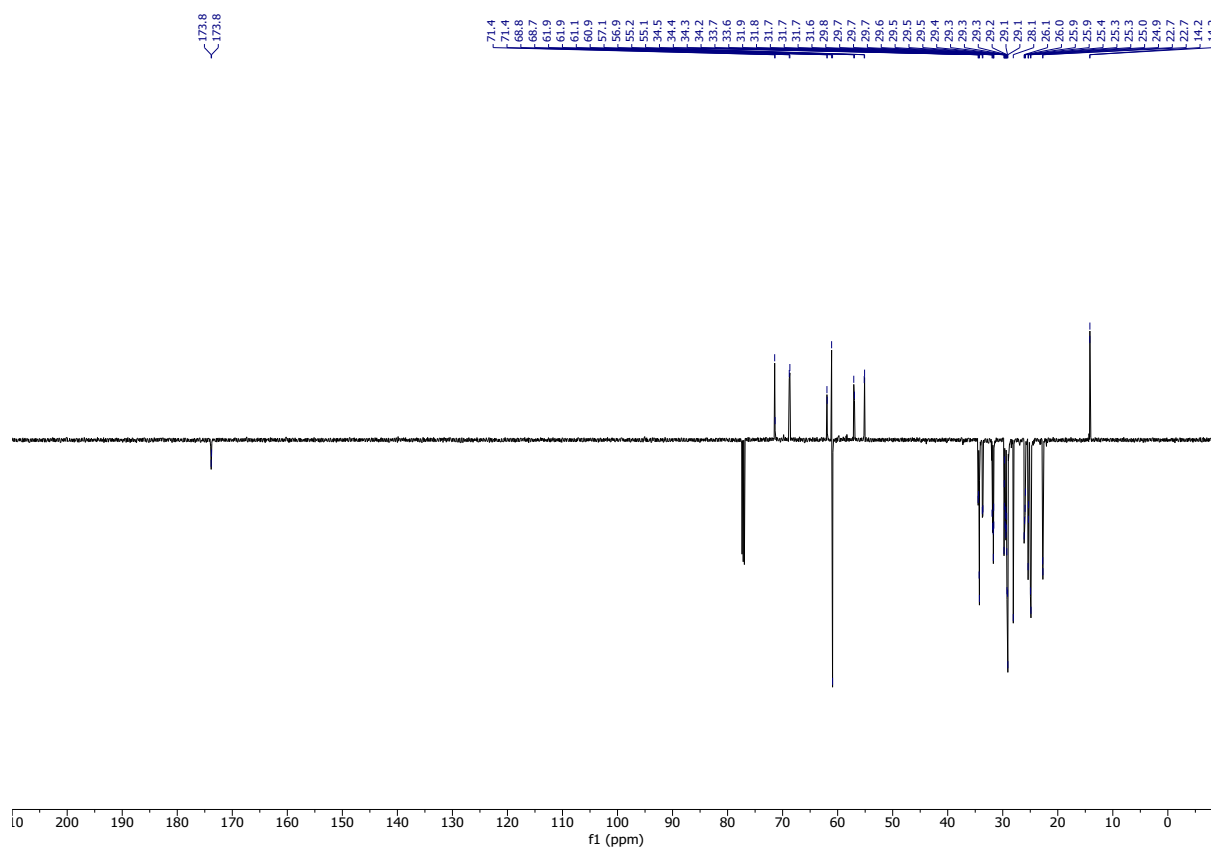
^{13}C NMR (151 MHz, CDCl₃) of DO-EpAlc.
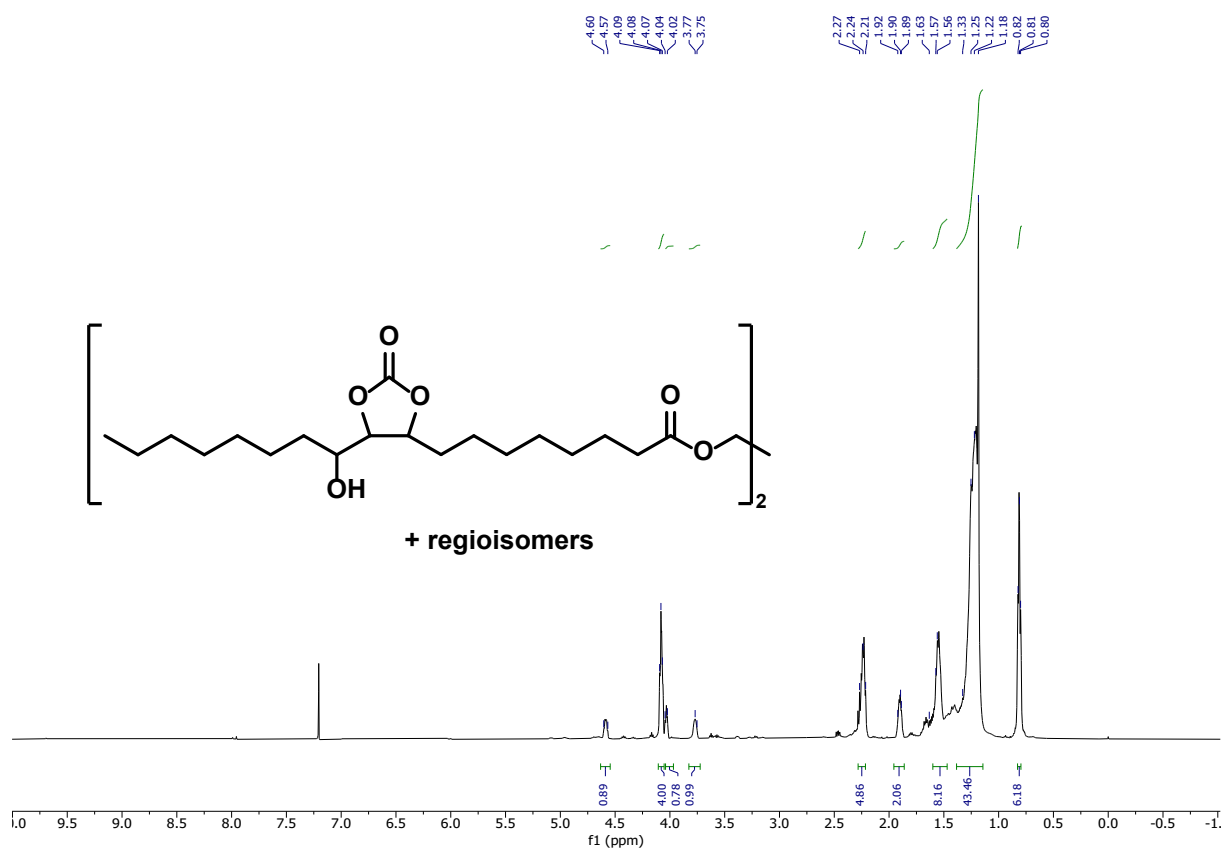
^{1}H NMR (300 MHz, CDCl₃) of DO-CC.

+ regioisomers
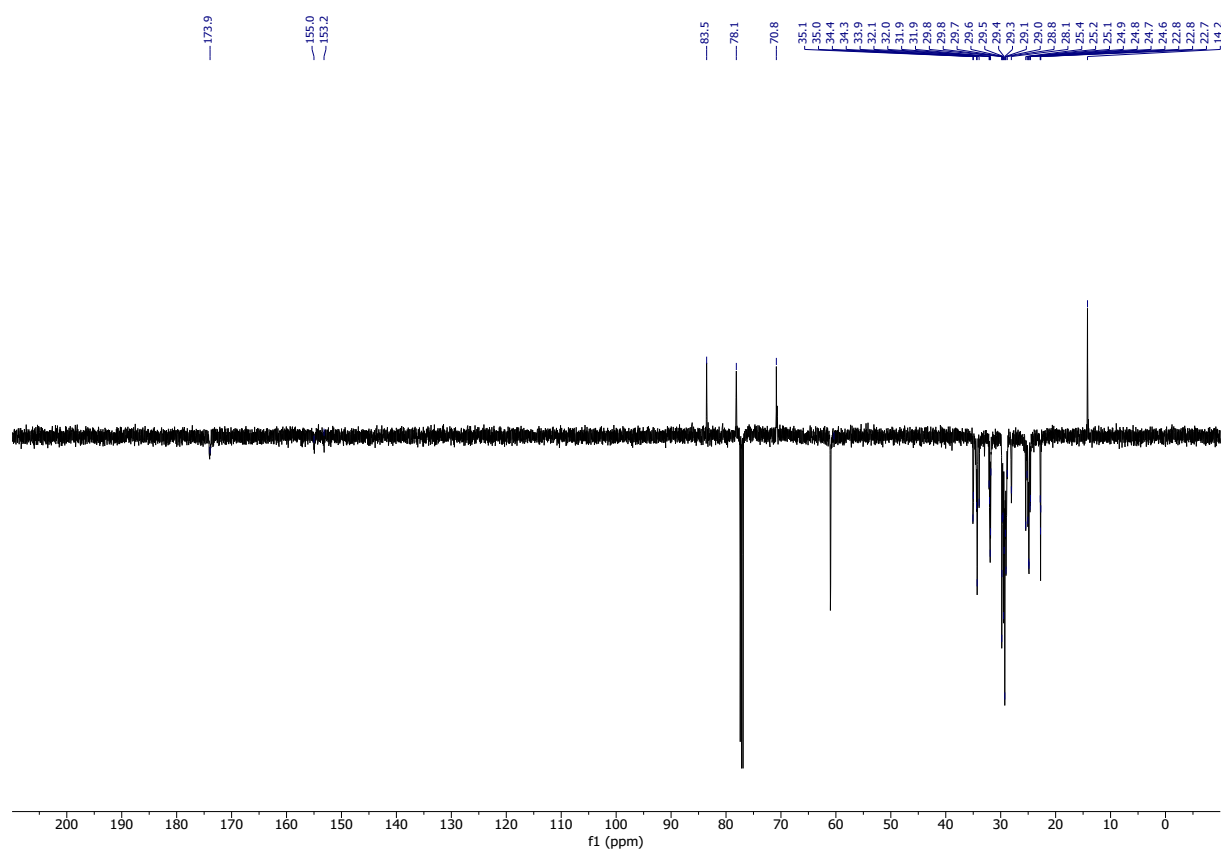
^{13}C NMR (101 MHz, CDCl₃) of DO-CC.
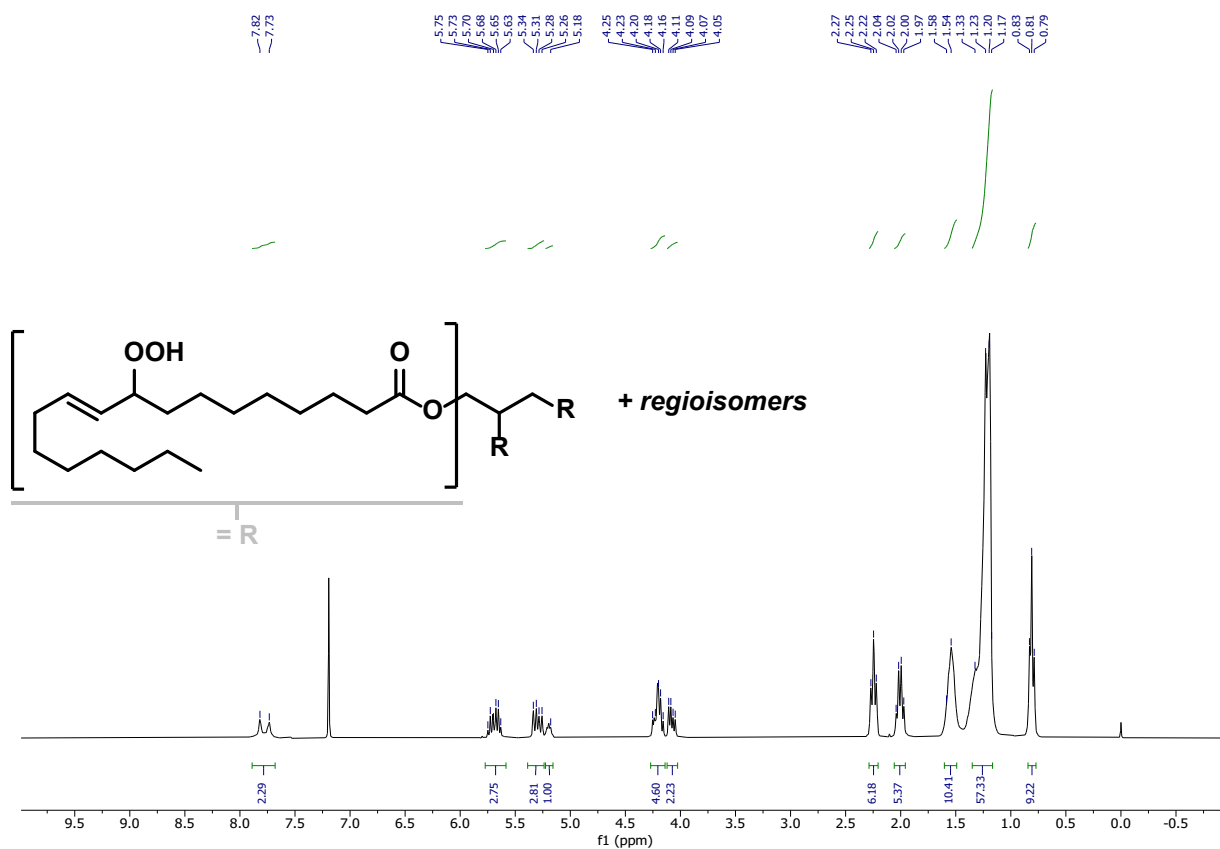
^{1}H NMR (300 MHz, CDCl$_3$) of TO-HYP.

^{1}H NMR (300 MHz, CDCl$_3$) of TO-EpAlc.

^{13}C NMR (151 MHz, CDCl$_3$) of TO-EpAlc.
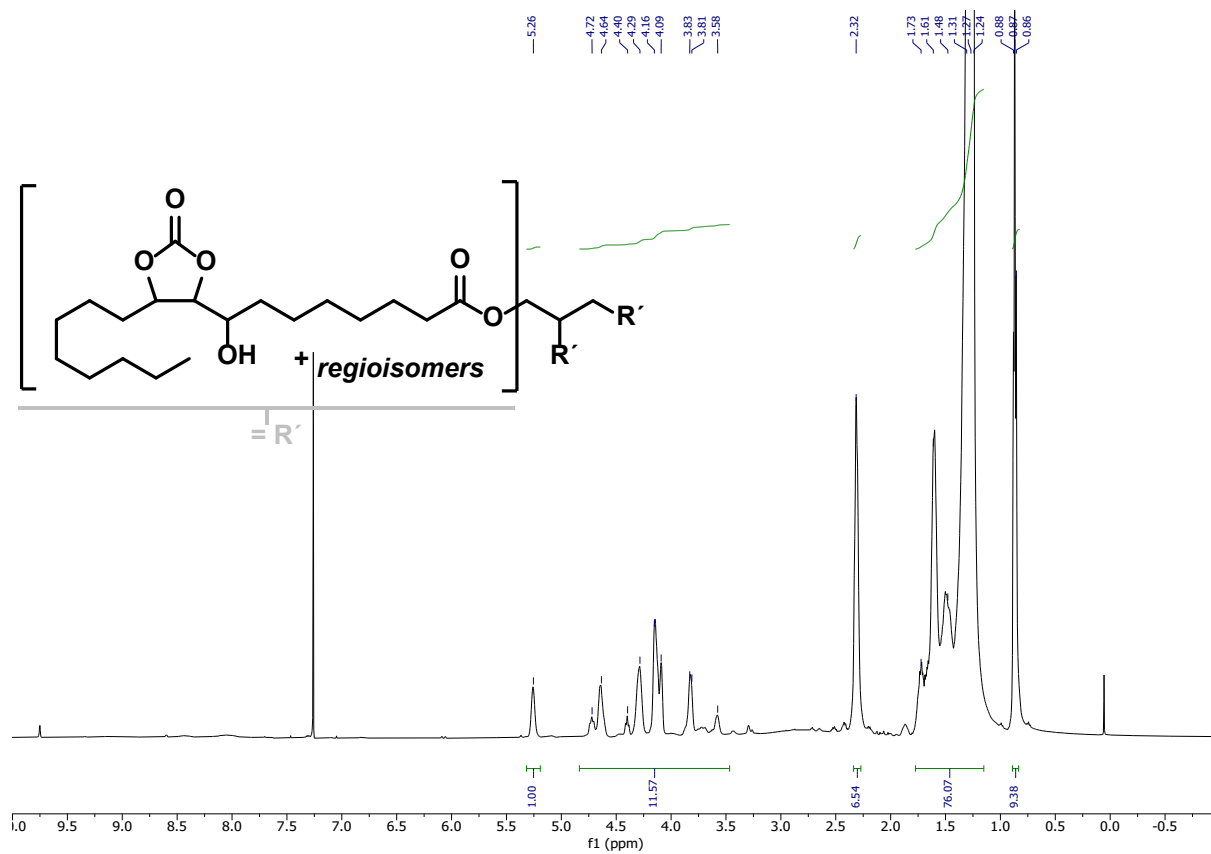
^{1}H NMR (300 MHz, CDCl$_3$) of TO-CC.
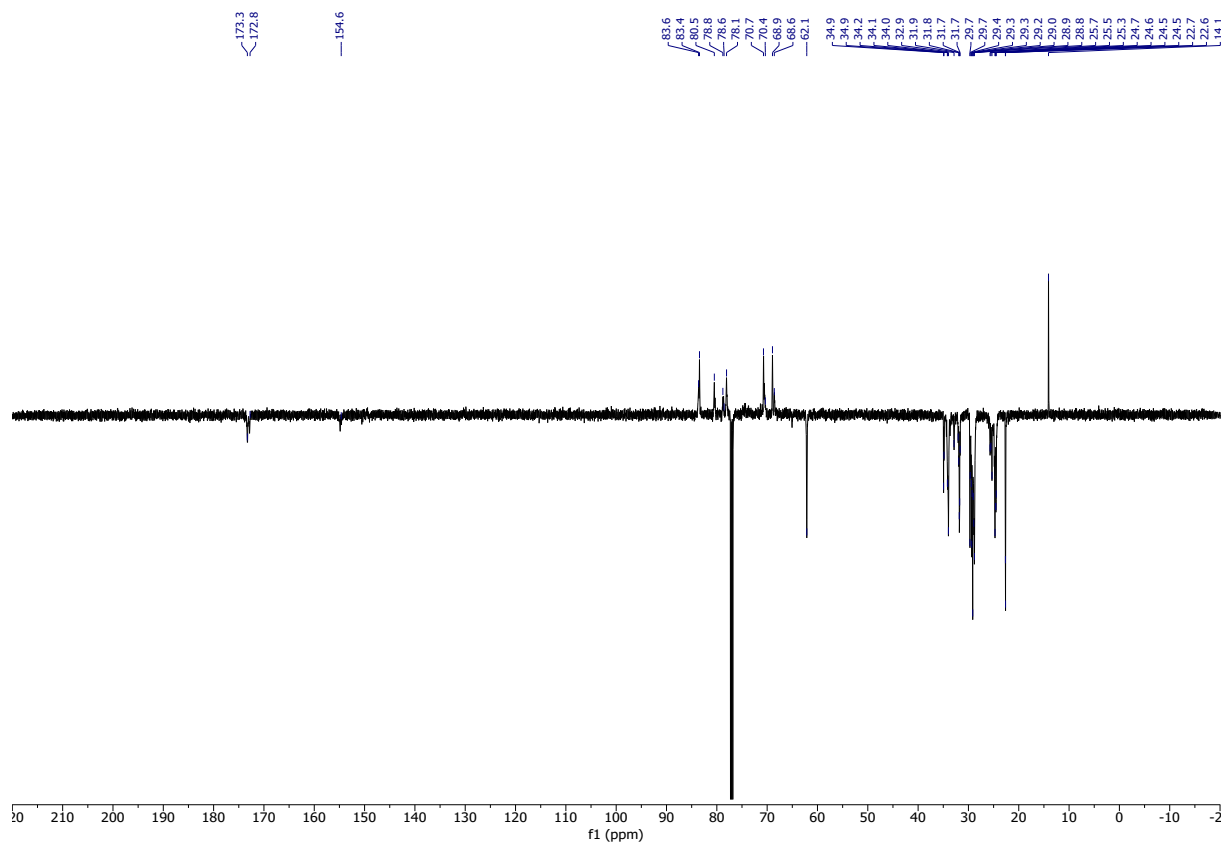
^{13}C NMR (151 MHz, CDCl$_3$) of TO-CC.

133

7. Organic Photoredox Carbonylation of Arenediazonium Salts under Mild Conditions
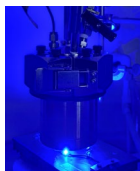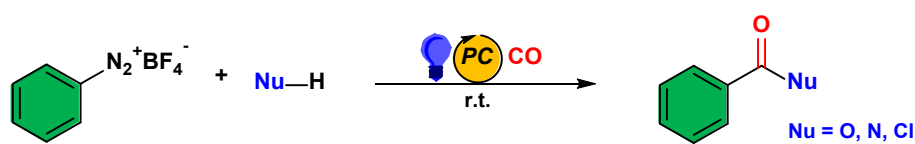
- *visible light-mediated, metal-free, organic photocatalyst*
- *lower pressure, room temperature*
- *broad scope: alcohol, diol, water, amine, chloride*

Abstract. The modular synthesis of diverse carbonyl compounds is a central aspect of organic synthesis. An optimized protocol for photoredox carbonylation was developed that operates under milder conditions with mesitylacridinium as a photocatalyst. Arenediazonium salts were converted into benzoates (with alcohols), benzoic acids (with water), benzamides (with amines), and chlorides (with 1-butyl-3-methylimidazolium chloride) at 20 bar CO and 20 °C.

7.1 Introduction

Carboxylate derivatives such as esters, amides, acids are ubiquitous structural motifs in natural products, pharmaceuticals, and fine chemicals and exhibit great synthetic utility by virtue of their special stereoelectronic properties and distinct modes of reactivity. Numerous synthetic strategies have been developed. Among them, carbonylations with the inexpensive technical gas carbon monoxide (CO) constitute an especially modular and versatile access to a wide variety of carboxyl derivatives.[1] Such protocols generally include rare and expensive late transition metal catalysts (Rh, Ir, Pd).[2] Metal-free reactions, on the other hand, are scarce and often rely on harsh reaction conditions (strong bases, UV light, high temperatures, high pressures).[3] Recently, the renaissance of photo(redox) chemistry has enabled new carbonylation pathways. The first metal-free and base-free photoredox-catalyzed carbonylation of aromatic electrophiles to benzoate esters was reported in 2014 by Xiao and us.[4] Subsequently, a handful reports on light-mediated synthesis of carboxyl derivatives with very limited substrate scopes were developed (aryl indoles, maleates, etc.).[5] However, an operationally facile protocol that utilizes simple, commercial reagents and provides access to a broad range of carboxylate derivatives (esters, acids, amides, acyl chlorides) has not yet been reported.
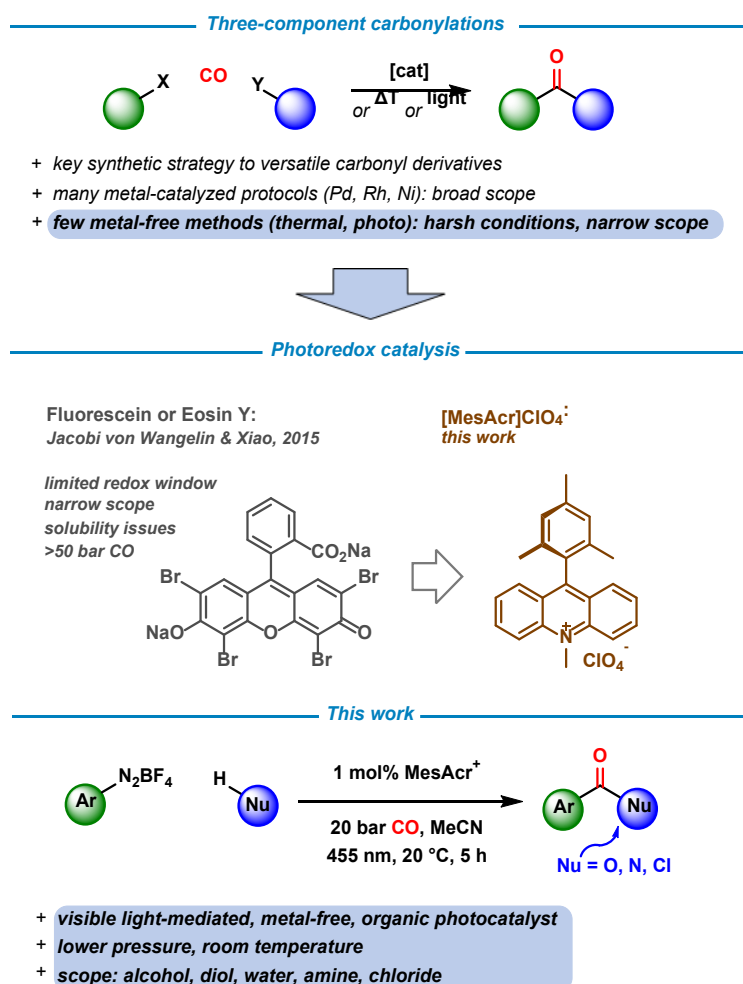
Scheme 7.1. Overview of three-component carbonylation syntheses.

Visible light-mediated reactions between liquid and gaseous reagents pose special challenges to the design of an operational reaction set-up. The precise control over the feed, mixing, and stoichiometry of the three distinct entities liquid, gas, and light resembles the difficulties of operating a three-phase reaction. We have resorted to a stainless-steel high-pressure reactor that is equipped with thermal and pressure control and a quartz glass window at the bottom (Figure 7.1). Reaction vials can be placed inside the reactor and illuminated from the outside by any available light source. This set-up enabled safe operation and independent variation of substrates, reaction conditions (T, t, p), and irradiation source. The reaction volume, however, is restricted by the inner volume of the autoclave but even more by the attenuation of the light (Lambert-Beer law).
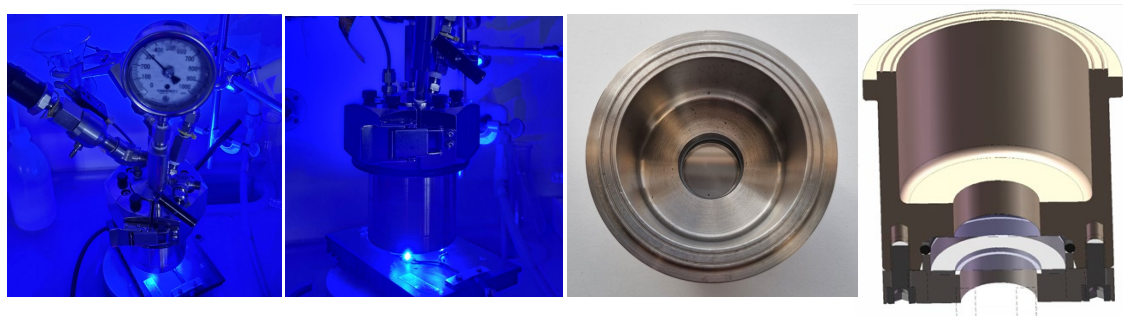
Figure 7.1. Autoclave equipped with gas inlet, manometer, temperature probe and quartz glass window at the bottom. The reactor is placed on an aluminum plate holding a blue LED and is magnetically stirred from below.

7.2   Results and Discussion

Previously, we reported a successful photoredox-catalyzed carbonylation strategy to transform arenediazonium salts into various alkyl benzoates.[4a] While being an effective method of synthesis for esters, the protocol suffered from several draw-backs, including the limitation to alcohols, the narrow redox window of the photocatalyst, low solubility of the photocatalyst, and a high CO pressure of 50 bar. For example, amines could not be employed as nucleophilic components; electron-poor arene-diazonium would not give product formation as the critical 1e-oxidation of the intermediate aroyl radical is beyond the redox potential of the photocatalyst eosin Y; lipophilic alcohols could not dissolve the photocatalyst. Therefore, we aimed at the development of an optimized procedure that would eliminate the aforementioned limitations. The use of a different photocatalyst was believed to make the biggest impact on the observed limitations. We studied the model reaction between 4-methoxy-benzenediazonium tetrafluoroborate (**1a**), gaseous carbon monoxide, and methanol as nucleophile (Table 7.1). The reproduction of our previously reported protocol in the presence of eosin Y confirmed the requirement of high CO pressures (4 mol% eosin Y, 525 nm, 40 bar CO, 2 equiv. MeOH; entry 1, Table 7.1), possibly due to a turnover-limiting CO addition to the intermediate aryl radical. Significantly lower yields of the methyl 4-methoxybenzoate (**2a**) were obtained at decreased pressure (20 bar, entry 2). Our previous mechanistic proposal involved a thermodynamically strongly favored 1e-reduction of the arene-diazonium salts while the back-electron transfer from the intermediate aroyl radical to the reduced state of the photo-catalyst was identified as rate-determining step (eosin Y is a weak oxidant: EY[+•]/EY: –

0.8 V *vs.* SCE; see below).[4] Therefore, a stronger photo-oxidant could obviate the need for high CO pressures by facilitating the oxidation of the aroyl radical, which is the adduct of aryl radical and gaseous CO and in direct equilibrium with both precursors. Indeed, use of the stronger oxidizing catalyst 9-mesityl-10-methylacridinium perchlorate (MesAcr+/MesAcr•: 2.06 V *vs.* SCE)[6] afforded greatly enhanced yields at much lower CO pressure (entries 3, 4). The capacity of MesAcr+ to act as photo-oxidant required a co-catalytic reductant that would ensure formation of the 1e-reduced MesAcr• state to initiate the reaction (by arenediazonium reduction) but not interfere with the other steps of the photoredox mechanism. Electron-rich arenes are known to undergo photoredox reactions with MesAcr+, so that we employed anisole as an inexpensive sacrificial co-catalyst.[7] The mixture of [MesAcr]ClO$_4$ (1 mol%) and anisole (5 mol%) afforded high yields in the carbonylation of **1a**. Minimal to no product formation was observed in the absence of photo-catalyst, in the dark, at 10 bar CO, or without anisole, respectively (entries 5–8).

Table 7.1. Selected optimization experiments.

Entry	Deviation from optimized conditions	Yield [%]
1	4 mol% eosin Y, 40 bar CO	71
2	4 mol% eosin Y, 20 bar CO	<5
3	**40 bar CO**	**84**
4	**-**	**79**
5	10 bar CO	<5
6	No light	0
7	No photocatalyst	0
8	No anisole	<5

Optimized conditions: **1a** (0.1 mmol), [MesAcr]ClO$_4$ (1 mol%, 0.001 mmol), anisole (5 mol%, 0.005 mmol), MeCN (1 mL), MeOH (2 equiv., 0.2 mmol), CO (20 bar), LED (455 nm), 20 °C, 5 h.

We explored the scope of this reaction under the optimized conditions (Scheme 7.2; values in parentheses give results of previous eosin Y catalysis).[4a] *n*-, *sec*-, *tert*-alcohols, *sec*-amines, water, diols, and chloride were successfully employed as nucleophiles. A diverse range of functional groups in the arenediazonium salts, the nucleophiles, and the products were tolerated, including Cl, Br, MeO, water, NO$_2$, nitrile, ketone, ester, carboxylic acid, thiophene, allyl, and alkyne. Importantly, the electron-poor 2-NO$_2$ derivative gave good conversion which

was outside of the redox window of the photocatalyst eosin Y in our previously reported protocol (2b).[4] Alcohols as nucleophiles afforded generally very good yields of the resultant benzoates. The use of 0.5 equiv. of diol allowed the formation of diesters; the synthesized diethylene glycol dibenzoate (2g) is a commercial plasticizer for polyvinyl chloride.[8] The use of water as nucleophile gives access to functionalized benzoic acids (2h). Unlike the previously reported eosin Y catalysis,[4a] secondary amines can be employed for the synthesis of tertiary benzamides (2j, 2k). The use of the soluble organic chloride salt 1-butyl-3-methyl-imidazolium chloride, [bmim]Cl, resulted in the formation of benzoyl chlorides in very good yield (2l). This HCl-free reaction may prove highly versatile as it offers ample opportunities for further downstream substitution of the acyl chloride by any nucleophile. Benzoyl fluorides (2m) were obtained in low yields by the use of KF. The use of other salts (CsF) or crown ethers to increase the concentration of fluoride in the reaction mixture did not improve the yield.
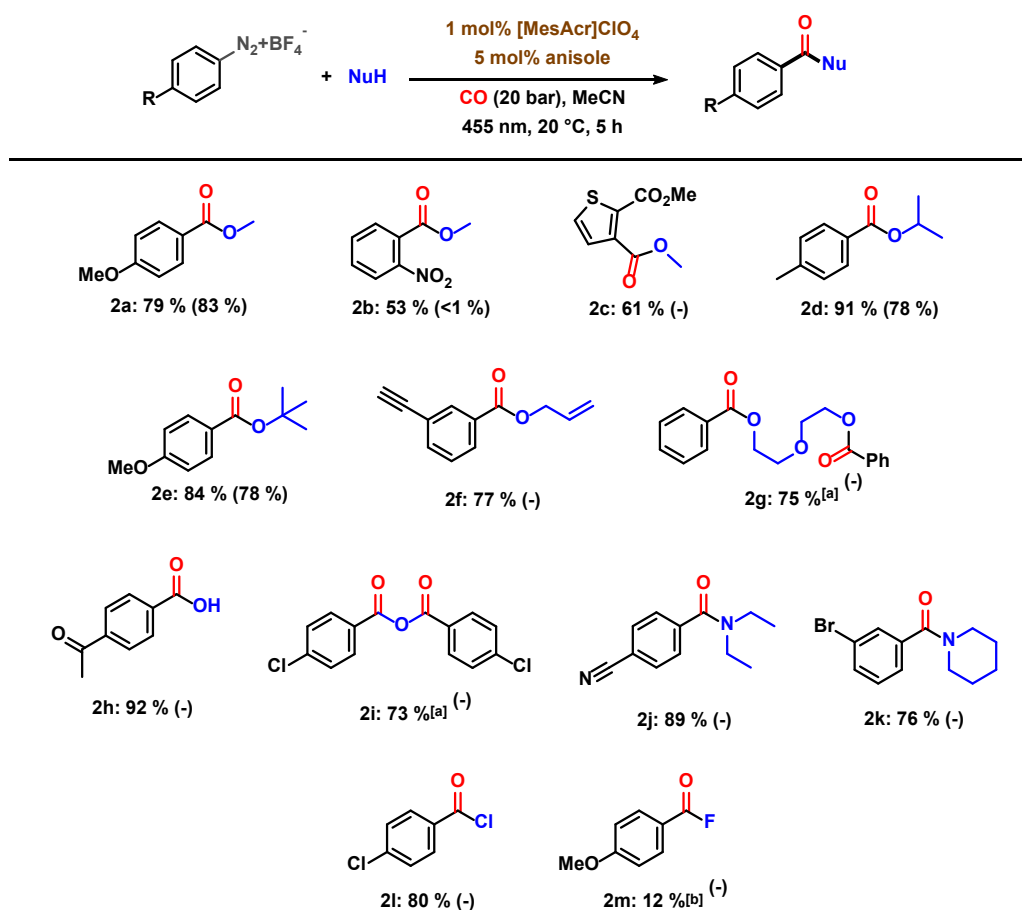
Scheme 7.2. Scope of the photocarbonylation. Reaction conditions: Diazonium salt (0.1 mmol), [MesAcr]ClO$_4$ (1 mol%, 0.001 mol), MeCN (1 mL), nucleophile (2 equiv., 0.2 mmol), CO (20 bar), LED (455 nm), anisole (5 mol%, 0.005 mol), 20 °C, 5 h. Isolated yields are reported. Yields of eosin Y catalyzed reaction at 50 bar CO with conditions from ref. [4a] are given in parentheses. [a] 0.5 eq. nucleophile [b] yield determined by ^{1}H NMR spectroscopy with hexamethylbenzene as standard.

Our previous studies on eosin Y catalyzed photo-carbonylations have strongly supported the notion of an overall redox-neutral catalytic cycle.[4] Here, we propose a similar mechanism involving three light-driven 1e-redox steps in the presence of the organic photo-catalyst MesAcr (Scheme 7.3). Activation of the employed photo-catalyst [MesAcr]+ (2.06 V),[6] occurs by photoredox with the sacrificial co-catalyst anisole (1.76 V *vs.* SCE, step *I*).[9] The resultant

MesAcr• (-0.57 V *vs.* SCE) is sufficiently reducing to initiate photocatalytic arenediazonium reduction (~0 V *vs.* SCE, step *II*). Reaction of the aryl radical with CO is limited by low mass transfer across the gas-liquid interface, low solubility of CO in short-chain alcohols (generally low solubility in polar media),[10,11] and low resonance stabilization of the resultant aroyl radical (step *III*). We reasoned that a thermodynamically strongly favored onward-oxidation to the acylium ion (step *IV*) may drive the turnover-limiting CO addition toward the aroyl side of the equilibrium (*III*). Upon employment of the significantly stronger photo-oxidant MesAcr+* (2.06 V *vs.* SCE) - in comparison with the previously used eosin Y (EY+*: –0.8 V *vs.* SCE) - enabled facile 1e-oxidation of all acyl radicals to the acylium ions (range of redox potentials calculated by DFT-B3LYP: -0.14 V to 1.7 V).[4a, 12] This change of photo-catalyst from eosin Y to MesAcr enabled good conversion of the so far unreactive electron-deficient 2-nitrobenzenediazonium (entry 2, Table 2) and generally a broader scope of nucleophiles, including water, amines, chloride.
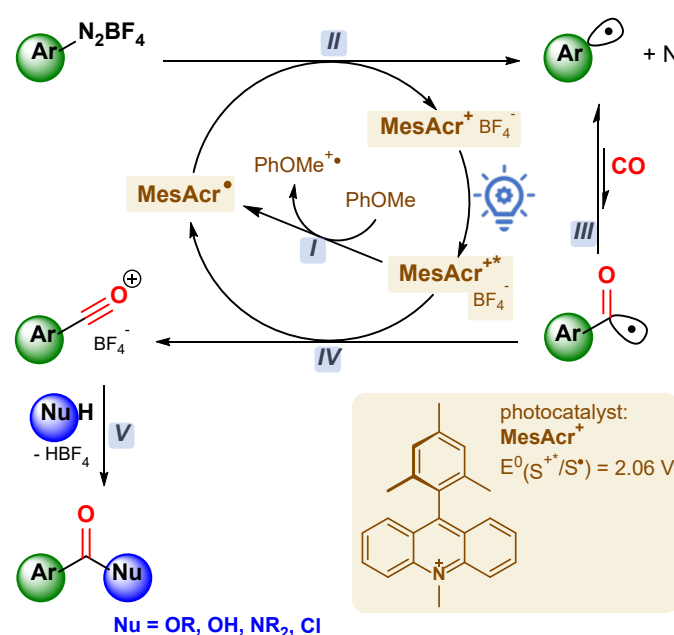
Scheme 7.3. Proposed photocatalysis mechanism: photo-catalyst activation by sacrificial reductant (*I*), SET mesolysis of diazonium salt (*II*), CO addition to aryl radical (*III*), SET oxidation of acyl radical (*IV*), nucleophilic addition (*V*).

7.3   Conclusion

In conclusion, we have developed optimized conditions for an organic photoredox carbonylation with visible light. Stable arene-diazonium salts are cleanly converted into various benzoic derivatives (ester, acid, amide, chloride). The use of mesityl-acridinium as photocatalyst addressed the major limitations of the previous procedure[4] by expanding the critical photo-oxidation window to electron-poor arenes, lowering the gas pressure from 50 bar to 20 bar, enabling reactions with water, amines, and chloride as nucleophiles, and eliminating solubility issues of the photo-catalyst. The utilization of the organic chloride [bmim]Cl afforded acyl chlorides under HCl-free conditions that can be subsequently substituted with any nucleophile so that this photo-carbonylation is a prime strategy to access a wide chemical space of carbonyl compounds.[13]

7.4 Experimental Section

7.4.1 Materials and methods

Commercial chemicals (> 98 % purity) were used as obtained without further purification unless specified otherwise. Diazonium salts were prepared by synthetic routes (*vide infra*), with the respective aniline precursors used without further purification as obtained from the vendors. TLC was performed using commercial silica gel coated aluminum plates (DC Kieselgel 60 F$_{254}$, *Merck*); visualization was done by the use of UV light. Staining was realized with a solution of phosphomolybdic acid in ethanol. Product yields were determined from isolated materials after flash chromatography on silica gel (Acros Organics, mesh 35–70). NMR spectral data was collected on a *Bruker* Fourier HD 400 (400 MHz for ^{1}H; 100 MHz for ^{13}C) at 25 °C. The quantification of ^{1}H cores was obtained by integration of resonance signals. Abbreviations used in ^{1}H NMR spectra: s – singlet, d – doublet, t – triplet, m – multiplet. Low-resolution mass spectroscopy was conducted on an *Agilent* 6890N GC-system coupled to a 5975 MSD unit and H$_2$ as carrier gas.
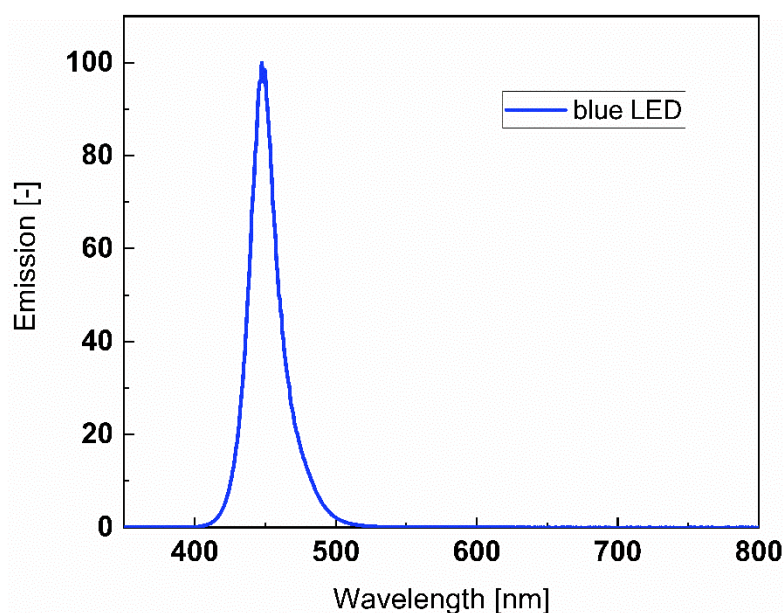
Scheme 7.4. Emission spectrum of used blue LED.

7.4.2 General procedures

Synthesis of diazonium salts

The parent aniline (4.5 mmol) was dissolved in glacial acetic acid (3 mL) and 48 % aqueous tetrafluoroboric acid (1.3 mL) at room temperature. Afterwards, isoamyl nitrite (1 mL) was dissolved in glacial acetic acid (2 mL) and added to the first solution over the course of five minutes. Then, diethyl ether (15 mL) was added and the mixture was cooled to -30 °C until the crystalline product precipitated. The precipitate was collected by filtration and re-dissolved in a minimum amount of acetone. Finally, the diazonium tetrafluoroborate was precipitated by addition of diethyl ether (15 mL), filtered, washed with diethyl ether (2x 10 mL) and dried in the air.

General procedure photocarbonylation

A glass vial (2 mL) was charged with a magnetic stirrer bar, arene diazonium salt (0.1 mmol), a 1 mM solution of [Mes-Acr]ClO$_4$ in MeCN (1 mL), anisole (0.005 mmol) and nucleophile (0.2 mmol). The rubber septum of the vial cap was punctured with a needle. Then, the vial was transferred to an autoclave containing a Quartz window bottom (*Parr Instruments*). The reactor was sealed, placed on a magnetic stirrer, and slowly filled with CO (20 bar). The reaction was irradiated with an external LED (λ_{max} = 455 nm). After 5 h at 20 °C, the gas was released, and the vial retrieved. Water (3 mL) was added, and the resulting mixture was extracted with ethyl acetate (2x5 mL). The organic phases were washed with brine (5 mL) and dried over Na$_2$SO$_4$. Volatiles were evaporated and the residues were purified by flash column chromatography on silica.

7.4.3   Analytical data of synthesized compounds

Methyl 4-methoxybenzoate (2a)
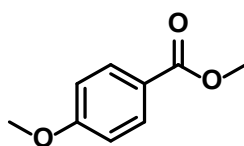
Following the general procedure, **methyl 4-methoxybenzoate** was isolated by flash chromatography on silica with ethyl acetate/pentane as eluent as a white solid (13.1 mg, 79 % yield).

¹H NMR (400 MHz, CDCl$_3$, ppm): δ = 8.01–7.98 (m, 2H), 6.93–6.90 (m, 2H), 3.88 (s, 3H), 3.85 (s, 3H). **¹³C NMR** (100 MHz, CDCl$_3$, ppm): δ = 167.0, 163.4, 131.7, 122.8, 113.7, 55.6, 52.0. **GC-MS (EI)** *m/z* (relative intensity): 166 (33) [M+], 135 (100), 107 (12), 92 (17), 77 (21).

The spectral data are consistent with literature values.[4a]

Methyl 2-nitrobenzoate (2b)
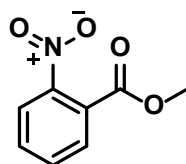
Following the general procedure, **methyl 2-nitrobenzene** was isolated by flash chromatography on silica with ethyl acetate/pentane as eluent as a yellowish liquid (9.6 mg, 53 % yield).

¹H NMR (400 MHz, CDCl$_3$, ppm): δ = 7.92–7.89 (m, 1H),7.76–7.60 (m, 3H), 3.92 (s, 3H). **¹³C NMR** (100 MHz, CDCl$_3$, ppm): δ = 166.0, 133.3, 132.2, 129.9, 128.4, 124.3, 53.7. **GC-MS (EI)** *m/z* (relative intensity): 181 (4) [M+], 150 (100), 92 (26), 79 (55), 77 (35).

The spectral data are consistent with literature values.[14]

Dimethyl 2,3-thiophendicarboxylate (2c)
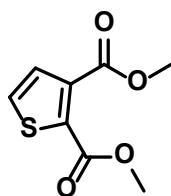
Following the general procedure, **dimethyl 2,3-thiophendicarboxylate** was isolated by flash chromatography on silica with ethyl acetate/pentane as eluent as a white solid (12.2 mg, 61 % yield).

^{1}H NMR (400 MHz, CDCl$_3$, ppm): δ = 7.46 (d, *J* = 5.1 Hz, 1H), 7.29 (d, *J* = 5.1 Hz, 1H), 3.92 (s, 3H), 3.90 (s, 3H). **^{13}C NMR** (100 MHz, CDCl$_3$, ppm): δ = 164.7, 161.7, 137.3, 134.0, 130.2, 128.9, 52.8, 52.8. **GC-MS (EI)** *m/z* (relative intensity): 200 (25) [M$^+$], 169 (100), 139 (44), 126 (8), 111 (9).

The spectral data are consistent with literature values.[15]

i-Propyl 4-methylbenzoate (2d)
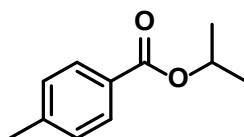
Following the general procedure, ***i*-propyl 4-methylbenzoate** was isolated by flash chromatography on silica with ethyl acetate/pentane as eluent as a colorless oil (16.2 mg, 91 % yield).

^{1}H NMR (400 MHz, CDCl$_3$, ppm): δ = 7.94–7.91 (m, 2H), 7.24–7.21 (m, 2H), 5.24 (hept, *J* = 6.3 Hz, 1H), 2.40 (s, 3H), 1.36 (d, *J* = 6.2 Hz, 1H). **^{13}C NMR** (100 MHz, CDCl$_3$, ppm): δ = 166.8, 143.7, 129.9, 129.4, 128.6, 68.5, 22.4, 22.0. **GC-MS (EI)** *m/z* (relative intensity): 178 (8) [M$^+$], 136 (34), 119 (100), 91 (57), 65 (22).

The spectral data are consistent with literature values.[4a]

t-Butyl 4-methoxybenzoate (2e)
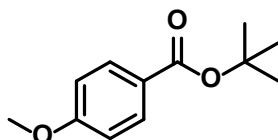
Following the general procedure, ***t*-butyl 4-methoxybenzoate** was isolated by flash chromatography on silica with ethyl acetate/pentane as eluent as a colorless oil (17.5 mg, 84 % yield).

^{1}H NMR (400 MHz, CDCl$_3$, ppm): δ = 7.91–7.88 (m, 2H), 7.45–7.42 (m, 2H), 1.41 (s, 9H). **^{13}C NMR** (100 MHz, CDCl$_3$, ppm): δ = 165.7, 163.1, 131.5, 124.6, 113.5, 80.6, 55.5, 28.4. **GC-MS (EI)** *m/z* (relative intensity): 208 (15) [M$^+$], 152 (100), 135 (71), 77 (10).

The spectral data are consistent with literature values.[4a]

Allyl 3-ethinyl benzoate (2f)
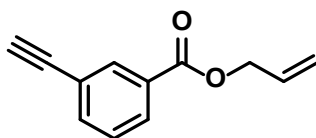
Following the general procedure, **allyl 3-ethinylbenzoate** was isolated by flash chromatography on silica with ethyl acetate/pentane as eluent as a colorless liquid (14.3 mg, 77 % yield).

^{1}H NMR (400 MHz, CDCl$_3$, ppm): δ = 8.19 (s, 1H), 8.05–8.03 (m, 1H), 7.68–7.66 (m, 1H), 7.44–7.39 (m, 1H), 6.10–5.97 (m, 1H), 5.44–5.29 (m, 2H), 4.84–4.82 (m, 2H), 3.12 (s, 1H). **^{13}C NMR** (100 MHz, CDCl$_3$, ppm): δ = 166.4, 136.5, 133.4, 132.2, 130.7, 130.0, 128.6, 122.8, 118.7, 78.3, 66.0. **GC-MS (EI)** m/z (relative intensity): 186 (2) [M$^+$], 129 (100), 101 (67), 75 (56), 74 (35).

The spectral data are consistent with literature values.[16]

Diethylene glycol dibenzoate (2g)
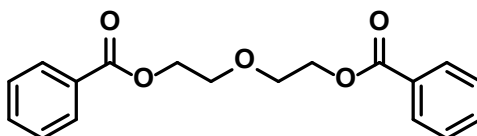
Following the general procedure with 0.5 eq. nucleophile, **diethylene glycol dibenzoate** was isolated by flash chromatography on silica with ethyl acetate/pentane as eluent as a colorless liquid (11.8 mg, 75 % yield).

^{1}H NMR (400 MHz, CDCl$_3$, ppm): δ = 8.05–8.03 (m, 2H), 7.57–7.52 (m, 1H),7.43–7.38 (m, 2H), 4.52–4.49 (m, 2H), 3.91–3.87 (m, 2H). **^{13}C NMR** (100 MHz, CDCl$_3$, ppm): δ = 167.2, 133.1, 130.2, 129.8, 128.5, 69.4, 64.1. **GC-MS (EI)** m/z (relative intensity): 149 (51), 105 (100), 77 (54), 51 (16).

The spectral data are consistent with literature values.[17]

4-Acetylbenzoic acid (2h)
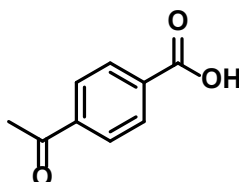
Following the general procedure, **4-acetyl benzoic acid** was isolated by flash chromatography on silica with ethyl acetate/pentane as eluent as a white solid (15.1 mg, 92 % yield).

^{1}H NMR (400 MHz, DMSO-d$_6$, ppm): δ = 13.29 (br s, 1H), 8.05 (s, 4H), 2.62 (3H). **^{13}C NMR** (100 MHz, DMSO-d$_6$, ppm): δ = 197.5, 166.3, 139.6, 134.3, 130.0, 128.1, 26.8.

The spectral data are consistent with literature values.[18]

4-Chloro benzoic anhydride (2i)
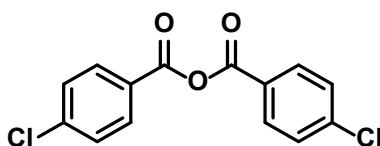
Following the general procedure with 0.5 eq. nucleophile, **4-chloro benzoic anhydride** was isolated by flash chromatography on silica with ethyl acetate/pentane as eluent as a white solid (10.8 mg, 73 % yield).

¹H NMR (400 MHz, CDCl₃, ppm): δ = 8.09–8.06 (m, 4H), 7.53–7.50 (m, 4H). **¹³C NMR** (100 MHz, CDCl₃, ppm): δ = 161.3, 141.4, 131.9, 129.4, 127.1. **GC-MS (EI)** *m/z* (relative intensity): 294 (2) [M⁺], 141 (34), 139 (100), 113 (13), 111 (36).

The spectral data are consistent with literature values.[19]

N,N-Diethyl 4-cyanobenzamide (2j)
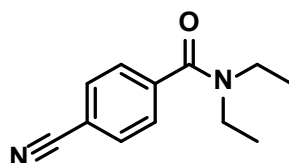
Following the general procedure, ***N,N*-diethyl 4-cyanobenzamide** was isolated by flash chromatography on silica with ethyl acetate/pentane as eluent as a white solid (18.0 mg, 89 % yield).

¹H NMR (400 MHz, CDCl₃, ppm): δ = 7.59–7.57 (m, 2H), 7.47–7.45 (m, 2H), (q, *J* = 7.2 Hz,4H), 1.33–1.24 (m, 6H). **¹³C NMR** (100 MHz, CDCl₃, ppm): δ = 168.3, 154.7, 133.1, 121.0, 119.8, 107.5, 49.5, 41.7, 14.4, 11.2. **GC-MS (EI)** *m/z* (relative intensity): 202 (10) [M⁺], 130 (15), 102 (100), 75 (25).

The spectral data are consistent with literature values.[20]

N-(3-Bromobenzoyl) piperidine (2k)
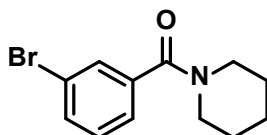
Following the general procedure, ***N*-(3-Bromobenzoyl) piperidine** was isolated by flash chromatography on silica with ethyl acetate/pentane as eluent as a white solid (20.5 mg, 76 % yield).

¹H NMR (400 MHz, CDCl₃, ppm): δ = 7.60 (m, 1H), 7.40–7.32, 7.40–7.32 (m, 1H), 7.26–7.24 (m, 1H), 7.21–7.15 (m, 1H), 3.80–3.78 (m, 4H), 1.72–1.70 (m, 6H). **¹³C NMR** (100 MHz, CDCl₃, ppm): δ = 168.3, 130.2, 128.3, 127.6, 123.0, 122.9, 120.0, 46.3, 25.7, 24.5. **GC-MS (EI)** *m/z* (relative intensity): 269 (3) [M⁺], 267 (3), 185 (8), 183 (8), 157 (89), 155 (91), 76 (100).

The spectral data are consistent with literature values.[21]

4-Chlorobenzoyl chloride (2l)
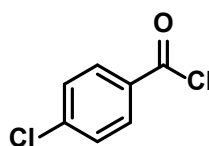
Following the general procedure using 1-butyl-3-methylimidazoliumchloride (0.2 mmol) as nucleophile, the crude reaction mixture was obtained after the autoclave reaction. The work-up differed from the general procedure. The solvent was removed under reduced pressure and **4-chlorobenzoyl chloride** was isolated by Kugelrohr-distillation of the residue as colorless liquid (14.0 mg, 80 % yield).

¹H NMR (400 MHz, CDCl₃, ppm): δ = 8.08–8.05 (m, 2H), 7.51–7.48 (m, 2H). **¹³C NMR** (100 MHz, CDCl₃, ppm): δ = 167.6, 142.5, 132.8, 131.8, 129.5. **GC-MS (EI)** *m/z* (relative intensity): 174 (6) [M⁺], 141 (34), 139 (100), 113 (13), 111 (39).

The spectral data are consistent with literature values.[22]

4-Methoxybenzoyl fluoride (2m)
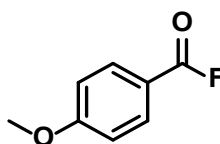
Following the general procedure using potassium fluoride (0.2 mmol) as nucleophile, the crude reaction mixture was obtained after the autoclave reaction. The work-up differed from the general procedure. The solvent was removed under reduced pressure and the crude reaction mixture was analyzed. The yield was determined by ¹H NMR spectroscopy with hexamethylbenzene as standard. **4-methoxybenzoyl fluoride** was obtained in 12 % yield (0.012 mmol). Isolation by column chromatography or distillation was not successful; NMR spectra of the crude mixture are given.

¹H NMR (400 MHz, CDCl₃, ppm): δ = 8.01–7.98 (m, 2H), 7.00–6.97 (m, 2H), 3.90 (s, 3H). **¹⁹F NMR** (376 MHz, CDCl₃, ppm): δ = 15.99. **GC-MS (EI)** *m/z* (relative intensity): 154 (100) [M⁺], 135 (25), 126 (62), 111 (25), 83 (41).

The spectral data are consistent with literature values.[23]

7.5   References

[1]   a) J. B. Peng, H. Q. Geng, X. F. Wu, *Chem* **2019**, *5*, 526–552. b) H.M. Colquhoun, D. J. Thompson, M.V. Twigg, *Carbonylation*, Plenum Press, New York, **1991**.

[2]   a) W. Bertleff, M. Roeper, X. Sava, *Carbonylation* in: Ullmann´s Encyclopedia of Industrial Chemistry, Wiley-VCH Verlag GmbH & Co. KGaA, Weinheim, **2007**. b) M. Beller, X.-F. Wu, *Transition Metal Catalyzed Carbonylation Reactions*, Springer Berlin, Heidelberg, **2013**. c) A. Brennführer, H. Neumann, M. Beller, *Angew. Chem. Int. Ed.* **2009**, *48*, 4114–4133.

[3]   For selected examples see: a) K. Nagahara, I. Ryu, M. Komatsu, N. Sonoda, *J. Am. Chem. Soc.* **1997**, *119*, 5465–5466. b) T. Kawamoto, A. Sato, I. Ryu, *Chem. Eur. J.* **2015**, *21*, 14764–14767. c) H. Zhang, R. Shi, A. Ding, L. Lu, B. Chen, A. Lei, *Angew. Chem. Int. Ed.* **2012**, *51*, 12542–12545. d) F. Xu, D. Li, W. Han, *Green Chem.* **2019**, *21*, 2911–2915. e) Z. Yin, J. Rabeah, A. Brückner, X.-F. Wu, *ACS Catal.* **2018**, *8*, 10926–10930. f) F. Jin, Y. Zhong, X. Zhang, H. Zhang, Q. Zhao, W. Han, *Green Chem.* **2016**, *18*, 2598–2603.

[4]   a) M. Majek, A. Jacobi von Wangelin, *Angew. Chem. Int. Ed.* **2015**, *54*, 2270–2274. b) W. Guo, L. Q. Lu, Y. Wang, Y. N. Wang, J. R. Chen, W. J. Xiao, *Angew. Chem. Int. Ed.* **2015**, *54*, 2265–2269.

[5]   For selected examples see: a) A. Cartier, E. Levernier, V. Corcé, T. Fukuyama, A. L. Dhimane, C. Ollivier, I. Ryu, L. Fensterbank, *Angew. Chem. Int. Ed.* **2019**, *58*, 1789–1793. b) X. Li, D. Liang, W. Huang, H. Zhou, Z. Li, B. Wang, Y. Ma, H. Wang, *Tetrahedron* **2016**, *72*, 8442–8448. c) A. Cartier, E. Levernier, A. L. Dhimane, T. Fukuyama, C. Ollivier, I. Ryu, L. Fensterbank, *Adv. Synth. Catal.* **2020**, *362*, 2254–2259. d) Z. Qi, L. Li, Y. K. Liang, A. J. Ma, X. Z. Zhang, J. B. Peng, *Org. Lett.* **2021**, *23*, 4769–4773.

[6]   T. Tsudaka, H. Kotani, K. Ohkubo, T. Nakagawa, N. V. Tkachenko, H. Lemmetyinen, S. Fukuzumi, *Chem. Eur. J.* **2017**, *23*, 1306–1317.

[7]   N. E. S. Tay, D. A. Nicewicz, *J. Am. Chem. Soc.* **2017**, *139*, 16100–16104.

[8]   W. D. Arendt, J. Lang, *J. Vinyl Addit. Technol*. **1998**, *4*, 184–188.

[9]   T. Fuchigami, S. Inagi, M. Atobe, *Fundamentals and Applications of Organic Electrochemistry*, Wiley, Chichester, **2015**.

[10]   C. Vogelpohl, C. Brandenbusch, G. Sadowski, *J. Supercrit. Fluids* **2013**, *81*, 23–32.

[11]   *Carbon Monoxide*, IUPAC Solubility Data Series, Vol. 43 (Ed. R. W. Cargill), Pergamon Press, Oxford, **1990**.

[12]   M.-H. Baik, R. A. Friesner, *J. Phys. Chem. A* **2002**, *106*, 7407–7412.

[13]   T. Maki, K. Takeda, *Benzoic Acid and Derivatives* in: *Ullmann's Encyclopedia of Industrial Chemistry*, Wiley-VCH Verlag GmbH & Co. KGaA, Weinheim, **2002**.

[14]   H. Aman, Y.H. Wang, G. J. Chuang, *ACS Omega* **2020**, *5*, 918–925.

[15]   E. Block, A. J. Yencha, M. Aslam, V. Eswarakrishnan, J. Luo, A. Sano, *J. Am. Chem. Soc.* **1988**, *110*, 4748–4753.

[16]   S. G. E. Amos, S. Nicolai, J. Waser, *Chem. Sci.* **2020**, *11*, 11274–11279.

[17]   L. N. D. Beardmore, S. L. Cobb, W. D. G. Brittain, *Org. Biomol. Chem*. **2022**, *20*, 8059–8064.

[18]   Q. Y. Meng, S. Wang, B. König, *Angew. Chem. Int. Ed.* **2017**, *56*, 13426–13430.

[19]   Y. Li, D. Xue, C. Wang, Z.-T. Liu, J. Xiao, *Chem. Commun.* **2012**, *48*, 1320–1322.

[20]   Y. S. Bao, L. Wang, M. Jia, A. Xu, B. Agula, M. Baiyin, B. Zhaorigetu, *Green Chem.* **2016**, *18*, 3808–3814.

[21]   F. Messa, S. Perrone, M. Capua, F. Tolomeo, L. Troisi, V. Capriati, A. Salomone, *Chem. Commun.* **2018**, *54*, 8100–8103.

[22]   AIST: Spectral Database for Organic Compounds SDBS; NMR spectra; SDBS No.: 2865; CAS RN: 122-01-0, https://sdbs.db.aist.go.jp (accessed **October 19, 2023)**

[23]   D. Kim, H. N. Lim, *Org. Lett.* **2020**, *22*, 7465–7469.

7.6 Experimental Spectra
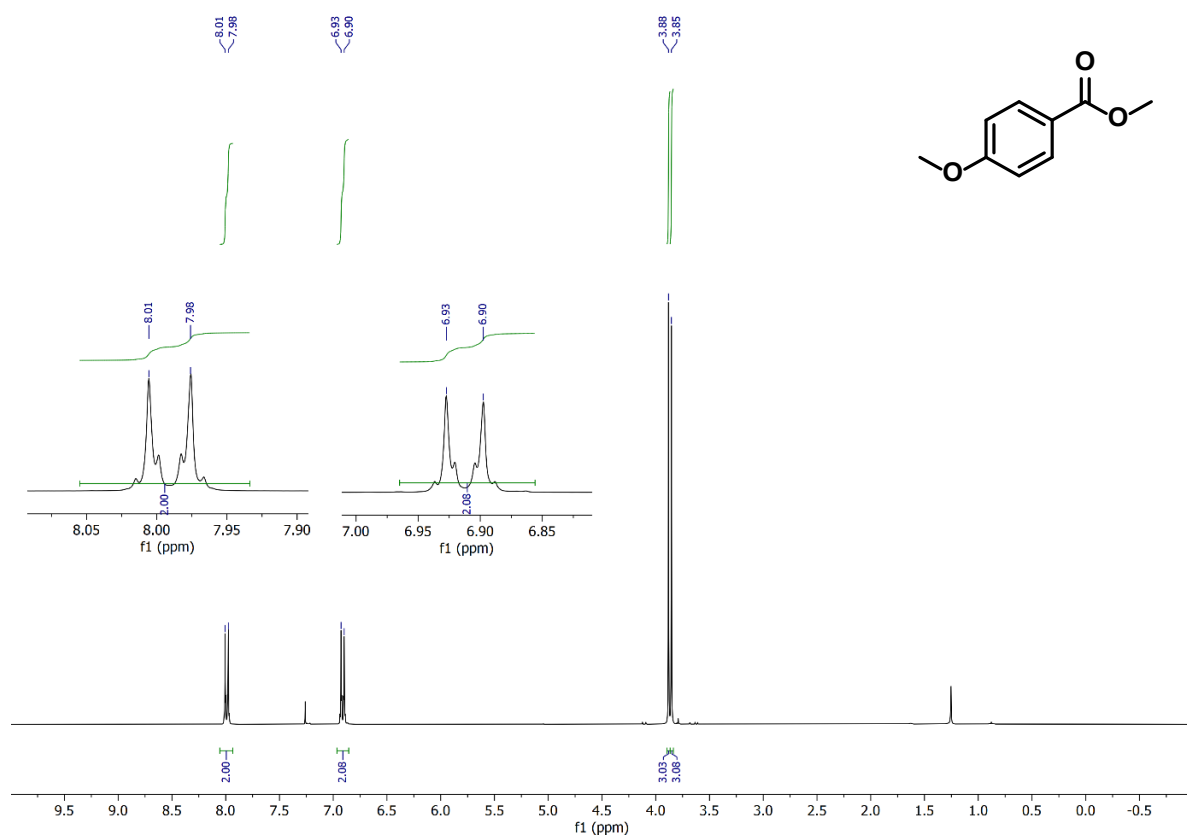
^{1}H NMR spectrum (400 MHz, CDCl$_3$) of Methyl 4-methoxybenzoate (2a).
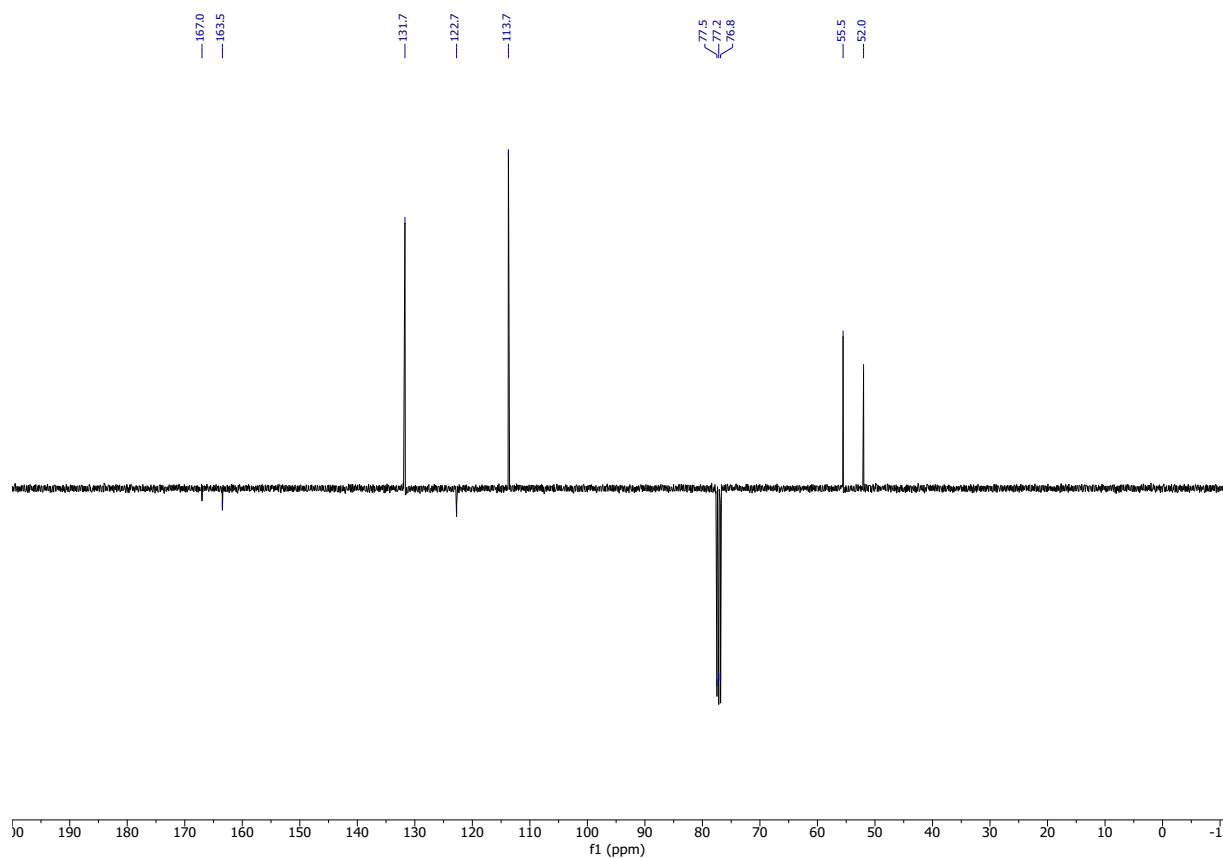
¹³C NMR spectrum (100 MHz, CDCl₃) of Methyl 4-methoxybenzoate.
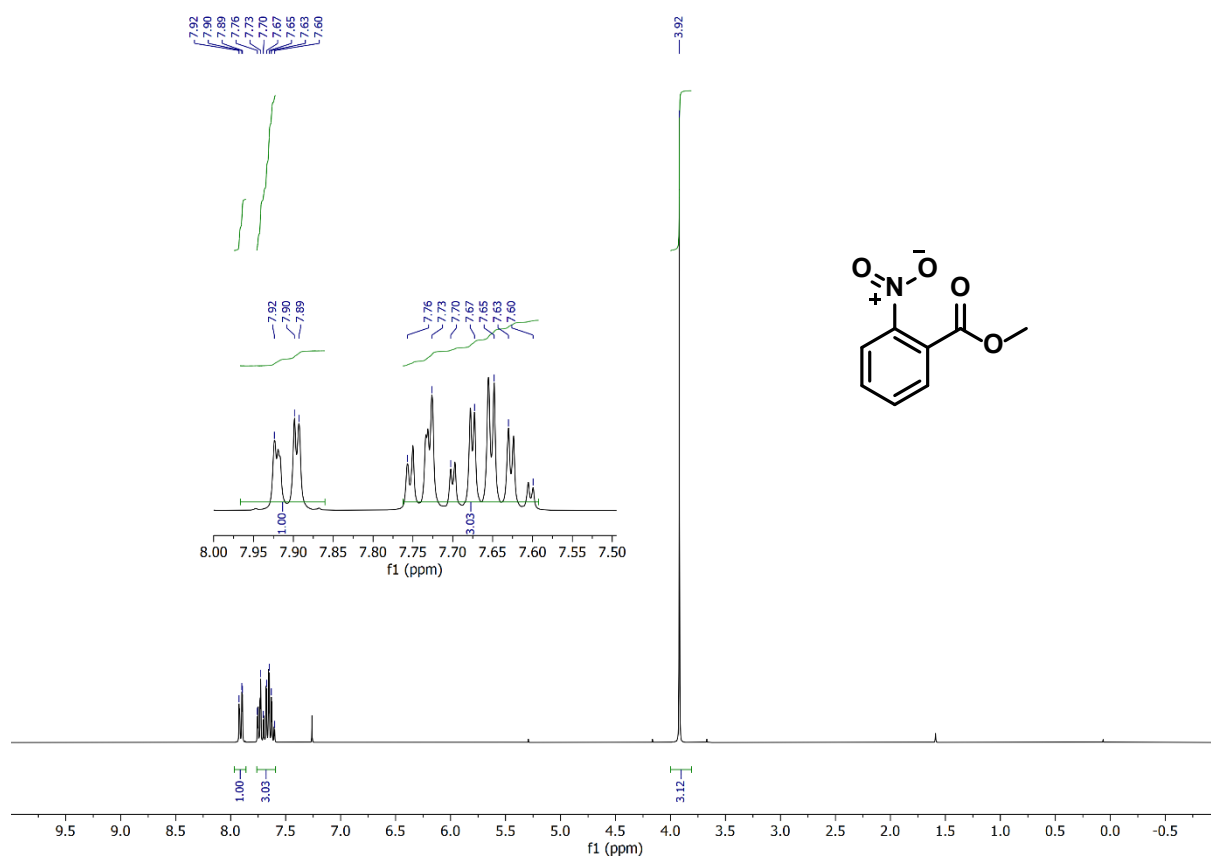
¹H NMR spectrum (400 MHz, CDCl₃) of Methyl 2-nitrobenzoate (2b).
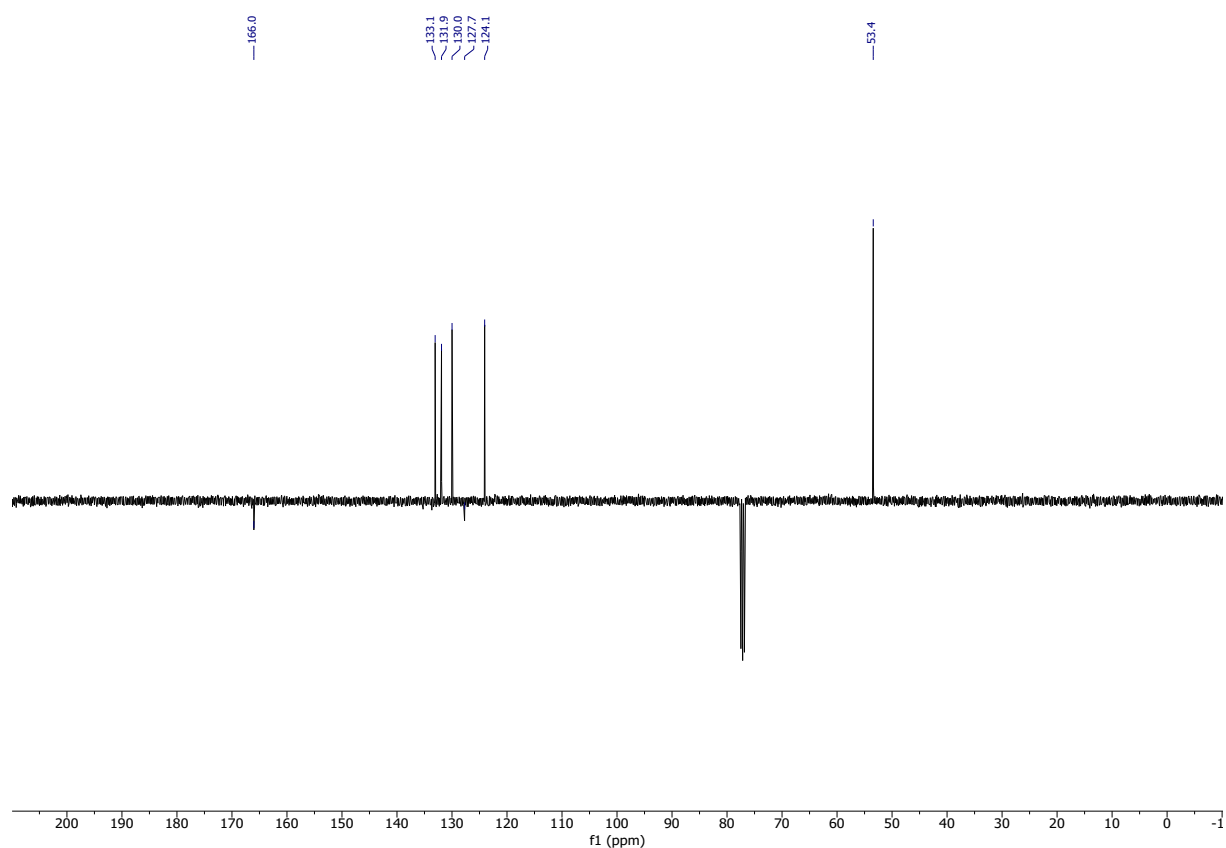
¹³C NMR spectrum (100 MHz, CDCl₃) of Methyl 2-nitrobenzoate.
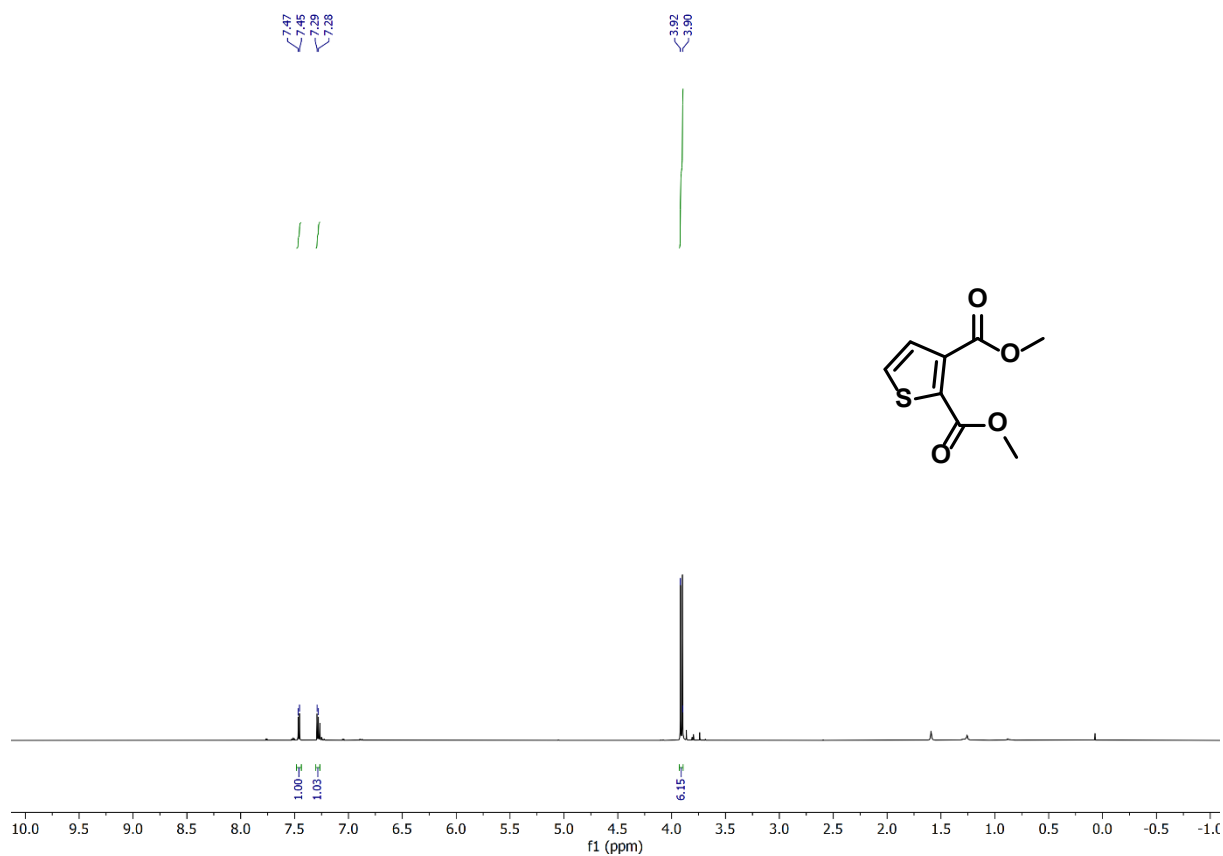
¹H NMR spectrum (400 MHz, CDCl₃) of Dimethyl 2,3-thiophendicarboxylate (2c).
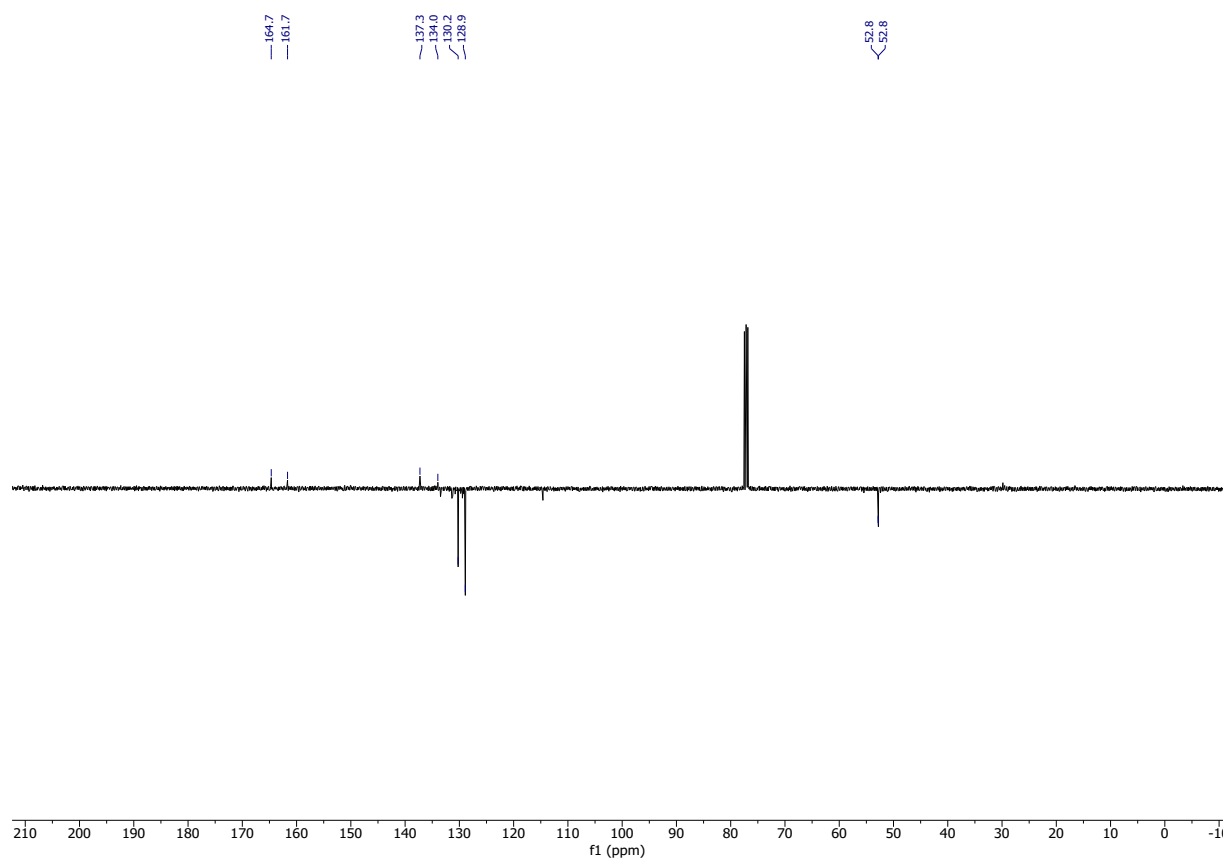
¹³C NMR spectrum (100 MHz, CDCl₃) of Dimethyl 2,3-thiophendicarboxylate.
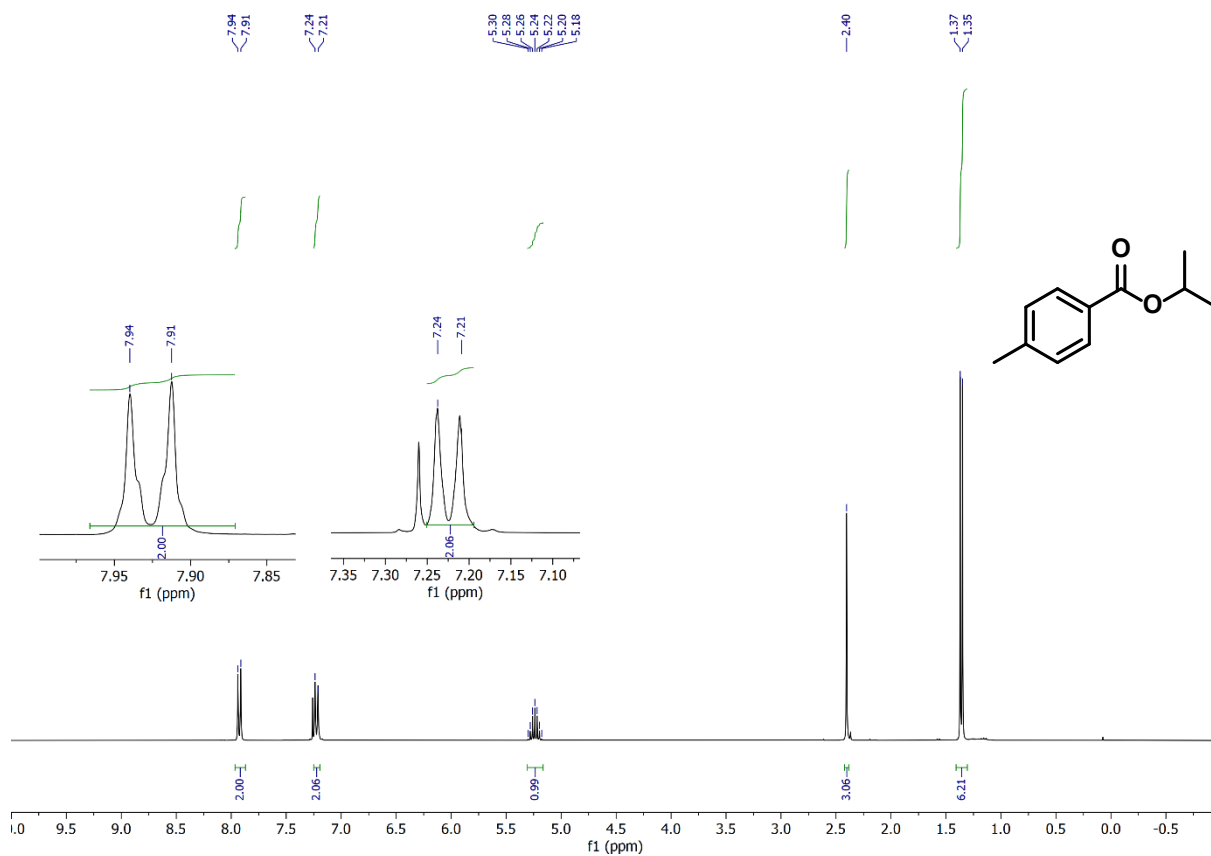
^{1}H NMR spectrum (400 MHz, CDCl$_3$) of *i*-Propyl 4-methylbenzoate (2d).
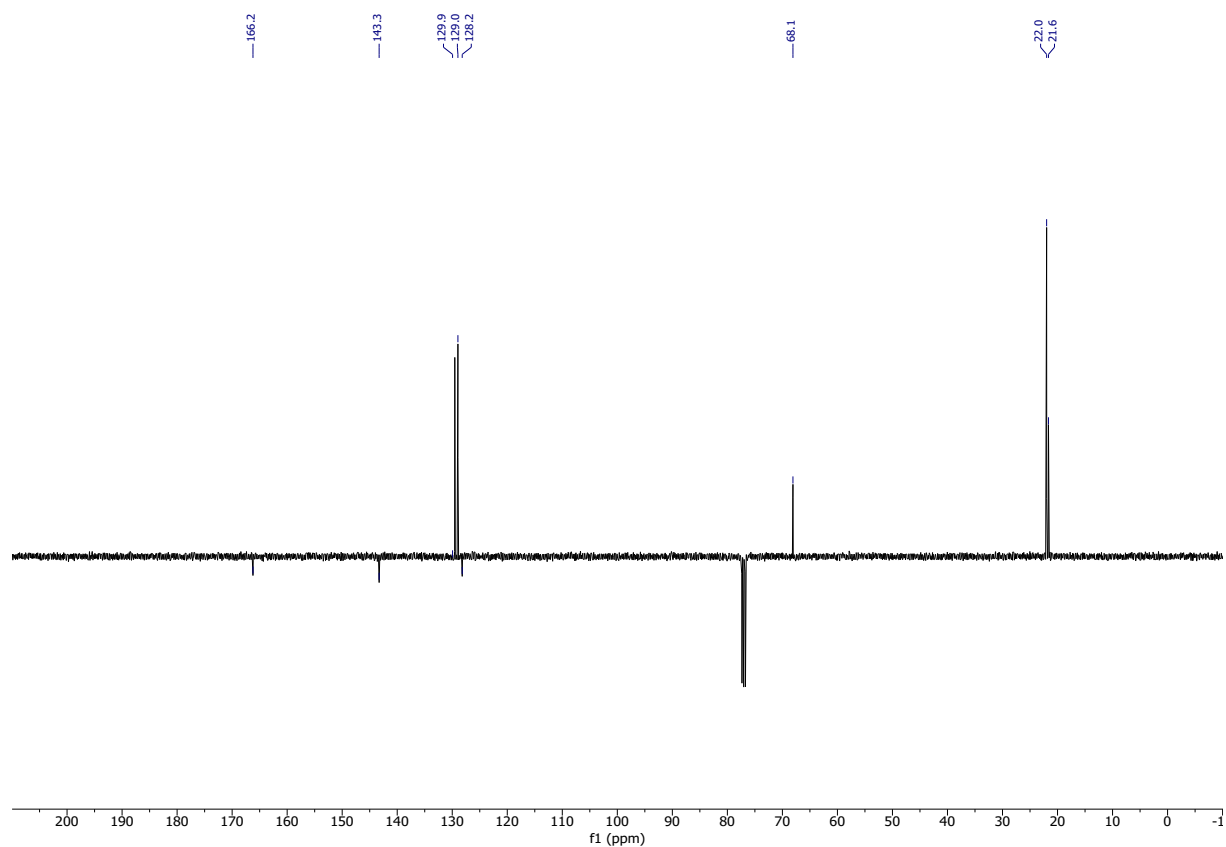
^{13}C NMR spectrum (100 MHz, CDCl$_3$) of *i*-Propyl 4-methylbenzoate.
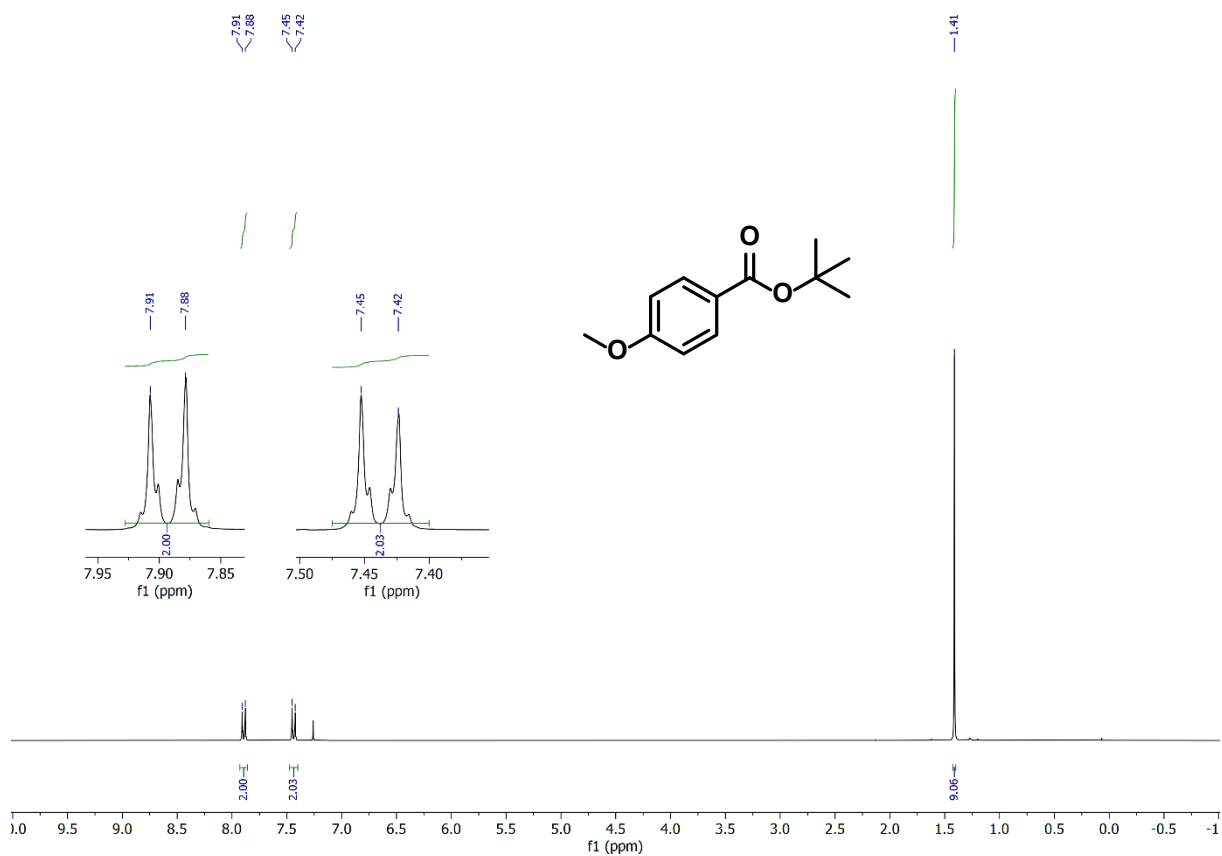
^{1}H NMR spectrum (400 MHz, CDCl$_3$) of *t*-Butyl 4-methoxybenzoate (2e).
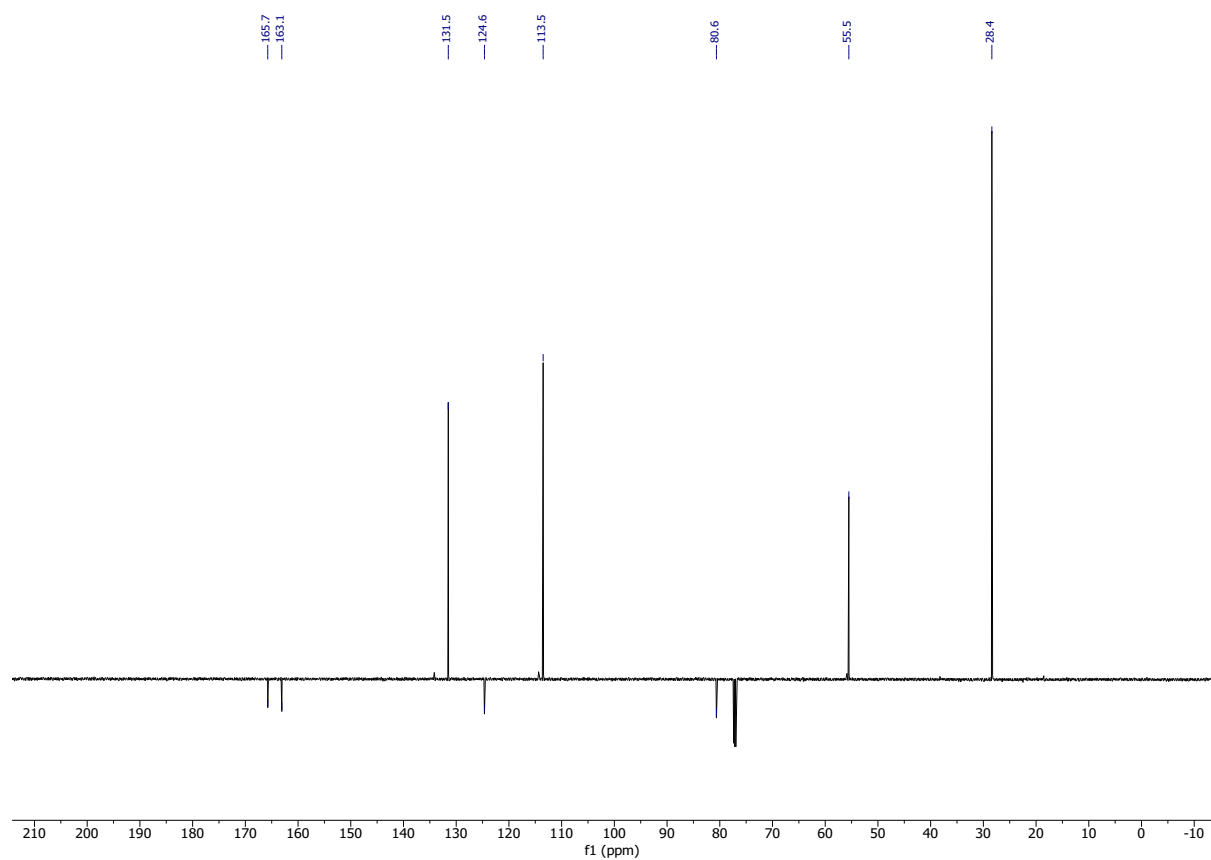
^{13}C NMR spectrum (100 MHz, CDCl$_3$) of *t*-Butyl 4-methoxybenzoate.
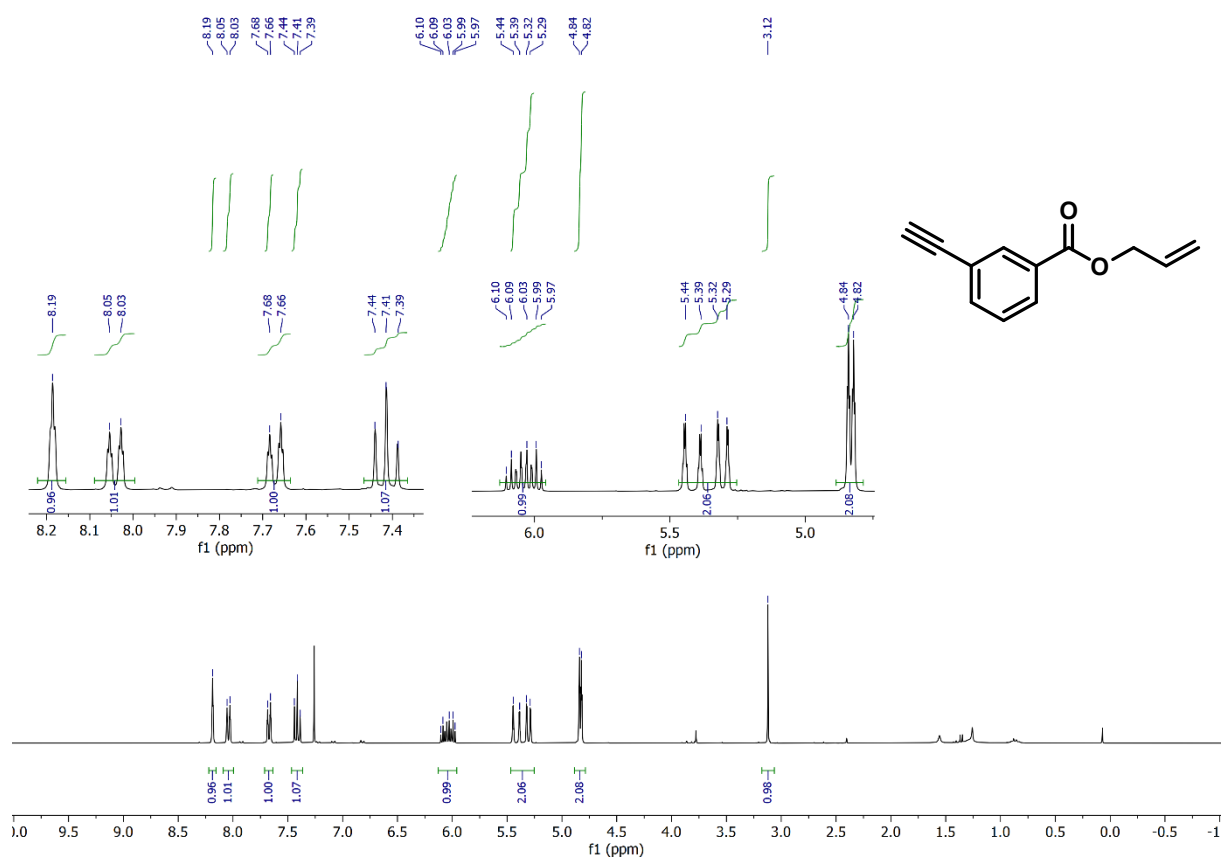
^{1}H NMR spectrum (400 MHz, CDCl$_3$) of Allyl 3-ethinylbenzoate (2f).
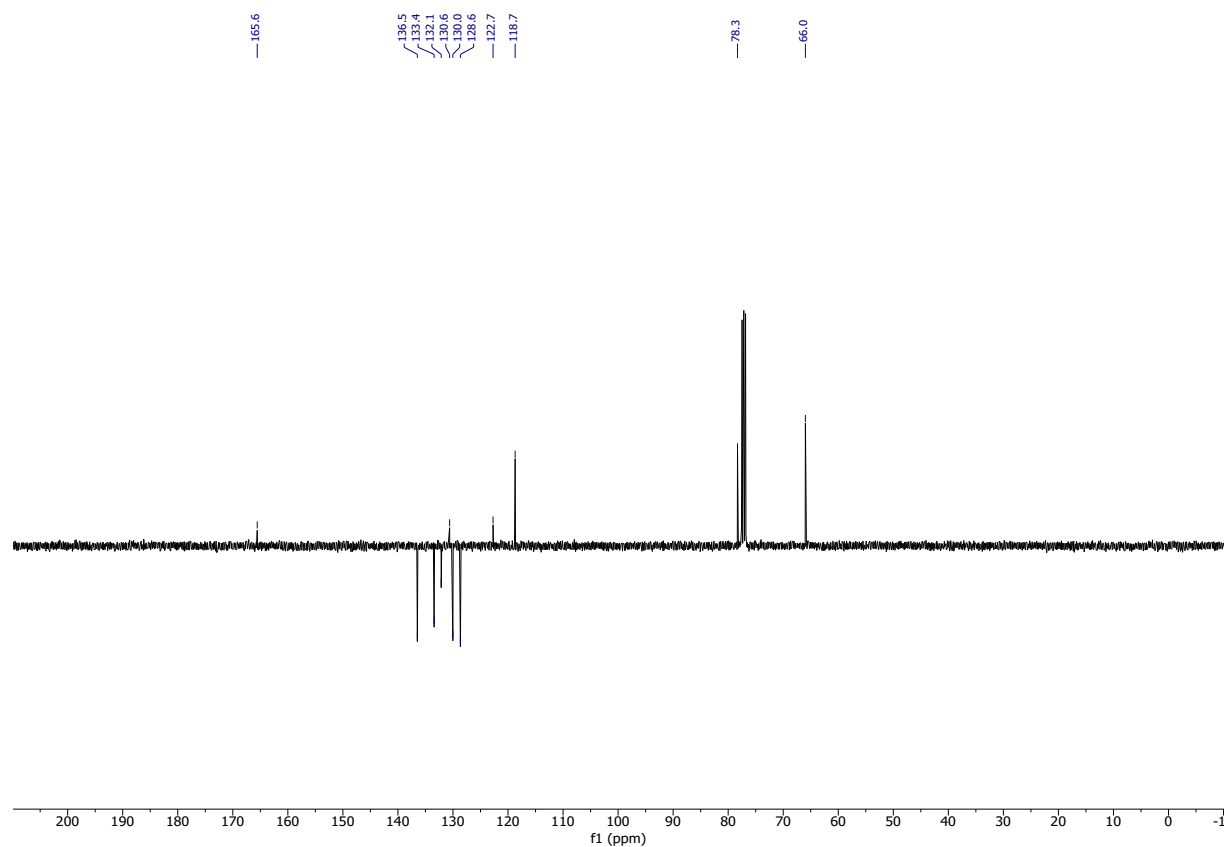
^{13}C NMR spectrum (100 MHz, CDCl$_3$) of Allyl 3-ethinylbenzoate.
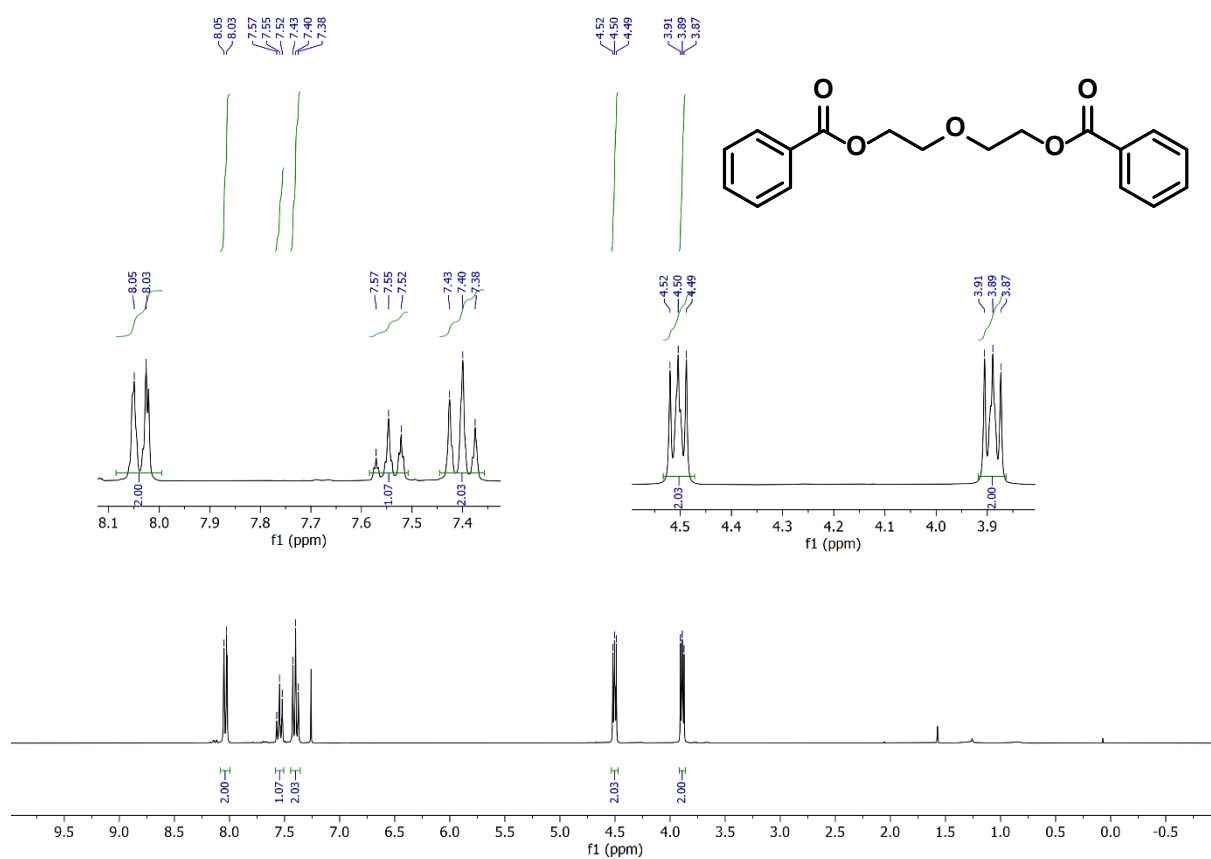
^{1}H NMR spectrum (400 MHz, CDCl$_3$) of Diethylene glycol dibenzoate (2g).
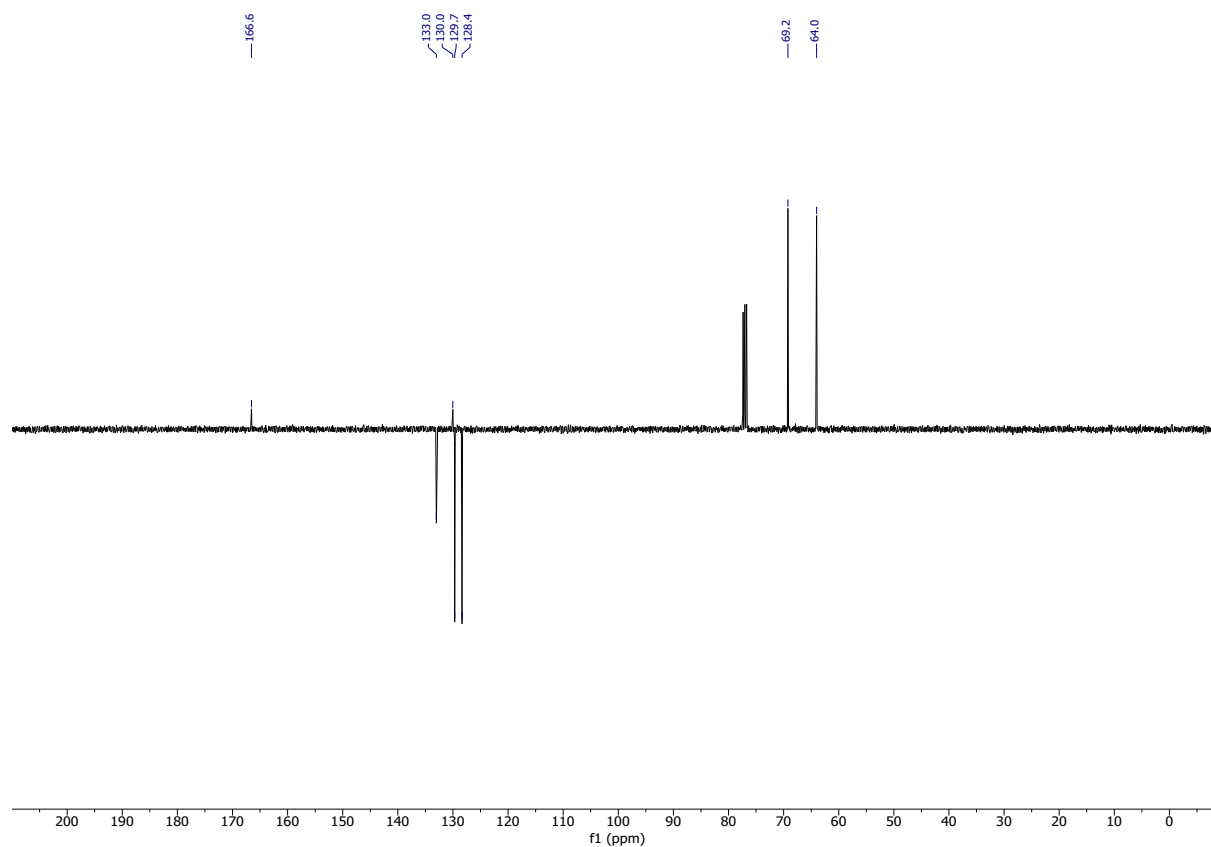
^{13}C NMR spectrum (100 MHz, CDCl$_3$) of Diethylene glycol dibenzoate.
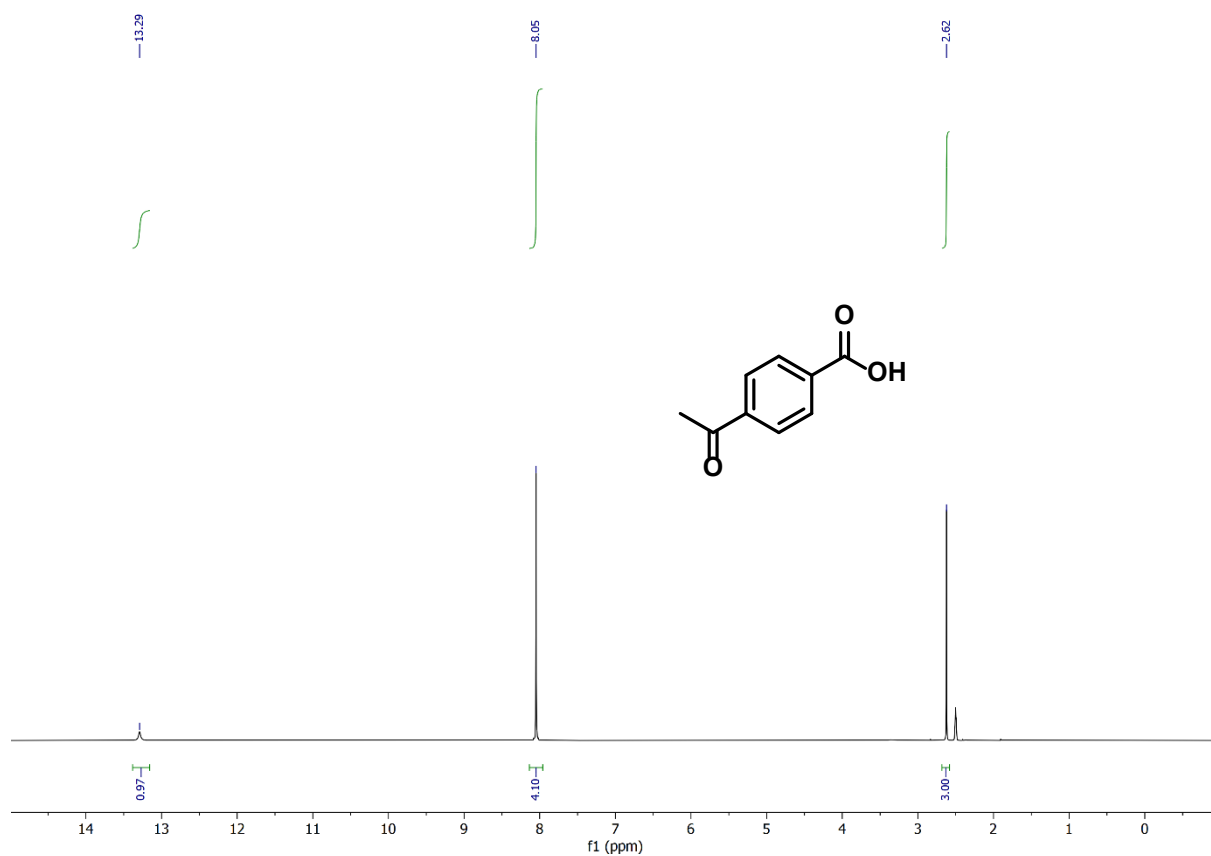
^{1}H NMR spectrum (400 MHz, DMSO-d$_6$) of 4-Acylbenzoic acid (2h).
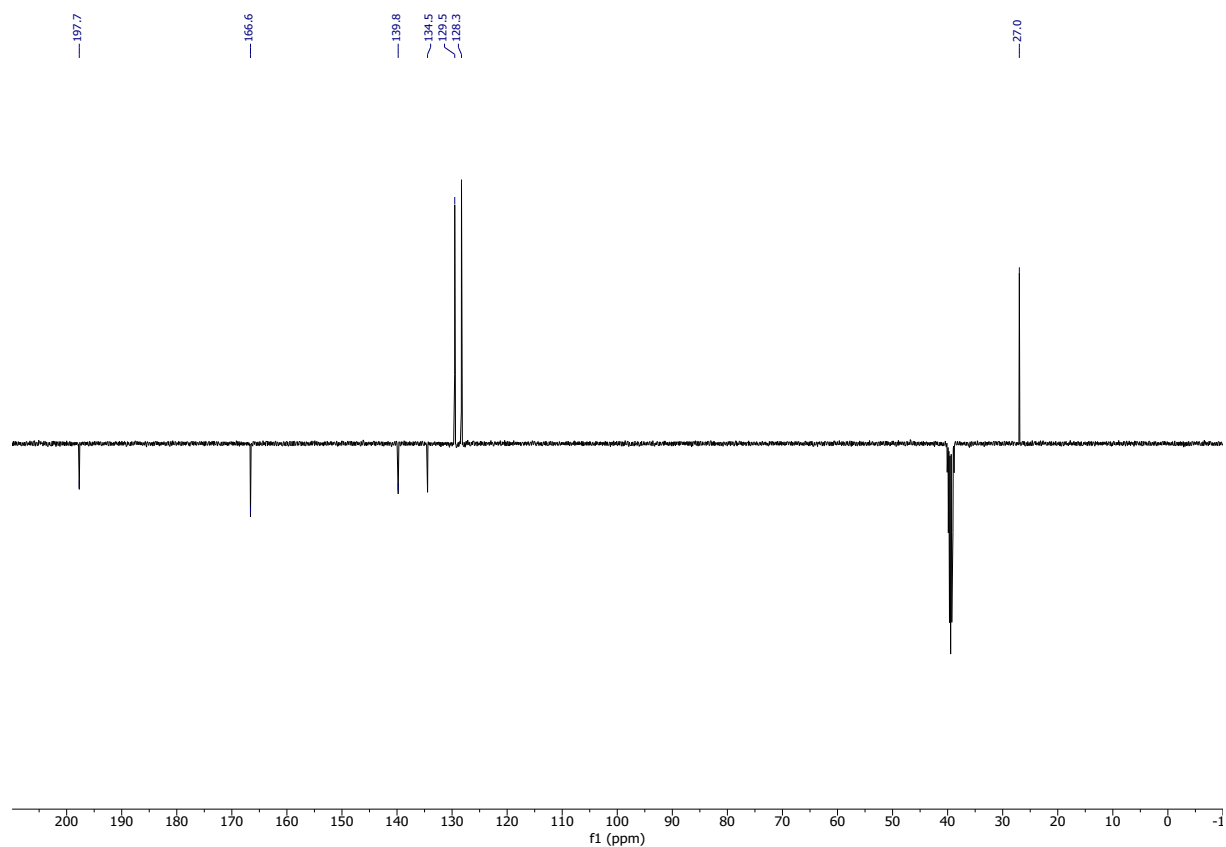
^{13}C NMR spectrum (100 MHz, DMSO-d$_6$) of 4-Acylbenzoic acid.
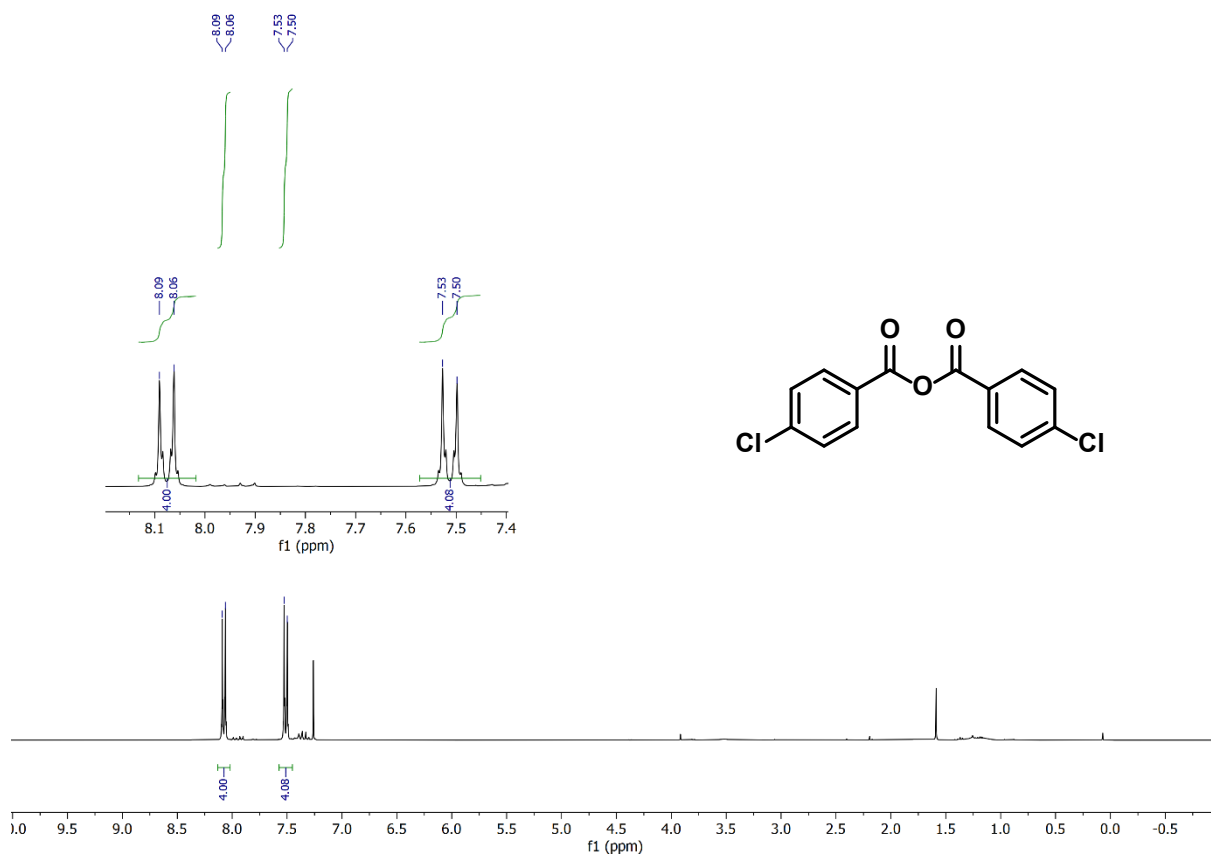
¹H NMR spectrum (400 MHz, CDCl₃) of 4-Chloro benzoic anhydride (2i).
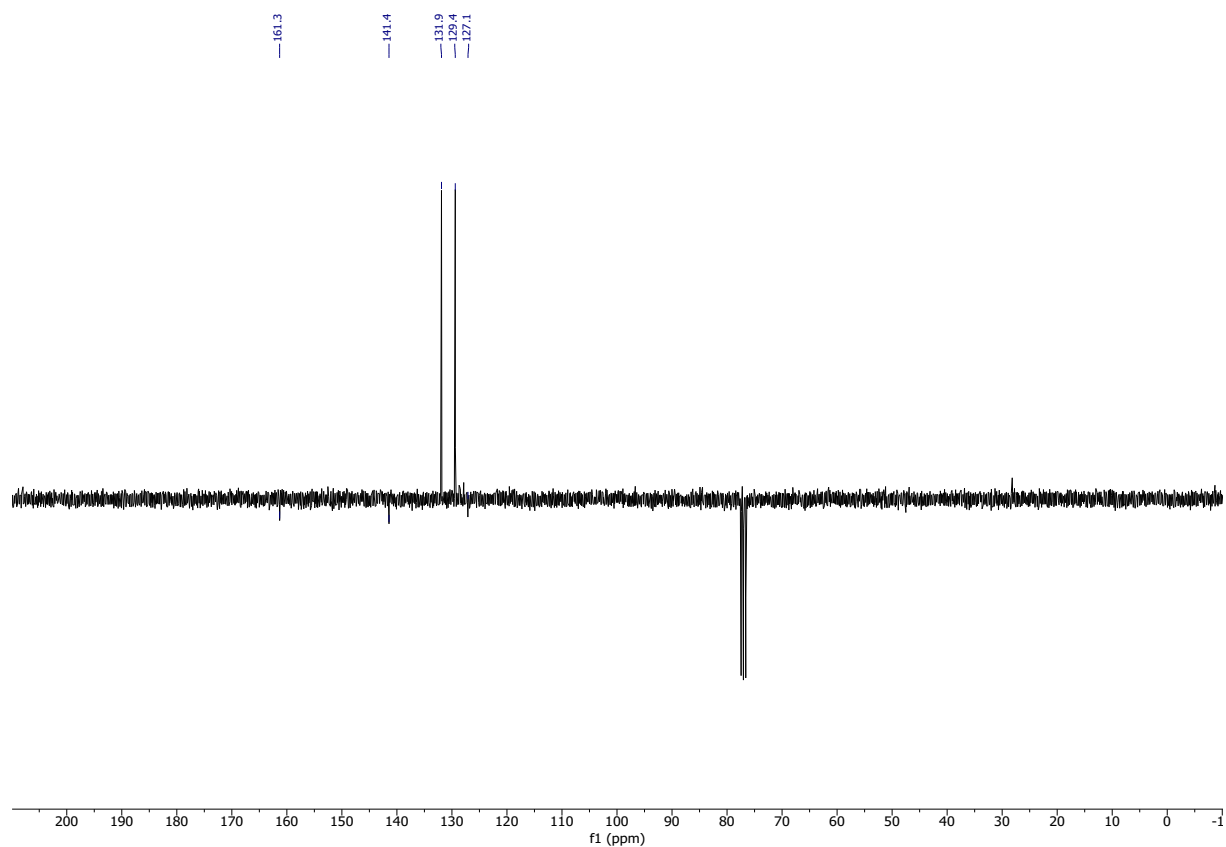
¹³C NMR spectrum (100 MHz, CDCl₃) of 4-Chloro benzoic anhydride.
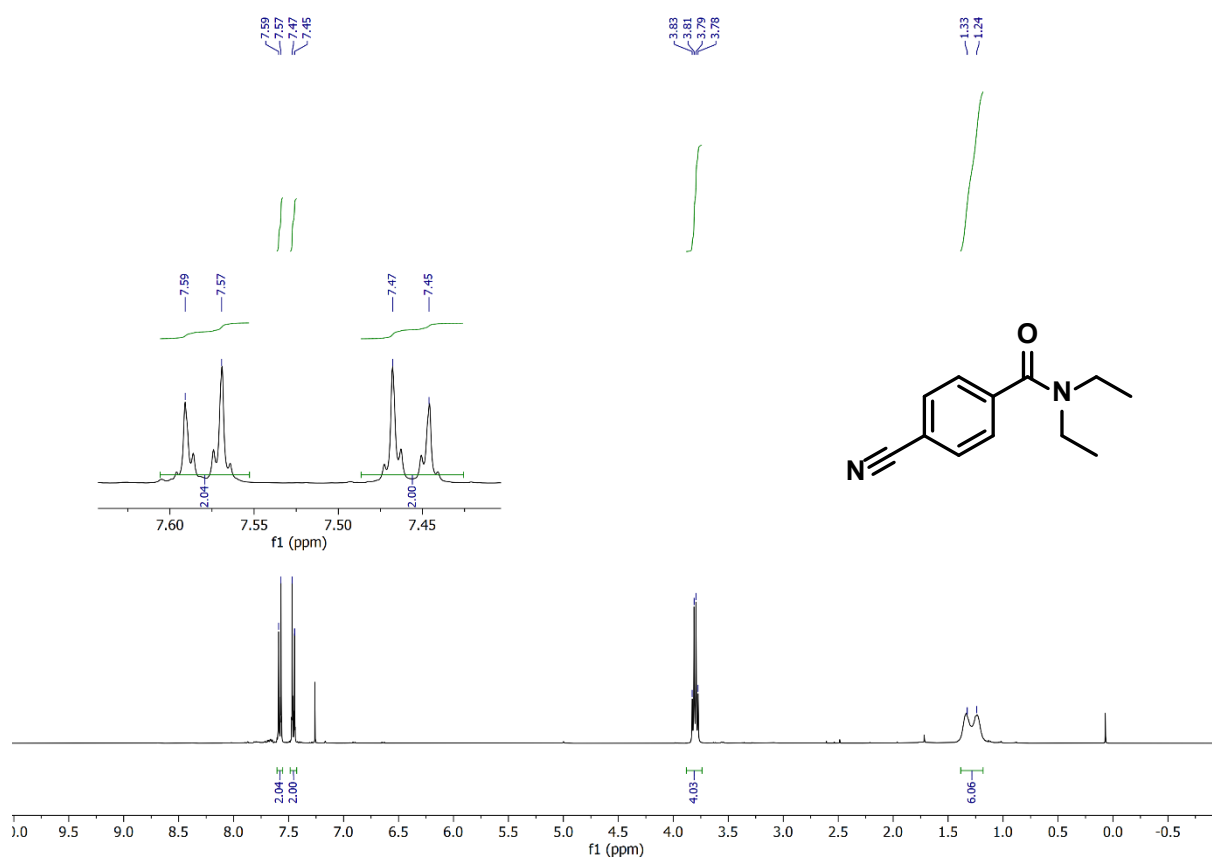
^{1}H NMR spectrum (400 MHz, CDCl$_3$) of *N,N*-Dimethyl 4-cyanobenzamide (2j).
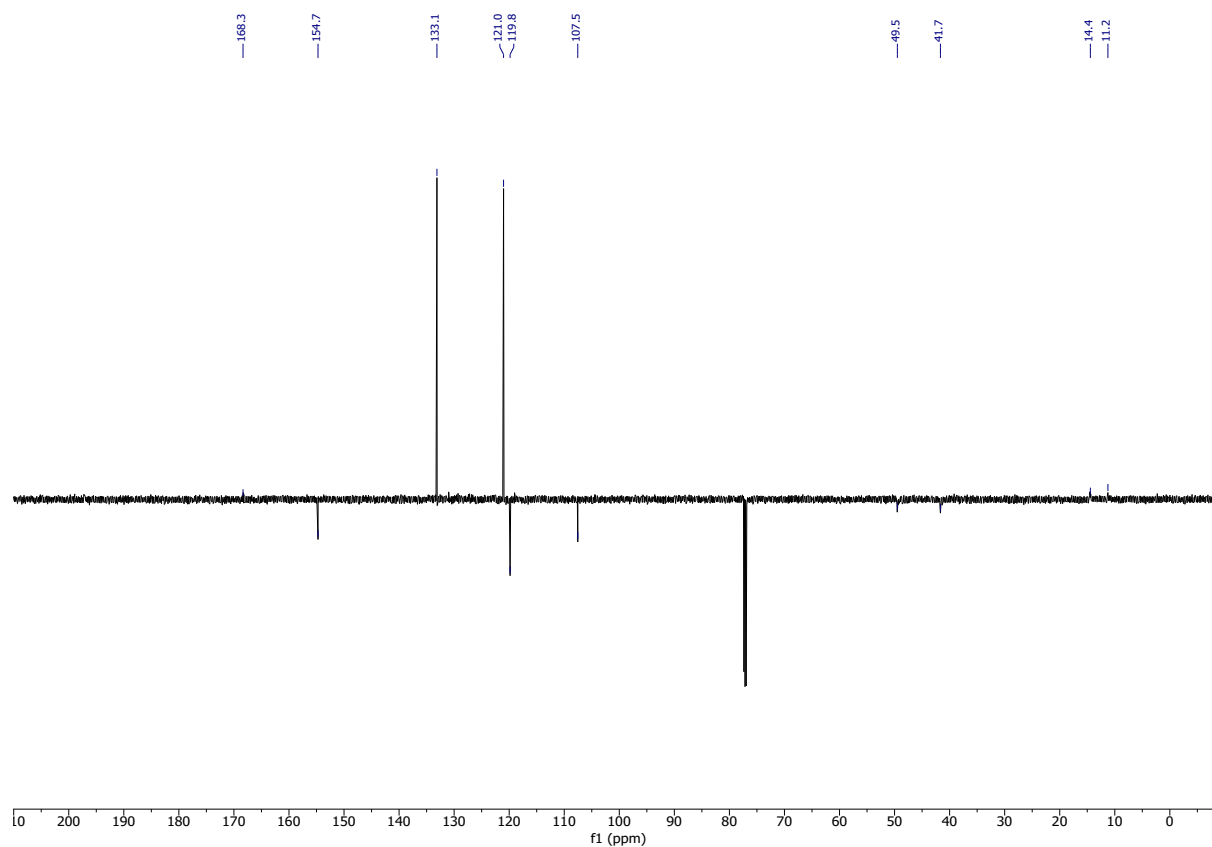
^{13}C NMR spectrum (100 MHz, CDCl$_3$) of *N,N*-Diethyl 4-cyanobenzamide.
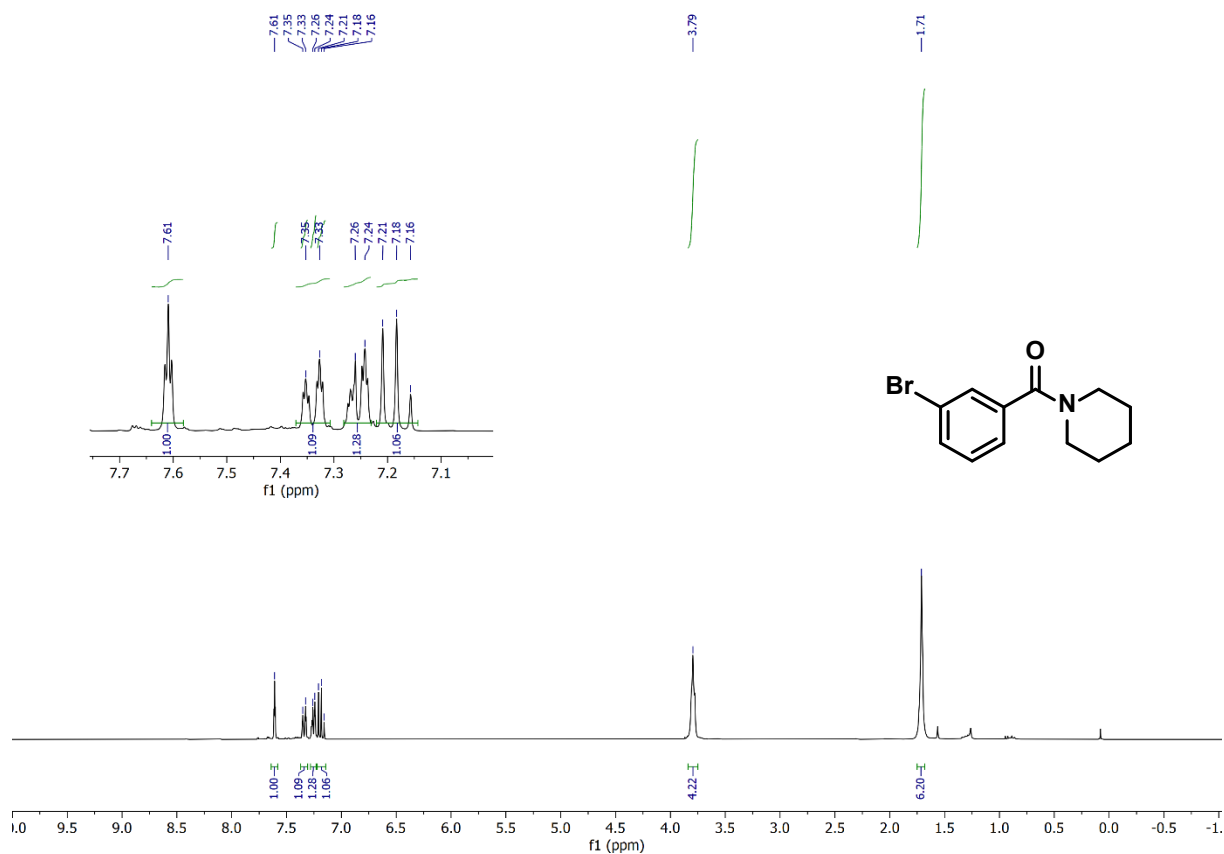
^{1}H NMR spectrum (400 MHz, CDCl$_3$) of *N*-(3-Bromobenzoyl)piperidine (2k).
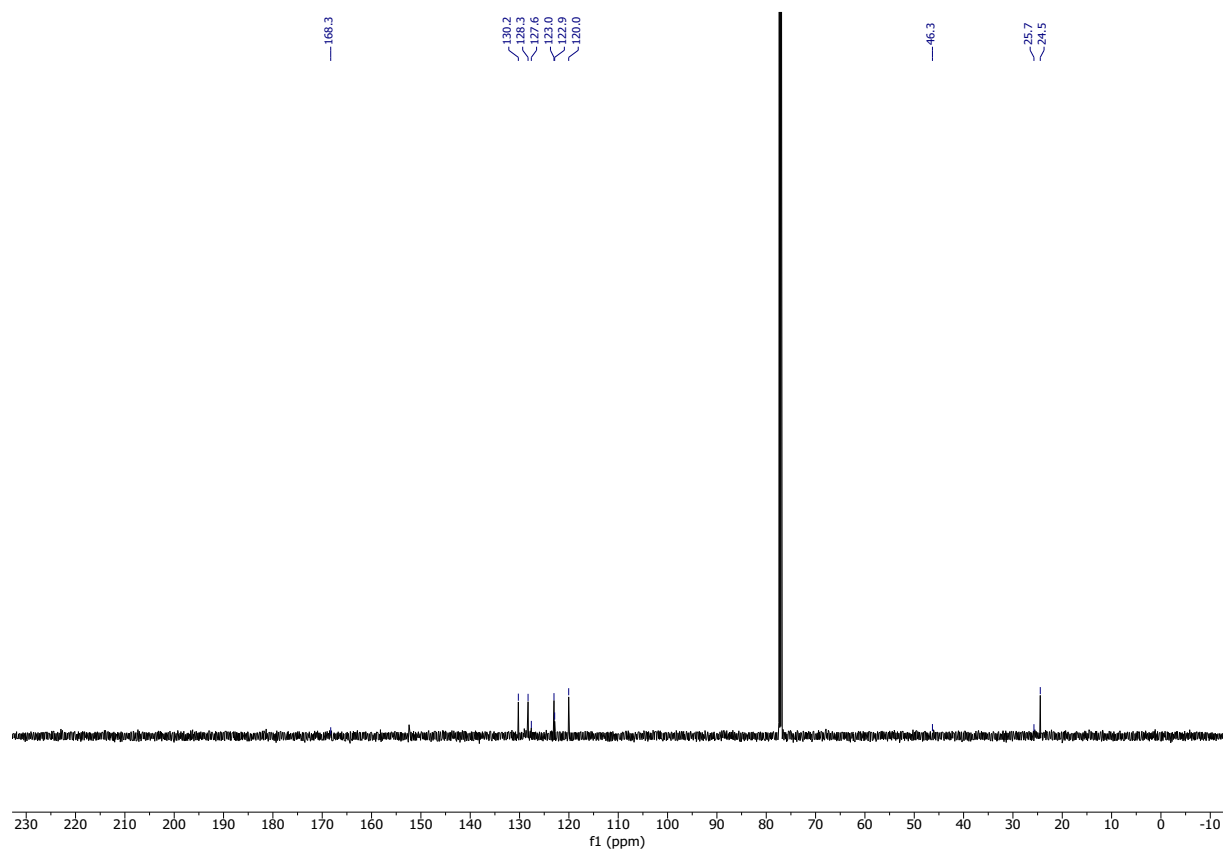
^{13}C NMR spectrum (100 MHz, CDCl$_3$) of *N*-(3-Bromobenzoyl)piperidine.
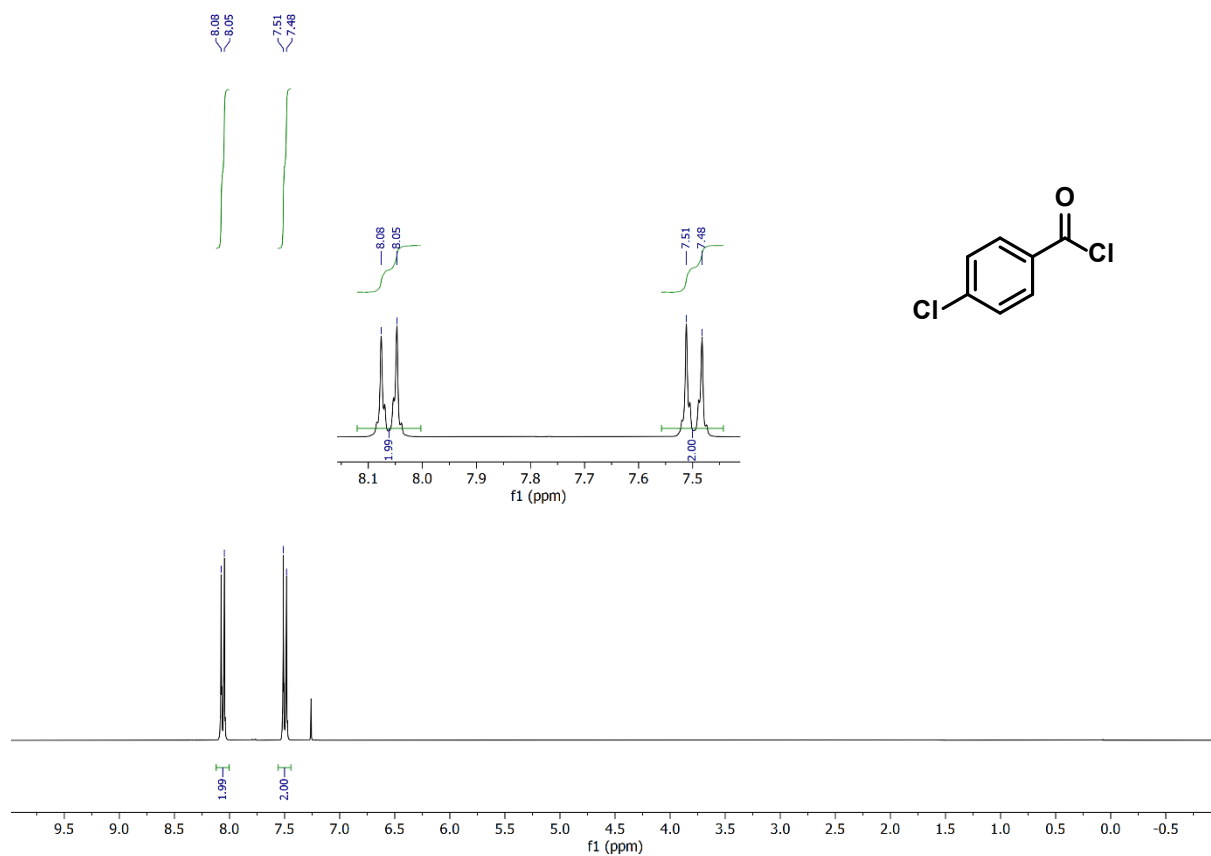
^{1}H NMR spectrum (400 MHz, CDCl$_3$) of 4-Chlorobenzoyl chloride (2l).
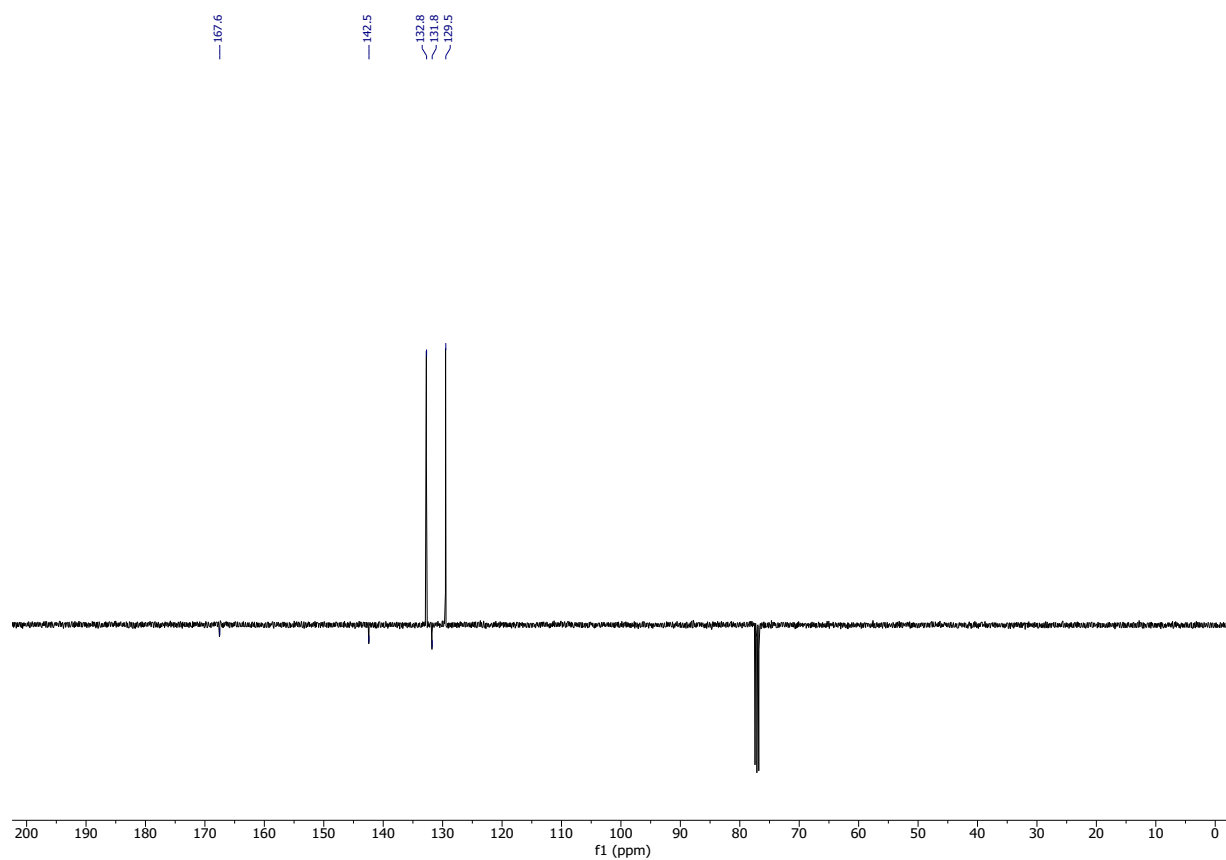
^{13}C NMR spectrum (100 MHz, CDCl$_3$) of 4-Chlorobenzoyl chloride.
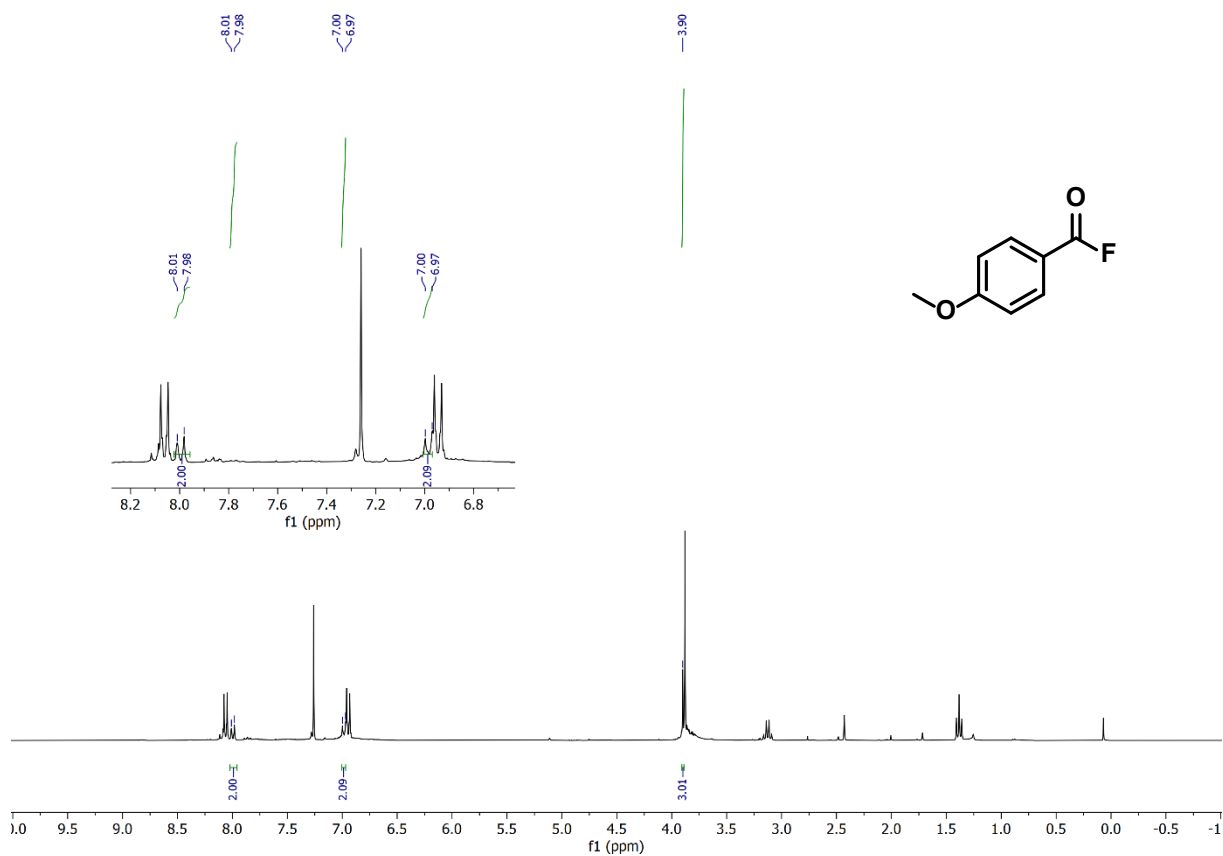
¹H NMR spectrum (400 MHz, CDCl₃) of crude reaction mixture of 4-Methoxybenzoyl fluoride (2m).

¹⁹F NMR spectrum (376 MHz, CDCl₃) of crude reaction mixture of 4-Methoxybenzoyl fluoride.

8. Highly Modular Photocatalytic Aromatic Carbonylations with Broad Scope

- mild conditions (r.t., 20 bar, 10 min)
- crystalline, stable starting material
- safe & scalable flow set-up
- modular & flexible reaction system
- broad scope (Nu = O,N,C,P,S,Cl,F,H)
- enabling telescoped reactions
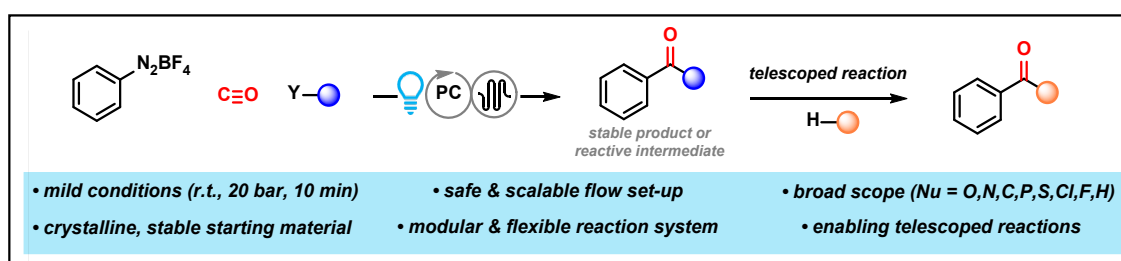
Abstract. The rapid access to carbonyl derivatives and their diverse modes of reactivity are at the heart of organic synthesis. Among the numerous syntheses of carbonyl derivatives, three-component assemblies from organic electrophiles, carbon monoxide, and nucleophilic reagents are especially attractive due to their modular nature and the use of easily available precursors. However, such methods are dominated by metal-mediated methods, harsh conditions, and narrow scopes. The utility of visible light to facilitate metal-free C–C bond-forming reactions has been only marginally explored in carbonylation reactions. This work details the development of a highly efficient photo-carbonylation of aromatic electrophiles with diverse sets of nucleophiles. An inexpensive organic catalyst operates under mild conditions (20 °C, 20 bar, 10 min) under visible light irradiation with high tolerance of functional groups. The selective access to aroyl chlorides enables preparations of virtually all conceivable carbonyl derivatives (X = O, N, S, P, Cl, F, C, H).

8.1   Introduction

Carbon monoxide (CO) is a natural and technical gas that is produced on huge scales (fires, volcanoes, petrochemistry). Beside its major applications in the production of fuels and bulk chemicals (e.g. alkanes, hydrogen, methanol, acetic acid, phosgene), the easy availability and low price render CO a most useful building block for the synthesis of many functionalized carbonyl derivatives.[1,2] Over the past century, several methods of carbonylations were developed, among which transition-metal catalyzed reactions are by far the most versatile. Such CO-insertion mechanisms operate under mild conditions with high tolerance of functional groups in the presence of noble metal catalysts (e.g. palladium, rhodium, iridium).[3] There are very few metal-free carbonylation strategies, often under harsh conditions (radical initiation, energy-intense UV light, strong bases, high temperatures, high pressures) or with narrow substrate scopes and low levels of structural diversifications.[4] Only very recently, visible light-mediated carbonylation reactions have complemented the arsenal of available methods.[5,6] The first metal- and base-free photoredox-catalyzed carbonylation of aromatic electrophiles to benzoate esters was reported in 2014 by our group.[7,8] Subsequently, further light-catalyzed metal-free carbonylation methods were developed, but with rather specific substrates and narrow product scopes (ketones,[9–12] amides,[13] phenyl indole-3-carboxylates[14]). However, a general photocatalytic method to access diverse sets of carboxyl derivatives containing widely varied substituents under mild conditions has so far not been reported. We surmised that an effective and synthetically useful extension of earlier methodologies would need to tackle the following challenges: *i)* formation of a broad scope of carbonyl and carboxyl derivatives with high tolerance of functional groups; *ii)* use of an inexpensive organic photocatalyst under visible light irradiation; *iii)* operation under mild conditions avoiding high pressures of gaseous carbon monoxide; *iv)* a technological solution of the low dispersion of the three distinct entities: gas, liquid, and light; *v)* safe operation and scalability of the process. Documented herein are the synthetic and mechanistic details of a new metal-free photocatalytic carbonylation protocol that presents tangible advances over the current state-of-the-art and fully addresses the aforementioned criteria. Under mild reaction conditions and without addition of metals or stoichiometric additives, a diverse set of easily available aromatic electrophiles underwent facile carbonylations in the presence of an inexpensive organic photocatalyst. Depending on the choice of the desired nucleophile (O, N, S, H, Cl, C, P), two methods of synthesis can be adopted: a direct three-component synthesis or a two-step process via an intermediate acid chloride. A simple flow reactor enabled effective mixing and short reaction times at low gas pressure (Scheme 8.1, bottom).
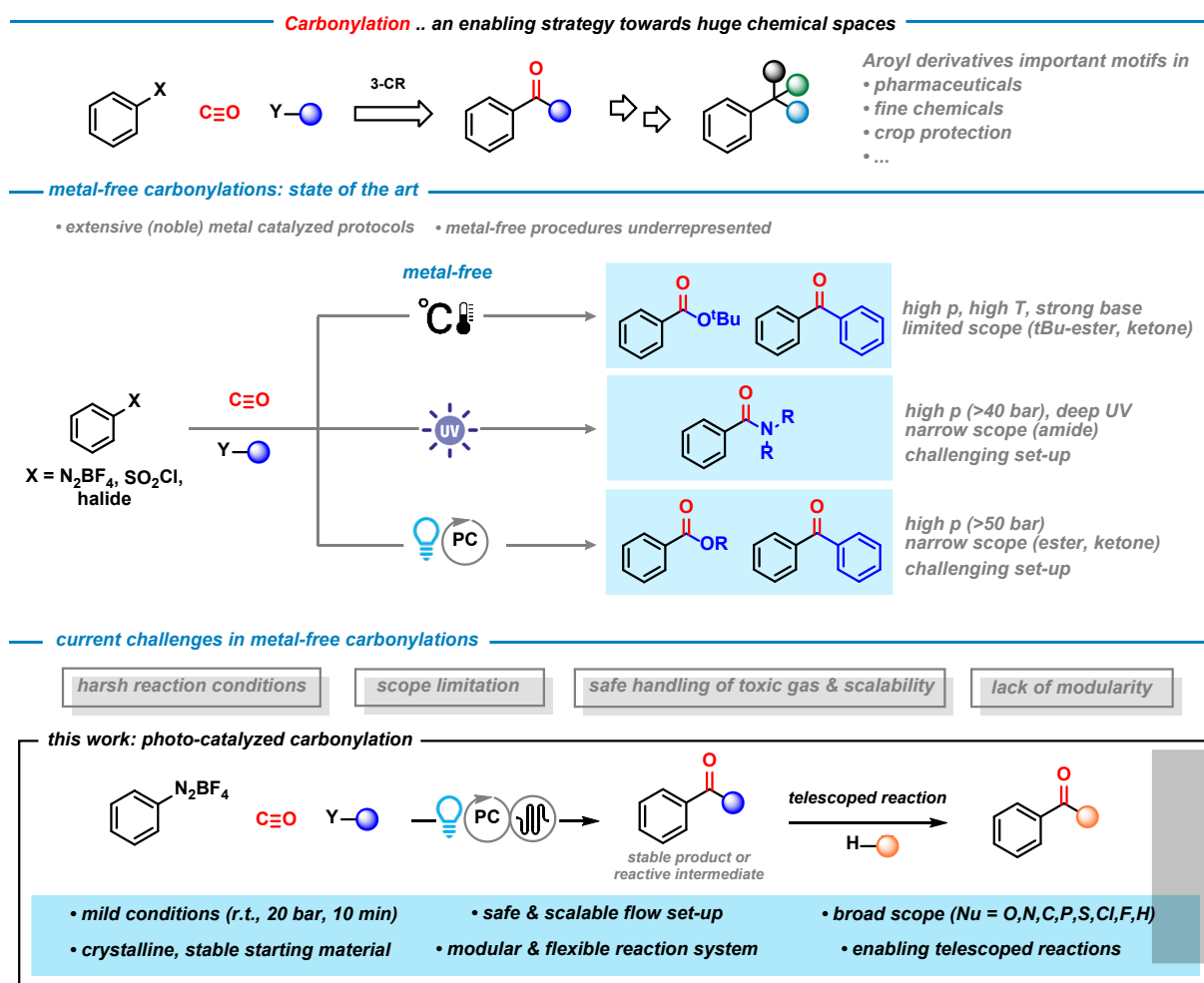
Scheme 8.1. Three-component carbonylations (3-CR) as versatile strategy of carbonyl derivative syntheses and various onward chemical diversifications (top), overview of metal-free carbonylations under thermal, photolytic, and photocatalytic conditions (middle), this development of a metal-free photoredox-catalyzed carbonylation with very broad scope under mild conditions in a safe flow reaction setup (bottom).

8.2   Results and Discussion

Our earlier report of a photoredox-catalyzed carbonylation[7] afforded benzoates in good yields, but displayed limitations with regard to other nucleophiles, the redox window of the photo-catalyst, and the required high CO pressure. We commenced our investigations into a more convenient and widely applicable protocol with the reaction of 4-methoxybenzene-diazonium tetrafluoroborate (**1a**), CO, and methanol (Table 8.1). Arenediazonium salts are stable crystalline materials that are readily prepared from an abundant library of commercial anilines with high tolerance of functional groups.[15–17] In an effort to enhance biphasic mixing, light penetration, and turnover at low gas pressures,[18] we used a home-built modular flow reactor.[19–21] The reactor was operated at 20 °C, 10–40 bar CO; the capillary coil (l = 13 m, inner d = 0.79 mm, inner v = 6.4 mL) was irradiated with LEDs over a residence time of 10–20 min. Consistent with our previous study,[7] the eosin Y catalyzed photo-carbonylation did not proceed effectively at pressures below 45 bar CO, short reaction times, and with low excess amounts of the nucleophile (4 mol% eosin Y, 525 nm, 40 bar CO, 2 equiv. MeOH; entry 1, Table

8.1).[22] The mechanistic study documented a photo-redox catalysis by eosin Y in which the initiating 1e-reduction of diazonium salts proceeded cleanly at ~0 V *vs.* SCE, while the moderate oxidation power of eosin Y (EY[+•]/EY: –0.8 V *vs.* SCE) enabled back-electron transfer with most substrates but prohibited the use of electron-poor arenes (e.g. 2-NO$_2$).[7] We employed the strong photo-oxidant 9-mesityl-10-methyl-acridinium perchlorate (MesAcr[+]/MesAcr[•]: 2.06 V *vs.* SCE)[23,24] that is easily converted into the sufficiently reducing radical state MesAcr[•] by simple sacrificial co-catalysts such as alcohols or arenes (*vide infra*).[25,26] Gratifyingly, [MesAcr]ClO$_4$ (1 mol%) and anisole (5 mol%) afforded a highly active photo-catalyst for efficient carbonylation of **1a** (0.1 M in MeCN) with MeOH (2 equiv.) to **2aa** at 20°C within 10 min (entry 2). Higher catalyst loading, catalyst anion exchange, longer reaction time, or higher CO pressure did not result in higher yields, respectively (entry 4–7). **2aa** was not observed at 10 bar CO, in the absence of photo-catalyst, in the dark, or without anisole, respectively (entry 8–11).

Table 8.1. Selected optimization experiments.
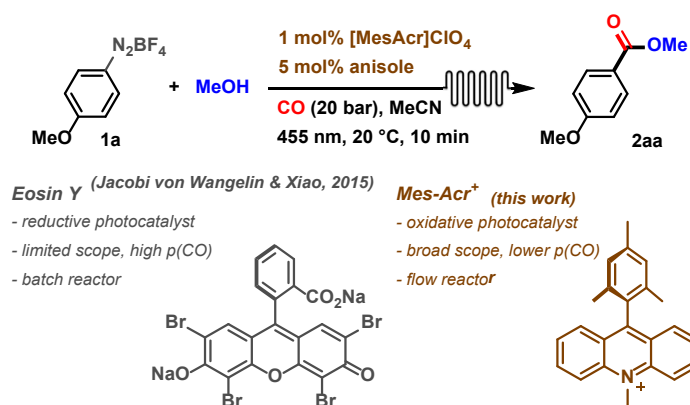
Entry	Deviation from standard conditions	2aa [%]
1	eosin Y (4 mol%), 525 nm, 40 bar CO	27 [a]
2	-	**83**
3	0.5 mol% [MesAcr]ClO$_4$	51
4	4 mol% [MesAcr]ClO$_4$	82
5	[MesAcr]BF$_4$	80
6	20 min residence time	82
7	40 bar CO	84
8	10 bar CO	0
9	in the dark	0
10	no dye	0
11	no anisole	<3

The optimized conditions were applied to a wide range of functionalized substrates (Scheme 8.2). The substitution pattern of the employed arenediazonium salts covered a large chemical space, including electron-donating, electron-deficient, and heteroarenes and various synthetically useful functional groups. The properties of the nucleophile governed the choice of the individual reaction conditions. Direct photo-carbonylation in the presence of the desired nucleophile was successful with a broad range of nucleophiles that exhibited *i)* sufficient solubility in acetonitrile, *ii)* no direct reaction with arenediazonium, and *iii)* an oxidation potential larger than that of the acyl radical intermediate. Nucleophiles with oxidation potentials lower than E(Mes-Acr$^+$) – such as benzyl alcohol, and *sec*. amines – acted as reductive activators of the photocatalyst and thus obviated the need for co-catalytic anisole (see mechanism below). The general protocol (entry 2, table 8.1) was applied to a wide range of *O*- and *N*-centered nucleophiles, cyanide, chloride, and fluoride anions. Excellent yields of the desired esters were obtained with *n*-, *sec*-, and *tert*-alkanols, including hydrophobic fatty alcohols and short-chain polar alcohols. Oxidation-sensitive alcohols with alkene and ketal groups gave very good yields, e.g. benzyl and allyl alcohol, citronellol, and 1,2:5,6-di-*O*-isopropylidene-α-D-glucofuranose. Carbonylation with 2 equiv. ethylene glycol gave the monoester; use of 0.5 equiv. glycol afforded the 1,2-diester. The same stoichiometric variation with water as nucleophile resulted in clean formation of the acid derivative (2 equiv. H_2O) or the acid anhydride (0.5 equiv. H_2O).[27] Various functional groups were tolerated (alkene, alkyne, halide, ester, ketone, CN, NO_2, CF_3, free OH, SO_2NH_2). Benzamides were formed in good yields from *sec*-amines, which is rather remarkable due to their potential to act as effective photocatalyst quenchers.[28] Nucleophiles with properties beyond the criteria *i)-iii)* above could not be employed: Primary amines gave only low yields of benzamides but afforded anilines via triazenes.[29] Other amines gave diazoarenes or underwent hydrodediazotation. Thiols, allyl silane, and tetrabutylammonium bromide were not productive (Scheme 2E). An important conceptual extension of this photo-carbonylation is the employment of aprotic nucleophiles which render the overall reaction a Bronsted-acid-free process that obviates any side reactions originating from acidic conditions. We have tested a range of available aprotic nucleophiles: The neutral silyl derivatives TMSCN and TMSN$_3$ afforded good yields of the aroyl products, respectively.[21,22] The ionic liquids 1-hexyl-3-methyl imidazolium fluoride, [hmim]F, and 1-butyl-3-methyl imidazolium chloride, [bmim]Cl, cleanly afforded the desired aroyl halides.
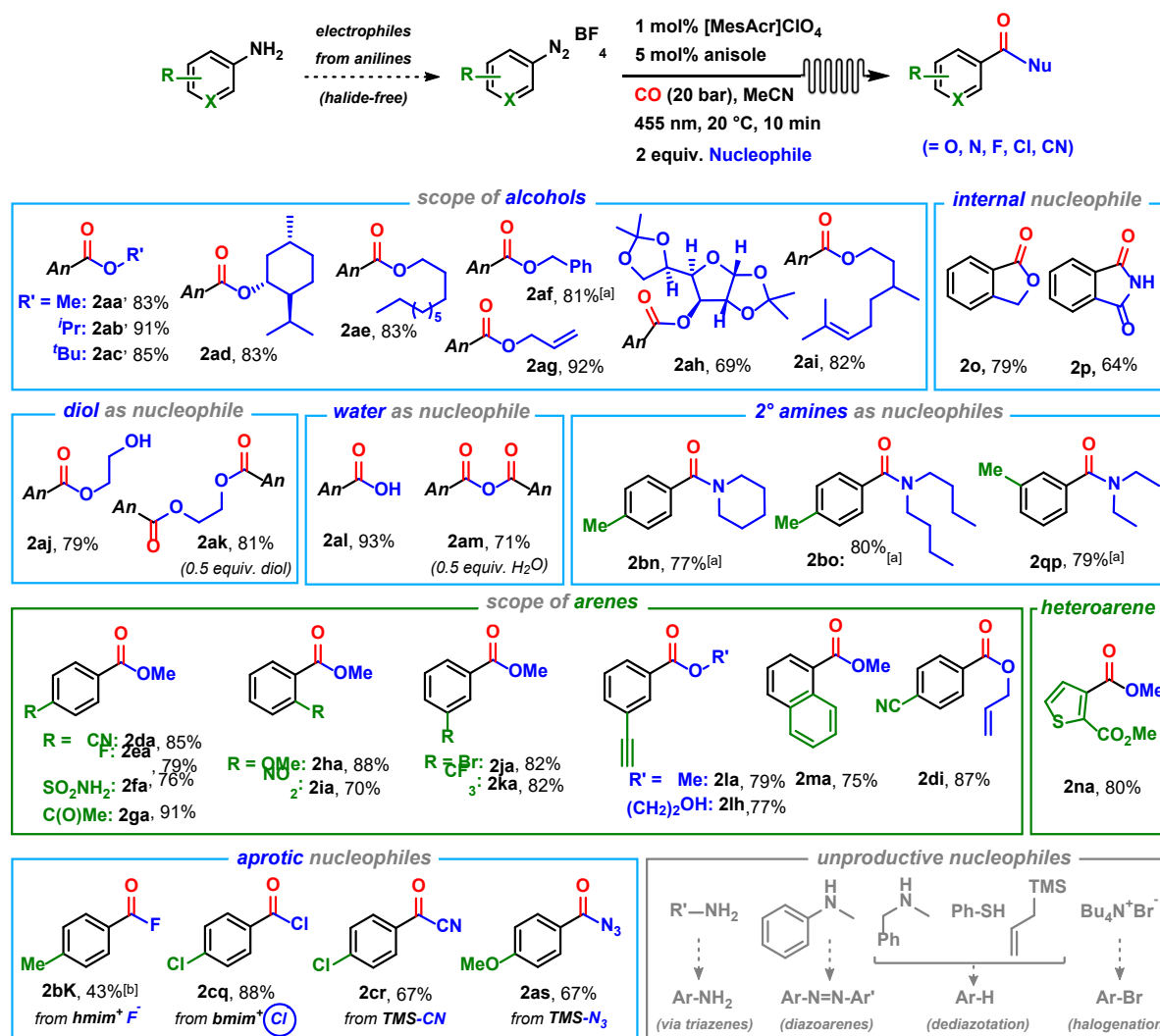
Scheme 8.2. Photo-carbonylation in the presence of suitable nucleophiles (top). Scope of O-, N-, Cl-, F-nucleophiles and arenes (bottom), [a] no anisole added [b] ^{1}H NMR yield. Arenediazonium tetrafluoroborates: *An* = 4-methoxyphenyl, *ClPh* = 4-chlorophenyl. *hmim* = 1-hexyl-3-methylimidazolium, *bmim* = 1-butyl-3-methylimidazolium.

The formation of benzoyl chlorides is especially noteworthy as this enables a most useful synthesis of virtually all carbonyl derivatives by subsequent nucleophilic substitution or other catalytic strategies (e.g. Acyl Suzuki cross-coupling).[33,34]

Metal-catalyzed formations of aliphatic acid halides from CO are well-known and employed e.g. in the Monsanto and Cativa processes for the production of acetic acid via intermediate formation of acetyl iodide.[3b] First carbonylation approaches for aroyl chlorides were reported by the group of Arndsten starting only in 2013 (Pd-catalysis, Pd/Photo process).[31,32] To our best knowledge, no metal-free synthesis routes to aroyl chlorides have been published, yet.

Multiple aroyl chlorides with electron-donating and -withdrawing substituents (OMe, Me, F, Cl, Br, Acetyl) in various positions (*ortho*, *meta*, *para*) were obtained in good yields (Scheme 8.3). Then, a multi-step strategy was applied. After photo-carbonylation with 1.5 equiv. [bmim]Cl, the resultant acyl chlorides were not worked up or isolated but - downstream of the flow reactor - reacted with the desired nucleophile (Scheme 8.3).

Such two-step protocol was suitable for nucleophiles that have limited solubility or exhibit no reactivity in the direct photo-carbonylation. This is illustrated by the successful use of various alcohols, thiols, peroxides, (hydroxyl)amines, phosphites, allylsilane, NaBH(OAc)₃. The tolerance of functional groups and the successful incorporation of complex nucleophiles such as 1,2:5,6-di-*O*-isopropylidene-α-D-glucofuranose, cholesterol (liquid crystalline esters),[35] sertraline (anti-depressant), or lumefantrine (anti-malarial drug) render this photo-carbonylation method a synthetic strategy for late-stage derivatizations. The use of poly-functional substrates offers ample opportunities for further diversifications.
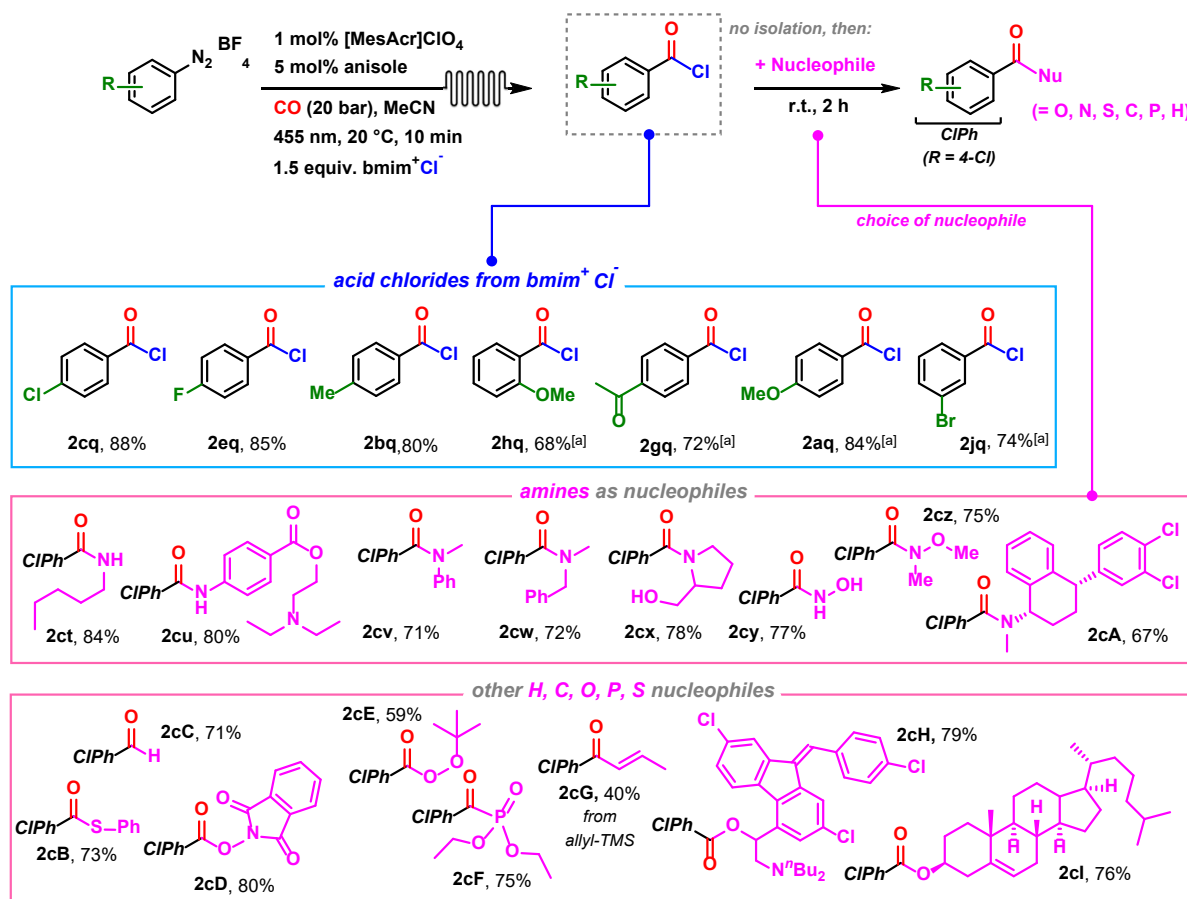
Scheme 8.3. Two-step protocol involving photo-carbonylation to aroyl chlorides with 1-butyl-3-methylimidazolium chloride (*bmimCl*) and subsequent addition of various H-, C-, N-, O-, P- and S-nucleophiles. [a] ¹H NMR yield. Arenediazonium tetrafluoro-borates: *ClPh* = 4-chlorophenyl.

Further synthetic utility of the photo-carbonylation under flow conditions was explored: A gram-scale reaction cleanly afforded the commercial insect repellant *N,N*-diethyl toluamide (DEET) in 77% yield from the inexpensive precursors *m*-toluidine, CO, and *N,N*-diethylamine (Scheme 8.4, top).[36] With a residence time of 10 min for the irradiated reaction volume (6.4 mL), continuous operation for 3 h enabled full conversion. The modular synthesis of aroyl derivatives by this photo-carbonylation offers ample opportunities for upstream variations of the electrophilic and nucleophilic components (aromatic substituents, heteroarenes; O- and N-nucleophiles, aprotic nucleophiles). Furthermore, down-stream manipulations of the carbonyl products enable additional diversification with molecular functions that are not tolerated by the photo-carbonylation. Ideally, the sequential reactions can be operated without isolation of the primary carbonylation products. We have demonstrated such strategy by the nucleophilic

substitution of aroyl chlorides with various H-, C-, N-, O-, P-, S-nucleophiles (Scheme 3C). Downstream manipulations at each of the three distinct skeletal units of the photo-carbonylation products can be applied, as exemplified in Scheme 8.4: Numerous methods are known for the nucleophilic substitution at benzoate derivatives. An aniline derivative was prepared without working up the photo-carbonylation reaction by a subsequent radical CH amination (60% yield over two steps).[37] The crude product mixture containing 4-bromobenzoyl azide was subjected to a Curtius rearrangement to give the herbicide metobromuron (62% yield, two steps).
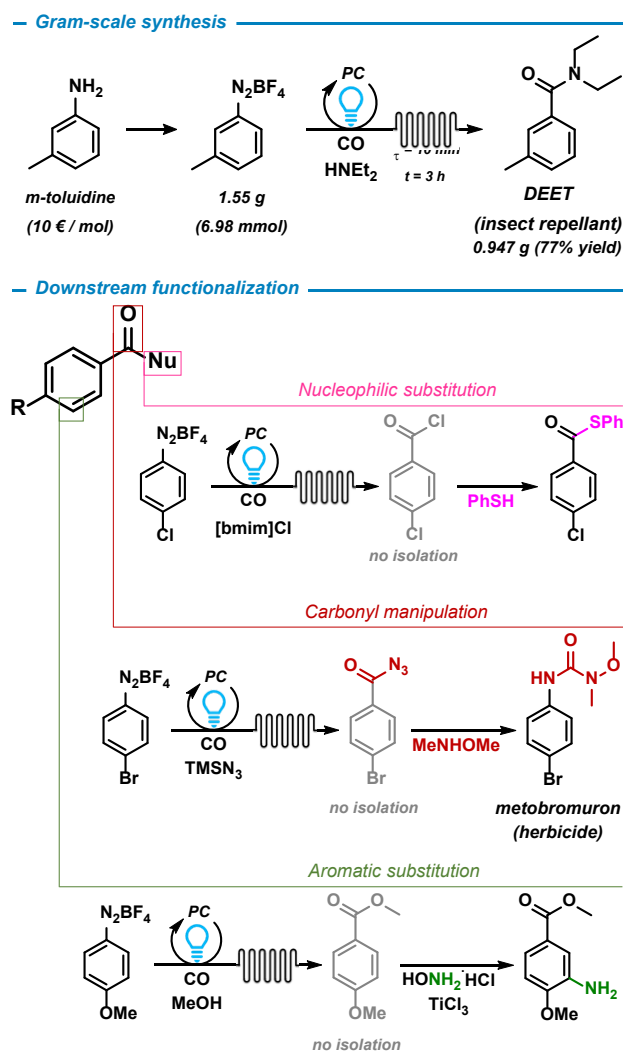
Scheme 8.4. Further synthetic applications of flow-photo-carbonylations: Gram-scale synthesis of the insect repellent DEET (top). Selected post-synthesis modifications (bottom).

Several insightful mechanistic experiments were performed (Scheme 8.5). Following our earlier report, we postulate the operation of an irreversible reductive 1e-activation of the arenediazonium by the photocatalyst which proceeds at ~0 V (vs. SCE). Aryl radical formation and CO addition give the acyl radical species which undergoes 1e-oxidation to the acylium ion. Nucleophilic attack furnishes the desired aroyl derivatives. While the chemical steps of this pathway have been described earlier,[7] the critical photoredox steps deserve special attention. With the employed pre-catalyst Mes-Acr+, a strong photooxidant (2.06 V),[38] the initial reductive activation of the arenediazonium substrate requires the presence of a co-

catalytic reductant. In many cases, the employed nucleophiles are also sufficiently reducing to effect pre-catalyst reduction. Carbonylations of nucleophiles that are outside this redox window require the addition of a sacrificial reductant. Gratifyingly, even poor reductants and rather inert reagents such as anisole (1.76 V) are effective reductants of the excited state Mes-Acr^{+*}.[41a,42a] The resultant Mes-Acr$^{\bullet}$ radical undergoes diazonium reduction (-0.57 V vs. SCE). The 1e-oxidation of the intermediate acyl radicals to the acylium ions (-0.14 V to 1.7 V)[7] by Mes-Acr^{+*} (2.06 V) is thermodynamically strongly favored. While the photo-reduction of the arenediazonium operates at very low potentials (~0 V), the back-electron transfer from the acyl radical is turn-over limiting, especially with electron-deficient substituents at the arene. Unlike the recently reported eosin- or fluorescein-catalyzed reactions, the higher oxidizing power of Mes-Acr^{+*} enabled even good conversion of the electron-poor 2-nitrobenzenediazonium.[7] Photo-carbonylations may operate without the addition of sacrificial anisole if the nucleophile itself acts as initiating reductant of the photo-catalyst. Such scenario can be realized if E(NuH) <2.06 V and if E(NuH) is higher than the oxidation potential of the intermediate acyl radical species, which includes benzyl alcohols and amines (Scheme 8.5, middle). A reliable alternative to any combination of substrates is the aroyl chloride strategy. Further key mechanistic studies involved the detection of TEMPO adducts of both radical intermediates, the aryl and aroyl species (Scheme 4, top). Stern-Volmer experiments showed the rapid quenching of photo-catalyst fluorescence (Mes-Acr+*) by piperidine (K_{SV} = 119 L mol^{-1}) or anisole (K_{SV} = 75 L mol^{-1}) but not by arenediazonium salts nor by mixtures of these with methanol (Scheme 8.5, bottom). This supports our hypothesis that sufficiently reducing nucleophiles initiate the reaction by photocatalyst activation. UV/Vis spectroscopic studies provided further insight.[39,40] Illumination of a solution of Mes-Acr^{+} and anisole in benzonitrile led to an immediate color change from yellow to orange. The corresponding UV/Vis spectrum can be assigned to the formed Mes-Acr$^{\bullet}$ radical.[39] Subsequent addition of arenediazonium regenerated the Mes-Acr^{+} state. (Experimental section, Figure 8.14, 8.15).

Scheme 8.5. Proposed reaction mechanism (top) involving critical photo-SET steps (colored dots) and TEMPO radical trapping of key intermediates (top, right). Photo-reactor setup: flow system with HPLC pump, gas supply, back-pressure valve, capillary coil and illumination. A slug flow of approx. 0.5 cm gas and liquid segments formed (center, right). Analyses of redox potentials for the critical photoredox steps involving Mes-Acr⁺ and Mes-Acr• (center). Photocatalyst quenching and Stern-Volmer analysis (bottom). Light on/off experiment (bottom, right). Redox potentials were taken from the literature.[42]

8.3   Conclusion

The modular synthesis of diverse sets of carbonyl compounds from easily available precursors (arenediazonium, CO, alcohols, amines) has been accomplished. A tailor-made flow reactor enabled very short reaction times at mild conditions (1 mol% cat., 20 bar CO, 20 °C, 10 min, blue light). An unprecedentedly wide scope of nucleophiles can be employed, importantly also including non-protic nucleophiles which expands the scope to include ionic nucleophiles, *i.e.* salts. The use of the ionic nucleophile [bmim]Cl enabled the formation of acid chlorides that can be subsequently reacted with various O-, N-, C-, S-, P- and H-nucleophiles and also enabled late-stage functionalizations of highly complex molecules. Mechanistic studies documented the reductive photocatalyst activation, the thermodynamic feasibility of all SET steps, the nature of the radical intermediates, and the absence of long radical-chain pathways.

8.4   Experimental Section

8.4.1   Materials and Methods

Commercial chemicals (>98 % purity) were used as obtained without further purification unless specified otherwise. Diazonium salts were prepared by synthetic routes (*vide infra*), with the respective aniline precursors used without further purification as obtained from the vendors. TLC was performed using commercial silica gel coated aluminum plates (DC Kieselgel 60 F$_{254}$, *Merck*); visualization was done by the use of UV light. Staining was realized with a solution of phosphomolybdic acid in ethanol. Product yields were determined from isolated materials after flash chromatography on silica gel (*Acros Organics*, mesh 35–70). NMR spectral data was collected on a *Bruker* FourierHD 300 (300 MHz for ^{1}H; 75 MHz for ^{13}C) at 25 °C. The quantification of ^{1}H cores was obtained by integration of resonance signals. Abbreviations used in ^{1}H NMR spectra: s – singlet, d – doublet, t – triplet, m – multiplet. Low-resolution mass spectroscopy was conducted on an *Agilent* 6890N GC-system coupled to a 5975 MSD unit and H$_2$ as carrier gas. UV/Vis spectra were measured on the Cary5000 spectrometer by *Agilent*. High resolution mass spectrometry (HRMS) was carried out by the Central Analytics at the department of chemistry, University of Hamburg.

A home-built flow reactor set-up was used. CO gas was applied with a *Brooks Instr*. mass-flow control, the system pressure was adjusted by an *IDEX* back-pressure cartridge. Commercial FEP tubing (1/16″ OD, 1/32″ ID) were purchased from *Bohlender*. The tubing (irradiated length 12.8 m) was wrapped around a glass cylinder (OD 65 mm). Temperature control (20 °C) was applied from the outside of the reactor coil by a temperature-controlled silicon oil bath. The reactor coil was irradiated from the inside by 24 water-cooled blue LEDs (λ_{max} = 455 nm). The reaction solution was pumped by a HPLC compact pump 3350 (*Bischoff*).

A detailed description of the flow reactor can be found in reference [19].

Figure 8.1. Flow reactor set-up (left), HPLC pump (right).
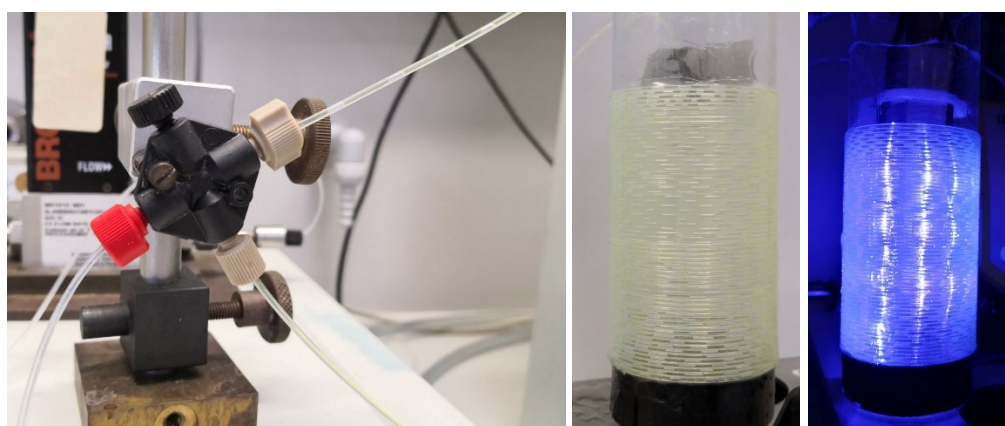
Figure 8.2. T-mixer combining gas and liquid flow (left), reactor coil filled with solvent and CO (middle), illuminated coil (right).
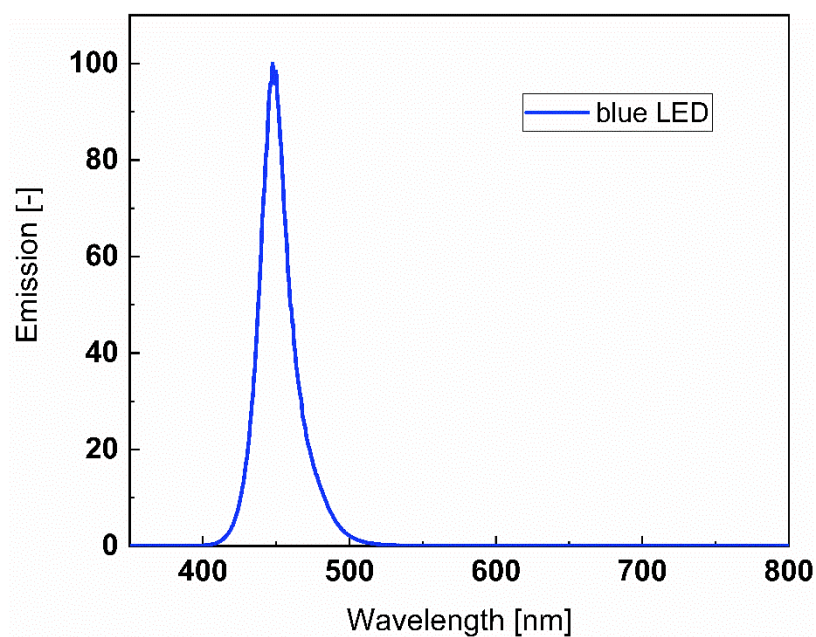
Figure 8.3. Emission spectrum of the used blue LEDs (λ_{max} = 455 nm).

8.4.2 General Procedures

Synthesis of Diazonium Salts

The parent aniline (4.5 mmol) was dissolved in glacial acetic acid (3 mL) and 48 % aqueous tetrafluoroboric acid (1.3 mL) at room temperature. Afterwards, isoamyl nitrite (1 mL) was dissolved in glacial acetic acid (2 mL) and added to the first solution over the course of five minutes. Then, diethyl ether (15 mL) was added and the mixture was cooled to -30 °C until the crystalline product precipitated. The precipitate was collected by filtration and redissolved in a minimum amount of acetone. Finally, the diazonium tetrafluoroborate was precipitated by addition of diethyl ether (15 mL), filtered, washed with diethyl ether (2x 10 mL) and dried in the air.

General procedure for Pathway A

The corresponding diazonium salt (0.5 mmol), anisole (5 mol%, 2.7 µL) and the nucleophile (1.0 mmol) were dissolved in a 1 mM solution of Mes-Acr-ClO$_4$ in MeCN (5 mL). The solution was then injected to the flow reactor at 20 °C and irradiated for 10 min with 24 blue LEDs (λ_{max} = 455 nm) in an approximately 13 m long 1/16 inch (0.79 mm inner diameter) FEP tubing at a CO pressure of 20 bar. Afterwards, the solvent was removed under reduced pressure and the crude product was purified via flash chromatography to give the clean compound.

General procedure for Pathway B

The corresponding diazonium salt (0.5 mmol), anisole (5 mol%, 2.7 µL) and [bmim]Cl (0.75 mmol) were dissolved in a 1 mM solution of Mes-Acr-ClO$_4$ in MeCN (5 mL). The solution was then injected to the flow reactor at 20 °C and irradiated for 10 min with 24 blue LEDs (λ_{max} = 455 nm) in an approximately 13 m long 1/16 inch (0.79 mm inner diameter) FEP tubing at a CO pressure of 20 bar. Afterwards, the nucleophile was added (1.0 mmol) and the mixture was stirred for two hours at room temperature if not specified otherwise. Finally, the solvent was removed under reduced pressure and the crude product was purified via flash chromatography to give the clean compound.

Large scale synthesis

3-methylbenzenediazonium tetrafluoroborate (7 mmol), anisole (5 mol%, 38 µL), and freshly distilled diethylamine (14 mmol) were dissolved in a 1 mM solution of Mes-Acr-ClO$_4$ in MeCN (70 mL). The solution was then injected to the flow reactor at 20 °C and irradiated for 10 min with 24 blue LEDs (λ_{max} = 455 nm) in an approximately 13 m long 1/16 inch (0.79 mm inner diameter) FEP tubing at a CO pressure of 20 bar. Afterwards, the solvent was removed under reduced pressure and the crude product was purified via flash chromatography to give the clean compound.
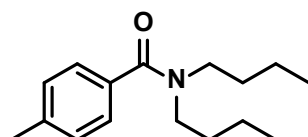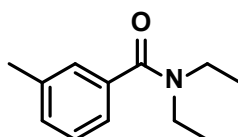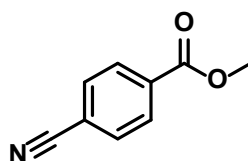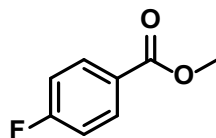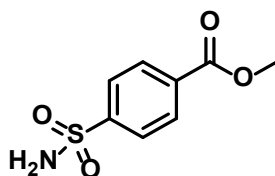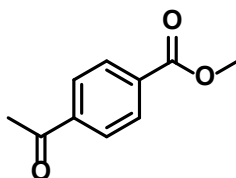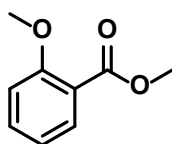
Methyl 4-methoxybenzoate (2aa)
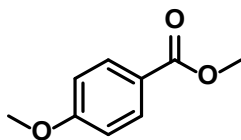
Following Pathway A with anisole, **2aa** was isolated by flash chromatography on silica with EA/pentane as eluent as a white solid (83 % yield).

¹H NMR (400 MHz, CDCl₃, ppm): δ = 8.01–7.98 (m, 2H), 6.93–6.90 (m, 2H), 3.88 (s, 3H), 3.85 (s, 3H). **¹³C NMR** (100 MHz, CDCl₃, ppm): δ = 167.0, 163.4, 131.7, 122.8, 113.7, 55.6, 52.0. **GC-MS (EI)** *m/z* (relative intensity): 166 (33) [M⁺], 135 (100), 107 (12), 92 (17), 77 (21).

The spectral data are consistent with literature values.[7]

i-Propyl 4-methoxybenzoate (2ab)
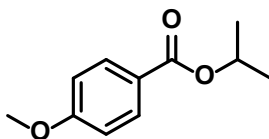
Following Pathway A with anisole, **2ab** was isolated by flash chromatography on silica with EA/pentane as eluent as a colorless oil (91 % yield).

¹H NMR (400 MHz, CDCl₃, ppm): δ = 8.00–7.98 (m, 2H), 6.92–6.90 (m, 2H), 5.22 (hept, *J* = 6.2 Hz, 1H), 3.86 (s, 3H), 1.35 (d, *J* = 6.2 Hz, 6H). **¹³C NMR** (100 MHz, CDCl₃, ppm): δ = 165.9, 163.4, 131.6, 123.3, 113.6, 68.1, 55.6, 22.1.

The spectral data are consistent with literature values.[7]

t-Butyl 4-methoxybenzoate (2ac)
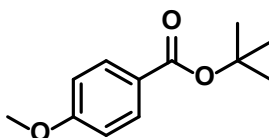
Following Pathway A with anisole, **2ac** was isolated by flash chromatography on silica with EA/pentane as eluent as a colorless oil (85 % yield).

¹H NMR (400 MHz, CDCl₃, ppm): δ = 7.95–7.93 (m, 2H), 6.90–6.88 (m, 2H), 3.85 (s, 3H), 1.58 (s, 9H). **¹³C NMR** (100 MHz, CDCl₃, ppm): δ = 165.7, 163.1, 131.5, 124.6, 113.5, 80.6, 55.5, 28.4. **GC-MS (EI)** *m/z* (relative intensity): 208 (15) [M⁺], 152 (100), 135 (71), 77 (10).

The spectral data are consistent with literature values.[7]
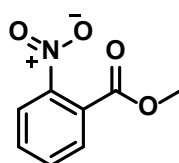
Menthyl 4-methoxybenzoate (2ad)
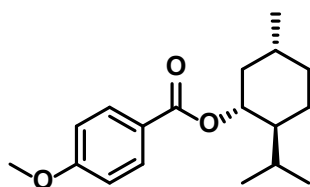
Following Pathway A with anisole, **2ad** was isolated by flash chromatography on silica with EA/pentane as eluent as a colorless oil (83 % yield).

¹H NMR (400 MHz, CDCl₃, ppm): δ = 8.01–7.98 (m, 2H), 6.93–6.90 (m, 2H), 4.95 – 4.83 (m, 1H), 3.85 (s, 1H), 2.16 – 2.08 (m, 2H), 1.97 – 1.89 (m, 1H), 1.76 – 1.69 (m, 2H), 1.58 – 1.47 (m, 2H), 1.15 – 1.05 (m, 2H), 0.92 (dd, *J* = 3.2, 6.8 Hz, 6H), 0.79 (d, *J* = 7.0 Hz, 2H). **¹³C NMR** (100 MHz, CDCl₃, ppm): δ = 166.0, 163.3, 131.7, 123.5, 113.7, 77.2, 74.6, 55.5, 47.5, 41.2, 34.5, 31.6, 26.7, 23.8, 22.2, 20.9, 16.7. **GC-MS (EI)** *m*/z (relative intensity): 152 (26), 138 (75), 135 (90), 123 (31), 95 (100), 81 (87).

The spectral data are consistent with literature values.[8]
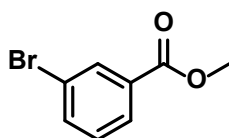
Decyl 4-methoxybenzoate (2ae)
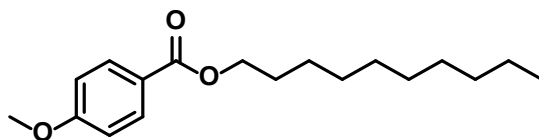
Following Pathway A with anisole, **2ae** was isolated by flash chromatography on silica with EA/pentane as eluent as a colorless oil (83 % yield).

¹H NMR (400 MHz, CDCl₃, ppm): δ = 8.01–7.99 (m, 2H), 6.93–6.90 (m, 2H), 4.28 (t, *J* = 6.7 Hz, 2H), 3.85 (s, 3H), 1.77–1.73 (m, 2H), 1.44–1.27 (m, 14H), 0.88 (m, 3H). **¹³C NMR** (100 MHz, CDCl₃, ppm): δ = 166.6, 163.4, 131.7, 123.1, 113.7, 65.0, 55.6, 32.0, 29.7, 29.4, 28.9, 26.2, 22.8, 14.3. **GC-MS (EI)** *m*/z (relative intensity): 292 (4) [M⁺], 153 (25), 152 (100), 135 (16), 107 (3).

The spectral data are consistent with literature values.[43]

Benzyl 4-methoxybenzoate (2af)
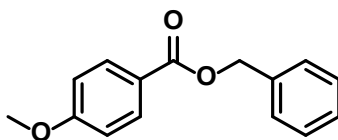
Following Pathway A without anisole, **2af** was isolated by flash chromatography on silica with EA/pentane as eluent as a colorless oil (81 % yield).

¹H NMR (400 MHz, CDCl₃, ppm): δ = 8.06–8.03 (m, 2H), 7.47–7.34 (m, 5H), 6.94–6.91 (m, 2H), 5.35 (s, 2H), 3.86 (s, 3H). **¹³C NMR** (100 MHz, CDCl₃, ppm): δ = 166.3, 163.6, 136.5, 131.9, 128.7, 128.3, 128.2, 122.7, 113.8, 66.5, 55.5.

The spectral data are consistent with literature values.[8]

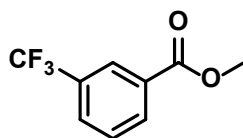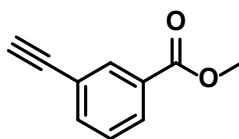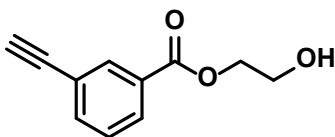## Allyl 4-methoxybenzoate (2ag)
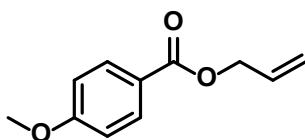
Following Pathway A with anisole, **2ag** was isolated by flash chromatography on silica with EA/pentane as eluent as a white solid (92 % yield).

¹H NMR (400 MHz, CDCl₃, ppm): δ = 8.04–8.01 (m, 2H), 6.93–6.91 (m, 2H), 6.03 (m, 1H), 5.40 (m, 1H), 4.80 (m, 1H), 3.86 (s, 3H). **¹³C NMR** (100 MHz, CDCl₃, ppm): δ = 166.2, 163.6, 132.6, 131.8, 122.8, 118.1, 113.8, 65.4, 55.6. **GC-MS (EI)** *m/z* (relative intensity): 192 (5) [M⁺], 135 (100), 107 (9), 92 (11), 91 (12), 77 (18).

The spectral data are consistent with literature values.[44]

3-(4-methoxybenzoate)-1,2:5,6-Di-*O*-isopropyliden-α-D-glucofuranose (2ah)
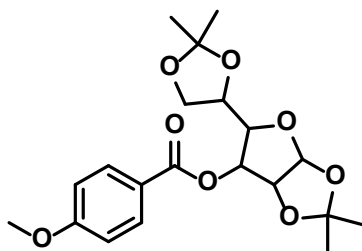
Following Pathway A with anisole, **2ah** was isolated by flash chromatography on silica with EA/pentane as eluent as a colorless oil (69 % yield).

¹H NMR (400 MHz, CDCl₃, ppm): δ = 7.98–7.96 (m, 2H), 6.93–6.91 (m, 2H), 5.93 (d, *J* = 3.7 Hz, 1H), 5.46 (d, *J* = 2.6 Hz 1H), 4.61 (d, *J* = 3.7 Hz, 1H), 4.36–4.31 (m, 2H), 4.11–4.08 (m, 2H), 3.86 (s, 3H), 1.55 (s, 3H), 1.41 (s, 3H), 1.31 (s, 3H), 1.26 (s, 3H). **¹³C NMR** (100 MHz, CDCl₃, ppm): δ = 165.0, 163.9, 131.9, 122.0, 113.9, 112.4, 109.5, 105.3, 83.6, 80.1, 76.5, 72.8, 67.3, 55.6, 26.9, 26.9, 26.3, 25.4. **HRMS** (ESI): *m/z* calculated for C₂₀H₂₆O₈+Na⁺: 417.1525 [M+Na]⁺; found 417.1527.

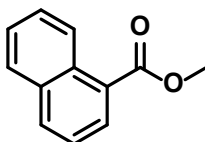## Citronellyl 4-methoxybenzoate (2ai)
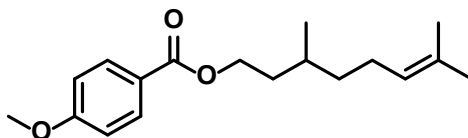
Following Pathway A with anisole, **2ai** was isolated by flash chromatography on silica with EA/pentane as eluent as a colorless oil (82 % yield).

¹H NMR (400 MHz, CDCl₃, ppm): δ = 8.00–7.97 (m, 2H), 6.93–6.90 (m, 2H), 5.12–5.06 (m, 1H), 4.35–4.30 (m, 2H), 3.86 (s, 3H), 2.05–1.96 (m, 2H), 1.83–1.75 (m, 2H), 1.67 (s, 3H), 1.64–1.51 (m, 1H), 1.44–1.34 (m, 2H), 1.25–1.20 (m, 2H), 1.60 (s, 3H), 0.96 (d, 3H). **¹³C NMR** (100 MHz, CDCl₃, ppm): δ = 166.6, 163.4, 131.7, 124.7, 123.3, 113.7, 63.3, 55.5, 37.2, 35.7, 29.7, 25.8, 25.6, 19.7, 17.8. **GC-MS (EI)** *m/z* (relative intensity): 152 (26), 138 (34), 135 (100), 123 (23), 109 (29), 95 (31), 81 (59).

The spectral data are consistent with literature values.[45]

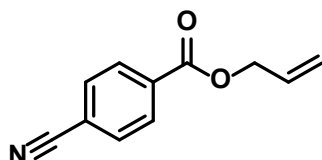## Isobenzofuran-1(3*H*)-one (2o)
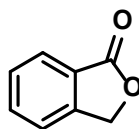
Following Pathway A with anisole, **2o** was isolated by flash chromatography on silica with EA/pentane as eluent as a white solid (79 % yield).

¹H NMR (400 MHz, CDCl₃, ppm): δ = 7.92 (d, J = 7.8 Hz, 1H), 7.71–7.66 (m, 1H), 7.56–7.49 (m, 2H), 5.32 (s, 2H). **¹³C NMR** (100 MHz, CDCl₃, ppm): δ = 171.1, 146.5, 134.0, 129.1, 125.8, 125.7, 122.1, 69.7. **GC-MS (EI)** *m/z* (relative intensity): 134 (37) [M⁺], 105 (100), 77 (45).

The spectral data are consistent with literature values.[46]

1*H*-Isoindole-1,3(2*H*)-dione (2p)
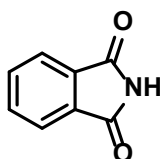
Following Pathway A with anisole, **2p** was isolated by flash chromatography on silica with EA/pentane as eluent as a white solid (64 % yield).

¹H NMR (400 MHz, CD₃CN, ppm): δ = 8.85 (br s, 1H), 7.83–7.77 (m, 4H). **¹³C NMR** (100 MHz, CD₃CN, ppm): δ = 173.5, 139.7, 138.3, 128.4.

The spectral data are consistent with literature values.[47]
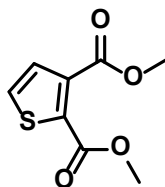
2-Hydroxyethyl 4-methoxybenzoate (2aj)
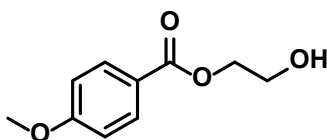
Following Pathway A with anisole, **2aj** was isolated by flash chromatography on silica with EA/pentane as eluent as a colorless oil (79 % yield).

¹H NMR (400 MHz, CDCl₃, ppm): δ = 8.02–8.00 (m, 2H), 6.93–6.91 (m, 2H), 4.44–4.43 (m, 2H), 3.95–3.93 (m, 2H), 3.86 (s, 3H). **¹³C NMR** (100 MHz, CDCl₃, ppm): δ = 166.9, 163.7, 131.9, 122.4, 113.8, 66.6, 61.7, 55.6. **GC-MS (EI)** *m/z* (relative intensity): 196 (9) [M⁺], 178 (16), 165 (9), 152 (47), 135 (100), 77 (26).

The spectral data are consistent with literature values.[8]

Ethylene glycol di-4-methoxybenzoate (2ak)

Following Pathway A with anisole, **2ak** was isolated by flash chromatography on silica with EA/pentane as eluent as a white solid (81 % yield).

¹H NMR (400 MHz, CDCl₃, ppm): δ = 8.03–8.00 (m, 4H), 6.93–6.90 (m, 2H), 4.62 (s, 4H), 3.85 (s, 6H). **¹³C NMR** (100 MHz, CDCl₃, ppm): δ = 166.3, 163.7, 131.9, 122.4, 113.8, 62.7, 55.6.

The spectral data are consistent with literature values.[48]

4-Methoxy benzoic acid (2al)

Following Pathway A with anisole, **2al** was isolated by flash chromatography on silica with EA/pentane as eluent as a white solid (93 % yield).

¹H NMR (400 MHz, CDCl₃, ppm): δ = 8.08–8.05 (m, 2H), 6.96–6.94 (m, 2H), 3.88 (s, 3H). **¹³C NMR** (100 MHz, CDCl₃, ppm): δ = 171.4, 164.2, 132.5, 121.8, 113.9, 77.2, 55.6. **GC-MS (EI)** *m/z* (relative intensity): 152 (97) [M⁺], 135 (100), 107 (21), 77 (27).

The spectral data are consistent with literature values.[49]

4-Methoxy benzoic anhydride (2am)

Following Pathway A with anisole, **2am** was isolated by flash chromatography on silica with EA/pentane as eluent as a white solid (71 % yield).

¹H NMR (400 MHz, CDCl₃, ppm): δ = 8.11–8.08 (m, 4H), 6.99–6.97 (m, 4H), 3.89 (s, 6H). **¹³C NMR** (100 MHz, CDCl₃, ppm): δ = 164.6, 162.3, 132.8, 121.3, 114.1, 55.6.

The spectral data are consistent with literature values.[50]

1-(4-Methylbenzoyl)-piperidine (2bn)

Ethylene glycol di-4-methoxybenzoate (2ak)

Following Pathway A with anisole, **2ak** was isolated by flash chromatography on silica with EA/pentane as eluent as a white solid (81 % yield).

¹H NMR (400 MHz, CDCl₃, ppm): δ = 8.03–8.00 (m, 4H), 6.93–6.90 (m, 2H), 4.62 (s, 4H), 3.85 (s, 6H). **¹³C NMR** (100 MHz, CDCl₃, ppm): δ = 166.3, 163.7, 131.9, 122.4, 113.8, 62.7, 55.6.

The spectral data are consistent with literature values.[48]

4-Methoxy benzoic acid (2al)

Following Pathway A with anisole, **2al** was isolated by flash chromatography on silica with EA/pentane as eluent as a white solid (93 % yield).

¹H NMR (400 MHz, CDCl₃, ppm): δ = 8.08–8.05 (m, 2H), 6.96–6.94 (m, 2H), 3.88 (s, 3H). **¹³C NMR** (100 MHz, CDCl₃, ppm): δ = 171.4, 164.2, 132.5, 121.8, 113.9, 77.2, 55.6. **GC-MS (EI)** *m/z* (relative intensity): 152 (97) [M⁺], 135 (100), 107 (21), 77 (27).

The spectral data are consistent with literature values.[49]

4-Methoxy benzoic anhydride (2am)

Following Pathway A with anisole, **2am** was isolated by flash chromatography on silica with EA/pentane as eluent as a white solid (71 % yield).

¹H NMR (400 MHz, CDCl₃, ppm): δ = 8.11–8.08 (m, 4H), 6.99–6.97 (m, 4H), 3.89 (s, 6H). **¹³C NMR** (100 MHz, CDCl₃, ppm): δ = 164.6, 162.3, 132.8, 121.3, 114.1, 55.6.

The spectral data are consistent with literature values.[50]

1-(4-Methylbenzoyl)-piperidine (2bn)

Following Pathway A without anisole, **2bn** was isolated by flash chromatography on silica with EA/pentane as eluent as a colorless oil (77 % yield).

¹H NMR (400 MHz, CDCl₃, ppm): δ = 7.30–7.27 (m, 2H), 7.20–7.17 (m, 2H), 3.68–3.37 (m, 4H), 2.37 (s, 3H), 1.62–1.44 (m, 6H). **¹³C NMR** (100 MHz, CDCl₃, ppm): δ = 170.6, 139.5, 133.7, 129.1, 127.1, 48.9, 43.1, 26.5, 25.6, 24.8, 21.5. **GC-MS (EI)** *m/z* (relative intensity): 203 (5) [M⁺], 119 (31), 91 (100), 65 (18).

The spectral data are consistent with literature values.[51]

N,N-Dibutyl-4-methylbenzamide (2bo)

Following Pathway A without anisole, **2bq** was isolated by flash chromatography on silica with EA/pentane as eluent as a colorless oil (80 % yield).

¹H NMR (400 MHz, CDCl₃, ppm): δ = 7.31–7.29 (m, 2H), 7.13–7.11 (m, 2H), 3.69–3.66 (m, 4H), 2.33 (s, 3H), 1.69–1.61 (m, 4H), 1.41–1.32 (m, 4H), 0.95 (t, *J* = 7.4 Hz, 6H). **¹³C NMR** (100 MHz, CDCl₃, ppm): δ = 172.0, 139.1, 134.6, 129.0, 125.1, 49.0, 44.6, 31.0, 29.8, 21.5, 20.5, 19.9, 14.1, 13.8. **GC-MS (EI)** *m/z* (relative intensity): 247 (13) [M⁺], 119 (27), 91 (100).

The spectral data are consistent with literature values.[52]

N,N-Diethyl-3-methylbenzamide (2qp)

Following Pathway A without anisole, **2qp** was isolated by flash chromatography on silica with EA/pentane as eluent as a colorless oil (79 % yield).

¹H NMR (400 MHz, CDCl₃, ppm): δ = 7.24 – 7.21 (m, 3H), 6.96 – 6.94 (m, 1H), 3.76 (q, *J* = 7.2 Hz), 2.36 (s, 3H), 1.26 (t, *J* = 7.2 Hz, 6H). **¹³C NMR** (100 MHz, CDCl₃, ppm): δ = 151.4, 138.6, 128.7, 126.0, 121.2, 117.7, 42.3, 21.6, 11.4. **GC-MS (EI)** *m/z* (relative intensity): 191 (17) [M⁺], 119 (36), 91 (100) 65 (13).

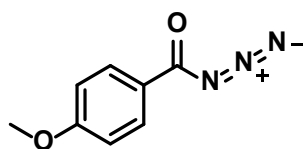The spectral data are consistent with literature values.[53]

Methyl 4-cyanobenzoate (2da)

Following Pathway A with anisole, **2da** was isolated by flash chromatography on silica with EA/pentane as eluent as a white solid (85 % yield).

¹H NMR (400 MHz, CDCl₃, ppm): δ = 8.15–8.13 (m, 2H), 7.75–7.73 (m, 2H), 3.95 (s, 3H). **¹³C NMR** (100 MHz, CDCl₃, ppm): δ = 165.6, 134.4, 132.4, 130.2, 118.1, 116.5, 52.9. **GC-MS (EI)** m/z (relative intensity): 161 (25) [M⁺], 130 (100), 102 (58), 75 (28).

The spectral data are consistent with literature values.[8]

Methyl 4-fluorobenzoate (2ea)
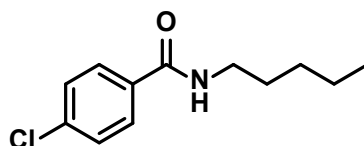

Following Pathway A with anisole, **2ea** was isolated by flash chromatography on silica with EA/pentane as eluent as a colorless liquid (79 % yield).

¹H NMR (400 MHz, CDCl₃, ppm): δ = 8.08–8.03 (m, 2H), 7.14–7.08 (m, 2H), 3.91 (s, 3H). **¹³C NMR** (100 MHz, CDCl₃, ppm): δ = 166.7, 166.3, 165.0, 132.3, 132.2, 126.5, 115.7, 115.6, 52.3. **GC-MS (EI)** m/z (relative intensity): 154 (22) [M⁺], 123 (100), 95 (66), 75 (41).

The spectral data are consistent with literature values.[54]

Methyl 4-aminosulfonylbenzoate (2fa)

Following Pathway A with anisole, **2fa** was isolated by flash chromatography on silica with EA/pentane as eluent as a white solid (76 % yield).

¹H NMR (400 MHz, CD₃CN, ppm): δ = 8.15–8.13 (m, 2H), 7.97–7.95 (m, 2H), 5.82 (br s, 2H), 3.91 (s, 3H). **¹³C NMR** (100 MHz, CD₃CN, ppm): δ = 166.6, 148.1, 134.5, 131.0, 127.3, 53.2. **GC-MS (EI)** m/z (relative intensity): 215 (27) [M⁺], 184 (100), 151 (12), 135 (18).

The spectral data are consistent with literature values.[55]

Methyl 4-Acylbenzoate (2ga)

Following Pathway A with anisole, **2ga** was isolated by flash chromatography on silica with EA/pentane as eluent as a white solid (91 % yield).

¹H NMR (400 MHz, CDCl₃, ppm): δ = 8.13–8.11 (m, 2H), 8.01–7.99 (m, 2H), 3.94 (s, 3H), 2.64 (s, 3H).**¹³C NMR** (100 MHz, CDCl₃, ppm): δ = 197.7, 165.9, 140.3, 134.0, 130.0, 128.3, 52.6, 27.0.

The spectral data are consistent with literature values.[56]

Methyl 2-methoxybenzoate (2ha)

Following Pathway A with anisole, **2ha** was isolated by flash chromatography on silica with EA/pentane as eluent as a colorless liquid (88 % yield).

¹H NMR (400 MHz, CDCl₃, ppm): δ = 7.81 – 7.78 (m, 1H), 7.49 – 7.45 (m, 1H), 7.00 – 6.96 (m, 2H), 3.91 (s, 3H), 3.89 (s, 3H). **¹³C NMR** (100 MHz, CDCl₃, ppm): δ = 167.0, 159.4, 133.7, 131.8, 120.3, 119.9, 112.1.

The spectral data are consistent with literature values.[58]

Methyl 2-nitrobenzoate (2ia)

Following Pathway A with anisole, **2ia** was isolated by flash chromatography on silica with EA/pentane as eluent as a yellowish liquid (70 % yield).

¹H NMR (400 MHz, CDCl₃, ppm): δ = 7.93–7.90 (m, 1H),7.76–7.60 (m, 3H), 3.92 (s, 3H). **¹³C NMR** (100 MHz, CDCl₃, ppm): δ = 166.0, 133.0, 131.9, 130.0, 127.7, 124.1, 53.4. **GC-MS (EI)** *m/z* (relative intensity): 181 (4) [M⁺], 150 (100), 92 (26), 79 (55), 77 (35).

The spectral data are consistent with literature values.[59]

Methyl 3-bromobenzoate (2ja)

Following Pathway A with anisole, **2ja** was isolated by flash chromatography on silica with EA/pentane as eluent as a white solid (82 % yield).

¹H NMR (400 MHz, CDCl₃, ppm): δ = 8.19–8.17 (m, 1H), 7.98–7.96 (m, 1H), 7.69–7.67 (m, 1H), 7.35–7.29 (m, 1H), 3.93 (s, 3H). **¹³C NMR** (100 MHz, CDCl₃, ppm): δ = 165.4, 136.0, 132.8, 132.2, 130.1, 128.3, 122.6, 52.6. **GC-MS (EI)** *m/z* (relative intensity): 214 (45) [M⁺], 216 (30), 185 (100), 183 (96), 157 (41), 155 (43).

The spectral data are consistent with literature values.[54]

Methyl 3-trifluoromethylbenzoate (2ka)

Following Pathway A with anisole, **2ka** was isolated by flash chromatography on silica with EA/pentane as eluent as a white solid (82 % yield).

¹H NMR (400 MHz, CDCl₃, ppm): δ = 8.31 (m, 1H), 8.24–8.22 (m, 1H), 7.83–7.80 (m, 1H), 7.61–7.56 (m, 1H), 3.96 (s, 3H). **¹³C NMR** (100 MHz, CDCl₃, ppm): δ = 165.5, 132.9, 131.1, 129.6, 129.2, 126.7, 52.7. **GC-MS (EI)** *m/z* (relative intensity): 204 (21) [M⁺], 185 (12), 173 (100), 145 (67).

The spectral data are consistent with literature values.[57]

Methyl 3-ethinylbenzoate (2la)

Following Pathway A with anisole, **2la** was isolated by flash chromatography on silica with EA/pentane as eluent as a white solid (79 % yield).

¹H NMR (400 MHz, CDCl₃, ppm): δ = 8.17 (m, 1H), 8.03–8.00 (m, 1H), 7.68–7.65 (m, 1H), 7.43–7.38 (m, 1H), 3.93 (s, 3H), 3.12 (s, 1H). **¹³C NMR** (100 MHz, CDCl₃, ppm): δ = 166.2, 136.4, 133.4, 130.6, 129.9, 128.6, 122.8, 82.3, 78.3, 52.4. **GC-MS (EI)** *m/z* (relative intensity): 160 (47) [M⁺], 129 (100), 101 (66), 79 (26).

The spectral data are consistent with literature values.[60]

2-Hydroxyethyl 2-ethinylbenzoate (2lh)

Following Pathway A with anisole, **2lh** was isolated by flash chromatography on silica with EA/pentane as eluent as a colorless oil (77 % yield).

¹H NMR (400 MHz, CDCl₃, ppm): δ = 8.18 (m, 1H), 8.05–8.02 (m, 1H), 7.69–7.67 (m, 1H), 7.45–7.39 (m, 1H), 4.49–4.46 (m, 2H), 4.01–3.94 (m, 2H), 3.13 (s, 1H). **¹³C NMR** (100 MHz, CDCl₃, ppm): δ = 166.2, 136.6, 133.4, 128.7, 122.8, 78.4, 67.0, 61.5. **HRMS** (ESI): *m/z* calculated for C₁₁H₁₀O₃+Na⁺: 213.0528 [M+Na]⁺; found 213.0523.

Methyl 1-naphthoate (2ma)

Following Pathway A with anisole, **2ma** was isolated by flash chromatography on silica with EA/pentane as eluent as a white solid (75 % yield).

¹H NMR (400 MHz, CDCl₃, ppm): δ = 8.93–8.91 (m, 1H), 8.20–8.18 (m, 1H), 8.04–8.01 (m, 1H), 7.90–7.88 (m, 1H), 7.65–7.60 (m, 1H), 7.56–7.51 (m, 1H), 7.53–7.48 (m, 1H), 4.01 (s, 3H). **¹³C NMR** (100 MHz, CDCl₃, ppm): δ = 168.2, 134.0, 133.5, 131.5, 130.3, 128.7, 127.9, 126.3, 126.0, 124.6, 52.3.

The spectral data are consistent with literature values.[59]

Allyl 4-cyanobenzoate (2di)

Following Pathway A with anisole, **2di** was isolated by flash chromatography on silica with EA/pentane as eluent as a colorless liquid (87 % yield).

¹H NMR (400 MHz, CDCl₃, ppm): δ = 8.17–8.15 (m, 2H), 7.76–7.74 (m, 2H), 6.08–5.98 (m, 1H), 5.45–5.31 (m, 1H), 4.86–4.85 (m, 1H). **¹³C NMR** (100 MHz, CDCl₃, ppm): δ = 164.8, 134.1, 133.0, 131.7, 130.3, 118.7, 118.1, 116.6, 66.5.

The spectral data are consistent with literature values.[61]

Dimethyl 2,3-thiophendicarboxylate (2na)

Following Pathway A with anisole, **2na** was isolated by flash chromatography on silica with EA/pentane as eluent as a white solid (80 % yield).

¹H NMR (400 MHz, CDCl₃, ppm): δ = 7.46 (d, J = 5.1 Hz, 1H), 7.29 (d, J = 5.1 Hz, 1H), 3.92 (s, 3H), 3.90 (s, 3H). **¹³C NMR** (100 MHz, CDCl₃, ppm): δ = 164.7, 161.7, 137.3, 134.0, 130.2, 128.9, 52.8, 52.8. **GC-MS (EI)** m/z (relative intensity): 200 (25) [M⁺], 169 (100), 139 (44), 126 (8), 111 (9).

The spectral data are consistent with literature values.[62]

4-Methylbenzoyl fluoride (2bK)
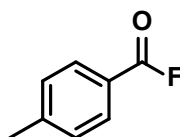
Following Pathway A with anisole and [hmim]F as nucleophile, **2bK** was obtained in a crude mixture. The yield was determined from the crude mixture by ¹H NMR spectroscopy with 1,3,5-trimethoxybenzene as standard (43 % ¹H NMR yield). After flash chromatography on

silica with EA/pentane as eluent a mixture of **2bK** and an unidentified substance was obtained as slightly yellow oil.

¹H NMR (400 MHz, CDCl₃, ppm): δ = 7.95–7.92 (m, 2H), 7.34–7.31 (m, 2H), 2.46 (s, 3H). **¹³C NMR** (151 MHz, CDCl₃, ppm): δ = 157.7 (J_{C-F} = 343.0 Hz), 146.7, 131.6 (J_{C-F} = 4.0 Hz), 129.9, 122.3 (J_{C-F} = 61.0 Hz), 22.8. **¹⁹F NMR** (565 MHz, CDCl₃, ppm): δ = 17.46.

The spectral data are consistent with literature values.[69]

4-Chlorobenzoyl chloride (2cq)
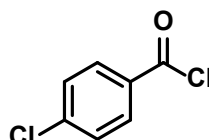
Following Pathway A with anisole and [bmim]Cl as nucleophile, **2cq** was isolated by distillation from the crude mixture as a colorless liquid (88 % yield).

¹H NMR (400 MHz, CDCl₃, ppm): δ = 8.07–8.05 (m, 2H), 7.51–7.49 (m, 2H). **¹³C NMR** (100 MHz, CDCl₃, ppm): δ = 167.6, 142.5, 132.8, 131.8, 129.5. **GC-MS (EI)** *m/z* (relative intensity): 174 (6) [M⁺], 141 (34), 139 (100), 113 (13), 111 (39).

The spectral data are consistent with literature values.[63]

4-Methoxybenzoyl chloride (2aq)
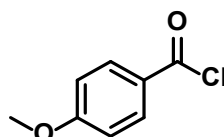
Following Pathway A with anisole and [bmim]Cl as nucleophile, **2aq** was obtained in a crude mixture. The yield was determined from the crude mixture by ¹H NMR spectroscopy with mesitylene as standard (84 % ¹H NMR yield).

¹H NMR (400 MHz, CDCl₃, ppm): δ = 8.10–8.07 (m, 2H), 6.99–6.96 (m, 2H). **¹³C NMR** (151 MHz, CDCl₃, ppm): δ = 167.2, 165.4, 134.0, 125.4, 113.8, 55.8.

The spectral data are consistent with literature values.[64]

4-Methylbenzoyl chloride (2bq)
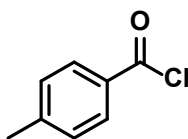
Following Pathway A with anisole and [bmim]Cl as nucleophile, **2bq** was isolated by distillation from the crude mixture as a colorless liquid (80 % yield).

¹H NMR (400 MHz, CDCl₃, ppm): δ = 8.03–8.00 (m, 2H), 7.32–7.29 (m, 2H). **¹³C NMR** (151 MHz, CDCl₃, ppm): δ = 168.3, 146.9, 131.7,130.8, 129.8, 22.0.

The spectral data are consistent with literature values.[65]

4-Acetylbenzoyl chloride (2gq)
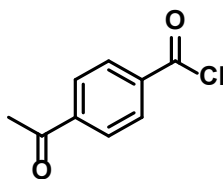
Following Pathway A with anisole and [bmim]Cl as nucleophile, **2gq** was obtained in a crude mixture. The yield was determined from the crude mixture by ^{1}H NMR spectroscopy with mesitylene as standard (72 % ^{1}H NMR yield).

^{1}H NMR (400 MHz, CDCl$_3$, ppm): δ = 8.21–8.19 (m, 2H), 8.07–8.04 (m, 2H), 2.66 (s, 3H). **^{13}C NMR** (151 MHz, CDCl$_3$, ppm): δ = 197.1, 168.0, 141.9, 136.6, 131.6, 1287, 27.1.

The spectral data are consistent with literature values.[66]

4-Fluorobenzoyl chloride (2eq)
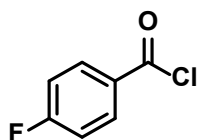
Following Pathway A with anisole and [bmim]Cl as nucleophile, **2eq** was isolated by distillation from the crude mixture as a colorless liquid (85 % yield).

^{1}H NMR (400 MHz, CDCl$_3$, ppm): δ = 8.19–8.14 (m, 2H), 7.22–7.17 (m, 2H). **^{13}C NMR** (151 MHz, CDCl$_3$, ppm): δ = 168.0, 166.7 (d, J_{C-F} = 117.2 Hz), 134.2 (d, J_{C-F} = 10.0 Hz), 129.6 (d, J_{C-F} = 2.8 Hz), 116.3 (d, J_{C-F} = 22.3 Hz). **^{19}F NMR** (565 MHz, CDCl$_3$, ppm): δ = -100.80.

The spectral data are consistent with literature values.[66]

2-Methoxybenzoyl chloride (2hq)
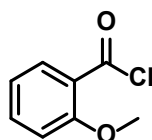
Following Pathway A with anisole and [bmim]Cl as nucleophile, **2hq** was obtained in a crude mixture. The yield was determined from the crude mixture by ^{1}H NMR spectroscopy with mesitylene as standard (68 % ^{1}H NMR yield).

^{1}H NMR (400 MHz, CDCl$_3$, ppm): δ = 8.11–8.08 (m, 1H), 7.62–7.56 (m, 1H), 7.08–6.99 (m, 2H), 3.94 (s, 3H). **^{13}C NMR** (151 MHz, CDCl$_3$, ppm): δ = 164.1, 159.8, 136.3, 134.8, 122.5, 120.5, 112.2, 56.2.

The spectral data are consistent with literature values.[67]

3-Bromobenzoyl chloride (2jq)
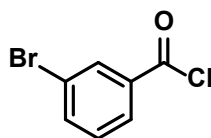
Following Pathway A with anisole and [bmim]Cl as nucleophile, **2jg** was obtained in a crude mixture. The yield was determined from the crude mixture by ^{1}H NMR spectroscopy with mesitilyene as standard (74 % ^{1}H NMR yield).

^{1}H NMR (400 MHz, CDCl$_3$, ppm): δ = 8.26–8.25 (m, 1H), 8.08–8.04 (m, 1H), 7.83–7.80 (m, 1H), 7.44–7.38 (1H). **^{13}C NMR** (151 MHz, CDCl$_3$, ppm): δ = 167.4, 138.3, 135.2, 134.2, 130.6, 129.4, 123.2.

The spectral data are consistent with literature values.[68]

4-Chlorobenzoyl cyanide (2cr)
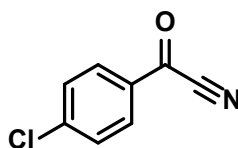
Following Pathway A with anisole and TMS-CN as nucleophile, **2cr** was isolated by flash chromatography on silica with EA/pentane as eluent as a white solid (66 % yield).

^{1}H NMR (400 MHz, CDCl$_3$, ppm): δ = 8.11–8.08 (m, 2H), 7.60–7.50 (m, 2H). **^{13}C NMR** (100 MHz, CDCl$_3$, ppm): δ = 166.7, 144.0, 131.8, 131.7, 130.1, 112.5.

The spectral data are consistent with literature values.[70]

4-Methoxybenzoyl azide (2as)

Following Pathway A with anisole and TMS-azide as nucleophile, **2as** was isolated by flash chromatography on silica with EA/pentane as eluent as a white solid (64 % yield).

^{1}H NMR (400 MHz, CDCl$_3$, ppm): δ = 8.00–7.97 (m, 2H), 6.94–6.91 (m, 2H), 3.87 (s, 3H). **^{13}C NMR** (100 MHz, CDCl$_3$, ppm): δ = 171.8, 164.8, 131.9, 123.4, 114.1, 55.7.

The spectral data are consistent with literature values.[71]
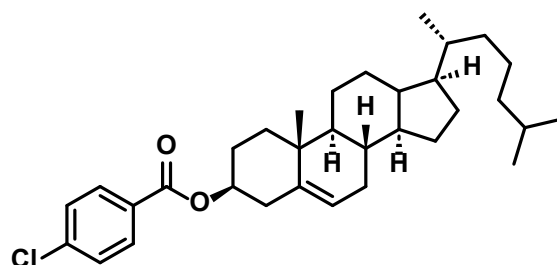
N-Pentyl-4-chlorobenzamide (2ct)

Following Pathway B, the reaction mixture was collected from the flow reactor, treated with pentylamine (2 eq.) and triethylamine (1 eq.) and stirred for two hours at room temperature. Then, **2ct** was isolated by flash chromatography on silica with EA/pentane as eluent as a colorless oil (84 % yield).

¹H NMR (400 MHz, CDCl₃, ppm): δ = 7.71–7.68 (m, 2H), 7.40–7.37 (m, 2H), 6.16 (br s, 1H), 3.46–3.39 (m, 2H), 1.63–1.56 (m, 2H), 1.37–1.35 (m, 2H), 0.93–0.88 (m, 3H). **¹³C NMR** (100 MHz, CDCl₃, ppm): δ = 166.6, 137.6, 133.4, 128.9, 128.4, 40.3, 29.5, 29.3, 22.5, 14.1. **GC-MS (EI)** *m/z* (relative intensity): 225 (5) [M⁺], 169 (16), 168 (17), 141 (32), 139 (100), 113 (8), 111 (24).

The spectral data are consistent with literature values.[72]

2-(Diethylamino)ethyl 4-[(4-chlorobenzoyl)amino]benzoate (2cu)
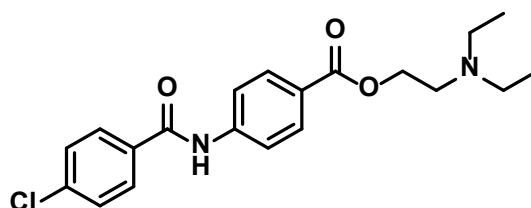
Following Pathway B, the reaction mixture was collected from the flow reactor, treated with procaine hydrochloride (2 eq.) and triethylamine (2 eq.) and stirred for two hours at room temperature. Then, **2cu** was isolated by flash chromatography on silica with EA/pentane as eluent as a white solid (77 % yield).

¹H NMR (400 MHz, CDCl₃, ppm): δ = 8.17, (s, 1H), 8.04–8.01 (m, 2H), 7.82–7.80 (m, 2H), 7.74–7.72 (m, 2H), 7.44–7.42 (m, 2H), 4.38 (t, *J* = 6.2 Hz, 2H), 2.86 (t, *J* = 6.2 Hz, 2H), 2.63 (q, *J* = 7.1 Hz, 4H), 1.07 (t, *J* = 7.1 Hz, 6H). **¹³C NMR** (100 MHz, CDCl₃, ppm): δ = 166.2, 164.9, 142.0, 138.7, 133.0, 131.1, 129.3, 128.7, 126.4, 119.4, 63.6, 51.2, 48.0, 12.2. **HRMS** (ESI): *m/z* calculated for C₂₀H₂₃ClN₂O₃+H⁺: 375.1475 [M+H]⁺; found 375.1485.

4-Chloro-*N*-Methyl-*N*-phenylbenzamide (2cv)
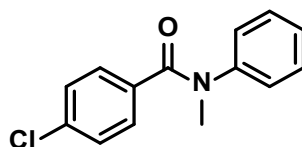
Following Pathway B, the reaction mixture was collected from the flow reactor, treated with *N*-Methyl-*N*-phenylbenzamide (2 eq.) and triethylamine (1 eq.) and stirred for two hours at room temperature. Then, **2cv** was isolated by flash chromatography on silica with EA/pentane as eluent as a white solid (71 % yield).

¹H NMR (400 MHz, CDCl₃, ppm): δ = 7.26–7.01 (m, 9H), 3.49 (s, 3H). **¹³C NMR** (100 MHz, CDCl₃, ppm): δ = 169.6, 144.8, 135.8, 134.4, 130.4, 129.5, 128.1, 127.0, 126.9, 38.6. **GC-MS (EI)** *m/z* (relative intensity): 245 (16) [M⁺], 141 (32), 139 (100), 113 (11), 111 (35).

The spectral data are consistent with literature values.[73]

N-methyl-N-(phenylmethyl)-4-methylbenzamide (2cw)
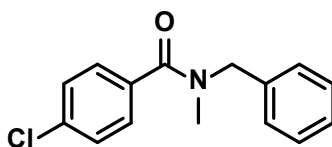
Following Pathway B, the reaction mixture was collected from the flow reactor, treated with N-Methyl-N-(phenylmethyl)-amine (2 eq.) and triethylamine (1 eq.) and stirred for two hours at room temperature. **2cw** was isolated by flash chromatography on silica with EA/pentane as eluent as a colorless solid (72 % yield).

¹H NMR (400 MHz, CDCl₃, ppm): δ = 7.42–7.30 (m, 9H), 4.74–4.50 (d, 2H), 3.03–2.86 (d, 3H). **¹³C NMR** (100 MHz, CDCl₃, ppm): δ = 170.6, 141.0, 136.9, 135.8, 134.7, 129.0, 128.9, 128.5, 128.3, 127.8, 126.7, 55.3, 51.0, 37.1, 33.5. **GC-MS (EI)** m/z (relative intensity): 259 (22) [M⁺], 258 (27), 141 (32), 139 (100), 120 (22), 113 (11), 111 (33), 91 (33).

The spectral data are consistent with literature values. [74]

1-(4-chlorobenzoyl)-2-pyrrolidinemethanol (2cx)
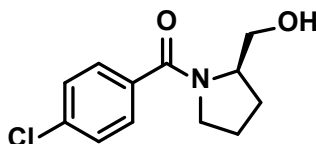
Following Pathway B, the reaction mixture was collected from the flow reactor, treated with prolinol (2 eq.) and triethylamine (1 eq.) and stirred for two hours at room temperature. Then, **2cx** was isolated by flash chromatography on silica with EA/pentane as eluent as a white solid (78 % yield).

¹H NMR (400 MHz, CDCl₃, ppm): δ = 7.46–7.45 (m, 2H), 7.39–7.37 (m, 2H), 4.73, (m, 1H), 4.40–4.35 (m, 1H), 3.80 (m, 1H), 3.74–3.72 (m, 1H), 3.49–3.45 (m, 2H), 2.20–2.14 (m, 1H), 1.91–1.85 (m, 1H), 1.79–1.72 (m, 1H), 1.69–1.61 (m, 1H). **¹³C NMR** (100 MHz, CDCl₃, ppm): δ = 171.0, 136.3, 135.0, 128.7, 128.6, 67.1, 61.6, 51.2, 28.5, 24.7. **HRMS** (ESI): m/z calculated for C₁₂H₁₄ClNO₂+Na⁺: 262.0611 [M+Na]⁺; found 262.0614.

Chloro-N-methoxybenzamide (2cy)
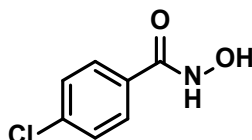
Following Pathway B, the reaction mixture was collected from the flow reactor, treated with hydroxylamine hydrochloride (2 eq.) and triethylamine (2 eq.) and stirred for two hours at room temperature. Then, the solvent was removed under reduced pressure, the residue was washed with pentane, acetone and water and **2cy** was collected as a white solid (77 % yield).

¹H NMR (400 MHz, DMSO-d₆, ppm): δ = 11.29 (s, 1H), 9.09 (s, 1H), 7.77–7.75 (m, 2H), 7.53–7.51 (m, 2H). **¹³C NMR** (100 MHz, DMSO-d₆, ppm): δ = 163.1, 135.9, 131.5, 128.8, 128.5.

The spectral data are consistent with literature values.[75]

4-Chloro-*N*-methoxy-*N*-methylbenzamide (2cz)
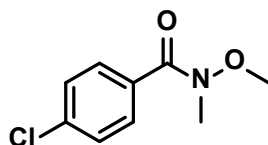
Following Pathway B, the reaction mixture was collected from the flow reactor, treated with *N,O*-dimethyl hydroxylamine hydrochloride (2 eq.) and triethylamine (1 eq.) and stirred for two hours at room temperature. **2cz** was isolated by flash chromatography on silica with EA/pentane as eluent as a colorless oil (75 % yield).

¹H NMR (400 MHz, CDCl₃, ppm): δ = 7.66–7.64 (m, 2H), 7.39–7.37 (m, 2H), 3.53 (s, 3H), 3.36 (s, 3H). **¹³C NMR** (100 MHz, CDCl₃, ppm): δ = 168.8, 136.9, 132.4, 130.0, 128.4 61.3, 33.7. **GC-MS (EI)** *m/z* (relative intensity): 199 (2) [M⁺], 141 (32), 139 (100), 113 (13), 111 (41).

The spectral data are consistent with literature values.[76]

N-[(1R,4R)-4-(3,4-dichlorophenyl)-1,2,3,4-tetrahydro-1-naphthalenyl]-*N*-methyl-4-chlorobenzamide (2cA)
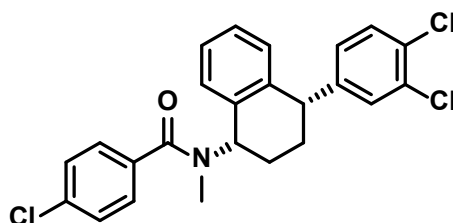
Following Pathway B, the reaction mixture was collected from the flow reactor, diluted with 5 mL dichloromethane, treated with sertraline hydrochloride (2 eq.) and triethylamine (2 eq.) and stirred for two hours at room temperature. **2cA** was isolated by flash chromatography on silica with EA/pentane as eluent as a white solid (67 % yield). The NMR spectra show the presence of two rotamers.

¹H NMR (400 MHz, CDCl₃, ppm): δ = 7.46–7.22 (m, 8H), 7.07 (br s, 1H), 7.07–6.97 (m, 1H), 6.87–6.84 + 6.77–6.75 (2x m, 1H), 6.04–6.01 + 4.94–4.90 (2x m, 1H), 4.24 + 4.16–4.15 (2x m, 1H), 2.86 + 2.71 (2x s, 3H), 2.39–1.63 (m, 4H). **¹³C NMR** (100 MHz, CDCl₃, ppm): δ = 171.9, 171.5, 147.0, 146.7, 138.5, 138.0, 138.0, 135.9, 135.8, 135.7, 125.6, 135.0, 132.6, 131.3, 131.1, 130.8, 130.7, 130.3, 130.3, 129.2, 128.9, 128.7, 128.2, 128.0, 128.0, 127.9, 127.8, 127.7, 127.3, 126.5, 58.9, 53.0, 43.2, 42.8, 33.3, 30.2, 30.1, 29.2, 22.8, 21.3.

S-Phenyl 4-chlorothiobenzoate (2cB)
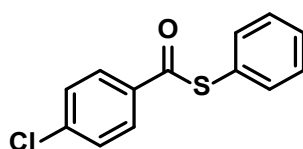
Following Pathway B, the reaction mixture was collected from the flow reactor, treated with thiophenol (2 eq.) and triethylamine (1 eq.) and stirred for two hours at room temperature. Then, **2cB** was isolated by flash chromatography on silica with EA/pentane as eluent as a white solid (73 % yield).

¹H NMR (400 MHz, CDCl₃, ppm): δ = 7.98–7.96 (m, 2H), 7.52–7.51 (m, 2H), 7.48–7.46 (m, 5H). **¹³C NMR** (100 MHz, CDCl₃, ppm): δ = 189.2, 140.2, 135.2, 135.1, 129.8, 129.5, 129.2, 129.0, 127.1.

The spectral data are consistent with literature values.[77]

4-Chlorobenzaldehyde (2cC)
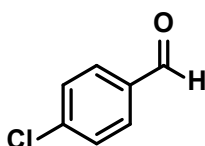
Following Pathway B, the reaction mixture was collected from the flow reactor, diluted with 5 mL THF, treated with Na[BH(OAc)₃] (1 eq.) and stirred for two hours at room temperature. The reaction was quenched with diluted HCl (1 M) and extracted with dichloromethane. Then, **2cC** was isolated by flash chromatography on silica with EA/pentane as eluent as a white solid (71 % yield).

¹H NMR (400 MHz, CDCl₃, ppm): δ = 9.98 (s, 1H), 7.84–7.81 (m, 2H), 7.53–7.51 (m, 2H). **¹³C NMR** (100 MHz, CDCl₃, ppm): δ = 191.6, 141.1, 134.9, 131.0, 129.6.

The spectral data are consistent with literature values.[78]

1,3-Dioxoisoindolin-2-yl 4-chlorobenzoate (2cD)
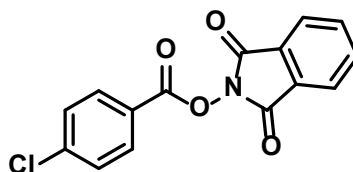
Following Pathway B, the reaction mixture was collected from the flow reactor, treated with N-hydroxy phthalimide (2 eq.) and triethylamine (1 eq.) and stirred for two hours at room temperature. Then, **2cD** was isolated by flash chromatography on silica with EA/pentane as eluent as a white solid (80 % yield).

¹H NMR (400 MHz, CDCl₃, ppm): δ = 8.14–8.12 (m, 2H), 7.94–7.92 (m, 2H), 7.83–7.81 (m, 2H), 7.53–7.51 (m, 2H). **¹³C NMR** (100 MHz, CDCl₃, ppm): δ = 162.2, 162.1, 141.8, 135.0, 132.1, 129.5, 129.1, 124.2, 123.9. **GC-MS (EI)** m/z (relative intensity): 141 (33), 139 (100), 111 (29), 76 (25).

The spectral data are consistent with literature values.[79]

tert-Butyl 4-chloroperbenzoate (2cE)
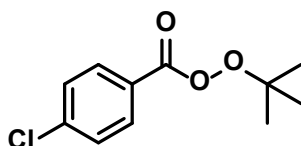
Following Pathway B, the reaction mixture was collected from the flow reactor, treated with *tert*-Butyl hydroperoxide (5.5 M in decane, 2 eq.) and triethylamine (1 eq.) and stirred for two hours at room temperature. **2cE** was isolated by flash chromatography on silica with EA/pentane as eluent as colorless oil (59 % yield).

^{1}H NMR (400 MHz, CDCl$_3$, ppm): δ = 7.90–7.88 (m, 2H), 7.45–7.43 (m, 2H), 1.41 (s, 9H). **^{13}C NMR** (100 MHz, CDCl$_3$, ppm): δ = 163.7, 140.0, 130.7, 129.2, 126.3, 84.3, 26.4.

The spectral data are consistent with literature values.[80]

P-(4-chlorobenzoyl)-phosphonic acid diethyl ester (2cF)
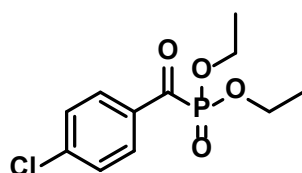
Following Pathway B, the reaction mixture was collected from the flow reactor. The solvent was removed under reduced pressure and substituted with dichloromethane. Triethylphosphite (1 eq.) was added and the mixture was stirred for 24 hours at room temperature. **2cF** was isolated by Kugelrohr-destillation as a white solid (75 % yield).

^{1}H NMR (400 MHz, CDCl$_3$, ppm): δ = 8.23–8.21 (m, 2H), 7.49–7.47 (m, 2H), 4.27 (m, 4H), 1.38 (t, *J* = 7.06 Hz, 6H). **^{13}C NMR** (100 MHz, CDCl$_3$, ppm): δ = 198.0, 141.6, 134.0, 131.4, 129.4, 64.3, 16.5. **^{31}P NMR** (162 MHz, CDCl$_3$, ppm): δ = -1.75.

The spectral data are consistent with literature values.[81]

(Z)-2-(dibutylamino)-1-(2,7-dichloro-9-(4-chlorobenzylidene)-9H-fluoren-4-yl)ethyl 4-chloro-benzoate (2cH)
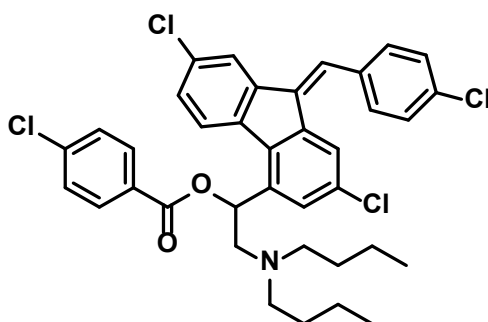
Following Pathway B, the reaction mixture was collected from the flow reactor, treated with lumefantrine (2 eq.) and triethylamine (1 eq.) and stirred for two hours at room temperature. Then, **2cH** was isolated by flash chromatography on silica with EA/pentane as eluent as a yellow solid (79 % yield).

^{1}H NMR (400 MHz, CDCl$_3$, ppm): δ = 8.05–8.00 (m, 3H), 7.77 (d, *J* = 2.0, 1H), 7.63 (s, 1H), 7.46–7.44 (m, 7H), 7.41–7.38 (m, 2H), 6.79 (br s, 1H), 3.07 (dd, *J* = 14.4, 8.2 Hz), 2.92 (dd, *J* = 14.4, 3.8 Hz), 2.54–2.51 (m, 4H), 1.36–1.33 (m, 4H), 1.26–1.20 (m, 4H), 0.83 (t, *J* = 7.3 Hz, 6H). **^{13}C NMR** (100 MHz, CDCl$_3$, ppm): δ = 165.0, 141.7, 139.9, 138.8, 136.6, 136.2, 135.0, 134.9, 134.2, 133.4,

132.9, 131.1, 130.7, 129.3, 129.0, 128.8, 128.6, 128.2, 124.6, 123.8, 120.8, 72.5, 58.8, 54.6, 29.5, 20.6, 14.2. **HRMS** (ESI): *m/z* calculated for $C_{37}H_{35}Cl_4NO_2+H^+$: 666.1500 [M+H]$^+$; found 666.1493.

Cholesteryl 4-methoxybenzoate (2cG)

Following Pathway B, the reaction mixture was collected from the flow reactor, diluted with dichloromethane (5 mL), treated with cholesterol (2 eq.) and triethylamine (1 eq.) and stirred for two hours at room temperature. **2cD** was isolated by flash chromatography on silica with EA/pentane as eluent as a white solid (76 % yield).

¹H NMR (400 MHz, CDCl₃, ppm): δ = 7.98–7.96 (m, 2H), 7.41–7.39 (m, 2H), 5.42–5.41 (m, 1H), 4.88–4.81 (m, 1H), 2.45 (d, *J* = 7.7 Hz, 2H), 2.04–1.97 (m, 3H), 1.93–1.90 (m, 1H), 1.86–1.81 (m, 1H), 1.76–1.68 (m, 1H), 1.59–0.99 (m, 24H), 0.92 (d, *J* = 6.5 Hz, 2H), 0.87 (dd, *J* = 6.6, 2.3 Hz, 6H), 0.69 (s, 3H). **¹³C NMR** (100 MHz, CDCl₃, ppm): δ = 165.3, 139.7, 139.3, 131.1, 129.4, 128.7, 123.1, 75.1, 56.8, 56.3, 50.2, 42.5, 39.9, 39.7, 38.3, 37.2, 36.8, 36.3, 35.9, 32.1, 32.0, 28.4, 28.2, 28.0, 24.4, 24.0, 23.0, 22.7, 21.2, 19.5, 18.9, 12.0.

The spectral data are consistent with literature values.[82]

8.4.4 Mechanistical Experiments

Radical trapping experiments

The experiment was conducted according to General procedure A with anisole, but with addition of TEMPO (3.0 equiv.). The obtained reaction mixture was analyzed by GC-MS.
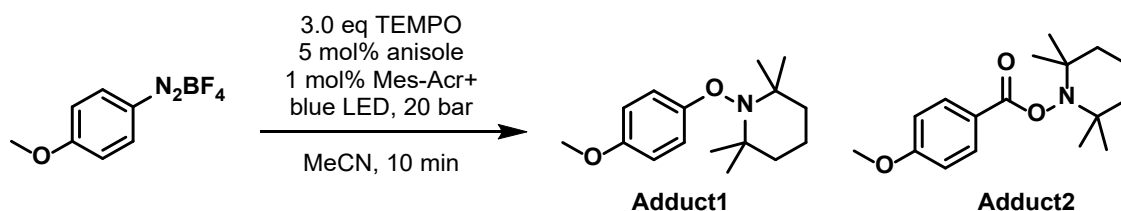
Scheme 8.6. TEMPO trapping experiment.

The TEMPO adducts of both the aryl and the acyl radical were detected and identified by molecular mass, fragmentation pattern and comparison with authentic samples.
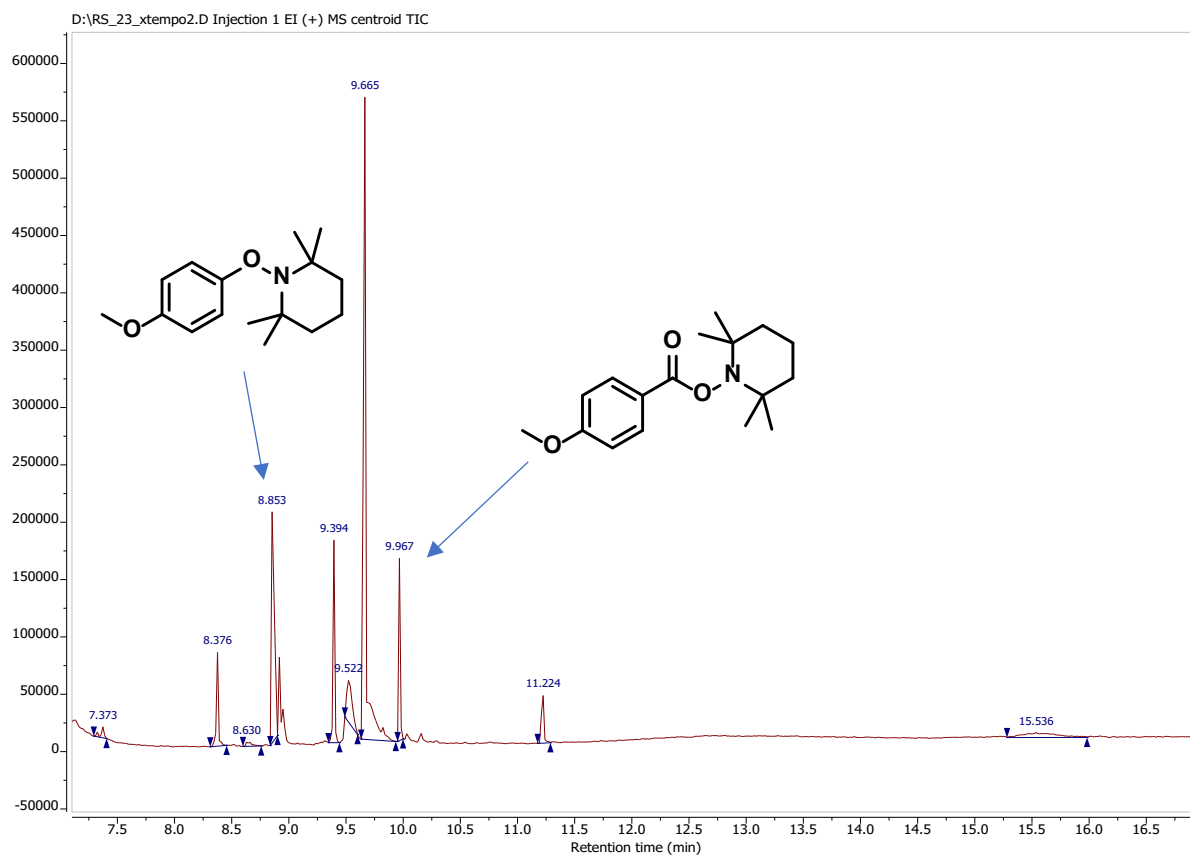
Figure 8.4. GC-MS trace of reaction mixture after radical trapping experiment.
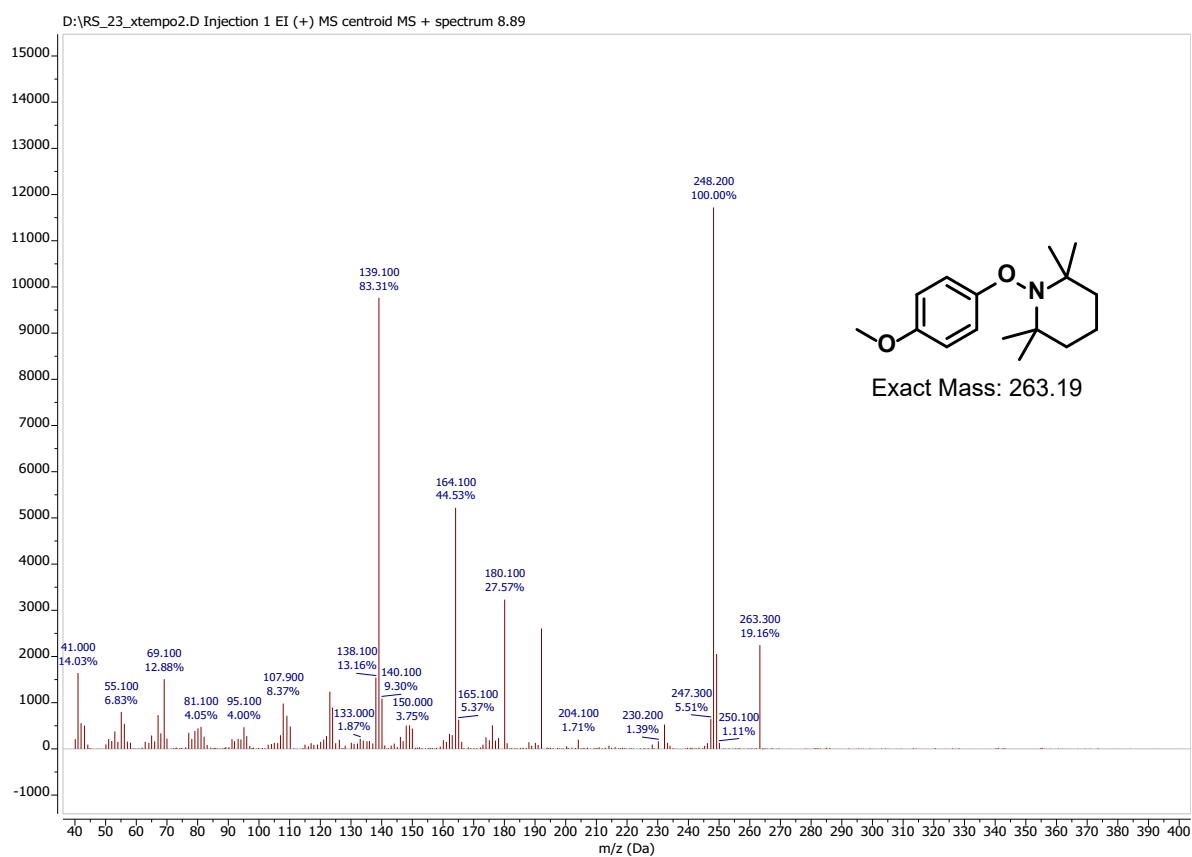
Figure 8.5. MS trace of Adduct1.
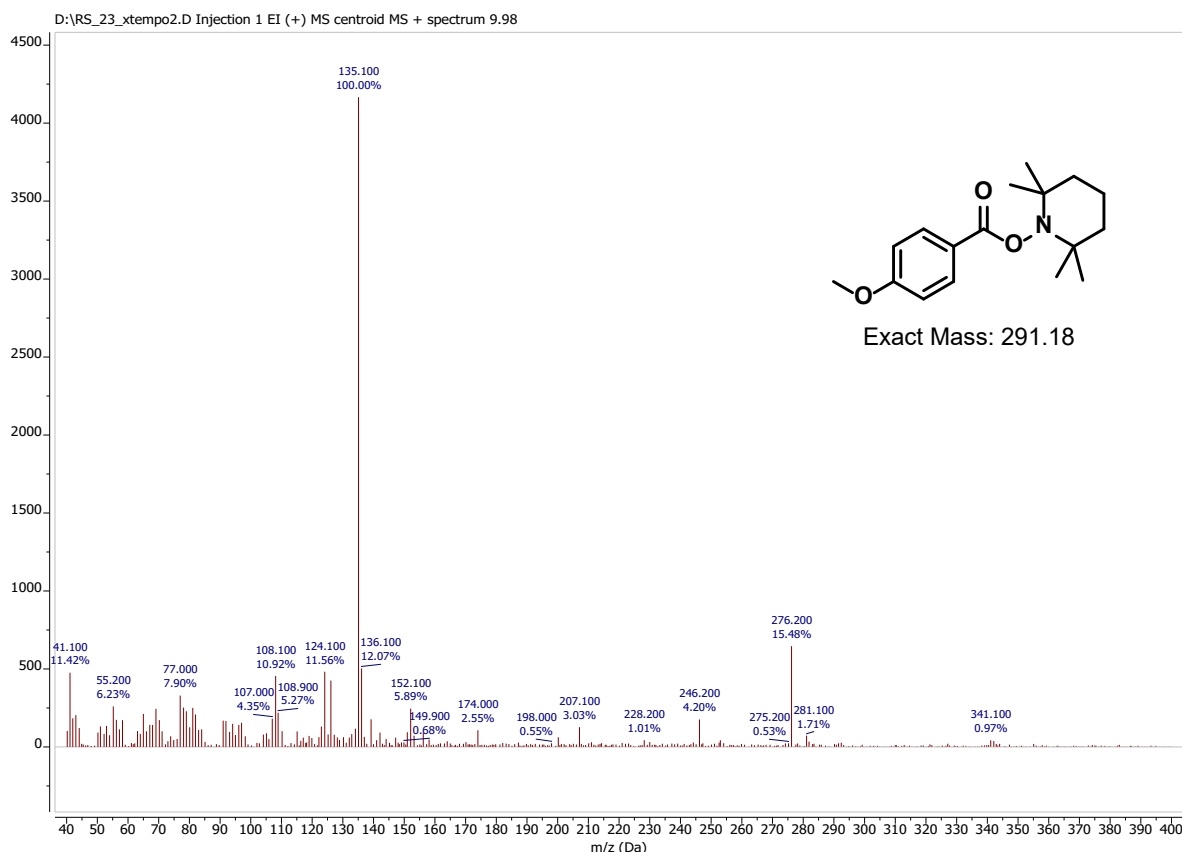
Figure 8.6. MS trace of Adduct 2. The molecular ion peak was not detected.

Stern-Volmer quenching

The Stern-Volmer quenching experiments were conducted according to a previously reported procedure.[83] UV/Vis absorption and fluorescence spectra were measured with a Specord 50 UV/Vis spectrophotometer (Analytic Jena) and a FluoroMax4 spectrofluorimeter (Horiba Scientific), respectively. The concentration of 9-mesityl-10-methylacridinium perchlorate was chosen such, that the absorbance at the excitation wavelength, 390 nm, did not exceed 0.1 absorbance units. Both excitation as well as emission slits were 20 nm wide. Emission spectra were recorded in the region 410 nm – 800 nm. Emission values were corrected taking into account the wavelength dependence of detector, and the internal filter effect of the quencher, where applicable. Corrected emission spectra were integrated, and the integral values were used to estimate the quenching constant K_{SV} using the Stern-Volmer equation[84]:

$$\frac{I_0}{I} - 1 = K_{SV} \cdot c(Q)$$

where I_0 and I is the total intensity of the fluorescence in the absence of quencher, and in the presence of quencher in concentration c(Q), respectively. It should be noted, that constant K_{SV} is derived from the life-time of the quenched excited species τ and from the rate constant of the bimolecular quenching k[84]:

$$K_{SV} = \tau \cdot k$$

When both quencher and the quenched excited species are charged, reaction rate is no longer constant with respect to quencher, as it is dependent on the total ionic strength of the solution, a behavior known as kinetic salt effect.[85] To take this into account, the Brønsted-Bjerrum equation[86] derived from the Debye-Hückel extended theory can be used:

$$
\ln(k) = \ln(k_0) + \frac{e^3 \sqrt{N_A}}{4\pi\sqrt{2 \cdot (\varepsilon_r \cdot \varepsilon_0 \cdot k_B \cdot T)^3}} \cdot \sqrt{1000} \cdot z_a \cdot z_b \cdot \frac{2\sqrt{I}}{1 + B\sqrt{I}}
$$
$$
= \ln(k_0) + A \cdot z_a \cdot z_b \cdot \frac{2\sqrt{I}}{1 + B\sqrt{I}}
$$

where e is the elementary charge; N_A is the Avogadro constant; ε_r is the relative permittivity of the solvent; ε_0 is the permittivity of vacuum; k_B is the Boltzmann constant; T is the thermodynamic temperature; z_A and z_B are the charges of the quencher and the quenched molecule and I is the ionic strength (using mol/dm^3 units). The factor $1000^{0.5}$ comes from the unit conversion of ionic strength (from 1000 mol/m^3 to the usual mol/dm^3). k_0 and k are quenching rates at ionic strengths of zero and I, respectively. Constant B is dependent on the size of the interacting species, but can be approximated in most cases as unity without any significant error.[86] For acetonitrile it can be calculated A = 3.351 at 300 K. Using this equation, the following can be written for Stern-Volmer quenching:

$$
\ln(K_{SV}) = \ln(\tau) + \ln(k) = \ln(\tau) + \ln(k_0) + A \cdot z_a \cdot z_b \cdot \frac{2\sqrt{I}}{1 + B\sqrt{I}} = \ln(K_{SV0}) + A \cdot z_a \cdot z_b \cdot \frac{2\sqrt{I}}{1 + B\sqrt{I}}
$$

where K_{SV0} is the Stern-Volmer quenching constant at zero ionic strength. Furthermore:

$$
\ln\left(\frac{I_0}{I} - 1\right) = \ln(K_{SV}) + \ln[c(q)] = \ln[c(q)] + \ln(K_{SV0}) + A \cdot z_a \cdot z_b \cdot \frac{2\sqrt{I}}{1 + B\sqrt{I}}
$$

$$
Q = \ln\left(\frac{I_0}{I} - 1\right) - A \cdot z_a \cdot z_b \cdot \frac{2\sqrt{I}}{1 + B\sqrt{I}} = \ln[c(q)] + \ln(K_{SV0})
$$

By plotting quantity Q (*vide supra*) against the natural logarithm of the quencher concentration, K_{SV0} – the Stern-Volmer quenching constant at zero ionic strength even for a charged pair quencher/luminescent dye can be obtained (Figure 8.10). In this case, it is the 9-mesityl-10-methylacridinium ion and the diazonium salts.
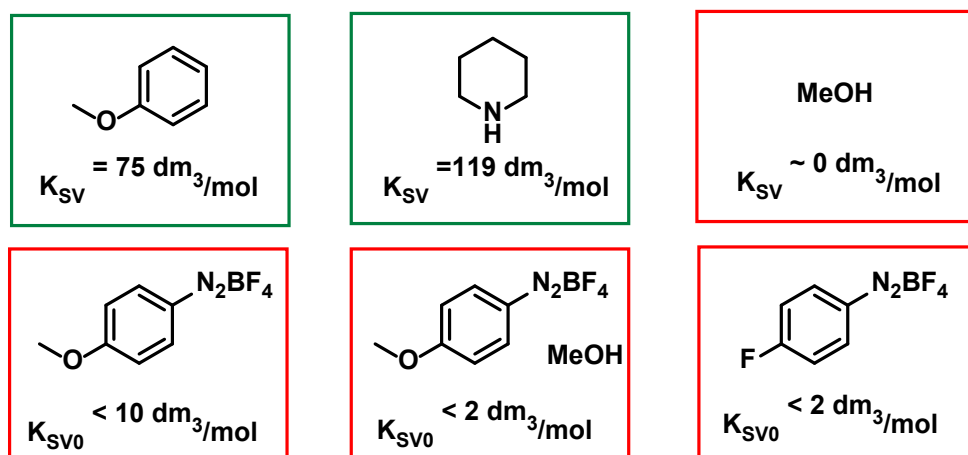
Figure 8.7. Stern-Volmer quenching constants K_{SV} and K_{SV0} for selected molecules.
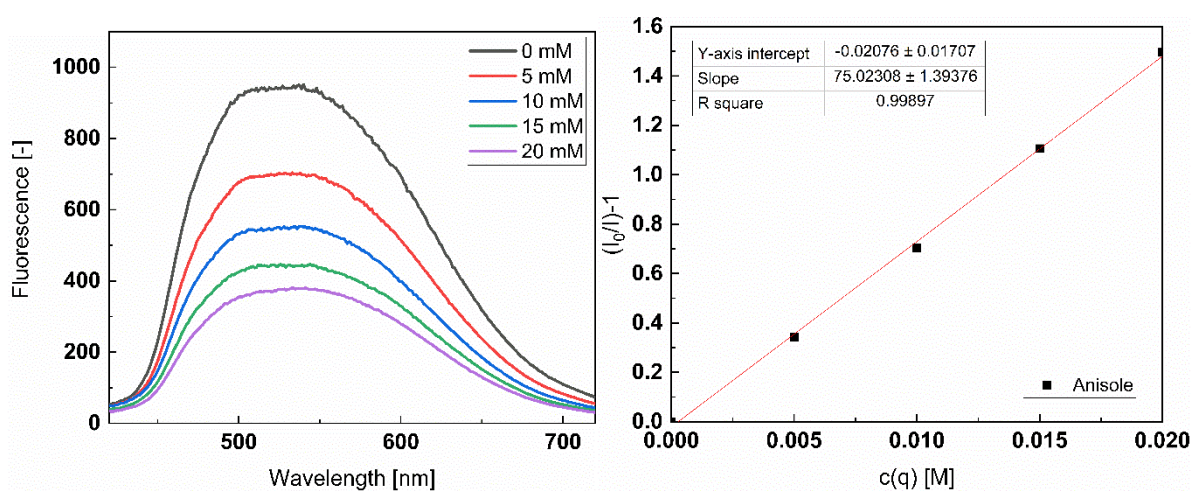
Figure 8.8. Fluorescence quenching of Mes-Acr+ with anisole (left) and linear fit (right).
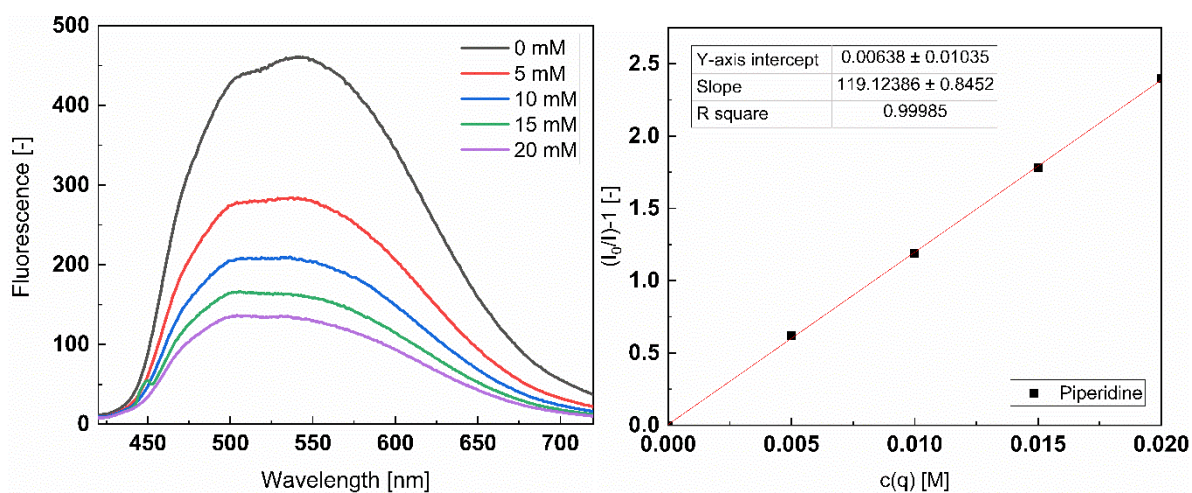
Figure 8.9. Fluorescence quenching of Mes-Acr+ with piperidine (left) and linear fit (right).
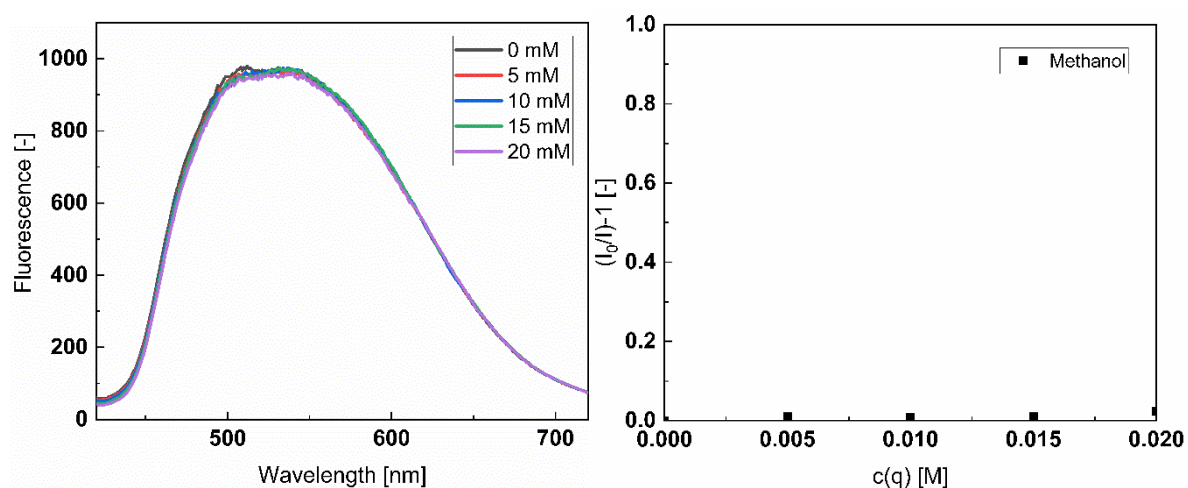
Figure 8.10. Fluorescence quenching of Mes-Acr+ with methanol (left) and linear fit (right).
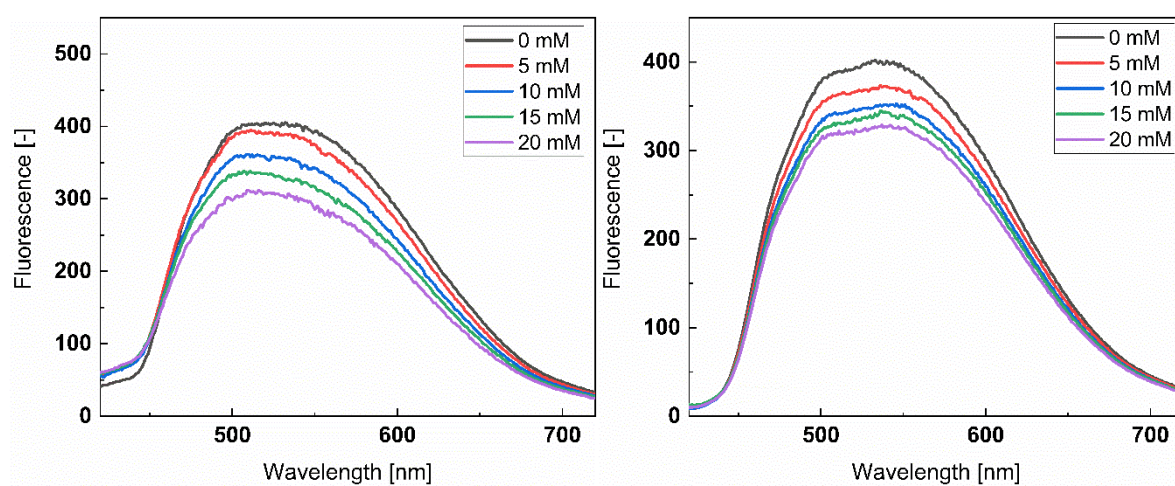
Figure 8.11. Fluorescence quenching of Mes-Acr+ with 4-OMe-phenyl diazonium salt (left) and 4-OMe-phenyl diazonium salt +MeOH (right).
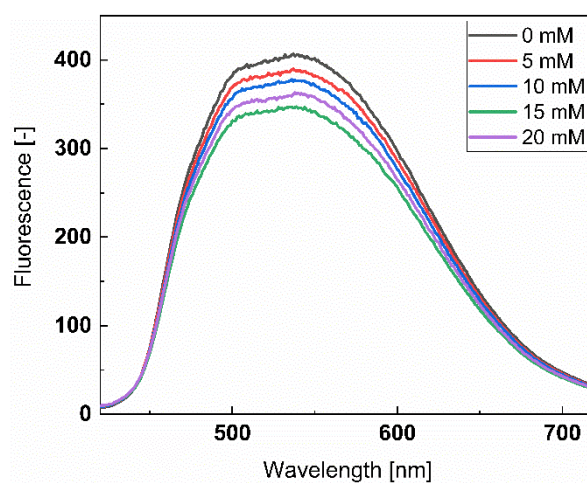
Figure 8.12. Fluorescence quenching of Mes-Acr+ with 4-F-phenyl diazonium salt.
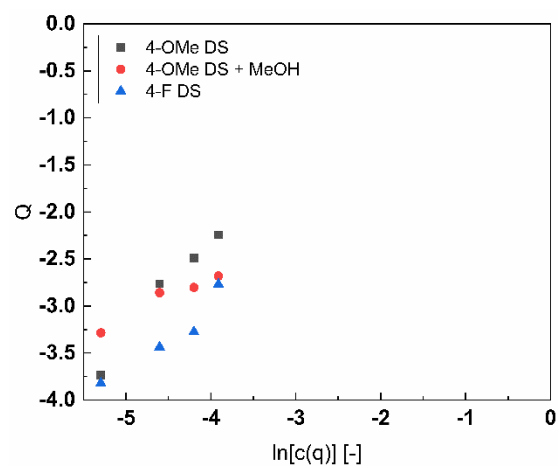
Figure 8.13. Modified Stern-Volmer-Plot for quenching of Mes-Acr+ with diazonium salts.

Benzonitrile (PhCN) was distilled, passed over acidic alumina and degassed prior to use. Mes-Acr+ was dissolved in PhCN under nitrogen atmosphere. The solution was transferred into an air-tight UV/Vis cuvette and the first UV/Vis spectrum was recorded. Afterwards, the cuvette was irradiated by two blue LEDs (455 nm) for 20 minutes and the second spectrum was acquired.
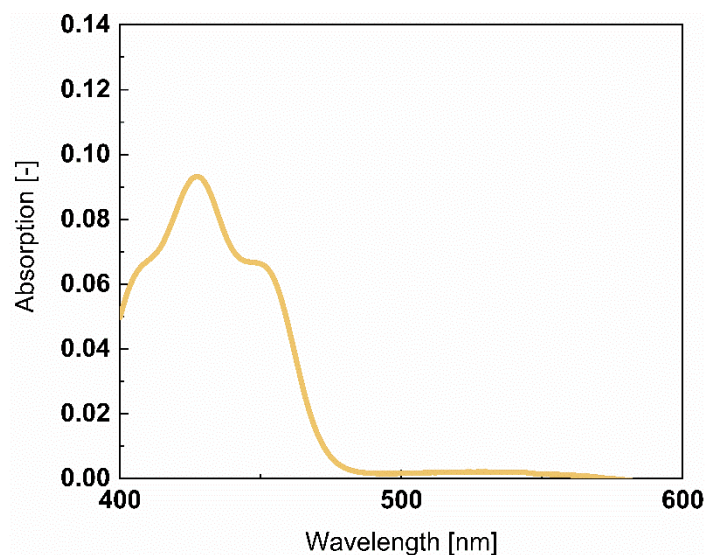
Figure 8.14. UV/Vis spectrum of Mes-Acr+ in PhCN.
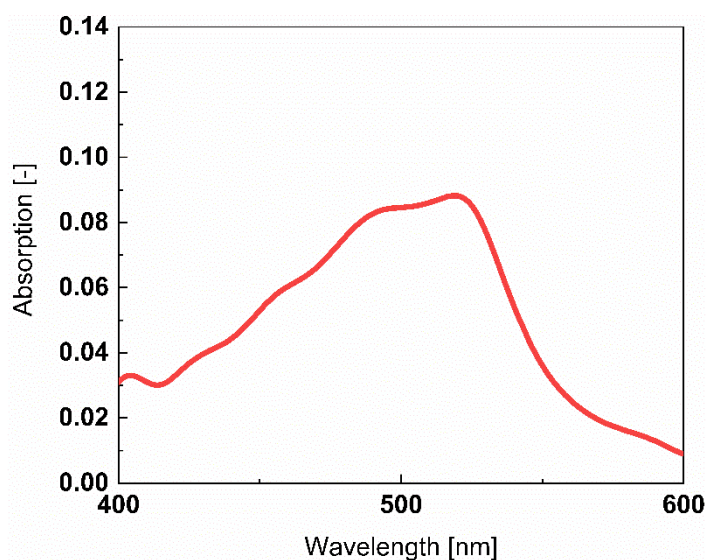
Figure 8.15. UV/Vis spectrum after addition of anisole and illumination.

Reaction kinetics

Experiments were conducted with different purities of diazonium salts and varying amounts of anisole. The flow reactor was filled with reaction mixture (0.1 M 4-methoxybenzene diazonium salt, varying mol% anisole in 1mM solution of Mes-Acr+ in MeCN) and CO in the dark. Then, the light was turned on and samples were collected at the reactor outlet for three seconds every 20 seconds. The samples were analyzed, and the amounts of starting material and product were quantified by GC-FID.
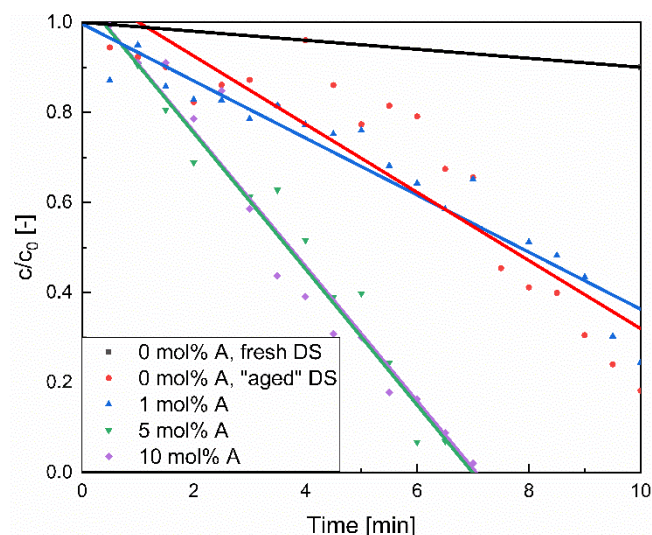
Figure 8.16. Decrease of starting material concentration under different conditions. A = anisole, DS = diazonium salt.

Light on/off experiment

The reactor was filled with reaction mixture (0.1 M 4-chlorobenzene diazonium salt, 5 mol% anisole in 1mM solution of Mes-Acr+ in MeCN) and CO in the dark. The light was turned on for four minutes. Then, a sample was collected, and the light was turned off. After three minutes the light was turned off and another sample was collected. The cycle was repeated two more times. The samples were analyzed, and the amounts of starting material and product were quantified by GC-FID.
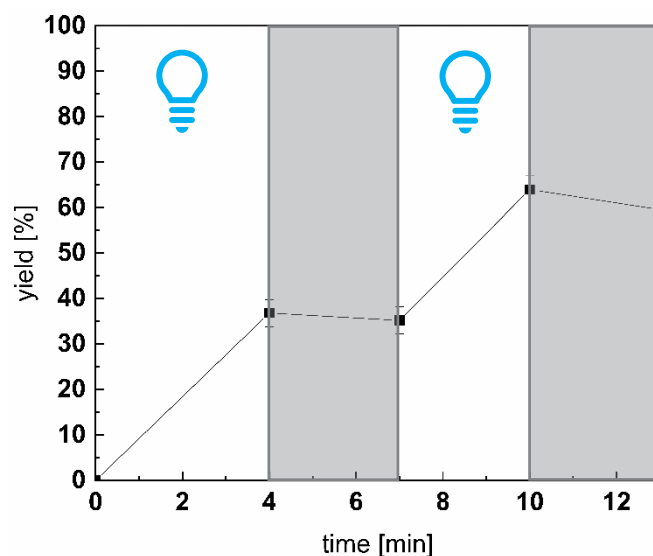
Figure 8.1. Light on/off experiment.

8.5 References

[1]   J. Bierhals, *Carbon monoxide* in: Ullmann's Encyclopedia of Industrial Chemistry, Wiley-VCH Verlag GmbH & Co. KGaA, Weinheim, **2012**.

[2]   J. B Peng. H. Q. Geng, X. F. Wu, *Chem* **2019**, *5*, 526–552.

[3]   a) H. M. Colquhoun, D. J. Thompson, M. V. Twigg *Carbonylation*, Plenum Press, New York, **1991**. b) W. Bertleff, M. Roeper, X. Sava, *Carbonylation* in: Ullmann's Encyclopedia of Industrial Chemistry, Wiley-VCH Verlag GmbH & Co. KGaA, Weinheim, **2012**. c) C. Zhu, J. Liu, M. B. Li, J. E. Bäckvall, *Chem. Soc. Rev.* **2020**, *49*, 341–353. d) A. Brennführer, H. Neumann, M. Beller, *Angew. Chem. Int. Ed.* **2009**, *48*, 4114–4133. e) *Transition Metal Catalyzed Carbonylation Reactions* (Eds. M. Beller, X. F. Wu), Springer Berlin, Heidelberg, **2013**. A recent example of Xanthphos/nickel-photoredox catalysis with alkyl iodides: f) K. El Chami, Y. Liu, M. A. Belahouane, Y. Ma, P.-L. Lagueux-Tremblay, B. A. Arndtsen, *Angew. Chem. Int. Ed.* **2023**, *62*, e202213297. DPEphos/palladium photoredox catalysis: g) Y. Liu, C. Zhou, M. Jiang, B. A. Arndtsen, *J. Am. Chem. Soc.* **2022**, *144*, 9413–9420.

[4]   a) K. Nagahara, I. Ryu, M. Komatsu, N. Sonoda, *J. Am. Chem. Soc.* **1997**, *119*, 5465–5466. b) T. Kawamoto, A. Sato, I. Ryu, *Chem. Eur. J.* **2015**, *21*, 14764–14767. c) H. Zhang, R. Shi, A. Ding, L. Lu, B. Chen, A. Lei, *Angew. Chem. Int. Ed.* **2012**, *51*, 12542–12545. d) F. Xu, D. Li, W. Han, *Green Chem.* **2019**, *21*, 2911–2915. e) Z. Yin, J. Rabeah, A. Brückner, X. F. Wu, *ACS Catal.* **2018**, *8*, 10926–10930. f) F. Jin, Y. Zhong, X. Zhang, H. Zhang, Q. Zhao, W. Han, *Green Chem.* **2016**, *18*, 2598–2603.

[5]   V. Botla, A. Voronov, E. Motti, C. Carfagna, R. Mancuso, B. Gabriele, N. Della Ca', *Catalysts* **2021**, *11*, 918, DOI 10.3390/catal11080918.

[6]   J. Singh, S. Sharma, A. Sharma, *J. Org. Chem.* **2021**, *86*, 24–48.

[7]   M. Majek, A. Jacobi von Wangelin, *Angew. Chem. Int. Ed.* **2015**, *54*, 2270–2274.

[8]   W. Guo, L. Q. Lu, Y. Wang, Y. N. Wang, J. R. Chen, W. J. Xiao, *Angew. Chem. Int. Ed.* **2015**, *54*, 2265–2269.

[9]   L. Gu, C. Jin, J. Liu, *Green Chem* **2015**, *17*, 3733–3736.

[10]   A. Cartier, E. Levernier, V. Corcé, T. Fukuyama, A. L. Dhimane, C. Ollivier, I. Ryu, L. Fensterbank, *Angew. Chem. Int. Ed.* **2019**, *58*, 1789–1793.

[11]   Y. Wang, H. Yang, Y. Zheng, M. Hu, J. Zhu, Z.-P. Bao, Y. Zhao, X,-F. Wu, *Nat. Catal* **2024**, DOI 10.1038/s41929-024-01204-6.

[12]   X. Li, D. Liang, W. Huang, H. Zhou, Z. Li, B. Wang, Y. Ma, H. Wang, *Tetrahedron* **2016**, *72*, 8442–8448.

[13]   A. Cartier, E. Levernier, A. L. Dhimane, T. Fukuyama, C. Ollivier, I. Ryu, L. Fensterbank, *Adv. Synth. Catal.* **2020**, *362*, 2254–2259.

[14]   Z. Qi, L. Li, Y. K. Liang, A. J. Ma, X. Z. Zhang, J. B. Peng, *Org. Lett.* **2021**, *23*, 4769–4773.

[15]   F. Mo, D. Qiu, L. Zhang, J. Wang, *Chem. Rev.* **2021**, *121*, 5741–5829.

[16]   A. Roglans, A. Pla-Quintana, M. Moreno-Mañas, *Chem. Rev.* **2006**, *106*, 4622–4643.

[17]   J. D. Firth, I. J. S. Fairlamb, *Org. Lett.* **2020**, *22*, 7057–7059.

[18]   T. Fukuyama, T. Totoki, I. Ryu, *Green Chem.* **2014**, *16*, 2042–2050.

[19]   J. Schachtner, P. Bayer, A. Jacobi von Wangelin, *Beilstein J. Org. Chem.* **2016**, *12*, 1798–1811.

[20]   R. Stuhr, P. Bayer, C. B. W. Stark, A. Jacobi von Wangelin, *ChemSusChem* **2021**, *14*, 3325–3332.

[21]   P. Bayer, J. Schachtner, M. Májek, A. Jacobi von Wangelin, *Org. Chem. Front*. **2019**, *6*, 2877–2883.

[22]   M. Majek, F. Filace, A. Jacobi von Wangelin, *Beilstein J. Org. Chem*. **2014**, *10*, 981–989.

[23]   S. Fukuzumi, H. Kotani, K. Ohkubo, S. Ogo, N. V. Tkachenko, H. Lemmetyinen, *J. Am. Chem. Soc*. **2004**, *126*, 1600–1601.

[24]   K. Ohkubo, K. Mizushima, R. Iwata, K. Souma, N. Suzuki, S. Fukuzumi, *Chem. Commun.* **2010**, *46*, 601–603.

[25]   P. P. Singh, J. Singh, V. Srivastava, *RSC Adv.* **2023**, *13*, 10958–10986.

[26]   A. Tlili, S. Lakhdar, *Angew. Chem. Int. Ed*. **2021**, *60*, 19526–19549.

[27]   C. Gosset, S. Pellegrini, R. Jooris, T. Bousquet, L. Pelinski, *Adv. Synth. Catal*. **2018**, *360*, 3401–3405.

[28]   J. W. Beatty, C. R. J. Stephenson, *Acc. Chem. Res.* **2015,** *48*, 1474–1484.

[29]   a) M. Balci, *Synthesis* **2018**, 50, 1373–1401; b) E. H. White, H. Scherrer, *Tetrahedron Lett.* **1961**, *2*, 758–762; c) K. Vaughan, M. T. H. Liu, *Can. J. Chem.* **1981**, *59*, 923–926.

[30]   S. Hünig, R. Schaller, *Angew. Chem. Int. Ed*. **1982**, *21*, 36–49.

[31]   J. S. Quesnel, B. A. Arndtsen, *J. Am. Chem. Soc*. **2013**, *135*, 16841–16844.

[32]   G. M. Torres, Y. Liu, B. A. Arndtsen, *Science* **2020**, *368*, 318–323.

[33]   *The chemistry of acyl halides* (Ed. S. Patai), John Wiley & Sons, London, **1972**.

[34]   J. Buchspies, M. Szostak, *Catalysts* **2019**, *53*, DOI 10.3390/catal9010053.

[35]   T. Itahara, S. Furukawa, K. Kubota, M. Morimoto, M. Sunose, *Liq. Cryst.* **2013**, *40*, 589–598.

[36]   M. Ditzen, M. Pellegrino, L. B. Vosshall, *Science* **2008**, *319*, 1838–1842.

[37]   Y. Y. See, M. S. Sanford, *Org. Lett*. **2020**, *22,* 2931–2934.

[38]   T. Tsudaka, H. Kotani, K. Ohkubo, T. Nakagawa, N. V. Tkachenko, H. Lemmetyinen, S. Fukuzumi, *Chem. Eur. J.* **2017**, *23*, 1306–1317.

[39]   A. C. Benniston, A. Harriman, P. Li, J. P. Rostron, J. W. Verhoeven, *Chem. Commun.* **2005**, 2701–2703.

[40]   K. Ohkubo, H. Kotani, S. Fukuzumi, *Chem. Commun*. **2005**, 4520–4522.

[41]   a) N. E. S. Tay, D. A. Nicewicz, *J. Am. Chem. Soc.* **2017**, *139*, 16100–16104. b) K. Margrey, A. Levens, D. A. Nicewicz, *Angew. Chem. Int. Ed.* **2017**, *56*, 15644–15648. c) J. B. McManus, D. A. Nicewicz, *J. Am. Chem. Soc.* **2017**, *139*, 2880–2883.

[42]   a) *Fundamentals and Applications of Organic Electrochemistry* (Eds. T. Fuchigami, S. Inagi, M. Atobe), Wiley, Chichester, **2015**. b) Y. Shiraishi, N. Saito, T. Hirai, *J. Am. Chem. Soc.* **2005**, *127*, 8304–8306. c) X. Cai, M. Sakamoto, M. Fujitsuka, T. Majima, *J. Phys. Chem. A* **2007**, *111*, 1788–1791.

[43]   H. Xu, C. Zhao, Q. Qian, W. Deng, H. Gong, *Chem. Sci.* **2013**, *4*, 4022–4029.

[44]   Z.-S. Chen, X.-H. Duan, P.-X. Zhou, S. Ali, J.-Y. Luo, Y.-M. Liang, *Angew. Chem. Int. Ed.* **2012**, *51*, 1370–1374.

[45]   Y. Bourne-Branchu, C. Gosmini, G. Danoun, *Chem. Eur. J.* **2017**, *23*, 10043–10047.

[46]   C. M. Nicklaus, P. H. Phua, T. Buntara, S. Noel, H. J. Heeres, J. G. de Vries, *Adv. Synth. Cat.* **2013**, *355*, 2839–2844.

[47]   U. B. Patil, A. S. Singh, J. M. Nagarkar, *RSC Adv.* **2014**, *4*, 1102–1106.

[48]   L. Wang, H. Neumann, A. Spannenberg, M. Beller, *Chem. Commun.* **2017**, *53*, 7469–7472.

[49]   T. Zweifel, J.-V. Naubron, H. Grützmacher, *Angew. Chem. Int. Ed.* **2009**, *48*, 559–562.

[50]   Y. Li, D. Xue, C. Wang, Z.-T. Liu, J. Xiao, *Chem. Commun.* **2012**, *48*, 1320–1322.

[51]   T. T. Dang, Y. Zhu, S. C. Ghosh, A. Chen. C. L. L. Chai, A. M. Seayad, *Chem. Commun.* **2012**, *48*, 1805–1807.

[52]   J. R. Martinelli, T. P. Clark, D. A. Watson, R. H. Munday, S. L. Buchwald, *Angew. Chem. Int. Ed.* **2007**, *46*, 8460–8463.

[53]   Y. Iyori, K. Takahashi, K. Yamazaki, Y. Ano, N. Chatani, *Chem. Commun.* **2019**, *55*, 13610–13613.

[54]   I. N. C. Kiran, K. Lalwani, A. Sudalai, *RSC Adv.* **2013**, *3*, 1695–1698.

[55]   V. Barton, S. A. Ward, J. Chadwick, A. Hill, P. M. O´Neill, *J. Med. Chem.* **2010**, *53*, 4555–4559.

[56]   D. W. Tan, H. X. Li, M. J. Zhang, J. L. Yao, J. P. Lang, *ChemCatChem* **2017**, *9*, 113–118.

[57]   C. Liu, J. Wang, L. Meng, Y. Deng, Y. Li, A. Lei, *Angew. Chem. Int. Ed.* **2011**, *50*, 5144–5148.

[58]   S. Ushijima, K. Moriyama, H. Togo, *Tetrahedron* **2012**, *68*, 4701–4709.

[59]   H. Aman, Y.H. Wang, G. J. Chuang, *ACS Omega* **2020**, *5*, 918–925.

[60]   H. Zou, L. Zhou, Y. Li, Y. Cui, H. Zhong, Z. Pan, Z. Yang, J. Quan, *J. Med. Chem.* **2010**, *53*, 994–1003.

[61]   Y. Wang, Q. Kang, *Org. Lett.* **2014**, *16*, 4190–4193.

[62]   E. Block, A. J. Yencha, M. Aslam, V. Eswarakrishnan, J. Luo, A. Sano, *J. Am. Chem. Soc.* **1988**, *110*, 4748–4753.

[63]   AIST: Spectral Database for Organic Compounds SDBS; NMR spectra; SDBS No.: 2865; CAS RN: 122-01-0, https://sdbs.db.aist.go.jp (accessed **April 22, 2024**).

[64]   AIST: Spectral Database for Organic Compounds SDBS; NMR spectra; SDBS No.: 6101; CAS RN: 100-07-2, https://sdbs.db.aist.go.jp (accessed **April 22, 2024**).

[65]   AIST: Spectral Database for Organic Compounds SDBS; NMR spectra; SDBS No.: 1876; CAS RN: 874-60-2, https://sdbs.db.aist.go.jp (accessed **April 22, 2024**).

[66]   J. A. Greenberg, T. Sammakia, *J. Org. Chem.* **2017**, 82, 3245–3251.

[67]   AIST: Spectral Database for Organic Compounds SDBS; NMR spectra; SDBS No.: 6100; CAS RN: 21615-34-9, https://sdbs.db.aist.go.jp (accessed **April 22, 2024**).

[68]   AIST: Spectral Database for Organic Compounds SDBS; NMR spectra; SDBS No.: 5579; CAS RN: 1711-09-7, https://sdbs.db.aist.go.jp (accessed **April 22, 2024**).

[69]   a) J. A. Birrell, J.-N. Desroisiers, E. N. Jacobsen, *J. Am. Chem. Soc.* **2011**, *133*, 13872–13875. b) Z. Wang, X. Wang, Y. Nishihara, *Chem. Commun.* **2018**, *54*, 13969–13972.

[70]   C. Duplais, F. Bures, I. Sapountzis, T. J. Korn, G. Cahiez, P. Knochel, *Angew. Chem. Int. Ed.* **2004**, *43*, 2968–2970.

[71]   F. M. Miloserdov, V. V. Grushin, *Angew. Chem. Int. Ed.* **2012**, *51*, 3668–3672.

[72]   K. S. Goh, C.-H. Tan, *RSC Adv.* **2012**, *2*, 5536–5538.

[73]   M. Cortigiani, A. Mereu, M. G. Healy, M. F. A. Adamo, *J. Org. Chem.* **2019**, *84*, 4112–4119.

[74]   T. Ohshima, Y. Hayashi, K. Agura, Y. Fuji, A. Yoshiyama, K. Mashima, *Chem. Commun.* **2012**, *48*, 5434–5436.

[75]   W. Li, R. Wang, Z. Li, J. Chen, Y. Zhang, N. Lu, *Chem. Commun.* **2023**, *59*, 4360–4363.

[76]   J. Davies, S. G. Booth, S. Essafi, R. A. W. Dryfe, D. Leonori, *Angew. Chem. Int. Ed.* **2015**, *54*, 14017–14021.

[77]   C. Liu, M. Szostak, *Chem. Commun*. **2018**, *54*, 2130–2133.

[78]   R.Kawahara, K. Fujita, R. Yamaguchi, *Angew. Chem. Int. Ed.* **2012**, *51*, 12790–12794.

[79]   B. Tan, N. Toda, C. F. Barbas III, *Angew. Chem. Int. Ed.* **2012**, *51*, 12538–12541.

[80]   W. Wei, C. Zhang, Y. Xu, X. Wan, *Chem. Commun.* **2011**, *47*, 10827–10829.

[81]   K. P. Jang, G. E. Hutson, R. C. Johnston, E. O. McCusker, P. H.-Y. Cheong, K. A. Scheidt, *J. Am. Chem. Soc.* **2014**, *136*, 76–79.

[82]   Z. Hu, X.-J. Wei, J. Handelmann, A.-K. Seitz, I. Rodstein, V. H. Gessner, L. J. Gooßen, *Angew. Chem. Int. Ed.* **2021**, *60*, 6778–6783.

[83]   L. Cardinale, M. Neumeier, M. Majek, A. Jacobi von Wangelin, *Org. Lett.* **2020**, *22*, 7219–7224.

[84]   P. Klán, J. Wirtz, *Photochemistry of Organic Compounds*, John Wiley and Sons, Chichester, **2009**.

[85]   M. A. R. Scandola, F. Scandola, A. Indelli, *J. Chem. Soc., Faraday Trans*. **1985**, *81*, 2967–2974.

[86]   J. T. Carstensen, *J. Pharm. Sci.* **1970**, *59*, 1140–1143.

8.6 Experimental Spectra
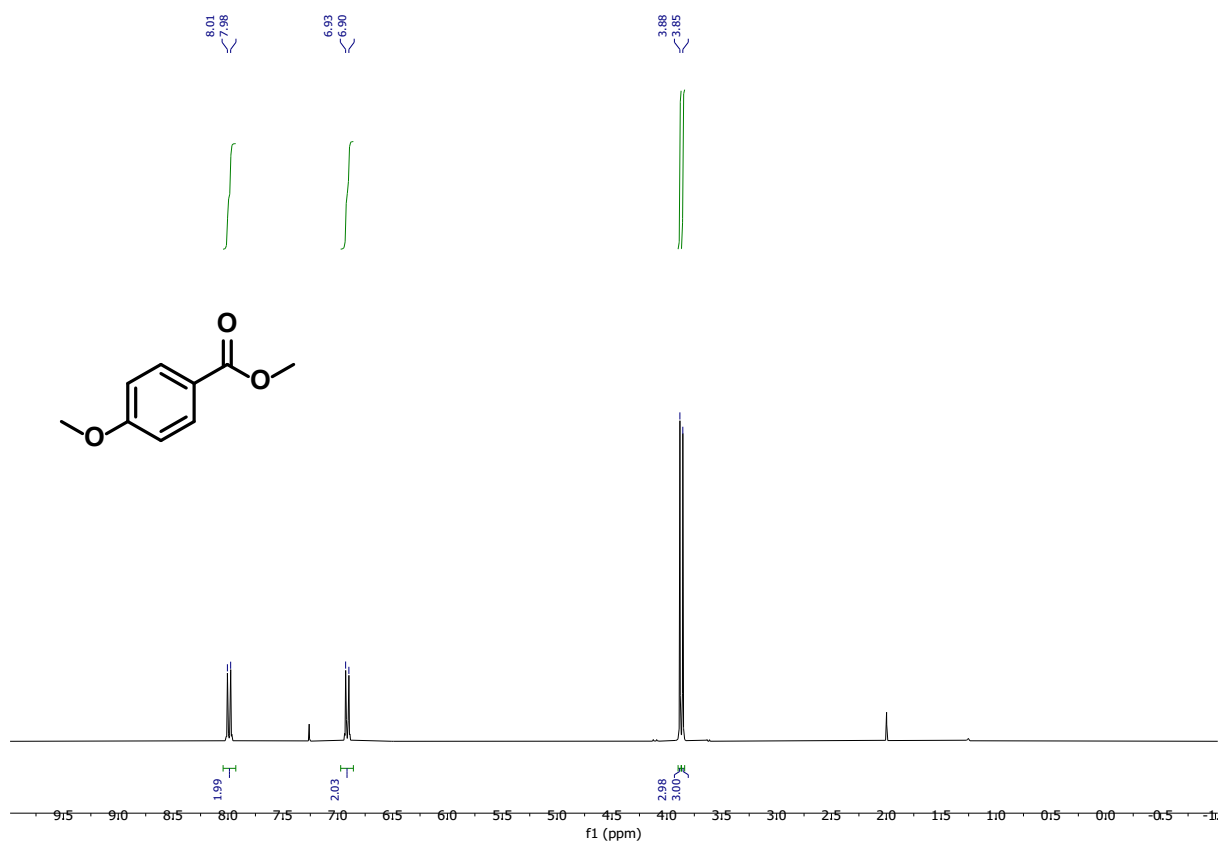
^{1}H NMR (300 MHz, CDCl$_3$) of Methyl 4-methoxybenzoate (2aa).
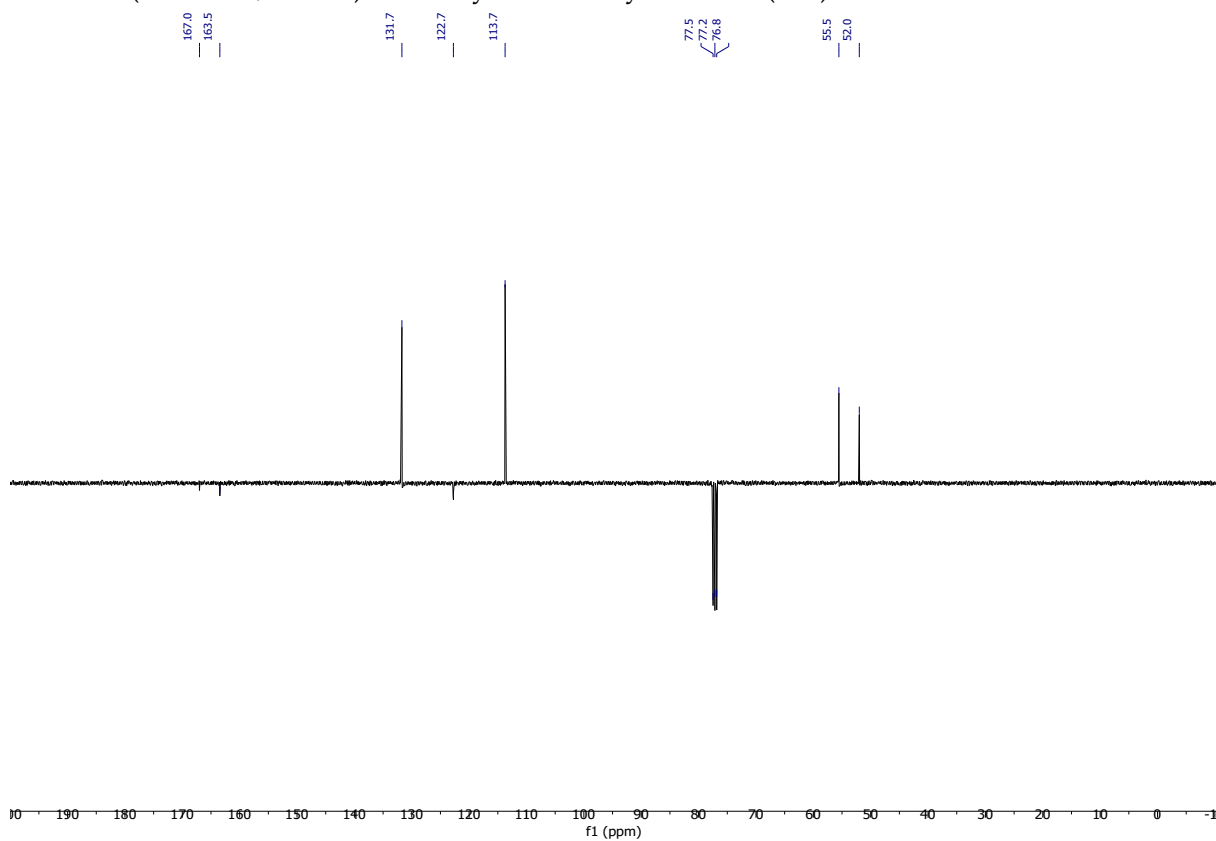
^{13}C NMR (75 MHz, CDCl$_3$) of Methyl 4-methoxybenzoate.
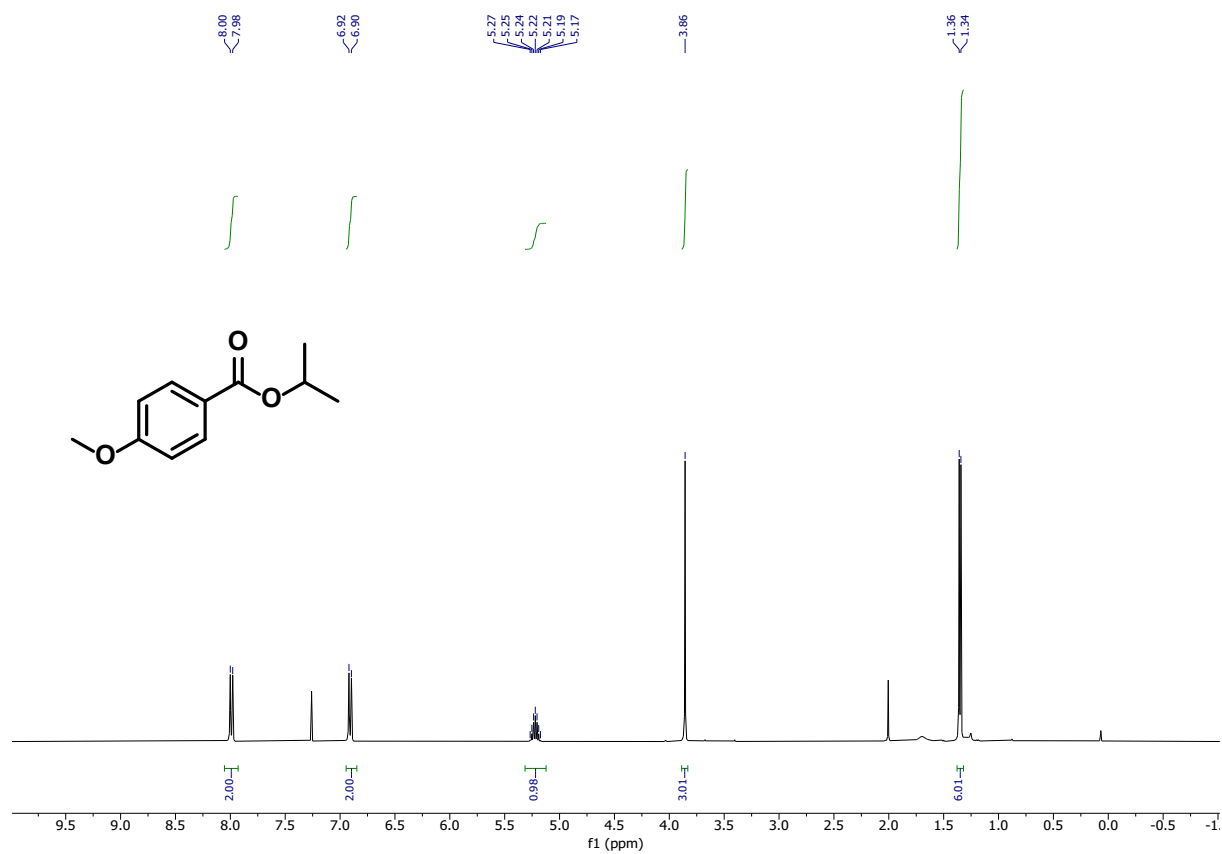
^{1}H NMR (300 MHz, CDCl$_3$) of Isopropyl 4-methoxybenzoate (2ab).

^{13}C NMR (75 MHz, CDCl$_3$) of Isopropyl 4-methoxybenzoate.

^{1}H NMR (300 MHz, CDCl₃) of *tert* Butyl 4-methoxybenzoate (2ac).
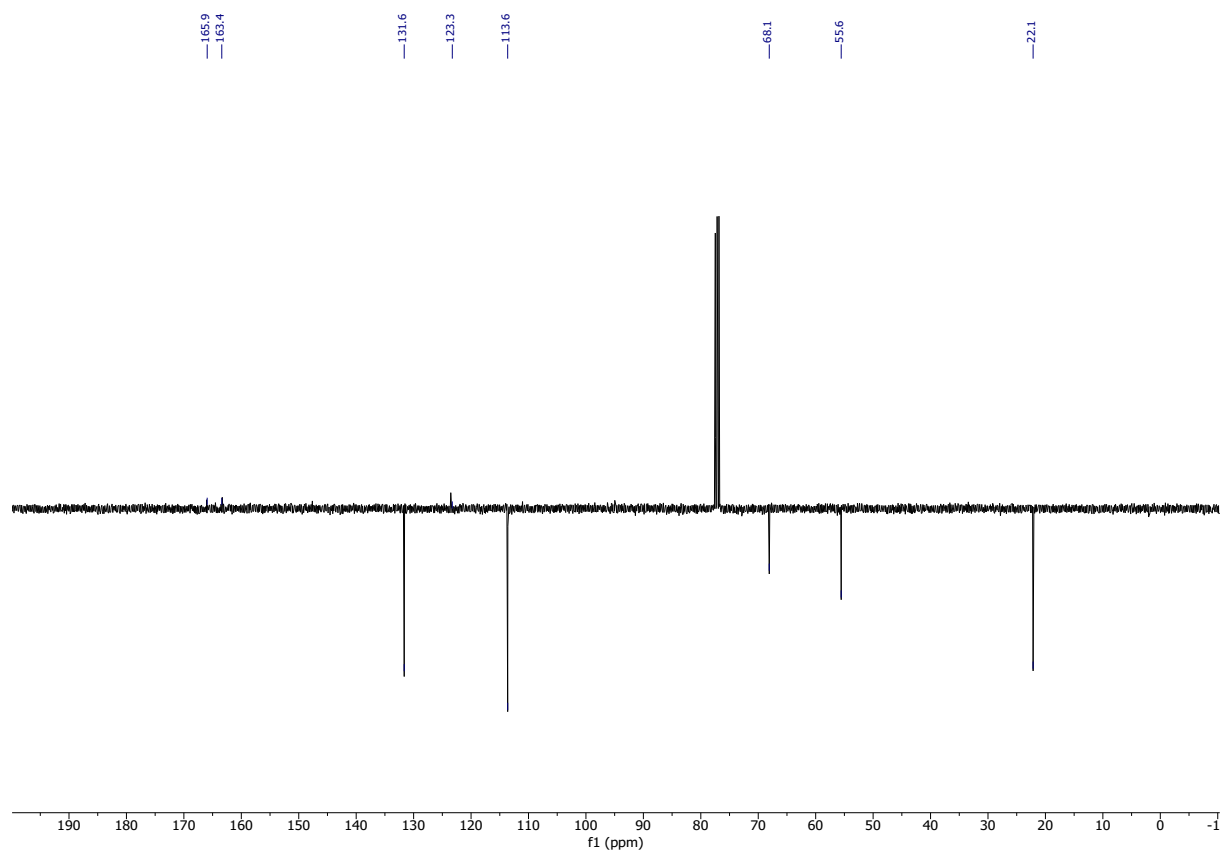
^{13}C NMR (75 MHz, CDCl₃) of *tert* Butyl 4-methoxybenzoate.
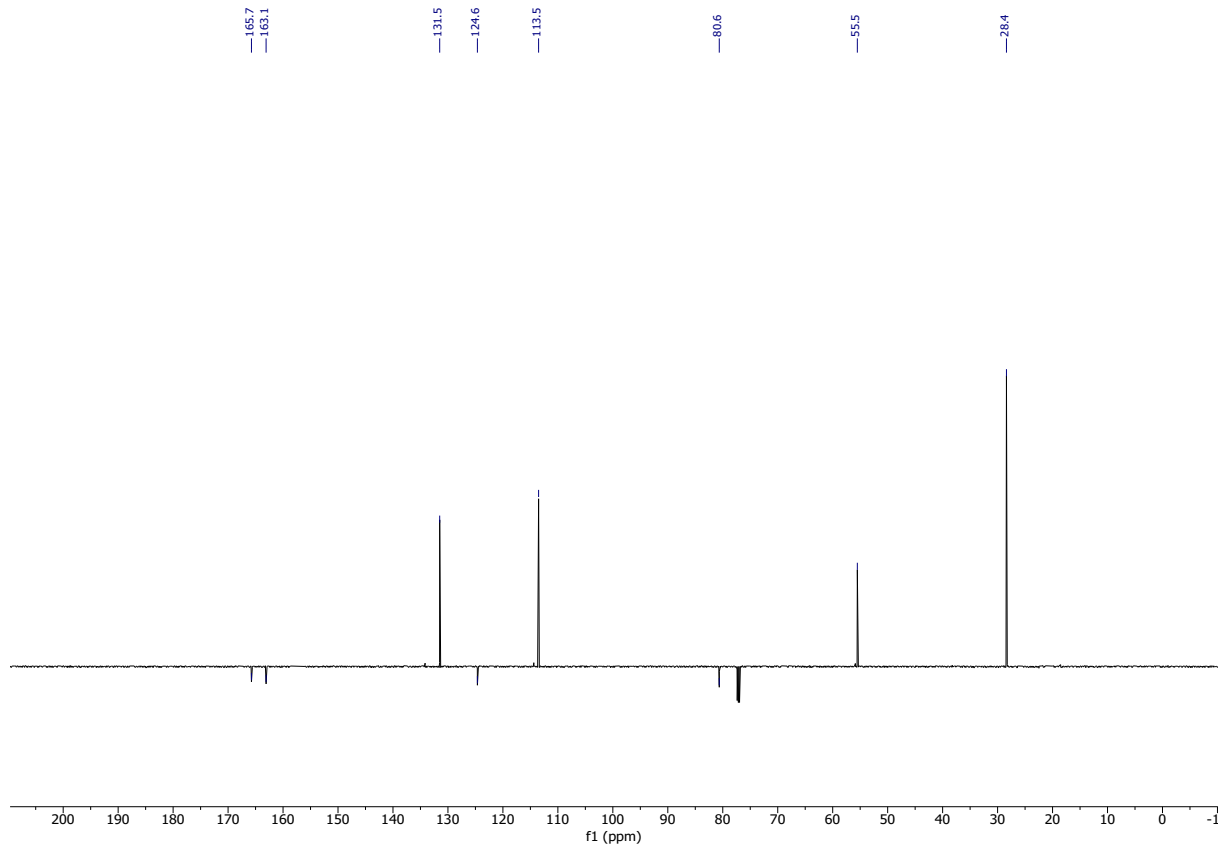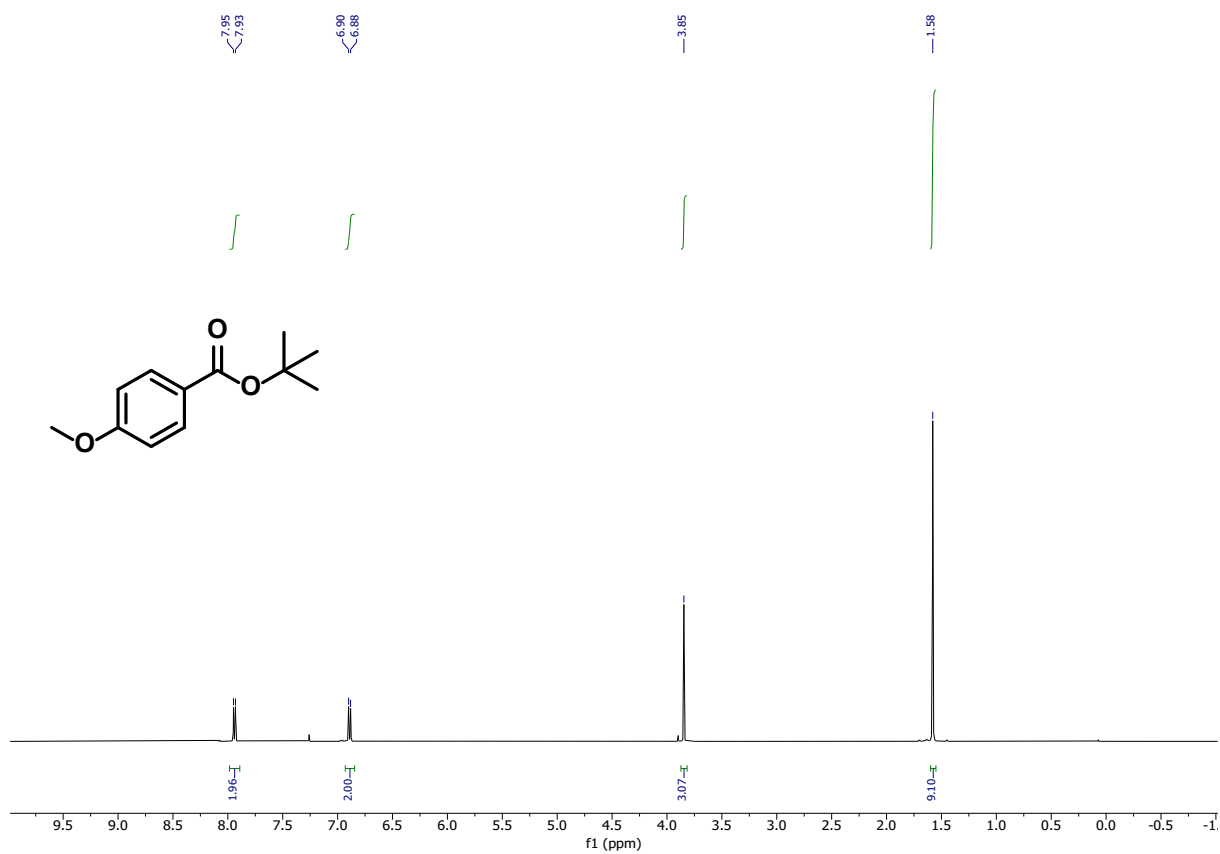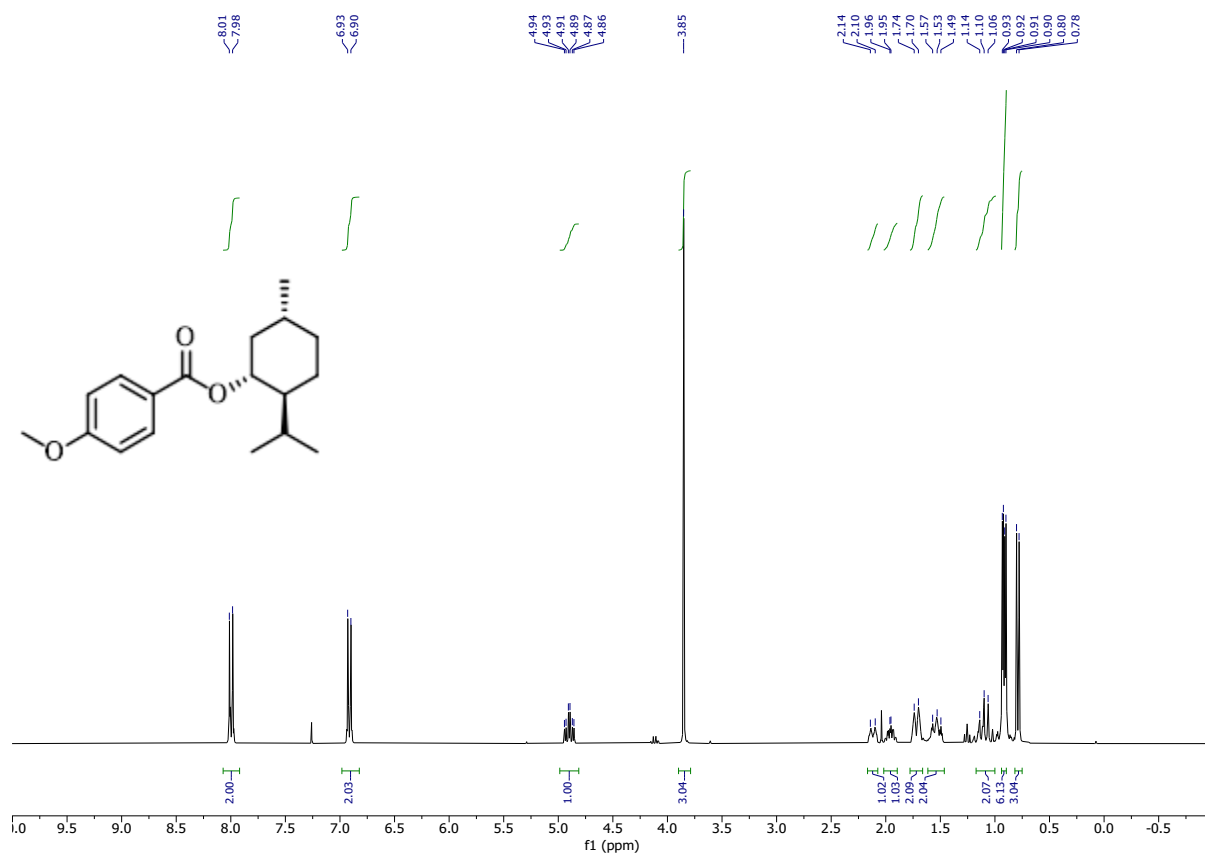
^{1}H NMR (300 MHz, CDCl$_3$) of Menthyl 4-methoxybenzoate (2ad).
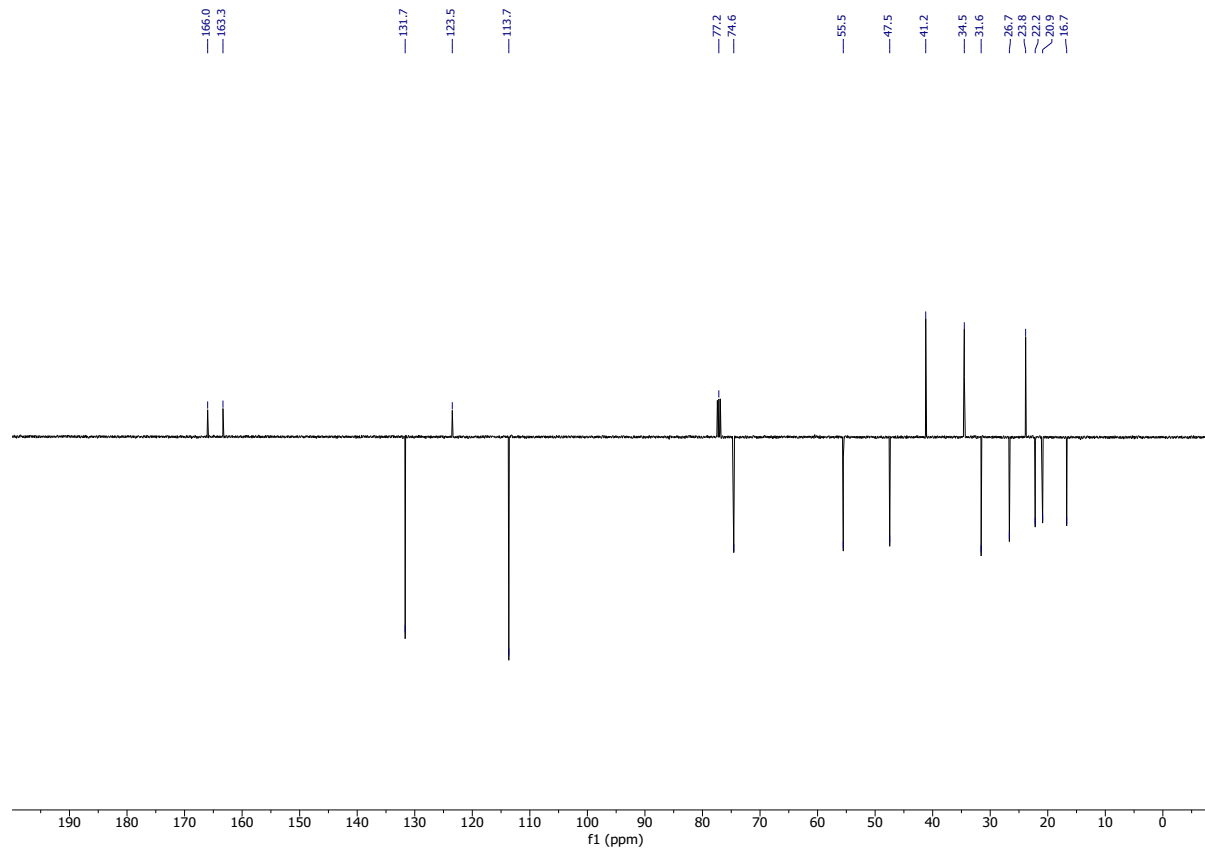
^{13}C NMR (75 MHz, CDCl$_3$) of Menthyl 4-methoxybenzoate.
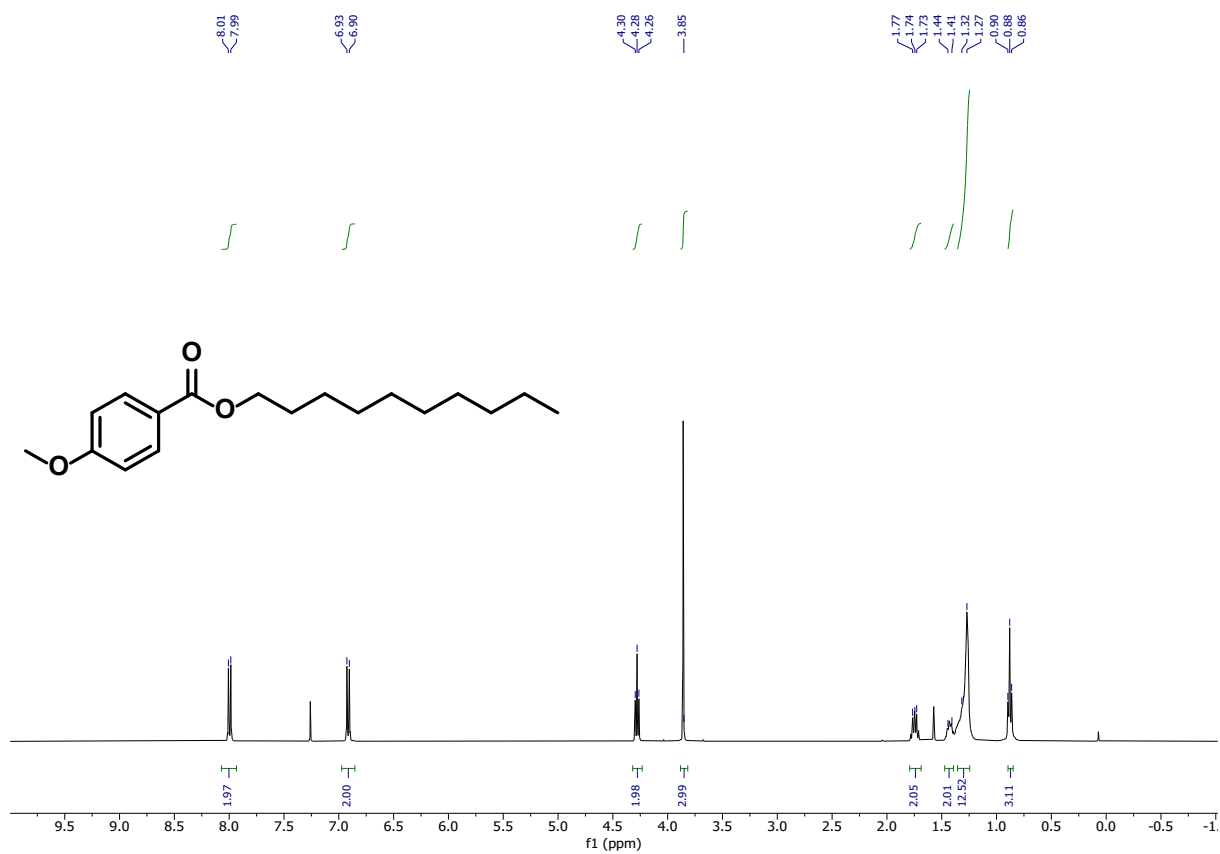
^{1}H NMR (300 MHz, CDCl₃) of Decyl 4-methoxybenzoate (2ae).
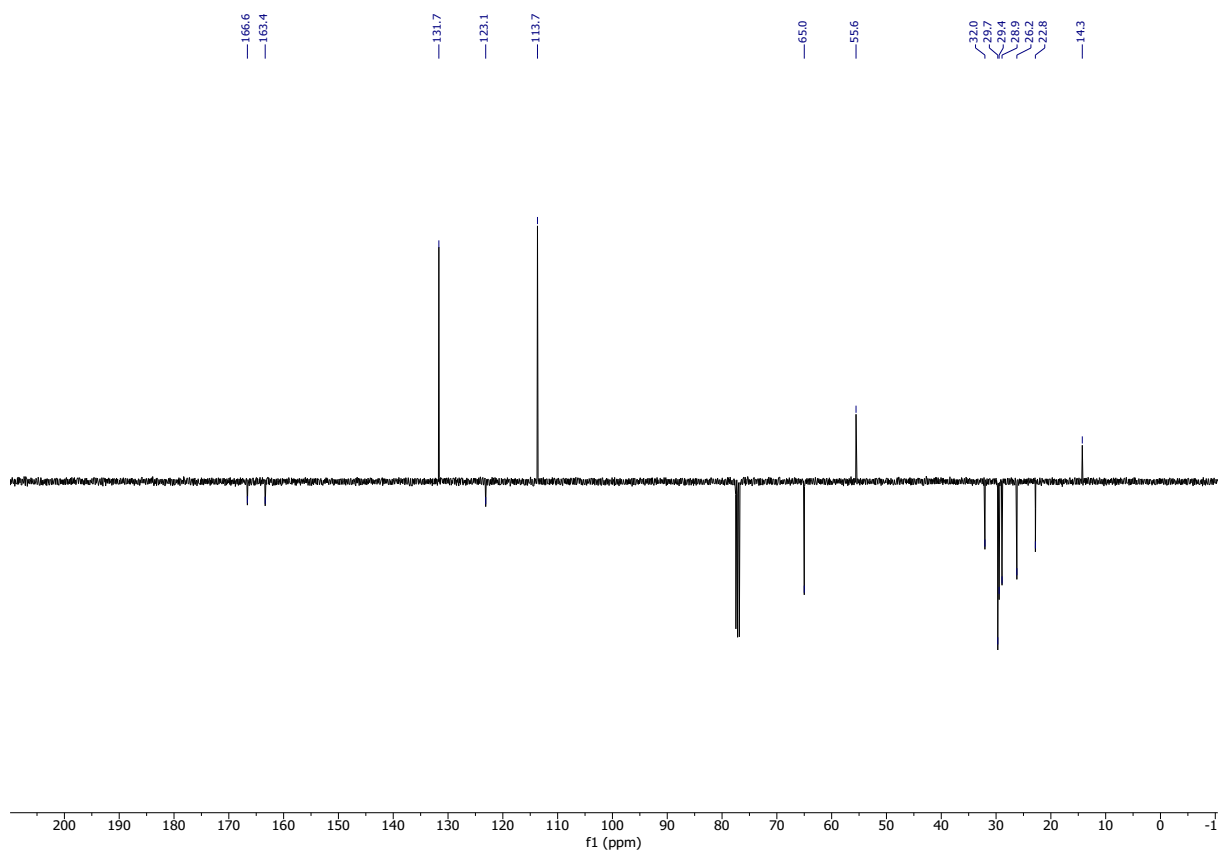
^{13}C NMR (75 MHz, CDCl₃) of Decyl 4-methoxybenzoate.
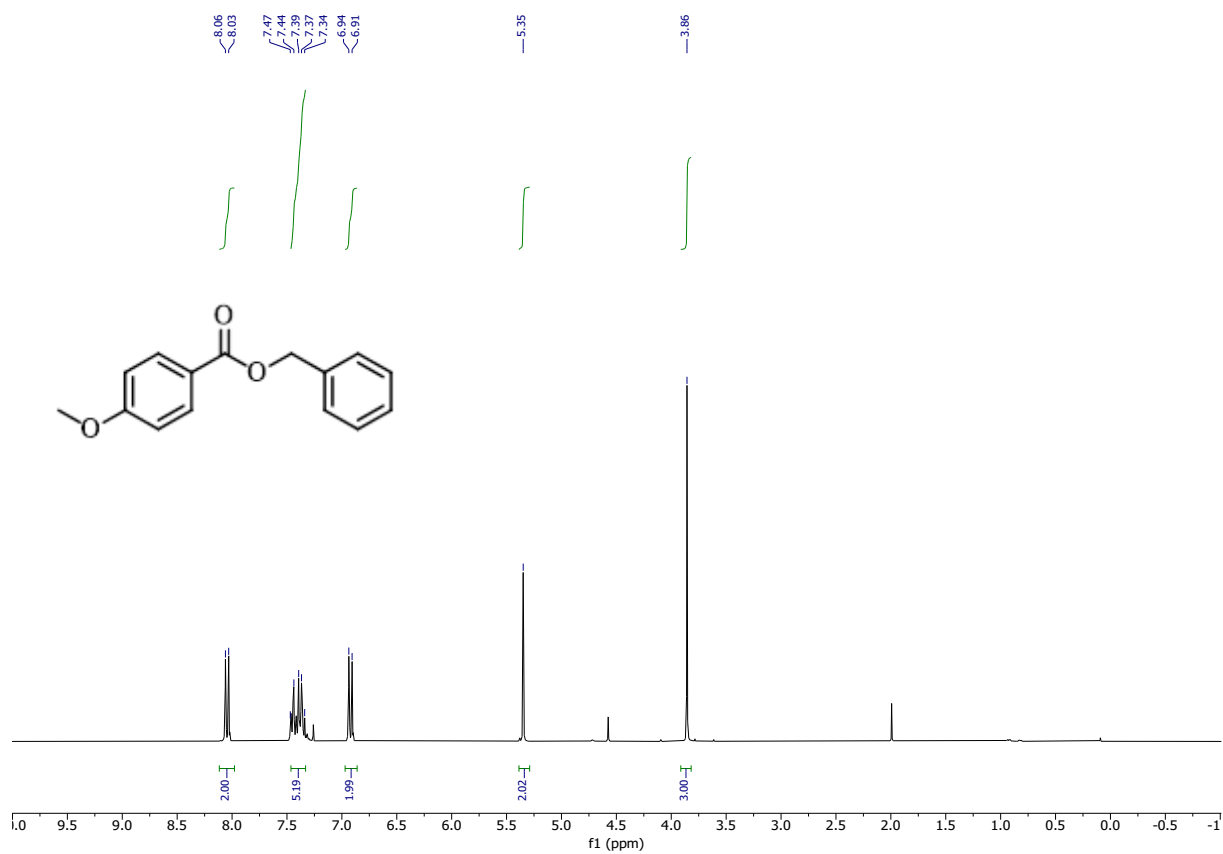
^{1}H NMR (300 MHz, CDCl$_3$) of Benzyl 4-methoxybenzoate (2af).
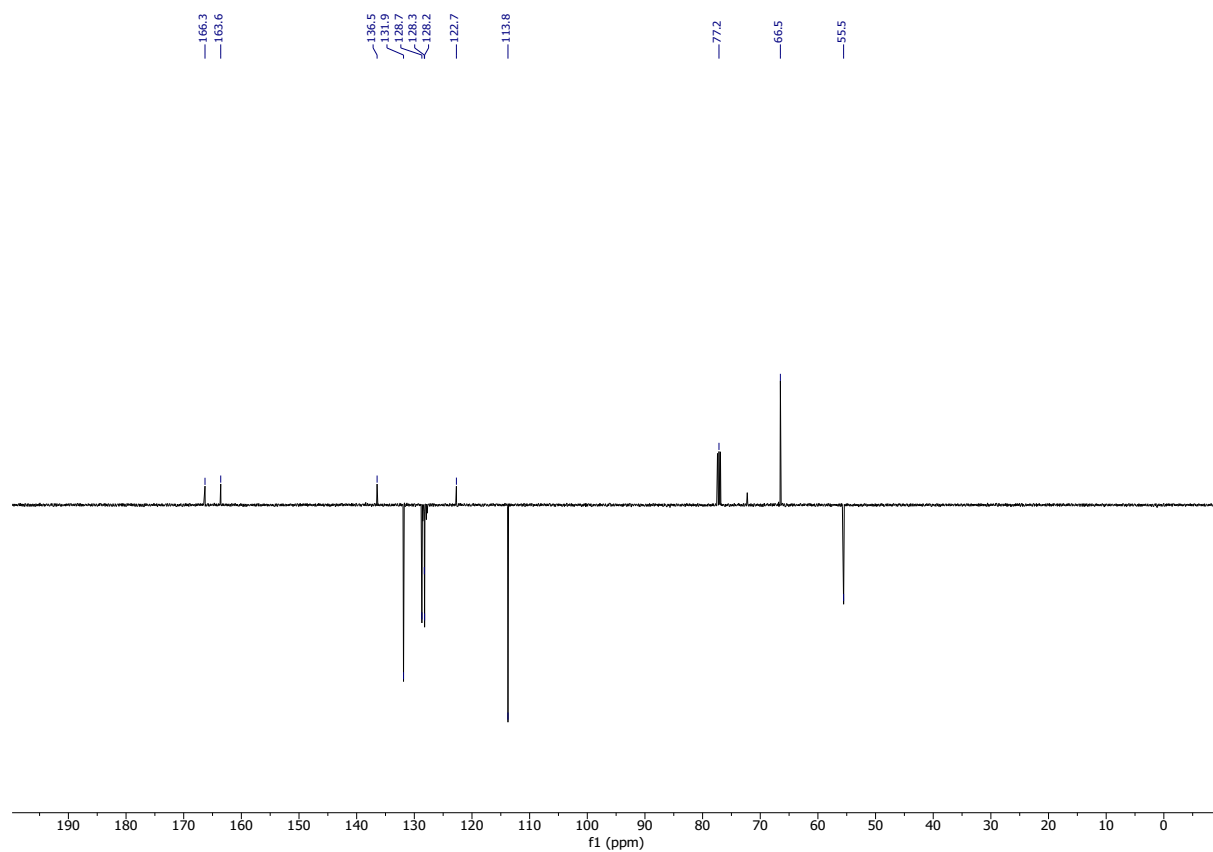
^{13}C NMR (75 MHz, CDCl$_3$) of Benzyl 4-methoxybenzoate.
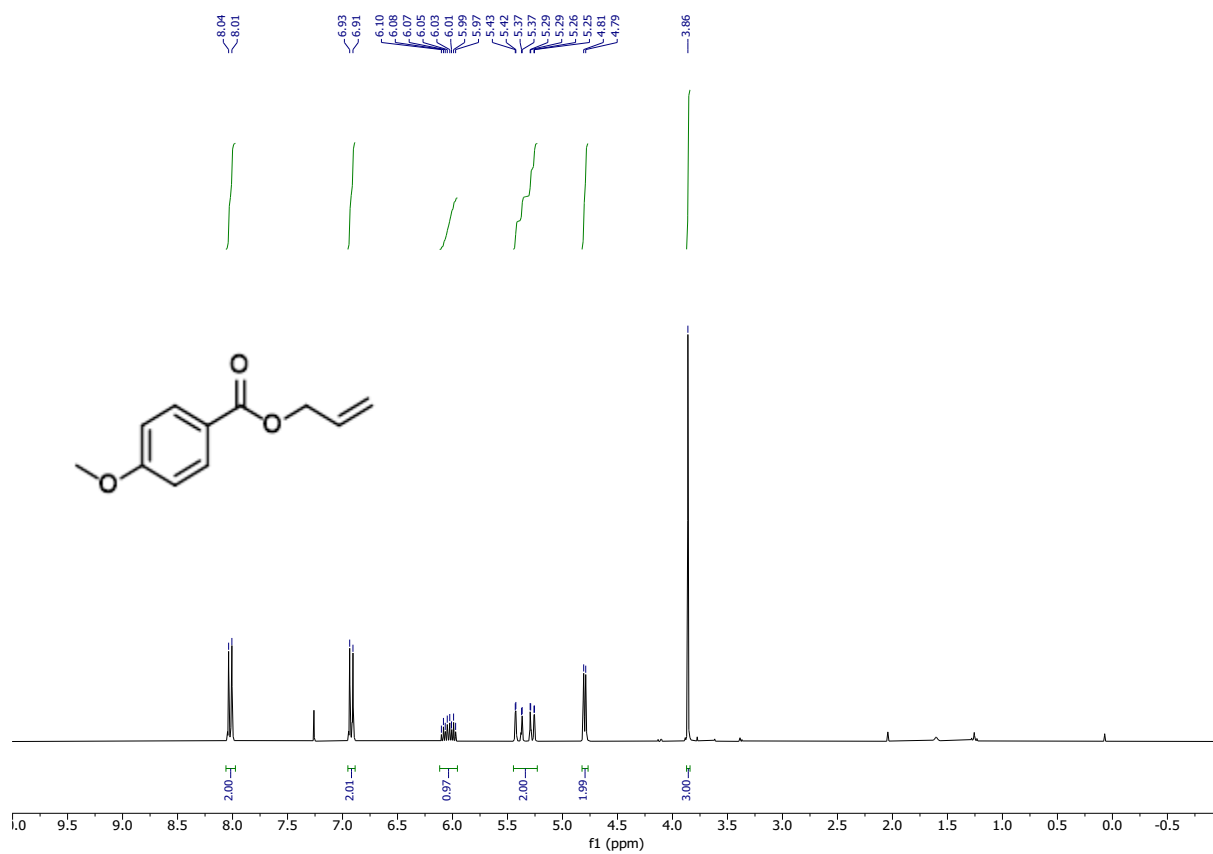
^{1}H NMR (300 MHz, CDCl$_3$) of Allyl 4-methoxybenzoate (2ag).

^{13}C NMR (75 MHz, CDCl$_3$) of Allyl 4-methoxybenzoate.

210
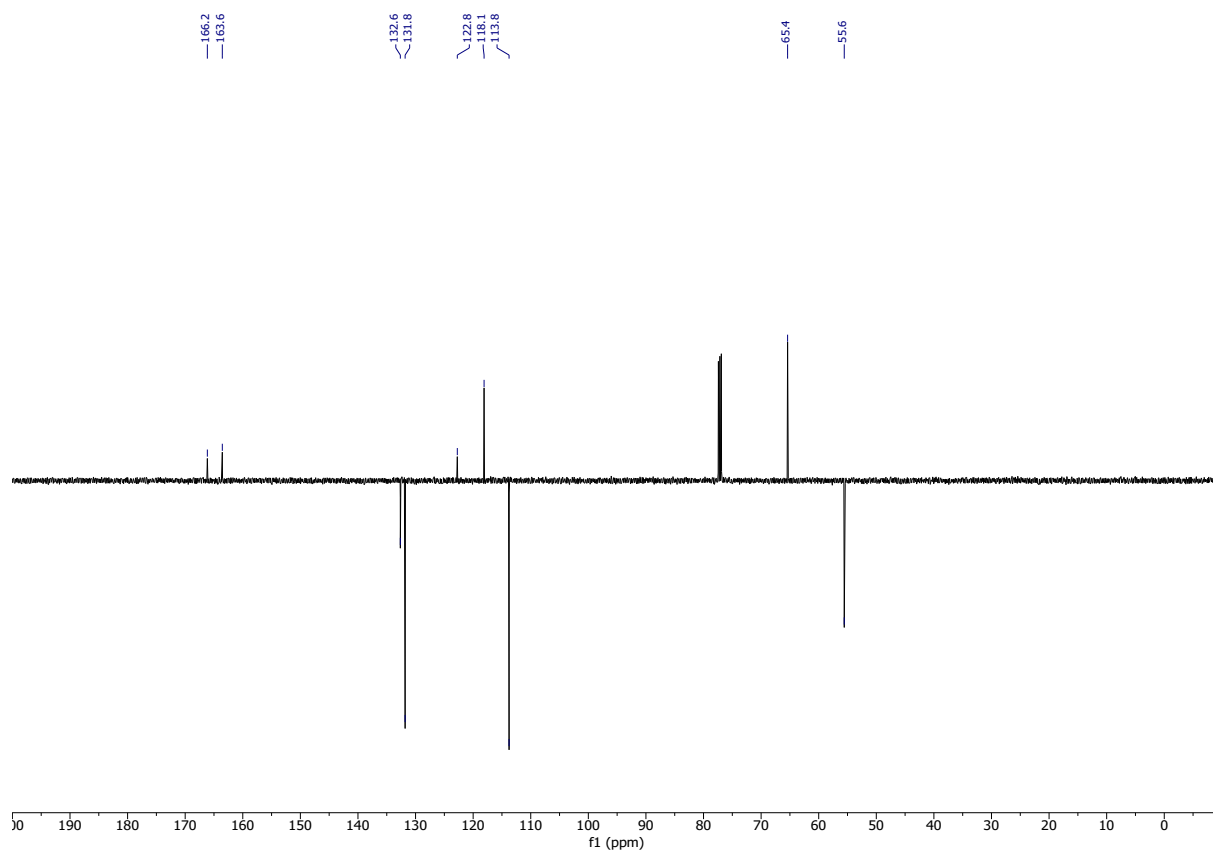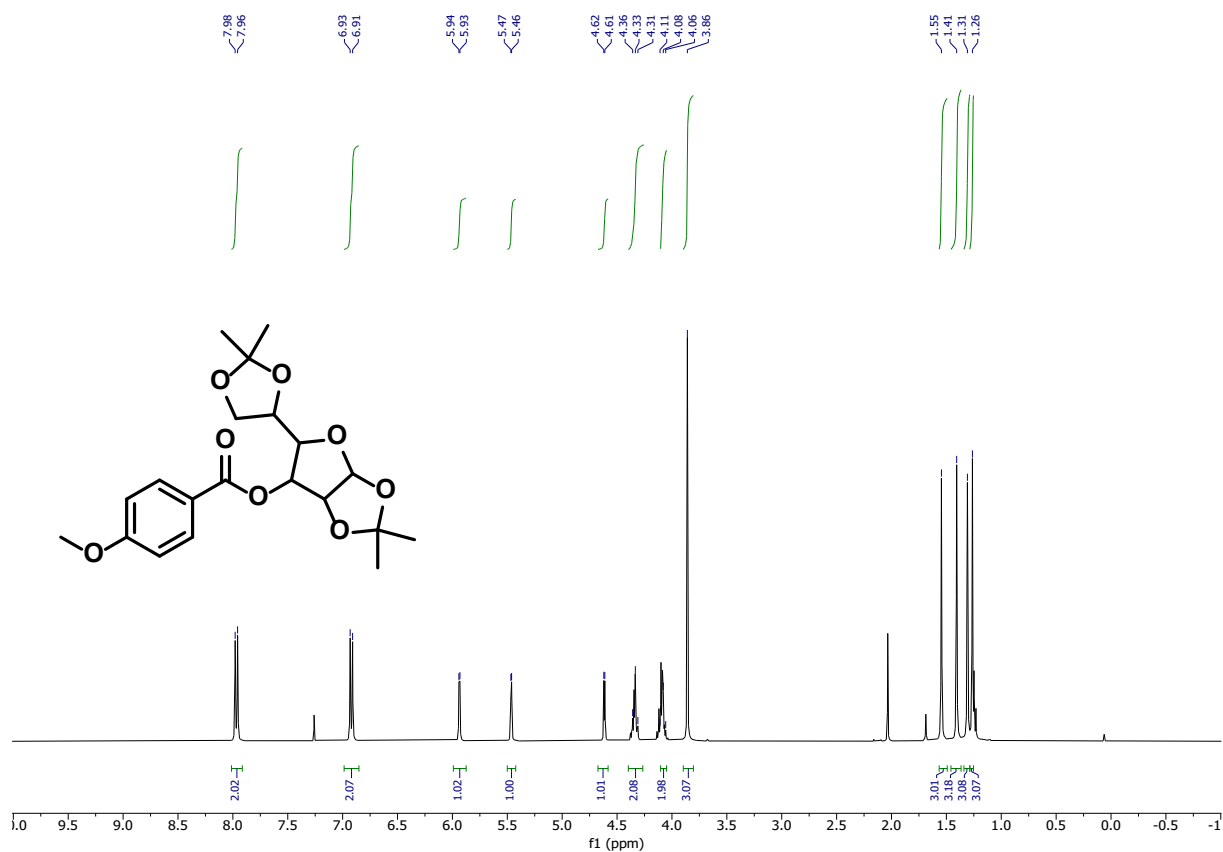
¹H NMR (300 MHz, CDCl₃) of 3-(4-methoxybenzoate)-1,2:5,6-Di-*O*-isopropyliden-*α*-D-glucofuranose (2ah).
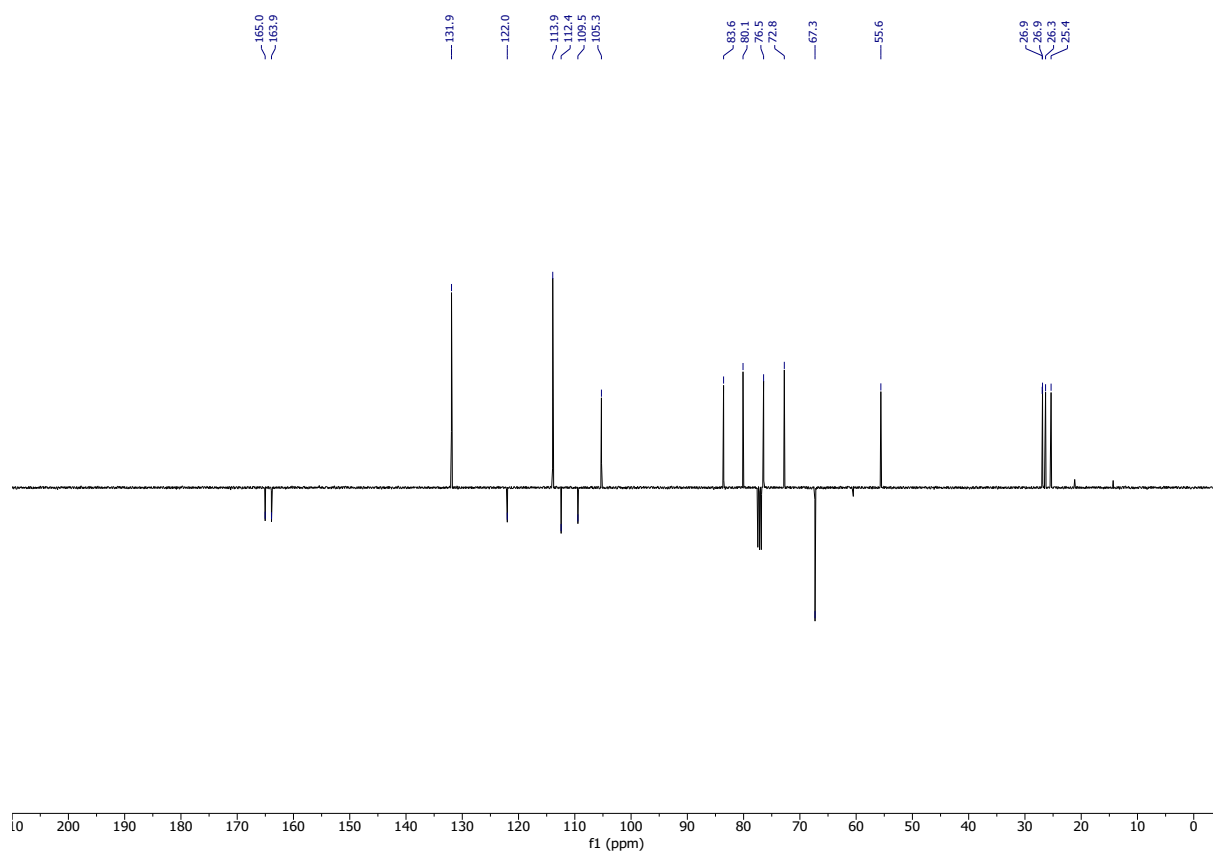
¹³C NMR (75 MHz, CDCl₃) of 2ah.

211
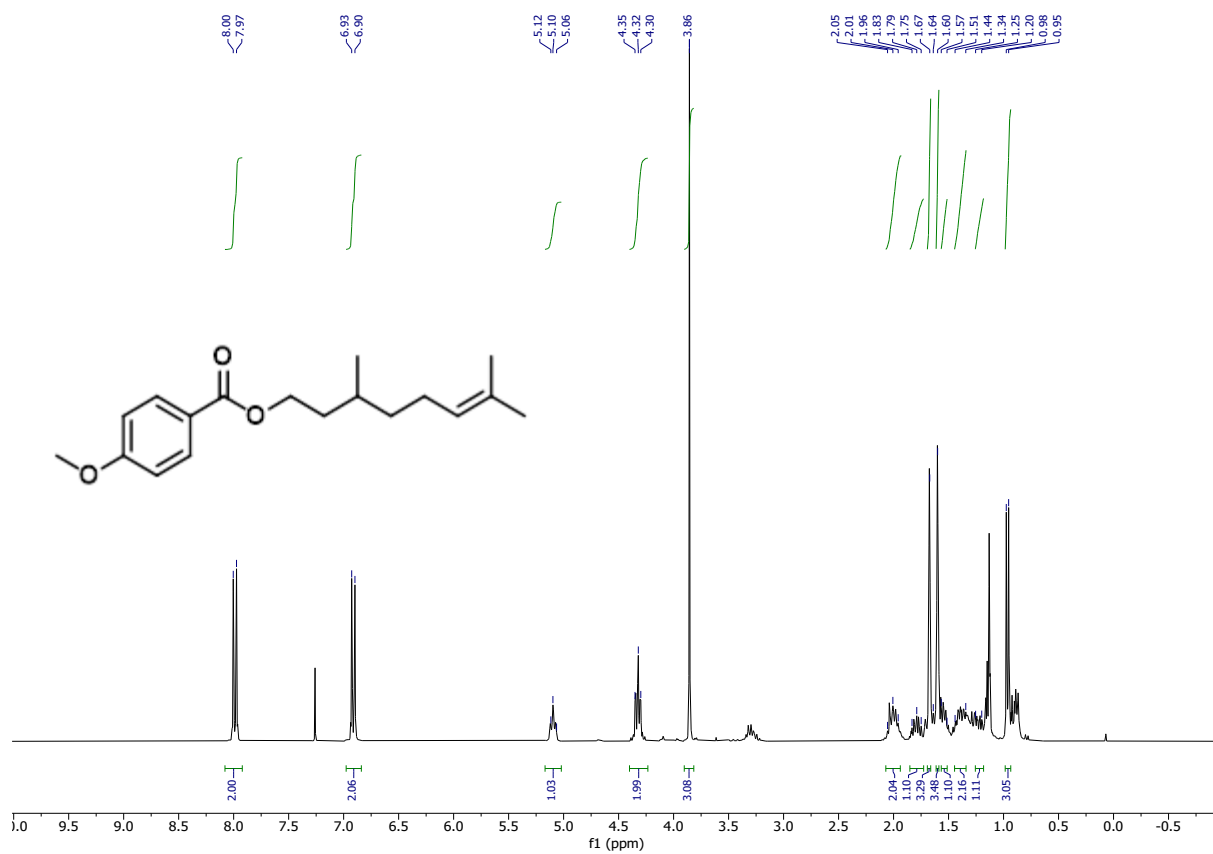
^{1}H NMR (300 MHz, CDCl$_3$) of Citronellyl 4-methoxybenzoate (2ai).
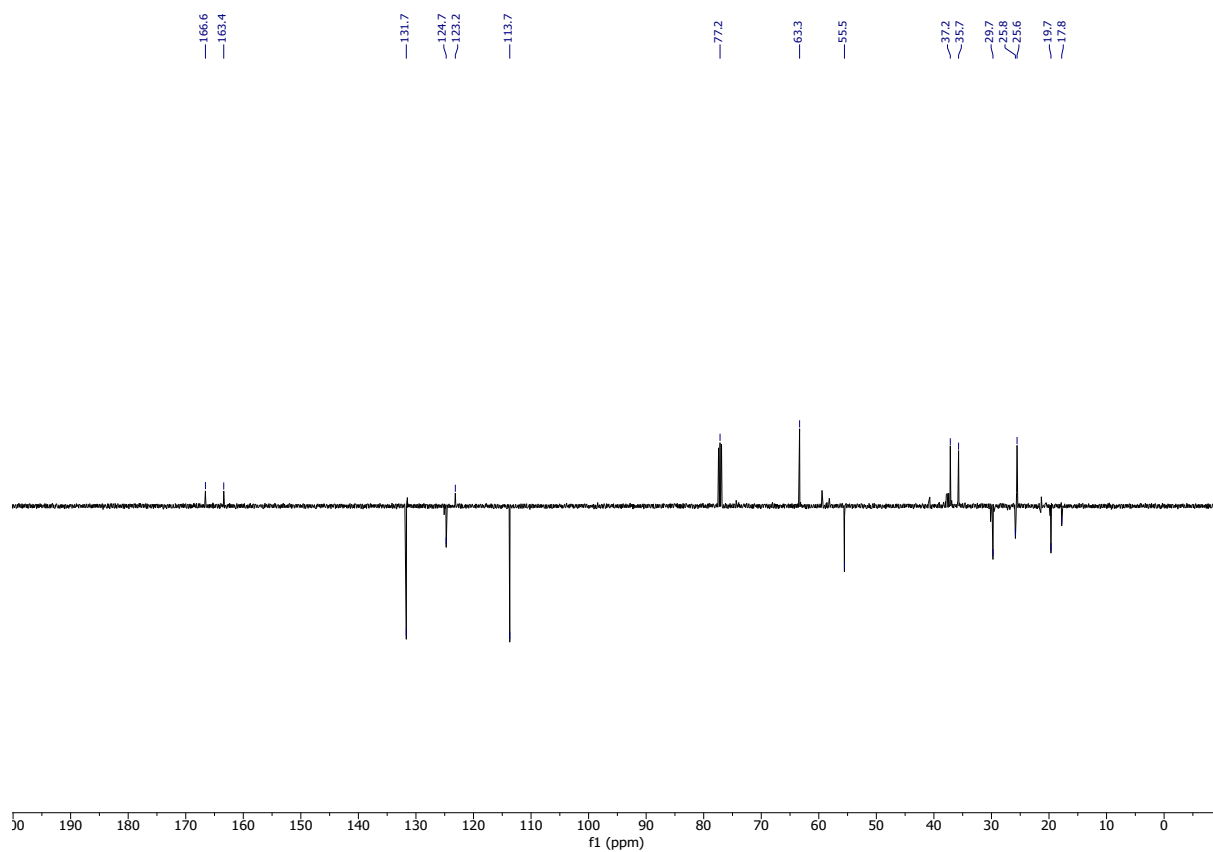
^{13}C NMR (75 MHz, CDCl$_3$) of Citronellyl 4-methoxybenzoate.
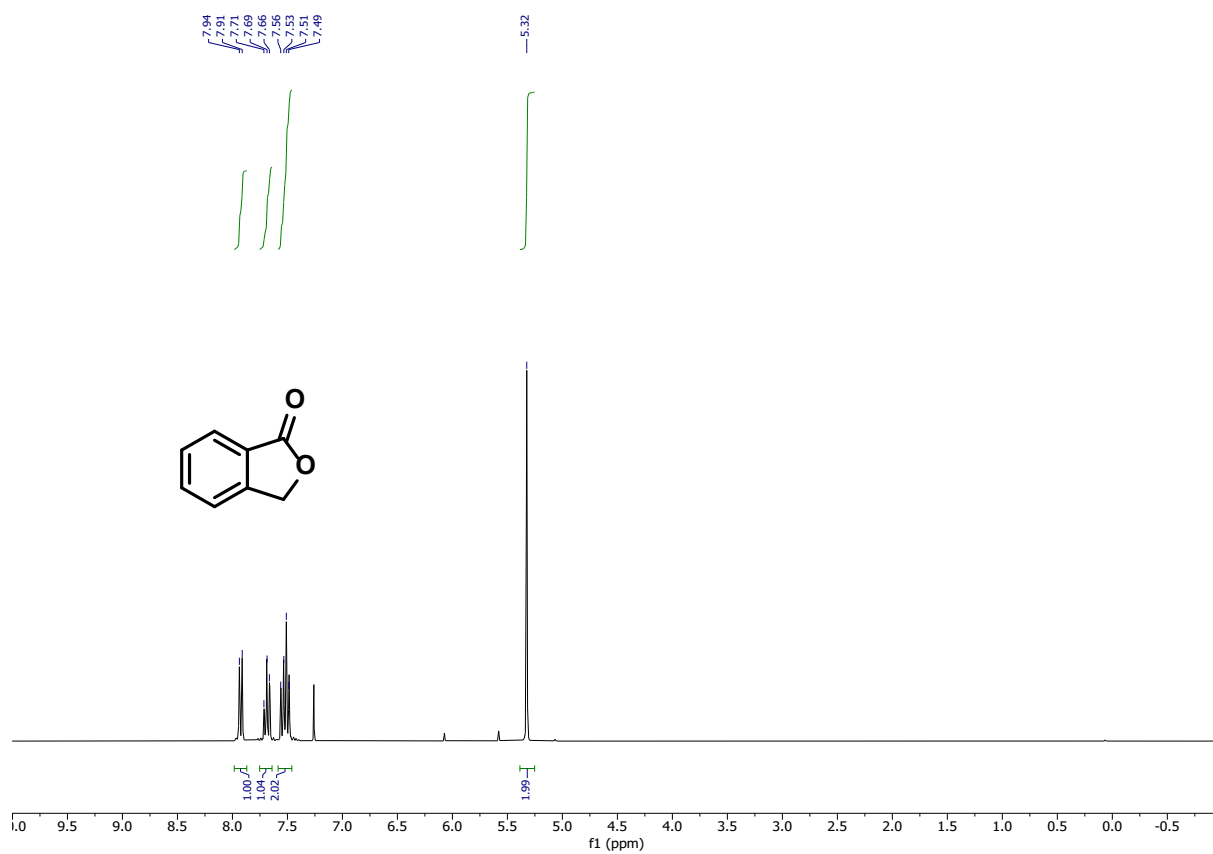
^{1}H NMR (300 MHz, CDCl$_3$) of Isobenzofuran-1(3H)-one (2o).
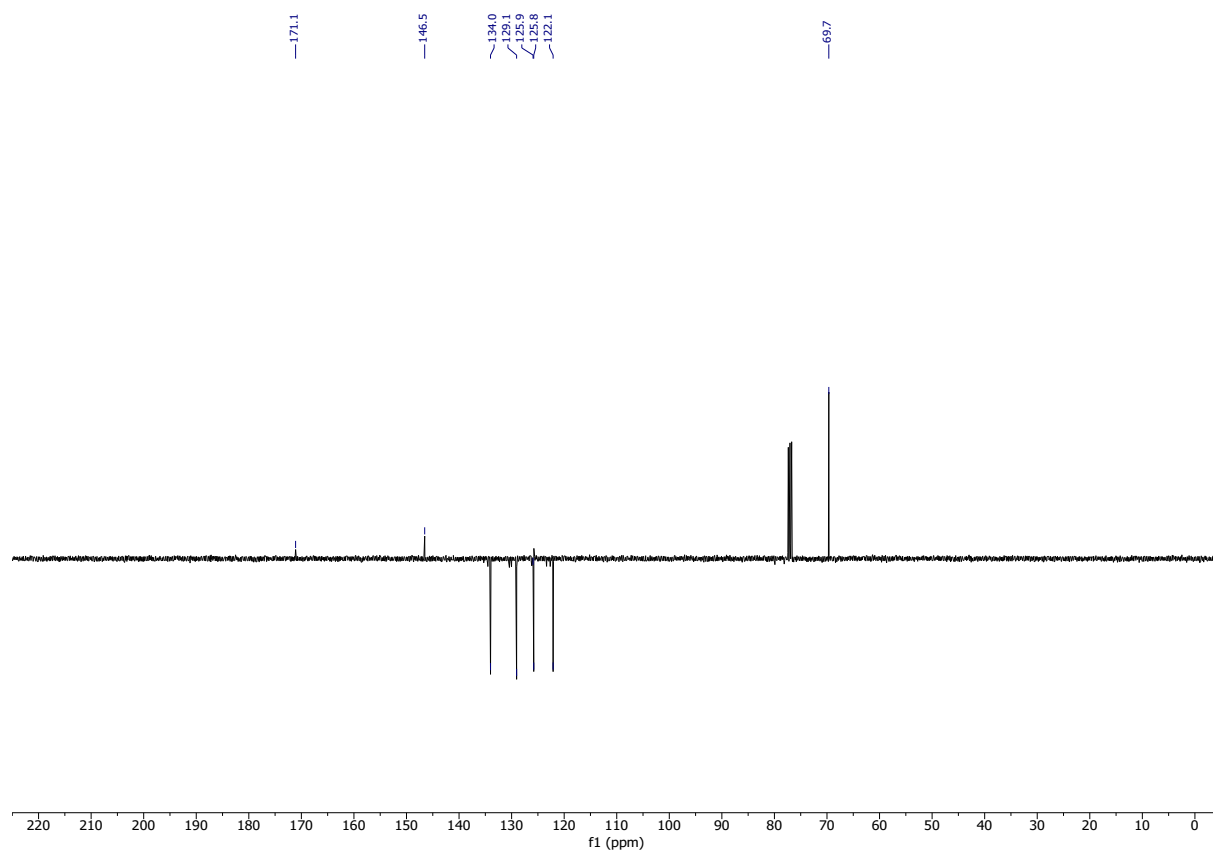
^{13}C NMR (75 MHz, CDCl$_3$) of Isobenzofuran-1(3H)-one.

213
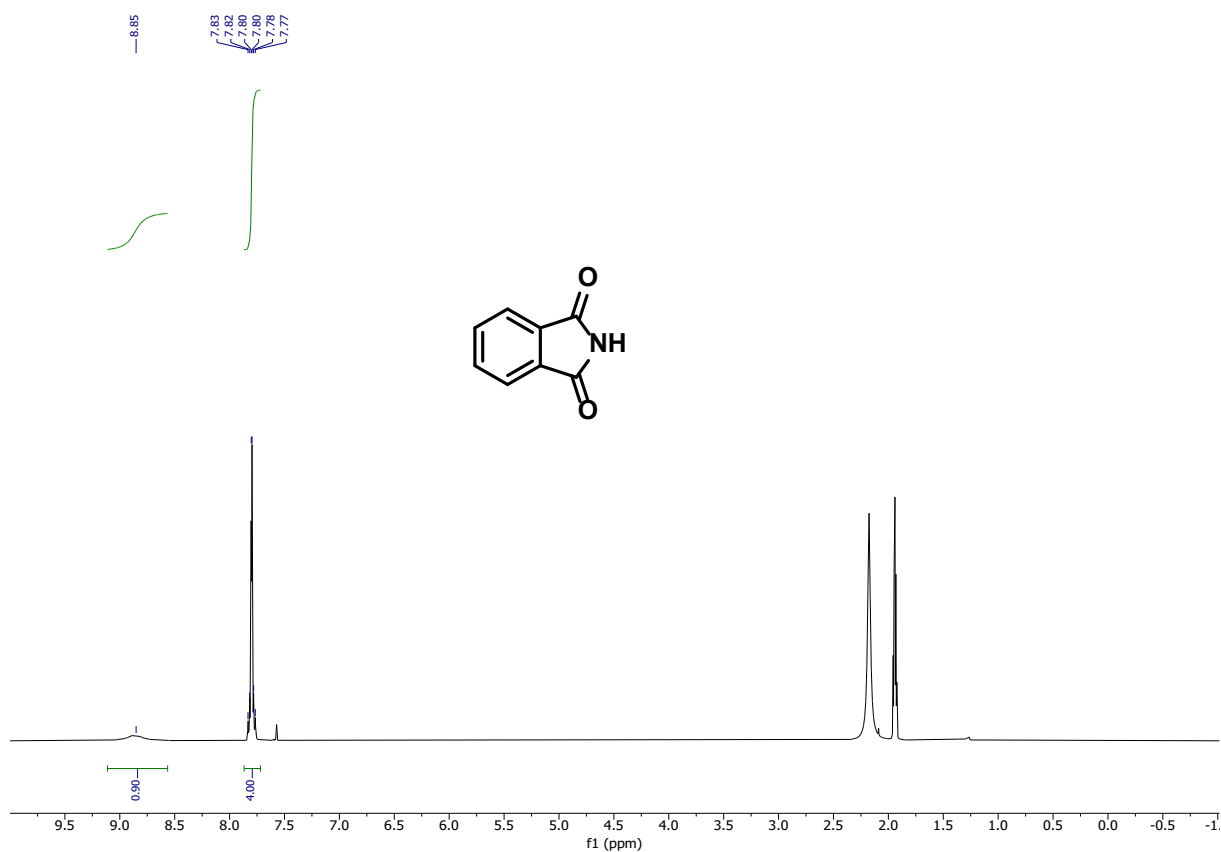
^{1}H NMR (300 MHz, CD₃CN) of 1H-Isoindole-1,3(2H)-dione (2p).
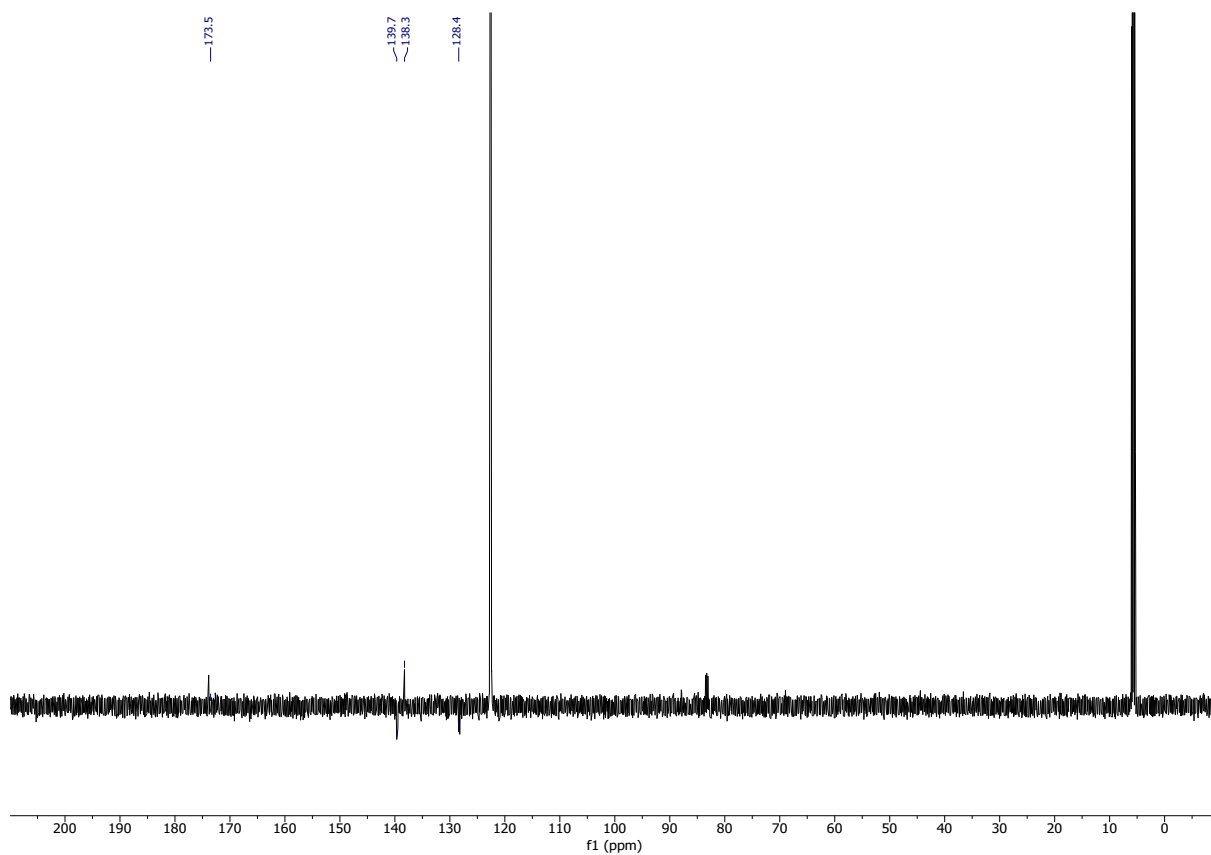
^{13}C NMR (75 MHz, CD₃CN) of 1H-Isoindole-1,3(2H)-dione.

214

^{1}H NMR (300 MHz, CDCl$_3$) of Ethylene glycol 4-methoxybenzoate (2aj).

^{13}C NMR (75 MHz, CDCl$_3$) of Ethylene glycol 4-methoxybenzoate.

215
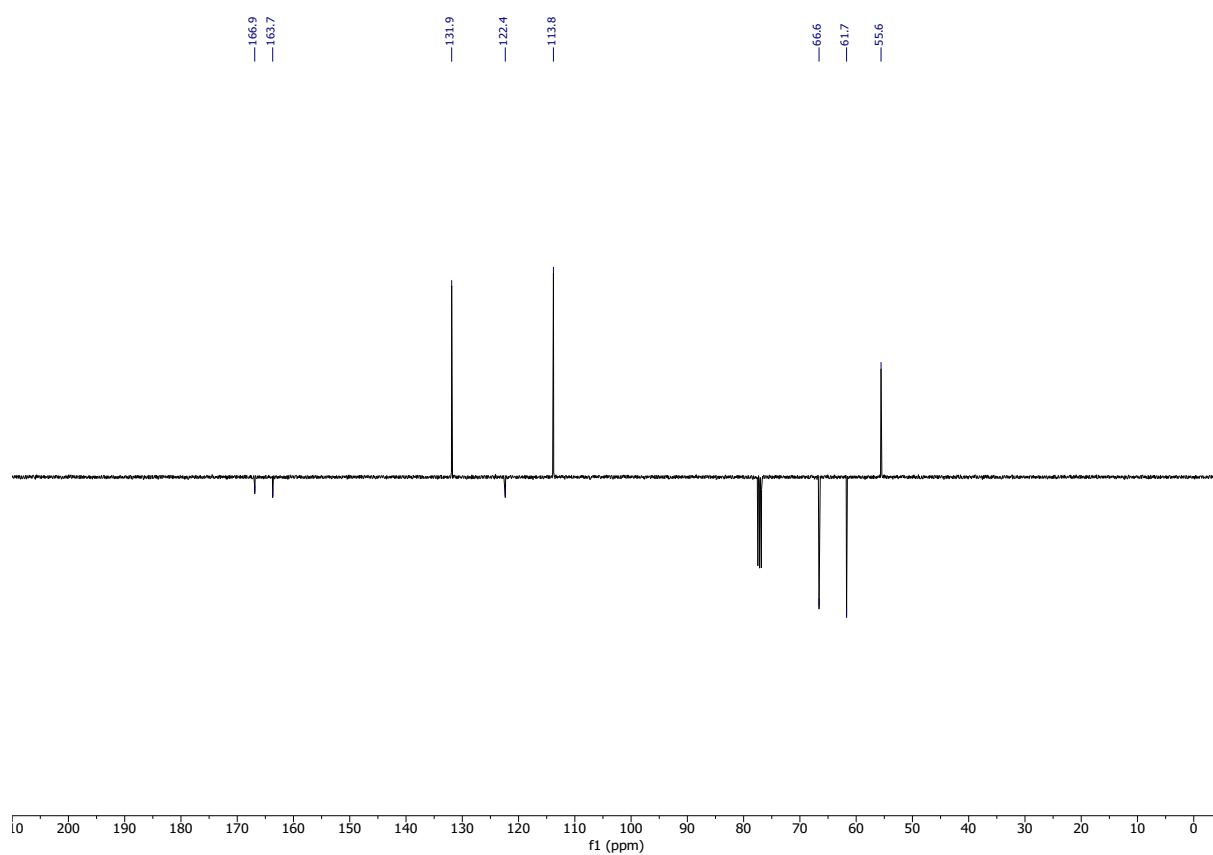
^{1}H NMR (300 MHz, CDCl$_3$) of Ethylene glycol di-4-methoxybenzoate (2ak).

^{13}C NMR (75 MHz, CDCl$_3$) of Ethylene glycol di-4-methoxybenzoate.
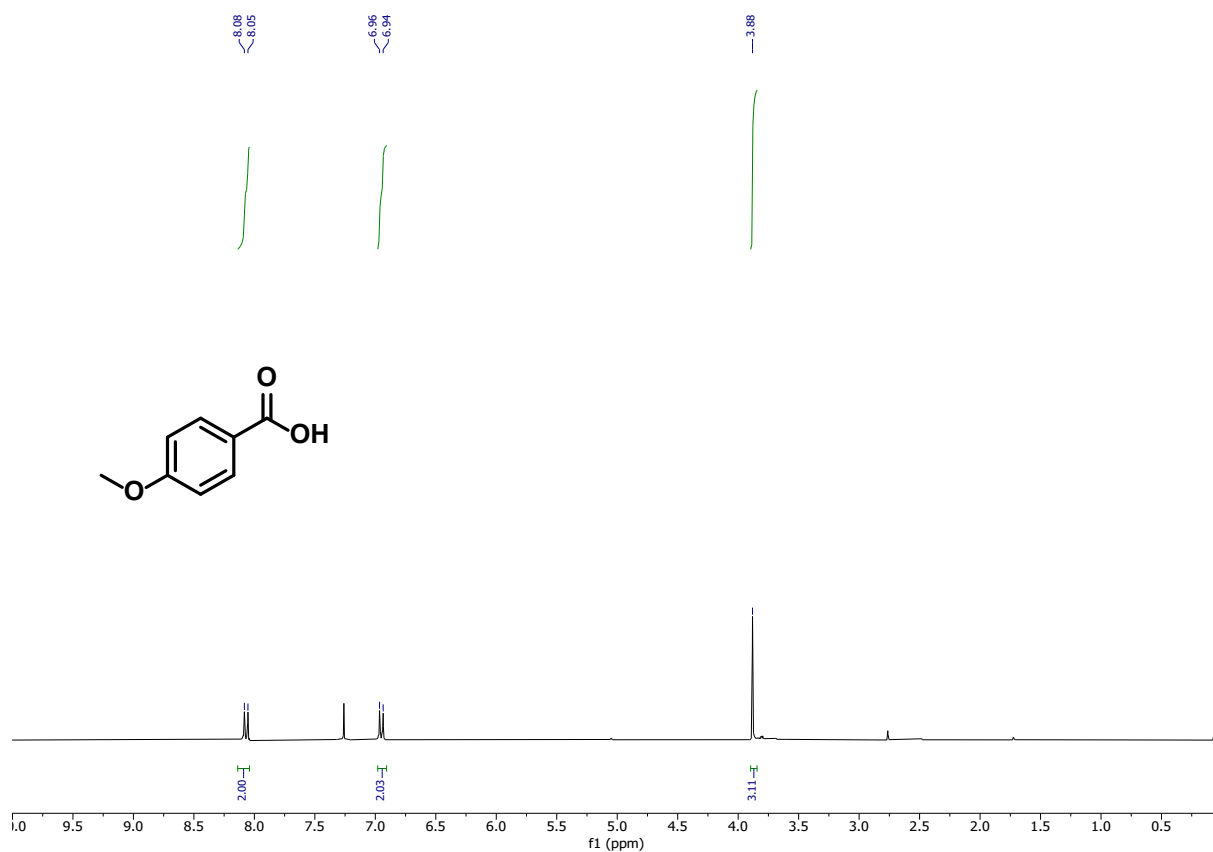
216

8.08
8.05
6.96
6.94
3.88

2.00
2.03
3.11

f1 (ppm)

¹H NMR (300 MHz, CDCl₃) of 4-Methoxybenzoic acid (2al).

171.4
164.2
132.5
121.8
113.9
77.2
55.6

f1 (ppm)
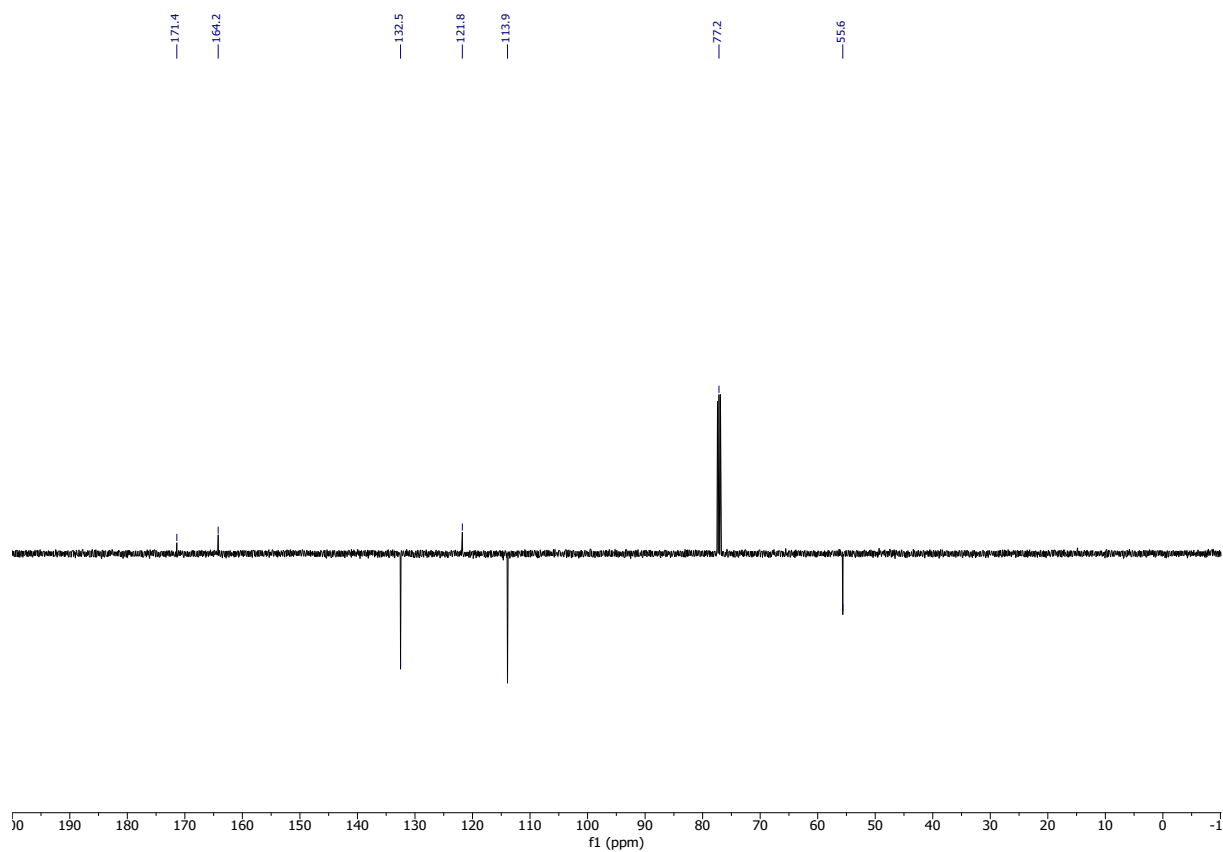
¹³C NMR (75 MHz, CDCl₃) of 4-Methoxybenzoic acid.
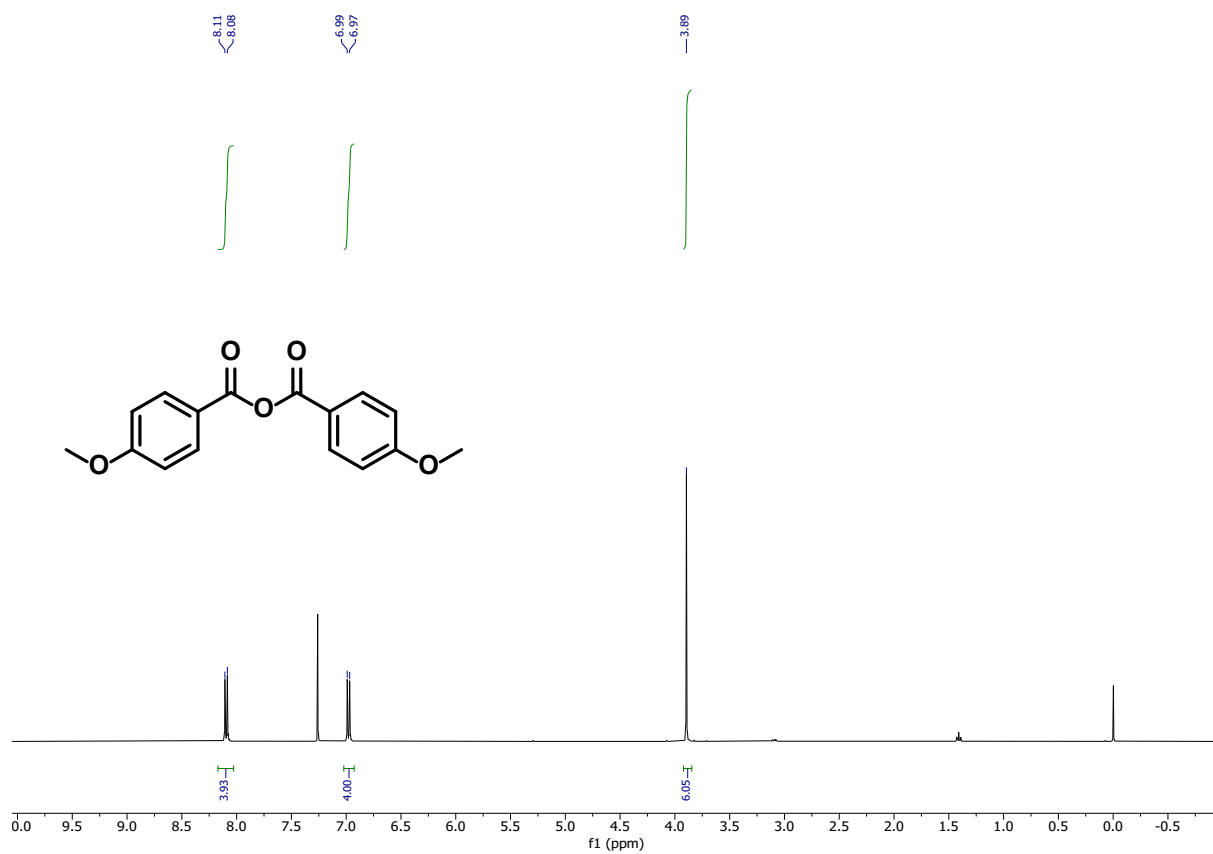
^{1}H NMR (300 MHz, CDCl$_3$) of 4-Methoxybenzoic anhydride (2am).

^{13}C NMR (75 MHz, CDCl$_3$) of 4-Methoxybenzoic anhydride.

218
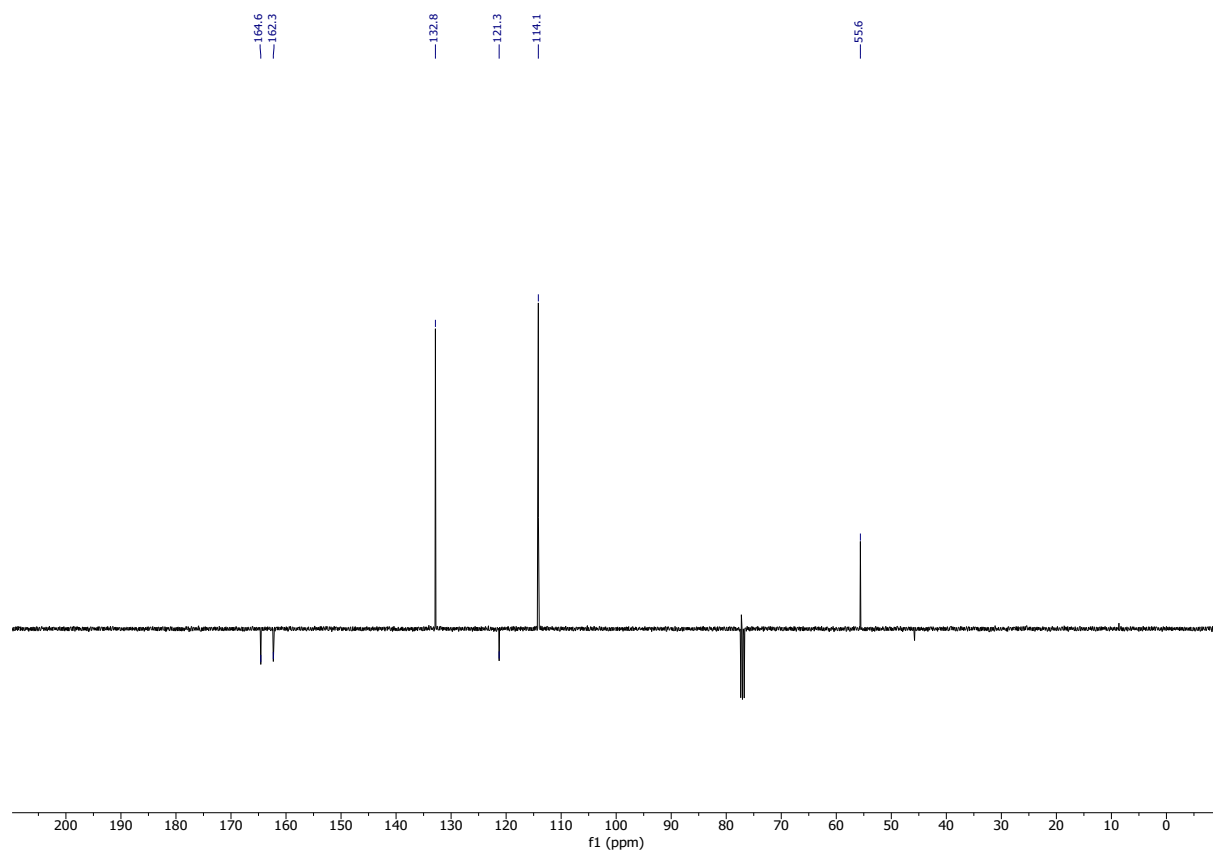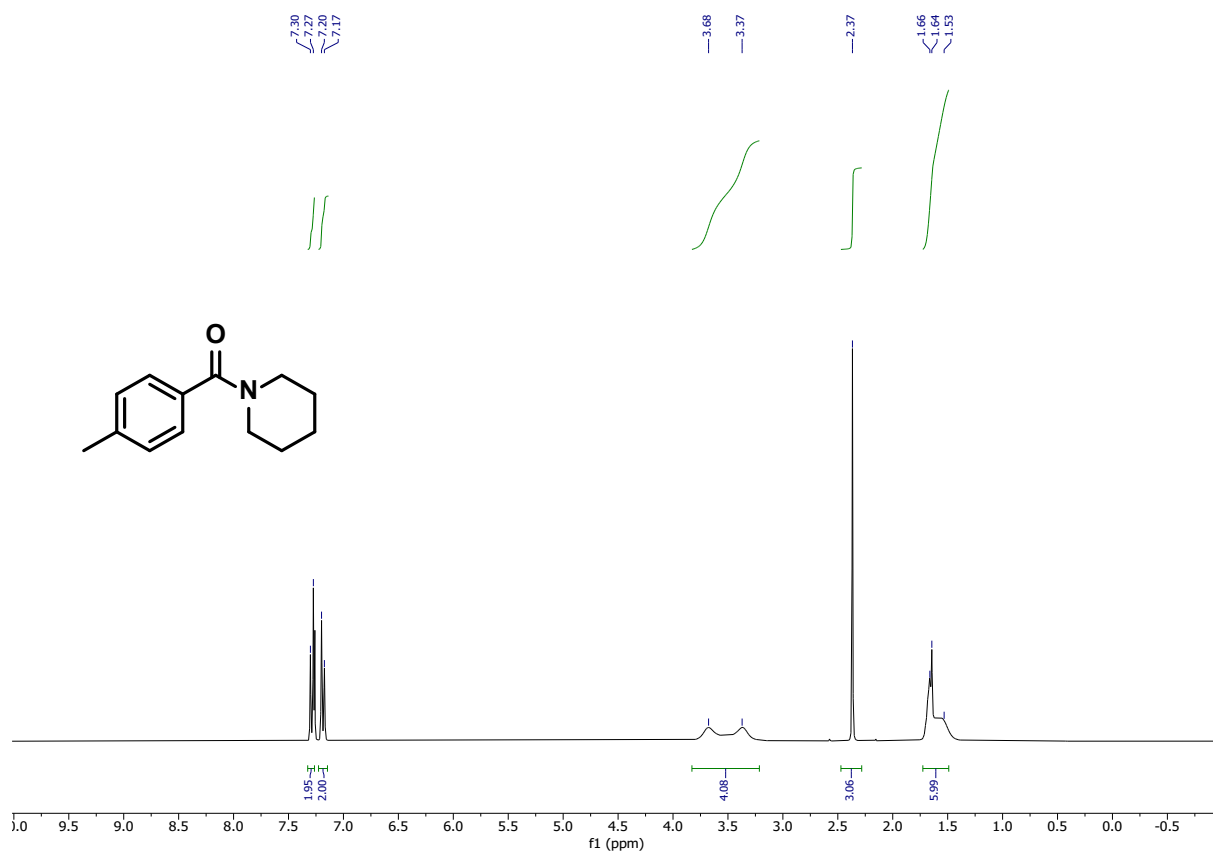
^{1}H NMR (300 MHz, CDCl$_3$) of 1-(4-Methylbenzoyl)-piperidine (2bn).
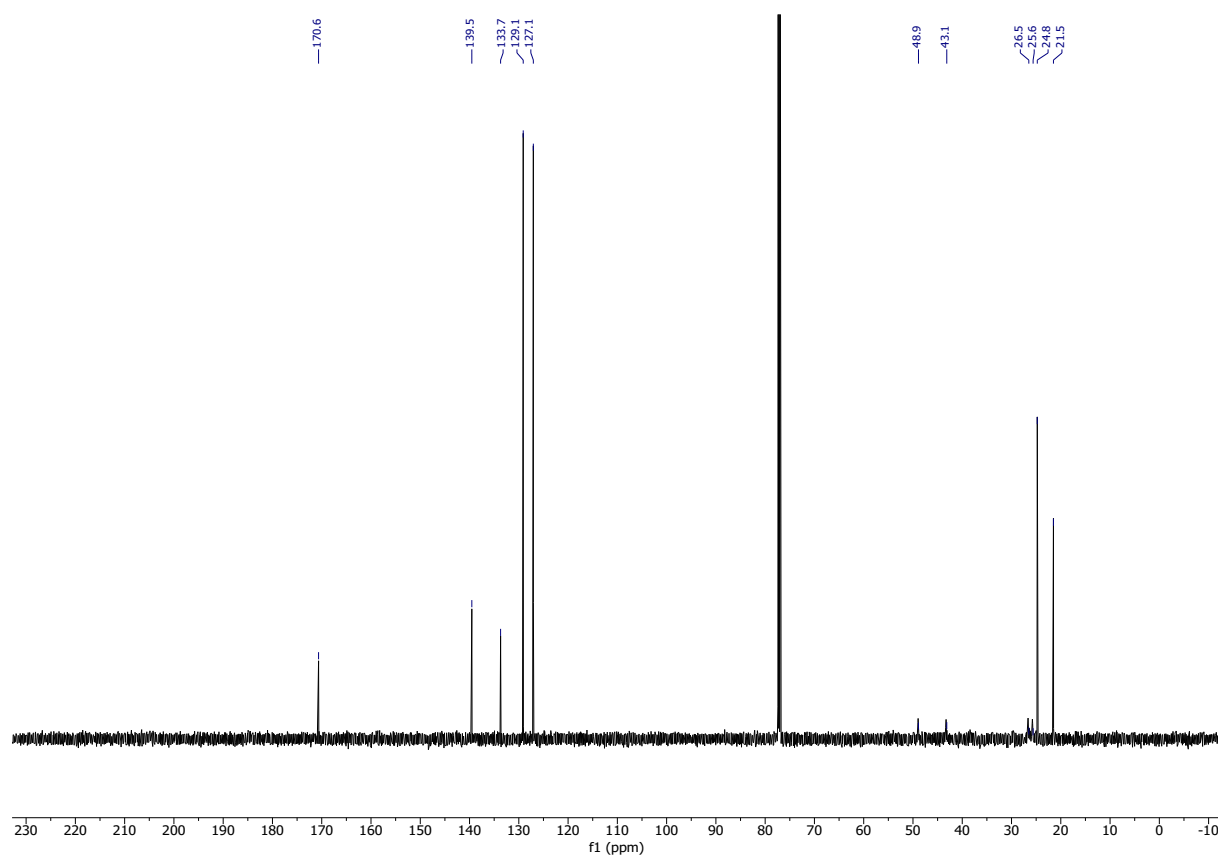
^{13}C NMR (75 MHz, CDCl$_3$) of 1-(4-Methylbenzoyl)-piperidine.
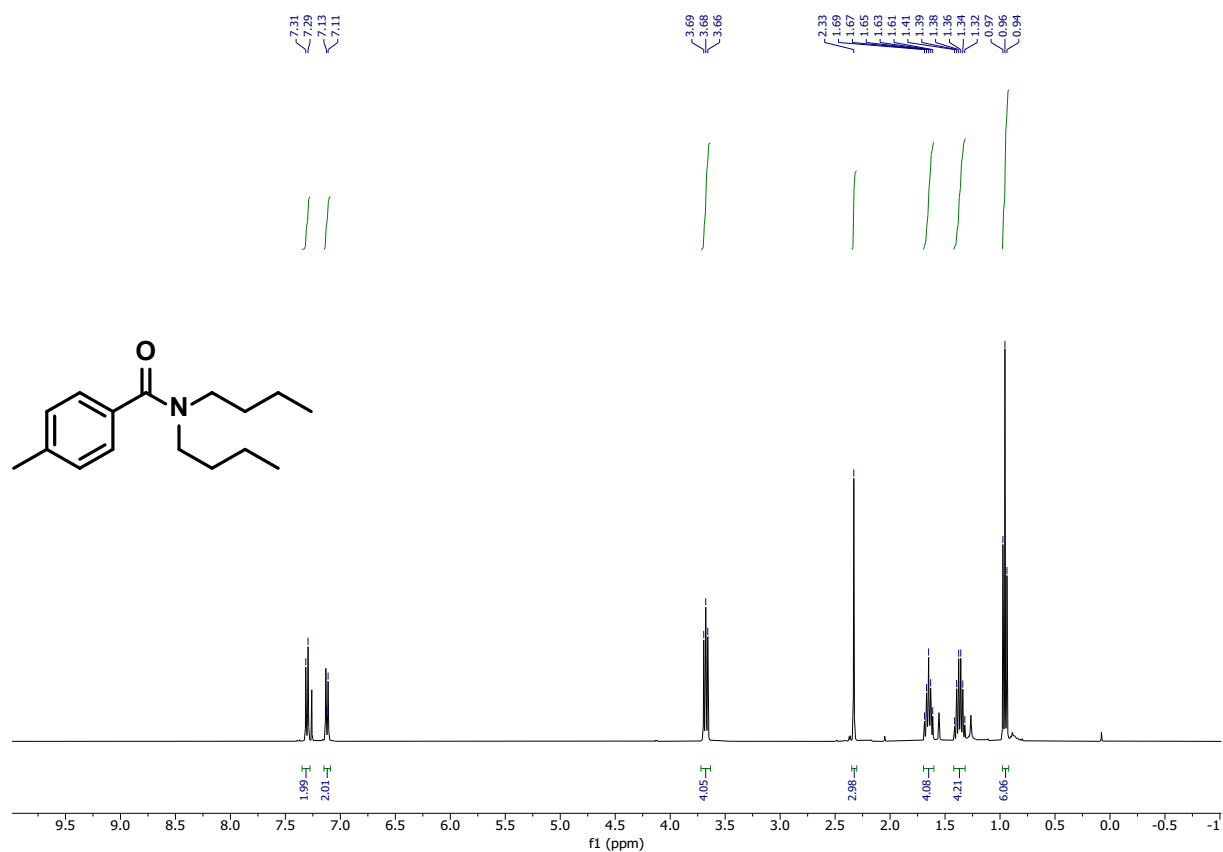
¹H NMR (300 MHz, CDCl₃) of *N,N*-Dibutyl-4-methylbenzamide (2bo).
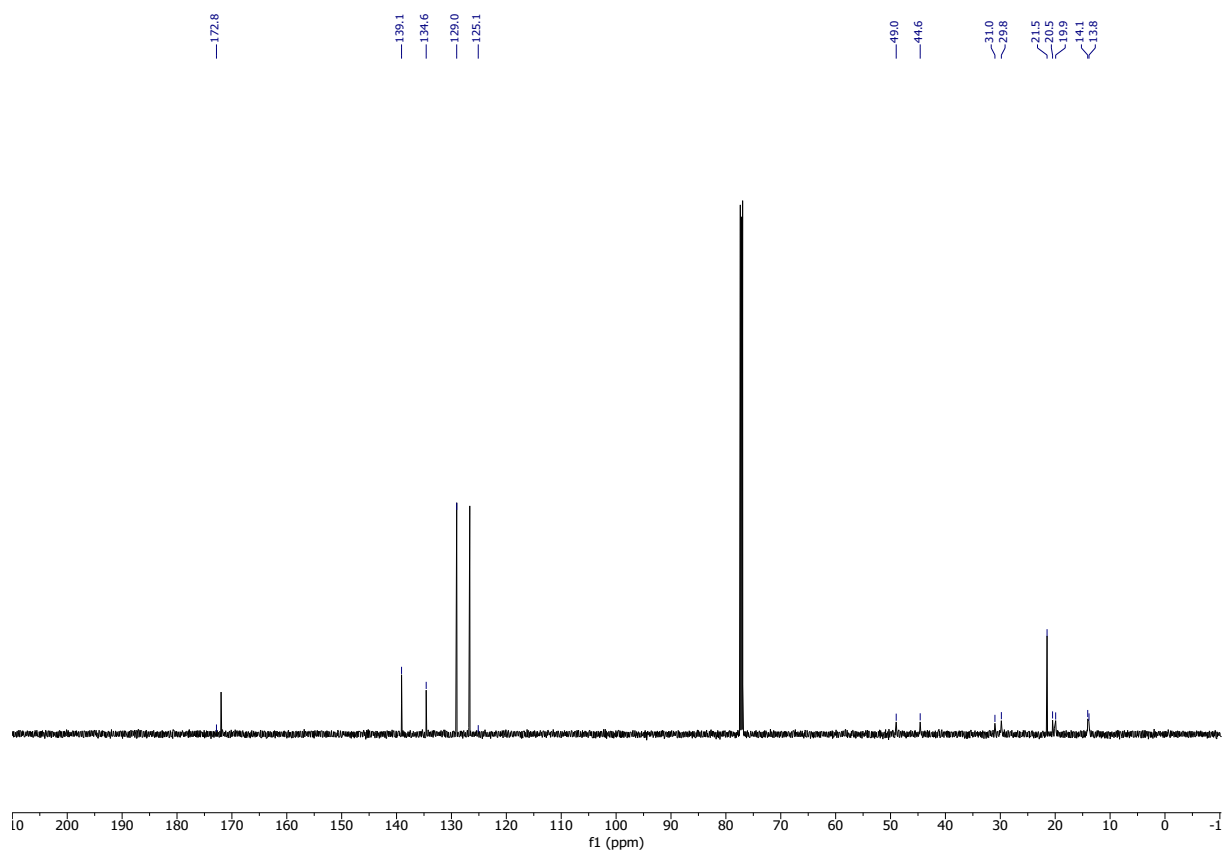
¹³C NMR (75 MHz, CDCl₃) of *N,N*-Dibutyl-4-methylbenzamide.

^{1}H NMR (300 MHz, CDCl$_3$) of DEET (2qp).

^{13}C NMR (75 MHz, CDCl$_3$) of DEET.
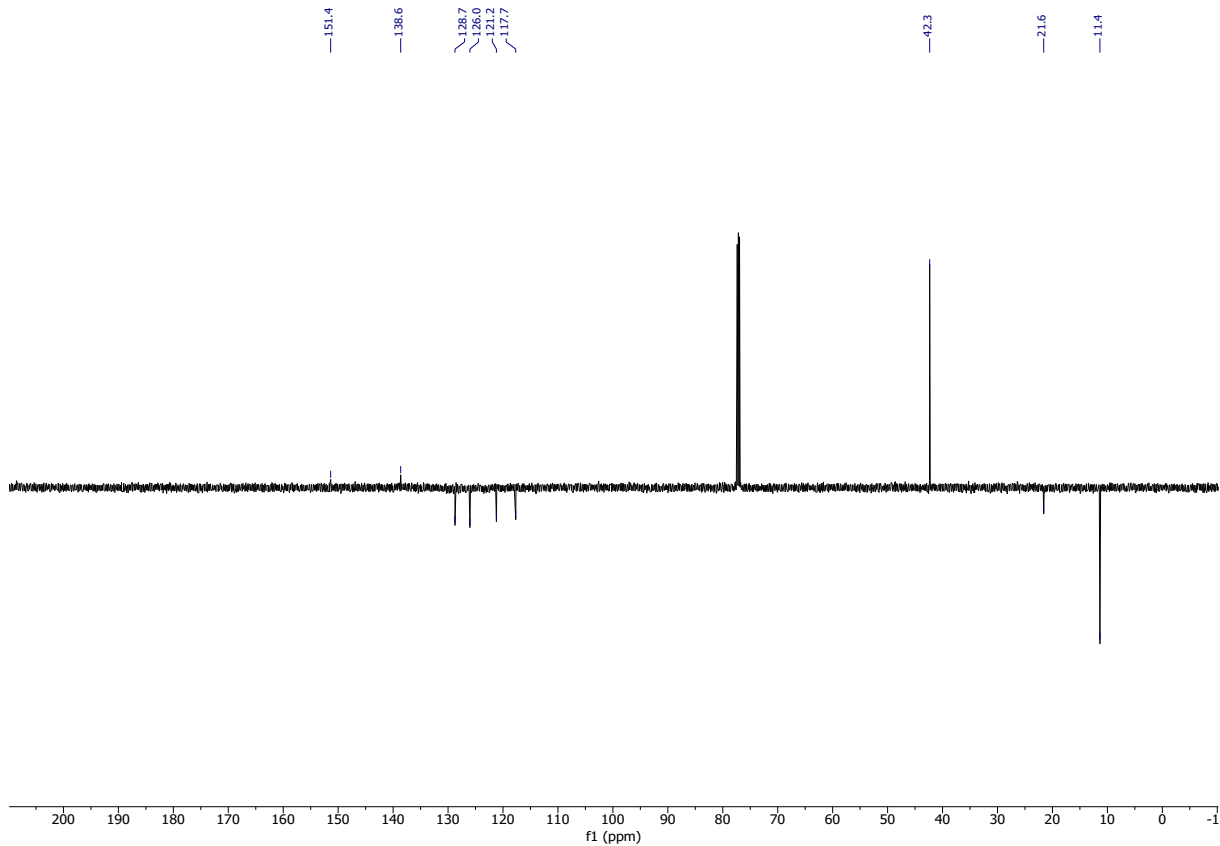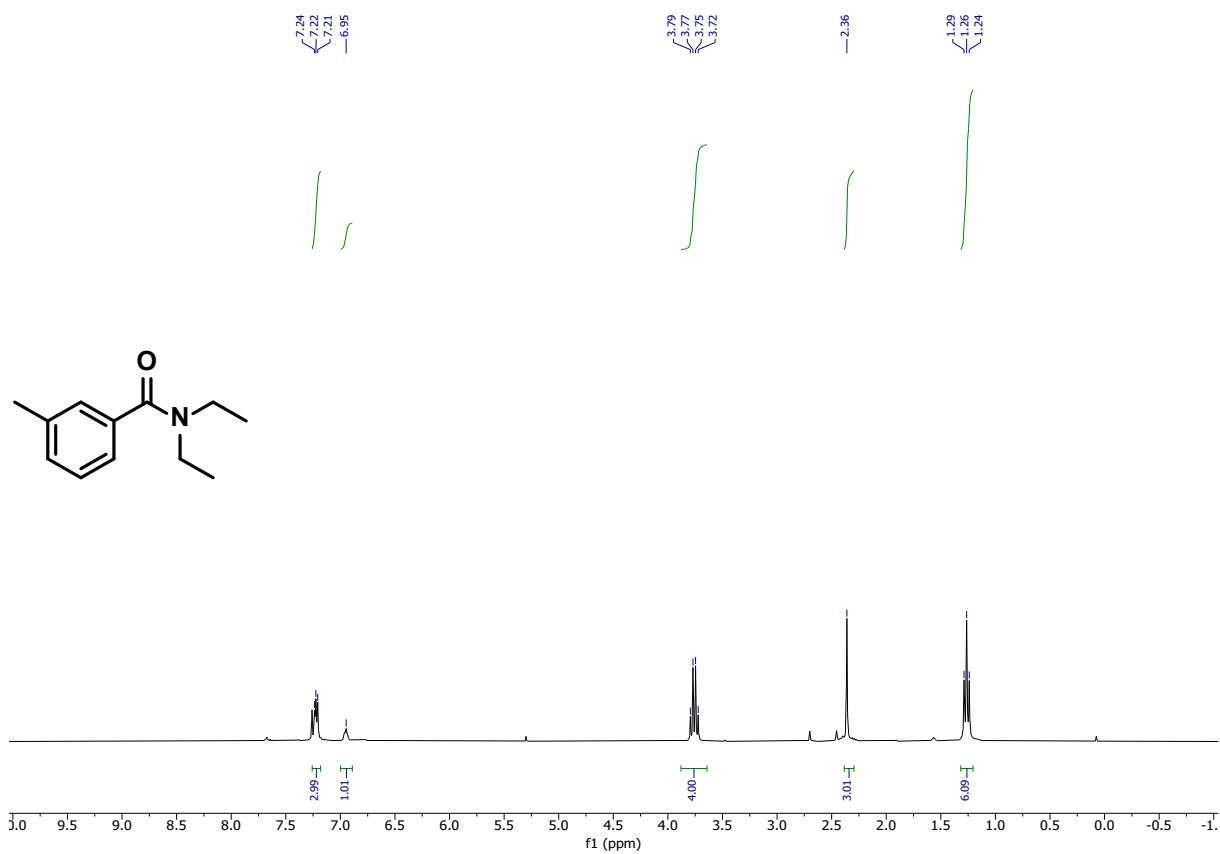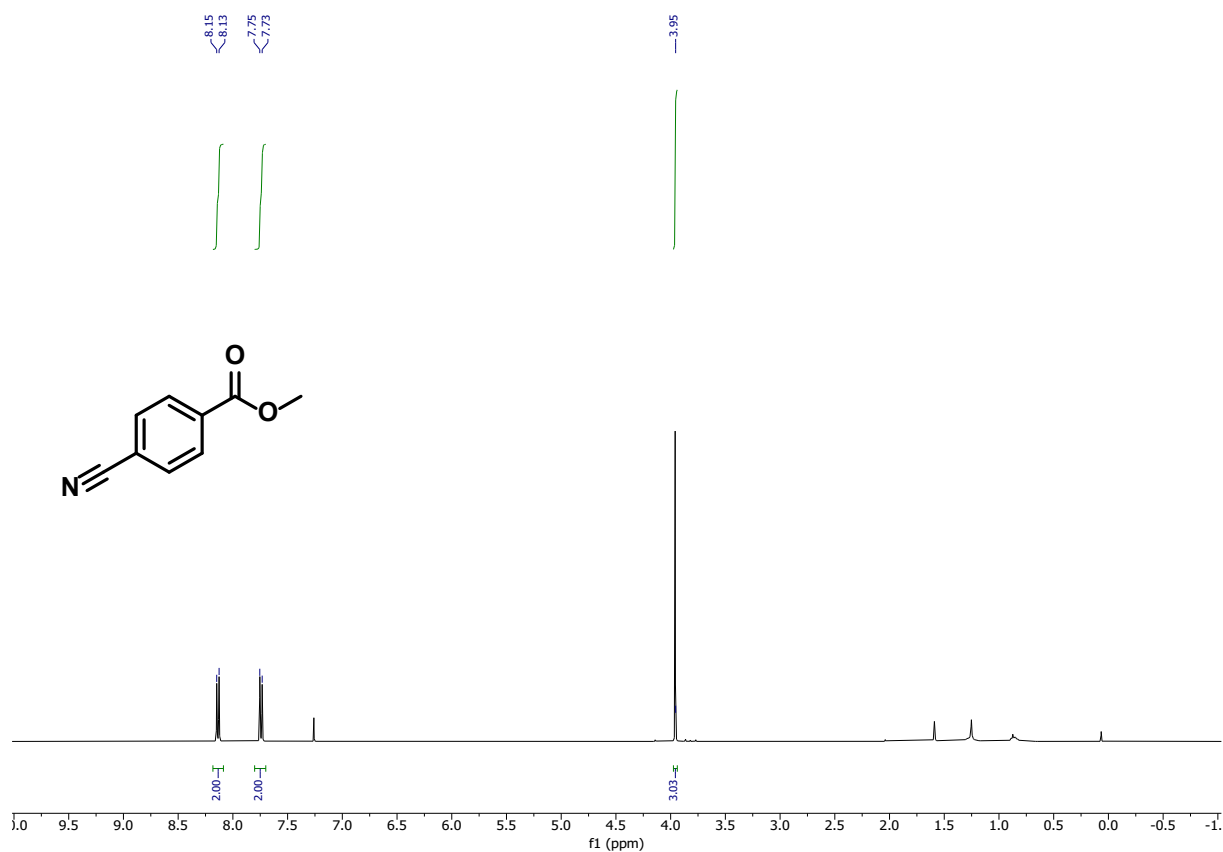
^{1}H NMR (300 MHz, CDCl₃) of Methyl 4-cyanobenzoate (2da).
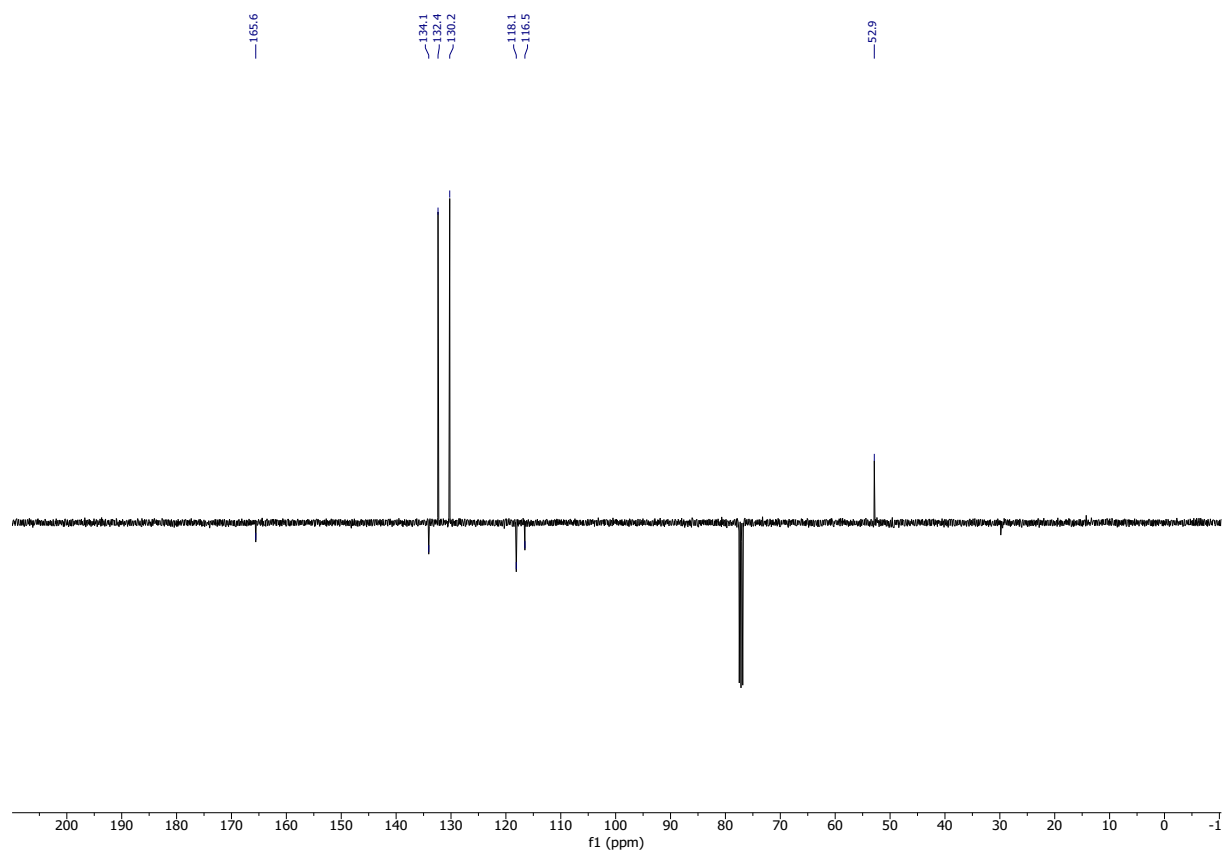
^{13}C NMR (75 MHz, CDCl₃) of Methyl 4-cyanobenzoate.
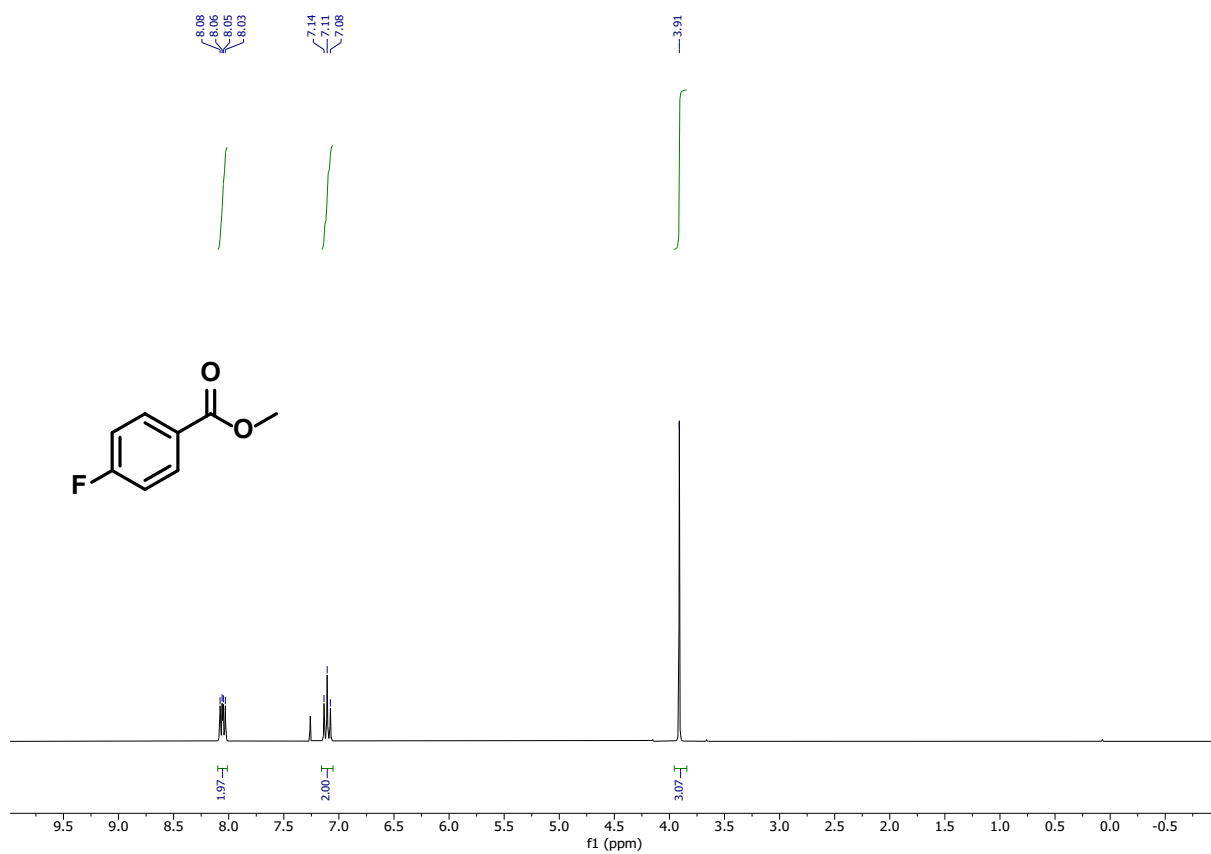
^{1}H NMR (300 MHz, CDCl$_3$) of Methyl 4-fluorobenzoate (2ea).
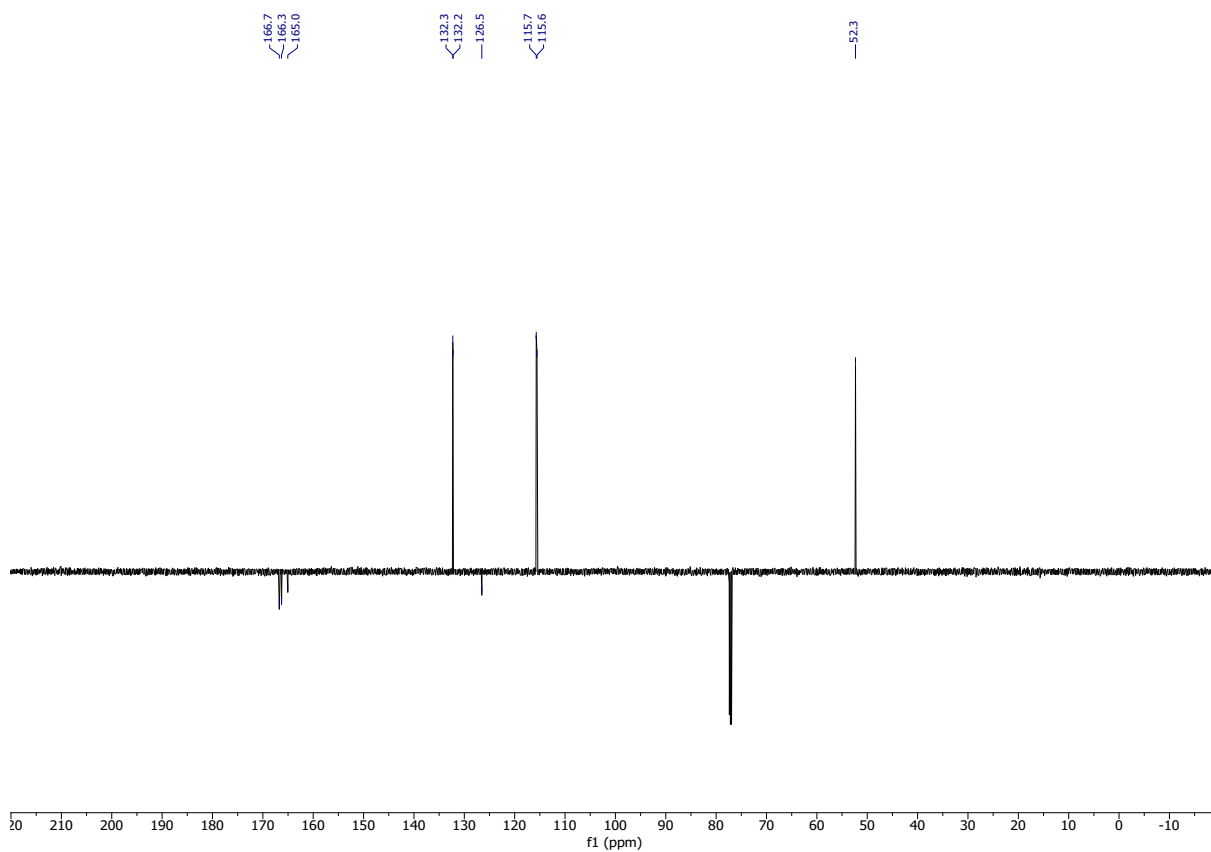
^{13}C NMR (75 MHz, CDCl$_3$) of Methyl 4-fluorobenzoate.
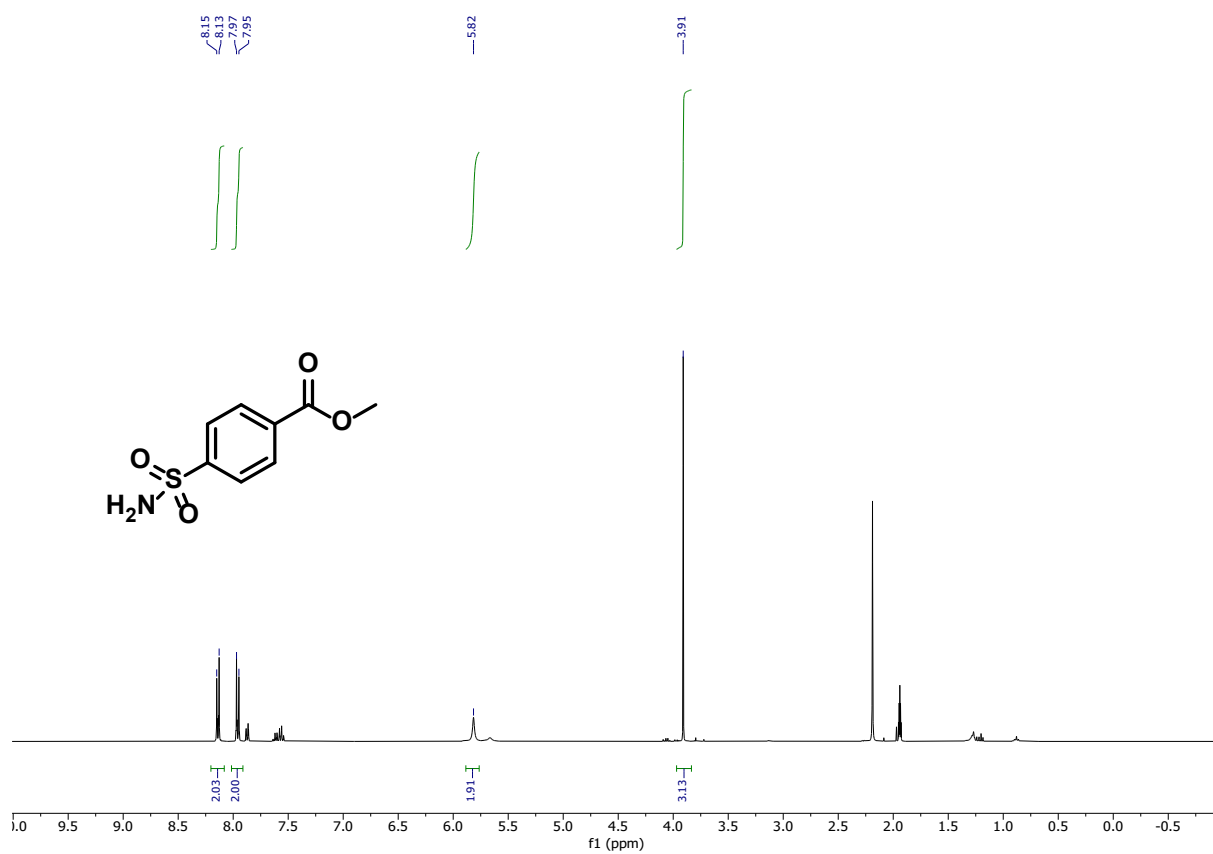
^{1}H NMR (300 MHz, CD₃CN) of Methyl 4-aminosulfonylbenzoate (2fa).
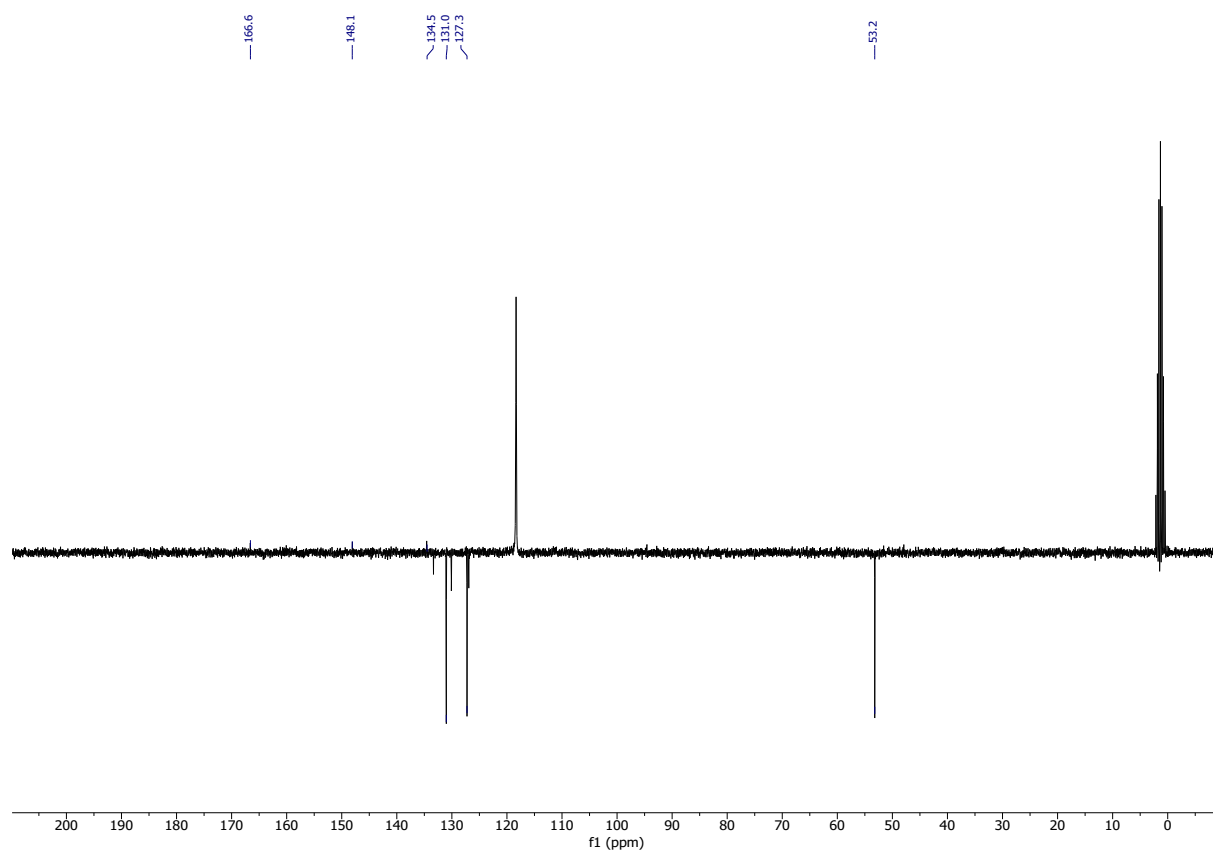
^{13}C NMR (75 MHz, CD₃CN) of Methyl 4-aminosulfonylbenzoate.

224
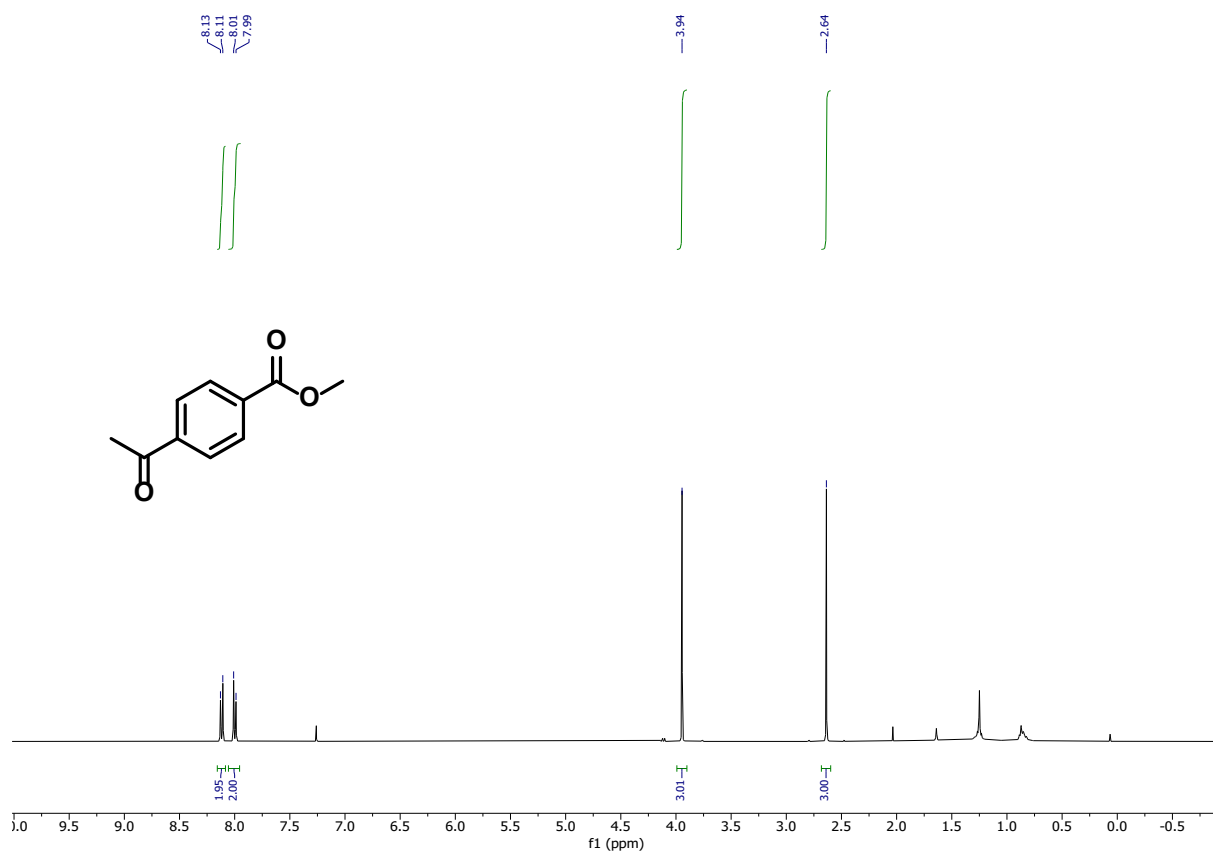
^{1}H NMR (300 MHz, CDCl$_3$) of Methyl 4-acetylbenzoate (2ga).
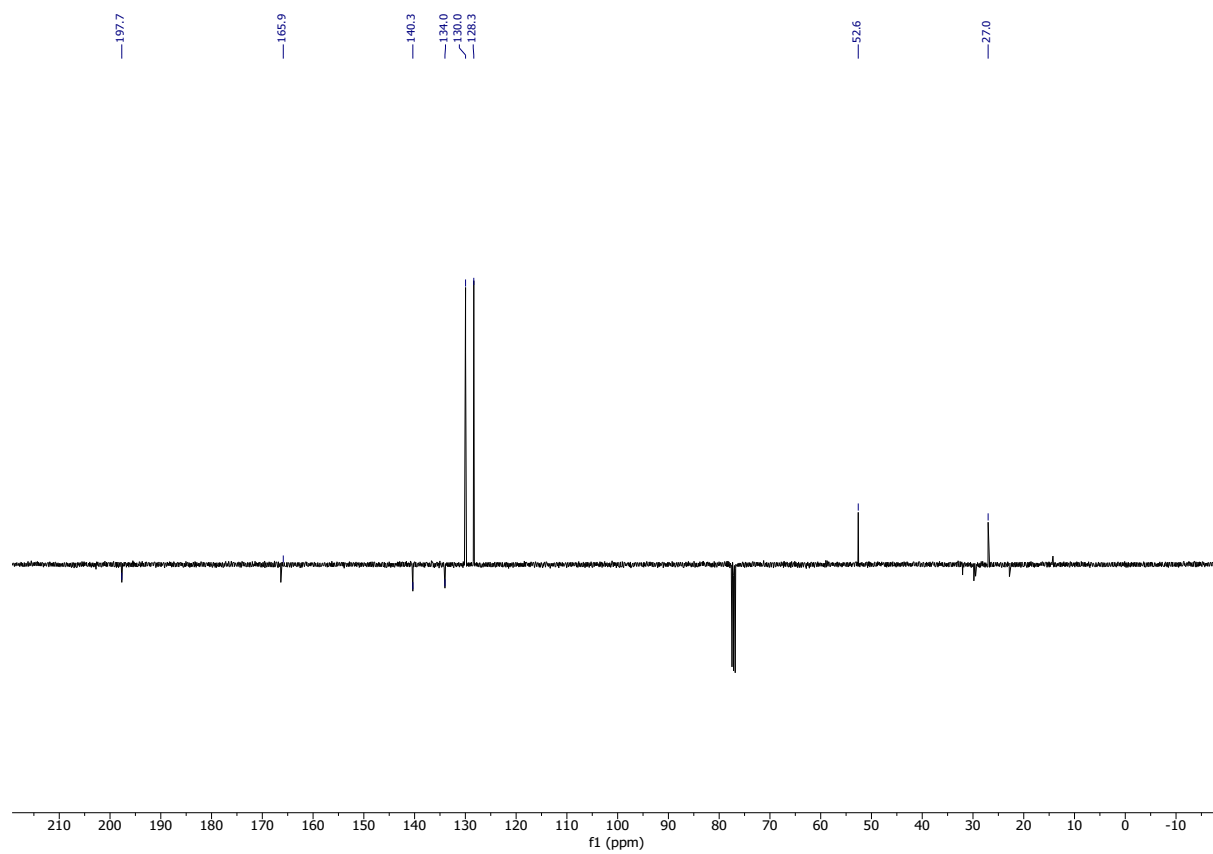
^{13}C NMR (75 MHz, CDCl$_3$) of Methyl 4-acetylbenzoate.
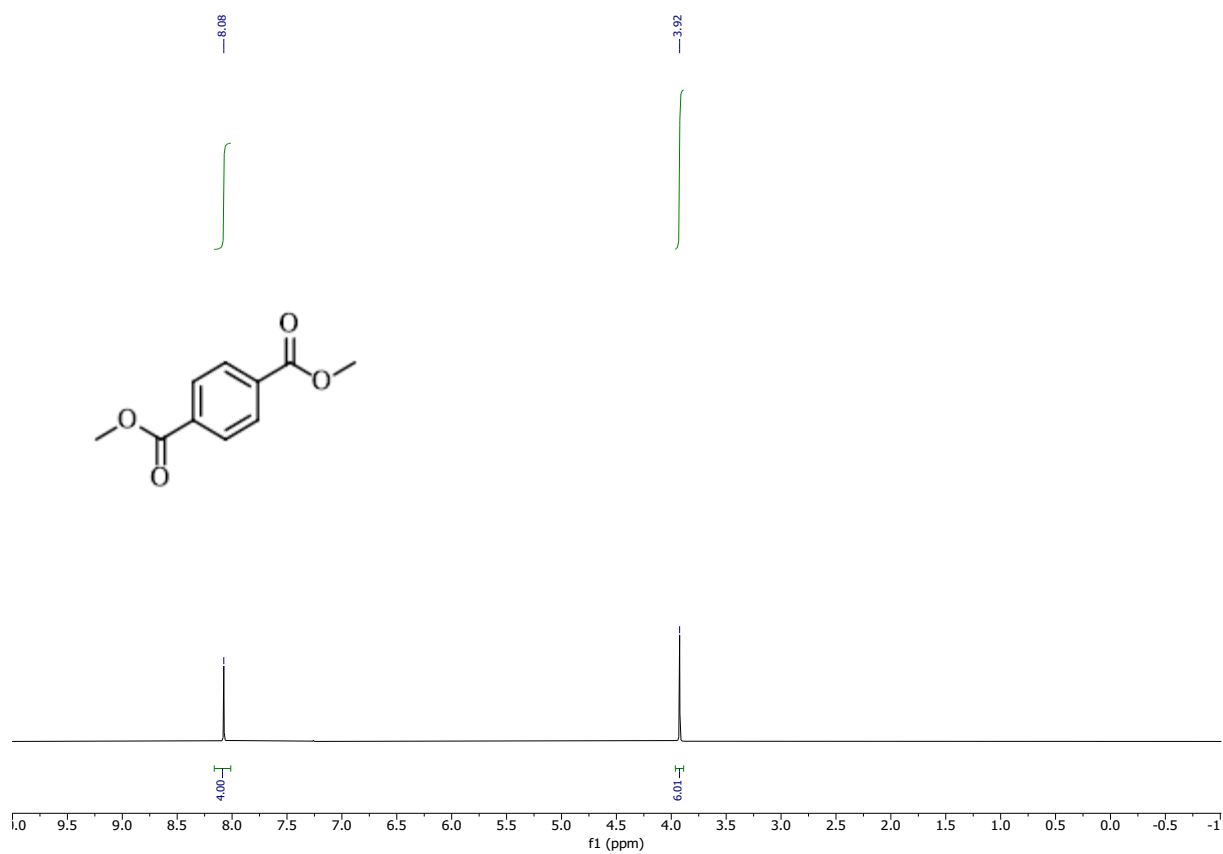
^{1}H NMR (300 MHz, CDCl$_3$) of Terephthalic acid dimethyl ester.
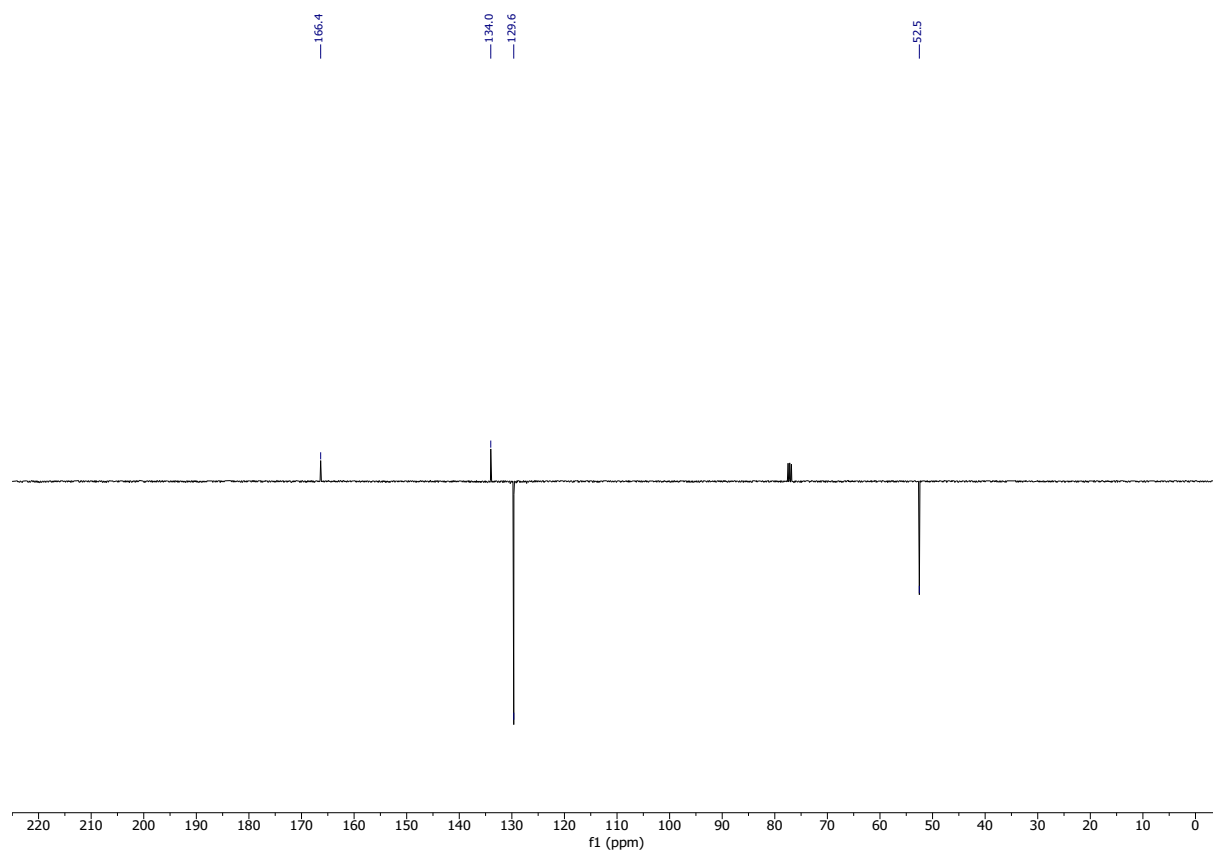
^{13}C NMR (75 MHz, CDCl$_3$) of Terephthalic acid dimethyl ester.
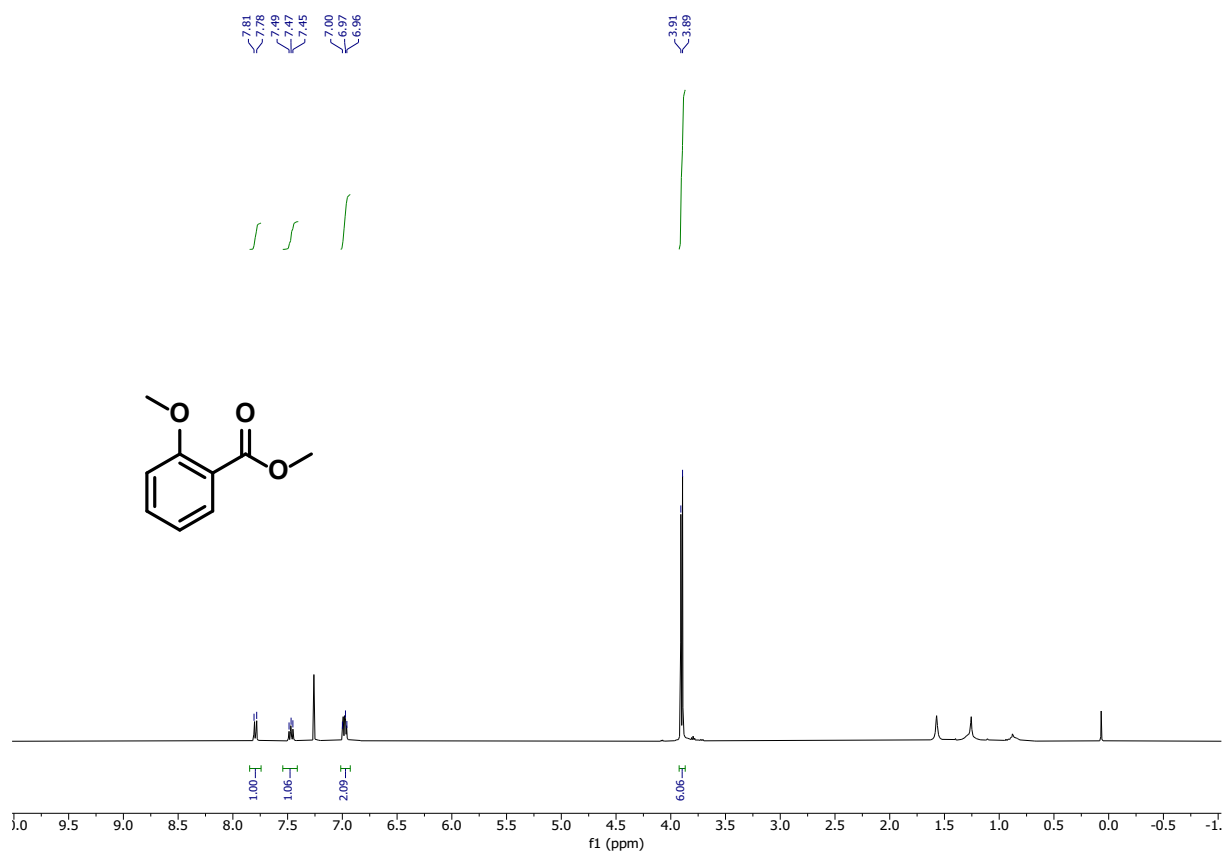
¹H NMR (300 MHz, CDCl₃) of Methyl 2-methoxybenzoate (2ha).
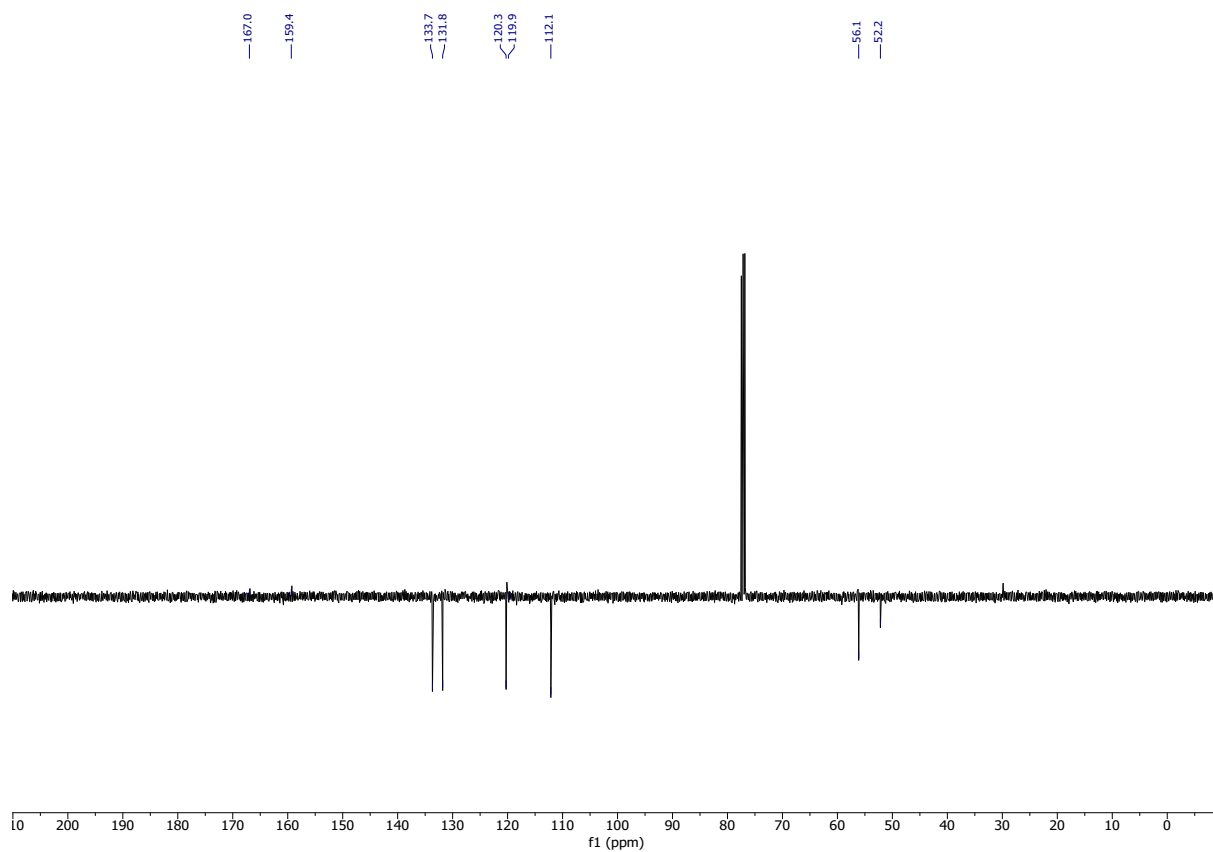
¹³C NMR (75 MHz, CDCl₃) of Methyl 2-methoxybenzoate.
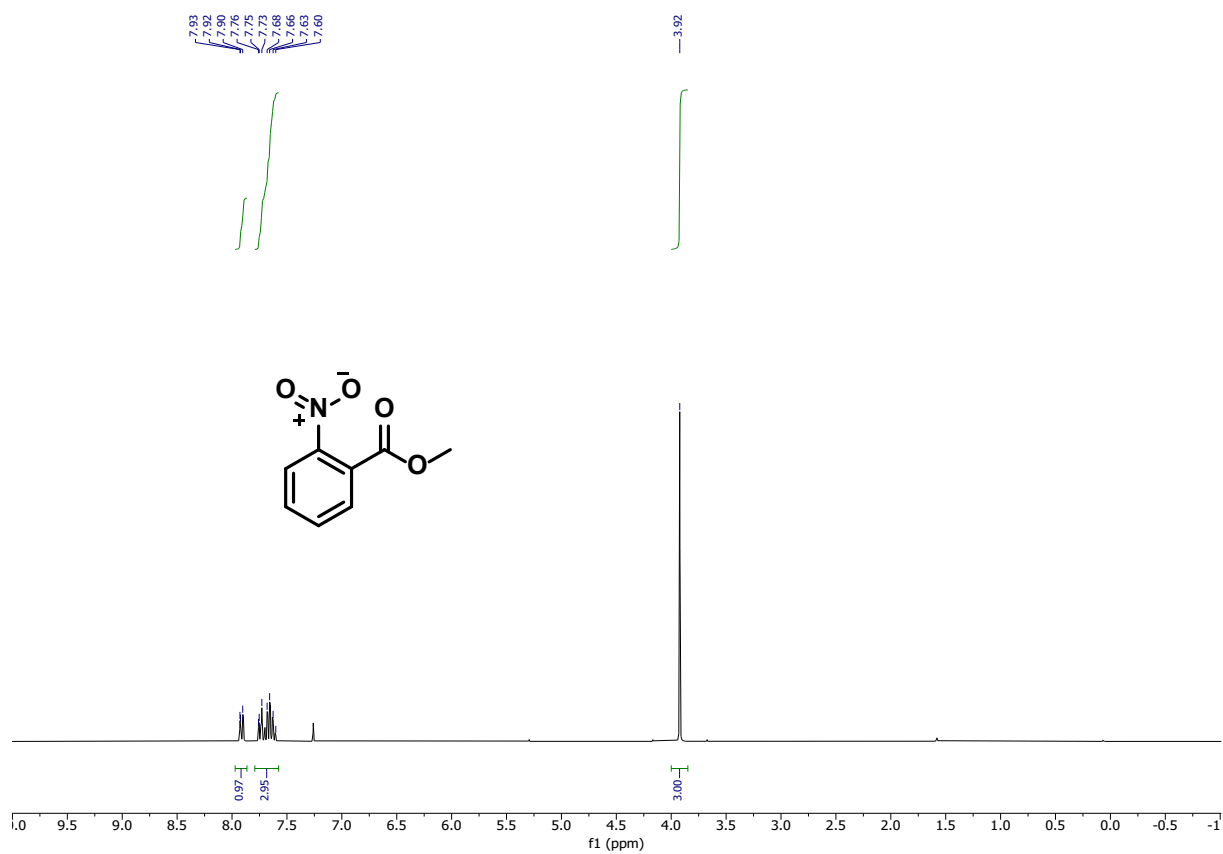
^{1}H NMR (300 MHz, CDCl$_3$) of Methyl 2-nitrobenzoate (2ia).

^{13}C NMR (75 MHz, CDCl$_3$) of Methyl 2-nitrobenzoate.

228
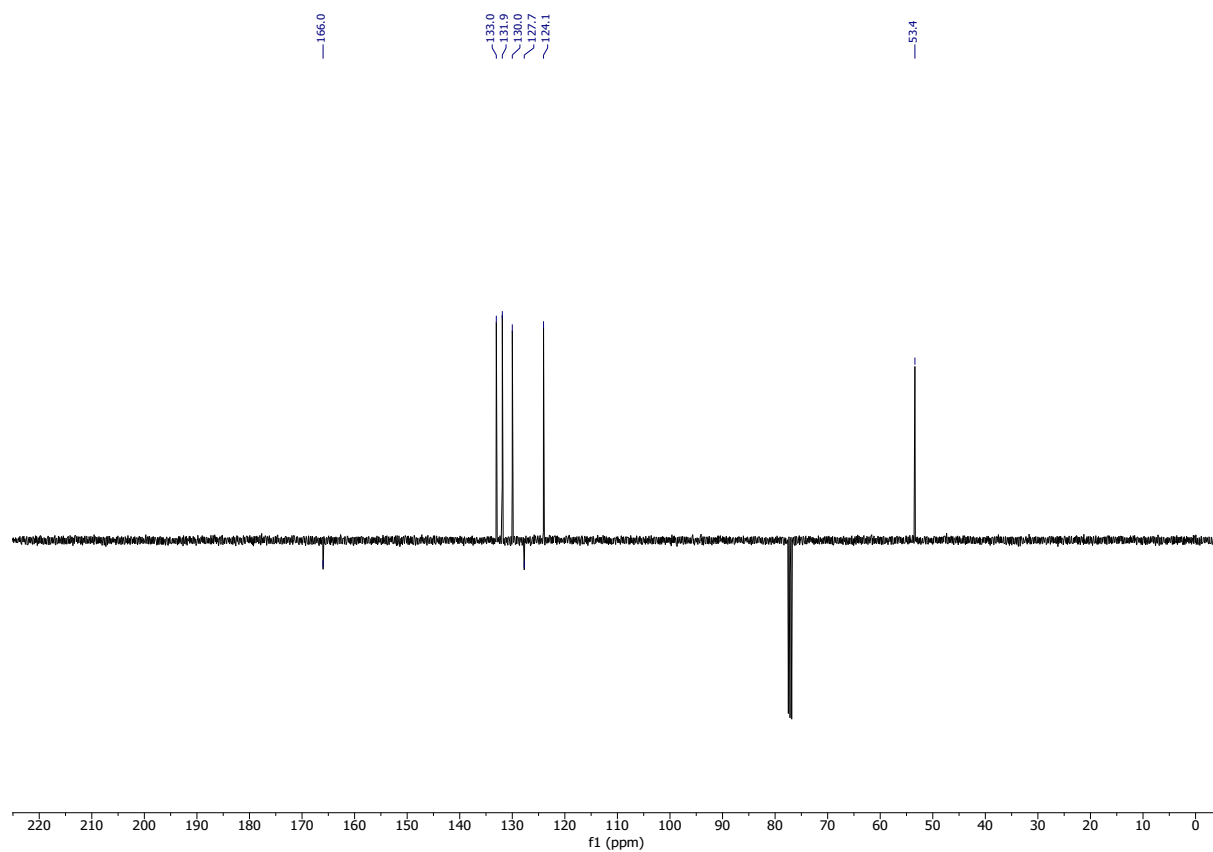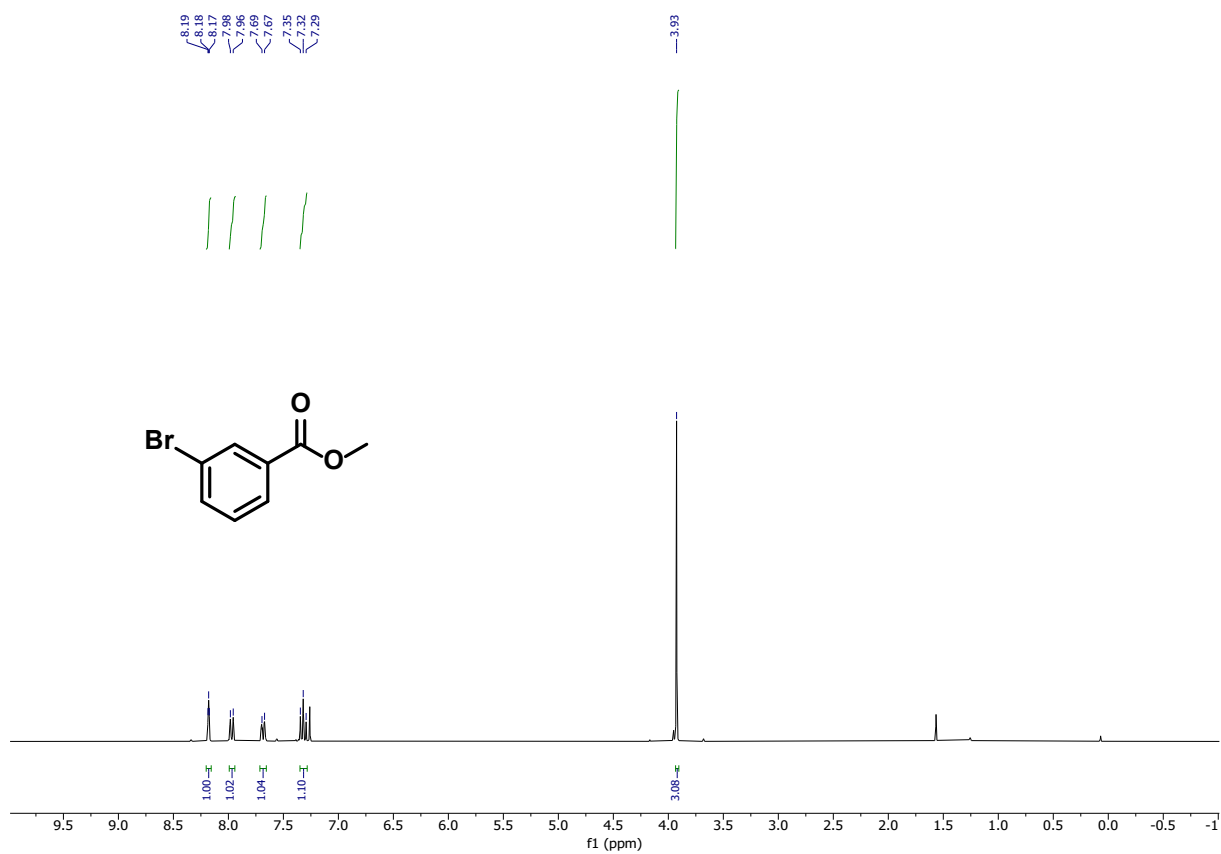
^{1}H NMR (300 MHz, CDCl$_3$) of Methyl 3-bromobenzoate (2ja).
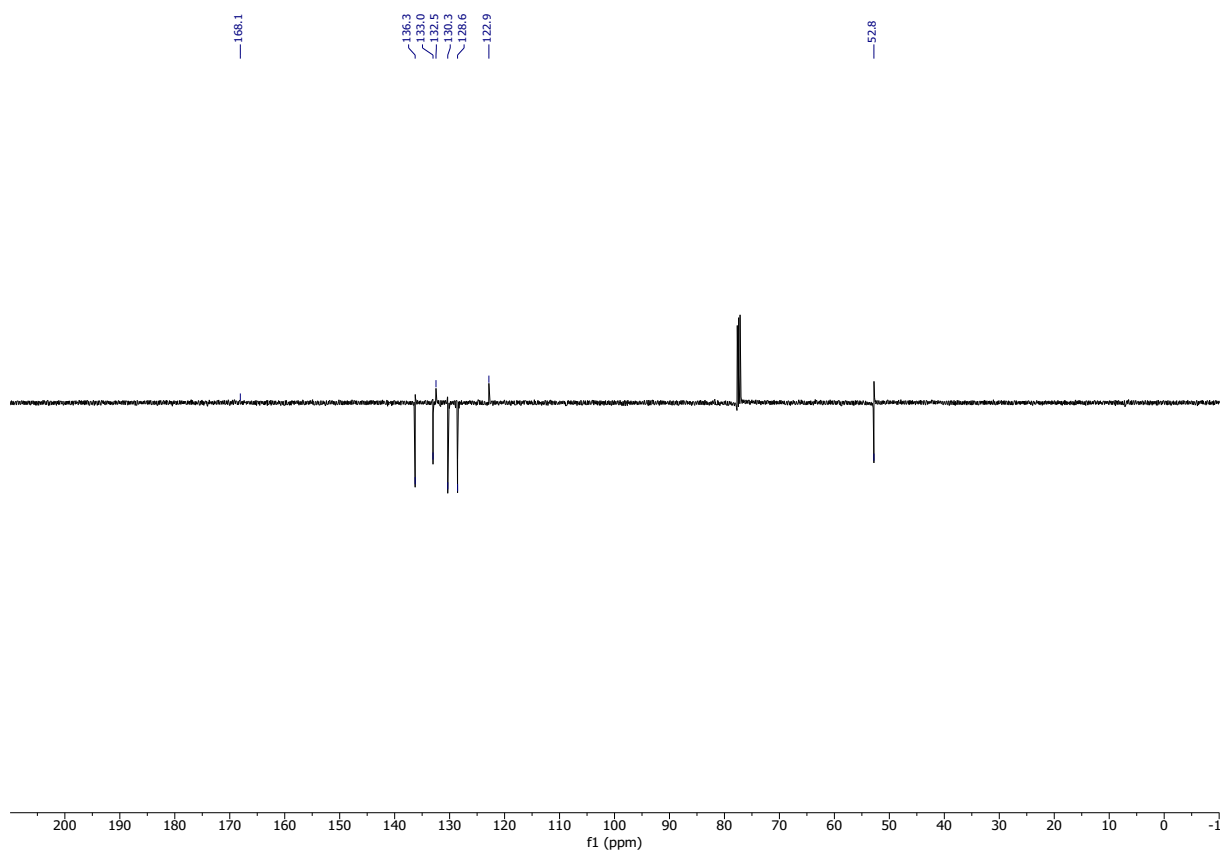
^{13}C NMR (75 MHz, CDCl$_3$) of Methyl 3-bromobenzoate.
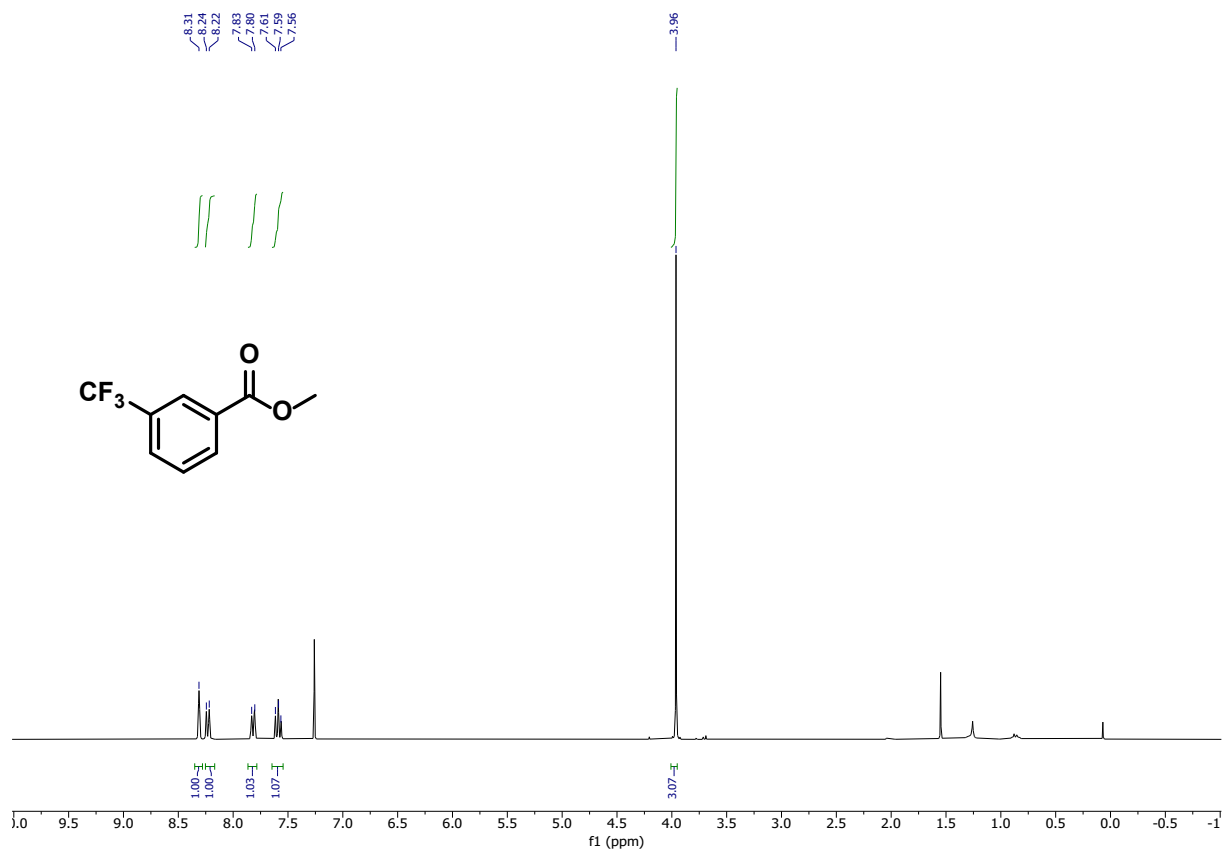
^{1}H NMR (300 MHz, CDCl$_3$) of Methyl 3-(trifluoromethyl)benzoate (2ka).
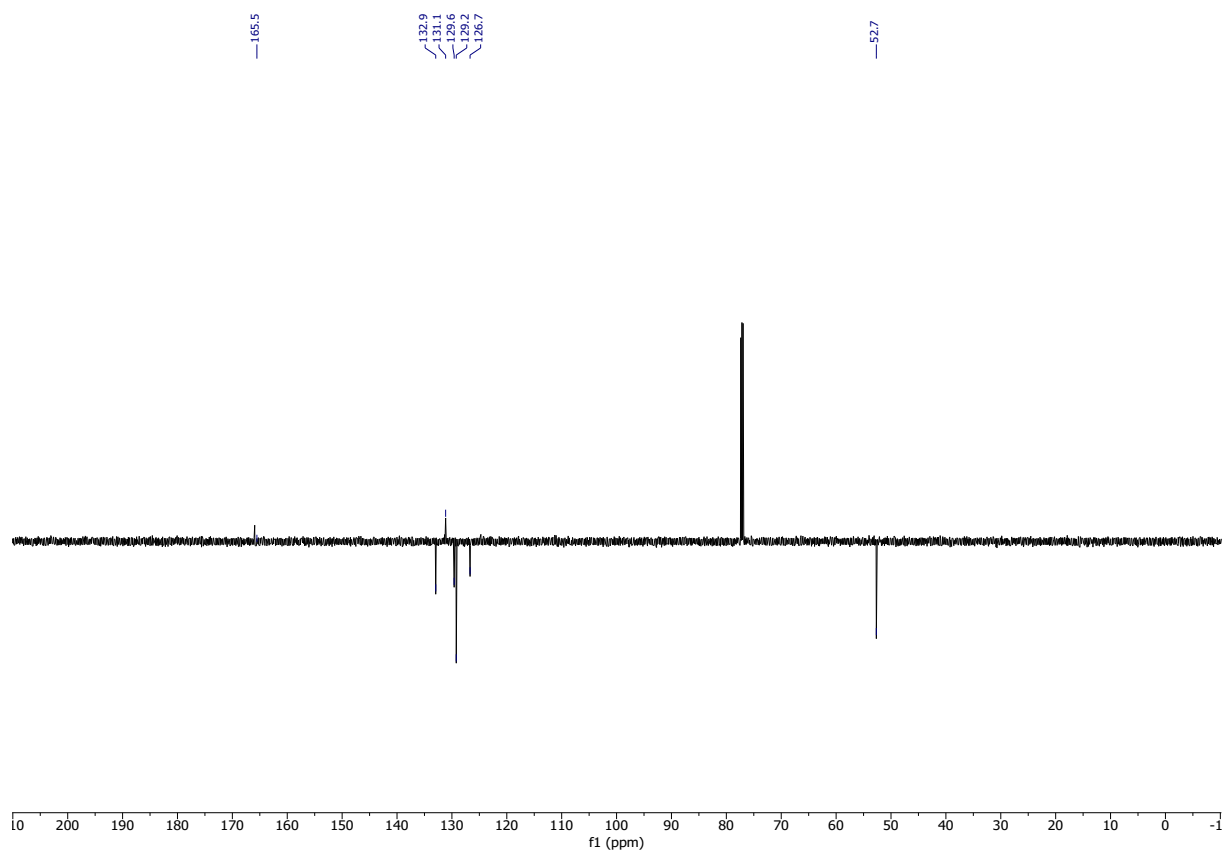
^{13}C NMR (75 MHz, CDCl$_3$) of Methyl 3-(trifluoromethyl)benzoate.
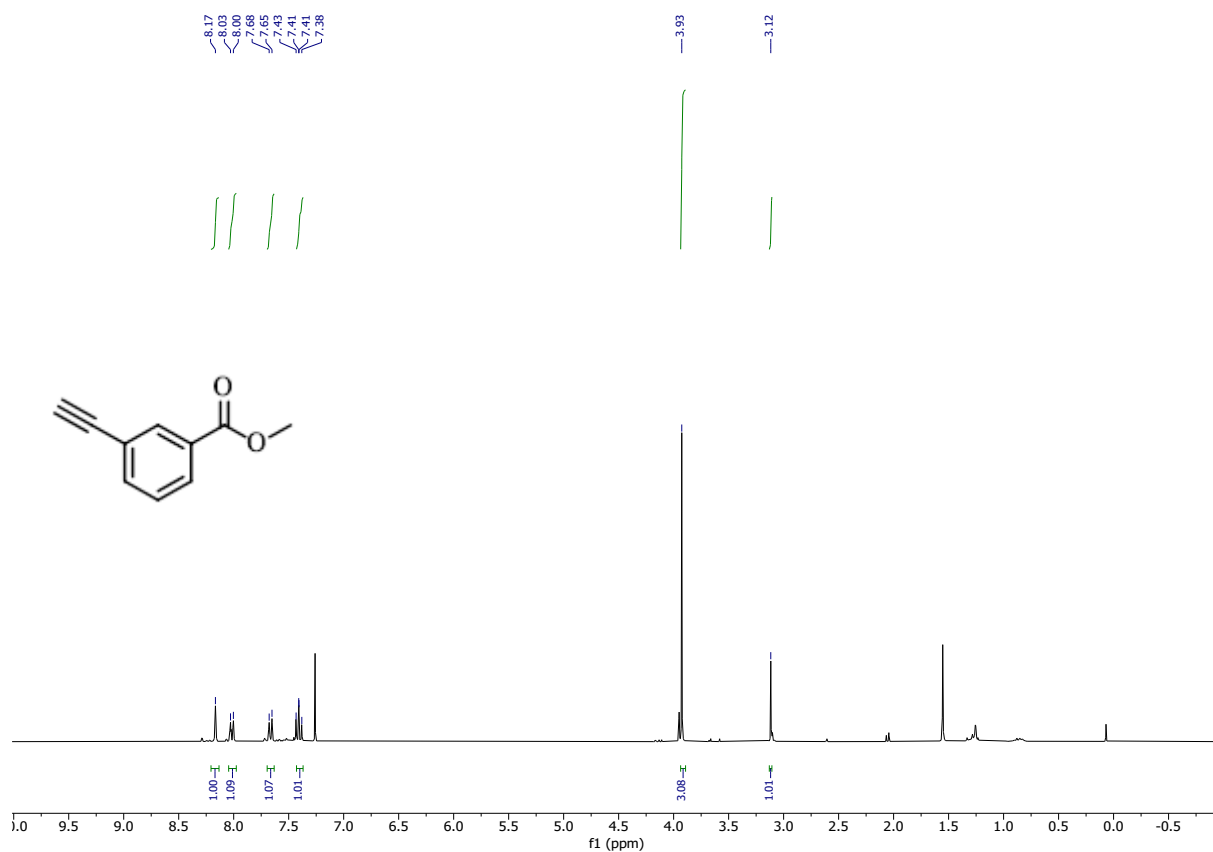
^{1}H NMR (300 MHz, CDCl$_3$) of Methyl 3-ethinylbenzoate (2la).

^{13}C NMR (75 MHz, CDCl$_3$) of Methyl 3-ethinylbenzoate.

231
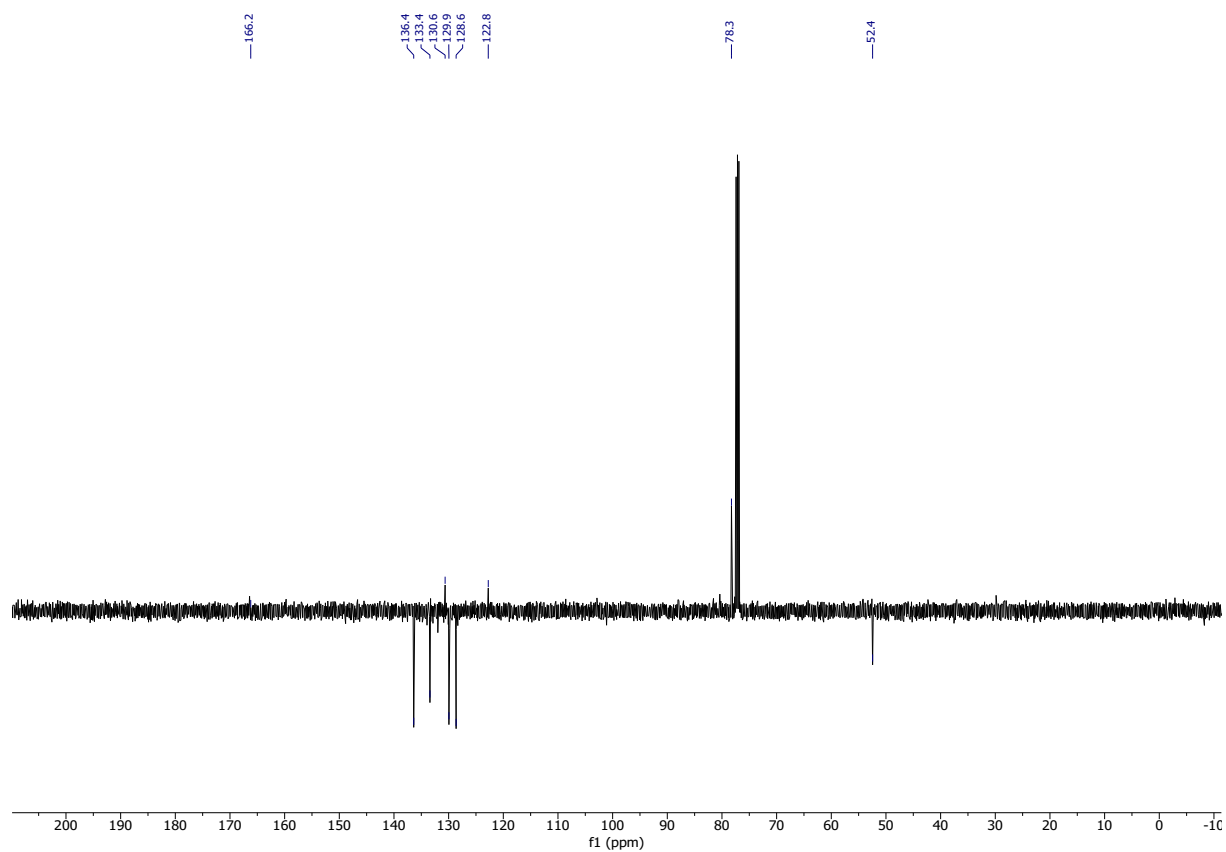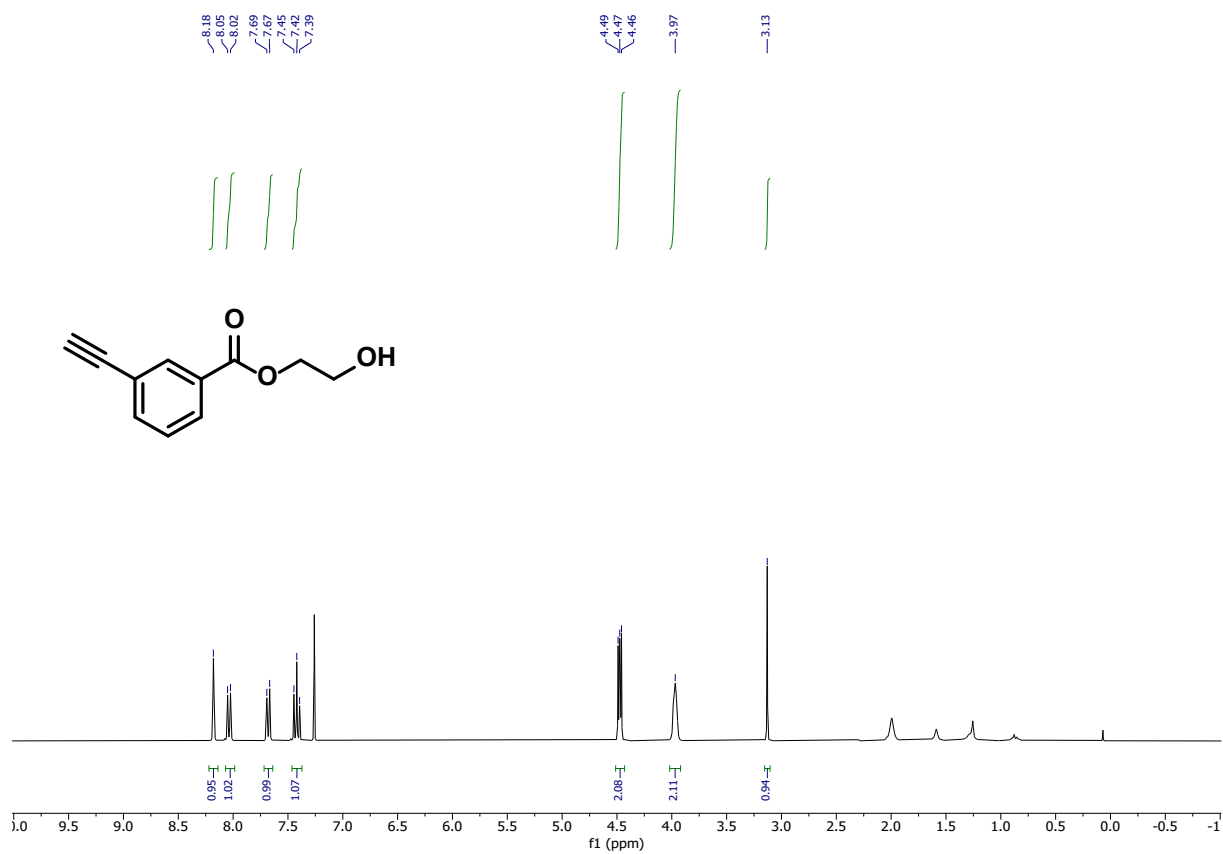
^{1}H NMR (300 MHz, CDCl$_3$) of 2-Hydroxyethyl 3-ethinylbenzoate (2lh).
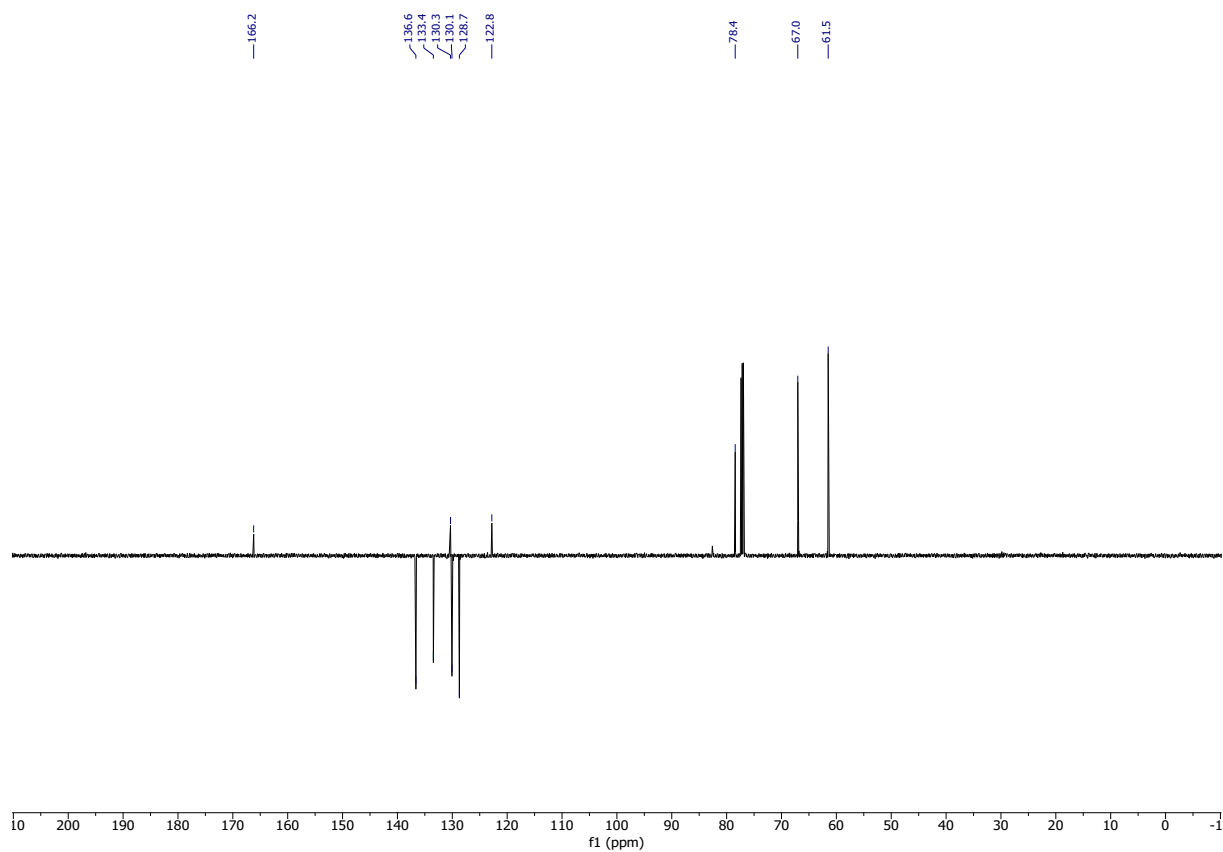
^{13}C NMR (75 MHz, CDCl$_3$) of 2-Hydroxyethyl 3-ethinylbenzoate.
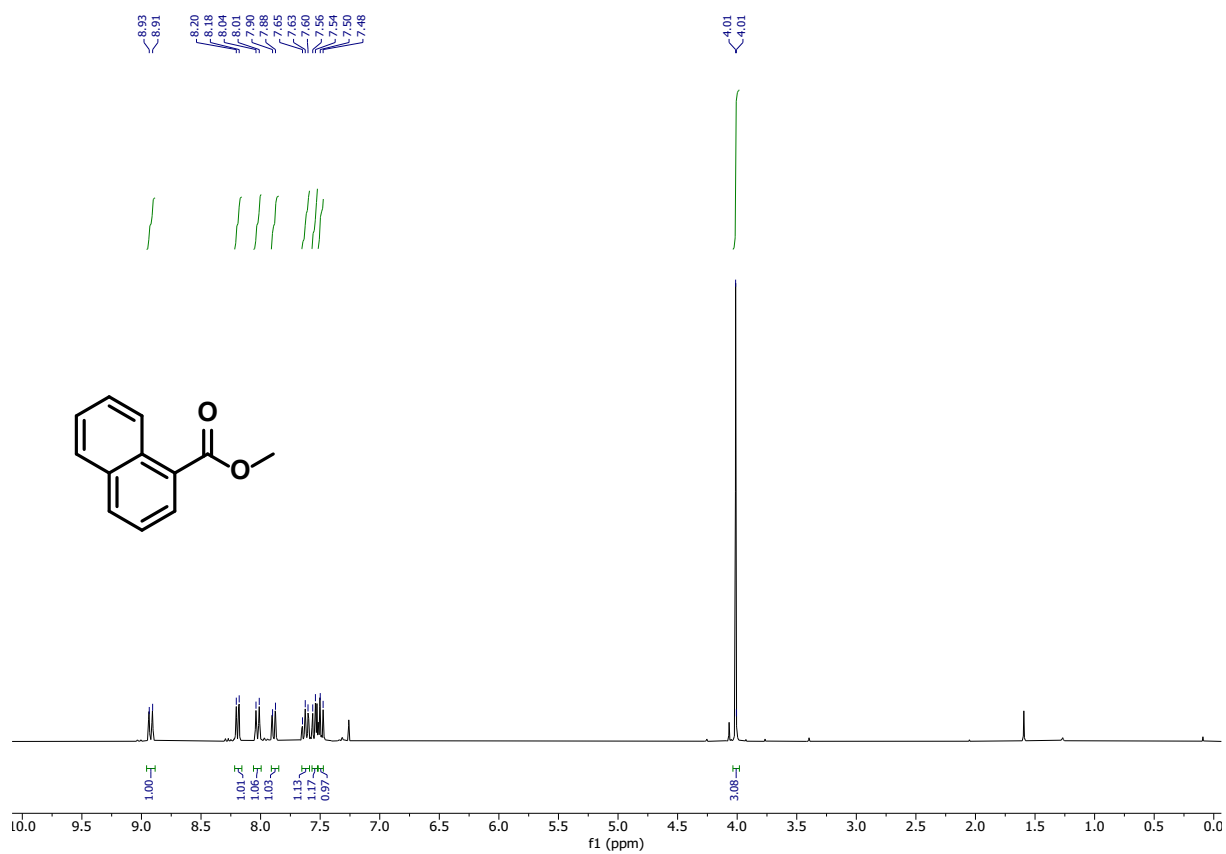
^{1}H NMR (300 MHz, CDCl$_3$) of Methyl 1-naphthoate (2ma).
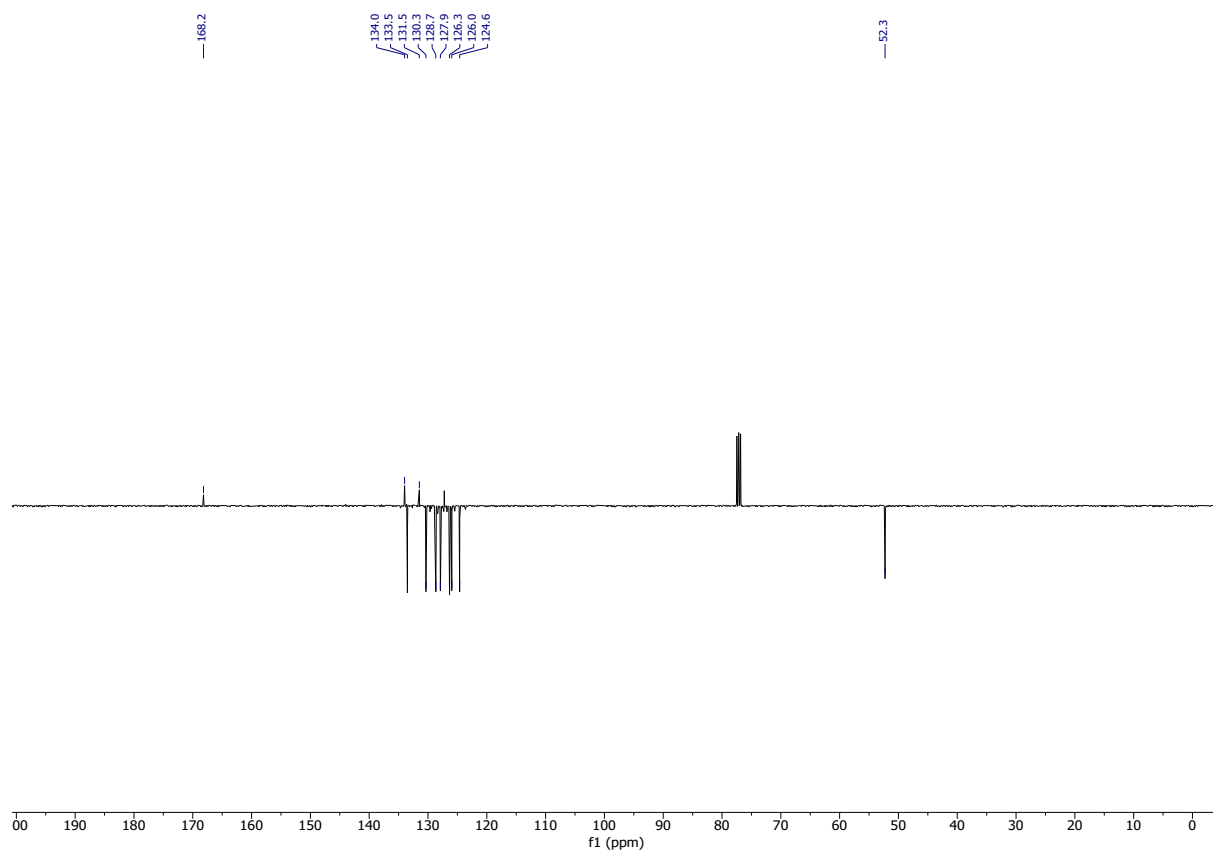
^{13}C NMR (75 MHz, CDCl$_3$) of Methyl 1-naphthoate.
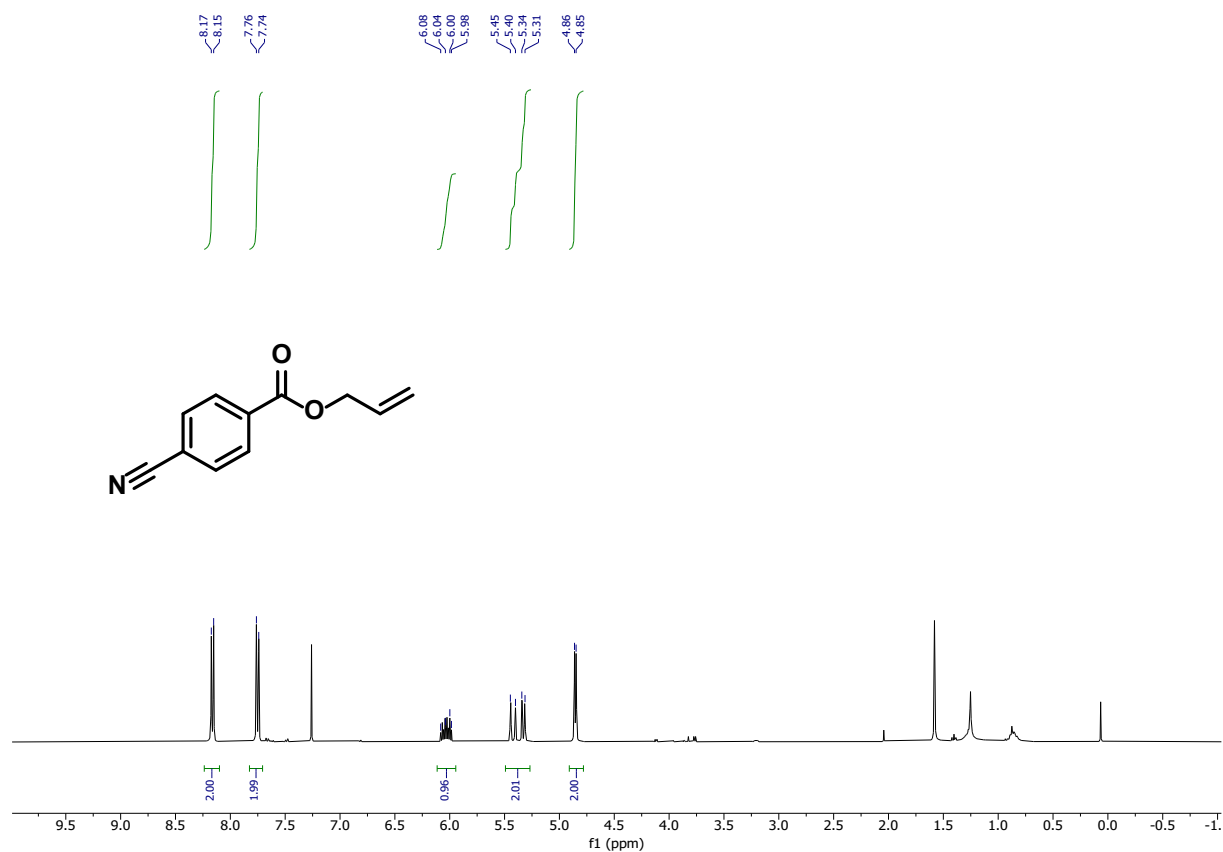
^{1}H NMR (300 MHz, CDCl₃) of Allyl 4-cyanobenzoate (di).
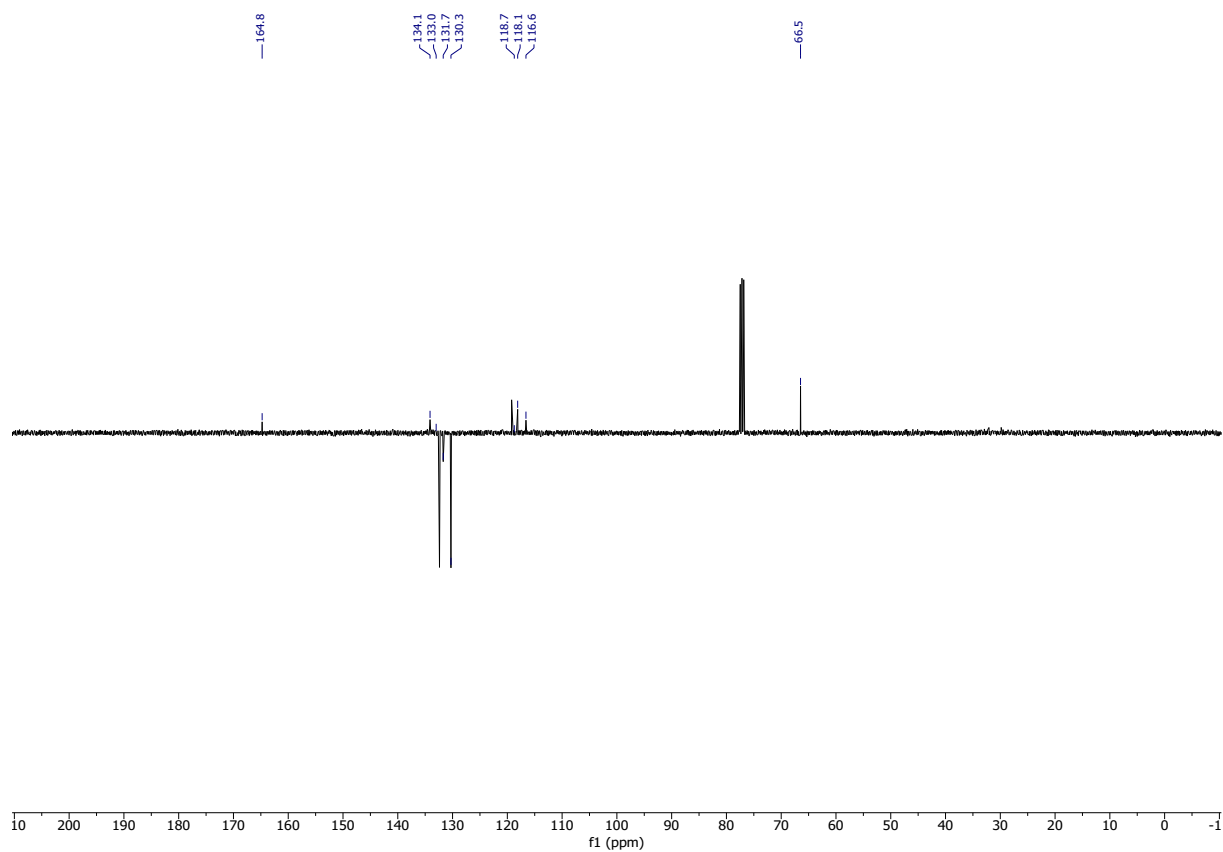
^{13}C NMR (75 MHz, CDCl₃) of Allyl 4-cyanobenzoate.
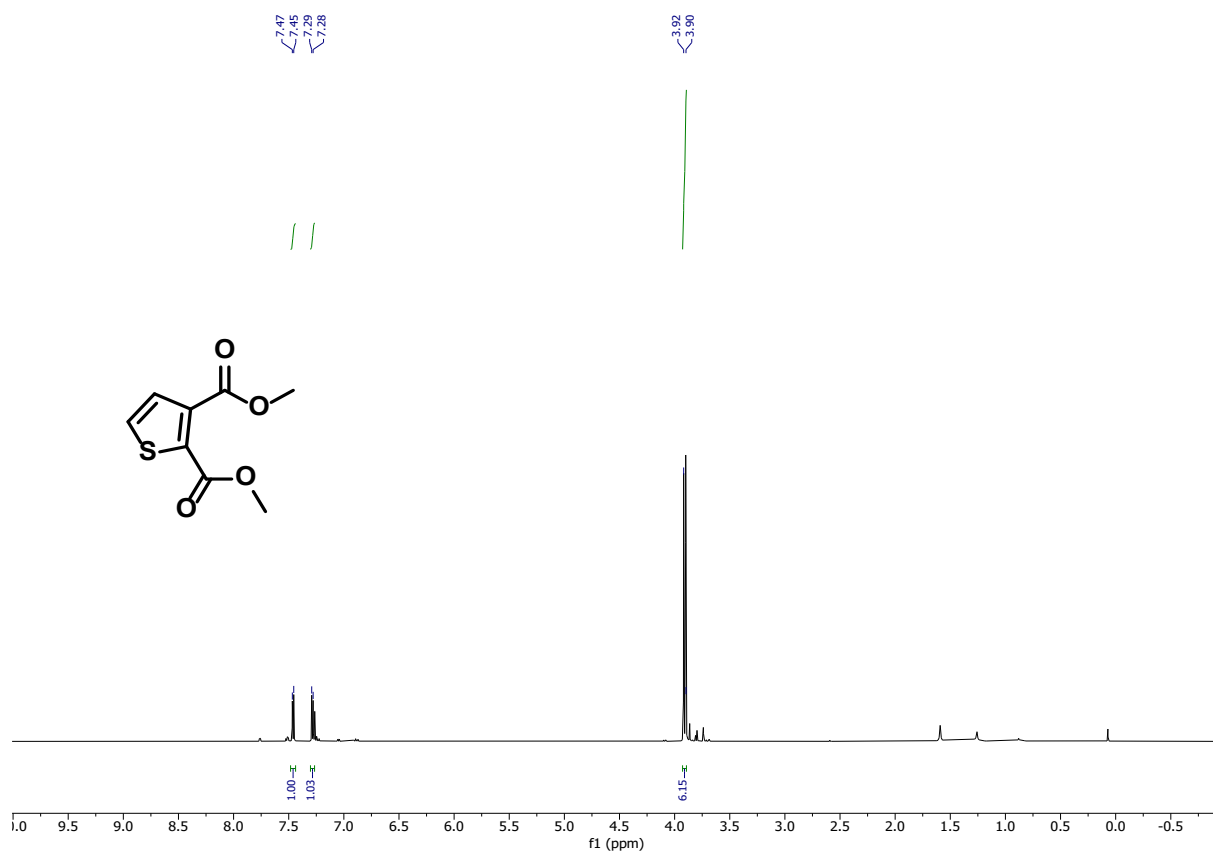
^{1}H NMR (300 MHz, CDCl$_3$) of Dimethyl 2,3-thiophendicarboxylate (2na).
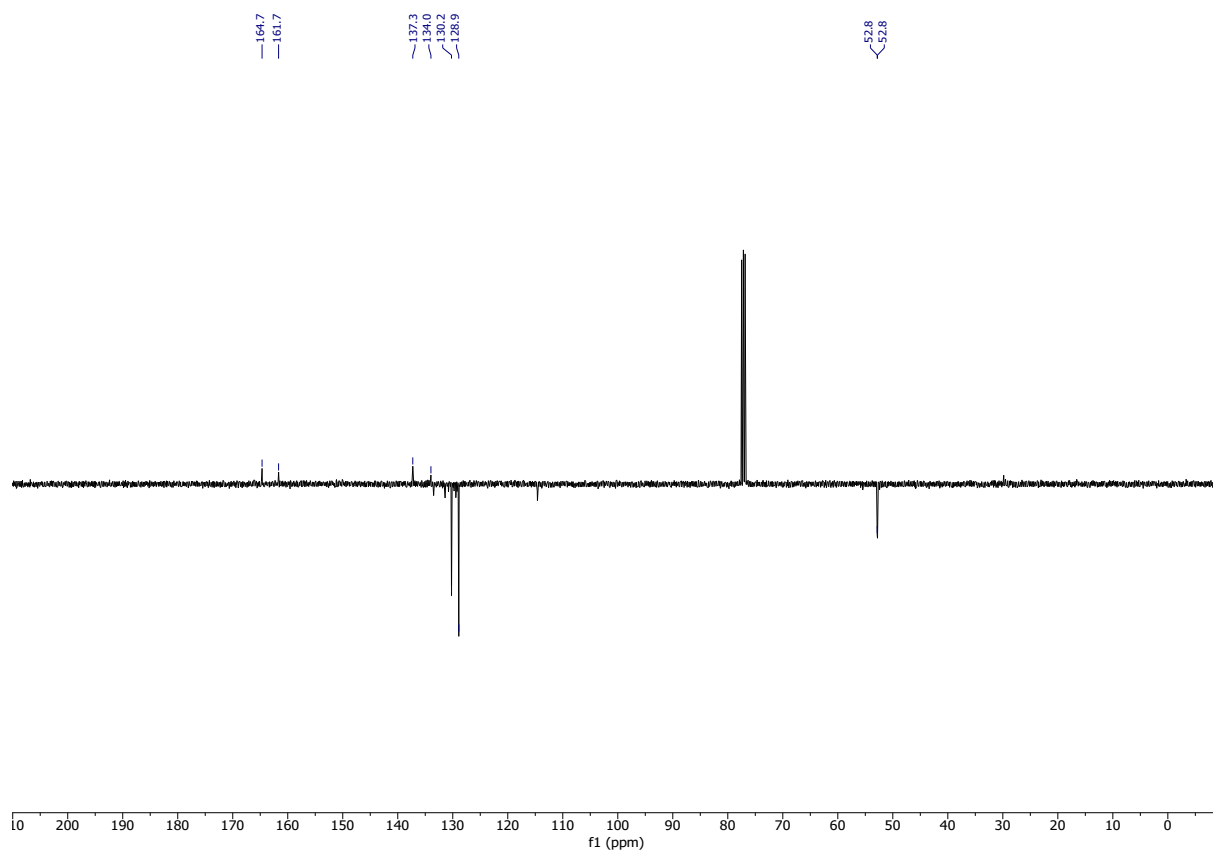
^{13}C NMR (75 MHz, CDCl$_3$) of Dimethyl 2,3-thiophendicarboxylate.
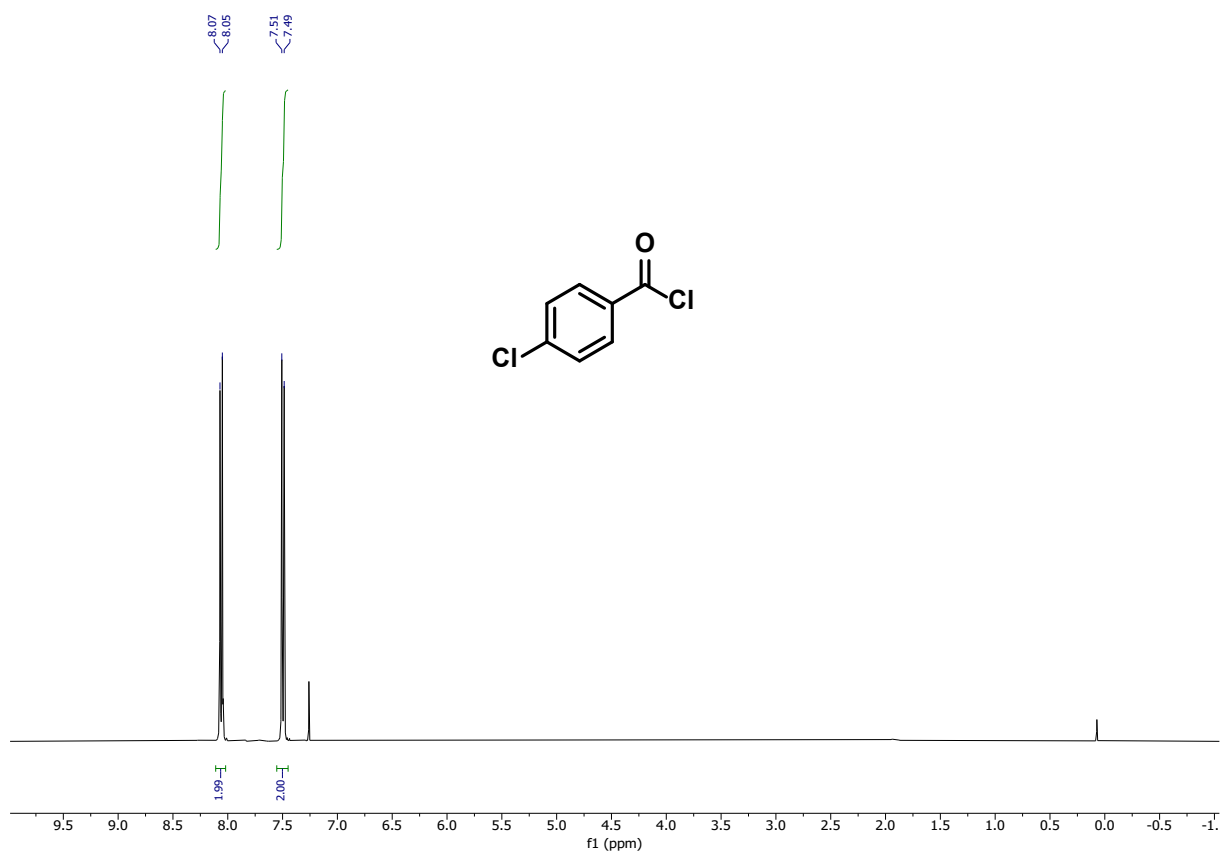
^{1}H NMR (300 MHz, CDCl$_3$) of 4-Chlorobenzoyl chloride (2cq).
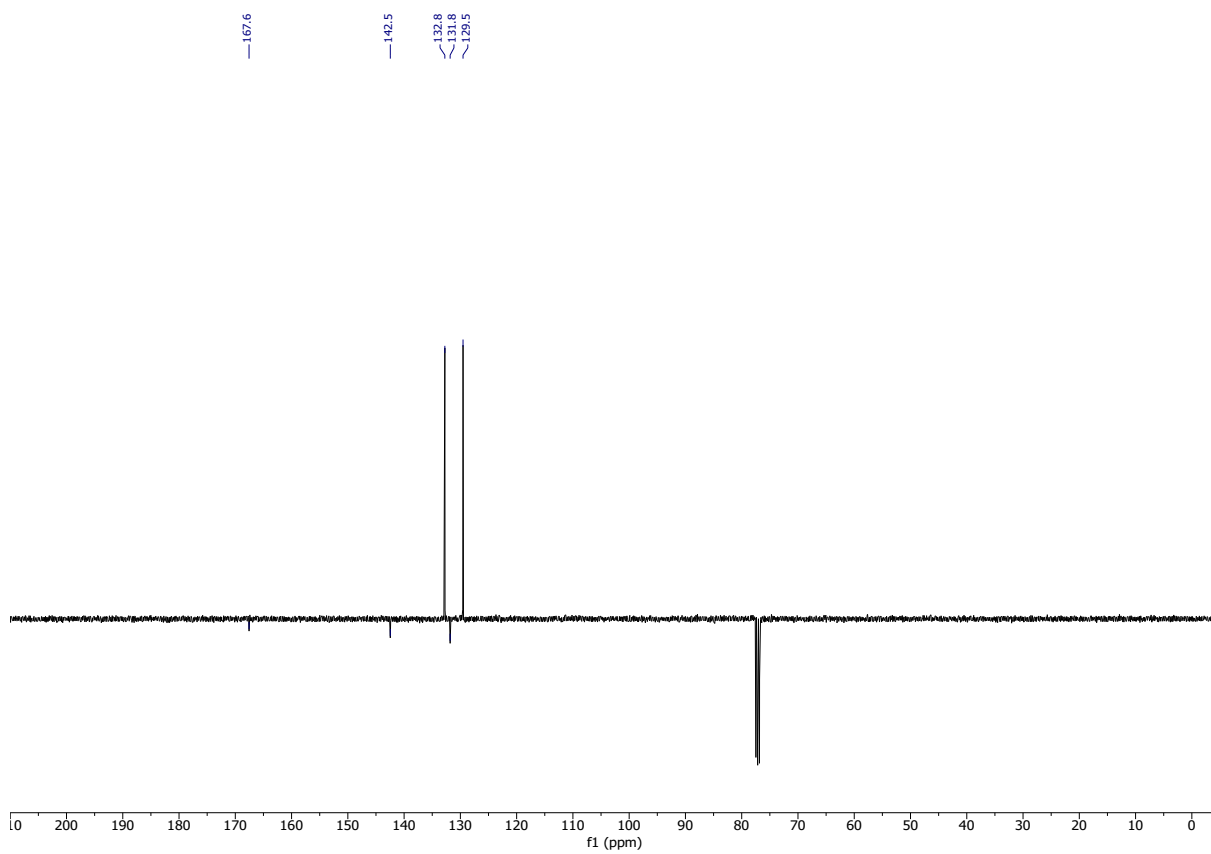
^{13}C NMR (75 MHz, CDCl$_3$) of 4-Chlorobenzoyl chloride.
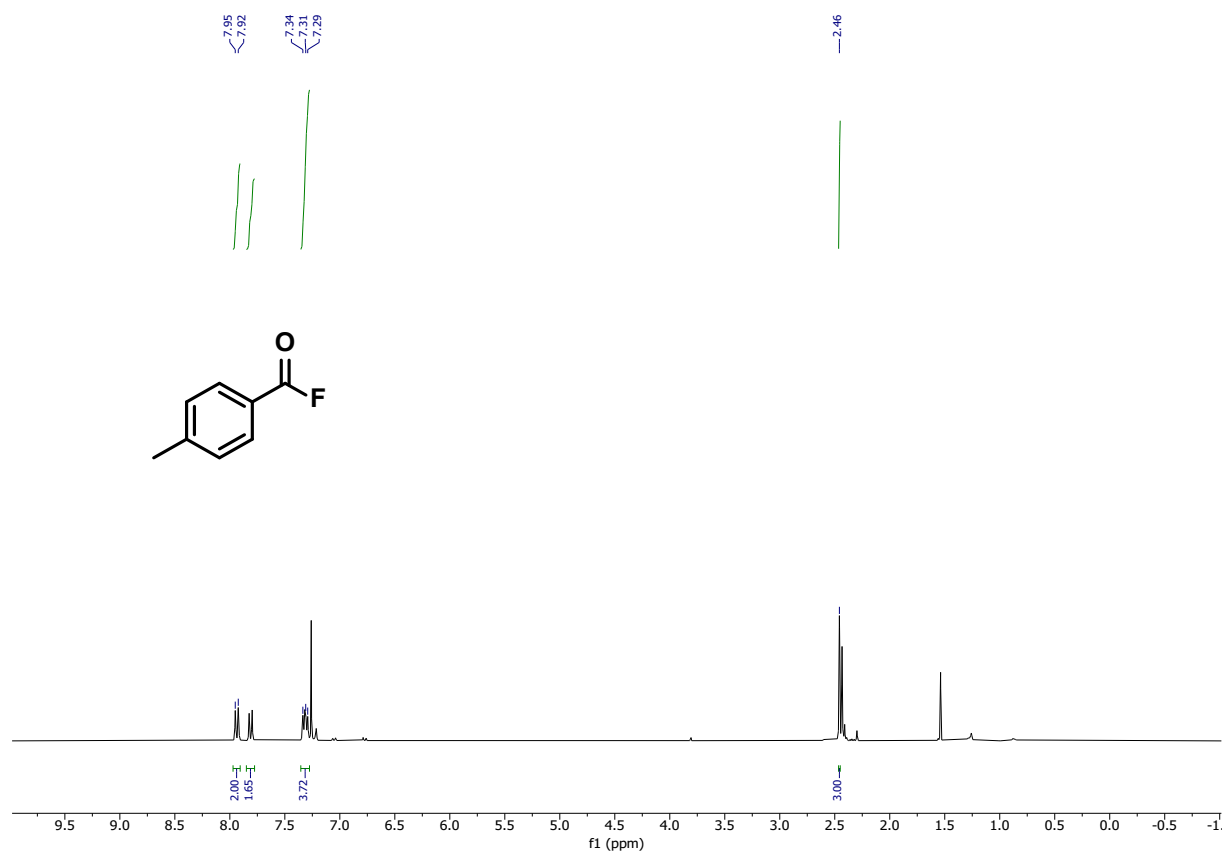
¹H NMR (300 MHz, CDCl₃) of 4-Methylbenzoyl fluoride (2bK), unidentified contamination.
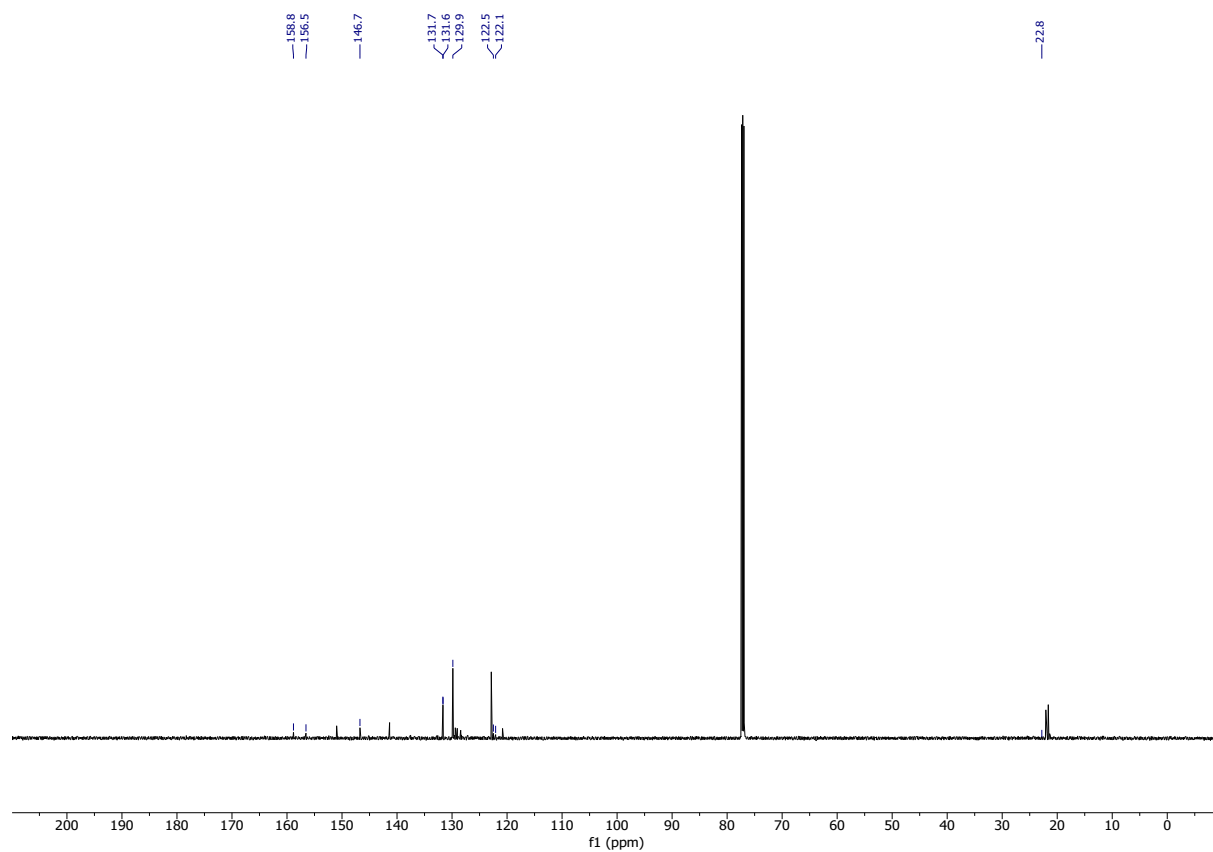
¹³C NMR (151 MHz, CDCl₃) of 4-Methylbenzoyl fluoride (2bK), unidentified contamination.
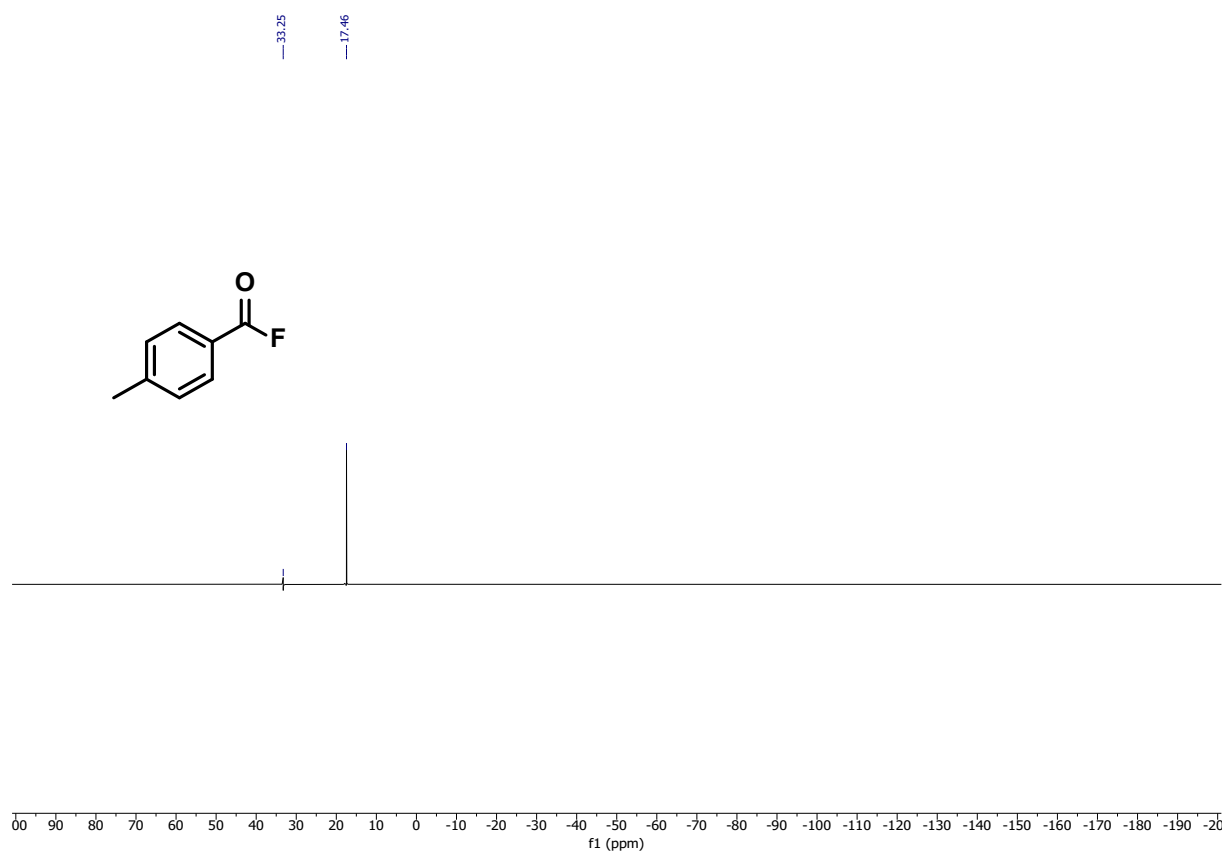
^{19}F NMR (565 MHz, CDCl$_3$) of 4-Methylbenzoyl fluoride (2bK), unidentified contamination.
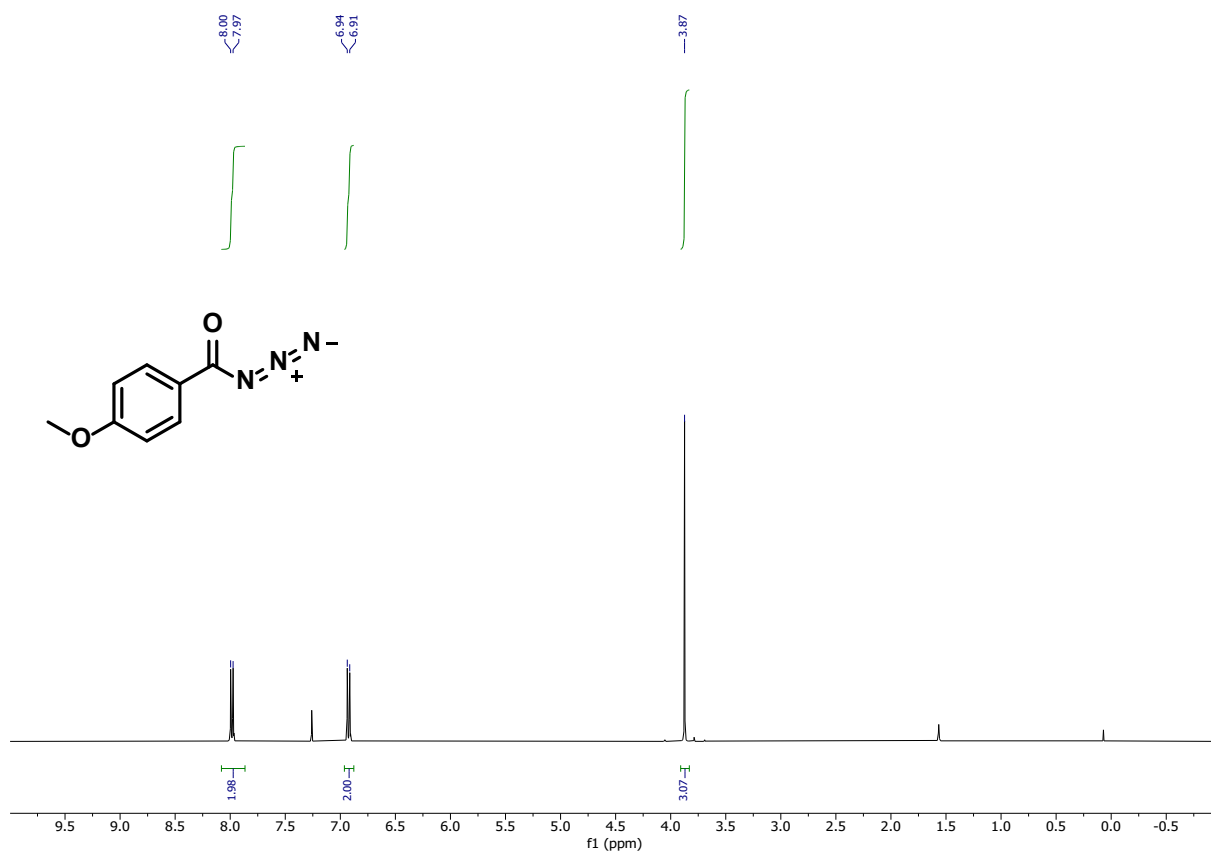
^{1}H NMR (300 MHz, CDCl$_3$) of 4-Methoxybenzoyl azide (2as).
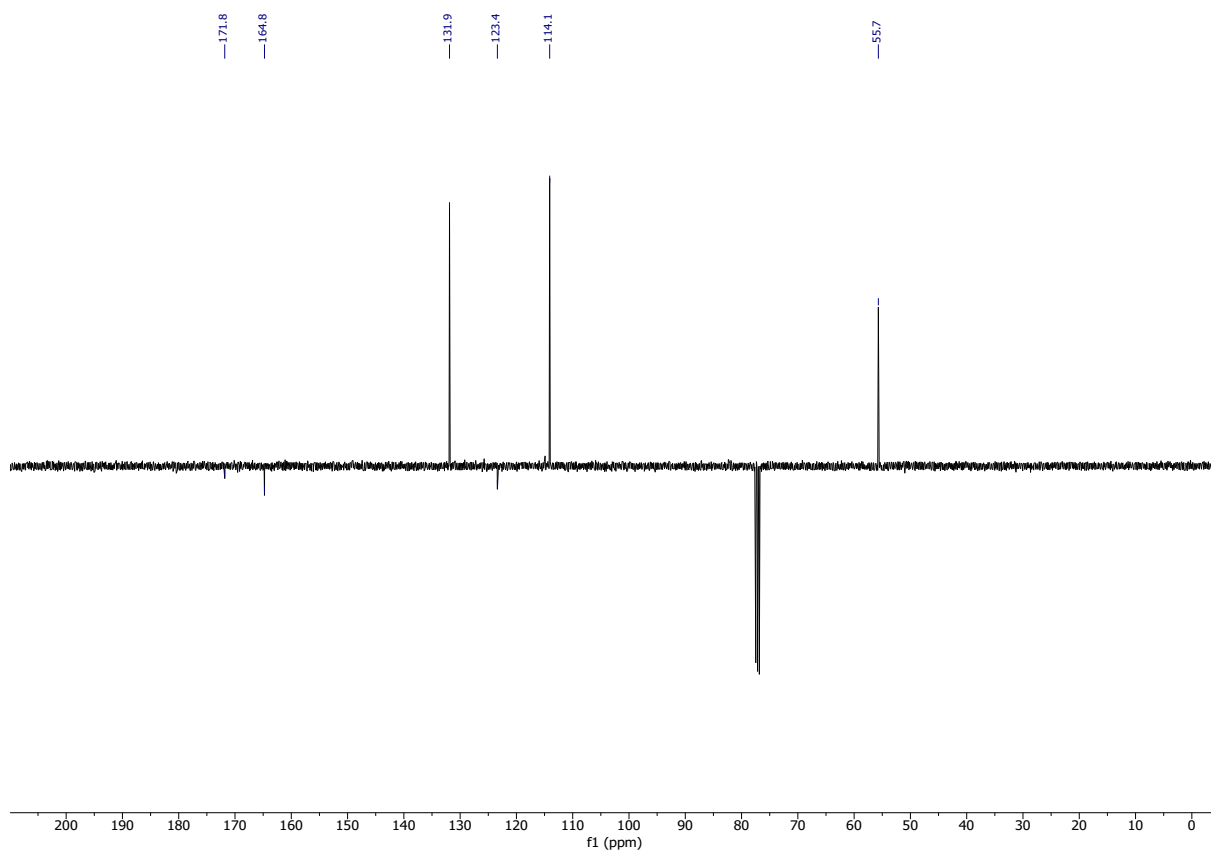
^{13}C NMR (75 MHz, CDCl$_3$) of 4-Methoxybenzoyl azide.
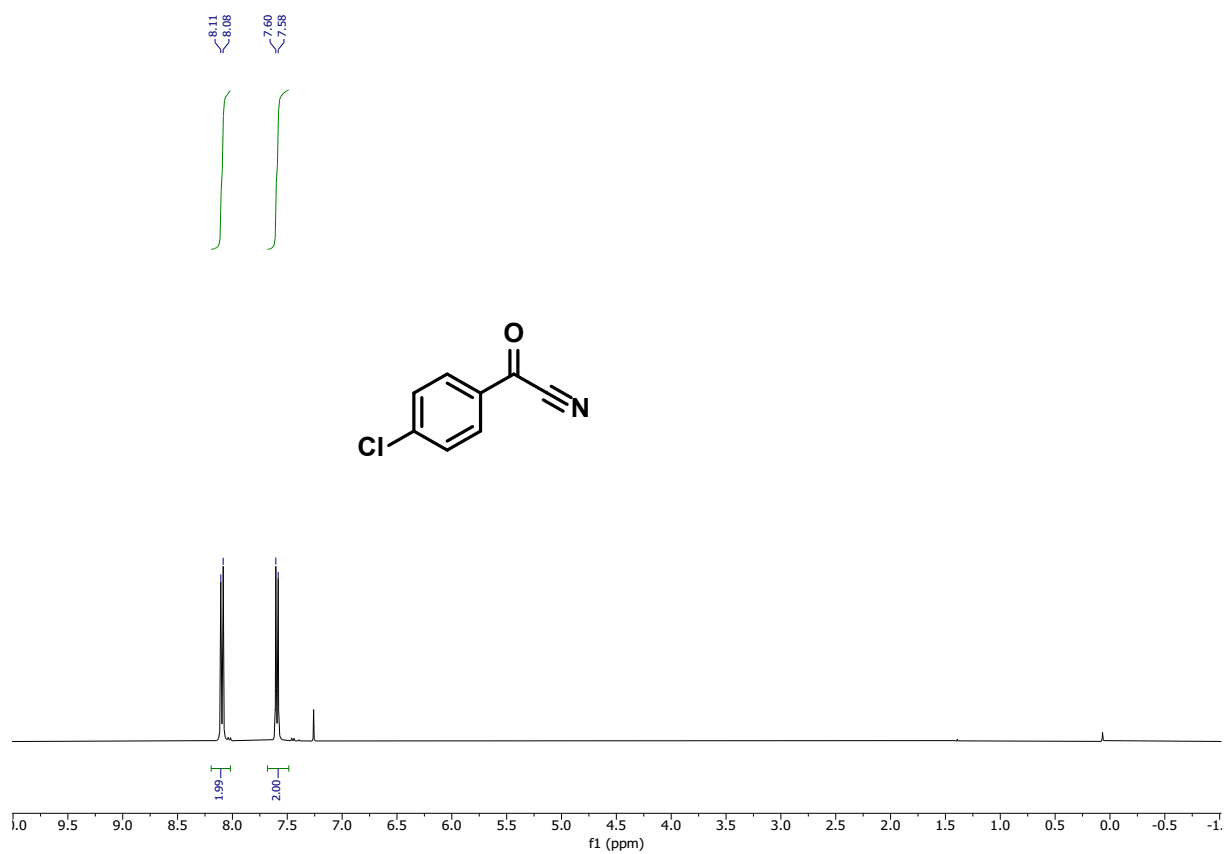
^{1}H NMR (300 MHz, CDCl$_3$) of 4-Chlorobenzoyl cyanide (2cr).
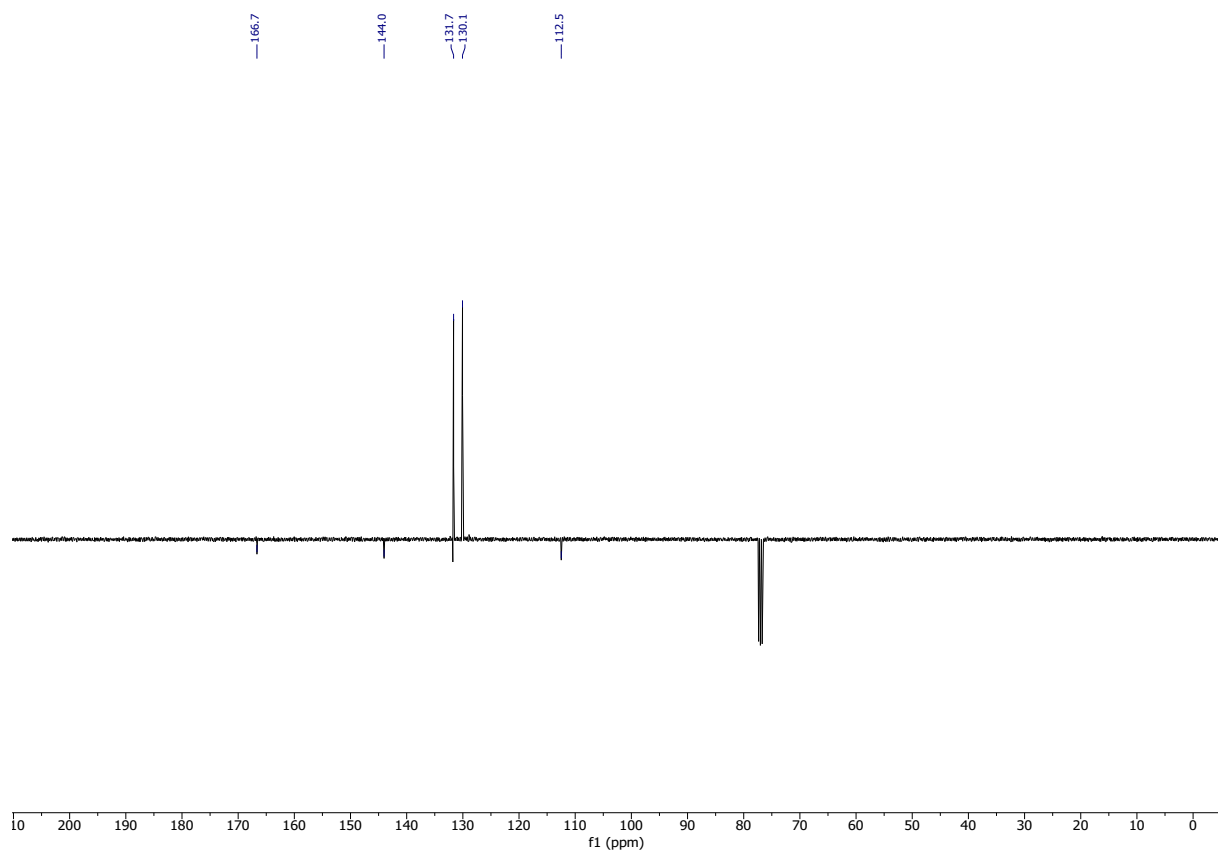
^{13}C NMR (75 MHz, CDCl$_3$) of 4-Chlorobenzoyl cyanide.
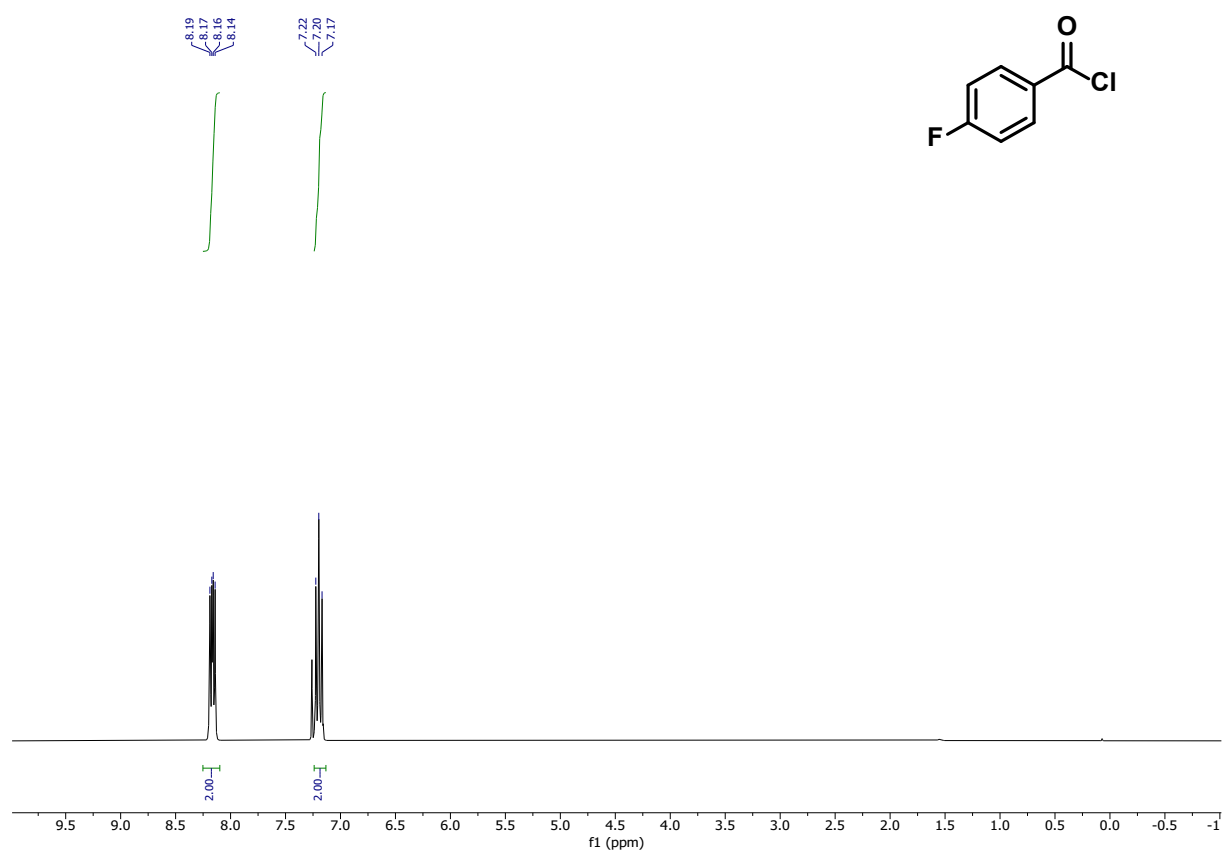
^{1}H NMR (300 MHz, CDCl$_3$) of 4-Fluorobenzoyl chloride (2eq).

^{13}C NMR (75 MHz, CDCl$_3$) of 4-Fluorobenzoyl chloride (2eq).

-100.80

60 50 40 30 20 10 0 -10 -20 -30 -40 -50 -60 -70 -80 -90 -100 -110 -120 -130 -140 -150 -160
f1 (ppm)
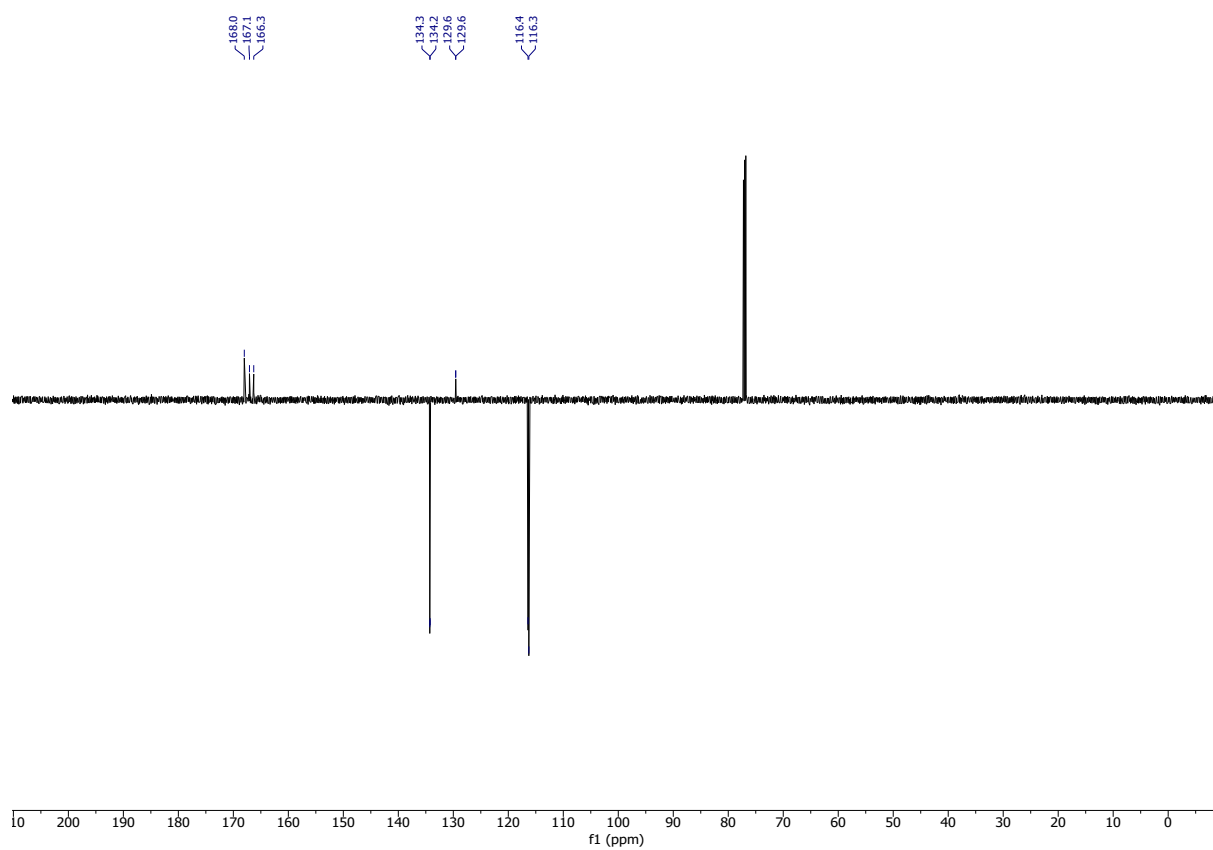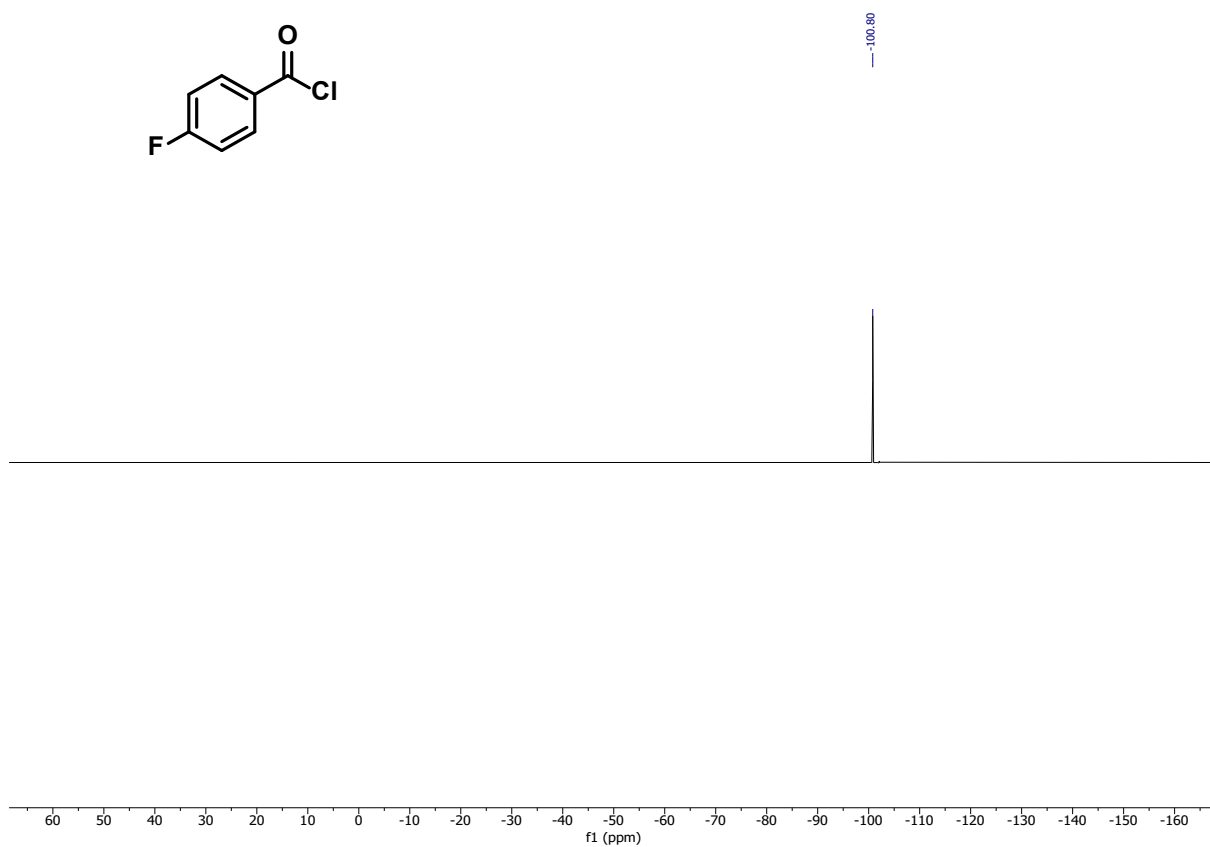
^{19}F NMR (565 MHz, CDCl$_3$) of 4-Fluorobenzoyl chloride (2eq).
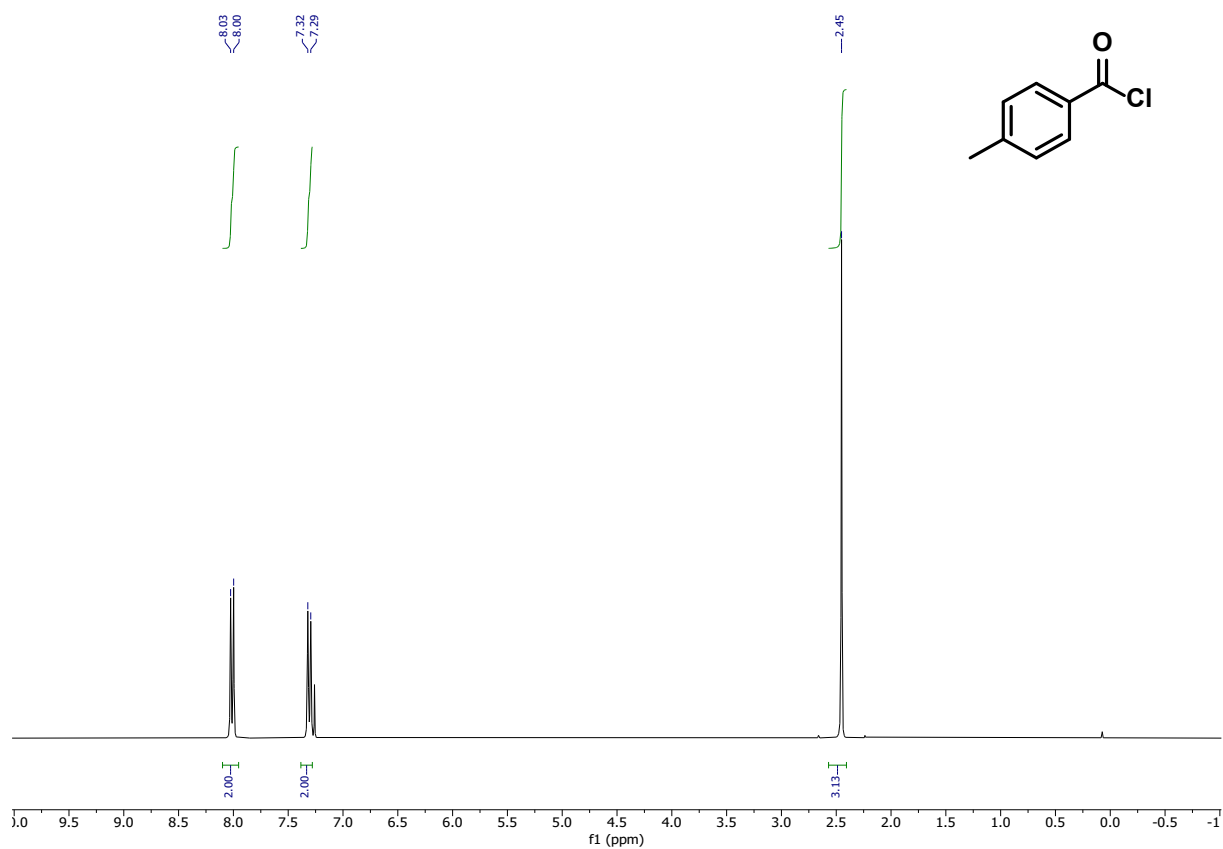
¹H NMR (300 MHz, CDCl₃) of 4-Methylbenzoyl chloride (2bq).
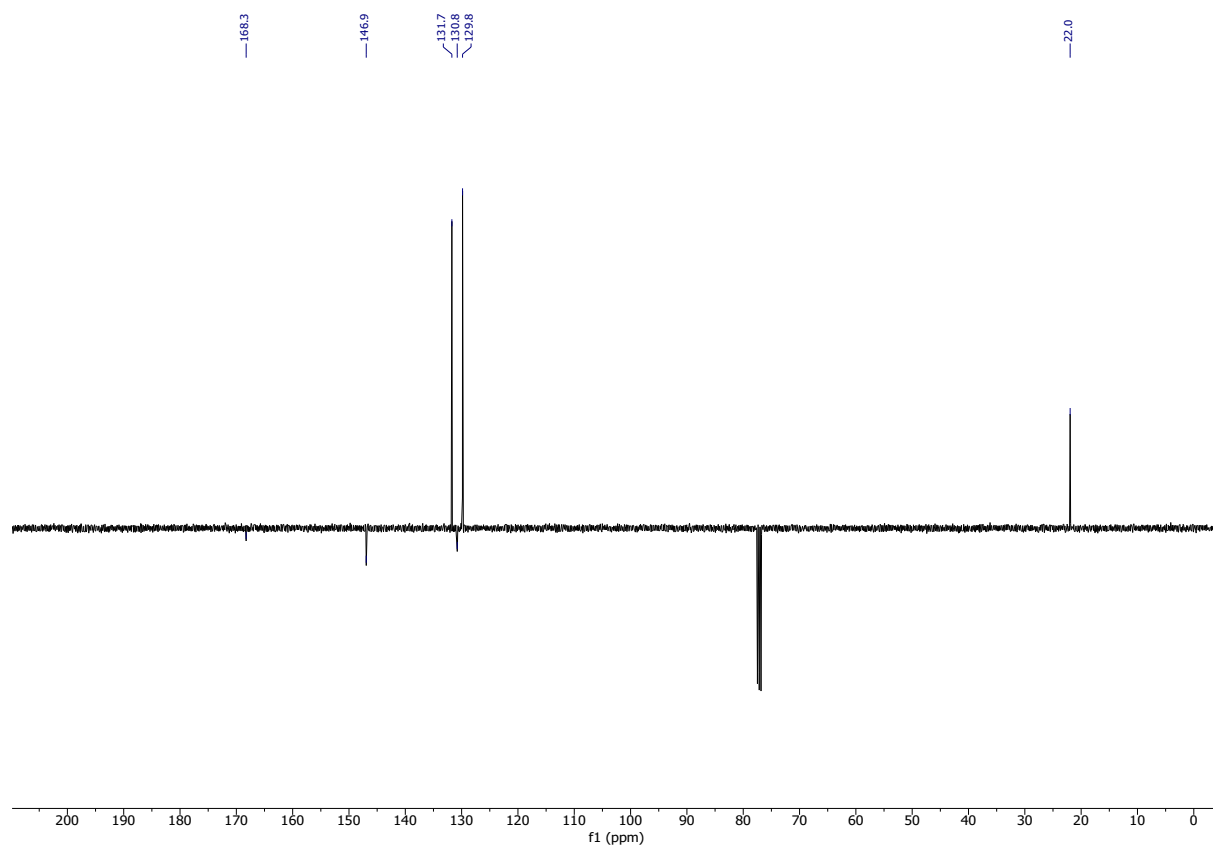
¹³C NMR (75 MHz, CDCl₃) of 4-Methylbenzoyl chloride (2bq).
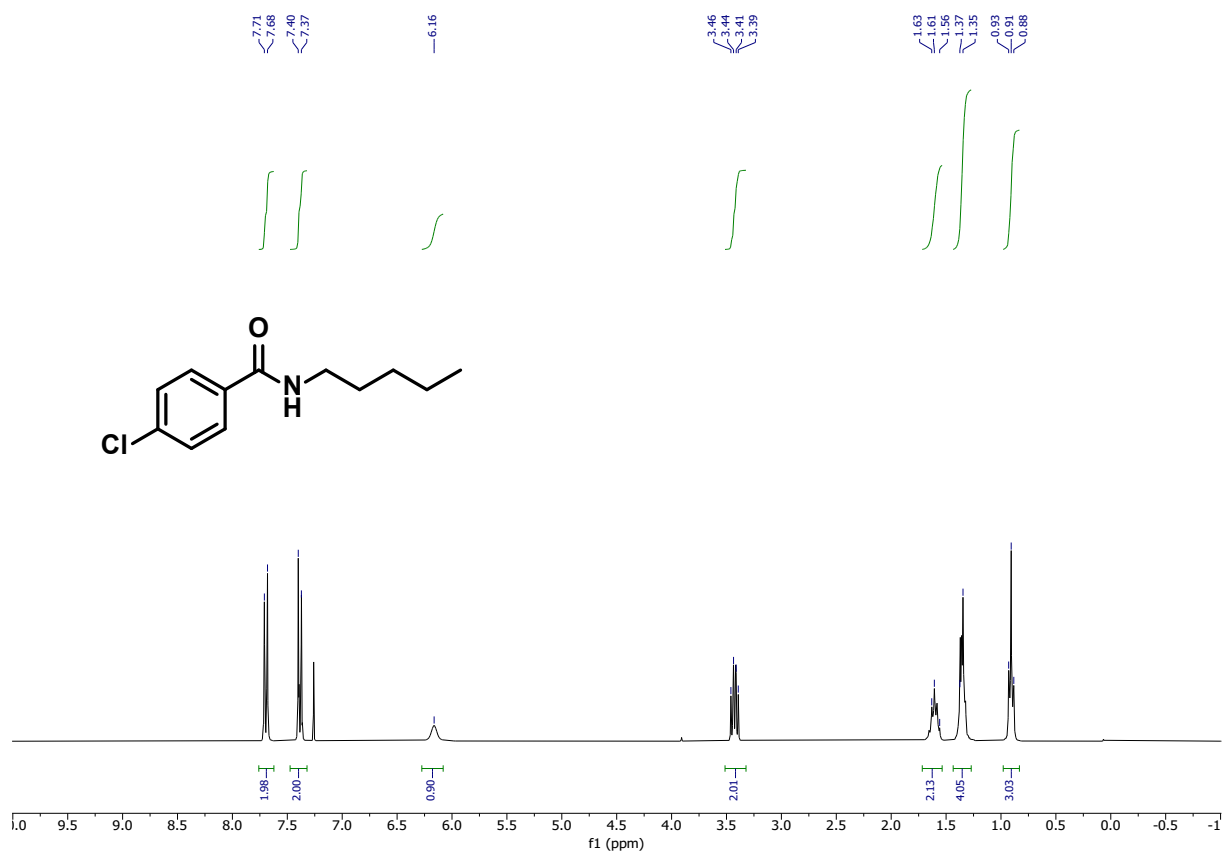
¹H NMR (300 MHz, CDCl₃) of *N*-Pentyl-4-chlorobenzamide (2ct).
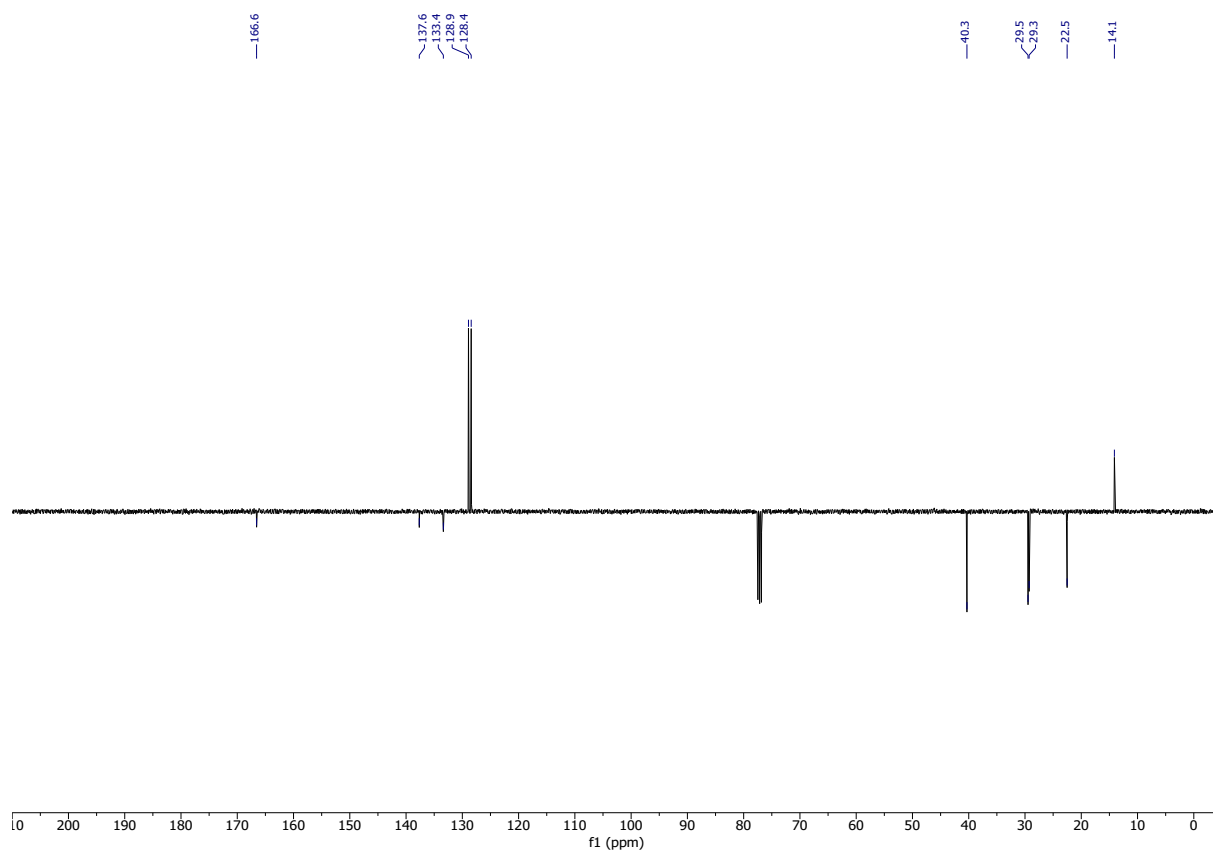
¹³C NMR (75 MHz, CDCl₃) of *N*-Pentyl-4-chlorobenzamide.

244

^{1}H NMR (300 MHz, CDCl₃) of 2-(Diethylamino)ethyl 4-[(4-chlorobenzoyl)amino]benzoate (2cu).

^{13}C NMR (75 MHz, CDCl₃) of 2-(Diethylamino)ethyl 4-[(4-chlorobenzoyl)amino]benzoate.
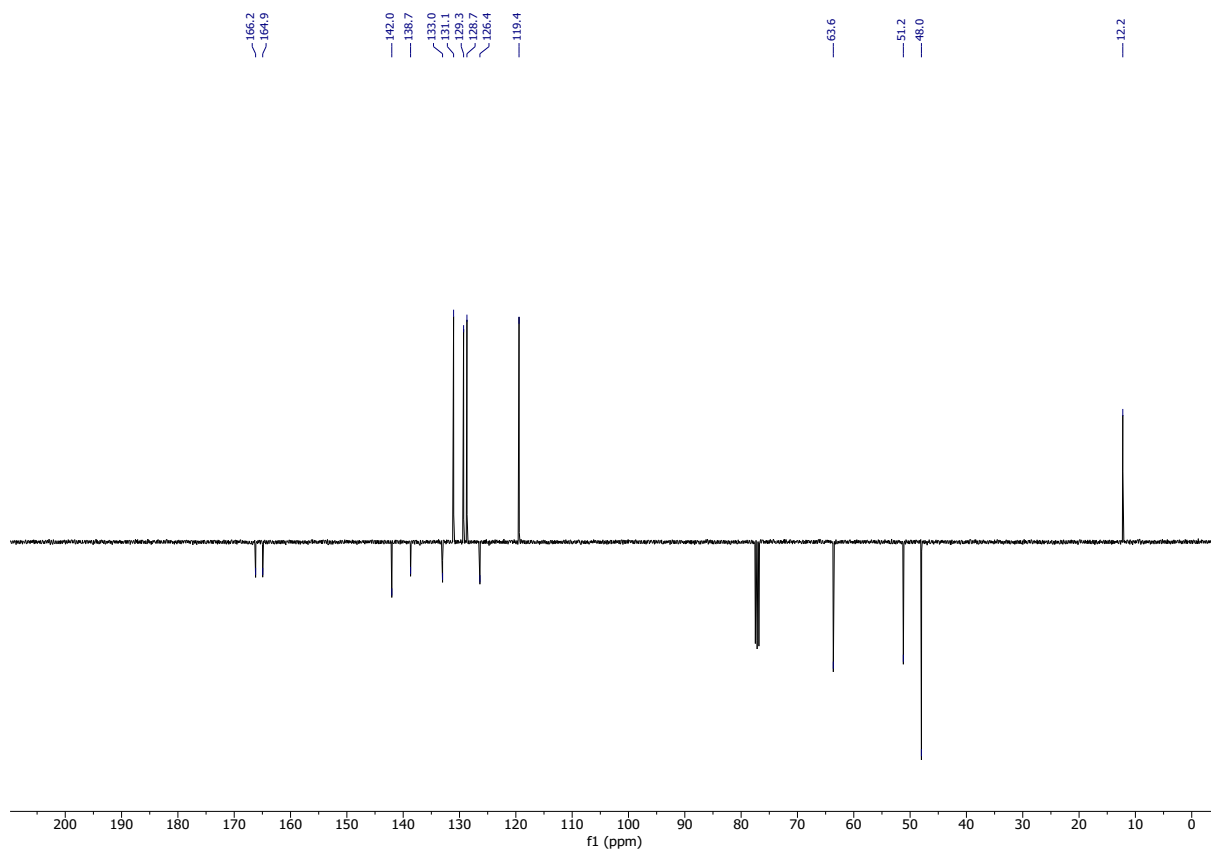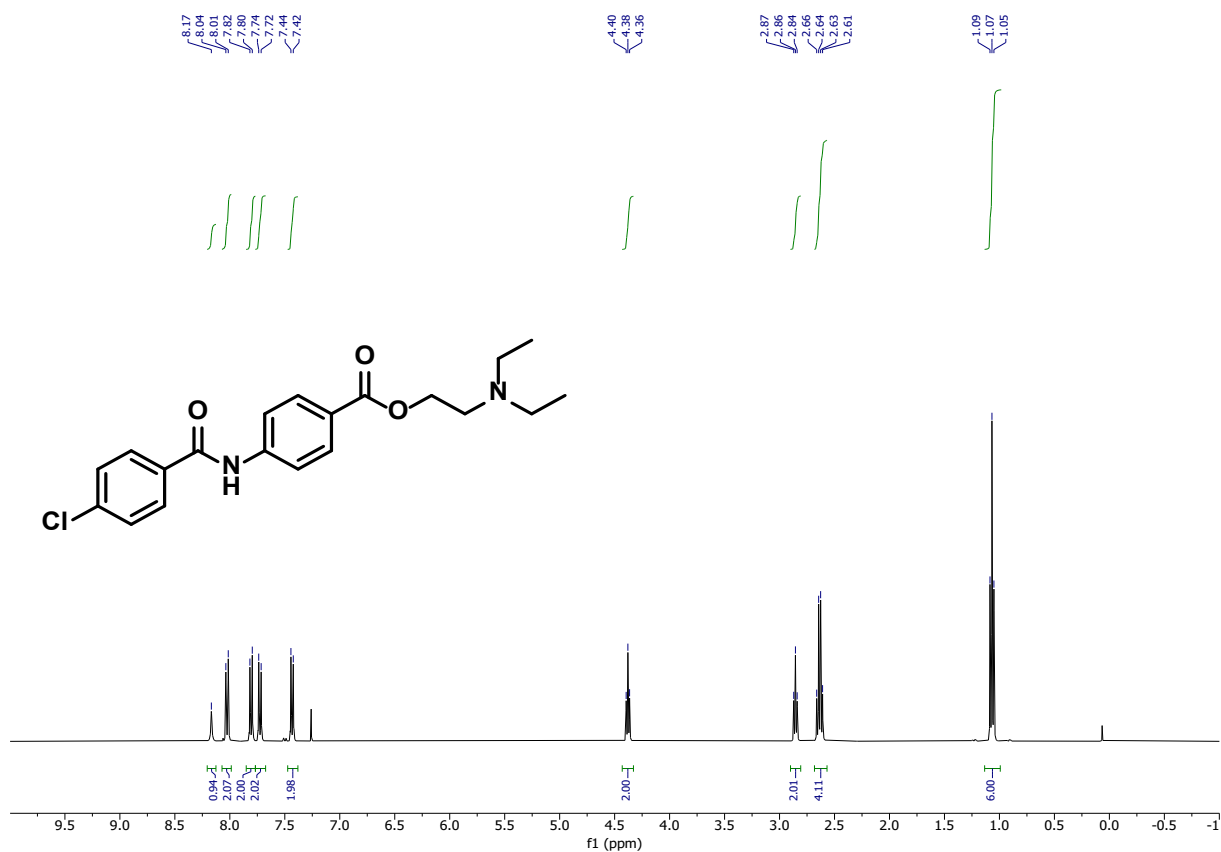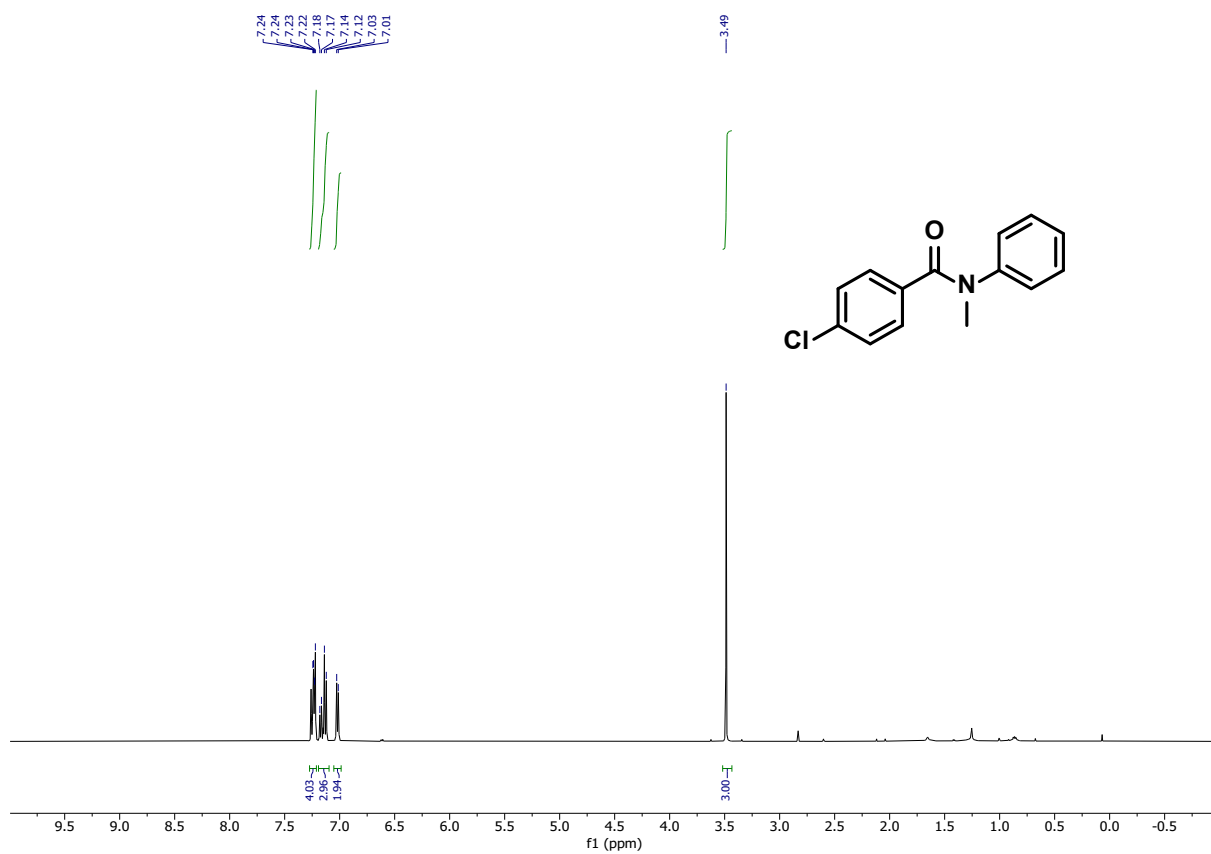
¹H NMR (300 MHz, CDCl₃) of 4-Chloro-*N*-methyl-*N*-phenylbenzamide (2cv).
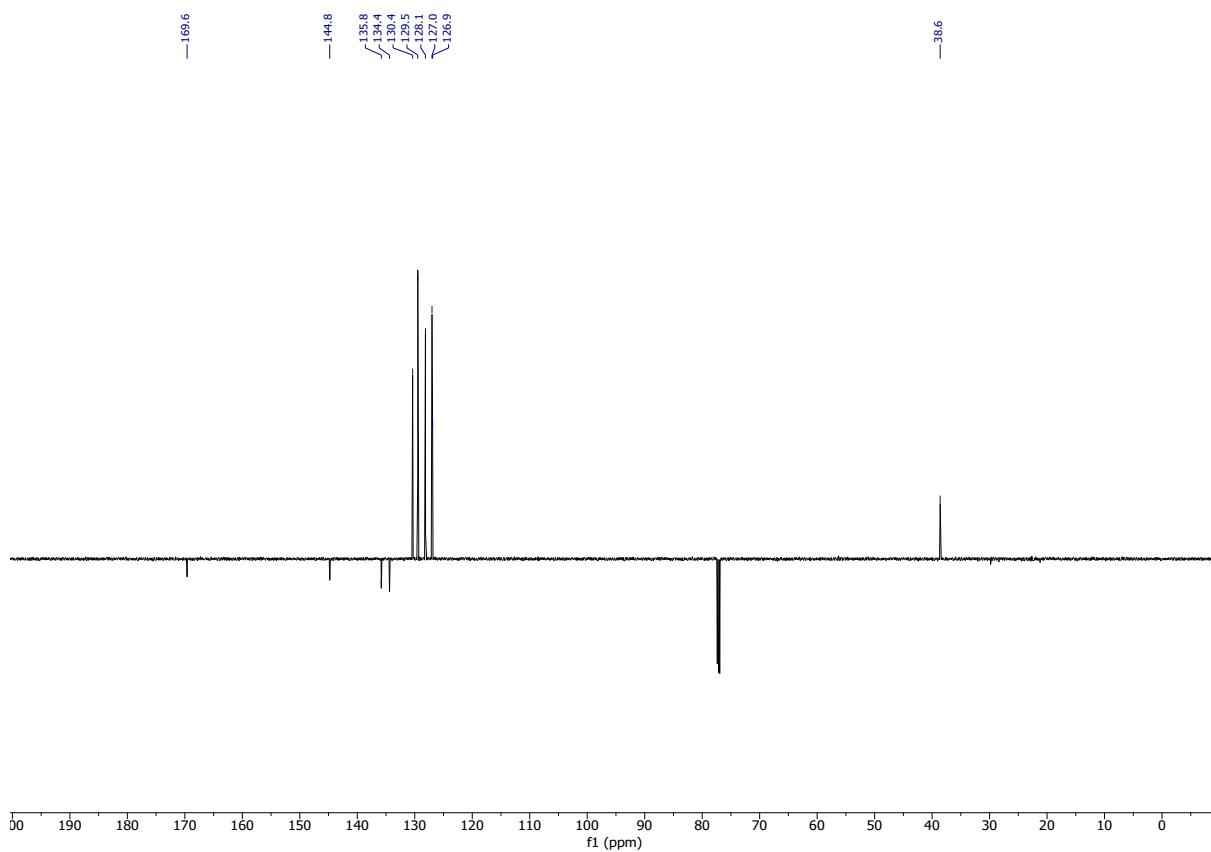
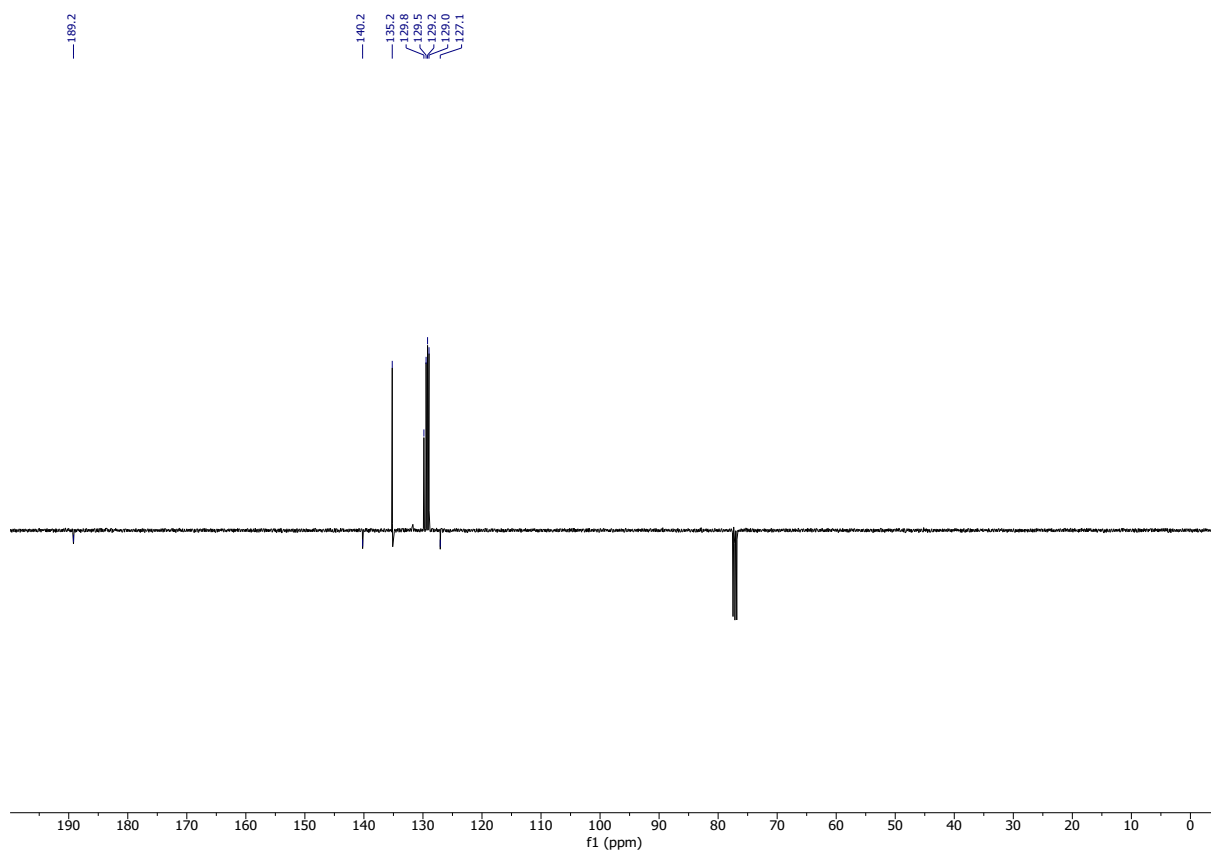¹³C NMR (75 MHz, CDCl₃) of 4-Chloro-*N*-methyl-*N*-phenylbenzamide.
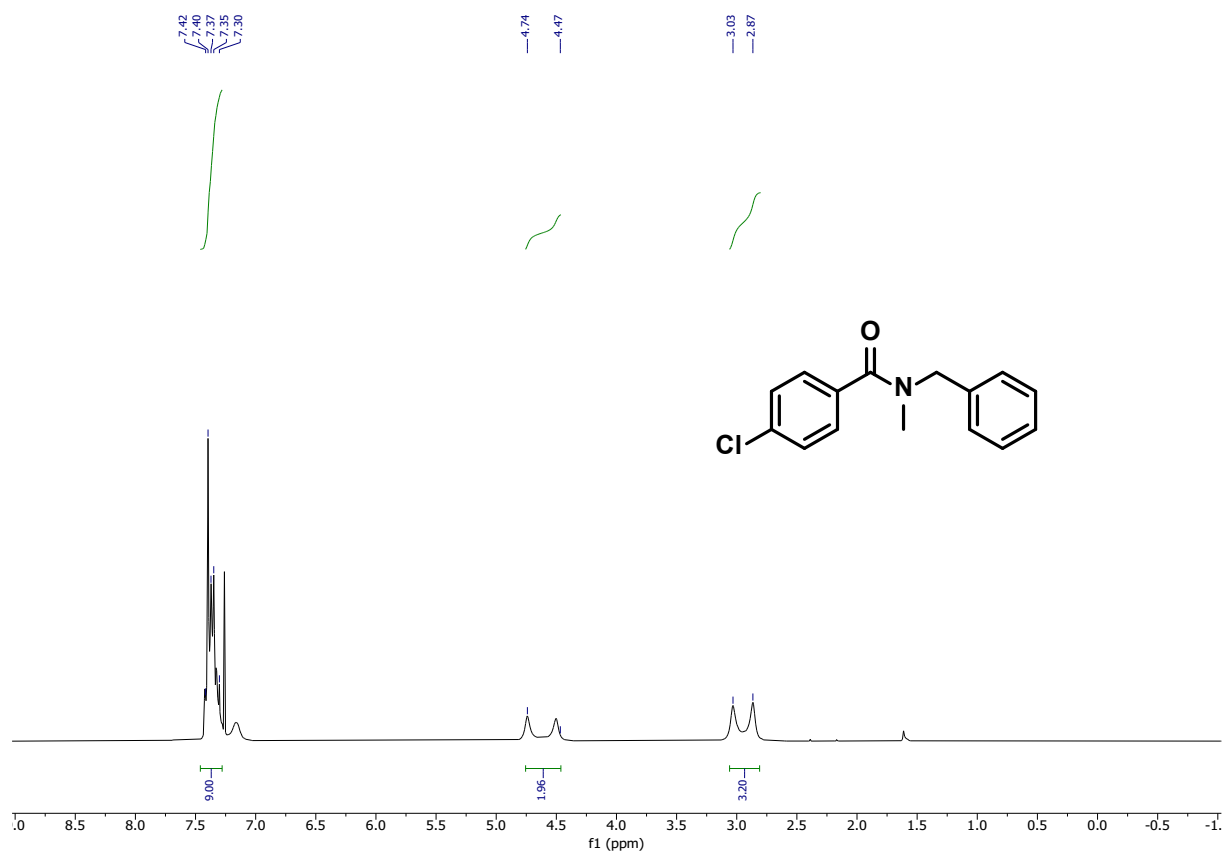
¹H NMR (300 MHz, CDCl₃) of 4-Chloro-*N*-methyl-*N*-(phenylmethyl)-benzamide (2cw).

¹³C NMR (75 MHz, CDCl₃) of 4-Chloro-*N*-methyl-*N*-(phenylmethyl)-benzamide.

247
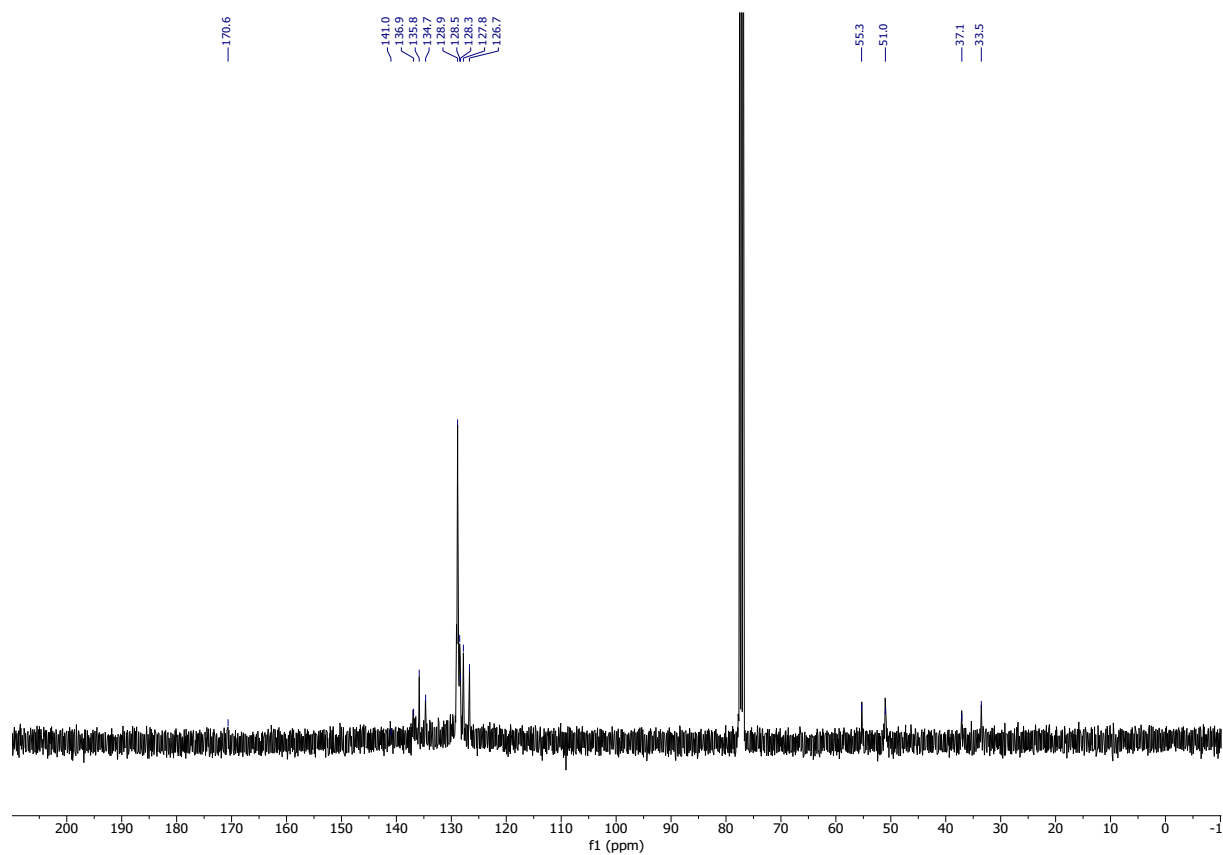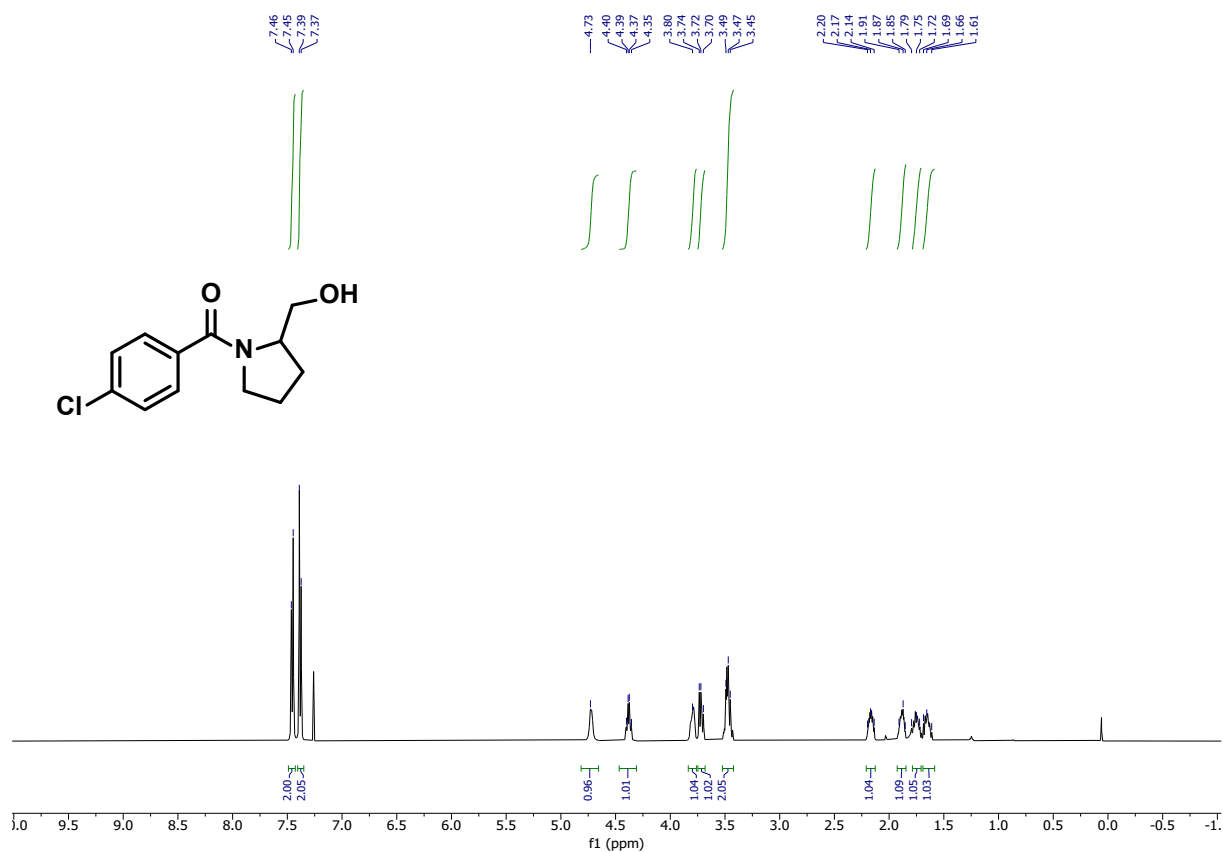
^{1}H NMR (300 MHz, CDCl$_3$) of 1-(4-Chlorobenzoyl)-2-pyrrolidinemethanol (2cx).
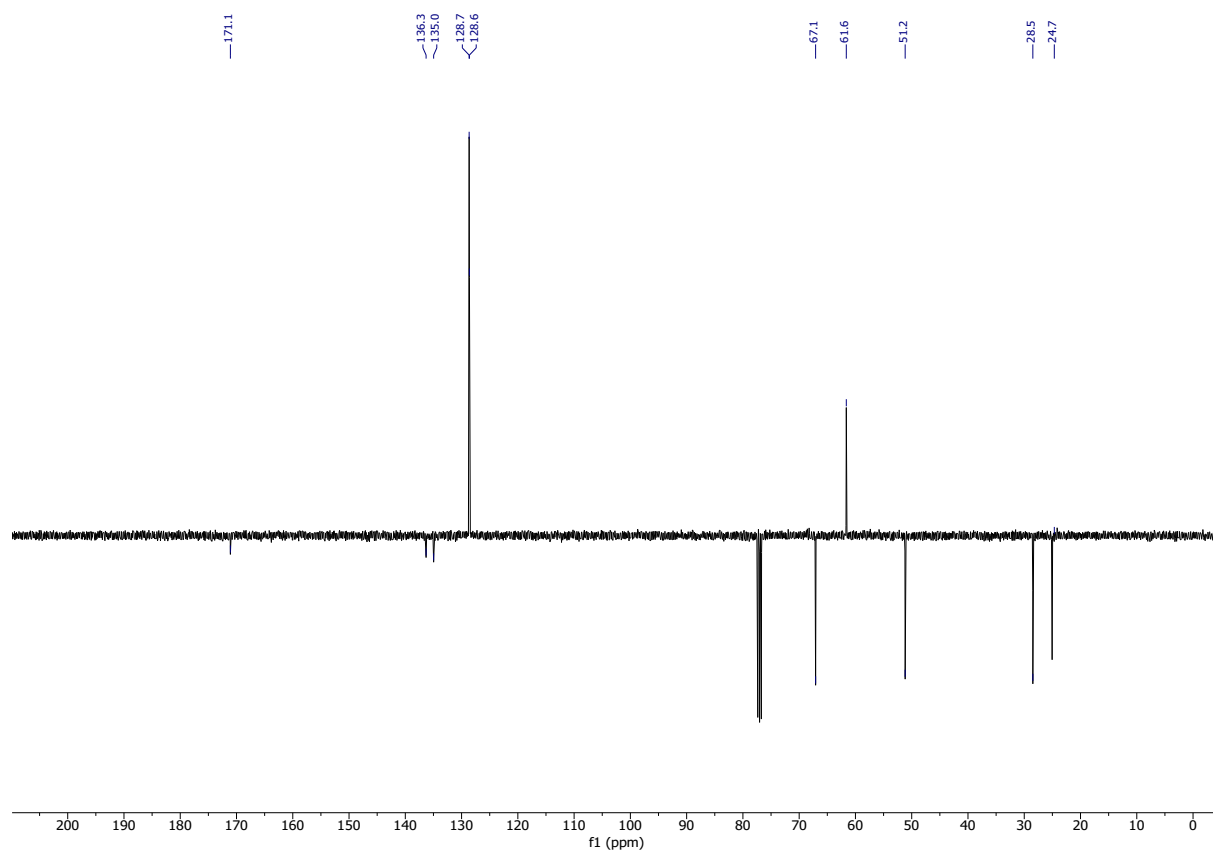
^{13}C NMR (75 MHz, CDCl$_3$) of 1-(4-Chlorobenzoyl)-2-pyrrolidinemethanol.

¹H NMR (300 MHz, DMSO-d₆) of 4-Chloro-*N*-methoxybenzamide (2cy).

¹³C NMR (75 MHz, DMSO-d₆) of 4-Chloro-*N*-methoxybenzamide.
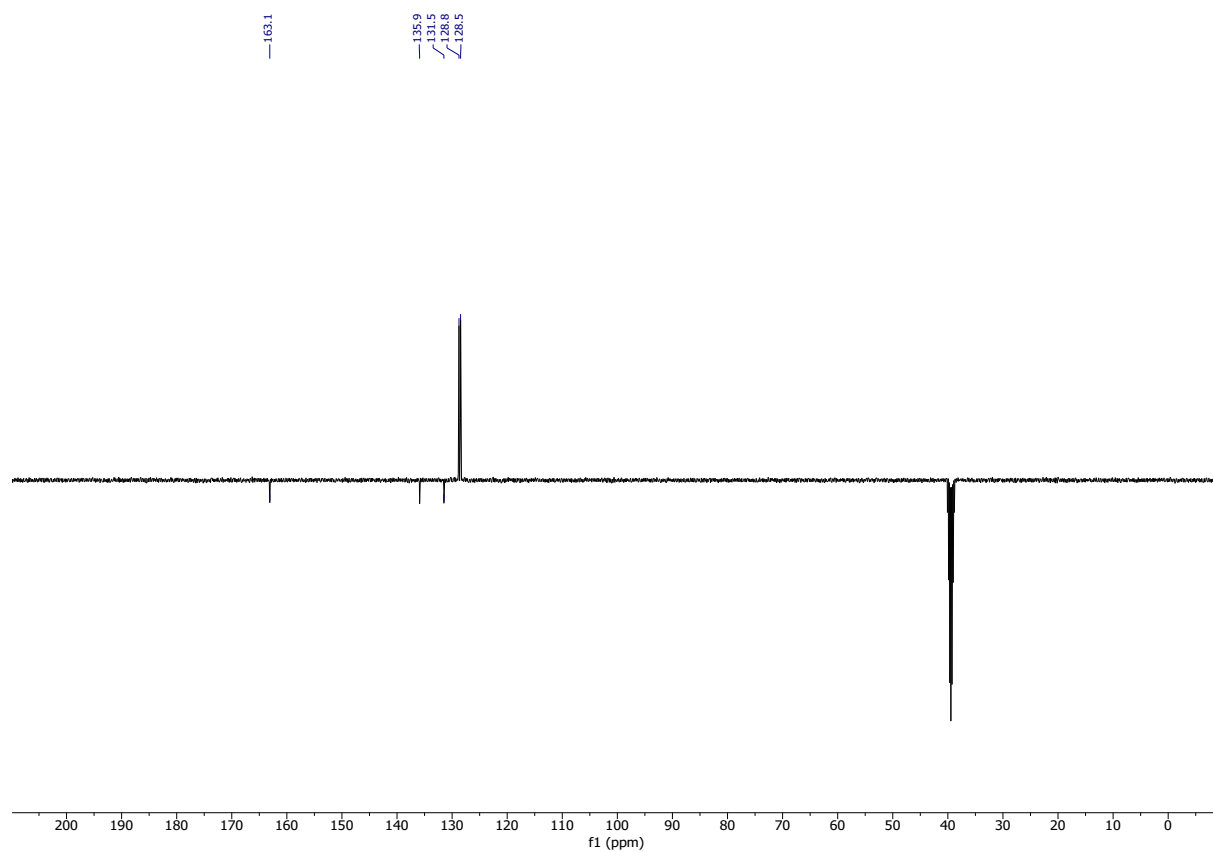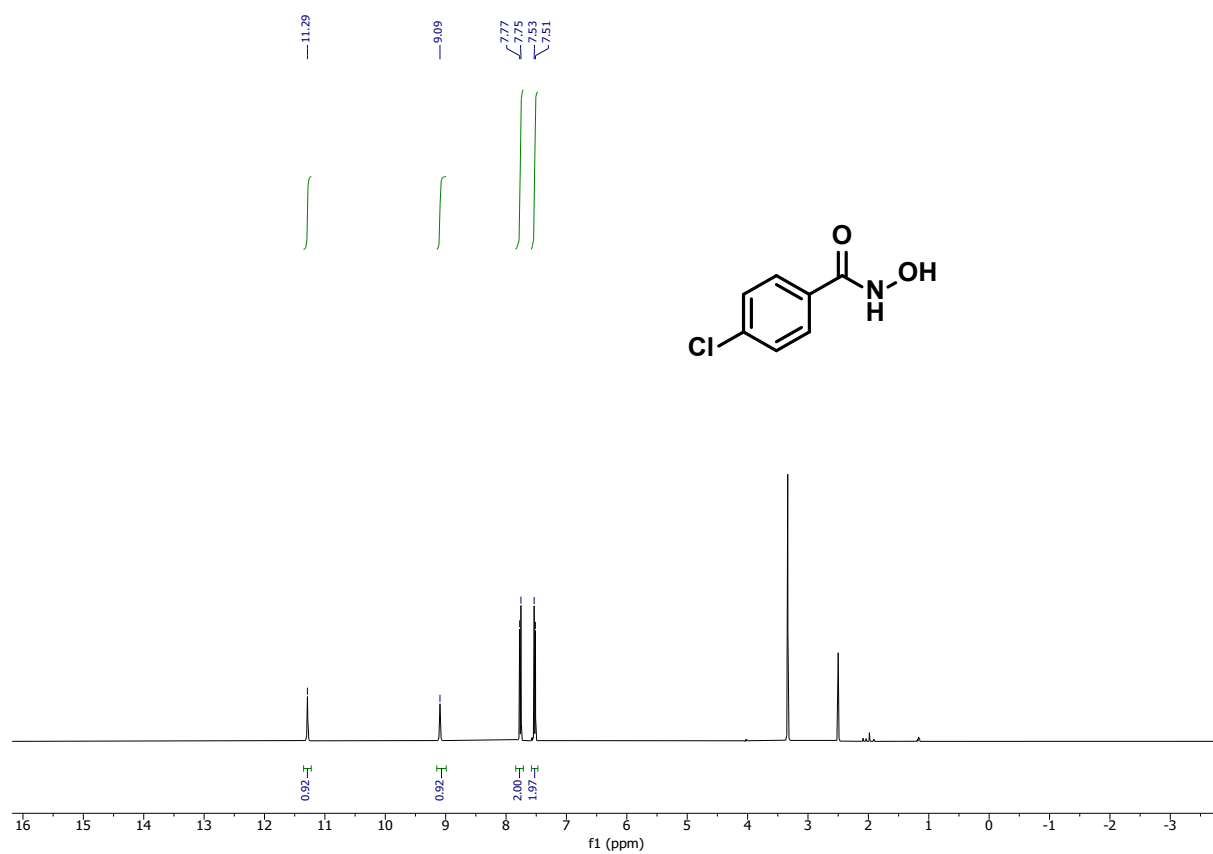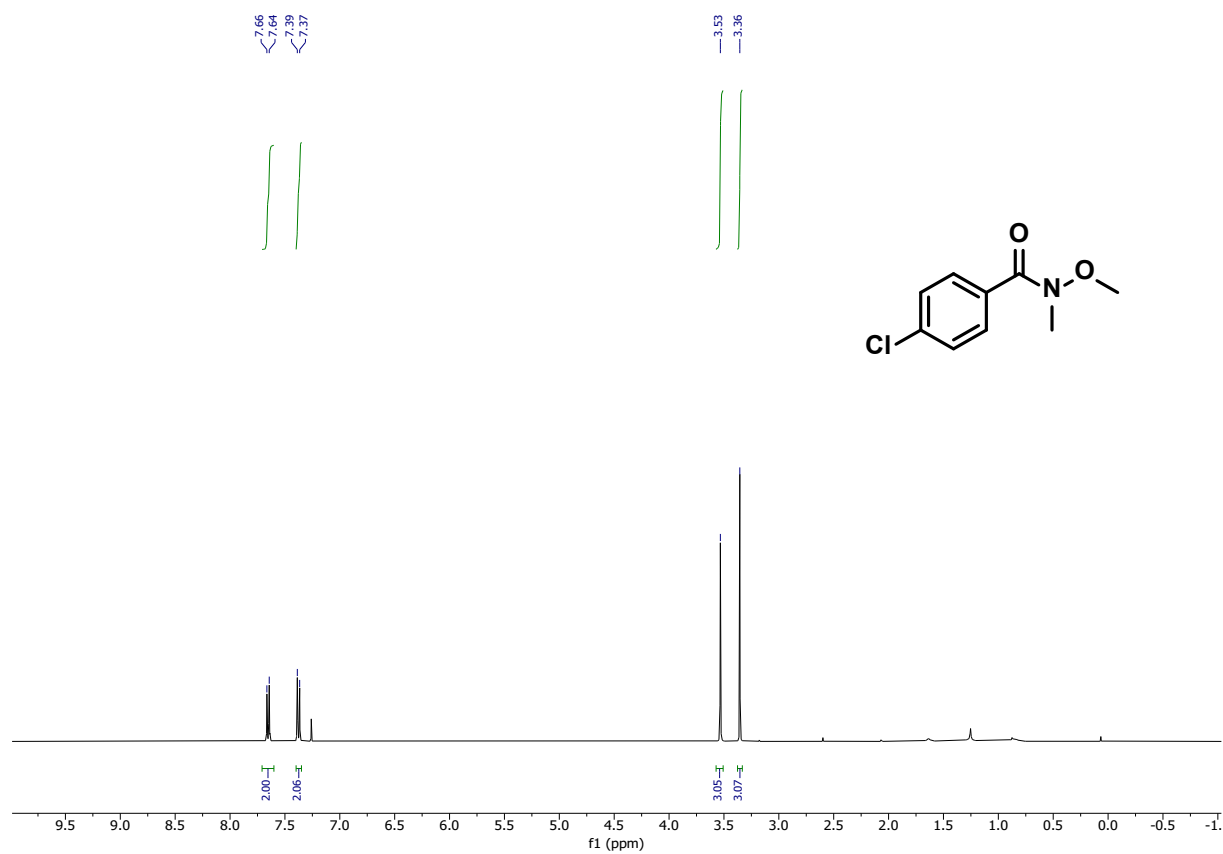
¹H NMR (300 MHz, CDCl₃) of 4-Chloro-*N*-methoxy-*N*-methylbenzamide (2cz).
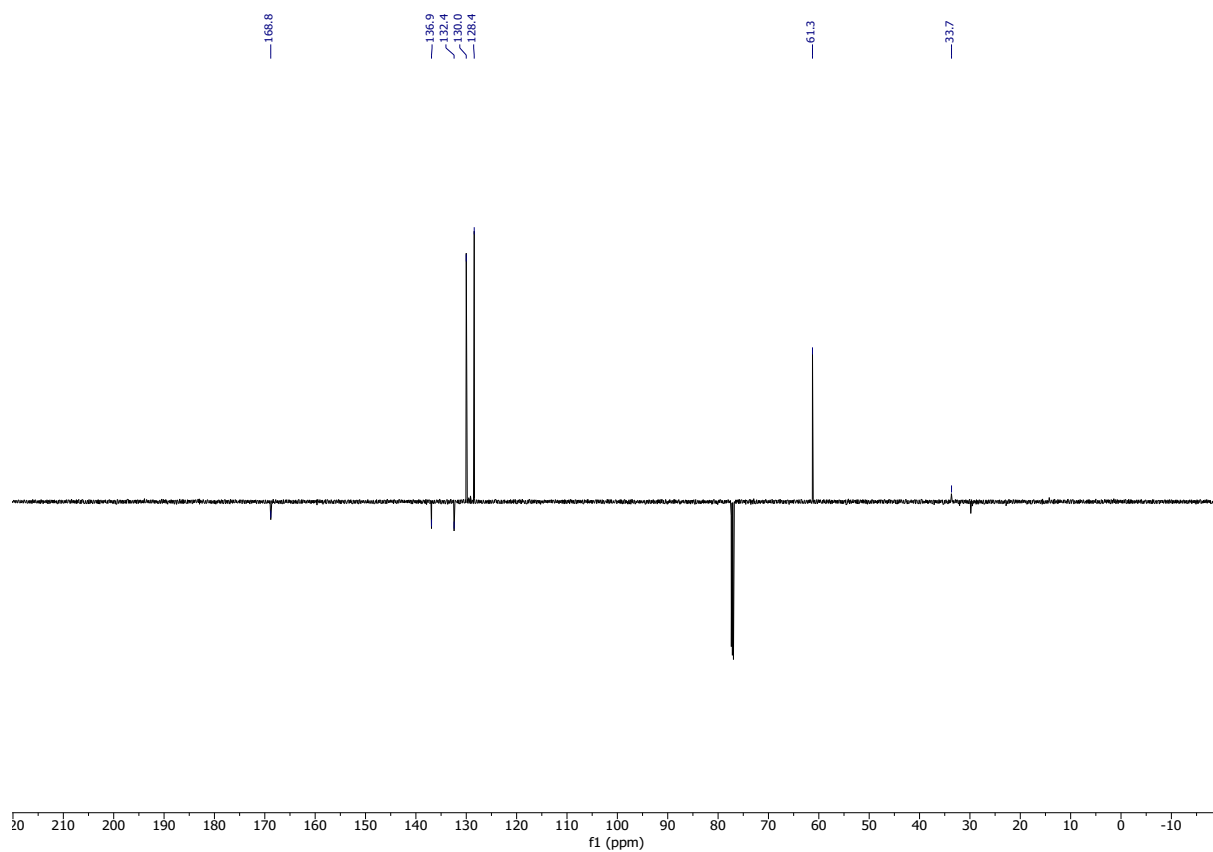
¹³C NMR (75 MHz, CDCl₃) of 4-Chloro-*N*-methoxy-*N*-methylbenzamide.
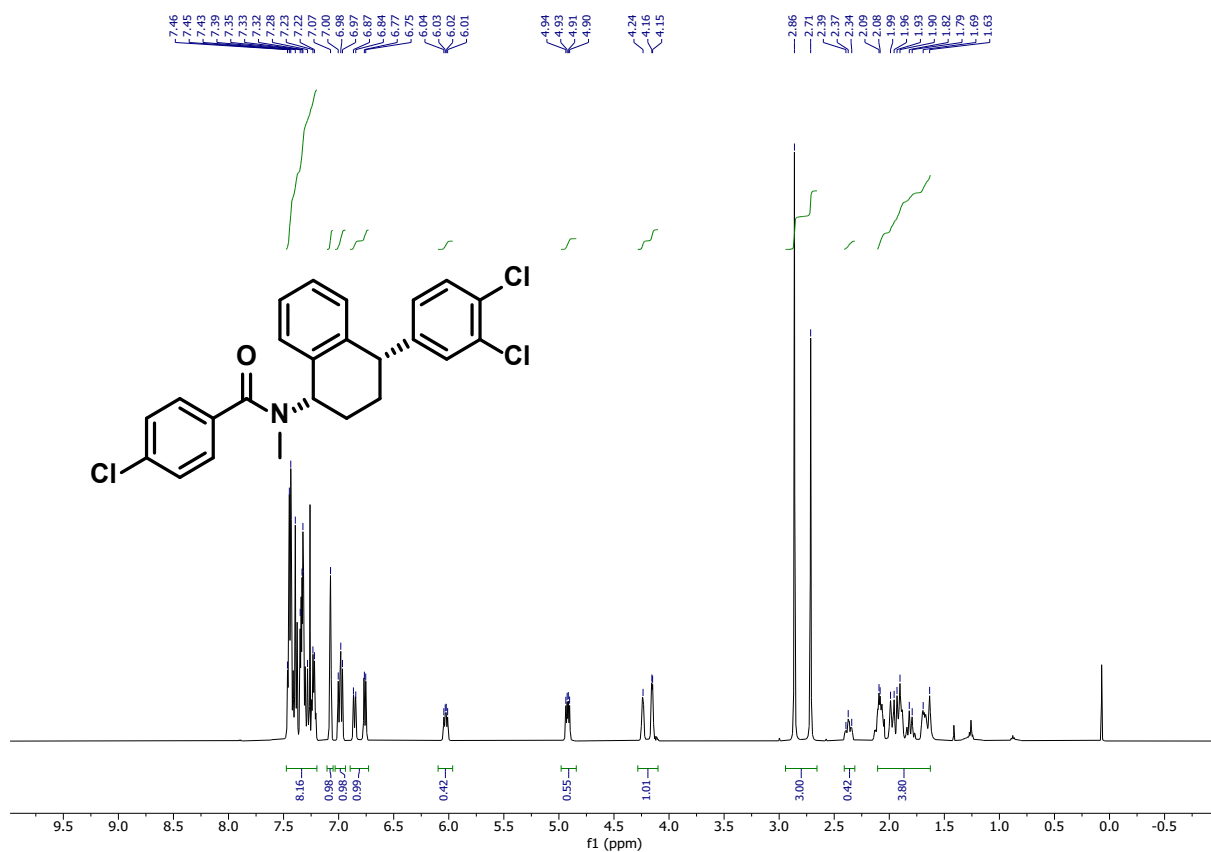
^{1}H NMR (300 MHz, CDCl$_3$) of N-[(1R,4R)-4-(3,4-dichlorophenyl)-1,2,3,4-tetrahydro-1-naphthalenyl]-N-methyl-4-chlorobenzamide (2cA).
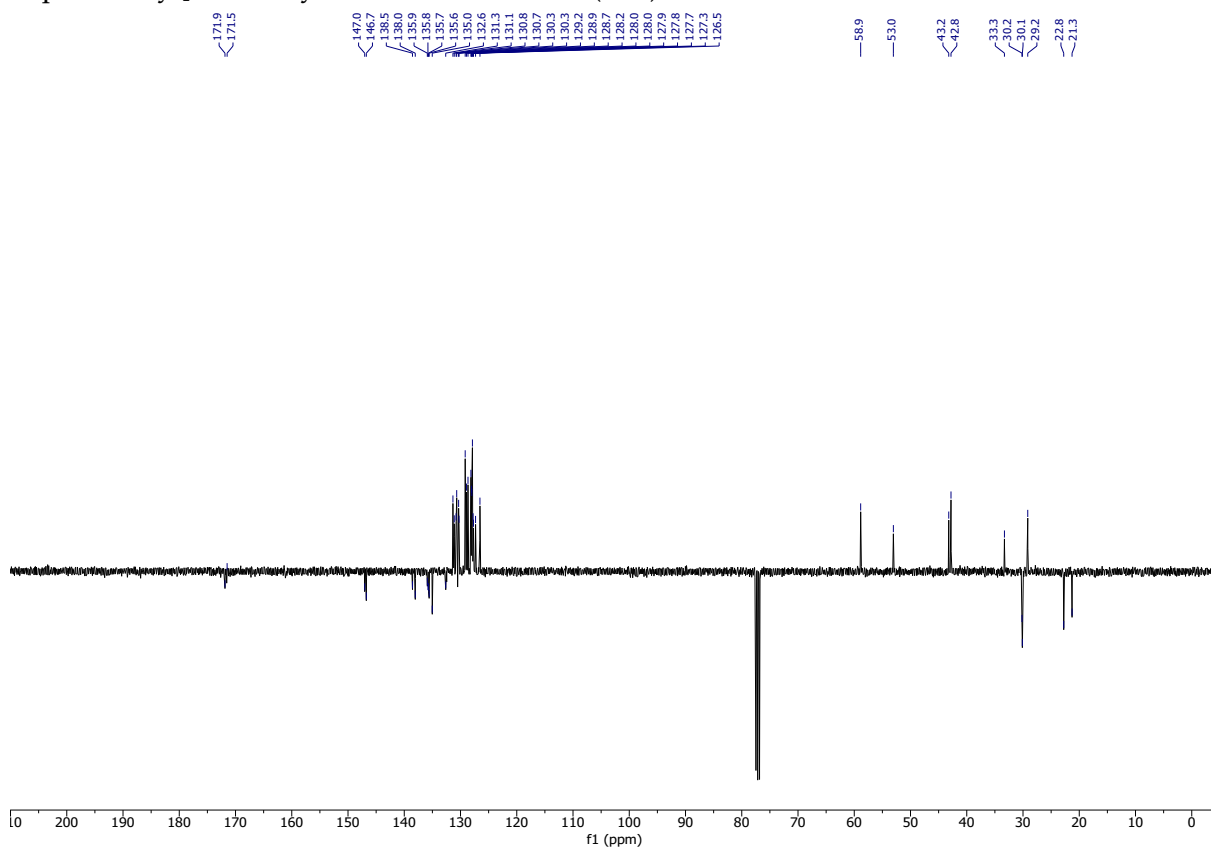
^{13}C NMR (75 MHz, CDCl$_3$) of 2cA.
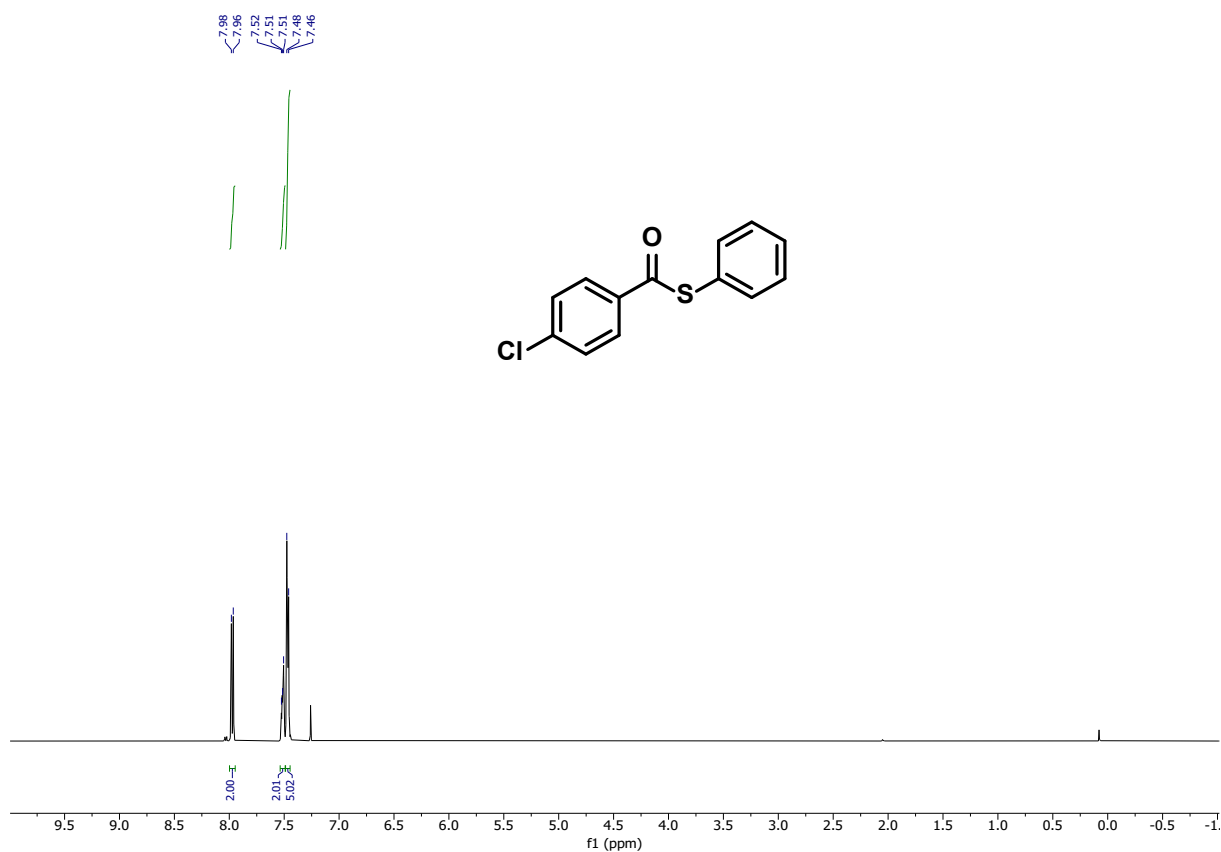
^{1}H NMR (300 MHz, CDCl$_3$) of *S*-Phenyl 4-chlorothiobenzoate (2cB).

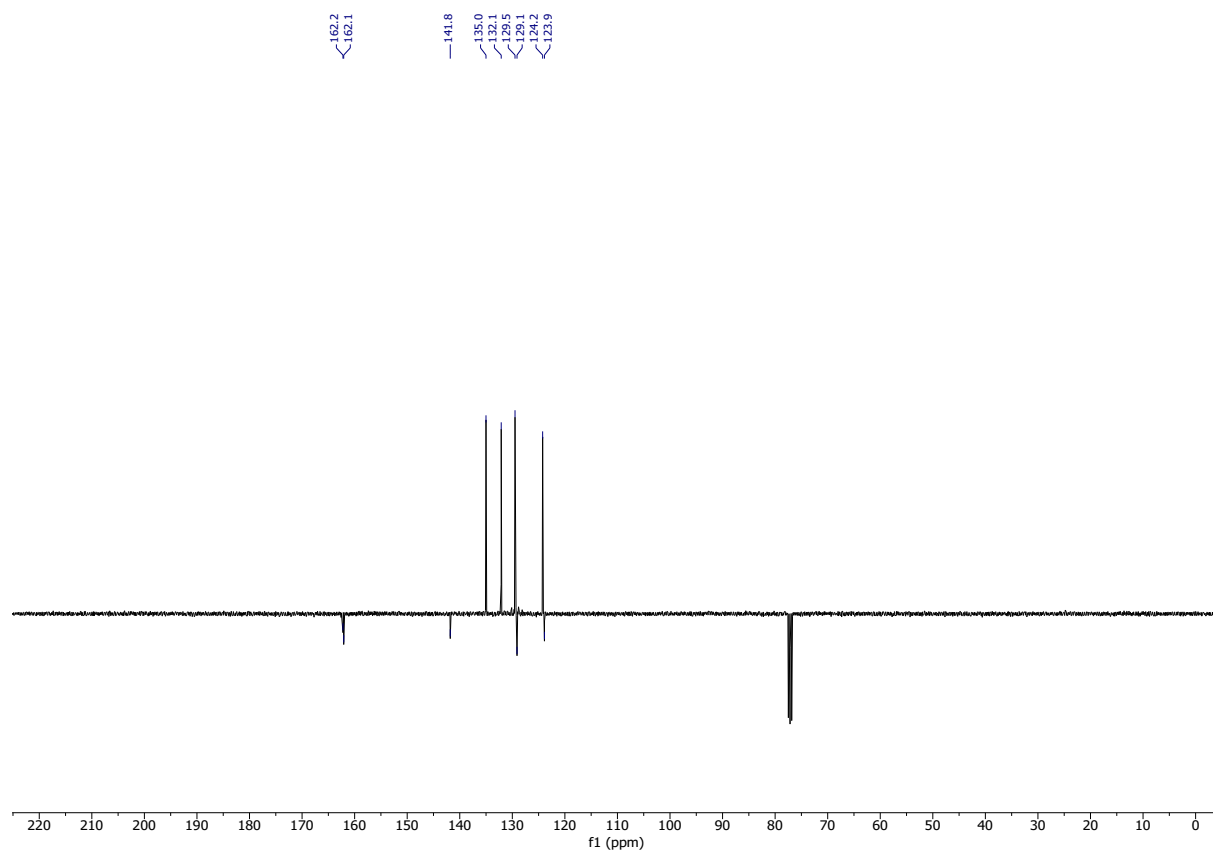^{13}C NMR (75 MHz, CDCl$_3$) of *S*-Phenyl 4-chlorothiobenzoate.
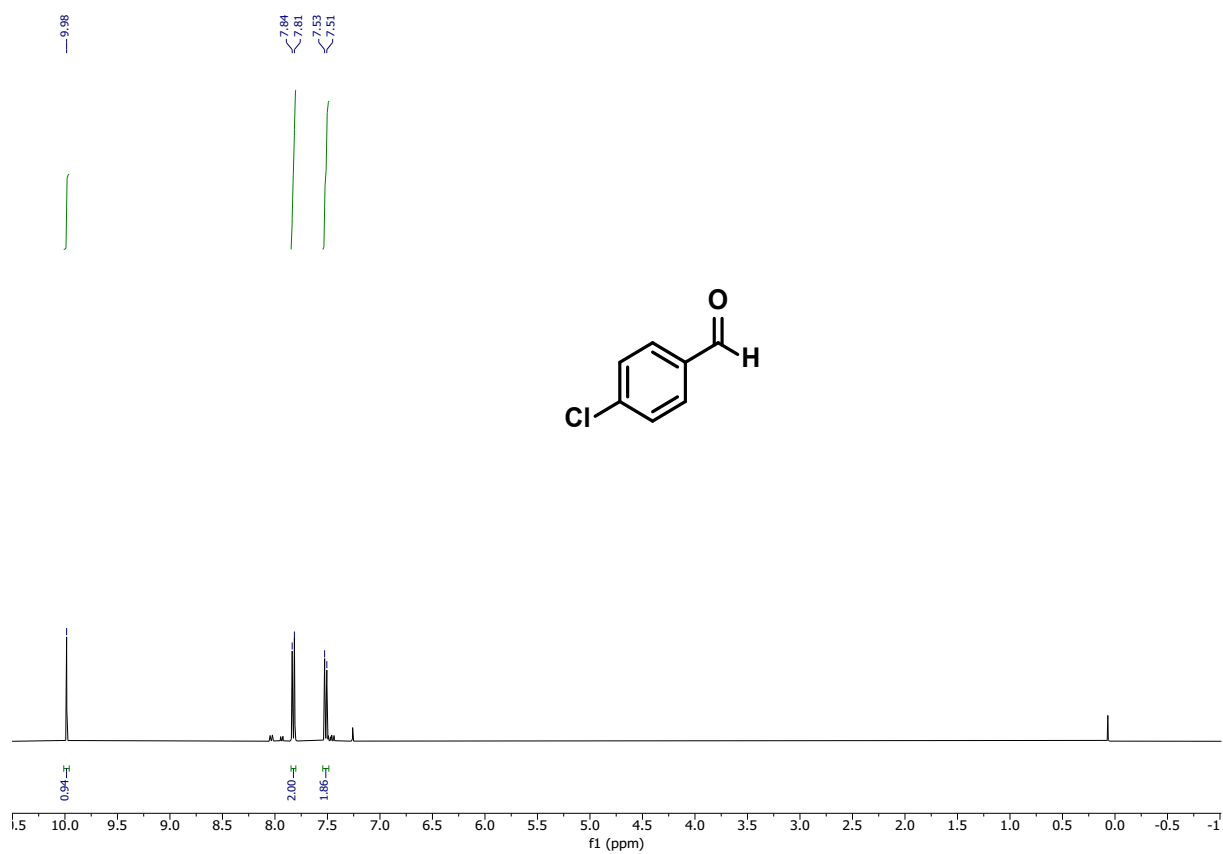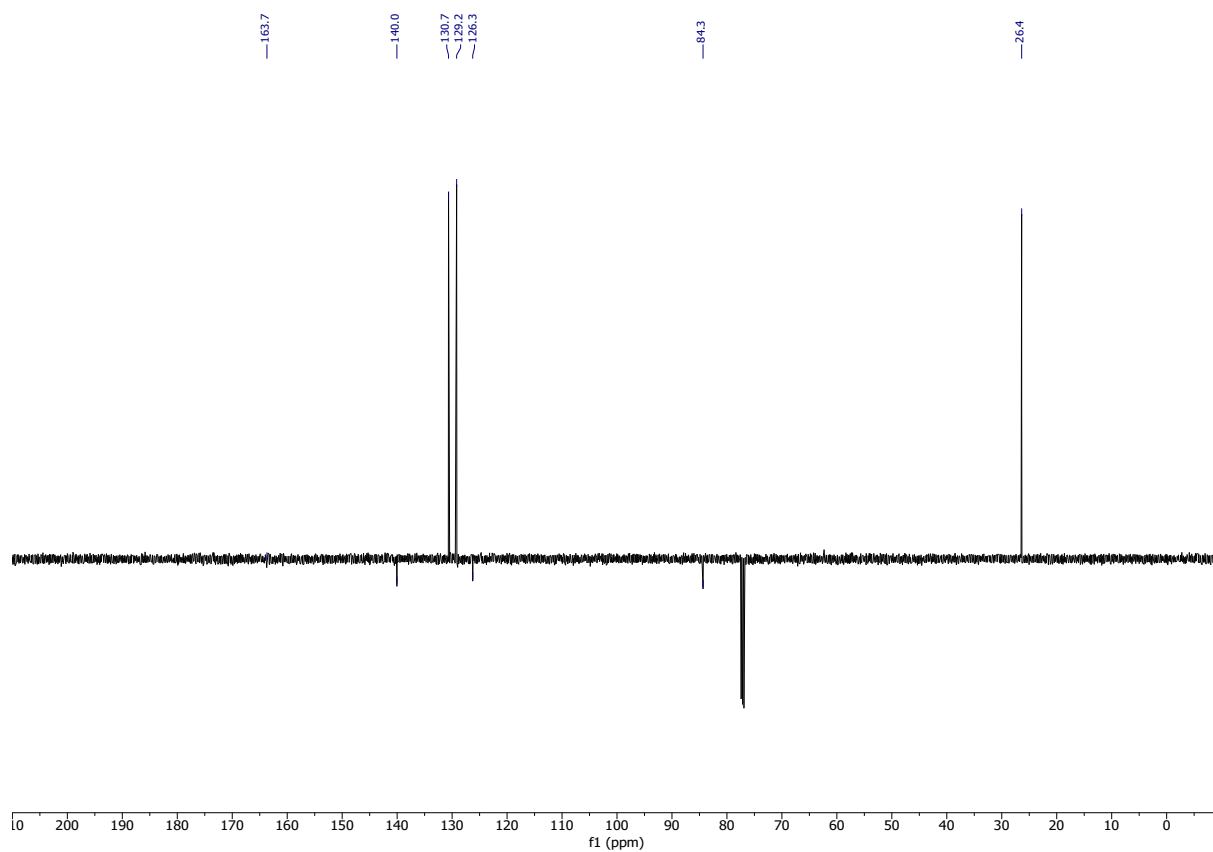
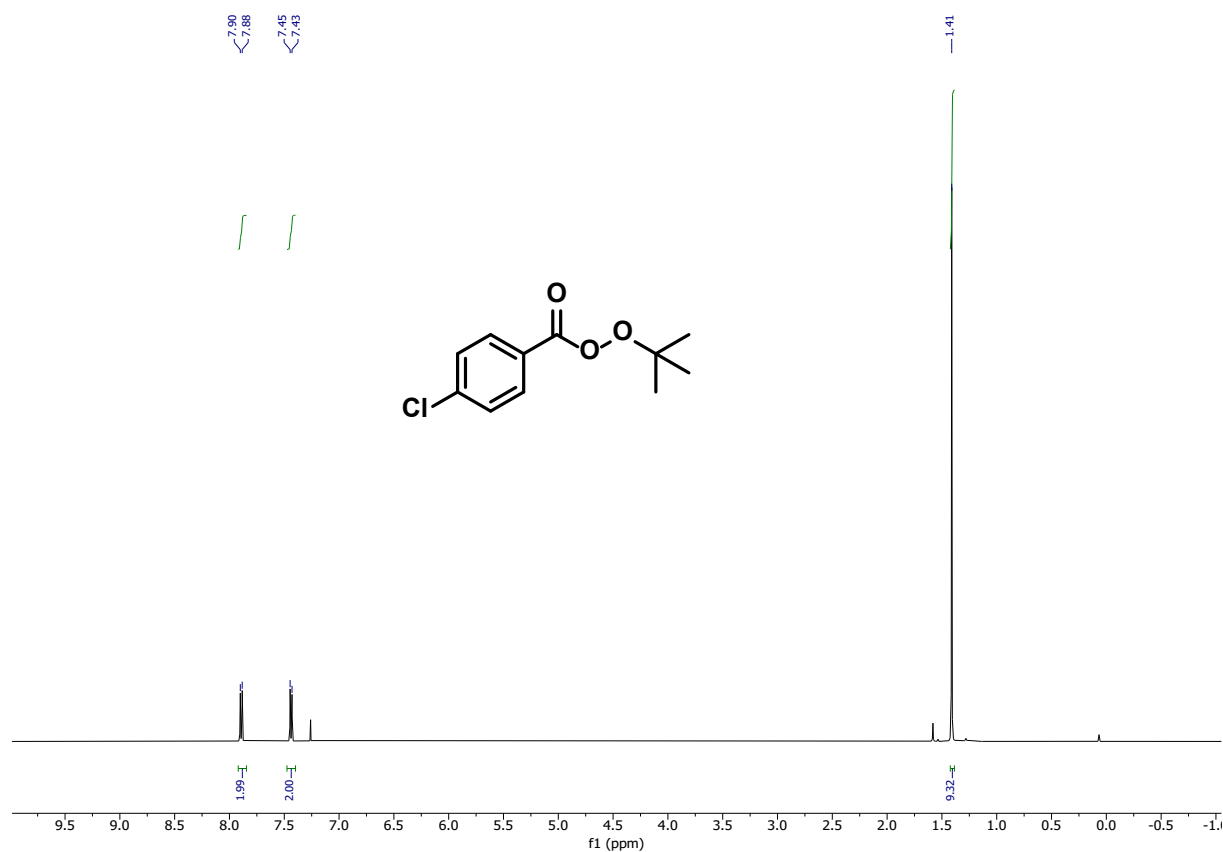^{1}H NMR (300 MHz, CDCl$_3$) of 4-Chlorobenzaldehyde (2cC).
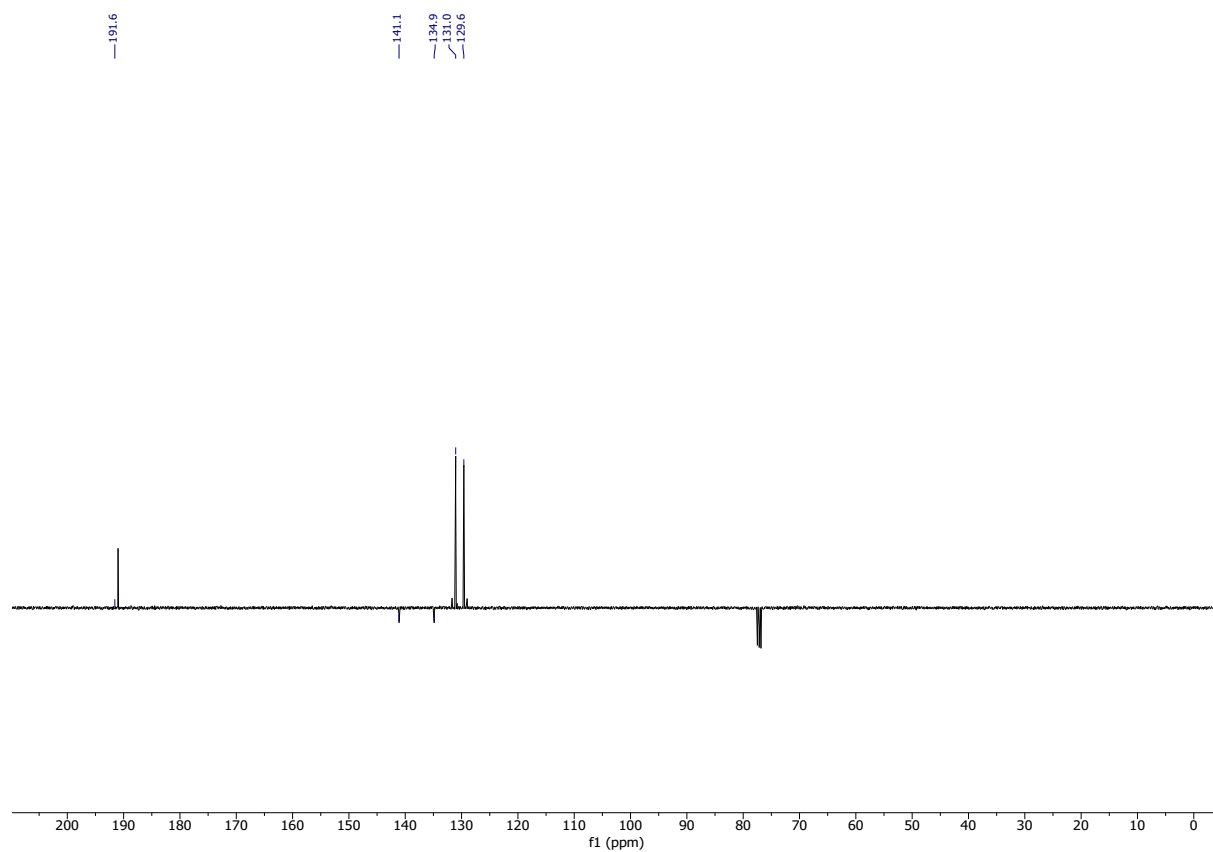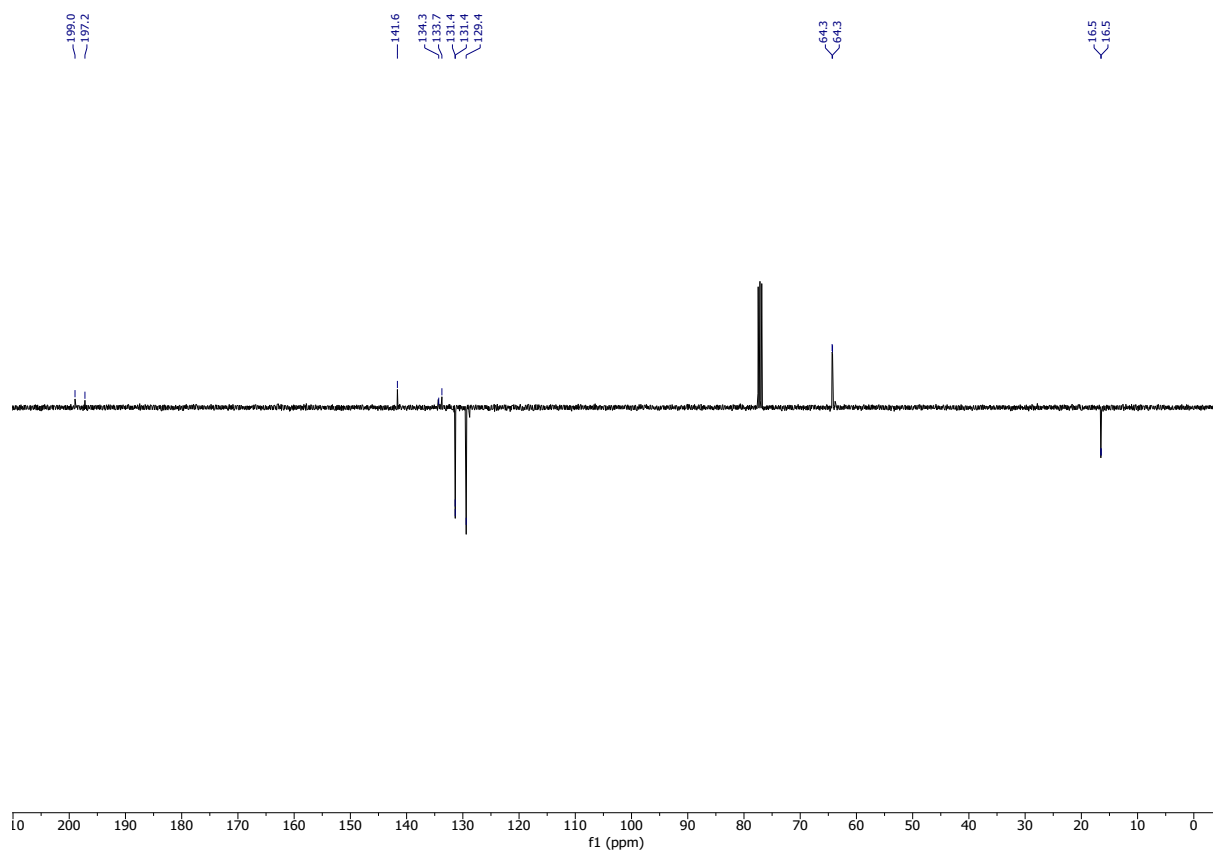

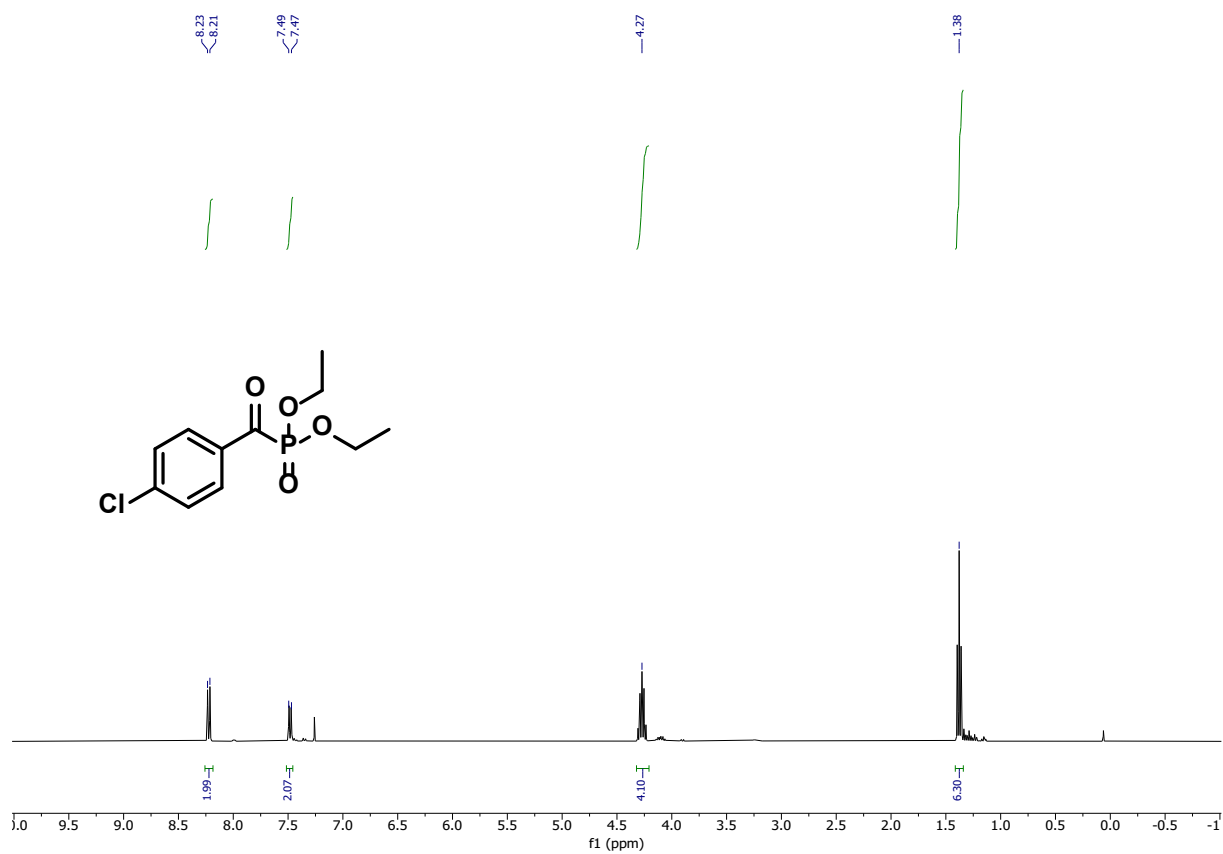
^{13}C NMR (75 MHz, CDCl$_3$) of 4-Chlorobenzaldehyde.
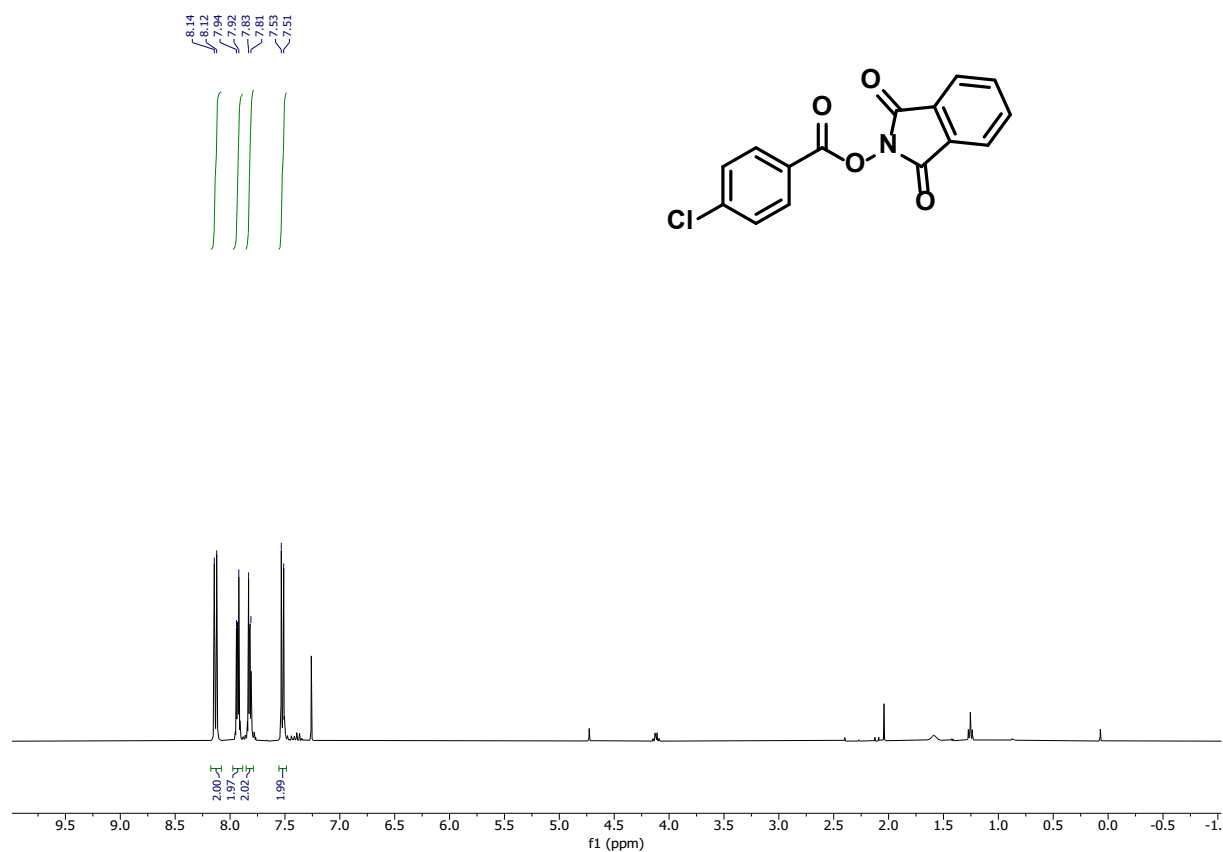
^{1}H NMR (300 MHz, CDCl$_3$) of 1,3-Dioxoisoindolin-2-yl 4-chlorobenzoate (2cD).

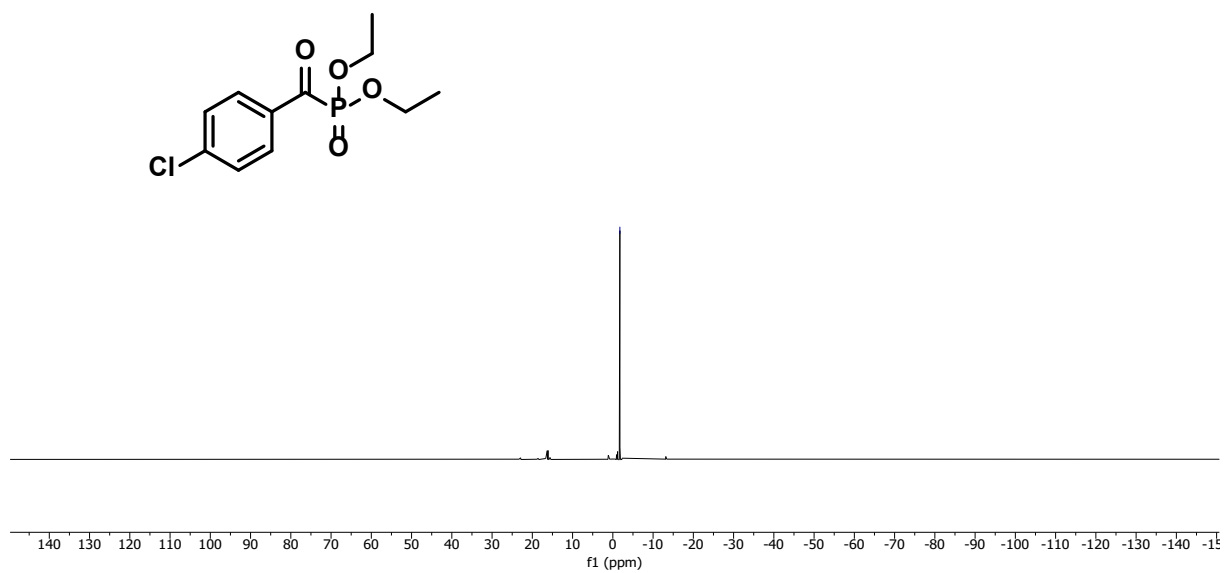^{13}C NMR (75 MHz, CDCl$_3$) of 1,3-Dioxoisoindolin-2-yl 4-chlorobenzoate.
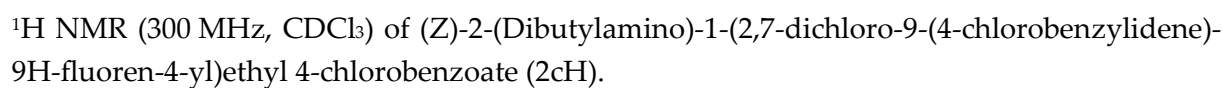
^{1}H NMR (300 MHz, CDCl$_3$) of *tert*-Butyl 4-chloroperbenzoate (2cE).

^{13}C NMR (75 MHz, CDCl$_3$) of *tert*-Butyl 4-chloroperbenzoate.

255

^{1}H NMR (300 MHz, CDCl₃) of *P*-(4-Chlorobenzoyl)-phosphonic acid diethyl ester (2cF).

^{13}C NMR (75 MHz, CDCl₃) of *P*-(4-Chlorobenzoyl)-phosphonic acid diethyl ester.

^{31}P NMR (162 MHz, CDCl$_3$) of *P*-(4-Chlorobenzoyl)-phosphonic acid diethyl ester.

^{1}H NMR (300 MHz, CDCl$_3$) of (Z)-2-(Dibutylamino)-1-(2,7-dichloro-9-(4-chlorobenzylidene)-9H-fluoren-4-yl)ethyl 4-chlorobenzoate (2cH).

^{13}C NMR (75 MHz, CDCl$_3$) of (Z)-2-(Dibutylamino)-1-(2,7-dichloro-9-(4-chlorobenzylidene)-9H-fluoren-4-yl)ethyl 4-chlorobenzoate.
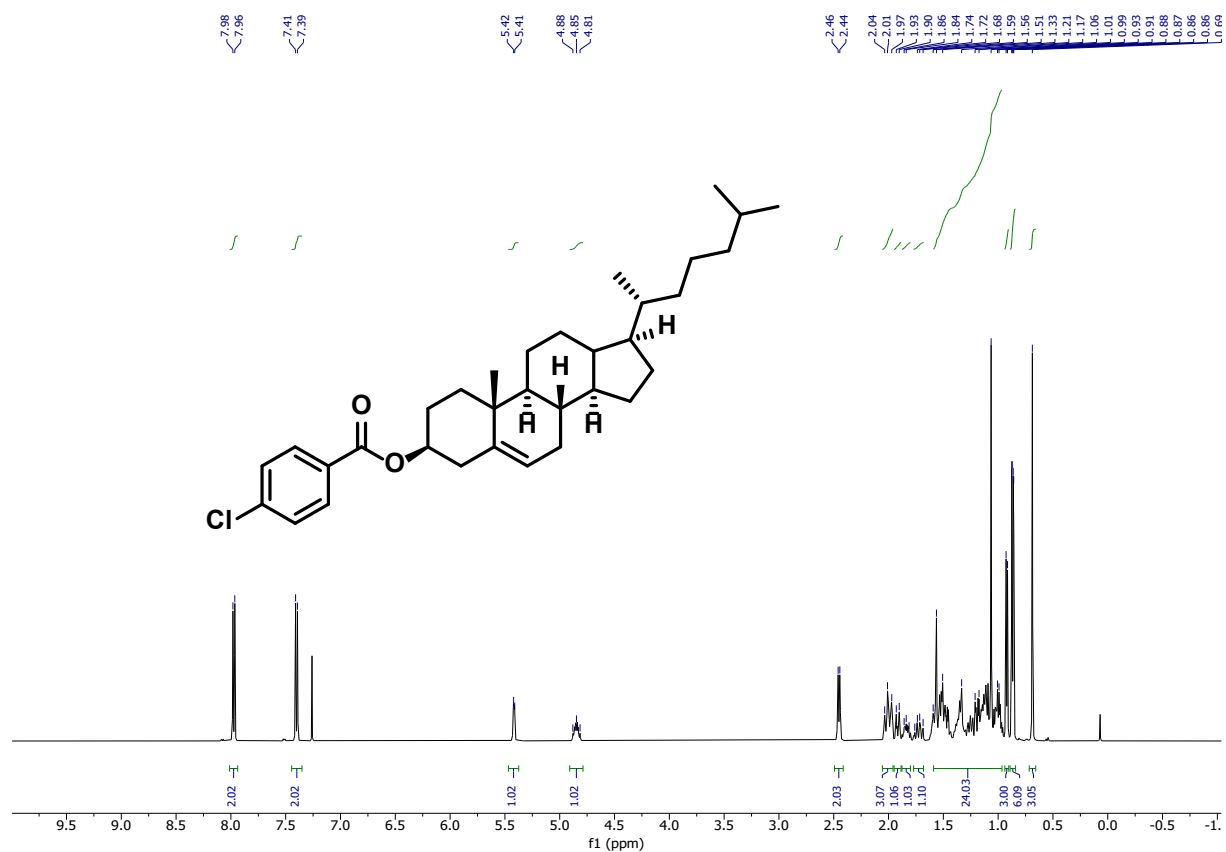
^{1}H NMR (300 MHz, CDCl$_3$) of Cholesteryl 4-chlorobenzoate (2cI).
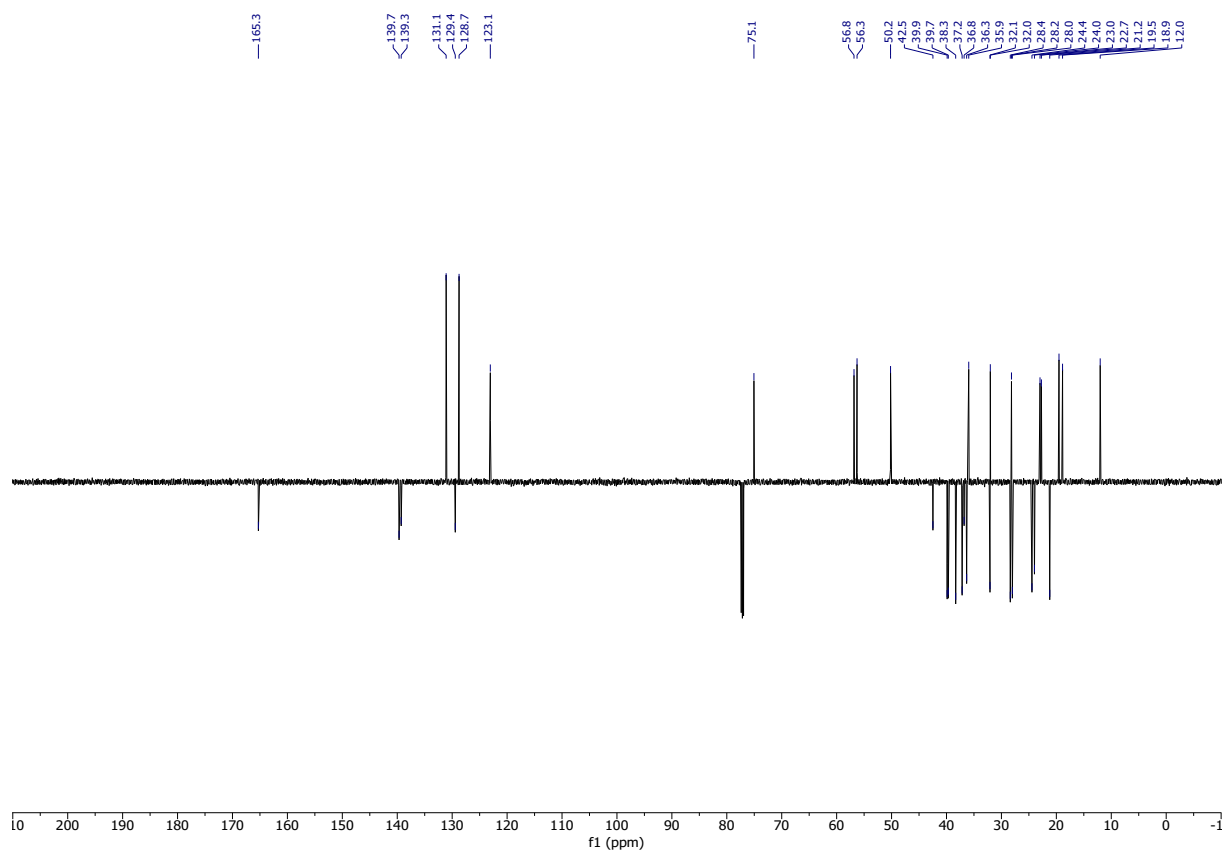
^{13}C NMR (75 MHz, CDCl$_3$) of Cholesteryl 4-chlorobenzoate.

259

9. Appendix

9.1 Chemicals and Safety

The chemicals used in this work and their classification according to GHS, including hazard and precautionary statements, are listed in **Table 9.1**. The GHS symbols and their assigned codes are shown in **Figure 9.1.**

Table 9.1. Chemicals used in this work and their classification according to GHS.[1-3]

Name and CAS-number	GHS symbols	Hazard statements	Precautionary statements
Acetic Acid 64-19-7	GHS02, GHS05	H226, H314	P210, P280, P301+P330+P331, P303+P361+P353, P305+351+P338, P310
Acetone 67-64-1	GHS02, GHS07	H225, H319, H336	P210, P233, P240, P241, P242, P305+P351+P338
Acetonitrile 75-05-8	GHS02, GHS06	H225, H302+H312, H319, H331	P210, P280, P301+P312, P303+P361+P353, P304+P340+P311, P305+P351+P338
4-Acetyl aniline 99-92-3	GHS07	H302	P264, P270, P301+312, P501
Acryloyl chloride 814-68-6	GHS02, GHS05, GHS06	H225, H290, H302, H314, H330	P210, P280, P301+P312, P303+P361+P353, P304+P340+P310, P305+P351+P338
Allyl alcohol 107-18-6	GHS02, GHS06, GHS09	H225, H301, H310, H330, H319, H335, H315, H400, H412	P210, P280, P303+P361+P353, P305+P351+P338
2-Aminobenzamide 88-68-6	GHS07	H319	P264, P280, P305+P351+P338, P337+P313
Aniline 62-53-3	GHS05, GHS06, GHS08, GHS09	H301, H311, H331, H317, H318, H341, H351, H372, H410	P273, P280, P301+P310, P302+P352+P312, P304+P340+P311, P305+P351+P338
2-Anisidine 90-04-0	GHS06, GHS08	H301, H311, H331, H341, H350	P201, P280, P301+P310+P330, P302+P352+P312, P304+P340+P311
4-Anisidine 104-94-9	GHS06, GHS08, GHS09	H300, H310, H330, H373, H400	P260, P284, P280, P301+P310+P330, P302+P352+P310, P361+P364, P304+P340+P310
Anisole 100-66-3	GHS02, GHS07	H226, H315, H319	P210, P233, P241, P243, P280, P305+P351+P338
Benzonitrile 100-47-0	GHS07	H302+H312	P264, P270, P280, P301+P312, P302+P352+P312, P362+P364

Name and CAS-number	GHS symbols	Hazard statements	Precautionary statements
Benzyl alcohol 100-51-6	GHS07	H302, H317, H319	P272, P280, P301+P312, P303+P361+P353, P305+P351+P338, P333+P313
Benzylamine 100-46-9	GHS05, GHS07	H302, H312, H314	P260, P264, P270, P280, P301+P312, P301+P330+P331, P302+P352, P303+P361+P353, P304+P340, P305+P351+P338, P310, P312, P321, P322, P330, P363, P405, P501
Bis(2,2,6,6-tetramethyl-4-piperidyl)sebacate 52829-07-9	GHS05, GHS06, GHS08, GHS09	H318, H330, H370, H410	P260, P273, P380, P304+P340+P310, P305+P351+P338, P308+P311, P403+P233
3-Bromo aniline 591-19-5	GHS07	H302, H312, H332, H315, H319, H335	P261, P280, P301+P312, P302+P352, P304+P340, P305+P351+P338
4-Bromo aniline 106-40-1	GHS06, GHS08, GHS09	H302, H311, H331, H373, H410	P260, P264, P273, P280, P391, P403+P233
Bumetrizole 3896-11-5	GHS07	H315, H319, H413	P264, P273, P280, P337+P313, P332+P313
1-Butyl-3-methyl-imidazolium chloride 79917-90-1	GHS06, GHS09	H301, H315, H319, H411	P264, P270, P273, P301+P310, P302+P352, P305+P351+P338
Carbon Dioxide 124-38-9	GHS04	H280	P403
Carbon Monoxide 630-08-0	GHS02, GHS04, GHS06, GHS08	H220, H280, H331, H360D, H372	P202, P210, P260, P304+P340+P315, P308+P313, P377, P381, P403, P405
4-Chloro aniline 106-47-8	GHS06, GHS08, GHS09	H301, H311, H317, H331, H350, H410	P201, P280, P302+P352, P304+P340, P308+P313, P273
Chloroform- d_1 865-49-6	GHS06, GHS08	H302, H315, H319, H331, H351, H361d, H372	P260, P280, P301+P312+P330, P304+P340+P311, P305+P351+P338, P403+P233
Cholesterol 57-88-5	Not classified as hazardous substance according to GHS		
Citronellol 106-22-9	GHS07	H315, H317, H319	P280, P302+P352, P333+P313, P337+P313
4-Cyano aniline 873-74-5	GHS07, GHS08	H302, H341, H412	P202, P264, P273, P280, P301+P312, P308+P313
Cyclododecane 294-62-2	Not classified as hazardous substance according to GHS		

Name and CAS-number	GHS symbols	Hazard statements	Precautionary statements
Cyclododecanone 830-13-7	GHS09	H411	P273
Decanol 112-30-1	GHS07	H319, H412	P264, P273, P280, P305+P351+P338, P337+P313
Dibutylamine 111-92-2	GHS02, GHS05, GHS06	H226, H301, H311, H330, H314, EUH071	P280, P301+P330+P331, P3022+P352, P304+P340, P305+P351+P338, P310
Dichloromethane 75-09-2	GHS07, GHS08	H315, H319, H336, H351	P201, P202, P261, P302+P352, P305+P351+P338, P308+P313
Diethylamine 109-89-7	GHS02, GHS05, GHS06	H225, H302, H332, H311, H314, H335	P210, P280, P301+P312, P303+P361+P353, P304+P340+P310, P305+P351+P338
Diethylene glycol 111-46-6	GHS07	H302	P264, P270, P310+P312
Diethylether 60-29-7	GHS02, GHS07	H224, H302, H336	P210, P261
N,O-Dimethyl hydroxylamine hydrochloride 6638-79-5	GHS07	H315, H319, H335	P261, P264, P271, P280, P302+P352, P305+P351+P338
Dimethylsulfoxide-d_6 2206-27-1	GHS07	H315, H319	P264, P280, P302+P352, P305+P351+P338, P337+P313
1,2:5,6-di-*O*-isopropylidene-*α-D*-glucofuranose 582-52-5		Not classified as hazardous substance according to GHS	
Eosin Y disodium salt 17372-87-1	GHS07	H317, H319	P261, P264, P272, P280, P302+P352, P305+P351+P338
Ethanol 64-17-5	GHS02, GHS07	H225, H319	P210, P280, P305+P351+P338, P337+P313, P403+P235
3-Ethinyl aniline 14235-81-5	GHS07	H315, H319, H335	P261, P264, P271, P280, P302+P352, P305+P351+P338
Ethylacetate 141-78-6	GHS02, GHS07	H225, H319, H336	P210, P233, P240, P305+P351+P338, P403+P235
Ethylene glycol 107-21-1	GHS07, GHS08	H302, H373	P301+P312+P330, P314
Ethyl 2-cyano-3,3-diphenylacrylate 5232-99-5	GHS07	H302, H312, H315, H319, H332	P261, P264, P280, P337+P313, P302+P352+P312, P304+P340+P312
4-Fluoroaniline 371-40-4	GHS05, GHS07, GHS08, GHS09	H302, H314, H373, H410	P280, P301+P330+P331, P305+P351+P338, P310, P303+P361+P353

Name and CAS-number	GHS symbols	Hazard statements	Precautionary statements
Hexamethylbenzene 87-85-4	Not classified as hazardous substance according to GHS		
Hexane 110-54-3	GHS02, GHS07, GHS08, GHS09	H225, H304, H315, H336, H361f, H373, H411	P201, P210, P273, P301+P310+P331, P302+P352, P308+P313
Hydrogen peroxide – urea 124-43-6	GHS03, GHS05	H272, H315, H318	P210, P220, P264, P280, P302+P352, P305+P351+P338
Hydroxylamine Hydrochloride 5470-11-1	GHS05, GHS07, GHS08, GHS09	H290, H302, H312, H315, H317, H319, H351, H373, H400	P273, P280, P301+P312, P302+P352+P312, P305+P351+P338, P308+P313
2-(Hydroxymethyl)-aniline 5344-90-1	GHS07	H315, H319	P264, P280, P302+P352, P337+P313, P362+P364, P332+P313
N-hydroxy phthalimide 524-38-9	GHS07	H315, H319	P264, P280, P302+P352, P337+P313, P362+P364, P332+P313
Iron(III)chloride 7705-08-0	GHS05, GHS07	H302, H315, H318	P280, P301+P312+P330, P302+P352, P305+P351+P338
Isoamyl nitrite 110-46-3	GHS02, GHS05, GHS07, GHS08	H225, H302, H314, H317, H332, H341	P210, P280, P301+P312, P303+P361+P353, P304+P340+P310, P305+P351+P338
Lumefantrine 82186-77-4	No classification according to GHS		
L-Menthol 2216-51-5	GHS07	H315, H319	P302+P352, P305+P351+P338
9-Mesitylacridinium perchlorate 674783-97-2	GHS03, GHS07	H315, H319, H272	P220, P210, P264, P280, P370+P378, P337+P313
Methanol 67-56-1	GHS02, GHS06, GHS08	H225, H301+H311+H331, H370	P210, P233, P280, P301+P310, P303+P361+P353, P304+P340+P311
Methyl 3-amino-2-thiophenecarboxylate 22288-78-4	GHS07	H315, H319, H335	P261, P264, P271, P280, P302+P352, P305+P351+P338
N-Methylbenzylamine 103-67-3	GHS05, GHS06	H301, H314	P280, P301+P330+P331, P303+P361+P353, P305+P351+P338, P310
Methylene blue 61-73-4	GHS07	H302	P301+P312
N-Methylaniline 100-61-8	GHS06, GHS08, GHS09	H301, H311, H331, H373, H410	P273, P280, P301+P310, P302+P352+P312, P304+P340+P311, P314

Name and CAS-number	GHS symbols	Hazard statements	Precautionary statements
1-Naphthylamine 134-32-7	GHS07, GHS09	H302, H411	P264, P273, P301+P312
2-Nitroaniline 88-74-4	GHS06, GHS08	H301, H311, H331, H373, H412	P273, P280, P301+P310, P302+P352+P312, P304+P340+P311, P314
cis-4-octene 7642-15-1	GHS02, GHS07, GHS08	H315, H319, H304, H225	P210, P233, P264, P370+P378, P331, P301+P310
trans-4-octene 14850-23-8	GHS02, GHS08	H225, H304	P210, P301+P310+P331
Octabenzone 1843-05-6	GHS07	H315, H319, H413	P264, P273, P280, P337+P313, P332+P313
Oleic acid 112-80-1	Not classified as hazardous substance according to GHS		
Oleyl alcohol 143-28-2	Not classified as hazardous substance according to GHS		
Oxygen 7782-44-7	GHS03, GHS04	H270, H280	P220, P244, P370+P376, P403
Pentaerythritol tetrakis[3-(3,5-di-*tert*-butyl-4-hydroxyphenyl)propionate] 6683-19-8	No classification according to GHS		
Pentane 109-66-0	GHS02, GHS07, GHS08, GHS09	H225, H304, H336, H411	P210, P273, P301+P310+P331
Pentylamine 110-58-7	GHS02, GHS05, GHS06	H225, H302, H312, H331, H314	P210, P280, P301+P330+P331, P303+P361+P353, P305+P351+P338, P310
Piperidine 110-89-4	GHS02, GHS05, GHS06	H225, H302, H311+H331, H314	P210, P280, P301+P312, P303+P361+P353, P304+P340+P310, P305+P351+P338
Potassium fluoride 7789-23-3	GHS06	H301, H311, H331	P280, P302+P352, P304+P340, P308+P310
Procaine hydrochloride 51-05-8	GHS06	H301, H317	P261, P264, P270, P280, P301+P310, P302+P352
(*S*)-Prolinol 23356-96-9	GHS05, GHS07	H302, H318, H335	P261, P264, P271, P280, P301+P312, P305+P351+P338
2-Propanol 67-63-0	GHS02, GHS07	H225, H319, H336	P210, P240, P305+P351+P338, P403+P233
Sertraline hydrochloride 79559-97-0	GHS07, GHS08, GHS09	H302, H373, H410	P260, P264, P270, P301+P312+P314

Name and CAS-number	GHS symbols	Hazard statements	Precautionary statements
Sodium borohydride 16940-66-2	GHS02, GHS05, GHS06, GHS08	H260, H301, H314, H360FD	P231+P232, P260, P280, P303+P361+P353, P304+P340+P310, P305+P351+P338
tert-Butanol 75-65-0	GHS02, GHS07	H225, H332, H319, H335, H336	P210, P240, P305+P351+P338, P403+P233
tert-Butylhydroperoxide 75-91-2	GHS02, GHS05, GHS06, GHS08, GHS09	H226, H242, H302, H311, H330, H314, H317, H341, H411	P210, P220, P280, P301+P330+P331, P303+P361+P353, P305+P351+P338, P310
Tetrabutylammonium bromide 1643-19-2	GHS07, GHS08	H302, H315, H319, H361fd, H412	P202, P273, P301+P312, P302+P352, P305+P351+P338, P308+P313
Tetrachloroethane-d_2 33685-54-0	GHS06, GHS09	H310, H330, H411	P262, P264, P273, P280, P302+P352+P310, P304+P340+P310
Tetrafluoroboric Acid 16872-11-0	GHS05	H314	P280, P303+P361+P353, P304+P340+P310, P305+P351+P338, P363
2,2,6,6-Tetramethyl, Piperidin-1-oxyl (TEMPO) 2564-83-2	GHS05	H314, H412	P260, P273, P280, P303+P361+P353, P304+P340+P310, P305+P351+P338
Tetraoctylammonium bromide 14866-33-2	GHS05	H315, H318	P264, P280, P302+P352, P305+P351+P338, P332+P313, P362+P364
Tetraphenylporphyrin 917-23-7	No classification according to GHS		
Thiophenol 108-98-5	GHS03, GHS05, GHS06, GHS07, GHS09	H226, H300, H301, H310, H311, H314, H315, H330, H410	P210, P233, P240, P241, P242, P243, P260, P262, P264, P270, P271, P273, P280, P284, P301+P310, P301+P330+P331, P302+P350, P302+P352, P303+P361+P353, P304+P340, P305+P351+P338, P310, P312, P320, P321, P322, P330, P332+P313, P361, P362, P363, P370+P378, P391, P403+P233, P403+P235, P405, P501
Titanium(III) chloride 7705-07-9	GHS02, GHS05	H250, H290, H314	P222, P280, P301+P330+P331, P303+P361+P353, P305+P351+P338, P422

Name and CAS-number	GHS symbols	Hazard statements	Precautionary statements
Titanium(IV) chloride 7550-45-0	GHS05, GHS06	H314, H330, H335, EUH014	P260, P271, P280, P303+P361+P353, P304+P340+P310, P305+P351+P338
3-Toluidine 108-44-1	GHS06, GHS08, GHS09	H301, H311, H331, H373, H410	P273, P280, P301+P310+P330, P302+P352+P312, P304+P340+P311, P314
4-Toluidine 106-49-0	GHS06, GH08, GHS09	H301, H311, H331, H317, H319, H351, H410	P273, P280, P301+P310, P302+P352+P312, P304+P340+P311, P305+P351+P338
1,2,4-Trichlorobenzene 120-82-1	GHS07, GHS09	H302, H315, H410	P264, P270, P273, P280, P301+P312, P302+P352
Triethylamine 121-44-8	GHS02, GHS05, GHS06	H225, H302, H311+H331, H314, H335	P210, P280, P301+P330+P331, P303+P361+P353, P304+P340+P311, P305+P351+P338+P310
Triethyl phosphite 122-52-1	GHS03, GHS07	H226, H302, H317, H412	P210, P233, P273, P280, P301+P312, P303+P361+P353
Trifluoroacetic anhydride 407-25-0	GHS05, GHS07	H332, H314, H412, EUH014	P261, P273, P280, P303+P361+P353, P304+P340+P310, P305+P351+P338
4-Trifluoromethyl aniline 98-16-8	GHS05, GH06, GHS08, GHS09	H302, H312, H330, H315, H318, H335, H373, H411	P280, P301+P330+P331, P302+P352, P304+P340, P305+P351+P338, P310, P332+P313
Trimethylsilyl azide 4648-54-8	GHS02, GHS06	H225, H301, H311, H331	P210, P233, P280, P301+P310, P303+P361+P353, P304+P340+P311
Trimethylsilyl diazomethane 18107-18-1	GHS02, GHS06, GHS08, GHS09	H225, H304, H315, H330, H336, H350, H361f, H370, H411	P202, P210, P273, P303+P361+P353, P304+P340+P310, P331
Trimethylsilyl cyanide 7677-24-9	GHS02, GHS06, GHS09	H225, H300, H310, H330, H410, EUH029	P210, P233, P273, P280, P303+P361+P353, P304+P340+P310
Tris(2,4-di-*tert*-butylphenyl)phosphite 31570-04-4	GHS07	H315, H319, H413	P264, P273, P280, P337+P313, P332+P313
Vanadyl Acetylacetonate 3153-26-2	GHS07	H302, H315, H319, H335	P261, P264, P271, P301+P312, P302+P352, P305+P351+P338

[1] *GESTIS-Stoffdatenbank*, www.gestis.dguv.de, accessed **August 29, 2024**. [2] *Sigma Aldrich Web Catalog*, www.sigmaaldrich.com, accessed **August 29, 2024**. [3] *TCI Web Catalog*, www.tcichemicals.com, accessed **August 29, 2024**.

Figure 9.1. GHS pictograms.

9.2 Curriculum Vitae

Lebenslauf aus datenschutzrechtlichen Gründen nicht enthalten.

Lebenslauf aus datenschutzrechtlichen Gründen nicht enthalten.

10.   Acknowledgements

11.　　Eidesstattliche Versicherung

Hiermit versichere ich an Eides statt, die vorliegende Dissertationsschrift selbst verfasst und keine anderen als die angegebenen Quellen und Hilfsmittel benutzt zu haben. Sofern im Zuge der Erstellung der vorliegenden Dissertationsschrift generative Künstliche Intelligenz (gKI) basierte elektronische Hilfsmittel verwendet wurden, versichere ich, dass meine eigene Leistung im Vordergrund stand und dass eine vollständige Dokumentation aller verwendeten Hilfsmittel gemäß der Guten wissenschaftlichen Praxis vorliegt. Ich trage die Verantwortung für eventuell durch die gKI generierte fehlerhafte oder verzerrte Inhalte, fehlerhafte Referenzen, Verstöße gegen das Datenschutz- und Urheberrecht oder Plagiate.

Hamburg, den 06.09.2024